(2)

RLE Progress Report

No. 133

January 1 - December 31, 1990

Submitted by

Professor Jonathan Allen
Professor Daniel Kleppner

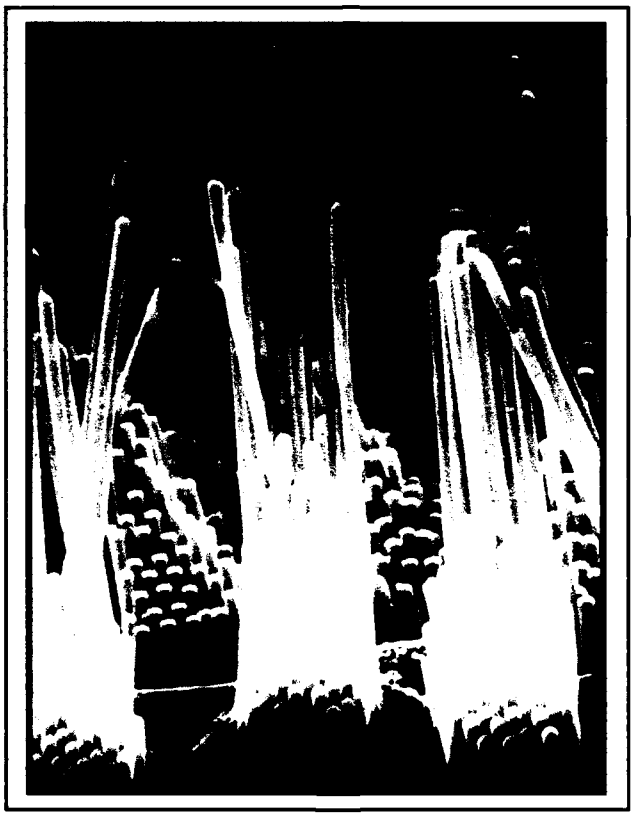

Research Laboratory of Electronics
Massachusetts Institute of Technology
Cambridge, Massachusetts

RLE Progress Report No. 133

Cover and title page: In 1991, we celebrate two big anniversaries—the RadLab's 50th and RLE's 45th. The Research Laboratory of Electronics, which was established in 1946, grew out of MIT's wartime Radiation Laboratory (1940-45). In honor of the milestones that we are sharing this year, the cover of *RLE Progress Report No. 133* notes the rich tradition of communications research in RLE.

In the early days of RLE, former RadLab staff member Professor Jerome B. Wiesner, collaborating with Professors Yuk Wing Lee and Norbert Wiener, developed practical applications for the theory of nonlinear systems. By combining the methods and techniques of mathematicians and communication engineers, the study of communication theory in RLE was not confined to electrical systems.

As new theories of modern communication were introduced in the 1950s, they were applied to new studies of the nervous system. Professor Walter A. Rosenblith worked with Professor Norbert Wiener to apply statistical communication techniques to the field of communication biophysics. This research established quantitative relations between neuroelectric data and the characteristics of sensory stimuli.

This tradition continues today. For example, members of RLE's Auditory Physiology Group are studying the sound-induced motions of mechanically sensitive cells (hair cells) in the inner ear, which contain microscopic hairs that vibrate when the ear is stimulated by sound. These vibrations are transduced by the hair cells to excite nerve fibers that carry the information about the sound stimulus to the brain. Shown on the cover is a scanning electron micrograph of the microscopic sensory hairs of a lizard, prepared by Dr. Ruth Anne Eatock. Approximately 60 hairs project from each sensory receptor cell, and the receptor cells are organized by length (2 to 20 microns for the cells shown) in an orderly staircase array. The mechanical properties of these sensory hairs play an important role in determining the neural code for sound.

Dr. Eatock, a former postdoctoral fellow in RLE under the direction of Professor Thomas F. Weiss, is presently an Assistant Professor in the Physiology Department at the University of Rochester.

Our special thanks to the following staff members of the RLE Communications Group: Mary J. Ziegler for her exceptional editing, formatting, and scanning; Mary S. Greene for proofreading and preparation of the publications and personnel chapters; and Rita C. McKinnon for her help with proofreading. We also want to thank David W. Foss, Manager of the RLE Computer Facility, for his technical assistance.

We thank the faculty, staff, and students of RLE for their generous cooperation.

Editor:	Barbara Passero
Design and Illustration:	Robert H. Priest
Photography:	John F. Cook
Printer:	DS Graphics, Pepperell, Massachusetts
Typesetting:	This report was produced with IBM's BookMaster Software. Mylar negatives were printed on an IBM 4250-II electro-erosion printer.

ISSN 0163-9218

REPORT DOCUMENTATION PAGE

Form Approved
OMB No. 0704-0188

1. AGENCY USE ONLY (Leave blank)	2. REPORT DATE	3. REPORT TYPE AND DATES COVERED
	August 1991	Technical 1 Jan 1990 - 31 Dec 1990

4. TITLE AND SUBTITLE

Research Laboratory of Electronics Progress Report No. 133

5. FUNDING NUMBERS

DAAL03-89-C-0001

6. AUTHOR(S)

Jonathan Allen and Daniel Kleppner

7. PERFORMING ORGANIZATION NAME(S) AND ADDRESS(ES)

Massachusetts Institute of Technology
Research Laboratory of Electronics
Cambridge, MA 02139

8. PERFORMING ORGANIZATION REPORT NUMBER

9. SPONSORING/MONITORING AGENCY NAME(S) AND ADDRESS(ES)

U. S. Army Research Office
P. O. Box 12211
Research Triangle Park, NC 27709-2211

10. SPONSORING/MONITORING AGENCY REPORT NUMBER

ARO 26213.96-EL

11. SUPPLEMENTARY NOTES

The view, opinions and/or findings contained in this report are those of the author(s) and should not be construed as an official Department of the Army position, policy, or decision, unless so designated by other documentation.

12a. DISTRIBUTION/AVAILABILITY STATEMENT

Approved for public release; distribution unlimited.

12b. DISTRIBUTION CODE

13. ABSTRACT *(Maximum 200 words)*

RLE Progress Report Number 133 describes research programs at RLE for the period January 1 through December 31, 1990. Each chapter of the *Progress Report* contains both a statement of research objectives and a summary of research efforts for research projects listed. Faculty, research staff, students and others who participated in these projects are identified at the beginning of each project, along with sources of funding.

There are three appendices at the end of the report: Appendix A is a bibliography of RLE publications and papers presented by RLE staff during 1989; Appendix B is a roster of current RLE staff; and Appendix C is an index of RLE sponsors. In addition, the Project Staff and Subject Index provides access to the information in this report.

14. SUBJECT TERMS

Electronics, Solid State Physics, Optics, Applied Physics, Radio Astronomy

15. NUMBER OF PAGES

390

16. PRICE CODE

17. SECURITY CLASSIFICATION OF REPORT	18. SECURITY CLASSIFICATION OF THIS PAGE	19. SECURITY CLASSIFICATION OF ABSTRACT	20. LIMITATION OF ABSTRACT
UNCLASSIFIED	UNCLASSIFIED	UNCLASSIFIED	UL

Table of Contents

● Sponsored by the Joint Services Electronics Program

APPENDICES

Introduction

The Research Laboratory of Electronics

The Research Laboratory of Electronics (RLE) was established in 1946 as the Institute's first interdepartmental laboratory. Originally organized under the joint sponsorship of the Departments of Physics and Electrical Engineering, RLE has broadened its interests to cover a wide range of research.

The RLE environment provides both the freedom of action essential in an academic institution and the availability of large-scale laboratory facilities and services required by researchers. RLE's interdisciplinary setting offers many opportunities for creative and collaborative research. By fostering this powerful combination of research and education, RLE effectively penetrates beyond the horizon of new ideas and information.

RLE Progress Report

RLE Progress Report Number 133 describes research programs at RLE for the period January 1 through December 31, 1990. Each chapter of the *Progress Report* contains both a statement of research objectives and a summary of research efforts for research projects listed. Faculty, research staff, students and others who participated in these projects are identified at the beginning of each project, along with sources of funding.

There are three appendices at the end of the report: Appendix A is a bibliography of RLE publications and papers presented by RLE staff during 1989; Appendix B is a roster of current RLE staff; and Appendix C is an index of RLE sponsors. In addition, the Project Staff and Subject Index provides access to the information in this report.

RLE Progress Report Number 133 was produced by the RLE Communications Office. Further inquiries may be addressed to:

Research Laboratory of Electronics
Communications Office
Room 36-412
Massachusetts Institute of Technology
Cambridge, Massachusetts 02139-4307
Tel. (617) 253-2566
Fax (617) 258-7864

Part I Solid State Physics, Electronics and Optics

Section 1 Materials and Fabrication

Chapter 1. Submicron Structures Technology and Research

Academic and Research Staff

Professor Henry I. Smith, Professor Dimitri A. Antoniadis, James M. Carter, Professor Jesus A. del Alamo, Professor Marc A. Kastner, Professor Terry P. Orlando, Dr. Mark L. Schattenburg, Professor Carl V. Thompson, Isobe Takashi

Visiting Scientists and Research Affiliates

Dr. Khalid Ismail,[1] C.T. Liu,[2] Yang Zhao[2]

Graduate Students

Phillip F. Bagwell, Martin Burkhardt, Gregory A. Carlin, William Chu, Kathleen R. Early, Christopher C. Eugster, Hao Fang, Stuart B. Field, Jerrold A. Floro, Reza A. Ghanbari, Hang Hu, Harold Kahn, Yao-Ching Ku, Arvind Kumar, Ady Levy, Yachin Liu, Hai P. Longworth, Udi E. Meirav, Alberto M. Moel, Haralabos Papadopoulos, Samuel L. Park, George E. Rittenhouse, John H.F. Scott-Thomas, David G. Steel, Lisa Su, Siang-Chun The, Kenneth Yee, Anthony Yen

Undergraduate Students

JoAnne M. Gutierrez, Chee-Heng Lee, Kenneth P. Lu, Euclid E. Moon, Pablo Munguia, Lee-Peng Ng, Daniel B. Olster, Shahir R. Salyani, Flora S. Tsai, Lead Wey

Technical and Support Staff

Donna R. Martinez, Mark K. Mondol, Jeanne M. Porter

1.1 Submicron Structures Laboratory

The Submicron Structures Laboratory at MIT develops techniques for fabricating surface structures with linewidths in the range from nanometers to micrometers and uses these structures in a variety of research projects. These projects of the laboratory, which are described briefly below, fall into four major categories: (1) development of submicron and nanometer fabrication technology; (2) nanometer and quantum-effect electronics; (3) crystalline films on non-lattice-matching substrates; and (4) periodic structures for x-ray optics, spectroscopy and atomic interferometry.

1.2 Microfabrication at Linewidths of 100 nm and Below

Sponsors

Joint Services Electronics Program
Contract DAAL03-89-C-0001
National Science Foundation
Grant ECS 87-09806

Project Staff

Martin Burkhardt, James M. Carter, William Chu, Kathleen R. Early, Reza A. Ghanbari, Yao-Ching Ku, Alberto M. Moel, Dr. Mark L. Schattenburg, Professor Henry I. Smith, Siang-Chun The, Anthony Yen

A variety of techniques for fabricating structures with characteristic dimensions of 0.1 μm (100 nm) and below are investigated. These include: x-ray nanolithography, holographic lithography, achro-

[1] IBM Corporation, Thomas J. Watson Research Center, Yorktown Heights, New York.

[2] Princeton University, Princeton, New Jersey.

matic holographic lithography, electron-beam lithography, focused-ion-beam lithography, reactive-ion etching, electroplating, and liftoff. Development of such techniques is essential if we are to explore the rich field of research applications in the deep-submicron and nanometer domains.

X-ray nanolithography is of special interest because it can provide high throughput and broad process latitude at linewidths of 100 nm and below. Figure 1 shows the replication of a 100 nm period grating (40 nm linewidths) using the C_k x ray at 4.5 nm. We are developing a new generation of x-ray masks made from inorganic membranes, primarily SiN_x, in order to eliminate pattern distortion and avoid mask breakage during handling. Figure 2 shows our most recent mask architecture. The mesa rim is composed of Si (what remains of a Si wafer that has been etched away). The SiN_x membrane is under moderate tension and is optically flat to better than 0.25 μm.

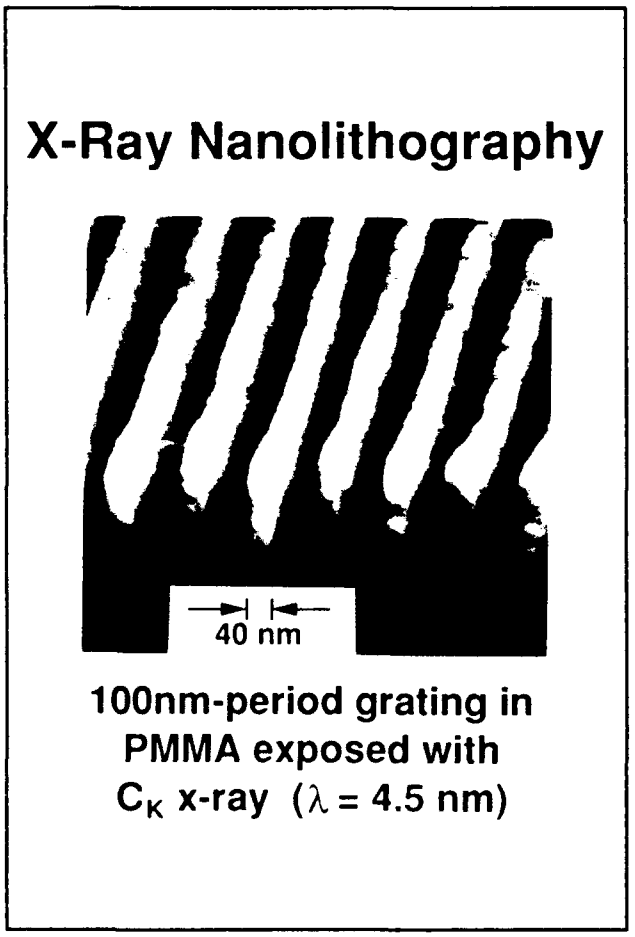

Figure 1. Scanning electron micrograph of a 100 nm-period grating (40 nm lines, 60 nm spacers) exposed in PMMA using the C_k x-ray (4.5 nm) and a mask made with tungsten absorbers. Previously, the finest grating period replicated was 200 nm, although linewidths below 30 nm are routinely replicated.

To achieve gaps of 5 μm and below, we can use spacer studs on the mesa rim. Such gaps are routinely achieved and allow us to replicate sub-100 nm features using the Cu_L line at 1.34 nm. To achieve multiple-mask alignment we currently use a dark field optical imaging system. In the future, in order to produce alignments compatible with 50 nm linewidths, we will fix the mask-sample gap at 4 μm, translate the mask piezoelectrically, and detect alignment to < 10 nm by a dual-grating interferometric scheme.

Phase-shifting x-ray masks should permit us to achieve sub-50 nm linewidths at gaps ~ 4 μm. In previous studies, we showed that a pi-phase-shifting mask improves process latitude by increasing the irradiance slope at feature edges. For linewidths below 50 nm, we bring the mask membrane into soft contact with the substrate by electrostatic means.

A variety of techniques are used to pattern the x-ray masks including e-beam lithography, focused-ion-beam lithography (FIBL), holographic lithography and sidewall shadowing. Figure 3 shows the process used, and figure 4a shows the result of e-beam lithography in a collaborative effort with S. Rishton of IBM. Using a single-layer resist, 250 nm thick, we were able to expose 50 nm lines and spaces of a quantum-effect device pattern and subsequently electroplate 200 nm of gold, suitable for the Cu_L x-ray at 1.34 nm. Reduced electron back-scattering from the 1

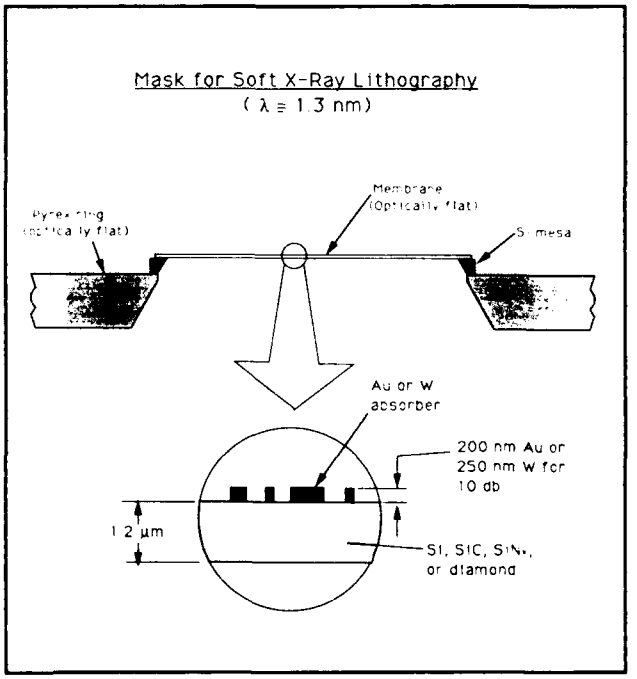

Figure 2. Schematic of the mesa-rim x-ray mask architecture. The mesa rim is composed of Si etched from a Si wafer that had been anodically bonded to the pyrex frame. The membrane is stress-controlled SiN_x.

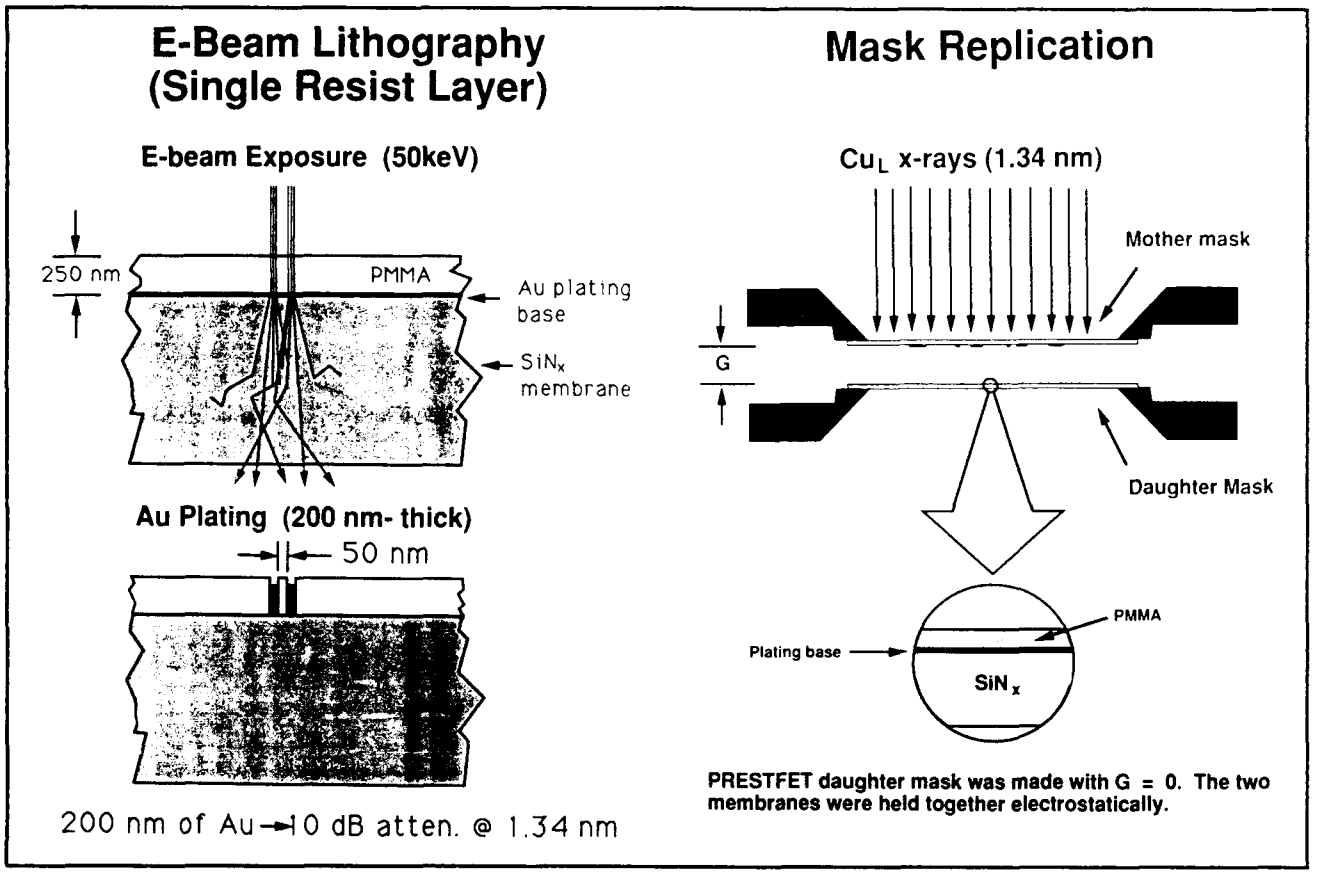

Figure 3. Schematic depiction of process used to make x-ray masks of 50 nm lines and spaces. The e-beam lithography depicted (left) achieves fine pitch by virtue of the thin (1 μm) substrate which reduces backscattering. The electroplating (right) is done under conditions that produce zero stress.

μm-thick SiN_x membrane played a crucial role in achieving such a result. This mask was then replicated with x rays and the "opposite polarity" pattern obtained (figure 4b).

We have further developed the achromatic holographic lithography (AHL), which enables us to achieve 100 nm period gratings (50 nm nominal linewidth). New anti-reflection resists have been developed and tested. This technology will be used to make gratings for x-ray spectroscopy and atom beam interferometry, and to fabricate new classes of quantum-effect electronic devices.

1.3 Improved Mask Technology for X-Ray Lithography

Sponsors

Semiconductor Research Corporation
Contract 90-SP-080
U.S. Navy - Naval Research Laboratory
Contract N00014-90-K-2018

Project Staff

JoAnne M. Gutierrez, Yao-Ching Ku, Kenneth P. Lu, Lee-Peng Ng, Shahir R. Salyani, Professor Henry I. Smith, Lisa Su, Flora S. Tsai, Lead Wey

In order to utilize x-ray lithography in the fabrication of submicron integrated electronics, distortion in the x-ray mask must be eliminated. Distortion can arise from stress in the absorber, which is usually gold or tungsten. Tungsten is preferred because it is a closer match in thermal expansion to Si, SiC, SiN_x and other materials used as mask membranes. However, W is usually under high stress when deposited by evaporation or sputtering. Earlier, we demonstrated that for a given type of substrate, zero stress (i.e., less than 5 x 107 dynes/cm^2) can be achieved by controlling the sputtering pressure to within one-tenth of a militorr. This year we have developed a computer-controlled system for monitoring *in situ*, during deposition, the stress in sputtered W on x-ray mask membranes. Stress is determined from the resonant frequency of the membrane. By monitoring the membrane resonant frequency during deposition and taking into account the mass

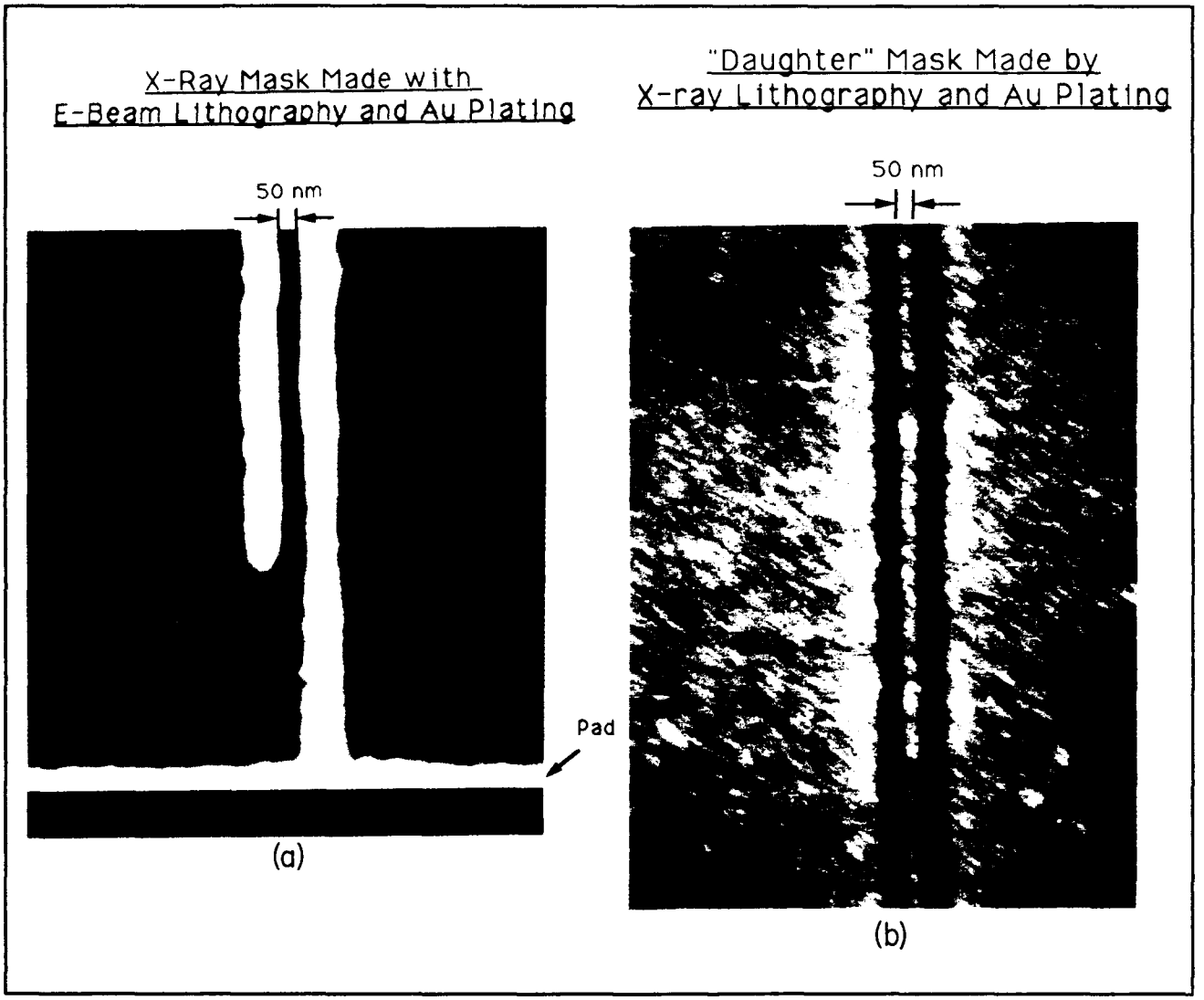

Figure 4. (a) Scanning electron micrograph of the absorber pattern on an x-ray mask, fabricated by the process depitcted in figure 3. The lines and spaces are ~ 50 nm. (b) Scanning electron micrography of a "daughter" x-ray mask made by replication of the mask in (a) followed by electroplating. The 50 nm lines and spaces are preserved in this replication process.

loading and temperature shifts, we can achieve zero stress (i.e., below 5 x 107 dynes/cm^2).

We are also investigating mask membranes including: SiN_x, SiC, and laminates of SiO_2/Si_3N_4. The strongest membranes were Si rich Si_3N_4. A 1.2 μm thick membrane of this material can sustain a full atmosphere pressure differential across a span of 20 mm. Because of its unusual strength we now use SiN_x as a vacuum window, 20 mm in diameter. We have also investigated the radiation hardness of SiN_x (in collaboration with the University of Wisconsin) and found very minor changes in resonant frequency as a result of over one million equivalent x-ray exposures.

1.4 Study of Electron Transport in Si MOSFETs with Deep-Submicron Channel Lengths

Sponsor

Joint Services Electronics Program
Contract DAAL03-89-C-0001

Project Staff

Professor Dimitri A. Antoniadis, Gregory A. Carlin, Hao Fang, Hang Hu, Professor Henry I. Smith, Siang-Chun The

We have continued to use x-ray lithography to fabricate NMOS devices with effective channel lengths down to 50 nm. As channel lengths decrease below about 150 nm, velocity overshoot has been observed both at room and liquid nitrogen temperatures. It appears that a necessary condition for this phenomenon is high surface mobility which we have achieved in our devices by utilizing a sharp, retrograde doping of the channel. Our initial devices used a single, moderately deep boron ion implant followed by a very short thermal activation step that also grew the gate oxide. More recently, we have used indium implants to achieve improved results. Indium, by virtue of its heavier mass, gives much sharper retrograde doping than boron. Also, it is a slower diffuser than boron, allowing more flexibility in subsequent thermal processing. Finally, it tends to segregate and diffuse through silicon dioxide, and thus it is better suited to give a low interface doping concentration.

Record saturated transconductances (710 mS/mm) were obtained with the new In-doped devices. This underscores the achievement of increased surface mobility with the steeper retrograde channel doping. Velocity overshoot and reduction of impact ionization rate with channel length reduction, which were observed earlier in boron-doped NMOS devices, were also observed in the In-doped devices.

During this reporting period we have also developed a technology for self-aligned silicided NMOS device fabrication. We have used cobalt deposition on the exposed silicon of source/drain and gate electrodes, with a subsequent two-step (450°C and 750°C) rapid thermal annealing, to form $CoSi_2$ self-aligned to the exposed silicon. Thin oxide or silicon nitride spacers around the gate electrode have been used to prevent shorts between sources/drains and gates. These process improvements were tested first with conventional lithography where the short gate was achieved by resist erosion in an O_2 plasma after resist exposure and development. More recently, an inorganic x-ray mask technology was developed and has allowed us to use x-ray lithography for the definition of the gates. Fabrication of devices with the new technologies is now in progress.

Work is also in progress to develop a corresponding deep-submicron self-aligned PMOS process. This should give us 100 nm-channel-length CMOS circuits fabricated by an x-ray lithography technology compatible with commercial mass production.

1.5 Studies of Electronic Conduction in One-Dimensional Semiconductor Devices

Sponsors

Joint Services Electronics Program
Contract DAAL03-89-C-0001
National Science Foundation
Grant ECS 85-03443

Project Staff

Professor Dimitri A. Antonaidis, Stuart B. Field, Professor Marc A. Kastner, Samuel L. Park, John H.F. Scott-Thomas, Professor Henry I. Smith

Sophisticated processing techniques and advanced lithography have allowed us to enter what we believe is a fundamentally new regime in the study of electronic conduction in one-dimensional systems. A slotted-gate MOSFET structure (figure 5) was used to produce an electron gas at the Si/SiO_2 interface beneath the gap in the lower-gate. This was done by biasing the upper gate positively, while keeping the slotted gate just below threshold. Fringing fields around the lower gate confined the electron gas to a width substantially narrower ($\sim$ 25 nm) than the distance separating the two halves of the slotted gate ($\sim$ 70 nm). The slotted gate was produced using x-ray nanolithography and liftoff. It was composed of refractory metals to allow a subsequent high temperature anneal. This anneal removed damage created by the e-beam evaporation of the refractory metal, so that the electron gas had a mobility of 15,000 cm^2/V-sec at 4.2K. The electrical conductance of the 1-D gas was measured as a function of the upper gate voltage for temperatures less than 1K, and a surprising series of periodic oscillations was seen in the conductance (figure 6).

Changing the gate voltage can be thought of as changing the number of electrons per unit length of electron gas. Since the conductance is thermally activated, the oscillations reflect a periodic change in the activation energy of the electron gas as the electron density is changed. Computer simulations solving Poisson's equation and the single particle Schrodinger wave equation strongly suggest that the electron gas is dynamically one-dimensional when the oscillations are most strongly seen. That is, the electrons are in the lowest quantum energy level of the potential well created by the fringing fields of the slotted gate.

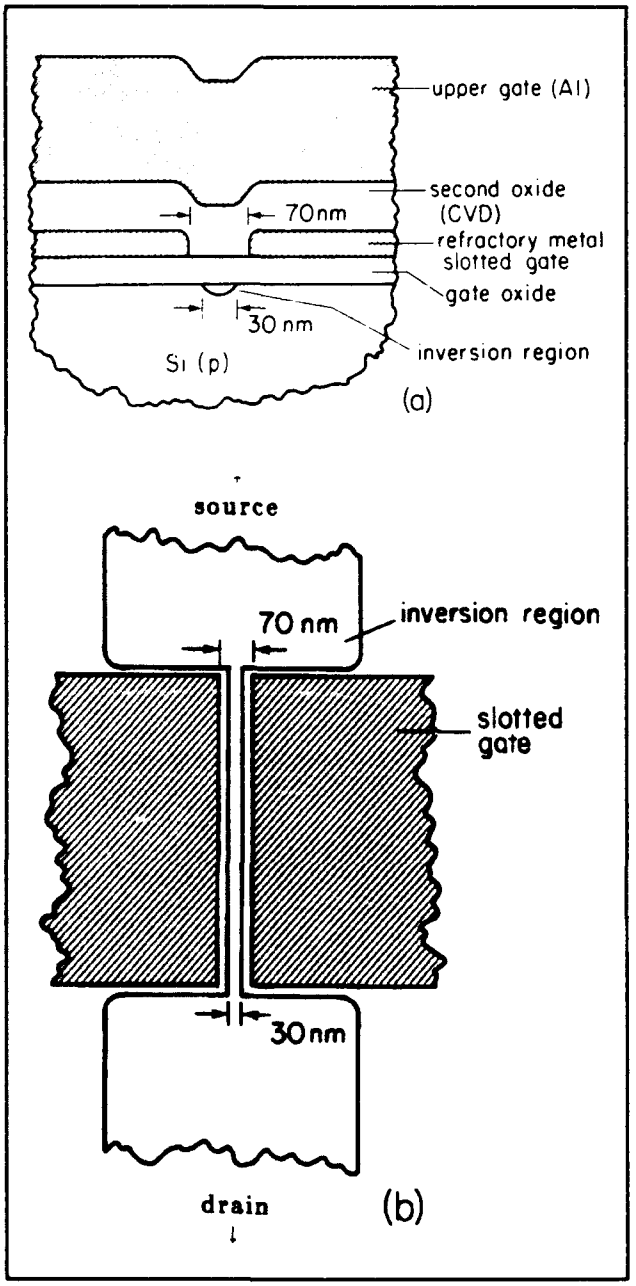

Figure 5. (a) Schematic cross section and (b) top view of the slotted-gate device. The inversion layer, formed by the positively biased upper gate is confined by the lower gate. The thermal oxide and refractory metal lower gate are both 30 nm thick, and the chemical vapor deposition oxide is 45 nm thick. The width of a narrow inversion layer is exaggerated in (b).

The period of the oscillations varies randomly from device to device. Additionally, the period changes when the same device is heated to room temperature and then cooled. This suggests that impurities are responsible for the conductance oscillations. The impurities delimit a segment of the channel that is capacitively coupled to the gates of the device. The electrostatic energy required to move an electron into this segment (and hence carry current) changes periodically with the gate voltage. This so-called Coulomb Blockade model of the oscillations is strongly supported by recent experiments in similar GaAs devices. It should be stressed that these oscillations are seen with no magnetic field, implying that the phenomenon is fundamentally different from phenomena requiring Landau quantization (such as the Quantum Hall Effect).

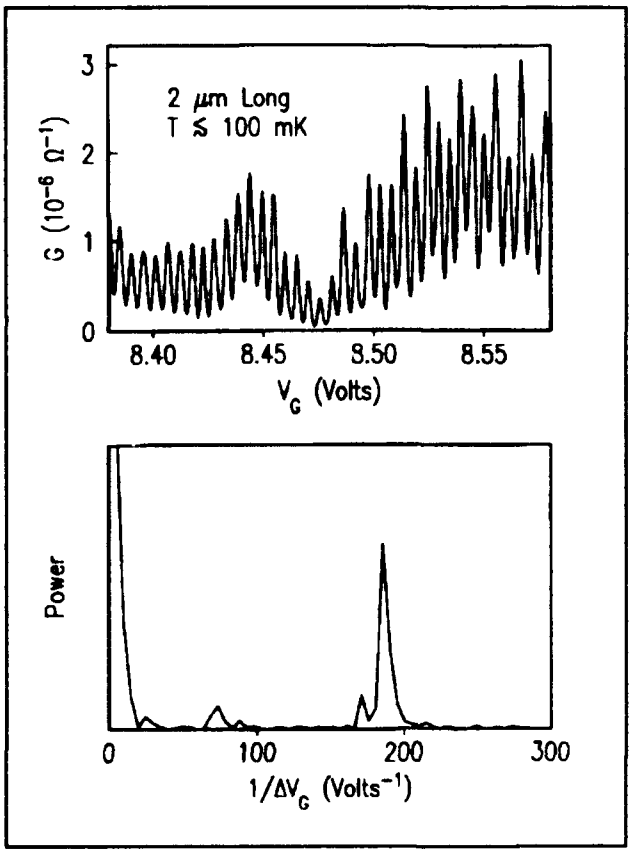

Figure 6. Top Panel. Conductance G versus gate voltage V_G for a 2 μm-long inversion layer. Bottom panel: Fourier power spectrum of the top panel data.

1.6 Lateral-Surface-Superlattice and Quantum Wire Arrays in Si

Sponsors

Joint Services Electronics Program
Contract DAAL03-89-C-0001
U.S. Air Force - Office of Scientific Research
Grant AFOSR 88-0304

Project Staff

Professor Dimitri A. Antoniadis, Phillip F. Bagwell, Professor Terry P. Orlando, Professor Henry I. Smith

We have been studying quantum mechanical effects in electrical conduction using the silicon grating gate field effect transistor (GGFET). The Si GGFET is a dual stacked-gate MOS type structure in which the gate closest to the inversion layer (bottom gate) is a 200 nm period grating made of refractory metal. A SiO_2 insulating layer separates the grating gate and the inversion layer from a second continuous aluminum gate (top gate). Using this dual gate structure, we can gradually vary the electron geometry in the inversion layer from many narrow wires in parallel, to a superlattice, and to a two-dimensional electron gas.

Electron weak localization becomes much more pronounced as the device is electrostatically pinched from a 2D inversion layer into many narrow 1D wires in parallel, proving that the wire width can be reduced below the electron phase coherence length. For fixed intermediate magnetic field of 1-10 Tesla, there is a large drop in the current of 90% or more, which persists to room temperature as electrons are added to the device, so that it opens electrostatically from many narrow inversion layers in parallel into a 2D electron gas. This is due to electrostatically changing the boundary conditions on the classical Drude magnetoconductance tensor from those of a long and narrow to a short and wide MOSFET. At high magnetic fields edge states form in the wire array, so that the conductance versus gate voltage evolves into Hall steps having a height of $4e^2/h$ multiplied by the number of wires in parallel. In contrast to a wide MOSFET, the conduction band valley degeneracy is not resolved, giving rise to Hall steps of twice the expected size.

1.7 Study of Surface Superlattice Formation in GaAs/GaAlAs Modulation Doped Field-Effect Transistors

Sponsor

U.S. Air Force - Office of Scientific Research
Grant AFOSR 88-0304

Project Staff

Professor Dimitri A. Antoniadis, Martin Burkhardt, William Chu, Professor Jesus A. del Alamo, Reza A. Ghanbari, Dr. Khalid Ismail, Professor Marc A. Kastner, Professor Terry P. Orlando, Professor Henry I. Smith, Kenneth Yee, Anthony Yen

We have used the modulation-doped field-effect transistor (MODFET) as a test vehicle for studying quantum effects such as electron back diffraction in a GaAs/AlGaAs material system. In a conventional MODFET, the current transport is modulated by a continuous gate between source and drain. In our studies, we have used Schottky metal gratings and grids for the gate, as illustrated in figure 7. Such gates produce a periodic potential modulation in the channel.

The grid was produced by x-ray nanolithography and liftoff. The x-ray mask of the grid was produced by two successive x-ray exposures at 90 degrees to one another, using a master mask that was fabricated via holographic lithography. The latter yields coherent gratings over areas several centimeters in diameter. A new technique was developed that yields grating and grid patterns only in the channel region between source and drain. This has simplified the overall process and enhanced its reliability.

The MODFET is normally on; that is, a negative gate bias of about -0.2 V must be applied to pinch off conductance from source to drain. As the gate bias is raised above this threshold point, the height of the periodic potential modulation is reduced and, simultaneously, the Fermi energy is raised (or, equivalently, the electron wavelength is reduced) in the 2D electron gas residing at the AlGaAs/GaAs interface. When the electron wavelength phase-matches the periodic potential, electron back-diffraction occur provided the inelastic length (i.e., the coherence or phase breaking length) is longer than the grating-period. Such back diffraction is manifested by a drop in the conductance. A stronger back diffraction effect is observed in the case of a grid because true minigaps are formed. The measurements of conductance modulation of grating and grid-gate MODFETs agrees with the theoretical predictions. In the grid gate devices it was also possible to

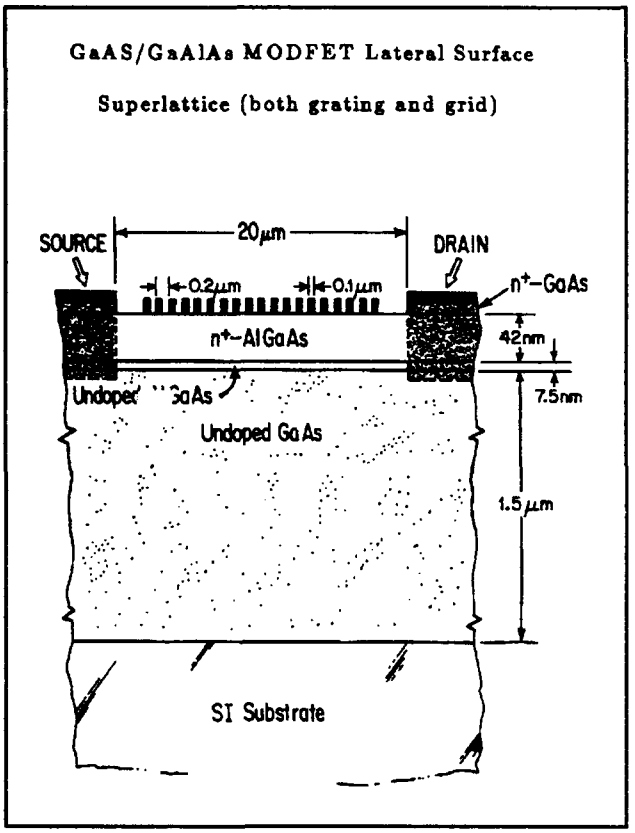

Figure 7. Schematic cross section of a grid-gate MODFET device. Contacts to the grid are made by pads off to the sides of the conduction channel.

observe negative differential resistance which might be due to sequential resonant tunneling.

We plan to decrease the periodicity of the gratings and grids by a factor of two, to 100 nm period. For devices with such fine grating periodicity, the superlattice effect might become more pronounced and observable at higher temperatures. We will also conduct magnetotransport measurements with devices of 100 and 200 nm periodicity.

We will also take advantage of a back-gate technology, illustrated in figure 8. This will give us the ability to independently control the confining potential experienced by the electrons, as well as the electron density in the channel. This will allow for much more quantitative understanding of device operation.

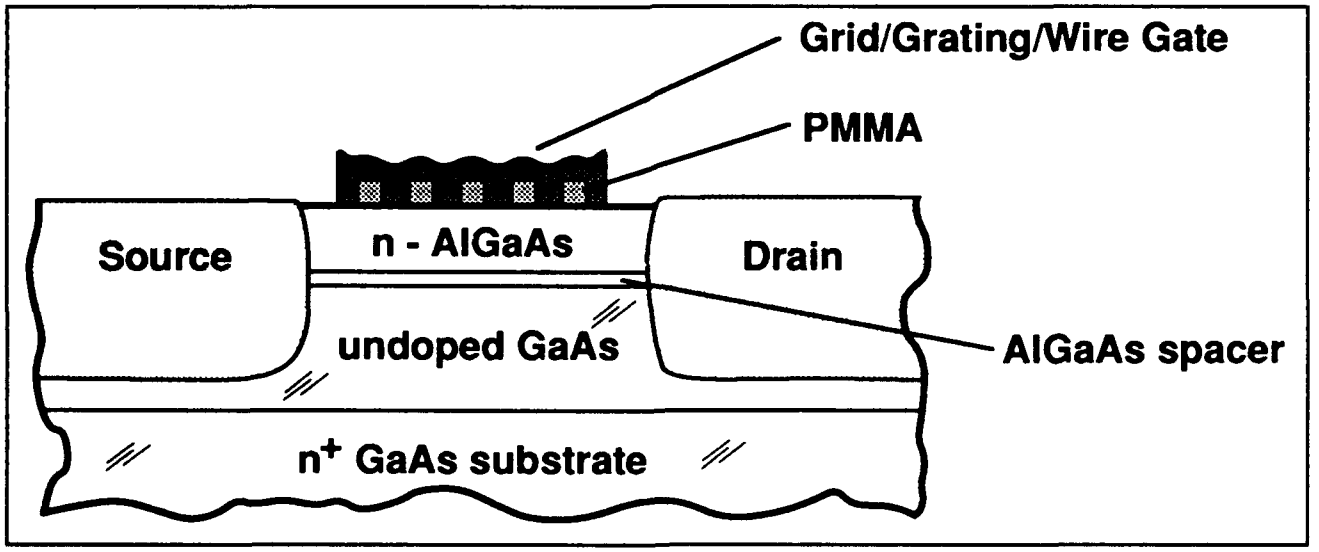

Figure 8. Schematic showing a cross section of our new configuration for studying grid-gate or grating-gate MODFETs and arrays of quantum wires. The substrate is n^+ doped, allowing us to apply a back bias to sweep the Fermi energy while keeping the potential modulation constant.

1.8 Study of One-Dimensional Subbands and Mobility Modulation in GaAs/AlGaAs Quantum Wires

Sponsors

Joint Services Electronics Program
Contract DAAL03-89-C-0001
U.S. Air Force - Office of Scientific Research
Grant AFOSR 88-0304

Project Staff

Professor Dimitri A. Antoniadis, Phillip F. Bagwell, Dr. Keith Evans, Reza A. Ghanbari, Dr. Khalid Ismail, Professor Terry P. Orlando, Professor Henry I. Smith

In order to study one-dimensional conductivity in the AlGaAs/GaAs modulation-doped structure, but without the conductance fluctuations normally associated with single microscopic systems, we previously fabricated arrays of 100 parallel quantum wires (MPQW) by etching the wires into the MODFET structure. The devices were then ground thin from the back side so that the charge concentration in the quantum wires could be increased by applying a positive bias to a back-side contact or by illumination. The devices were not optimal because the degree confinement was set by the etch and not electrostatically. Also, thinning the samples was haphazard at best.

To overcome these difficulties, we have developed a technology that allows us to electrostatically confine the electrons to QID channels. In parallel, in collaboration with K. Evans at the Wright-Patterson Air Force Base, we are developing the technology to give us the backside gating by growing the epitaxial layers on n^+ GaAs instead of the traditional semi-insulating GaAs. A schematic of the device is shown in figure 8.

Using this approach, we can explore the regime from a regular 2D gas ($V_{TG} \approx 0$) to weakly coupled QID wires ($V_{TG} \approx 0.5V$) to strongly isolated QID wire ($V_{TG} < 1V$), while at the same time using the backgate to sweep the electron density and hence, "probe" the confining potential.

1.9 Arrays of Field-Effect-Induced Quantum Dots

Sponsors

Joint Services Electronics Program
Contract DAAL03-89-C-0001
U.S. Air Force - Office of Scientific Research
Grant AFOSR 88-0304

Project Staff

Professor Dimitri A. Antoniadis, Martin Burkhardt, Reza A. Ghanbari, Dr. Khalid Ismail, Professor Marc A. Kastner, C.T. Liu, Professor Terry P. Orlando, Professor Henry I. Smith, Dr. M. Shayegan, T.P. Smith, Dr. Daniel Tsui, Yang Zhao

A metal grid on a modulation-doped AlGaAs/GaAs substrate (depicted in figure 9a) produces a two-dimensional periodic potential modulation at the AlGaAs/GaAs interface via the Schottky effect. If a gate electrode is attached to the grid, the potential can be further modified with an external voltage source. By changing the gate voltage from positive to negative values, the potential seen by the electrons located at the AlGaAs/GaAs interface can be varied from uniform (in which case the electrons behave as a 2-D electron gas), to weakly coupled zero-D quantum wells (figure 9b), to isolated zero-D quantum dots (figure 9c). We have made such structures with spatial periods of 200 nm in both orthogonal directions using technology similar to that described in Section 1.7, but now the grid gate occupies an area of several square millimeters. The isolated quantum dots and the attendant zero-dimensional electronic subbands were examined in collaboration with D. Tsui at Princeton University using far-infrared (FIR) cyclotron resonance. Transitions between the discrete energy levels in the quantum dots were observed as a function of magnetic field. Results were in agreement with a theoretical model.

Currently, we are continuing our study using extremely high quality samples prepared by M. Shayegan's group at Princeton. With typically greater than $10^6 cm^2/Vsec$, the resolution of the experiments should improve dramatically.

We are currently fabricating a new set of grid-gate MODFETS, using an improved fabrication process and will study their transport, capacitance, and absorption properties as a function of magnetic field.

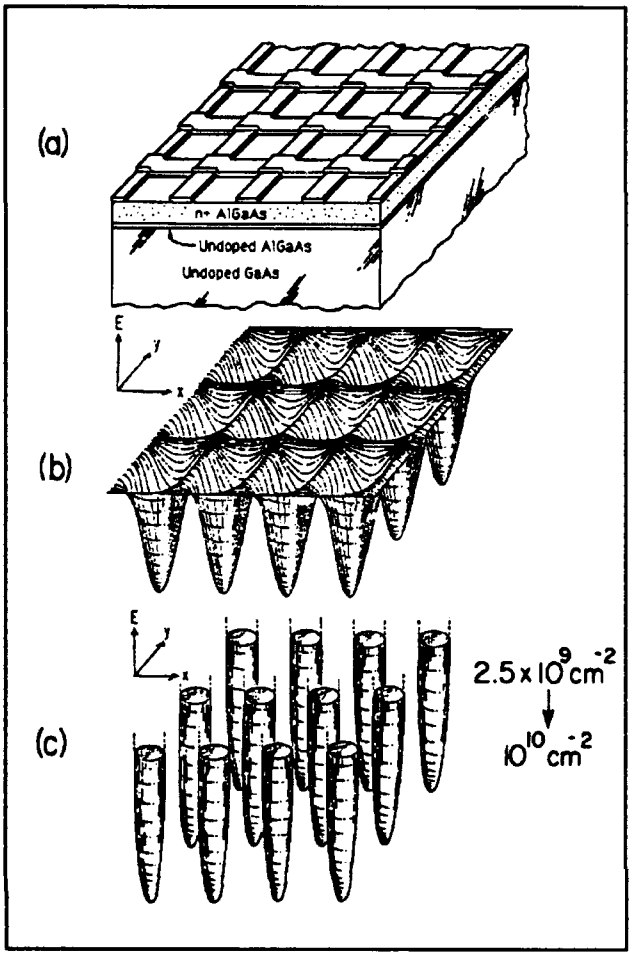

Figure 9. (a) Metal grid gate on a modulation-doped AlGaAs/GaAs substrate; (b) Depiction of potential seen by electrons at the AlGaAs/GaAs interface for weakly coupled quantum dots; (c) Potential for the case of isolated quantum dots.

1.10 Planar-Resonant-Tunneling Field-Effect Transistors (PRESTFET)

Sponsor

U.S. Air Force - Office of Scientific Research
Grant AFOSR 85-0154

Project Staff

Professor Dimitri A. Antoniadis, William Chu, Dr. Khalid Ismail, Professor Henry I. Smith

Previously, we reported on the performance of a planar-resonant-tunneling field-effect transistor (PRESTFET) depicted in figure 10, in which the gate electrodes were 60 nm long and separated by 60 nm. Clear evidence of resonant tunneling

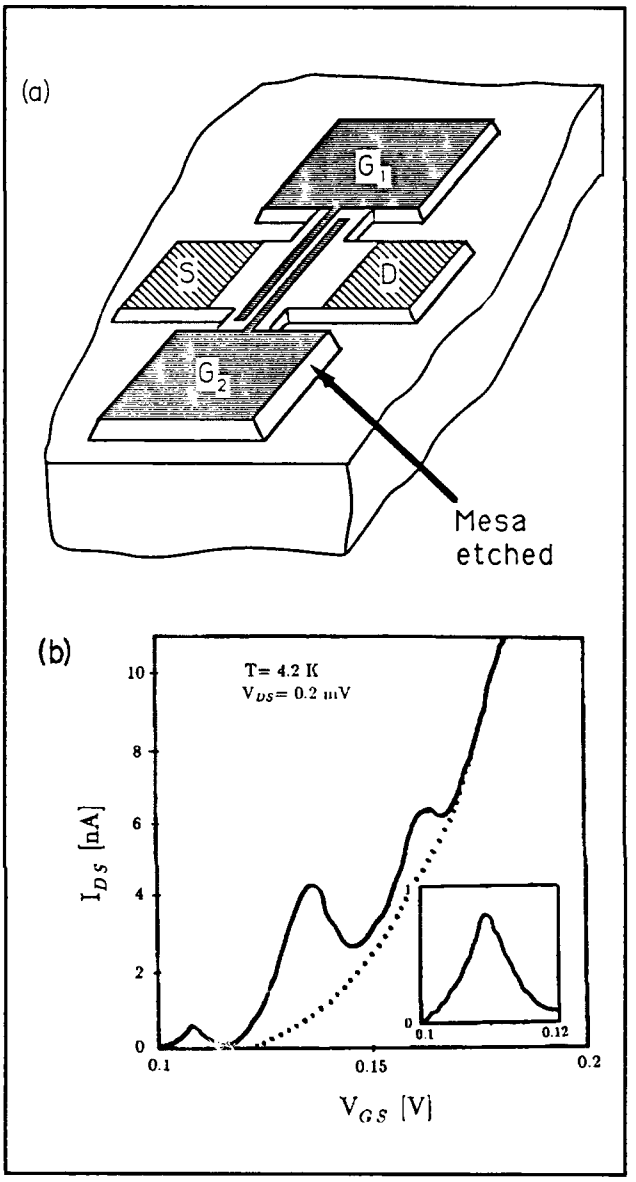

Figure 10. (a) Layout of a 4-terminal double-barrier planar-resonant-tunneling field-effect transistor (PRESTFET). (b) Plot of source-drain current versus gate voltage for a PRESTFET with 60 nm well width.

through the bound states in the well between electrodes was observed, as shown in figure 10b.

In order to reduce the electrode separation while retaining a large process latitude, we have chosen to pursue a new technology for making the PRESTFET. In collaboration with S. Rishton of IBM, a high-performance e-beam nanolithography system was used to write PRESTFET paterns on SiN_x x-ray mask membranes, 1 μm thick. Reduced backscattering from the thin membrane allows finer linewidths to be obtained, as shown in figure 3. The written masks are then processed and replicated at MIT. We have succeeded in making and replicating masks with PRESTFET patterns of 50

nm linewidth. The masks can be aligned to GaAs substrates using an adapted deep-UV aligner and exposed with the Cu_L x-ray (1.3 nm). Liftoff of appropriate Schottky electrodes will complete the device fabrication.

1.11 Submicrometer-Period Transmission Gratings for X-Ray and Atom-Beam Spectroscopy and Interferometry

Sponsors

Joint Services Electronics Program
Contract DAAL03-89-C-0001
X-OPT, Inc.

Project Staff

Dr. Mark L. Schattenburg, Professor Henry I. Smith, James M. Carter, Anthony Yen

Transmission gratings with periods of 0.1-1.0 nm are finding increasing utility in applications such as x-ray, vacuum-ultraviolet, and atom-beam spectroscopy and interferometry. Over 20 laboratories around the world depend on MIT-supplied gratings in their work, and this project constitutes the sole source for these diffractors. For x-ray and VUV spectroscopy, gratings are made of gold or tungsten and have periods of 0.1-1.0 μm and thicknesses ranging from 0.1-1 μm. They are most commonly used for spectroscopy of the x-ray emission from high-temperature plasmas. Transmission gratings are supported on thin (1μm) polyimide membranes or made self supporting ("free standing") by the addition of crossing struts (mesh). (For short x-ray wavelengths, membrane support is desired, while for the long wavelengths a mesh support is prefered in order to increase efficiency.) Fabrication is generally performed by holographic lithography, x-ray lithography and electroplating. Progress in this area tends to focus on decreasing the period and improving the yield and flexibility of the fabrication procedures.

Another application is the diffraction of long-de Broglie-wavelength (0.17Å) neutral sodium beams by mesh-supported gratings. Professor Pritchard's group at MIT has clearly demonstrated atomic diffraction with these gratings, and work is in progress to use these gratings to divide and recombine an atomic beam coherently, thus realizing an atom wave interferometer. Because good spatial coherence (low distortion) of the grating is critical to ensure measurable interference of the beams, efforts are concentrating on fabrication with low stress and high stiffness materials such as tungsten, silicon nitride, and silicon oxide.

1.12 High-Dispersion, High Efficiency Transmission Gratings for Astrophysical X-Ray Spectroscopy

Sponsor

National Aeronautics and Space Administration
Contract NAS8-36748

Project Staff

Professor Claude R. Canizares, Dr. Mark L. Schattenburg, Professor Henry I. Smith

This work involves a collaboration between the Center for Space Research and the Submicron Structures Laboratory (SSL), providing transmission gratings for the Advanced X-ray Astrophysics Facility (AXAF) x-ray telescope, currently scheduled for launch in 1998. Many hundreds of low-distortion, large area transmission gratings of 0.2 μm period (gold) and 0.6 μm period (silver) are required. These will provide high resolution x-ray spectroscopy of astrophysical sources in the 100 eV to 10 keV band.

Because of the requirements of low distortion, high yield, and manufacturability, a fabrication procedure involving the replication of x-ray masks has been selected. Masks are made of high-stiffness silicon nitride membranes to eliminate distortion. Masks are patterned using a process involving holographic lithography, reactive-ion etching, and electroplating. The masks are then replicated using soft x-rays (10 - 15 Å), and the resulting patterns electroplated with gold or silver. An etching step then yields membrane-supported gratings suitable for space use. Flight prototype gratings have been fabricated and continue to undergo space-worthiness tests. Progress in this area focuses on increasing the yield and flexibility of the fabrication procedures and perfecting various mask and grating evaluation tests.

1.13 Epitaxy via Surface-Energy-Driven Grain Growth

Sponsor

AT&T Bell Laboratories

Project Staff

Jerrold A. Floro, Professor Henry I. Smith, Professor Carl V. Thompson

Epitaxial grain growth (EGG) in polycrystalline thin films on single crystal substrates is being investigated as an alternative process for obtaining and studying epitaxy. EGG can produce smoother ultra-thin expitaxial films than those produced in conventional epitaxy and may yield lower defect densities as well. In addition, EGG can produce unique non-latticed-matched orientations not observed in conventional epitaxy.

The mechanism of epitaxial grain growth is simple. The anisotropic film/single-crystal substrate interfacial energy selects one film crystallographic orientation as having lowest total free energy. Grains in this orientation have the largest driving force for growth and will predominate as the system coarsens.

We have continued our work on model materials systems, i.e., metals on mica and alkali halides. We made extensive use this year of x-ray pole figure analysis for quantitative measurement of texture and epitaxy. Using this technique we measured the expitaxial fraction transformed versus film thickness, verifying the rate of EGG increases with decreasing film thickness as predicted by theory.

In order to achieve perfect epitaxy, the EGG process must be highly orientation selective, with a small fraction of iso-orientation grains in the initial population growing extremely large. We have shown that by proper treatment of a mica substrate surface prior to deposition, the selectivity can be greatly increased, and the final grain size can be as large as 50 μm, an order of magnitude larger than previously obtained. This increased selectivity is apparently due to modification of the mica surface chemistry.

We have performed extensive numerical analysis of EGG using mean field coarsening theory, we are trying to determine under what conditions (interface energy, boundary pinning, etc.) significant selectivity in grain growth rates can occur.

1.14 Publications

Journal Articles

Anderson, E.H., V. Bögli, M. Schattenburg, D. Kern, and H.I. Smith. "Metrology of Electron Beam Lithography Systems using Holographically Produced Reference Samples." Submitted to the 35th International Symposium on Electron, Ion and Photon Beams, Seattle, Washington, May 28-31, 1991.

Bagwell, P.F. "Evanescent Modes and Scattering in Quasi-One-Dimensional Wires." *Phys. Rev. B* 41: 354-371 (1990).

Bagwell, P.F., and A. Kumar. "Comment on Effects of Channel Opening and Disorder on the Conductance of Narrow Wires." Submitted to *Phys. Rev B.*

Bagwell, P.F., A. Yen, S.L. Park, D.A. Antoniadis, H.I. Smith, T.P. Orlando, and M.A. Kastner. "Magnetotransport in Multiple Narrow Silicon Inversion Channels Opened Electrostatically into a 2-Dimensional Electron Gas." In preparation.

Bagwell, B.F. "Solution of Dyson's Equation in a Quasi-One-Dimensional Wire." *J. Phy. Condens. Matter* 2: 6179 (1990).

Bagwell, P.F., T.P.E. Broekaert, T.P. Orlando, and C.G. Fonstad. "Resonant Tunneling Diodes and Transistors with a One, Two, and Three Dimensional Electron Emitter." *J. Appl. Phys.* 68: 4634-4646 (1990).

Chu, W., S.A. Rishton, M.L. Schattenburg, D.P. Kern, and H.I. Smith. "Fabrication of 50 nm Line and Space X-ray Masks in Thick Au using a 50 keV Electron Beam." Submitted to the 35th International Symposium on Electron, Ion and Photon Beams, Seattle, Washinton, May 28-31, 1991.

del Alamo, J.A., and C.C. Eugster. "Quantum Field-Effect Directional Coupler." *Appl. Phys. Lett.* 56: 78 (1990)

Field, S.B., M.A. Kastner, U. Meirav, J.H.F. Scott-Thomas, D.A. Antoniadis, H.I. Smith, and S.J. Wind. "Conductance Oscillations Periodic in the Density of One-Dimensional Electron Gases." *Phys. Rev. B* 42: 3523-3536 (1990).

Geis, M.W., and H.I. Smith. "Large-Area Mosaic Diamond Films Approaching Single-Crystal Quality." Submitted to *Appl. Phys. Lett.*

Ismail, K., F. Legoues, N.H. Karam, J. Carter, and H.I. Smith. "High Quality GaAs on Sawtooth-Patterned Si Substrates." Submitted to *Appl. Phys. Lett.*

Ismail, K., M. Burkhardt, H.I. Smith, N.H. Karam, and P.A. Sekula-Moise. "Patterning and Characterization of Large-Area Quantum-Wire Arrays." *Appl. Phys. Lett.* 58(14): 1539-1541 (1991).

Ismail, K., P.F. Bagwell, T.P. Orlando, D.A. Antoniadis, and H.I. Smith. "Quantum Phenonema in Field-Effect-Controlled Semiconductor Nanostructures." *IEEE Proc.* (1991). Forthcoming.

Ku, Y.C., L.-P. Ng, R. Carpenter, K. Lu, and H.I. Smith. "In-Situ Stress Monitoring and Deposition of Zero Stress W Absorber for X-ray Masks." Submitted to the 35th International Symposium on Electron, Ion and Photon Beams, Seattle, Washington, May 28-31, 1991.

Kumar, A., and P.F. Bagwell. "Resonant Tunneling in a Quasi-One-Dimensional Wire: Influence of Evanescent Modes." Submitted to *Phys. Rev. B*.

Kumar, A., and P.F. Bagwell. "Resonant Tunneling in a Multi-Channel Wire." *Solid State Commun.* 75 (12): 949-953 (1990).

Kumar, A., S.E. Laux, and F. Stern. "Electron States in a GaAs Quantum Dot in a Magnetic Field." Submitted to *Phys. Rev.*

Liu, C.T., D.C. Tsui, M. Shayegan, K. Ismail, D.A. Antoniadis, and H.I. Smith. "Guiding-Center-Drift Resonance of Two-Dimensional Electrons in a Grid-Gate Superlattice Potential." Submitted to *Appl. Phys. Lett.*

Liu, C.T., K. Nakamura, D.C. Tsui, K. Ismail, D.A. Antoniadis, and H.I. Smith. "Far-Infrared Transmission Measurements on Grid-Gate GaAs/AlGaAs Lateral-Surface-Superlattice Structures." *J. Surface Sci.* 228: 527 (1990).

Liu, C.T., D.C. Tsui, M. Shayegan, K. Ismail, D.A. Antoniadis, and H.I. Smith. "Oscillatory Density-of-States of Landau Bands in a Two-Dimensional Lateral Surface Superlattice." *Solid State Commun.* 75: 395-399 (1990).

Meirav, U., M.A. Kastner, and S.J. Wind. "Single Electron Charging and Periodic Conductance Resonances in GaAs Nanostructures." *Phys. Rev. Lett.* 65: 771-774 (1990).

Moel, A., M.L. Schattenburg, J.M. Carter, and H.I. Smith. "A Compact, Low-Cost System for Sub-100 nm X-ray Lithography." *J. Vac. Sci. Technol.* B8: 1648-1651 (1990).

Moel, A., W. Chu, K. Early, Y.C. Ku, E.E. Moon, M.L. Schattenburg, J.M. Bauer, F. Tsai, F.W. Griffith, L.E. Haas, and H.I. Smith. "Fabrication and Characterization of High-Flatness Mesa-Etched Silicon Nitride X-ray Masks." Submitted to the 35th International Symposium on Electron, Ion and Photon Beams, Seattle, Washington, May 28-31, 1991.

Schattenburg, M.L , K. Early, Y.C. Ku, W. Chu, M.I. Shepard, S.C. The, H.I. Smith, D.W. Peters, R.D. Frankel, D.R. Kelly, and J.P. Drumheller. "Fabrication and Testing of 0.1 μm-Linewidth Microgap X-ray Masks." *J. Sci. Technol.* B8: 1604-1608 (1990).

Schattenburg, M.L., C.R. Canizares, and H.I. Smith. "X-ray/VUV Transmission Gratings for Astrophysical and Laboratory Applications." *Phys. Scripta* 41: 13-20 (1990).

Schattenburg, M.L., C.R. Canizares, D. Dewey, K.A. Flanagan, M.A. Hamnett, A.M. Levine, K.S.K. Lum, R. Manikkalingam, T.H. Markert, and H.I. Smith. "Transmission Grating Spectroscopy and the Advanced X-ray Astrophysics Facility (AXAF)." Submitted to *Opt. Eng.*.

Schattenburg, M.L., K. Li, R.T. Shin, J.A. Kong, and H.I. Smith. "Electromagnetic Calculation of Soft-X-ray Diffraction from Nanometerscale Gold Structures." Submitted to the 35th International Symposium on Electron, Ion and Photon Beams, Seattle, Washington, May 28-31, 1991.

Smith, H.I., Scott D. Hector, M.L. Schattenburg, and E.H. Anderson. "A New Approach to High Fidelity E-Beam Lithography Based on an In-Situ, Global Fiducial Grid." Submitted to the 35th International Symposium on Electron, Ion and Photon Beams, Seattle, Washinton, May 28-31, 1991.

Smith, H.I., and H.G. Craighead. "Nanofabrication." *Phys. Today*, pp. 24-30 (February 1990).

Smith, H.I., and D.A. Antoniadis. "Seeking a Radically New Electronics." *Tech. Rev.* 93: 26-40 (1990).

Thompson, C.V., J. Floro, and H.I. Smith. "Epitaxial Grain Growth in Thin Metal Films." *J. Appl. Phys.* 67: 4099-4104 (1990).

Toriumi, A., K. Ismail, M. Burkhardt, D.A. Antoniadis, and H.I. Smith. "Resonant Magneto-Capacitance in a Two-Dimensional Lateral-Surface Superlattice." *Phys. Rev. B* 41: 12346-12349 (1990).

Published Meeting Papers

Early, K., M.L. Schattenburg, and H.I. Smith. "Absence of Resolution Degradation in X-ray Lithography from 1 from 4.5 nm to 0.83 nm." Microcircuit Engineering '89, Cambridge, England, September 26-28, 1989. *Microelectron. Eng.* 11: 317-321 (1990).

Floro, J.A., C.V. Thompson. "Epitaxial Grain Growth and Orientation Metals Metastability in Heteroepitaxial Thin Films." Materials Research Society Spring Meeting, San Francisco, California, April 17, 1990.

Karam, N.H., A. Mastrovita, V. Haven, K. Ismail, S. Pennycock, and H.I. Smith. "Patterning and Overgrowth of Nanostructure Quantum Well Wire Arrays by L.P. Movpw." Fifth International Conference on Metallorganic Vapor Phase Epitaxy, Aachen, Germany, June 18-21, 1990.

Ku, Y.C., H.I. Smith, and I. Plotnik. "Low Stress Tungsten Absorber for X-ray Masks." Microcircuit Engineering '89, Cambridge, England, September 26-28, 1989. *Microelectron. Eng.* 11: 303-308 (1990)

Liu, C.T., D.C. Tsui, M. Shayegan, K. Ismail, D.A. Antoniadis, and H.I. Smith. "Observation of Landau Level Splitting in Two-Dimensional Lateral Surface Superlattices." 20th International Conference on the Physics of Semiconductors, Thessaloniki, Greece, August 6-10, 1990.

Liu, C.T., D.C. Tsui, M. Santos, M. Shayegan, K. Ismail, D.A. Antoniadis, and H.I. Smith. "Magnetoresistance of Two-Dimensional Electrons in a Two-Dimensional Lateral Surface Superlattice." Materials Research Society Fall Meeting, Boston, Massachusetts, 1990.

Smith, H.I., K. Ismail, M.L. Schattenburg, and D.A. Antoniadis. "Sub-100 nm Electronic Devices and Quantum-Effects Research using X-ray Nanolithography." Microcircuit Engineering '89, Cambridge, England, September 26-28, 1989. *Microelectron. Eng.* 11: 53-59 (1990).

Toriumi, A., K. Ismail, M. Burkhardt, D.A. Antoniadis, and H.I. Smith. "Resonant Magneto-Conductance in a Two-Dimensional Lateral-Surface-Superlattice." 20th International Conference on the Physics of Semiconductors, Thessaloniki, Greece, August 6-10, 1990.

Yen, A., R.A. Ghanbari, E.H. Anderson, and H.I. Smith. "Fabrication of 100 nm-Period Gratings using Achromatic Holographic Lithography." Microcircuit Engineering '89, Cambridge, England, September 26-28, 1989. Microelectronic *Microelectron. Eng.* 11: 201-205 (1990).

Yen, A., R.A. Ghanbari, Y.-C. Ku, W. Chu, and M.L. Schattenburg. J.M. Carter, and H.I. Smith. "X-ray Masks with Large-Area 100nm-Period Gratings for Quantum-Effect Device Applications." Proceedings of the International Conference on Microlithography, Microcircuit Engineering 90, Leuven, Belgium, September 18-20, 1990; *Microelectron. Eng.*. Forthcoming.

Meetings Papers Presented

Bagwell, P.F., A. Kumar, and T.P. Orlando. "Evanescent Modes and Scattering in Quasi-One-Dimensional Wires." *Bull. Amer. Phys. Soc.* 35: 298 (1990).

Bagwell, P.F., T.P. Orlando, and A. Kumar. "Low-Dimensional Resonant Tunneling." Paper presented at the NATO Advanced Research Workshop on Resonant Tunneling in Semiconductors: Physics and Applications, El Escorial, Spain (1990).

Bagwell, P.F., A. Kumar. "Evolution of the Quantized Ballistic Conductance with Increasing Disorder in Narrow Wire Arrays." Submitted for the March Meeting of the American Physical Society, 1991.

Broekaert, T.P.E., P.F. Bagwell, T.P. Orlando, and C.G. Fonstad. "Resonant Tunneling Diodes and Transistors with a One, Two, or Three Dimensional Electron Emitter." *Bull. Amer. Phys. Soc.* 35: 298 (1990).

Eugster, C.C., J.A. del Alamo, and M.J. Rooks. "Ballistic Transport in a Novel Gated Quantuam Wire." Paper presented at Device Research Conference, Santa Barbara, California, June 1990.

Eugster, C.C., J.A. del Alamo, and M.J. Rooks. "Ballistic Transport in a Novel Grated Quantum Wire." Paper presented at the 48th Annual

Device Research Conference, Santa Barbara, California, June 25-27, 1990.

Kumar, A., and P.F. Bagwell. "Resonant Tunneling in a Q1-Dimensional Wire." Paper presented at Techcon, October 1990.

Liu, C.T., D.C. Tsui, M. Shayegan, K. Ismail, D.A. Antoniadis, and H.I. Smith. "Observation of Landau Level Splitting in Magneto-Capacitance Measurements on GaAs/AlGaAs Two-Dimensional Surface Superlattice Structures." *Bull. Amer. Phys. Soc.* 35: 597 (1990).

Liu, C.T., S. Luryi, and P.A. Garbinski. "Quench of Hot-Electron Real-Space-Transfer by Electronic Screening." Submitted for March Meeting of the American Physical Society, 1991.

Markert, T., M.L. Schattenburg, T. Isobe, J. Bauer, C. Canizares, J. O'Connor, J. Porter, and H.I. Smith. "Investigations of Materials for Ultra-Thin Window X-ray Detectors." Paper presented at 177th Meeting of the American Astronomical Society, Philadelphia, Pennsylvania, January 13-17, 1991.

Meirav, U., M.A. Kastner, M. Heiblum, and S.J. Wind. "Single Electron Charging and Conductance Oscillations in GaAs Nanostructures." *Bull. Phys. Soc.* 35: 721 (1990).

Meirav, U., M.A. Kastner, M. Heiblum, and S.J. Wind. "Single Electron Charging and Conductance Oscillations in GaAs Nanostructures." *Bull. Phys. Soc.* 35: 721 (1990).

Park, S.L., P.F. Bagwell, A. Yen, D.A. Antoniadis, H.I. Smith, T.P. Orlando, and M.A. Kastner. "Magnetotransport in Multiple Narrow Si Inversion Channels Opened Electrostatically Into a Two-Dimensional Electron Gas." Submitted for the March Meeting of the American Physical Society, 1991.

Rittenhouse, G., H.I. Smith, J.M. Graybeal, and B. Meyerson. "A Novel Structure for a Three-Terminal Superconducting Resonant Tunneling Device." Submitted for the March Meeting of the American Physical Society, 1991.

Scott-Thomas, J.H.F., M.A. Kastner, S.B. Field, H.I. Smith, and D.A. Antoniadis. "Conductance Oscillations of 1-Dimensional Hole and Electron Gases." *Bull. Phys. Soc.* 35: 731 (1990).

Schattenbrug, M.L., K. Li, R.T. Shin, J.A. Kong, and H.I. Smith. "Calculation of Soft X-ray Diffraction from Nanometer-Scale Gold Structures Using a Finite-Element Time-Domain Method." Submitted to the Progress in Electromagnetics Research Symposium, July 1991.

Smith, H.I., K. Ismail, and D.A. Antoniadis. "Investigations of Field-Effect-Controlled Mesoscopic Structures Fabricated with X-ray Nanolithography" Paper presented at the Advanced Heterostructure Transistors Conference, December 1990.

Zhao, Y., D.C. Tsui, S.J. Allen, K. Ismail, H.I. Smith, and D.A. Antoniadis. "Spectroscopy of 2-Deg in a Grid Gate Patterned Heterostructure." Submitted for the March Meeting of the American Physical Society, 1991.

Theses

Bagwell, P.F. *Quantum Mechanical Transport in Submicron Electronic Devices.* Ph.D. diss. Dept. of Electr. Eng. and Comput. Sci., MIT, 1990.

Meirav, U. *Single Electron Charging and Periodic Conductance Oscillations in Gallium Arsenide Nanostructures.* Ph.D. diss. Dept. of Physics, MIT, 1990.

Park, S.L. *The Anomalous Magnetoresistance of the Electron Gas in a Restricted Geometry.* Ph.D. diss. Dept. of Physics, MIT, 1990.

Scott-Thomas, J. *Conductance Oscillations Periodic in the Charge Density of One-Dimensional MOSFET Structures.* Ph.D. diss. Dept. of Physics, MIT, 1990.

The, S.C. *A Self-Aligned NMOS Process using X-ray Lithography.* M.S. thesis. Dept. of Electr. Eng. and Comput. Sci., MIT, 1990.

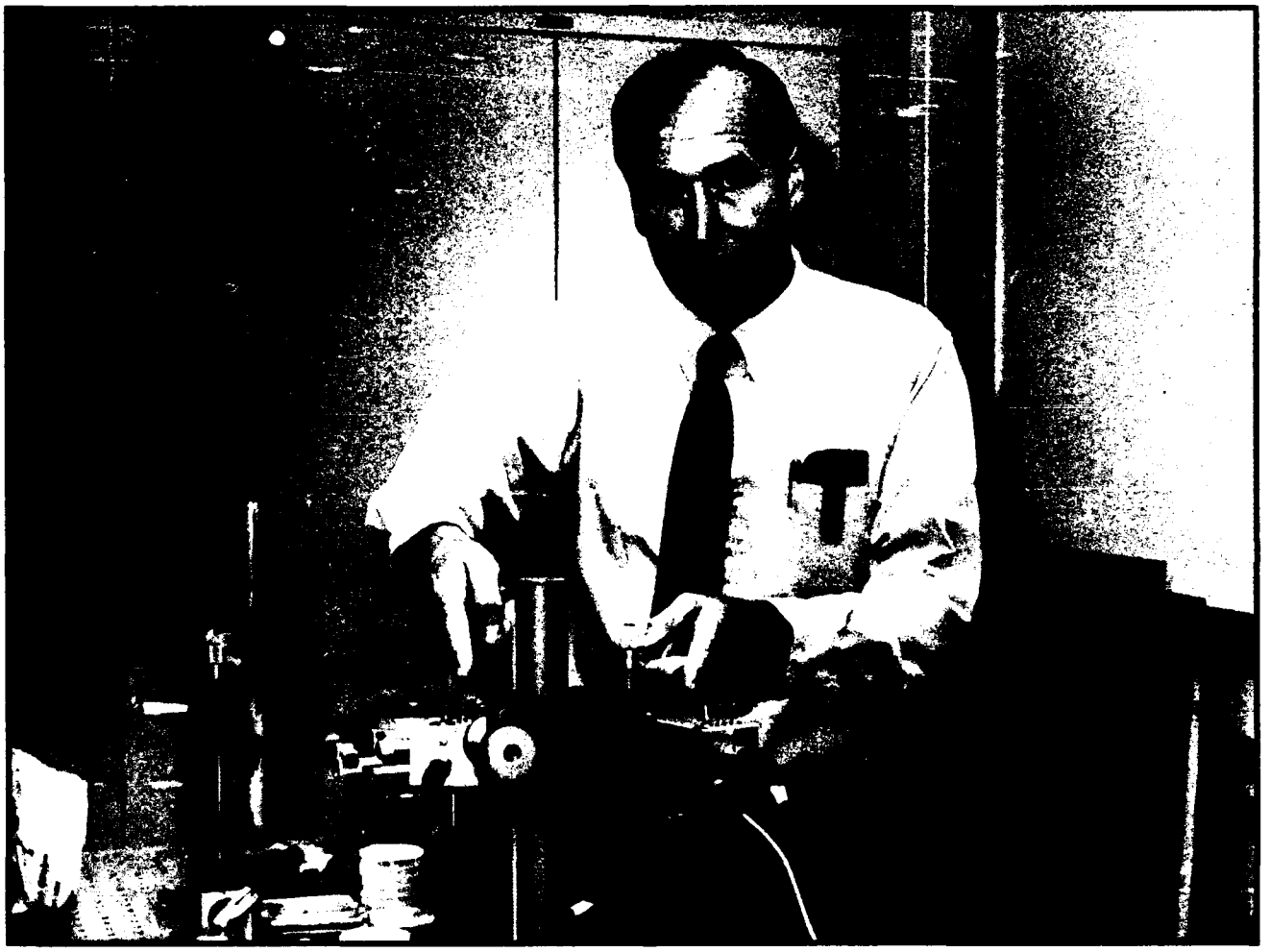

Professor Henry I. Smith explains the development of an alignment system for x-ray nanolithography that should be capable of 100-angstrom precision.

Chapter 2. Microstructural Evolution in Thin Films of Electronic Materials

Academic and Research Staff

Professor Carl V. Thompson, Professor Henry I. Smith, Dr. Paul Evans, Dr. En Ma, Dr. John Melngailis, Dr. H. Miura

Visiting Scientists and Research Affiliates

David J. Edell,[1] Harold J. Frost,[2] David A. Smith,[3] King-N. Tu[3]

Graduate Students

Jaeshin Cho, S. Cooperman, Andrew D. Dubner, Jerrold A. Floro, H. Inglefield, Y-C. Joo, Harold Kahn, Yachin Liu, Hai P. Longworth, Jaesang Ro

Technical and Support Staff

Celia Slattery

2.1 Coarsening of Particles on a Planar Substrate

Sponsor

National Science Foundation

Project Staff

Professor Carl V. Thompson, Yachin Liu

Very small particles on a planar substrate can exchange material by atomic diffusion of the particle constituent on the substrate surface. This generally leads to an increase in the average particle size and spacing and can also lead to the development of restricted crystallographic orientations. This process can be very important in the early stages of the formation of a thin film. We have developed a theory to describe the evolution of particle sizes and orientations and are testing this theory by experimentally characterizing particle coarsening in model systems. We have shown that Au particles on amorphous SiN membranes annealed in air undergo a coarsening process which is described well by the theory for interface-reaction-limited coarsening. We have also shown that differences in the gaseous ambient strongly affect the coarsening rate.

2.2 Epitaxial Grain Growth

Sponsors

National Science Foundation
U.S. Air Force - Office of Scientific Research

Project Staff

Jerrold A. Floro, H. Inglefield, Professor Carl V. Thompson

We have demonstrated that grain growth in polycrystalline films on single crystal substrates can lead to epitaxial films. This new approach to obtaining heteroepitaxial films can lead to ultrathin films with reduced defect densities compared to films deposited using conventional techniques. In epitaxial grain growth, ultrathin polycrystalline films are deposited on single crystal substrates. When these polycrystalline films are heated to elevated temperatures, epitaxial grains with low film-substrate interface energies grow and consume misoriented grains. Because the initial polycrystalline films are deposited at low temperatures, fully continuous ultrathin films can be obtained. Conventional Volmer-Weber epitaxy which is carried out at higher deposition temperatures can not be used to obtain equivalently thin epitaxial films. We have developed kinetic analyses for epitaxial grain growth and are testing these analyses through experiments on model systems,

---

[1] Harvard-MIT Health Sciences Program, Cambridge, Massachusetts.

[2] Thayer School of Engineering, Dartmouth College, Hanover, New Hampshire.

[3] IBM Corporation, Thomas J. Watson Research Center, Yorktown Heights, New York.

including Au and Ag films on mica and NaCl. Experiments on epitaxial grain growth are providing a means of characterizing the film-substrate interface energy, as a function of crystal orientation.

2.3 Modeling of Microstructural Evolution in Thin Films

Sponsors

Joint Services Electronics Program
Contract DAAL03-89-C-0001
National Science Foundation
U.S. Air Force - Office of Scientific Research

Project Staff

Professor Carl V. Thompson, Harold J. Frost, Jerrold A. Floro

We are developing analytic models for normal and secondary grain growth in continuous thin films as well as particle coarsening in discontinuous films. The effects of surface or interface energy anisotropy play especially important roles in these processes. We have developed computer models for film formation by crystal nucleation and growth to impingement under a variety of conditions. We have shown that topology and geometry of grain structures strongly depend on the conditions of film formation.

We have also developed a computer model for two-dimensional grain growth. This simulation has been modified to account for the important effects that the surfaces of a film have on grain growth. We have shown that when formation of grain boundary surface grooves leads to stagnation of normal grain growth, lognormal grain size distributions with average grain size two to three times the film thickness result. This is in agreement with well-established experimental observations. We have also successfully modeled abnormal grain growth caused by anisotropy of the surface energy of grains.

2.4 Properties of Grain Boundaries in Zone Melted Silicon Thin Films

Sponsor

IBM Corporation

Project Staff

Dr. Paul Evans, David A. Smith, Professor Carl V. Thompson

We are using zone melting recrystallization (ZMR) of thin silicon films on oxidized silicon wafers to prepare thin film bicrystals in order to study the electronic properties of grain boundaries in silicon. We are correlating electronic properties with structural features, as revealed using high resolution electron microscopy. We have found that in these samples, (100) tilt boundaries with tilts up to 25.5 degrees are electrically inactive. This surprising result indicates that even polycrystalline ZMR films might be useful for silicon-on-insulator (SOI) majority carrier devices.

2.5 Kinetics of Thin Film Silicide Formation

Sponsors

Hitachi Corporation
IBM Corporation

Project Staff

Professor Carl V. Thompson, Dr. En Ma, Dr. H. Miura, King-N. Tu

Currently, there is considerable interest in the use of refractory metals or refractory metal silicides as interconnects, as gate materials in MOS devices and for low contact resistance diffusion barriers at metal-silicon contacts in integrated circuits. One method of silicide formation is through the reaction of metallic thin films with silicon substrates or polycrystalline silicon films. This application raises fundamental questions about the rate and products of thin film metal-silicon reactions.

There are four critical parameters in analysis and modeling of these reactions: (1) interdiffusivities, (2) free energy changes, (3) surface energies, and (4) interface reaction constants. Of these, the first two parameters are fairly well understood and predictable. The purpose of this project is to develop a better understanding and predictive capability for the last two parameters. Surface energies are being determined through silicide precipitation experiments and the kinetics of thin film reactions

are being studied through thermal, TEM, and x-ray analysis of reactions in multilayer thin films.

We have used differential scanning calorimetry, transmission electron microscopy, electron beam microanalysis, and thin film x-ray diffractometry to study the thermodynamics and kinetics of reactions in multilayer thin films. In Pt/amorphous-Si (Pt/a-Si), Ni/a-Si, V/a-Si and Ti/a-Si multilayers, amorphous silicides are the first phases to form, even though these phases are thermodynamically stable only if crystalline silicide formation is kinetically suppressed.

We have demonstrated that calorimetric analysis of multilayer films can be used to detect and analyze crystalline silicide nucleation during reactions in multilayers. Evidence for crystal nucleation has been observed in the cases listed above as well as in Co/a-Si and Ni/Al multilayers in which crystalline phases are the first phases to form. We have accumulated experimental and theoretical evidence which suggests that nucleation is preceded by interdiffusion and that it is the kinetic constraints of these sequential processes which govern phase selection during interfacial reactions.

We have also observed explosive reactions in multilayer metal/a-Si films and fully crystalline Ni/Al multilayers. These reactions can propagate in a room temperature ambient at velocities over 20 meters per second. This self-rapid-thermal-annealing process results in homogeneous films composed of the stable high temperature product phase.

2.6 Reliability and Microstructures of Interconnects

Sponsors

Joint Services Electronics Program
Contract DAAL03-89-C-0001
Semiconductor Research Corporation

Project Staff

Jaeshin Cho, Harold Kahn, Hai P. Longworth, Professor Carl V. Thompson

We are developing new techniques which allow statistical characterization of failure of contact vias and interconnects for integrated circuits. We are using these techniques to correlate failure rates and mechanisms with microstructures of interconnect lines, contact diffusion barriers and via plugs.

We are also investigating techniques for controlling microstructures in order to improve contact and interconnect reliability, especially under conditions which can lead to electromigration.

We have recently shown that in interconnect lines with uniform microstructures, increasing the grain size results in an increase of both the median time to electromigration-induced failure and the lognormal standard deviation in the time to failure. The net result, in large populations of lines, is little or no change in the time to the first failure. We have explained these results in terms of a "failure unit model" in which grain boundaries are taken to be the individual units which are responsible for the reliability of a line. The successful application of this model indicates the importance of the properties of individual grain boundaries in controlling interconnect reliability.

This interpretation is further supported by the observation that interconnects with bimodal grain size distributions (leading to grain size discontinuities) have greatly reduced reliabilities. On the other hand, lines which are completely free of grain boundary triple junctions have greatly improved reliabilities compared to lines with comparable grain sizes but also with triple junctions. We are now investigating the development of electromigration-induced damage in lines with individual grain boundaries of controlled types and locations. This will allow characterization of the failure mechanisms and rates for the fundamental units that control the reliability of interconnect systems.

2.7 Focused Ion Beam Induced Deposition

Sponsor

IBM Corporation

Project Staff

Dr. John Melngailis, Andrew D. Dubner, Jaesang Ro, Professor Carl V. Thompson

It is now possible to produce ion beams with diameters as small as 500 Å. This permits use of focused ion beams for high spatial resolution implantation, sputtering and deposition. In principal, the latter can be used in integrated circuit mask repair or high resolution direct writing of interconnects. We are investigating the mechanisms of ion-beam-induced chemical vapor deposition from metal-bearing gases.

2.8 Protective Coatings for Integrated Circuits in an in vitro Environment

Sponsor

National Institutes of Health

Project Staff

David J. Edell, Professor Carl V. Thompson

We are investigating the use of various coating materials to prevent Na diffusion into integrated circuits to be used in biomedical applications. We are correlating processing conditions, microstructural characteristics and diffusion barrier properties to develop standard methodologies for deposition and characterization of protective coatings.

2.9 Publications

Cammarata, R.C., C.V. Thompson, C. Haydelden, and K.N. Tu. "Silicide Precipitation and Silicon Crystallization in Nickel Implanted Amorphous Silicon Thin Films." *J. Mater. Res.* 5: 2133 (1990).

Cho, J., and C.V. Thompson. "Electromigration-Induced Failures in Interconnects with Bimodal Grain Size Distributions." *J. Electron. Mater.* 19: 1207 (1990).

Clevenger, L.A., and C.V. Thompson. "Explosive Silicidation in Nickel/Amorphous-Silicon Multilayer Thin Films." *J. Appl. Phys.* 67: 2894 (1990).

Clevenger, L.A., and C.V. Thompson. "Nucleation Limited Phase Selection During Reactions in Nickel Amorphous-Silicon Multilayer Thin Films." *J. Appl. Phys.* 67: 1325 (1990).

Clevenger, L.A., C.V. Thompson, R.R. De Avillez, and E. Ma. "Nucleation Controlled Phase Selection in Vanadium/Amorphous-Silicon Multilayer Thin Films." *J. Vac. Sci. Tech.* A 8 (3): 1566 (1990).

De Avillez, R.R., L.A. Clevenger, C.V. Thompson, and K-N. Tu. "Quantitative Investigation of Titanium/Amorphous-Silicon Multilayer Thin Film Reactions." *J. Mater. Res.* 4: 593 (1990).

Frost, H.J., C.V. Thompson, and D.T. Walton. "Simulation of Thin Film Grain Structures: I. Grain Growth Stagnation," *Acta Metall. Mater.* 38: 1455 (1990).

Jiran, E., and C.V. Thompson. "Capillary Instabilities in Thin Films." *J. Electron. Mater.* 19: 1155 (1990).

Kim, H.-J., and C.V. Thompson. "The Effects of Dopants on Surface-Energy-Driven Secondary Grain Growth in Silicon Films." *J. Appl. Phys.* 67: 757 (1990).

Ma, E., and C.V. Thompson. "Self-Propagating Explosive Reactions in Al/Ni Multilayer Thin Films." *Appl. Phys. Lett.* B7: 1262 (1990).

Thompson, C.V. "Grain Growth in Thin Films." *Ann. Rev. Mater. Sci.* 20: 245-68 (1990).

Thompson, C.V., J. Floro, and H.I. Smith. "Epitaxial Grain Growth in Thin Metal Films." *J. Appl. Phys.* 67 (9): 4-99 (1990).

Theses

Cho, J. *Effect of Microstructure of Aluminum Alloys on the Electromigration-Limited Reliability of VLSI Interconnects,* Ph.D. diss. Dept. of Mater. Sci. and Eng., MIT, 1990.

Dubner, A.D. *Mechanisms of Ion Beam Induced Deposition.* Ph.D. diss. Dept. of Mater. Sci. and Eng., MIT, 1990.

Jiran, E. *Capillary Instabilities in Thin, Solid Films.* Ph.D. diss. Dept. of Mater. Sci. and Eng., MIT, 1990.

Chapter 3. Focused Ion Beam Fabrication

Academic and Research Staff

Dr. John Melngailis, Professor Dimitri A. Antoniadis, Mark I. Shepard, Dr. Tao Tao, Professor Carl V. Thompson, Dr. Xin Xu

Graduate Students

Andrew D. Dubner, Jeung-Soo Huh, Henri J. Lezec, Kenneth S. Liao, James E. Murguia, Christian R. Musil, Haralabos Papadopoulos, Jaesang Ro

Technical and Support Staff

Donna R. Martinez

3.1 Focused Ion Beam Fabrication

The focused ion beam research program at MIT has developed around two machines: a high energy 150 kV system used mainly for implantation and lithography and a 50 kV system used mainly for development of processes related to repair of masks and integrated circuits. The high energy system includes automated patterning capability over wafers up to six inches in diameter. Alignment of the focused ion beam writing to within ± 0.1 μm of existing features on a wafer has been demonstrated. Software has been developed which permits patterns to be transferred from the layout system used in the Microsystems Technologies Laboratory to the focused ion beam machine. Accordingly, this permits flexible, mixed fabrication where standard steps have been carried out in the integrated circuits laboratory at MIT and special implantation or lithography steps have been carried out on the focused ion beam system. Similar mixed fabrication has also been carried out with Ford Aerospace and with Raytheon Research Laboratory. The ion species available for implantation include the principal dopants of GaAs and of Si. The minimum beam diameter available is on the order of 0.1 μm at an ion current of 20 pA. In many of the implantation projects where the minimum diameter is not needed, a higher beam current can be used.

The lower energy 50 kV system has mainly been used to develop ion induced deposition. This technique uses a local ambient of a precursor gas, usually organometallic or metal halide, to permit deposition to be carried out with minimum linewidth of 0.1 mm. The local patterned deposition complements material removal by ion milling and is used to add missing absorber material in the repair of photomasks and x-ray lithography masks or to rewire local connections in integrated circuits. Our efforts have focused on gold and platinum deposition and on understanding the fundamentals of the process.

3.2 Tunable Gunn Diode

Sponsor

Defense Advanced Research Projects Agency/
U.S. Army Research Office
Contract DAAL03-88-K-0108

Project Staff

Henri J. Lezec, Christian R. Musil, Leonard J. Mahoney,[1] Dr. Alex Chu,[2] Larry Chu,[3] Mark I. Shepard, Professor Dimitri A. Antoniadis, Dr. John Melngailis

A tunable Gunn diode has been designed and built using the focused ion beam to implant a doping gradient in the direction of current flow. The output frequency of the diode changes from 6 to 23 GHz as the DC bias across the device is varied. The output power is in the range of -10 to -15 dBm. The devices have been extensively tested at M/ACom. Significant power in the second and

[1] MIT Lincoln Laboratory, Lexington, Massachusetts.

[2] Mitre Corporation, Bedford, Massachusetts.

[3] M/ACom, Burlington, Massachusetts.

third harmonics has been measured. Using a specia[1] high speed oscilloscope, the waveform of the output has been observed. It agrees with the triangular forms predicted by simulations. The potential applications of the tunable Gunn diode, which have been identified as a result of those tests, include collision avoidance radans, electronic countermeasures, and built-in frequency response test circuits for GaAs monolithic microwave integrated circuits.

3.3 Light Emission From Tunable Gunn Diodes

Sponsor

Defense Advanced Research Projects Agency/
U.S. Army Research Office
Contract DAAL03-88-K-0108

Project Staff

Christian R. Musil, Henri J. Lezec, Dr. George W. Turner,[4] Leonard J. Mahoney, Professor Dimitri A. Antoniadis, Dr. John Melngailis

Somewhat surprisingly, we have observed light emission from the tunable Gunn diodes when they are oscillating. The light comes only from the rectangular area where the Gunn domain is propagating. As the frequency is changed, the length of the rectangle changes. The spectrum of the light is roughly Gaussian with some structure and peaks at about 1.3 eV, which is below the 1.43 eV bandgap. The tail of the spectrum extends into the visible. The mechanism of emission is thought to be avalance breakdown and the shift in the spectrum away from the band gap is attributed to local heating.

3.4 Effect of Dose Rate on Activation of Si Implanted in GaAs

Sponsor

Defense Advanced Research Projects Agency/
U.S. Army Research Office
Contract DAAL03-88-K-0108

Project Staff

Henri J. Lezec, Christian R. Musil, Mark I. Shepard, Leonard J. Mahoney, John D. Woodhouse,[4] Dr. John Melngailis

The instantaneous current density in focused ion beam implantation is typically between 0.1 and 3 A/cm^2 while in conventional broad beam implantation the current density is in the range of μA/cm^2. We have found that in the case of Si ion implantation into GaAs this large difference in current density leads to differences in the properties of the material. The implantations were generally carried out at 140 and 280 keV and with doses varying from 1×10^{12} to 1×10^{14} ions/cm^2. SIMS analysis indicates that the broad beam implants penetrate somewhat deeper than the focused ion beam implants. This is thought to be due to the fact that the high current density of the focused ion beam causes amorphization to occur at lower doses than in the broad beam case. Thus channeling would be inhibited for focused ion beam implantation. In addition, the sheet resistance of conventionally implanted material saturates at a dose of about 10^{13} ions/cm^2 while for the focused ion beam implants the sheet resistance (after anneal) actually decreases above 10^{13} ions/cm^2. This has been further examined by Hall sectioning. The drop-off in sheet resistance appears to be mainly due to a lack of activated carriers above doses of 10^{13} ions/cm^2, i.e., in the case of broad beam implantation the carrier density saturates at 10^{18} ions/cm^3, while for focused ion beams it actually drops. Thus for practical applications the focused ion beam dose should be kept below 10^{13} ions/cm^2, or the beam should be scanned rapidly over the area implanted.

[4] MIT Lincoln Laboratory, Lexington, Massachusetts.

3.5 Focused Ion Beam Implantation of GaAs MMICs and MESFETs

Sponsor

National Science Foundation
Grant ECS 89-21728

Project Staff

Kenneth S. Liao, Christian R. Musil, Mark I. Shepard, Dr. Tom Kazior,[5] Dr. Robert Mozzi,[5] Dr. John Melngailis

A potentially cost effective application of focused ion beams is the implantation of GaAs monolithic microwave integrated circuits (MMICs). In some cases MMICs require as many as five implantation steps to be carried out during fabrication, and the area implanted in each step may be small. With a focused ion beam system, all implantations can be carried out in one step. Because high resolution is not needed and a high current ion beam can be used, the focused ion beam implantation times are expected to be acceptable. The first device patterns have been transferred from Raytheon to MIT, the alignment capability verified, and the first devices implanted.

3.6 Doping Gradients in GaAs MESFETs

Sponsor

Defense Advanced Research Projects Agency/
U.S. Army Research Office
Contract DAAL-03-88-0108

Project Staff

Christian R. Musil, Leonard J. Mahoney, Mark I. Shepard, Professor Dimitri A. Antoniadis, Dr. John Melngailis

Focused ion beam implantation permits the dose to be varied from point to point with a resolution of 0.1 μm. This may permit device optimization. GaAs MESFETs with graded dopant distributions under 0.5 μm-long gate electrodes have been fabricated. When compared with the conventional constant channel implant, increasing the doping towards the source is found to significantly increase transconductance (up to 60%) with little effect on gate capacitance or drain current. Reversing the gradient has the potential to increase power handling capabilities by increasing the gate-drain breakdown voltage. Carrier dynamics including Gunn oscillations have been simulated using a nonstationary, hydrodynamic solution to the Boltzman transport equation which takes into account short channel effects. These simulations have been effectively used to visualize the influence of doping gradients and formation of domains. Using the focused ion beam to also expose resist and define the gate, gate lengths down to 0.1 μm have been fabricated.

3.7 CMOS Transistors Fabricated by Focused Ion Beam Implantation and Lithography

Sponsor

Defense Advanced Research Projects Agency/
U.S. Army Research Office
Contract DAAL-03-88-0108

Project Staff

James E. Murguia, Mark I. Shepard, Professor Dimitri A. Antoniadis, Dr. John Melngailis

Focused ion beam implantation has been used to dope the channels of both NMOS and PMOS transistors. A large number of geometries and doses have been fabricated and tested. For example, in NMOS devices, implantation of a line dose of boron adjacent to the source causes the maximum electric field to appear next to the source rather than next to the drain. This results in a 20% increase in transconductance and a more than ten-fold decrease in output conductance. The result of the boron implant is a 20-fold increase in open circuit gain. One of the key features of this work was the precise ($\pm$0.1 μm) alignment of the focused ion beam implant to the structures fabricated by conventional optical lithography.

To fabricate short gates in the Integrated Circuits Laboratory, a process has been developed which permits combined focused ion beam lithography and optical lithography. The focused ion beam is used only to expose the gate, while all of the other exposures are carried out with conventional lithography. Standard KTI-820 resist is used which is positive in optical lithography but negative when exposed by the ion beam (i.e., the exposed area does not develop out). With this process, transis-

[5] Raytheon Research Laboratory, Lexington, Massachusetts.

tors with gate lengths down to 0.2 μm have been made on top of an optical lithography process which supports minimum dimensions of 1.75 μm.

3.8 Charge Coupled Devices with Focused Ion Beam Implanted Doping Gradients in the Channel

Sponsors

Defense Advanced Research Projects Agency/
U.S. Army Research Office
Contract DAAL-03-88-0108
MIT Lincoln Laboratory
Innovative Research Program

Project Staff

Dr. Analisa L. Lattes,[6] Dr. Scott C. Munroe,[6] James E. Murguia, Mark I. Shepard, Dr. John Melngailis

The main factor that determines the charge transfer efficiency and the maximum clocking speed of CCDs is the time taken by the residual charge to diffuse from one well to its neighboring, lower potential well. This is particularly true in longer channel CCDs. If a slight doping gradient is implanted in the direction of current flow, then a built in electric field is created which will speed up the charge transfer. CCDs with 26-μm-long channels were fabricated in which the doping gradient was created with an As implant dose varying from 0 to 1.5×10^{11} ions/cm^2. The gradient implanted CCDs had a maximum clocking frequency of 41 MHz while the uniformly implanted devices had a maximum clocking frequency of only 2.5 MHz. Such long channel CCDs are used in infrared detectors and in some signal processing applications.

3.9 Focused Ion Beam Lithography

Sponsor

SEMATECH
Contract 90-MC-503

Project Staff

Jeung-Soo Huh, Haralabos Papadopoulos, Mark I. Shepard, Dr. John Melngailis

A number of resists have been exposed with Be and Si ions at various energies to determine their suitability for focused ion beam lithography. The resists included PMMA, Microposit 2400, HEBR, and KTI 820. Both Microposit and HEBR act as positive resist, for low doses but become negative resists at higher doses due to cross linking. Unfortunately, the window between the positive and negative operation is only about a factor of 2, making them unsuitable for most applications. KTI acts as a negative resist and features down to 0.2 μm line width have been successfully exposed. PMMA, in which we have in the past succeeded in exposing 0.05 μm wide features, acts as a positive resist and was tested here for its sensitivity and ion penetration range. Be ions at 200 keV expose PMMA to a depth of 1.2 μm, while Si ions at 200 keV expose PMMA to a depth of 0.5 μm. We are in the process of testing other resists such as Ray PF. Preliminary results indicate that it acts as a positive resist with a factor of about 10 higher sensitivity than PMMA.

3.10 Focused Ion Beam Exposure Combined With Silylation

Sponsor

SEMATECH
Contract 90-MC-503

Project Staff

Dr. Mark Hartney,[6] Dr. David C. Shaver,[6] Mark I. Shepard, Jeung-Soo Huh, Dr. John Melngailis

In the silylation process the top layer of a resist such as SAL 601 from Shipley is cross linked by exposing it with a dose of ions. The resist is then exposed to a silylating agent in gaseous form which diffuses onto the surface where it is not cross linked. The resist is "developed" by reactive ion etching in oxygen which removes the resist that had been exposed by the ions. This process is sketched out in figure 1. Since only the top surface of the resist needs to be cross linked, the range of ions is unimportant. As a result, we have successfully used Be, Si, Au and Ga ions. The minimum dose needed to expose is 1×10^{12} ions/cm^2 for the heavier ions, i.e., about an order of magnitude lower than required for PMMA. Thus Ga ions can be used which have a current density in the beam an order of magnitude higher than the lighter ions. Proximity effects were

[6] MIT Lincoln Laboratory, Lexington, Massachusetts.

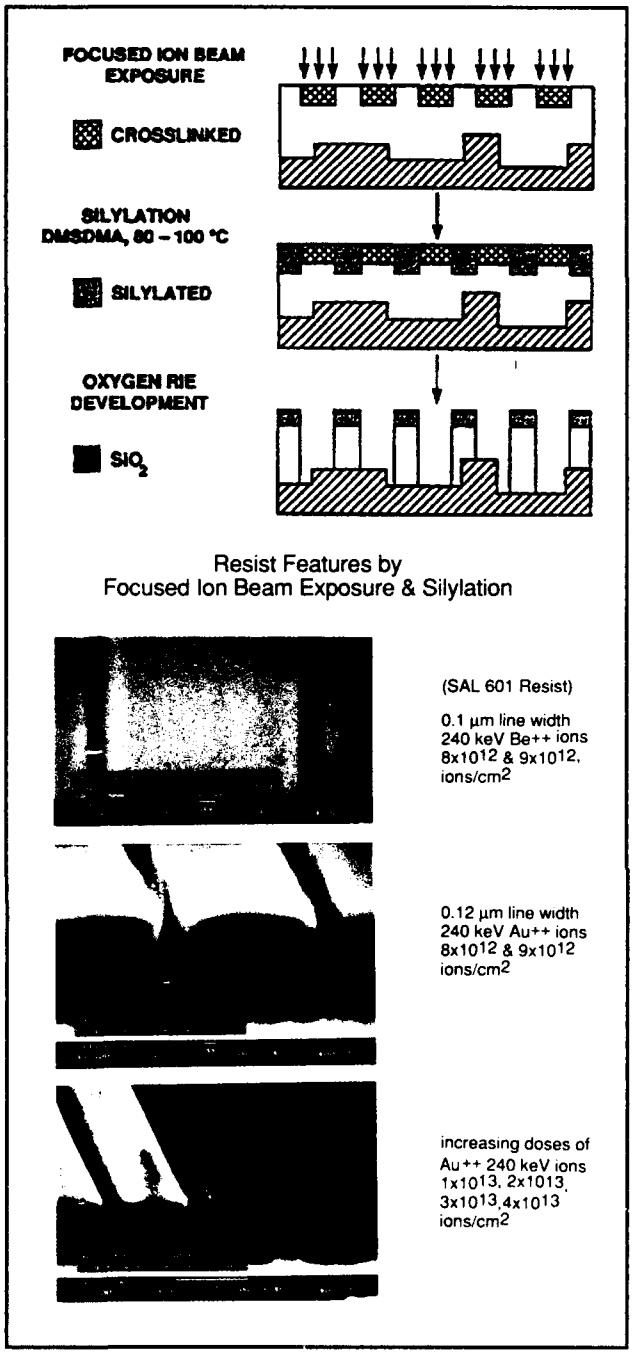

Figure 1. (Top) Schematic of the silylation process. Where the ions strike, the resist becomes cross linked, impeding the silylation. Reactive ion etching then removes the unsilylated resist. (Bottom) Series of scanning electron micographs of the resist features. First, top view of lines exposed with 240 keV Be^{++} ions showing smooth sidewalls and lines of 0.08 μm and 0.1 μm width. Second, resist lines of about 0.15 μm width in profile exposed with 240 keV Au ions. The resist sidewalls are almost vertical. Third, profiles of resist lines also exposed with Au ions at 240 keV. Line widths are varied from 0.2 μm to 0.4 μm from left to right.

also found to be absent, and features down to 0.08 μm linewidth were exposed. Because of its high sensitivity and potentially fast writing speed, focused ion beam exposure combined with silylation may be preferable to the more commonly used electron beam lithography.

3.11 Focused Ion Beam Induced Deposition of Platinum

Sponsors

Micrion
Contract M08774
U.S. Army Research Office
Contract DAAL03-87-K-0126

Project Staff

Dr. Tao Tao, William Wilkinson, Dr. John Melngailis

Platinum has been deposited using a precursor gas of (methylcyclopentadienyl) trimethyl platinum and creating a local gas ambient using a capillary feed tube directed at the surface where the ion beam is incident. Pt is of interest for x-ray mask repair because it is a high density material. It also has advantages for integrated circuit repair since it is compatible with Si processing and has shown a relatively low resistivity. We have used Pt to rewire circuits by first milling contact vias through the passivation layer and then depositing a "jumper" of Pt to connect two metal lines. Since in circuit repair, and even more so in x-ray mask repair, deposition will need to be performed over existing topography, the deposition rate as a function of the angle of incidence is important. Accordingly, we have measured the deposition as a function of angle of incidence by scanning the ion beam across a glass fiber and measuring the thickness of the deposit at various angles using a scanning electron microscope (SEM). As expected, the deposition yield (number of atoms deposited/incident ion) increases sharply as grazing incidence is approached. See figure 2.

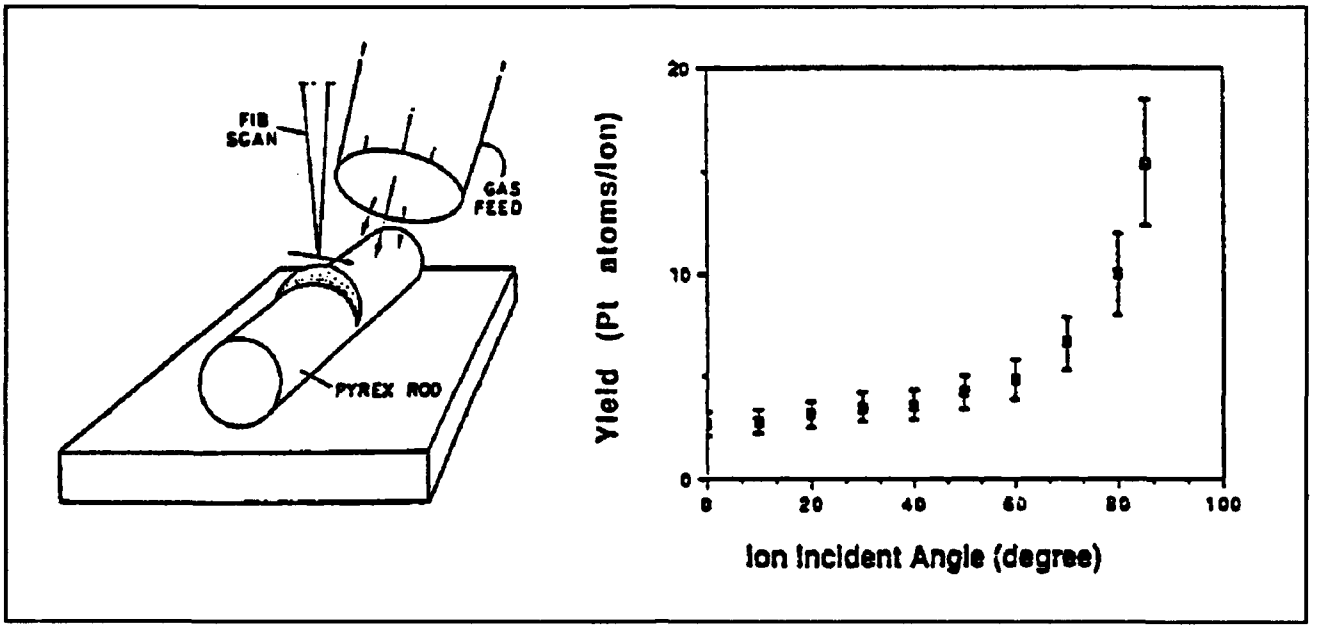

Figure 2. Measurement of focused ion beam deposition yield as a function of incidence angle. The results were obtained by depositing over a pyrex fiber 3 μm in diameter as shown schematically (on the left). The yield is found to increase as the angle of incidence approaches 90°. Incidentally the sputtering yield similarly increases as grazing incidence is approached.

3.12 Ion Induced Deposition of Gold, Results and Models for the 2 to 10 keV Energy Range

Sponsor

IBM Corporation

Project Staff

Andrew D. Dubner, Dr. Alfred Wagner,[7] Professor Carl V. Thompson, Dr. John Melngailis

To study the mechanism of ion induced deposition, a UHV apparatus was constructed with a 2 to 10 kV ion source directed at a quartz crystal microbalance acting as the sample. The adsorption of the precursor gas, dimethylgold hexafluoroacetylacetonate, the deposition rate of gold and the milling rate of gold could be measured accurately and quickly, *in-situ*. Data was taken for all of the noble gas ions from He to Xe at energies between 2 and 10 kV. Numerous observations pointed to the fact that the process by which adsorbed gas molecules are dissociated is substrate mediated. Two models of the process, the thermal spike and the collision cascade model, were analyzed and used to fit the observed data. In the thermal spike model, the instantaneous temperature rise surrounding the point of ion impact is calculated and assumed to cause the dissociation. In the Monte-Carlo collision-cascade model, the excitation of individual surface atoms is calculated and assumed to cause the dissociation. The collision-cascade model fits the observed data well and supports the view that this is the atomic process by which ion induced deposition occurs.

3.13 Ion Induced Deposition of Gold, Results and Models for the 50 to 100 keV Energy Range

Sponsors

Micrion
Contract M08774
U.S. Army Research Office
Contract DAAL03-87-K-0126

Project Staff

Jaesang Ro, Professor Carl V. Thompson, Dr. John Melngailis

The ion induced gold deposition yield and the sputter yield have been measured using a special gas cell apparatus constructed to fit in the endstation of an implanter. Noble gas ions were used. The film composition and microstructure

[7] IBM Corporation Research Division, Yorktown Heights, New York.

have been measured under various conditions. The heavier mass ions Kr to Xe yield films that are 80% Au and 20% carbon, while the lower mass ions yield films that are near 50-50. Preliminary calculations indicate that the differences of dissociation yield on ion mass and ion energy appears to fit the collision cascade model. In addition, the dissociation and sputter yield has been calculated as a function of ion incidence angle. The results appear to fit the observed increases in yield as grazing incidence is approached.

3.14 Publications

Hartney, M.A., D.C. Shaver, M.I. Shepard, J.S. Huh, and J. Melngailis. "Silylation of Focused Ion Beam Exposed Resists." *Appl. Phys. Lett.* Forthcoming.

Huh, J.S., M.I. Shepard, and J. Melngailis. "Focused Ion Beam Lithography." *J. Vac. Sci. Technol.* B1: 173-175 (1991).

Lezec, H.J., C.R. Musil, J. Melngailis, L.J. Mahoney, and J.D. Woodhouse. "Dose-Rate Effects in Focused-Ion Beam Implantation of Si into GaAs." *J. Vac. Sci. Technol. B.* Forthcoming.

Melngailis, J., P.G. Blauner, A.D. Dubner, J.S. Ro, T. Tao, and C.V. Thompson. "Focused Ion Beam Induced Depositon." *Proceedings of International Symposium on Process Physics and Modeling in Semiconductor Technology.* Forthcoming.

Melngailis, J. "Focused Ion Beam Induced Depositon - A Review." *SPIE Proc.* 1465 (1991). Forthcoming.

Murgia, J.E., C.R. Musil, M.I. Shepard, H. Lezec, D.A. Antoniadis, and J. Melngailis. "Merging Focused Ion Beam Patterning and Optical Lithography in Device and Circuit Fabrication." *J. Vac. Sci. Technol.* B6: 1374-1379 (1990).

Murguia, J.E., M.I. Shepard, J. Melngailis, A.L. Lattes, and S.C. Munroe. "Increase in Speed of Silicon CCDs with Channels Implanted using a Focused Ion Beam." *J. Vac. Sci. Technol.* Forthcoming.

Tao, T., J.S. Ro, J. Melngailis, Z. Xue, and H.D. Kaesz. "Focused Ion Beam Induced Deposition of Platinum." *J. Vac. Sci. Technol.* B6: 1826-1829 (1990).

Tao, T., W. Wilkinson, and J. Melngailis. "Focused Ion Beam Induced Depositon of Platinum for Repair Processes." *J. Vac. Sci. Technol.* B1: 162-164 (1991).

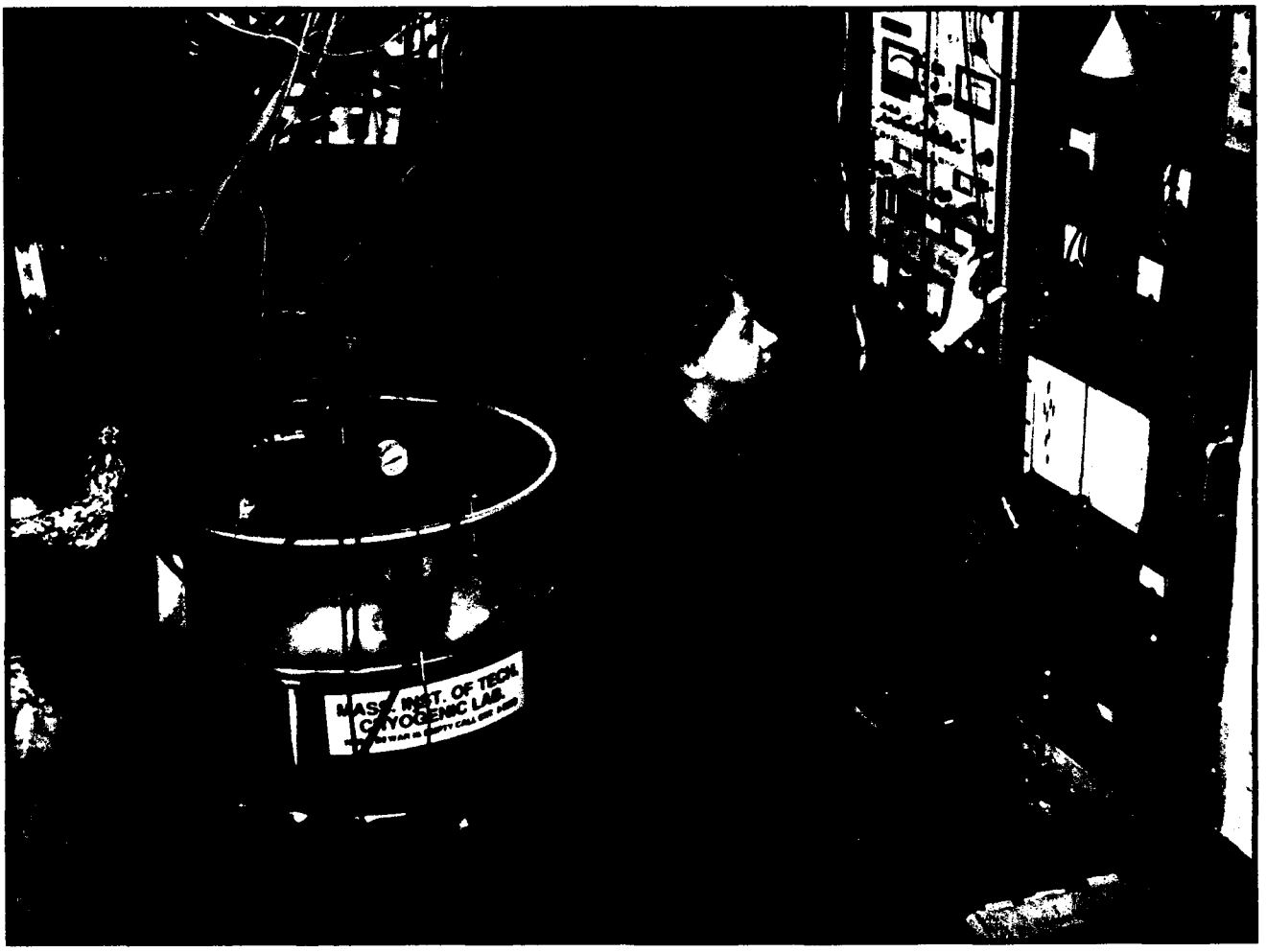

Professor Sylvia T. Ceyer conducts molecular beam surface scattering experiments in order to analyze the chemistry that occurs during the plasma etching of silicon and gallium arsenide.

Chapter 4. Chemical Reaction Dynamics at Surfaces

Academic and Research Staff

Professor Sylvia T. Ceyer, Dr. Kenneth B. Laughlin, Dr. Yulin Li, Dr. Kevin J. Maynard, Dr. David P. Pullman

Graduate Students

Sean P. Daley, Andrew D. Johnson, Michelle T. Schulberg, Julius J. Yang

Undergraduate Student

Gerald R. Cain

4.1 Dynamics of the Reaction of Fluorine with Si(100)

Sponsor

Joint Services Electronics Program
Contract DAAL03-89-C-0001

Project Staff

Professor Sylvia T. Ceyer, Dr. Kenneth B. Laughlin, Dr. Yulin Li, Dr. David P. Pullman, Michelle T. Schulberg, Gerald R. Cain

It has long been believed that molecular fluorine, F_2, would not react with or etch Si. To overcome this problem, scientists used a plasma environment. Because the plasma dissociates the molecular F_2 or other fluorine containing molecules into F atoms, it was believed that these species are responsible for reacting with the Si surface to form the volatile product SiF_4. While atomic fluorine, F, certainly does react with Si, we have shown that, contrary to popular belief, molecular F_2 also reacts with Si(100) with very close to unity probability ($\sim$ 0.95).

With support from the Joint Services Electronics Program, we used our molecular beam-ultrahigh vacuum surface scattering apparatus to direct a well-characterized, monoenergetic beam of F_2 molecules at a Si(100) surface. Not only have we shown that fluorine reacts via the well-known mechanism in which both F atoms of the incident F_2 molecule adhere to the surface (known as dissociative chemisorption), but also that some of the incident F_2 reacts so that only one of the F atoms sticks to the surface while the other atom is scattered from the surface. This latter mechanism is called an abstraction reaction and, while its existence has been predicted theoretically, we were the first group to demonstrate it experimentally.

In essence, the dangling bonds on the Si surface strip off one of the F atoms as the F_2 molecule flies by it. We were able to observe this mechanism in the angular and time-of-flight distribution measurements only as the direct consequence of the high resolution, the high signal to noise, and the collisionless environment of the detector in our apparatus. This mechanism could not have been observed with any other existing apparatus either custom-built or commercially available. As expected, the surface temperature has no effect on the abstraction process, but the incident energy of the F_2 molecule does determine the branching ratio between F atom abstraction and dissociative chemisorption.

Presently, we are continuing our angular and time-of-flight (energy) distribution measurements of the scattered F and F_2 signal to more accurately quantify this ratio as a function of the kinetic energy of the incident F_2 molecule. These accurate measurements are necessary because the F atom abstraction mechanism has implications for models of the plasma environment during etching reactions. The abstraction of F_2 by the Si surface provides an additional source of F atoms, in addition to the known source of F atoms from the gas phase decomposition of F_2 in the plasma. Therefore, this source of reactive species must now be included in a quantitative model of the plasma etching environment.

Publications

Ceyer, S.T. "New Mechanisms for Chemistry at Surfaces." *Sci.* 249:133 (1990).

Ceyer, S.T., D.J. Gladstone, M. McGonigal, and M.T. Schulberg. "Molecular Beams: Probes of the Dynamics of Reactions on Surfaces." In *Physical Methods of Chemistry*. 2nd ed. Eds. B.W. Rossiter, J.F. Hamilton and R.C. Baetzold. New York: Wiley, 1991. Forthcoming.

Gladstone, D.J., M.T. Schulberg, K.B. Laughlin, M. McGonigal, and S.T. Ceyer. "Design of a Power

Supply for Resistive Heating of Semiconductor Crystals." In preparation.

4.2 Dynamics of the Reaction of Fluorine with Fluorinated Si(100)

Sponsor

Joint Services Electronics Program
Contract DAAL03-89-C-0001

Project Staff

Professor Sylvia T. Ceyer, Dr. Kenneth B. Laughlin, Dr. Yulin Li, Dr. David P. Pullman, Michelle T. Schulberg, Gerald R. Cain

While the reaction probability of F_2 with a clean Si(100) surface is near unity, we have shown that the probability for reaction decays to zero as the fluorine coverage increases to one monolayer. That is, F_2 is not unreactive with Si but it is unreactive with a fluorinated surface of Si. This lack of reactivity with the fluorinated Si surface is the source of the misconception that F_2 does not react with Si. The lack of reactivity with the fluorinated surface precludes the build up of a sufficient layer of fluorine to produce the volatile etch product, SiF_4. However, we have shown that if the kinetic energy of the incident F_2 molecule is increased above a threshold value of 6 kcal/ mol ($\sim$ 0.25 eV), the reaction probability of F_2 with a fluorinated Si surface increases linearly with the normal component of kinetic energy. The enhancement in the reaction probability allows enough fluorine to be deposited to form the volatile etch product, SiF_4. Therefore, we have observed efficient etching of Si(100) at 300K for an incident F_2 normal kinetic energy of 15 kcal/mol (0.5 eV). This energy is two orders of magnitude below the energies used in plasmas. This result establishes that Si can be etched with low energies using molecular beam techniques without the use of plasmas. The low energies afforded by molecular beam techniques prevent the introduction of radiation damage or defects into the Si lattice, which is a typical result of plasma etching.

Publication

Schulberg, M.T. *The Reaction of Molecular Fluorine with Silicon (100): Adsorption, Desorption, and Scattering Dynamics.* Ph.D. diss., Dept. of Chem., MIT, 1990.

4.2.1 New Mechanisms for Surface Processes

Sponsors

MIT Energy Laboratory
Synthetic Fuels Center
National Science Foundation
Grant CHE 85-08734
Petroleum Research Fund
Contract 19014-AC5

Project Staff

Professor Sylvia T. Ceyer, Dr. Kevin J. Maynard, Andrew D. Johnson, Sean P. Daley

With partial support from the Joint Services Electronics Program (JSEP), we have found that the kinetic energy of an inert gas atom incident on CH_4 physisorbed on Ni(111) activates the dissociative chemisorption of CH_4 just as the translational energy of the CH_4 molecule incident on the surface. This process occurs because the impact of the inert gas atom pounds the molecularly adsorbed CH_4 into the distorted shape of the transition state that leads to dissociation. The products of the dissociative chemisorption event after collision induced activation, identified by high resolution electron energy loss spectroscopy as an adsorbed methyl radical and an adsorbed hydrogen atom, are identical to those observed after translational activation. This observation represents the discovery of a new mechanism for dissociative chemisorption: collision induced dissociation of adsorbates. These results for translational and collision induced activation as well as the translational activation of F_2 on fluorinated Si(100) signal the demise of the long-standing and pervasive notion in surface science that the surface is the all-important and sole source of energy in activating the dissociation of a molecule at or adsorbed on a surface.

With the goal of uncovering the detailed mechanism and dynamics of this new process, the absolute cross section for collision induced dissociation of CH_4 physisorbed on Ni(111) is measured over a wide range of kinetic energies and angles of incidence of a Ne, Ar and Kr atom beam. Unlike the translational activation of CH_4, which exhibits strict normal energy scaling, the collision induced dissociation cross section displays a complex dependence on the energy of the impinging inert gas atoms characteristic of neither normal nor total energy scaling. A two-step, dynamic model for the mechanism for collision induced dissociation provides excellent agreement with the energy and angular dependence of the cross section for dissociation. The model shows that the origin of the breakdown in normal energy scaling in the inert gas kinetic energy is the range

of impact parameters which contribute to the dissociation cross section. By properly summing over the impact parameter, the model calculations allow the previous translational activation results to be mapped onto the cross sections for collision induced dissociation. In this way, translational activation and collision induced activation are shown to be completely consistent. They are simply different ways to provide the energy to deform the CH_4 molecule but, once deformed, the mechanism for the dissociation is the same.

In competition with collision induced dissociation, another process, collision induced desorption, occurs. Previously, the desorption of adsorbates by the impact of an inert, neutral species has been predicted, but ours was the first experimental observation of this process. Specifically, the absolute cross section for collision induced desorption of CH_4 physisorbed on Ni(111) is measured as a function of the kinetic energy and incident angle of an Ar beam. The mechanism for desorption is shown to involve a direct and impulsive, bimolecular collision between Ar and CH_4. Molecular dynamics simulations show that the complicated energy and incident angle dependence of the desorption cross section are the consequence of the competition between the decrease in the energy transferred in the normal direction and the increase in the collision cross section as the incident angle increases. The results of detailed trajectory calculations also assess the minor roles of multiple and mirror collisions, normal energy accommodation and neighboring molecules.

The impact of the observations of collision induced chemistry and desorption for understanding surface chemistry in a high pressure environment is potentially large because, in a high pressure environment, an adsorbate-covered surface is continually bombarded by a large flux of high energy molecules. Therefore, having shown that collision induced processes occur, we believe that no mechanism for surface reactions under high pressure conditions including those that occur in plasma environments, can now be considered complete without an assessment of the importance of collision induced processes as a major reaction step. In fact, there are many unexplained observations in the literature of effects of inert gases on the rates of high pressure, heterogeneous catalytic reactions. It is now important to reinvestigate these reactions in light of the knowledge that these collision induced processes occur. Collision induced chemistry and desorption are additional reasons why surface chemistry at high pressures is often very different from the chemistry in UHV environments.

Knowledge of these microscopic origins for the pressure gap has allowed us to develop a scheme to bypass the high pressure requirement by simply raising the energy of the incident molecule or collisionally inducing dissociation. We have used the former trick to synthesize and identify spectroscopically by high resolution electron energy loss spectroscopy, an adsorbed CH_3 radical for the first time under low pressure, ultrahigh vacuum conditions. More recently, higher resolution and higher sensitivity spectra of CH_3, CH_2D and CD_3 have confirmed a Fermi resonance between the overtone of the asymmetric deformation and the low frequency or "soft" C-H symmetric stretch. These spectra have also allowed a symmetry analysis to be carried out that establishes that the CH_3 species is adsorbed with C_{3v} symmetry in a threefold hollow site with the hydrogens either eclipsed over or staggered between the surrounding Ni atoms.

Because of our unique ability to produce a CH_3 species, we have been able to probe its stability. Above 150 K, CH_3 begins to dissociate to adsorbed CH. An unambiguous identification of the spectrum as that of CH is only possible because of the high resolution ($32cm^{-1}$ FWHM) and high sensitivity (5×10^6 counts/sec for the elastically scattered electron beam) of our spectrometer. This assignment is also supported by the spectra measured after the thermal decomposition of the mixed isotope CH_2D. This work rectifies a previous assignment of a spectrum in the literature to a CH species.

Our ability to bypass the high pressure requirement has allowed us to carry out a high pressure reaction at low pressure: the synthesis of C_6H_6 from CH_4. In addition, because this reaction is carried out at low pressure, we have been able to identify the adsorbed intermediates by high resolution electron energy loss spectroscopy and to determine the mechanism of this reaction. The synthesis is effected by exposing a monolayer of CH_4 physisorbed on Ni(111) at 47 K to a beam of Kr atoms. The collision of the incident Kr with the physisorbed CH_4 distorts the CH_4 from its tetrahedral configuration, thereby lowering the barrier to dissociation into an adsorbed methyl radical and an adsorbed hydrogen atom. As the surface temperature is raised to 230 K, all the adsorbed CH_3 dissociates to CH and the CH recombines to form adsorbed C_2H_2. Some of the C_2H_2 trimerizes to adsorbed C_6H_6 and at 410 K and 425 K, respectively, the atomically adsorbed hydrogen desorbs as H_2 and some of the chemisorbed C_6H_6 desorbs. The gas phase benzene is detected mass spectrometrically in a thermal desorption experiment. These data also provide mechanistic information useful to the possible extrapolation of this synthesis from molecular beam-UHV environments to more practical conditions.

Publications

Beckerle, J.D., A.D. Johnson, and S.T. Ceyer. "Collision Induced Desorption of Physisorbed CH_4 from Ni(111): Experiments and Simulations." *J. Chem. Phys.* 93:4047 (1990).

Ceyer, S.T. "New Mechanisms for Chemistry at Surfaces." *Sci.* 249:133 (1990).

Ceyer, S.T. "The Activation and Reactions of CH_4 on Ni(111)." Paper presented at the Gordon Conference on Organometallic Chemistry, June 1990.

Ceyer, S.T. "Collision Induced Absorption of H into Ni(111)." Paper presented at the American Chemical Society Meeting, Washington, D.C., August 1990.

Ceyer, S.T. "Adsorbate Synthesis with Molecular Beams." Paper presented at the Chemistry at Surfaces Symposium, University of California, Irvine, October 1990.

Chapter 5. Measurement of Electron-phonon Interactions Through Large-amplitude Phonon Excitation

Academic and Research Staff

Professor Keith A. Nelson

Visiting Scientists and Research Affiliates

Dr. Andrew M. Weiner,[1] Dan E. Leard[1]

Graduate Students

Matthew J. Banet, Gary P. Wiederrecht

5.1 Introduction

Sponsor

Joint Services Electronics Program
Contract DAAL03-89-C-0001

The main goal of this project is to determine the responses of electronic materials to input signals which are not only fast (i.e., pulses of short duration) but also high in repetition rate (i.e., many short pulses in rapid succession) as is directly relevant to ultrafast electronics applications. This is accomplished through direct measurement using terahertz-frequency sequences of femtosecond pulses. The responses are heavily dependent on electron-phonon interactions whose strength can be determined.

5.2 High Repetition-rate Signals and Resonant Responses of Electronic Materials

Much of the current work in ultrafast spectroscopy of electronic materials involves irradiation of the sample with a single femtosecond pulse followed by probing of the sample's time-dependent response. This has taught us a great deal about the fundamental properties and ultrafast dynamical responses of semiconductors, metals, and, more recently, superconductors. What does this type of spectroscopy tell us about the performance of the material in a real ultrafast device?

Most ultrafast signal processing and communications applications involve not just one very fast signal followed by a long waiting period, then another isolated very fast signal, another long waiting period, etc. The main purpose of developing ultrafast devices is to make possible *high-density* signal processing, i.e., processing of very high (terahertz) repetition rate signals. For a material to be appropriate for this type of application, its response to terahertz-frequency signals must be suitable. Usually "suitable" means fast, without long-lived or spurious components.

Ultrafast spectroscopy generally measures material responses to single, isolated ultrafast optical signals. Certainly, if the response to this kind of signal is unsuitable (slow, or a fast initial response with substantial slow "trailing edge" components), then the material can be ruled out for many ultrafast device applications. However, successful performance in this type of test does not ensure successful response to high-density signal inputs of interest in real ultrafast devices. How can we use spectroscopy to provide a better "real-world" test of material performance?

It is now possible to generate complex terahertz frequency signals through femtosecond "pulse-

[1] Bell Communications Research (Bellcore).

shaping" techniques[2] developed at Bell Communications Research (Bellcore). Recognizing the importance of these techniques for ultrafast electronic materials characterization, we worked in collaboration with Bellcore scientists to conduct the first spectroscopic experiments in which material responses to terahertz-frequency signals were recorded.[3] The experiments showed how a crystalline solid could give a very fast response to a single ultrafast input signal, with minimal "trailing edge," and yet give a clearly unacceptable response to a terahertz-frequency sequence of input signals. The sample showed a "spurious" response (due to lattice vibrations) with an amplitude that was very small after one input signal, but which was amplified by successive input signals in the sequence. After the terahertz-frequency sequence was over, the spurious signal dominated the response! This signal was amplified by an "impulsive" driving force on the lattice vibrations exerted by each of the successive input signals. The mechanism for this force, "impulsive stimulated Raman scattering," was discovered and elucidated with earlier RLE support.[4]

Our initial experiments on organic molecular crystals, supported through RLE, received wide publicity through publication (by us and by journalists) in *Science*,[3] *Physics News in 1990*,[5] *Optics News*,[6] *Science News*,[7] *Chemistry and Industry*,[8] *Chemical and Engineering News*,[9] and other "semi-popular" as well as technical journals.[10] We have now imported the Bellcore technology into our own lab, as illustrated in figure 1. The figure shows a terahertz repetition-rate sequence of femtosecond pulses generated in our lab using the pulse-shaping method developed at Bellcore.

Our current experiments are focused on semiconductors and high-Tc superconductor materials for which the results will be of immediate practical importance. We expect very substantial "spurious" responses to terahertz-frequency frequency inputs in semiconductor multiple-quantum-well structures due to lattice resonances associated with the layer thicknesses. Similarly, in "quantum dot" structures formed by semiconductor clusters, resonances associated with the cluster size will likely lead to spurious responses to high-density input signals. The size of these responses will probably be large due to strong electron-phonon interactions in semiconductors. High-Tc superconductors have recently been shown to have very strong electron-phonon interactions as well, with specific lattice phonons coupling strongly to the low-energy electronic continuum. We expect that these materials too will show important responses to high-density signals which are not apparent when an isolated, ultrafast signal is used.

In addition to providing a direct test of material performance in ultrafast device applications, the experiments permit characterization of the

---

[2] A.M. Weiner, J.P. Heritage, and E.M. Kirschner, "High-resolution Femtosecond Pulse Shaping," *J. Opt. Soc. Am. B* 5(8): 1563-1572 (1988).

[3] A.M. Weiner, D.E. Leaird, G.P. Wiederrecht, and K.A. Nelson, "Femtosecond Pulse Sequences Used for Optical Manipulation of Molecular Motion," *Science* 247: 1317-1319 (1990).

[4] For a recent review see: K.A. Nelson and E.P. Ippen, "Femtosecond Coherent Spectroscopy," *Adv. Chem. Phys.* 75: 1-35 (1989).

[5] A.M. Weiner, D.E. Leaird, G.P. Wiederrecht, and K.A. Nelson, "Femtosecond Optical Control Over Molecular Motion," in *Physics News in 1990,* ed. P.F. Schewe (New York: American Institute of Physics, 1990), pp. 25-26.

[6] A.M. Weiner, D.E. Leaird, G.P. Wiederrecht, and K.A. Nelson, "Femtosecond Multiple Pulse Impulsive Stimulated Raman Scattering," *Opt. News* 15(12): 29-31 ("Optics in 1989" section).

[7] "Sculpting Light to Maneuver Molecules," *Sci. News* 137(14): 223 (1990).

[8] "Molecule Motions," *Chem. Ind. News* 7: 202 (1990).

[9] "Lasers Manipulate Molecular Motion," *Chem. Eng. News* 68(12): 21 (1990).

[10] K.A. Nelson, "Impulsive Stimulated Raman Scattering with Single-pulse and Multiple-pulse Excitation," in *Proceedings of the 12th International Conference on Raman Spectroscopy,* ed. J.R. Durig and J.F. Sullivan (Chichester: Wiley, 1990), pp. 19-22; A.M. Weiner, D.E. Leaird, G.P. Wiederrecht, M.J. Banet, and K.A. Nelson, "Spectroscopy with Shaped Femtosecond Pulses: Styles for the 1990s," in *Picosecond and Femtosecond Spectroscopy from Laboratory to Real World,* ed. K.A. Nelson (Bellingham, Washington: SPIE, 1990), *SPIE Proc. Ser.* 1209: 185-197 (1990); A.M. Weiner, D.E. Leaird, G.P. Wiederrecht, and K.A. Nelson, "Femtosecond Multiple-pulse Impulsive Stimulated Raman Spectroscopy," *J. Opt. Soc. Am. B*, forthcoming.

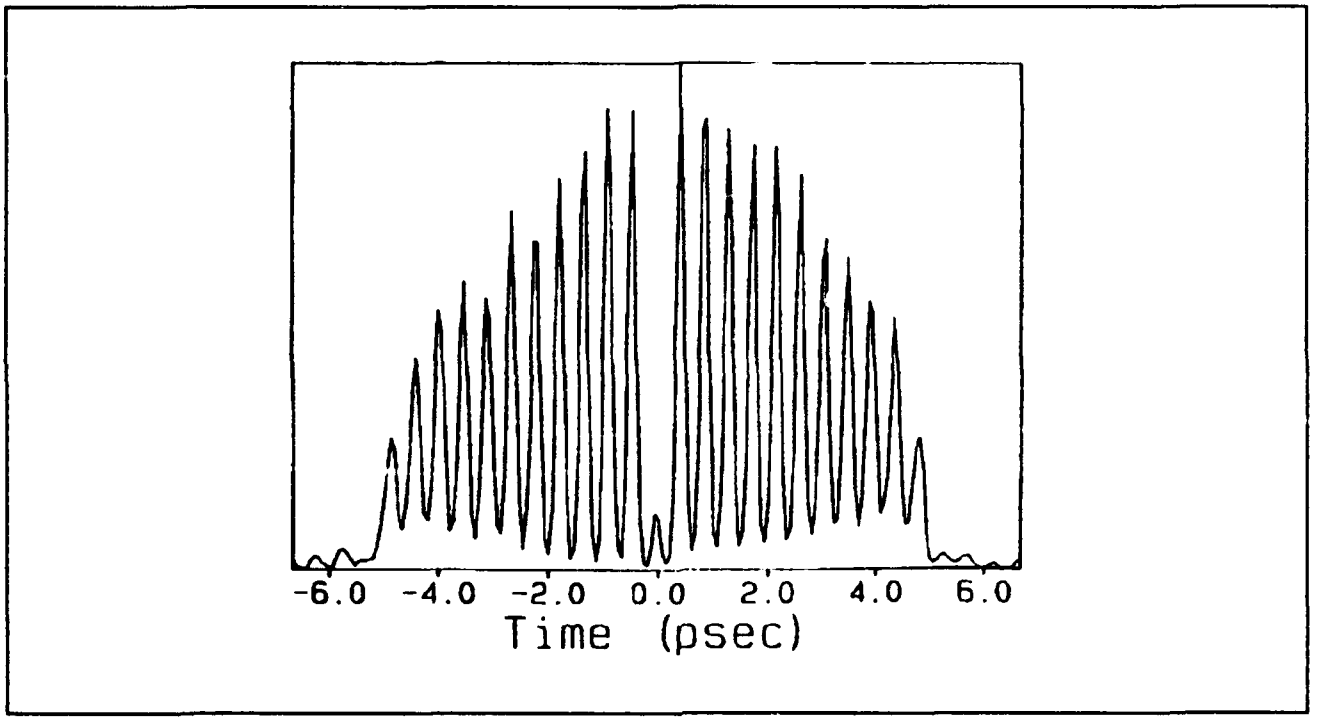

Figure 1. A 2.1-terahertz repetition rate pulse sequence produced through pulse-shaping techniques. The responses of electronic materials to high-density signals of this type are examined to provide a realistic test of their performance characteristics in ultrafast device applications.

electron-phonon interactions of the samples. These are important in mediating carrier mobility at different temperatures (i.e., different levels of phonon excitation). In high-Tc superconductors, the mechanism for strong electron-phonon coupling and its importance in superconductivity are not well understood. Our experiments may resolve these issues since they provide a unique opportunity to examine the effects of specific phonon modes on electronic energies.

As of November 1, 1990, this work is no longer sponsored through the RLE Joint Services Electronics Program. Support for our work on semiconductor and superconductor responses to terahertz frequency signals is currently being sought.

Publications

Nelson, K.A. "Impulsive Stimulated Raman Scattering with Single-pulse and Multiple-pulse Excitation." In *Proceedings of the 12th International Conference on Raman Spectroscopy*. Ed. J.R. Durig and J.F. Sullivan. Chichester: Wiley, 1990, pp. 19-22.

Weiner, A.M., D.E. Leaird, G.P. Wiederrecht, and K.A. Nelson. "Femtosecond Pulse Sequences Used for Optical Manipulation of Molecular Motion." *Sci.* 247: 1317-1319 (1990).

Weiner, A.M., D.E. Leaird, G.P. Wiederrecht, M.J. Banet, and K.A. Nelson. "Spectroscopy with Shaped Femtosecond Pulses: Styles for the 1990s." In *Picosecond and Femtosecond Spectroscopy from Laboratory to Real World*. Ed. K.A. Nelson. Bellingham, Washington: SPIE, 1990. *SPIE Proc. Ser.* 1209: 185-197 (1990).

Weiner, A.M, D.E. Leaird, G.P. Wiederrecht, and K.A. Nelson. "Femtosecond Optical Control Over Molecular Motion." In *Physics News in 1990*, Ed. P.F. Schewe. New York: American Institute of Physics, 1990, pp. 25-26.

Professor Leslie A. Kolodziejski's research is focused on the fabrication of semiconductor lasers based on II-VI compounds. (Photo by Paul McGrath)

Chapter 6. Chemical Beam Epitaxy of Compound Semiconductors

Academic and Research Staff

Professor Leslie A. Kolodziejski, Stephen C. Shepard

Visiting Scientists and Research Affiliates

Dr. Hidehito Nanto,[1] Dr. Carmen Huber[2]

Graduate Students

Christopher A. Coronado, Easen Ho

Technical and Support Staff

Angela R. Odoardi

6.1 Chemical Beam Epitaxy Facility

Sponsors

3M Company Faculty Development Grant
AT&T Research Foundation
Special Purpose Grant
Defense Advanced Research Projects Agency
Subcontract 216-25013 and 542383
Joint Services Electronics Program
Contract DAAL03-89-C-0001
National Science Foundation
Grants ECS 88-46919 and ECS 89-05909
U.S. Navy - Office of Naval Research
Contract N00014-88-K-0564

Our new laboratory for the chemical beam epitaxy (CBE) of both II-VI and III-V compound semiconductors finally began to take the form of a working research facility in 1990. The substantial laboratory renovation was completed in February; the CBE system hardware was delivered in March and installed throughout most of the summer; ZnSe was deposited onto GaAs substrates in early August. However, the modular CBE system is not complete yet. We are anticipating delivery of the analytical/metalization chamber and a III-V-dedicated gas source molecular beam epitaxy (GSMBE) system. Both chambers will be attached to the periphery of the ultrahigh vacuum (UHV) transfer chamber. Figure 1 shows the system footprint complete with all chambers which are currently expected. In the future, we plan to add an in situ patterning chamber for further processing of the samples prior to removal from the UHV environment. The analytical metalization chamber will contain Auger Electron Spectroscopy, reflection high energy electron diffraction, electron beam evaporators for metals, and ports for photon illumination of the sample. The GSMBE system will be dedicated to the growth of arsenides, phosphides, and antimonides; solid elemental sources of In, Ga, Sb and Al will be utilized with gaseous hydrides of As and P. The chamber will be employed for the fabrication of sophisticated quantum-effect electronic devices, a variety of optoelectronic devices, and advanced II-VI/III-V multilayered heterostructures.

6.2 Metalorganic Molecular Beam Epitaxy (MOMBE) of ZnSe

Sponsors

Charles Stark Draper Laboratories
Contract DL-H-418484
Defense Advanced Research Projects Agency
Subcontract 542383
Joint Services Electronics Program
Contract DAAL-03-89-C-0001
National Science Foundation
Grant ECS 88-46919
U.S. Navy - Office of Naval Research
Contract N00014-88-K-0564

---

[1] Department of Electronics, Kanazawa Institute of Technology, Kanazawa, Japan.

[2] Physics Department, University of Puerto Rico, Rio Piedras, Puerto Rico.

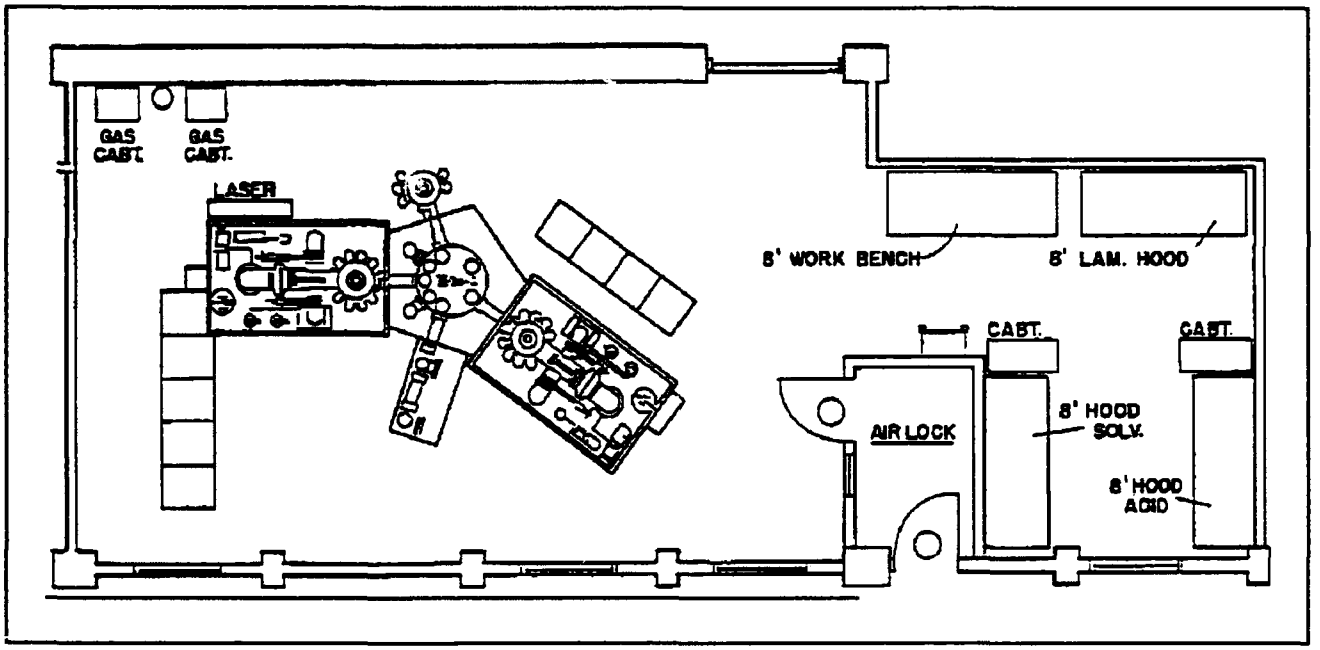

Figure 1. Layout of the CBE laboratory showing the footprint of the modular UHV system. The five chambers are the introduction, transfer, analytical/metalization, II-VI CBE reactor, and III-V GSMBE reactor. Also indicated in the drawing is the wet chemical station for substrate preparation.

The II-VI semiconductor ZnSe is currently receiving considerable attention due to the recently reported success of p-type doping. Once ZnSe is successfully doped, both n- and p-type, various optical devices such as laser diodes, optical modulators, etc., can take advantage of the 2.67 eV bandgap to provide operation in the blue/blue-green portion of the spectrum. The most successful n-type dopant has been Cl with 10^{19} electron carrier concentrations reported for molecular beam epitaxy (MBE) growth. Thus far, incorporation of Li has been demonstrated to result in p-type ZnSe. Electrical measurements to confirm the presence of holes are complicated due to the small hole concentrations and the problem associated with forming ohmic contacts to p-type material. However, pn junctions formed in ZnSe have emitted blue light at room temperature. Due to significant problems of Li interdiffusion, investigations are currently focusing on incorporating dopant species other than Li to provide shallow acceptors. A potential candidate is nitrogen, although this volatile atom is difficult to incorporate due to its small sticking coefficient and stable dimer bonding.

Our objective is to study controlled substitutional doping of ZnSe, both n- and p-type, by employing the growth technique of chemical beam epitaxy. CBE offers many advantages compared to MBE or metalorganic chemical vapor deposition and emphasizes the use of gaseous sources in an ultrahigh vacuum environment. In the CBE growth technique, the gaseous sources which are utilized are both hydrides and metalorganics. It is anticipated that precise flux control of each specie via mass flow control of the gas will be a significant advantage in the growth of the high vapor pressure II-VI compounds.

We have grown ZnSe thin films on GaAs bulk substrates by metalorganic molecular beam epitaxy (MOMBE). MOMBE differs from CBE due to the absence of the gaseous hydride sources. The metalorganic gaseous sources which have been employed at present are diethylzinc (DEZn) and diethylselenide (DESe). In the growth experiments, the metalorganics are "cracked" or thermally decomposed prior to impingement onto the GaAs. The Zn and Se atoms are removed from the hydrogen and carbon atoms to allow the use of a lower growth temperature and to more closely approximate the MBE growth approach.

Figure 2 shows the reflection high energy electron diffraction pattern obtained from a 500Å ZnSe film grown on GaAs. The presence of Kikuchi lines and a strongly streaked pattern suggest that the ZnSe is of high quality and single crystalline. The two-fold reconstruction lines observed in the [010] indicate a Zn-stabilized surface. For the growth of the thin ZnSe shown here, the substrate temperature was approximately 300°C with 1.0 and 0.30 sccm flow rates of DEZn and DESe, respectively. Investigations of the surface morphology with Nomarski interference microscopy has indicated the presence of a featureless surface at 1000x magnification. Additional experiments are in progress to increase the growth rate, as well

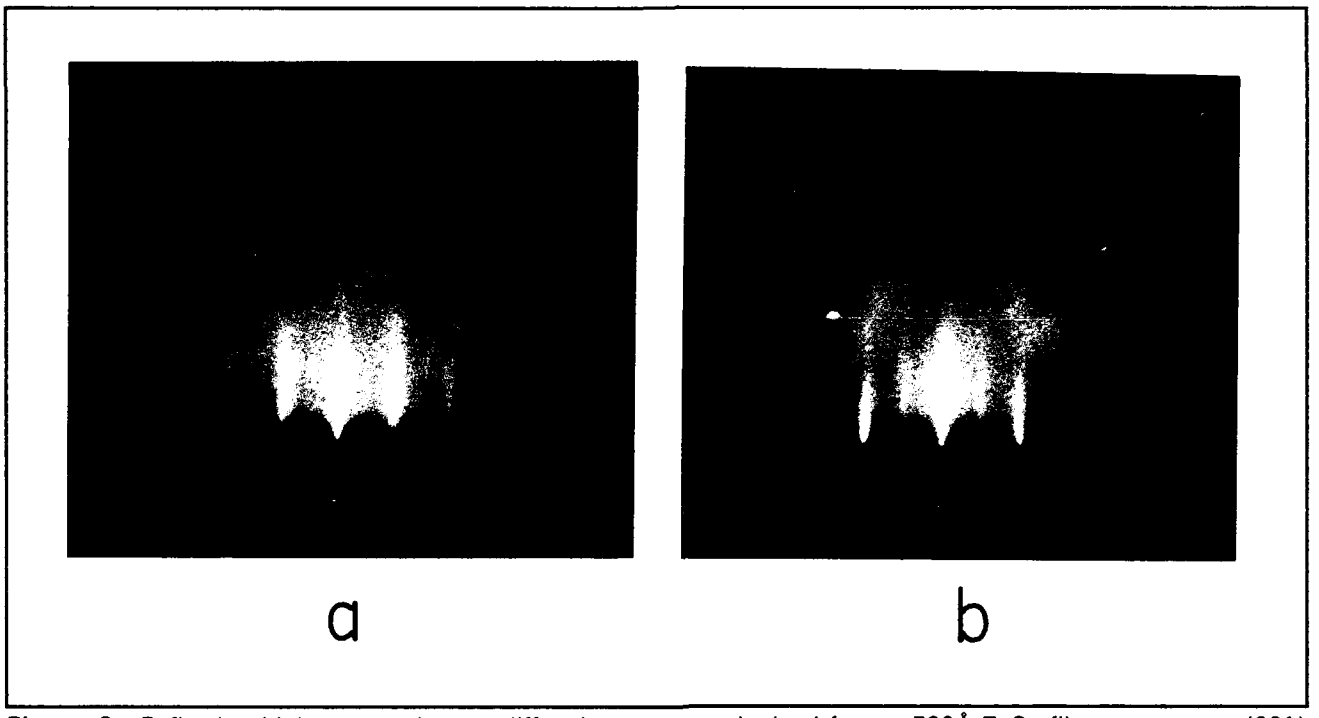

Figure 2. Reflection high energy electron diffraction patterns obtained from a 500Å ZnSe film grown on a (001) GaAs substrate. (a) [110] azimuth and (b) [010] azimuth.

as to investigate the growth using sources of dimethylzinc and hydrogen selenide.

6.3 Photon-assisted MOMBE of Wide Bandgap II-VI Compound Semiconductors

Sponsors

Defense Advanced Research Projects Agency
Subcontract 530-0716-07
National Science Foundation
Grant ECS 88-46919

To achieve our objective of fabricating p-type ZnSe, we are employing state-of-the-art epitaxial growth techniques, such as CBE and MOMBE, to take advantage of the nonequilibrium nature of the growth. At the same time, we are employing a variety of coherent photon sources to illuminate a portion of the GaAs substrate during growth. Photon-assisted MBE of ZnSe has been demonstrated to have an effect on (1) the incorporation of various atoms, (2) the stoichiometry of the growing surface front, and (3) the density of defects. In our laboratory, the CBE reactor has viewports positioned so that a photon source can illuminate the substrate either perpendicular to or parallel to the surface. In our preliminary experiments, we have employed the visible 4579Å line of an argon ion laser perpendicular to the GaAs surface during MOMBE growth of ZnSe. The laser beam was defocused to partially illuminate a 1 cm diameter area of the wafer, providing a power density of approximately 100 mW/cm^2. The power density is sufficiently low so that there was very little temperature increase. Following growth, no visible differences in the surface morphology were detected. However, a significant enhancement in the growth rate was observed from thickness measurements made by selectively etching away the ZnSe layer from the GaAs substrate. In the area illuminated by the laser, the growth rate was three times greater than in the area which was unilluminated. At the growth temperature of ~ 325°C, the wavelength of the laser is at an energy above that of the ZnSe bandgap. We are currently preparing experiments to study in detail the physical phenomena, for example electronic or photochemical, responsible for the growth rate enhancement.

The above mentioned results on the MOMBE of ZnSe, with and without photon assistance, are preliminary and not at all conclusive. These data represent the very first results on films grown by the MOMBE technique in our new CBE reactor. Additional microstructural, electrical, and optical characterizations of the ZnSe films are currently being prepared to provide further insight into the properties of this very important wide bandgap semiconductor.

6.4 Publications

Kolodziejski, L. A. "Modern Growth Technologies of Semimagnetic Semiconductors." Paper presented at the International School on Physics of Semiconducting Compounds, Jaszoweic, Poland, April 1990.

Kolodziejski, L. A. "Chemical Beam Epitaxy for Advanced Optoelectronic Devices." Paper presented at the Optical Society of America Meeting, Boston, Massachusetts, November 1990.

Chapter 7. High-Frequency InAlAs/InGaAs Metal-Insulator-Doped Semiconductor Field-Effect Transistors (MIDFETs) for Telecommunications

Academic and Research Staff

Professor Jesus A. del Alamo

Graduate Student

Sandeep R. Bahl

Undergraduate Students

Walid Azzam, Michael H. Leary

Technical and Support Staff

Angela R. Odoardi

7.1 Introduction

Sponsors

Charles S. Draper Laboratory
Contract DL-H-418488
Joint Services Electronics Program
Contract DAAL03-89-C-0001

The goals of this project are to design, fabricate, test, and model submicron InAlAs/InGaAs Heterostructure Field-Effect Transistors (HFETs) on InP. These devices are of great interest for applications in long-wavelength lightwave communication systems and ultra-high frequency microwave telecommunications.

Metal-Insulator-Doped semiconductor Field-Effect Transistors (MIDFETs) in which the InGaAs channel is heavily doped but the InAlAs insulator is undoped were pioneered by del Alamo and Mizutani at NTT Laboratories.[1] These devices have been found to display a performance comparable to InAlAs/InGaAs Modulation-Doped FETs (MODFETs) of similar gate length. They additionally offer unique benefits not found in other device structures: reduced g_m and f_T collapse, higher breakdown voltage, and enhanced freedom for optimization of gate insulator parameters.

During the past year, we have studied the effect of increasing the InAs composition in the channel of the device in an effort to enhance its performance. In the process of carrying out this research, we have uncovered serious isolation problems that will need dedicated process technology work in the future. We have also continued our study of strain-insulator MIDFETs and examined the impact of dislocations on device performance. A detailed description of these experiments is presented in this report.

7.2 Strained-channel InAlAs/n$^+$-InGaAs MIDFETs

In this work, we investigated the effect of increasing the InAs mole fraction (x) in the $In_xGa_{1-x}As$ channel from that required to lattice match to InP (x=0.53). This work is motivated by the expected improvement in electron transport

[1] J.A. del Alamo and T. Mizutani, "An $In_{0.52}Al_{0.48}As/n^+$-$In_{0.53}Ga_{0.47}As$ MISFET with a Heavily-Doped Channel," *IEEE Electron Device Lett.* EDL-8 (11): 534-536 (1987); J.A. del Alamo and T. Mizutani, "Bias Dependence of f_T and f_{max} in an $In_{0.52}Al_{0.48}As/n^+$-$In_{0.53}Ga_{0.47}As$ MISFET," *IEEE Electron Device Lett.* EDL-9 (12): 654-656 (1988); J.A. del Alamo and T. Mizutani, "A Recessed-Gate $In_{0.52}Al_{0.48}As/n^+$-$In_{0.53}Ga_{0.47}As$ MIS-type FET," *IEEE Trans. Electron Devices* ED-36 (4): 646-650 (1989).

properties[2] and the enhanced conduction band discontinuity between the channel and the insulator[3] as the InAs composition increases.

Three wafers were grown by molecular-beam epitaxy in MIT's Riber 2300 system with cross sections shown in figure 1. The InAs mole fraction in the $In_{0.53}Ga_{0.47}As$ channel and subchannel were 0.53, 0.6, and 0.7. The 100Å subchannel is undoped and the 100Å channel is Si doped to a level of about 4.5×10^{18} cm^{-3}. The $In_{0.52}Al_{0.48}As$ gate insulator and buffer are undoped as is the $In_{0.53}Ga_{0.47}As$ cap. Device fabrication is similar to that described by del Alamo and Mizutani.[4]

I-V characteristics were measured for devices with a nominal gate length of 1 μm and width of 30 μm. The gate diode characteristics were measured with the drain and source shorted. Specially designed gate-diode structures were also measured in order to investigate the gate-channel leakage paths.

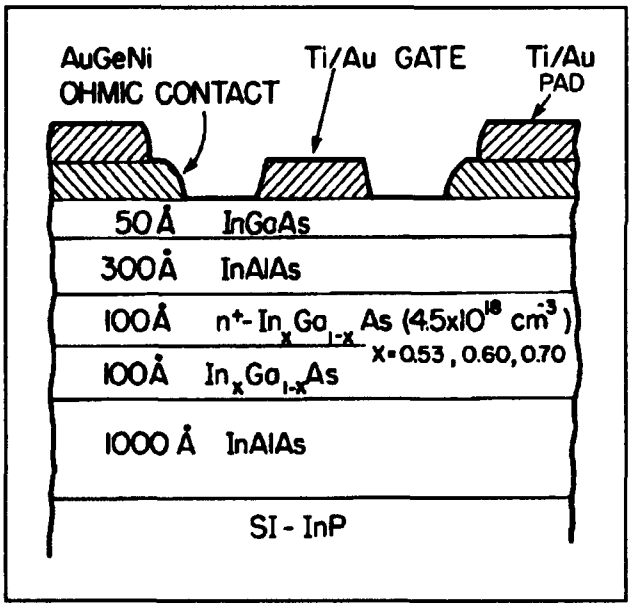

Figure 1. Cross section of $In_{0.52}Al_{0.48}As/n^+\text{-}In_xGa_{1-x}As$ MIDFETs.

Figure 2 shows a plot of the tranconductance versus gate-source voltage of representative devices from the three wafers at a drain-source voltage of 3 V. For devices with x=0.53, 0.6, and 0.7, the peak g_m's measured (averaged over 10 devices) were 200 $\pm$ 22, 250 $\pm$ 14, and 296 $\pm$ 15 mS/mm respectively. The threshold voltages are -1.05 ± 0.09, -1.28 ± 0.20, and -2.09 ± 0.24 V respectively. Figure 3 shows the drain current versus V_{gs} at $V_{ds} = 3$ V. The peak drain currents measured over 10 devices were 320 $\pm$ 42, 424 $\pm$ 37, and 656 $\pm$ 69 mA/mm respectively, demonstrating the tremendous improvement in electron transport properties as the InAs mole fraction in the channel increases. However, as x increases, as seen in figure 3, the leakage current below threshold increases, preventing the transistor from shutting off.

Figure 4 shows the gate diode characteristics for $V_{ds} = 0$ V (for a clearer presentation, the forward scale has been expanded). The increased InAs mole fraction in the channel results in larger forward and reverse currents. In forward bias, this is contrary to what is expected from the enhanced ΔE_c between channel and insulator. The values of reverse breakdown voltage are -12.6,

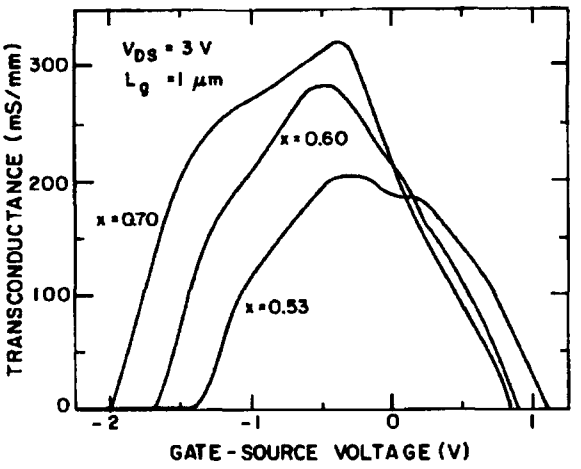

Figure 2. g_m versus V_{gs} with $V_{ds} = 3$ V for the three InAs mole fractions.

[2] U.K. Mishra, A.S. Brown, and S.E. Rosenbaum, "DC and RF Performance of 0.1μm Gate Length AlInAs-GaInAs Pseudomorphic HEMTs," *Proceedings of the International Electron Devices Meeting*, 1988, pp. 180-183.

[3] F.L. Schuermeyer, P. Cook, E. Martinez, and J. Tantillo, "Band-Edge Alignment in Heterostructures," *Appl. Phys. Lett.* 55 (18): 1877-1878 (1989).

[4] J.A. del Alamo and T. Mizutani, "An $In_{0.52}Al_{0.48}As/n^+\text{-}In_{0.53}Ga_{0.47}As$ MISFET with a Heavily-Doped Channel," *IEEE Electron Device Lett.* EDL-8 (11): 534-536 (1987).

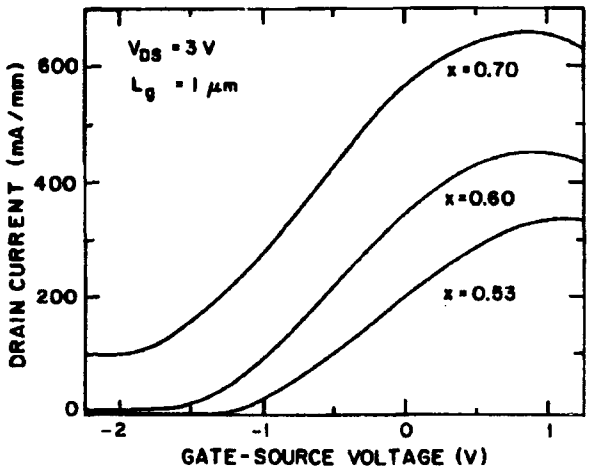

Figure 3. I_D versus V_{gs} with V_{ds} = 3V for the three InAs mole fractions.

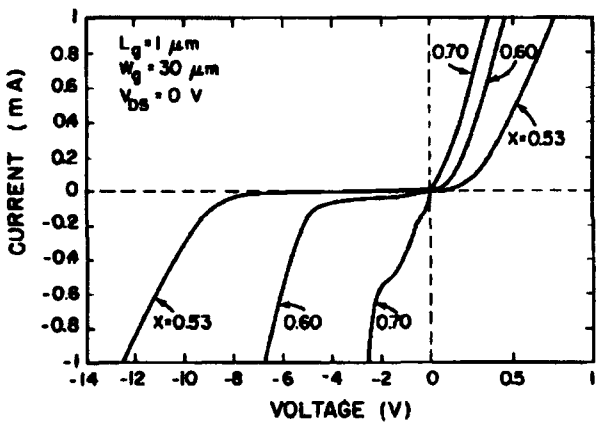

Figure 4. Forward and reverse diode characteristics of 1-μm MIDFETS for the three InAs mole fractions.

−6.7, and −2.6 V for x=0.53, 0.6, and 0.7 respectively. We have defined breakdown at a reverse gate current of 1 mA, which is about 10 percent of the peak drain current carried by the reference (x=0.53) device. The increased gate leakage current represents a serious shortcoming of enhanced InAs channels devices.

We have investigated the origin of this extra leakage current, and we attribute it to the presence of a direct leakage path between the gate and the channel at the edge of the mesa, as shown in figure 5. At the mesa edges, where the gate metal goes onto and off the mesa, there is no isolation between the edge of the channel and the gate metal. The problem exists for $In_{0.53}Ga_{0.47}As$ because it has a Schottky barrier height of 0.2 eV with the metal. As x increases, this gets smaller, about 0.1 eV for x=0.6, and 0.03 eV for x=0.7,[5] and this isolation problem becomes even more severe.

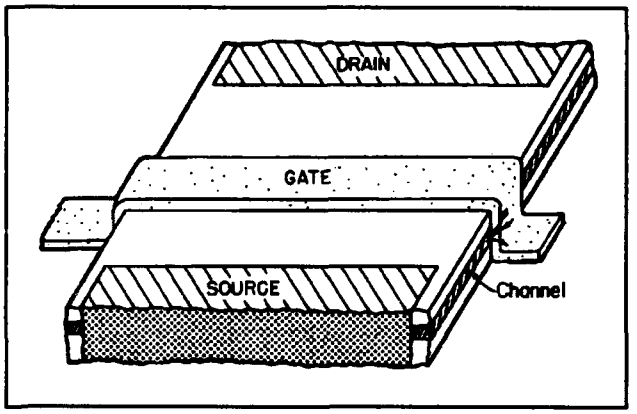

Figure 5. Perspective of the intrinsic device region.

To investigate this *edge leakage* path, we have fabricated heterojunction diodes with an inner square gate area of 10,000 μm². In one diode there is no gate-edge overlap, i.e., the gate is entirely on the mesa. In another diode, a 600 μm long edge overlap has been obtained by producing three cuts of the mesa structure underneath the gate. In this manner, the only difference between these diodes is the gate-edge overlap.

Figure 6 shows the forward and reverse characteristics of these two diodes. Without edge overlap, the forward current decreases with increasing x, as expected from the larger ΔE_c. With edge overlap, however, we see a marked increase in the forward current and a reversal in x dependence. This implies that edge leakage dominates the forward characteristics in the actual FETs. In the reverse characteristics of these diodes, for x=0.53, the edge overlap marginally contributes to the total reverse current. At x=0.6, the presence of three regions in the reverse characteristics becomes evident: pre-threshold, plateau, and breakdown. The edge overlap influences the reverse current in the pre-threshold region and then saturates at the threshold voltage, i.e., when the channel gets totally depleted underneath the gate. Far into the breakdown region, the reverse characteristics of both the structures with and without edge overlap at x=0.6 do not differ much either. For the x=0.7 diodes, edge leakage strongly affects the entire reverse characteristics. For this device, the edge

[5] H.H. Wieder, "Fermi Level and Surface Barrier of GaInAs Alloys," *Appl. Phys. Lett.* 38(3): 170-171 (1981).

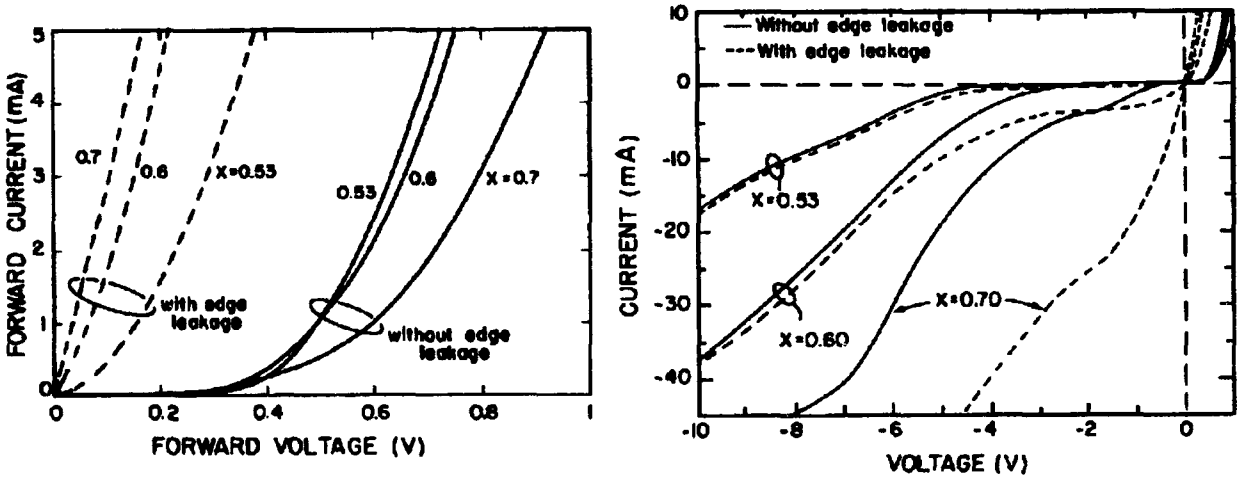

Figure 6. Forward (left) and reverse (right) diode characteristics with and without edge overlap.

leakage definitely exacerbates the loss of pinchoff. Significant gains could be made in pinchoff quality and reverse breakdown voltage by using some form of isolation that prevents edge gate-mesa overlap.

In conclusion, $In_{0.52}Al_{0.48}/n^+\text{-}In_xGa_{1-x}As$ MIDFETs have shown markedly improved peak currents and transconductances as the InAs mole fraction in the channel is increased. Devices with $L_g = 1\mu m$ and x=0.7 display an unprecedented I_D of 656 mA/mm and g_m of 296 mS/mm. As x is increased, however, there is an increase in the gate current, a dramatic decrease in the breakdown voltage, and a degradation of pinch-off. Leakage at the gate-mesa edge overlap is found to be partially responsible for these effects. To achieve the substantial gains in transport that higher InAs fractions offer, better isolation technology is required.

7.3 Orientation Dependence of Mismatched-Insulator InAlAs/n⁺-InGaAs MIDFETs

In this work,[6] a device perspective is applied to the issue of critical layer thickness and the impact of strain relaxation on electrical characteristics. The critical layer thickness of a strained semiconductor layer is ultimately determined by its application. For devices, performance is the ultimate goal. In many III-V semiconductor devices, the use of intentionally mismatched layers has the potential of significantly improving device characteristics. The appearance of misfit dislocations, however, is expected to degrade device performance, but to determine how much and in what manner, there is no substitute to studying the devices fabricated using these mismatched layers.

In an effort to increase the conduction band discontinuity in the $In_{0.52}Al_{0.48}As/In_{0.53}Ga_{0.47}As$ system (lattice-matched to InP), we have strained the $In_xAl_{1-x}As$ layer to negative mismatch by reducing its InAs fraction. This results in many benefits to the device characteristics of $In_xAl_{1-x}As/n^+\text{-}In_{0.53}As_{0.47}As$ HFETs.[7] Here we focus on the effect of mismatch on device performance. Our main result is the finding of strong orientation

[6] S.R. Bahl, W.J. Azzam, and J.A. del Alamo, "Orientation Dependence of Mismatched $In_xAl_{1-x}As/In_{0.53}Ga_{0.47}As$ HFETs," *J. Cryst. Growth*, forthcoming.

[7] J.A. del Alamo and T. Mizutani, "An $In_{0.52}Al_{0.48}As/n^+In_{0.53}Ga_{0.47}As$ MISFET with a Heavily-Doped Channel," *IEEE Electron Device Lett.* EDL-8 (11): 534-536 (1987); S.R. Bahl, W.J. Azam, and J.A. del Alamo, "Strained-Insulator $In_xAl_{1-x}As/n^+\text{-}In_{0.53}Ga_{0.47}As$ Heterostructure Field Effect Transistors," submitted to *IEEE Trans. Electron Devices.*

dependence in device characteristics beyond the Matthews-Blakeslee critical layer thickness.[8]

A cross section of the device structure is shown in figure 7. Four wafers were grown by MBE in MIT's Riber 2300 system with InAs mole fractions in the $In_xAl_{1-x}As$ gate insulator layer of 0.52 (lattice-matching), 0.48, 0.40 and 0.30. The starting material was S.I. (100) InP. The device structure consists (from bottom to top) of a 1000Å undoped $In_{0.52}Al_{0.48}As$ buffer layer, a 100Å undoped $In_{0.53}Ga_{0.47}As$ subchannel, a 100Å heavily Si doped ($N_D = 4 \times 10^{18}\ cm^{-3}$) $In_{0.53}Ga_{0.47}As$ channel, a 300Å undoped $In_xAl_{1-x}As$ gate insulator layer, and an undoped 50Å $In_{0.53}Ga_{0.47}As$ cap. The four wafers were grown subsequently, and device processing was carried out simultaneously. Device processing is described by Bahl et al.[9]

HFETs were fabricated with gate-widths of 30 μm and gate lengths of 1.5 μm with current flow along the [0$\bar{1}$1] (defined here as 0° with respect to the flat), [001] (45°), and [011] (90°) directions.

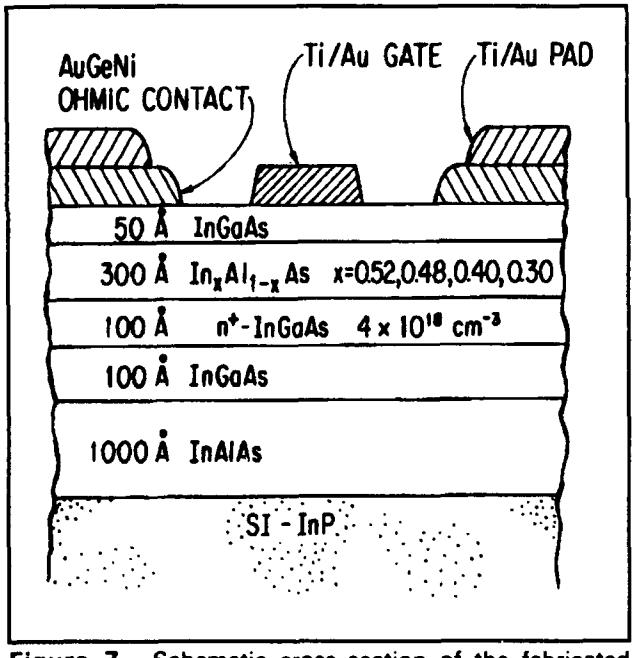

Figure 7. Schematic cross-section of the fabricated $In_xAL_{1-x}As/n^+$-$In_{0.53}Ga_{0.47}As$ MIDFETs.

Figure 8 shows the channel sheet resistance, R_{sh}, on each of the four wafers as a function of orientation. R_{sh} was measured using the actual MIDFETs by the all-electrical Floating Gate Transmission-Line Model (FGTLM).[10] Each point represents an average over five FGTLMs. For wafers with InAs mole fractions, x, of 0.52, 0.48, and 0.40, R_{sh} remains constant at approximately 850 Ω/□ independent of orientation. However, upon decreasing x from 0.40 to 0.30, the channel sheet resistance increases for all three orientations, showing a very pronounced orientation dependence with $R_{sh}[011] > R_{sh}[001] > R_{sh}[0\bar{1}1]$.

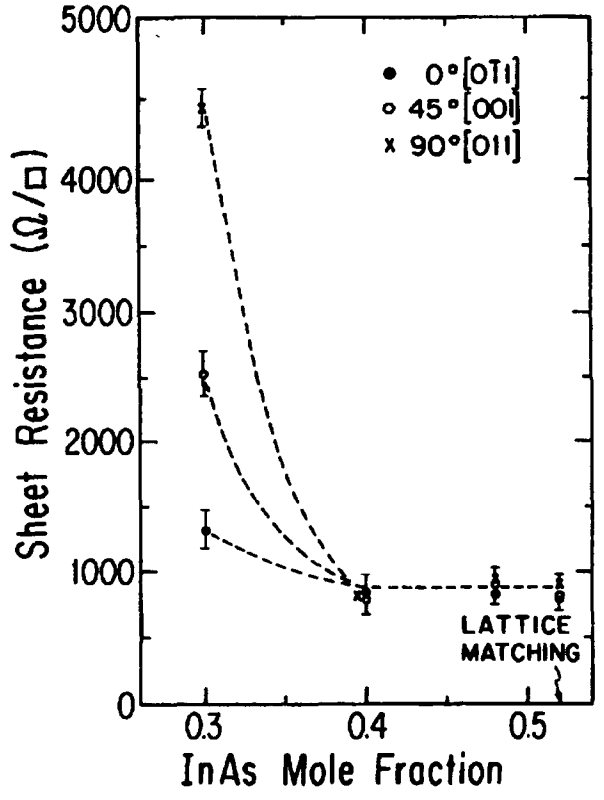

Figure 8. Channel sheet resistance versus InAs mole fraction, x, in the $In_xAl_{1-x}As$ insulator layer, for current flow along the various directions.

8 J.W. Matthews, A.E. Blakeslee, and S. Mader, "Use of Misfit Strain to Remove Dislocations from Epitaxial Thin Films," *Thin Solid Films* 33: 253-266 (1976).

9 S.R. Bahl, W.J. Azam, and J.A. del Alamo, "Strained-Insulator $In_xAl_{1-x}As/n^+$ - $In_{0.53}Ga_{0.47}As$ Heterostructure Field Effect Transistors," submitted to *IEEE Trans. Electron Devices*.

10 W.J. Azzam and J.A. del Alamo, "An All-Electrical Floating-Gate Transmission Line Model Technique for Measuring Source Resistance in Heterostructure Field-Effect Transistors," *IEEE Trans. Electron Devices* 37(9): 2105-2107 (1990).

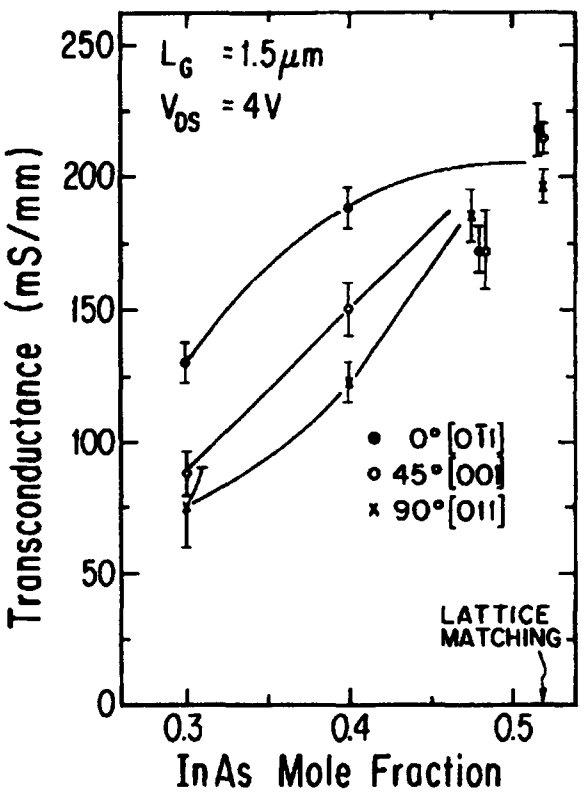

Figure 9. Peak transconductance versus x along the various directions at V_{ds}=4 V.

Figure 9 shows the average peak transconductance, g_m, over ten devices versus x for the three orientations measured at $V_{ds} = 4$ V. The x=0.52 and 0.48 devices do not show any orientation dependence (the x=0.40 devices have a high source resistance and are anomalously low in g_m). A pronounced orientation dependence is seen for devices with both x=0.40 and 0.30, with the 0° device being the best and the 90° device the most degraded. An additional significant result is that g_m (0°, x=0.40) is 189 mS/mm, which is very close to the average $g_m = 209$ mS/mm of the x=0.52 sample.

The x=0.40 and 0.30 devices were grown with thicknesses greater than the Matthews-Blakeslee critical layer limit.[11] This suggests that, in these devices, misfit dislocations may be responsible for the decrease in g_m and the appearance of orientation dependence. Since the presence of misfit dislocations has been correlated to the appearance of a cross-hatched surface,[12] we have taken dark field microscope images of the surface of the four wafers (figure 10). Figures 10(a) and 10(b) are the surfaces of the x=0.52 and x=0.48 wafers respectively. There are no ridges or cross-hatches on the surface. Figures 10(c) and 10(d) are the surfaces of the x=0.40 and x=0.30 wafers respectively. We see the appearance of a unidirectional array of surface ridges, faint and short, in figure 10(c), and brighter and longer in figure 10(d), running along the [0$\bar{1}$1] direction. This is the direction of current flow in the better (0°) devices. We could not distinguish any ridges along the [011] direction, neither in the Nomarski, nor in the dark-field mode of the microscope. The ridges could not be imaged at higher magnification, so a density count was impossible. Brighter and longer streaks would result from greater surface relief, indicating a higher dislocation density, with a greater bunch of dislocations associated with each surface streak.[13] The unidirectional hatch observed is consistent with that reported[14] for thin strained samples.

In III-V semiconductors, orthogonal 60° dislocations in the zinc-blende lattice occur on different sublattices and show an asymmetry relative to each other.[13] The so-called α dislocations have an extra half plane ending on a row of group-III atoms, and the β dislocations have an extra half plane ending on a row of group-V atoms.[15] For strained (100) InGaAs/GaAs, it has been shown

[11] J.W. Matthews, A.E. Blakeslee, and S. Mader, "Use of Misfit Strain to Remove Dislocations from Epitaxial Thin Films," *Thin Solid Films* 33: 253-266 (1976).

[12] K.H. Chang, R. Gibala, D.J. Srolovitz, P.K. Bhattacharya, and J.F. Mansfield, "Crosshatched Surface Morphology in Strained III-V Semiconductor Films," *J. Appl. Phys.* 67(9): 4093-4098 (1990).

[13] M.S. Abrahams, J. Blanc, and C.J. Buiocchi, "Like-Sign Asymmetric Dislocations in Zinc-Blende Structure," *Appl. Phys. Lett.* 21(5): 185-186 (1972).

[14] K.L. Kavanagh, M.A. Capano, L.W. Hobbs, J.C. Barbour, P.M.J. Maree, W. Schaff, J.W. Mayer, D. Pettit, J.M. Woodall, J.A. Stroscio, and R.M. Feenstra, "Asymmetries in Dislocation Densities, Surface Morphology and Strain of GaInAs/GaAs Single Heterolayers," *J. Appl. Phys.* 64 (10): 4843-4852 (1988).

[15] A.L. Esquivel, S. Sen, and W.N. Lin, "Cathodoluminescence and Electrical Anisotropy from α and β Dislocations in Plastically Deformed Gallium Arsenide," *J. Appl. Phys.* 47(6): 2588-2603 (1976).

that the first dislocations to form are 60° α dislocations along the [011] direction.[16] For our samples, in contrast, the dislocations run unidirectionally along the [0$\bar{1}$1] direction, perpendicular to the preferred dislocation direction we have seen reported in the literature. However,

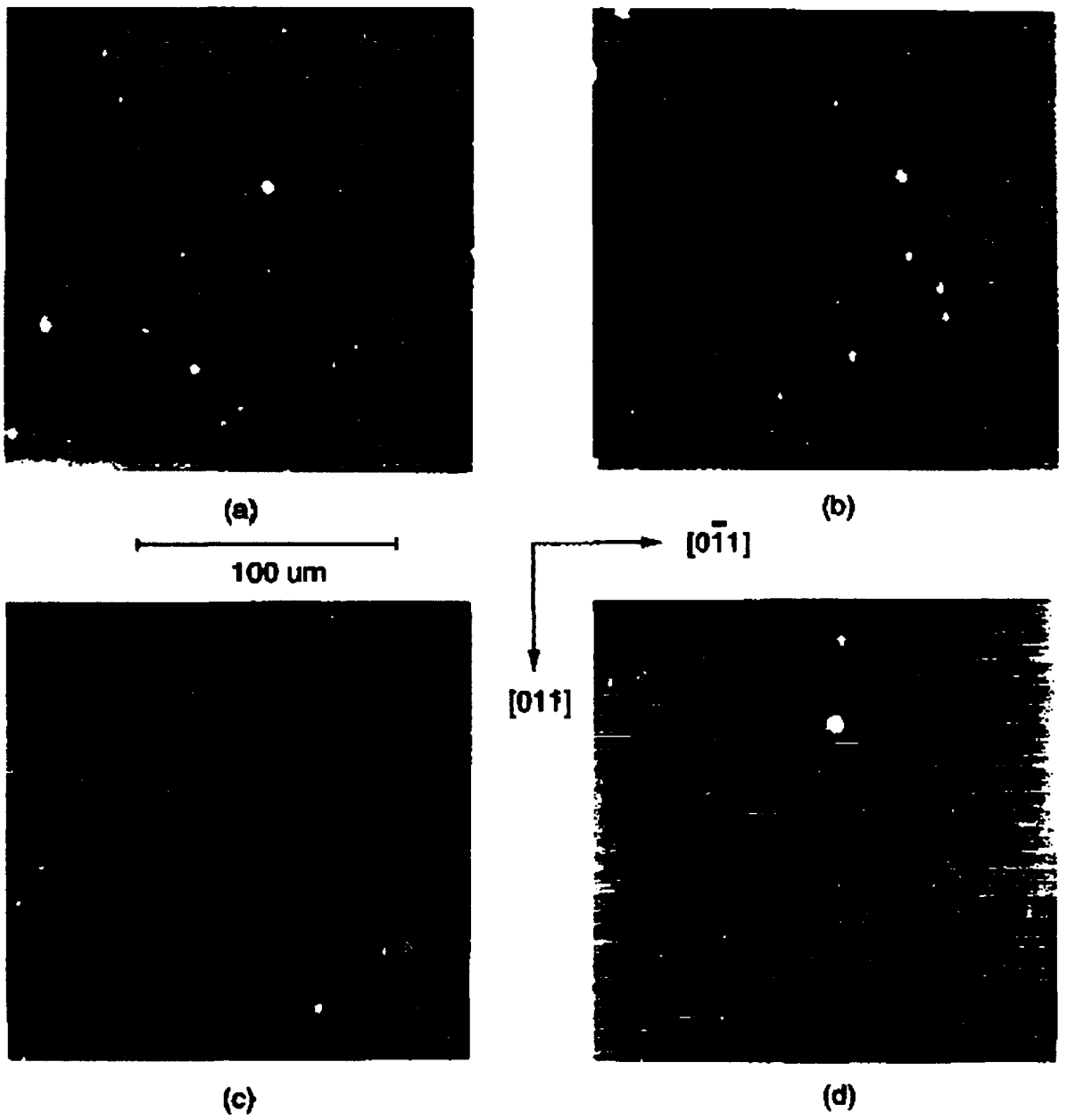

Figure 10. Dark field optical microscope photographs of the surface of the MIDFET layer structure for (a) x=0.52, (b) x=0.48, (c) x=0.40, and (d) x=0.30.

[16] K.L. Kavanagh, M.A. Capano, L.W. Hobbs, J.C. Barbour, P.M.J. Maree, W. Schaff, J.W. Mayer, D. Pettit, J. M. Woodall, J.A. Stroscio, and R.M. Feenstra, "Asymmetries in Dislocation Densities, Surface Morphology and Strain of GaInAs/GaAs Single Heterolayers," *J. Appl. Phys.* 64(10): 4843-4852 (1988); E.A. Fitzgerald, G.P. Watson, R.E. Proano, D.G Ast, P.D. Kirchner, G.D. Pettit, and J.M. Woodall, "Nucleation Mechanisms and the Elimination

these reports[16] have been done for epilayers under compression, i.e., the relaxed lattice constant for the epilayer is larger than that of the substrate. It has also been suggested that the 60° α and β dislocations should interchange directions when the epilayer is grown in tension,[17] which is consistent with our results, assuming that the α dislocations still nucleate preferentially. We believe we are the first to report observations of this behavior.

Our 0° devices, which have current flowing along the dislocations, are better than our 90° devices, which have current flowing perpendicular to them. The 45° devices fall in between. Our results are in agreement with the findings of Esquivel et al.[15] who show a decrease in mobility for current flow perpendicular to the α dislocations.

Woodall et al.[18] have proposed that misfit dislocations pin the Fermi-level, depleting a cylindrical region around them. Figure 11 shows a schematical cross-section of the dislocation depletion regions in a semiconductor slab with misfit dislocations running along the [0$\bar{1}$1] direction. Based on this figure, we can hypothesize an explanation for our observations. For our 0° devices, current flows along the dislocation direction [0$\bar{1}$1], while for our 90° device, current flow along [011] is normal to it. If the dislocation density is low, as in the x=0.40 sample, a dislocation would be associated with a small depletion region in the channel. If this depletion depth is smaller than the equilibrium depletion associated with Fermi-level pinning at the wafer surface or underneath the gate, then R_{sh} should not be affected by the presence of the dislocations. However, the pinning at the dislocation would prevent the gate voltage from modulating the portion of the channel underneath it. This should result in the more severe degradation of g_m for current flow perpendicular to the dislocations, because of their constricting effect, than for flow parallel to them. For a higher misfit (such as in the x=0.30 sample), the surface relief becomes more pronounced, indicating a greater bunching of the dislocations,[19] and producing depletion regions that exceed the depth of the one associated with the wafer surface. This should result in an asymmetry in both R_{sh} and g_m.

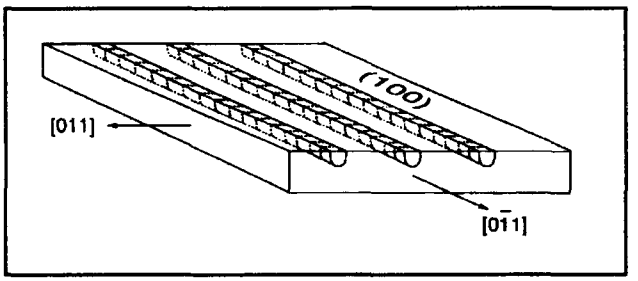

Figure 11. Schematic cross-section of the channel region of the MIDFET under tension, showing the effect of the depletion regions of misfit dislocations on current flowing parallel and perpendicular to them.

$In_{0.40}Al_{0.60}As/n^+$-$In_{0.53}Ga_{0.47}As$ devices with $L_g = 1.5\ \mu m$ and current flow along the [0$\bar{1}$1] direction show excellent characteristics in spite of the presence of misfit dislocations: a reverse breakdown voltage of 23 V, a maximum drain current of 308 mA/mm, a peak transconductance of 189 mS/mm and reduced real-space transfer of hot electrons from the channel to the gate.[20] Our result shows that although dislocations degrade device performance, excellent devices may be obtained by orienting the current parallel to them, if they are sufficiently sparse.

In conclusion, we have studied the electrical properties of strained-insulator $In_xAl_{1-x}As/n^+$-$In_{0.53}Ga_{0.47}As$ HFETs with the insulator composition below and above the Matthews-Blakeslee criteria for dislocation formation. For devices with the $In_xAl_{1-x}As$ layer above its critical thickness, we see a unidirectional array of surface ridges and measure a strong orientation dependence of peak transconductance. By aligning the current in the direction of the ridges, the impact of dislocations is greatly minimized, resulting in excellent devices, if their density is not too high.

of Misfit Dislocations at Mismatched Interfaces by Reduction in Growth Area," *J. Appl. Phys.* 65(6): 2220-2237 (1989).

[17] W.J. Bartels and W. Nijman, "Asymmetry of Misfit Dislocations in Heteroepitaxial Layers of (001) GaAs Substrates," *J. Cryst. Growth* 37: 204-214 (1977).

[18] J.M. Woodall, G.D. Pettit, T.N. Jackson, and C. Lanza, "Fermi-Level Pinning by Misfit Dislocations at GaAs Interfaces," *Phys. Rev. Lett.* 51(19): 1783-1786 (1983).

[19] M.S. Abrahams, J. Blanc, and C.J. Buiocchi, "Like-Sign Asymmetric Dislocations in Zinc-Blende Structure," *Appl. Phys. Lett.* 21(5): 185-186 (1972).

[20] S.R. Bahl, W.J. Azam, and J.A. del Alamo, "Strained-Insulator $In_xAl_{1-x}As/n^+$ - $In_{0.53}Ga_{0.47}As$ Heterostructure Field Effect Transistors," submitted to *IEEE Trans. Electron Devices.*

7.4 Publications and Conference Papers

Azzam, W.J., and J.A. del Alamo. "An All-Electrical Floating-Gate Transmission Line Model Technique for Measuring Source Resistance in Heterostructure Field-Effect Transistors." *IEEE Trans. Electron Devices* 37(9): 2105-2107 (1990).

Bahl, S.R., W.J. Azzam, and J.A. del Alamo. "Orientation Dependence of Mismatched $In_xAl_{1-x}As/In_{0.53}Ga_{0.47}As$ HFETs." Paper presented at Sixth International Conference on Molecular Beam Epitaxy, San Diego, California, August 27-31, 1990. *J. Cryst. Growth*. Forthcoming.

Bahl, S.R., and J.A. del Alamo. "Strained InAlAs/n^+-InGaAs HFETs." Paper presented at the 1990 Workshop on Compound Semiconductor Materials and Devices (WOCSEMMAD), San Francisco, California, February 19-21, 1990.

Bahl, S.R., and J.A. del Alamo. "An $In_{0.52}Al_{0.48}As/n^+In_xGa_{1-x}$ Heterostructure Field-Effect Transistor with an In-Enriched Channel." *Proceedings of the Second International Conference on Indium Phosphide and Related Materials*, Denver, Colorado, April 23-25, 1990, pp. 100-103.

Bahl, S.R., and J.A. del Alamo. "A Quantized-Channel $In_{0.52}Al_{0.48}As/n^+$-$In_{0.53}Ga_{0.47}As$ HFET with High Breakdown Voltage." Paper presented at Symposium on Electronic, Optical and Device Properties of Layered Heterostructures of the 1990 Fall Meeting of the Materials Research Society, Boston, Massachusetts, November 28-December 1, 1990. *Extended Abstracts* EA-21: 117-120 (1990).

Professor Henry I. Smith (left) observing an x-ray lithography experiment being carried out by graduate students Anthony Yen and William Chu.

Chapter 8. Novel Superconducting Tunneling Structures

Academic and Research Staff

Professor John M. Graybeal, Professor Henry I. Smith

Visiting Scientists and Research Affiliates

Dr. Bernard S. Meyerson[1]

Graduate Student

George E. Rittenhouse

8.1 Project Description

Sponsor

Joint Services Electronics Program
Contract DAAL03-89-C-0001

Project Staff

Professor John M. Graybeal, Professor Henry I. Smith, Dr. Bernard S. Meyerson, George E. Rittenhouse

In this program, we seek to examine the behavior of electronically-gated resonant tunneling structures with superconducting source and drain electrodes. Specifically, we will examine whether superconducting Cooper pairs can participate in the resonant-tunneling channel. These three-terminal hybrid superconducting/semiconducting structures represent the first attempt at Josephson coupling via resonant tunneling. A significant potential technological consequence of this approach is that quantum confinement levels, not the semiconducting gap, set the characteristic energy scale for modulating the Josephson current. In addition, such structures may provide important insight into the behavior of "conventional" (i.e., single electron) resonant tunneling structures, as the Josephson channel is inherently coherent.

In previously fabricated electronically-gated hybrid superconducting/semiconducting devices, the energy scale in the semiconducting region was set by the semiconducting gap energy ($E_{semi} \approx 0.1\text{-}1\,eV$), while the energy scale for the Josephson coupling (and hence the output voltage) was set by the superconducting gap energy ($\Delta \approx 10^{-3}\,eV$). It is important to recognize that it is this energy mismatch which fundamentally leads to less than unity gain in such devices. As a result, the output voltage Δ is insufficient to drive the gate of another device downstream ($V_{gate} \approx E_{semi}/e$). On the contrary, the characteristic energy scale for a quantum confined structure is instead set by the device size, and is therefore tunable. For device dimensions on the scale of 10-100 nm, now experimentally accessible via advanced lithographic patterning techniques, these energies can thus more easily approach that of the superconducting gap energy.

The novel geometry of our hybrid resonant tunneling device is shown schematically in figure 1. The semiconducting quantum well is made of single crystal silicon, the tunnel barriers are ultrathin thermally-grown layers of SiO_2, and the superconducting electrodes are vacuum-deposited niobium (Tc(Nb)=9 K).

The Si quantum well is a high-aspect ratio structure and is etched into the surface of a single-crystal Si wafer using a highly anisotropic wet etch. A top view of this kind of wall is displayed in figure 2. Please note that this is a novel geometry, because the semiconducting well is oriented vertically and not horizontally. The fact that it is patterned via wet etching from single crystal silicon leads to almost no reduction in the electron mobility as compared to the starting bulk material. The patterning of this walled structure was produced via x-ray lithography. In order to fabricate such a structure, the mask must be aligned to crystalline axes of the silicon wafer with high precision. The anisotropic etch (in a potassium hydroxide solution) produces essentially atomically smooth surfaces, leading to parallel faces on either side of the quantum well. This is an essential ingredient for a resonant tunneling device, because

[1] IBM Corporation, Thomas J. Watson Research Center, Yorktown Heights, New York.

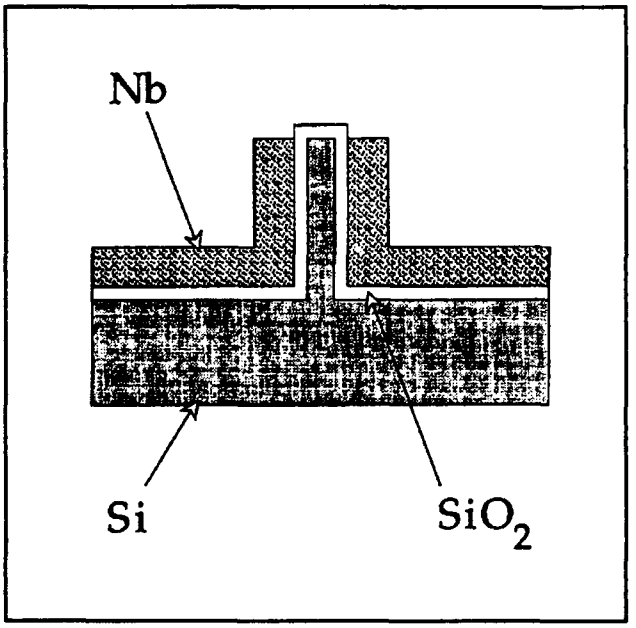

Figure 1. Schematic of device structure (not to scale) displaying Nb superconducting electrodes, SiO_2 tunneling barriers, and Si wafer and quantum well. Note quantum well is vertical and composed entirely of single-crystal Si. The gate (not shown) is offset laterally and is attached to the Si surface layer.

there are close analogies between it and an optical Fabry-Perot interferometer.

The ultrathin oxide tunneling barriers are grown thermally at 800°C in a dilute (0.8%) oxygen atmosphere. Using this technique, we can produce oxide thicknesses down to 15Å, and C-V analysis show them to be of very high quality. For our device to date, we have used 15-20Å oxide layers.

The Nb superconducting counterelectrodes are deposited in high vacuum via electron-beam deposition and are subsequently laterally patterned into cross-strips via standard lithographic processing techniques. The crucial and most difficult step is to remove the Nb over the top of the quantum well, in order to avoid superconducting shorts across the device. We have found that planarization is both convenient and appropriate for this task, and we reactively etch the top strip of Nb using chlorine gas (which stops at the ultrathin SiO_2 tunnel barrier).

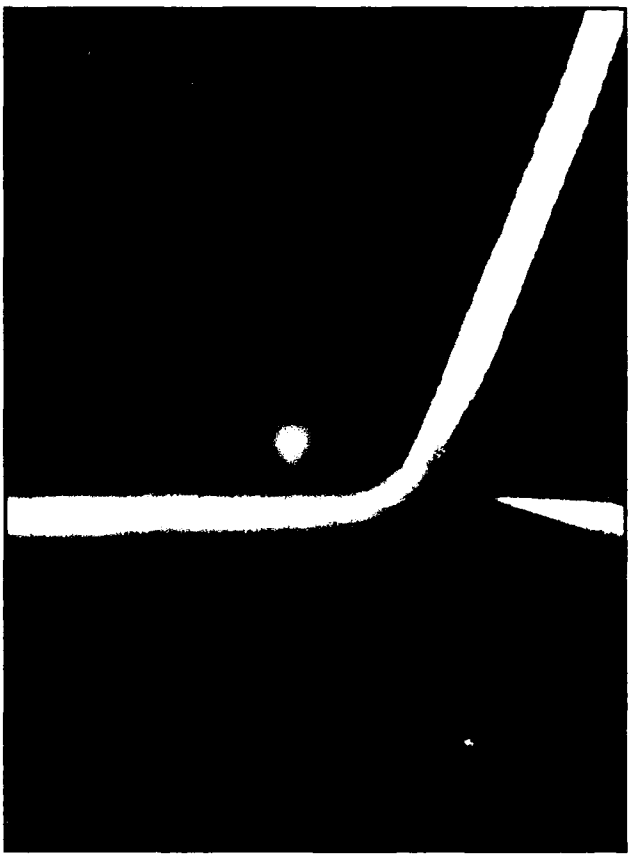

Figure 2. Scanning electron microscope picture of the top of such a wall, showing the extremely smooth and straight faces produced by the anisotropic etching.

We have just completed the fabrication trials. We have tested every key step of device fabrication and have put all the steps together to fabricate several test devices on very lightly doped Si wafers. The devices made had quantum well thicknesses ranging down to 750Å, with Si wall heights on the order of 5000Å. These test devices have successfully verified all aspects of the device fabrication, but unfortunately were too lightly doped for resonant tunneling conduction. Thus, the next step will be to fabricate these devices onto wafers with doped high-mobility epitaxially-grown Si layers. *In collaboration with Dr. Bernard* S. Meyerson at the IBM Thomas J. Watson Research Center, we are presently preparing to fabricate these devices using Si wafers on which high-mobility delta-doped epitaxial Si layers have been grown.

Chapter 9. Heterostructures for High Performance Devices

Academic and Research Staff

Professor Clifton G. Fonstad, Jr., Dr. Elias D. Towe

Visiting Scientists and Research Affiliates

Dr. Herve Blanck,[1] Jack Cunningham,[2] Victor Ehrenrich,[3] R. Victor Jones,[3] Michael Kim,[4] Bahman Meskoob,[5] James Mikkelson,[6] Dr. Sheila Prasad,[5] Masahi Usami[7]

Graduate Students

Thomas P.E. Broekaert, Geoffrey F. Burns, Woo-Young Choi, Isako Hoshino, Tanni Y. Kuo, Paul Martin, Patrick J. McCann, Lung-Han Peng, Yakov Royter, Krishna Shenoy, Richard A. Singer, Jurgen Smet, James C. Vlcek

Undergraduate Student

Clifford P. Stephens

Technical and Support Staff

Angela R. Odoardi, Ning Fang, Richard R. Perilli

9.1 Introduction

The broad objective of our research effort is to develop III-V quantum heterostructures for high performance electronic, optoelectronic, and photonic devices for high speed optical communications and signal processing. To this end, we are developing: (1) new, higher performance materials systems including InP-based InGaAlAs heterostructures and <111> oriented strained layer superlattices; (2) a new family of quantum-well-base, tunnel-barrier n-n-n transistors and near- and far-infrared optoelectronic devices; and (3) new damage-free *in situ* processing techniques for fabricating advanced quantum structure and embedded heterostructures.

The following sections describe our progress during the past year in the above research areas. Our group works closely with Professors Hermann A. Haus, Eric P. Ippen, and James G. Fujimoto to develop the optical device application, characterization, and modeling aspects of this program and with Professor Sylvia T. Ceyer to develop new *in situ* processing techniques.

---

[1] Thomson CSF, Orsay, France.

[2] AT&T Bell Laboratories, Holmdel, New Jersey.

[3] Harvard University, Cambridge, Massachusetts.

[4] TRW, Electronics and Technology Division, Redondo Beach, California.

[5] Northeastern University, Boston, Massachusetts.

[6] Vitesse Semiconductor, Camarillo, California.

[7] Kokusai Denshin Denwa Company, Ltd., Saitama, Japan.

9.2 Computer Controlled Growth of Lattice-Matched InGaAlAs Heterostructures on InP

Sponsors

Charles S. Draper Laboratory
Contract DL-H-418483
DARPA/NCIPT
Subcontract 542383
Joint Services Electronics Program
Contract DAAL03-89-C-0001

Project Staff

James C. Vlcek, Professor Clifton G. Fonstad, Jr.

In electronic and optical semiconductor devices, the need for both graded-composition and hyper-abrupt metallurgical junctions frequently arises. The use of graded-composition junctions allows for precise control of the confinement of charge carriers and optical fields through spatially varying bandgaps and refractive indices, respectively. On the other hand, hyper-abrupt junctions may be desired in some devices, most notably quantum effect devices, where a sharp interface is desired to reduce fluctuations in the confinement energy which might arise from graded interfaces due to shutter transients. Thus, optimal device designs can place tight constraints on the molecular beam epitaxial growth procedures – in particular, the ratios of the constituent and dopant fluxes during the growth — which will implement these complicated epitaxial layer structures.

The need to lattice-match, as to an InP substrate, further constrains the ratio of constituent fluxes. If the alloy composition is not sufficiently close to the lattice-matching composition, strain effects can significantly alter the electrical and optical properties of the material, and, in the extreme case, dislocations can be seeded. Thus, the constraints imposed by the need to lattice-match may be more stringent than those imposed by the composition gradients dictated by the device design. In this work, we have grown the quaternary $In_xGa_yAl_{1-y}As_{1-s}$, lattice-matched to InP substrates. This quaternary, which may be viewed as a binary alloy of the two ternaries InGaAs and InAlAs, spans the bandgap range of 0.75 – 1.5 eV and is better suited to solid-source MBE techniques than the $In_{1-x}Ga_xAs_yP_{1-y}$ alloy system, which spans a similar bandgap range.

We have implemented a computer-automated MBE control system (1) to provide precise control of the constituent and dopant fluxes necessary to achieve graded-composition alloys and (2) to maintain uniform compositions in the presence of shutter events. Key to this system are accurate models of the characteristics of the effusion cells, including not only the static flux versus temperature relationship, but also the time-dependent behavior of the cell in the presence of changes in either setpoint and/or shutter status. These models approximate the temporal response of the effusion cells to a setpoint change with a single-pole system function with the location of the pole determined by a direct measurement of the flux profile generated by a step change in the cell setpoint temperature.

In the case of graded-composition layers, the thermal lag time of the cell requires modification of the time-dependent effusion cell setpoint temperature profile. This modification is necessary to eliminate the over- and undershoot effects at the endpoints of the graded layer which would result if the effects of cell response time are neglected. With such modifications, we have achieved linearly graded flux profiles with deviations from the desired profile which can be held within one percent. The gradient of material composition in these layers corresponded to a conduction band gradient of 33 kV/cm.

To remove flux transients which arise from the operation of the cell shutters, we have structured the control system so that it seeks to maintain the flux in the effusion cell at a constant value, irrespective of the shutter status. In practice, this entails maintaining the setpoint temperature of the cell at a lower value with the shutter closed than open and performing an exponential ramp sequence upon change of shutter status. Using this technique, we have reduced cell shutter transients from 15 - 30% to one percent or less.

9.3 InGaAlAs Strained-Layer Heterostructures on 111 GaAs and InP for Optoelectronic Device Applications

Sponsors

DARPA/NCIPT
Subcontract 542383
Joint Services Electronics Program
Contract DAAL03-89-C-0001

Project Staff

Richard A. Singer, Professor Clifton G. Fonstad, Jr.

We have been interested in (111)-oriented strained-layer heterostructures because of the large piezoelectrically generated built-in electric fields that are present in these materials, as well as because of the possibility of enhanced optical

effects in (111)-oriented quantum structures. We have been very successful in growing layers on (111)B GaAs, routinely grow on these substrates, but we have had considerably more difficulty on InP substrates.

Mirror surfaces for both bulk InGaAs and InAlAs layers, grown by molecular beam epitaxy (MBE) on (111)B InP substrates, have recently been achieved. These materials have been characterized by photoluminescence (PL), Hall measurement, and double crystral diffraction, and, in the latter case, exhibit linewidths which compare favorably to both the InP substrates and to concurrently grown (100) epilayers. Nevertheless, the Hall mobilities of the (111) InGaAs samples are consistently an order of magnitude lower than their (100) counterparts, while the PL intensities are extremely weak. The InAlAs is essentially semiinsulating and shows no PL. These results, of course, indicate that the electrical and optical quality of these materials is still relatively low and, as a result, epilayers grown on (111)InP are not acceptable for use in p-i-n devices yet.

The difficulties associated with MBE grown on (111)InP arise because of the highly reactive (111) surface and the volatilty of the InP substrate and the indium alloys of the epitaxial layers. Unfortunately, the growth conditions, which address the issues described above, inhibit the surface mobility of the group III constituents. This results in material of poor surface morphology. To circumvent this problem, a quasi-migration enhanced epitaxy procedure was developed in which growth takes place at low substrate temperature, low As overpressure, and slow growth rate. We have, in fact, observed an increase in Hall Mobility when the growth rate was slowed. Therefore, this is a promising direction for continuing in our efforts to optimize the growth parameters for (111) epilayers.

9.4 Molecular Beam Epitaxy of GaAlAs Laser Diode Heterostructures on Silicon Substrates

Sponsors

DARPA/NCIPT
Subcontract 542383
IBM Corporation Fellowship

Project Staff

Geoffrey F. Burns, Dr. Herve Blanck, Professor Clifton G. Fonstad, Jr.

Prospects for monolithic integration of III-V electrical and optical devices with Si circuits have fueled vigorous research in direct heteroepitaxial growth of these compounds on Si substrates. Developing III-V optical sources useful for VLSI optical interconnects is one goal which has been pursued by several groups. Along these lines, we have focused upon the laser diode due to its capacity for high speed modulation and efficient electrical to optical power conversion. Using molecular beam epitaxy (MBE), we have developed a process for routine fabrication of (Ga,Al)As laser heterostructure lasers directly on Si substrates.

Unfortunately, active optical devices such as the laser exhibit degraded luminescent efficiency and reliability when fabricated in heteroepitaxial GaAs-on-Si; threshold currents and lifetimes presently obtained are insufficient for Si integration. These shortcomings are imposed primarily by limitations in the quality of heteroepitaxial GaAs-on-Si currently produced, including dislocation densities above 10^6 per square cm and residual strains above 10^9 dynes per square cm, resulting from the 4.2% lattice mismatch and $\sim$ 40% thermal expansion mismatch between GaAs and Si.

The thermal strain problem can be attacked by reducing the area of the III-V epitaxial layer in contact with the Si substrate during growth, as well as by significantly reducing the maximum growth temperature of the laser device. Following the first approach, we are evaluating lasers grown on substrates structured with oxide windows and ridges. Initial working devices have been produced on structured substrates and reduced threshold currents have been observed. Further evaluation of these devices will determine the degree of strain relief and reliability improvement. Additional process measures currently in development include an MBE growth process which lowers the laser device growth temperature in addition to post fabrication thermal annealing to reduce the residual dislocation density.

9.5 Integration of Vertical Cavity Surface Emitting Lasers on GaAs Integrated Circuits

Sponsors

DARPA/NCIPT
Subcontract 542383
IBM Corporation Fellowship
National Science Foundation Fellowship
Vitesse Semiconductor

Project Staff

Krishna Shenoy, Geoffrey F. Burns, Professor Clifton G. Fonstad, Jr., in collaboration with James Mikkelson

Vertical cavity surface emitting lasers (VCSELs) offer many advantages over in-plane lasers, both as discrete and integrated devices. Monolithic fabrication, on-wafer testing, inherent single longitudinal mode operation, low threshold currents, and low divergence angles (suitable for optical fiber coupling) are among VCSEL attributes. VCSELs can also form high-density two-dimensional arrays for high-speed parallel optical processing, and large-scale integrated circuit optical interconnections as a result of their vertical emission and small in-plane dimensions.

It is the purpose of this program to demonstrate that VCSELs can be integrated with state-of-the-art refractory metal gate GaAs VLSI integrated circuits by growing GaAlAs heterostructures selectively in windows, i.e., openings cut through the dielectric covering the electronic circuitry down to the underlying GaAs substrate. Solid source molecular beam epitaxy (MBE) is being used to grow the structures, and standard etchants and metalization procedures are being followed. The laser emission will occur normal to the wafer plane, either through the substrate or from the processed surface.

The basic low-threshold VCSEL design incorporates a single quantum well (SQW) active region between two distributed bragg reflector (DBR) mirrors. High mirror reflectivities (>95%), a thin active region (<10 nm), and adequate current confinement are crucial for low-threshold lasing. An InGaAs active region with alternating GaAs/AlAs DBRs is yielding the lowest threshold currents.

Three VCSEL integration issues are currently being investigated: (1) selective growth of GaAs/InGaAs/AlGaAs VCSEL heterostructures in insulator windows on GaAs substrates, (2) low temperature AlGaAs growth, and (3) VCSEL design optimization. As a first step, crystalline GaAs/AlGaAs layers have been successfully grown in a variety of window geometries on GaAs wafers provided by Vitesse Semiconductor. These initial growths look excellent. However, high optical quality AlGaAs is conventionally grown above 700°C, and even with refractory metal gates, GaAs electronic circuitry can not tolerate these growth temperatures for the times involved in MBE growth. Hence, we are growing lower temperature AlGaAs and characterizing it both electrically and optically to understand the lower acceptable bound on the growth temperature. At the same time, tests of Vitesse circuitry are planned to quantify its thermal tolerance. Given this information, VCSEL designs will be optimized to reach a balance between growth temperature-time demands and the device limitations, while, at the same time, meeting the necessary threshold, power output, and emission specifications.

9.6 MBE-Grown InGaAlAs/InP Long-Wavelength Laser Diodes for Narrow Linewidth Applications

Sponsor

Charles S. Draper Laboratory
Contract DL-H-418483

Project Staff

Woo-Young Choi, Yakov Royter, Professor Clifton G. Fonstad, Jr.

Semiconductor lasers emitting at a wavelength of 1.3 to 1.5 μm are a key element of low-loss optical fiber communication systems. The material system most often used for such laser diodes is the quaternary alloy InGaAsP lattice-matched to InP substrates. Liquid phase epitaxy (LPE) and metal-organic chemical vapor deposition (MOCVD) are the usual growth techniques for this material system.

The InGaAlAs material system, grown by conventional solid-source molecular beam epitaxy (MBE), is another promising candidate for laser diodes emitting in the 1.3 to 1.5 μm range. Significantly, the InGaAs/InAlAs heterojunction has a larger conduction band discontinuity than the InGaAs/InP heterojunction. This enhances the quantum confinement of elections, affording the device designer greater latitude in choosing layer structures for optimizing electrical and optical confinement profiles. This enhanced design latitude, in turn, can be used to achieve lower threshold currents, lower temperature variation (T_0), and narrower spectral line-width.

Using MBE, we have grown InGaAs/InAlAs double heterostructure (DH) 1.3 μm and 1.55 μm InGaAlAs graded-index separate confinement (GRIN-SCH) multiple quantum well (MQW) laser diodes. From these laser materials, we have fabricated broad-area and ridge-stripe laser diode devices. We have also characterized threshold currents, emission spectra, and far-field patterns. Our initial data indicate that our devices are comparable to other laser diodes of the same material system reported in the literature. Currently, we are focusing our efforts on the optimization of the GRIN-SCH MQW laser structure in terms of the

optical confinement structure, barrier height and width, and the number of quantum wells. With these optimizations, we believe that our device performance will be greatly enhanced.

In addition, we are investigating the possibility of additional performance enhancement with strained quantum wells. Strained quantum well devices have demonstrated exciting results in GaAs-based laser diodes, and we believe we can achieve similar improvements in InGaAlAs long-wavelength laser diodes with the excellent capacity of MBE to grow precisely-controlled strained layers.

Other possible applications for these devices include pure FM laser diodes with reduced AM noise, pure AM laser diodes with reduced chirping, laser diodes easily tunable over a wide band, and other non-laser devices like tunable narrow bandwith filters and light modulators.

The list of possible device applications shows that developing the basic idea of wells with different optical gain profiles and accessing them independently within a single device is quite general. Once the above narrow linewidth laser diode and the associated theory have been demonstrated, we expect this list to continue to grow.

9.7 Applications for New Three Terminal Laser Diodes with Dynamic Control of Gain and Refractive Index

Sponsor

DARPA/NCIPT
Subcontract 542383

Project Staff

Paul Martin, Professor Clifton G. Fonstad, Jr., in collaboration with Professor Hermann A. Haus

We are investigating a new class of devices in which the active region consists of two sets of quantum wells with different optical gain profiles. By designing structures in which the current injection into these two sets of quantum wells can be independently controlled, we gain a new, previously unexploited, degree of freedom in controlling light output from the device.

The immediate goal of this program is to use this new degree of freedom to design a ridge type laser diode with reduced alpha-parameter, which is the ratio of refractive index change to gain change associated with an injected current density change. Since the linewidth of a semiconductor laser diode is proportional to one plus alpha squared, a reduction in alpha from a typical value of three for QW laser diodes to near zero would give a reduction in laser linewidth on the order of ten. We expect narrow-linewidth lasers incorporating this scheme to find application in many optical communications systems where linewidth of the signal laser limits the transmission bit rate-distance product. New systems based on erbium-doped fiber are particularly sensitive to signal laser linewidth because optical signals are amplified but not regenerated or retimed. The recent explosion of interest in erbium-doped fiber communications systems thus makes this application especially timely.

9.8 Use of Graded Profiles to Improve InGaAlAs/InP Heterojunction Bipolar Transistor Performance

Sponsor

Joint Services Electronics Program
Contract DAAL03-89-C-0001

Project Staff

James C. Vlcek, Professor Clifton G. Fonstad, Jr.

Heterojunction Bipolar Transistors (HBTs) fabricated in the $In_xGa_yAl_{1-y}As_{1-x}$ alloy system, lattice matched to semi-insulating InP substrates, are emerging as promising candidates for microwave applications. By utilizing the advantages of the material properties of this alloy system, in particular the properties of the ternary alloy InGaAs, HBT device performance superior to that of GaAlAs HBTs may be realized. The $In_xGa_yAl_{1-y}As_{1-x}$ system is also better suited to the solid-source molecular beam epitaxial (MBE) growth techniques typically employed in HBT fabrication than the $In_{1-x}Ga_xAs_yP_{1-y}$ system, which also lattice matches to InP.

While, in its simplest form, an HBT needs to have only an emitter of a wider bandgap material than its base, such single heterojunction devices suffer from a number of drawbacks. Most important of these drawbacks is that the base-collector junction of such a device will have a lower turn-on voltage than the base-emitter junction, resulting in an "offset" voltage in the output characteristics. A single heterojunction HBT which uses the ternary InGaAs for both base and collector will also suffer from a high output conductance and low collector-emitter breakdown voltage due to the narrow gap collector material. Finally, the use of abrupt heterojunctions, at either of the two pn junctions in the device, introduces "spikes" in the

band edges at the junctions which could lead to carrier trapping and degraded device performance. For these reasons, an HBT fabricated in the $In_xGa_yAl_{1-y}As_{1-x}$ alloy system is best achieved with graded base-emitter and base-collector junctions.

Using advanced computer-controlled MBE growth techniques, we have successfully fabricated and characterized an $In_xGa_yAl_{1-y}As_{1-x}/InP$ emitter-up, doubly-graded heterojunction bipolar transistor. By using parabolic compositional gradings in the pn junctions, made possible by precise computer control of the constituent fluxes during the epitaxial growth, successful devices with characteristics much improved over abrupt single-heterojunction devices fabricated in this same material system. In particular, the "offset voltage" from which many single heterojunction devices suffer has been reduced from ≥ 500, mV to ≤ 20, mV; the Early voltage has been increased from < 5, V to 25, V; the collector breakdown voltage has been increased from $BV_{CEO} < 5$, V to $BV_{CEO} > 10$, V.

9.9 Applications of Delta-Doping to Heterojunction Bipolar Transistors

Sponsors

AT&T Bell Laboratories
Hertz Foundation Fellowship

Project Staff

Tanni Y. Kuo, Professor Clifton G. Fonstad, Jr., in collaboration with Jack Cunningham

In our research, we have grown heterostructure bipolar transistors (HBTs) by gas source molecular beam epitaxy in which the base is delta-doped with Be to concentrations ranging from $5 \times 10^{13}/cm^2$ to $6 \times 10^{14}/cm^2$. *Transmission* electron microscopy studies revealed that the Be is spatially confined to within 1.5 nm. To fabricate the HBT without inducing Be redistribution and avoid critical emitter mesa etching, we have developed a new low-temperature base-contacting procedure ($T_{max} = 420°C$) which requires no base emitter etching. We use a non-alloyed emitter contact facilitated by a delta-doped n-layer placed on the surface of the sample, eliminating the need for a doped cap layer. The base is contacted by depositing Au-Zn or Au-Be on the surface and alloying at 420° C for 10 seconds. This results in ohmic contact with the base, rectifying contact with the emitter. A 50 μm diameter delta-HBT shows a current gain of 20. After reducing the size of the emitter 3 x 8 μm, the current gain of the delta-HBT increases to 30. This is due to the fact that we have eliminated the critical base-emitter etch which reduces surface recombination. In order to completely planarize the HBTs, we grew and fabricated HBTs in holes which were pre-etched into the substrates. High quality material has been achieved in the holes.

We have also demonstrated the growth of the complete structure of high quality AlGaAs/GaAs heterostructure bipolar transistors (HBTs) by chemical beam epitaxy (CBE). This includes a non-alloyed delta-doped ohmic emitter contact and *in situ* Al emitter metalization which are accomplished by CBE using a new precursor, trimethylamine alane, as the Al source and trimethyl-Ga as the Ga source. Devices with both graded AlGaAs and uniform GaAs bases doped with carbon to the high $10^{19}/cm^3$ using trimethyl-Ga have been fabricated. A current gain of 10 at a current density of 2.5 kA/cm^2 is obtained for the uniform base HBTs. The DC performance of the grade base HBTs is comparable. Both types of devices display excellent output characteristics.

9.10 Microwave Characterization, Analysis, and Modeling of Emitter-Down Heterojunction Bipolar Transistors

Sponsors

National Science Foundation[8]
TRW

Project Staff

Dr. Sheila Prasad, Professor Clifton G. Fonstad, Jr., in collaboration with Bahman Meskoob, Michael Kim

Emitter-down InGaAs/InAlAs/InP heterojunction bipolar transistors have been characterized at microwave frequencies and small-signal equivalent circuit models have been obtained using the commercial Touchstone software. A comparison of the measured S-parameters and gain characteristics with the modeled values showed an error of about 5%. Since such a large percentage of error was

[8] Support of Dr. Prasad at Northeastern University.

not considered acceptable for optimization, other methods of optimization were considered.

A modification of the Touchstone program was suggested by Professor R. Trew at North Carolina State University. The technique uses the device cut-off frequency f_T, determined by the current gain h_{21} characteristic to establish the total emitter-to-collector delay time from the experimental data. This information was used to establish an equation that is then used to constrain the circuit elements, thereby facilitating the procedure for parameter extraction. The error between measured and modeled parameters was reduced to 0.05%. The simulated annealing algorithm has been used successfully in other modelling applications. Since it does not depend on good starting values for the elements, the error should be minimized further. Optimization using the simulated annealing method is now in progress.

Large signal-modeling of the HBT is also in progress. Small-signal S parameter measurements are being made for a large number of bias points on-wafer probing of the transistors using the Hewlett-Packard 8510B automatic network analyzer and the Cascade Microtech microwave probe station. The bias-dependence of each of the elements in the equivalent circuit will be determined so that an accurate large-signal model will obtained. Measurements are also in progress to determine the optimized model for high frequency third-order intermodulation product.

9.11 AlAs Etch-Stop Layers for InGaAlAs/InP Heterostructure Devices and Circuits.

Sponsor

Joint Services Electronics Program
Contract DAAL03-89-C-0001

Project Staff

Thomas P.E. Broekaert, Professor Clifton G. Fonstad, Jr.

Wet chemical etching solutions have been developed that allow the selective etching of InP lattice-matched InGaAlAs quaternary compounds using thin pseudomorphic AlAs layers as etch stops. The best results have been obtained for etchants consisting of succinic acid, ammonia, and hydrogen peroxide. The etchant is well buffered and can be used over a wide pH range, from 4.2 to 7.0, by varying the amount of ammonia added. In addition, the etchant is compatible with Cr/Au contact metallization and standard positive photoresists. Typically, the InGaAs etch rate is about 100 nm/min.

At a pH of 4.2, the etch rate of InGaAs is found to be over 1000 times the etch rate of AlAs, while the etch rate of InAlAs is over 500 times that of the AlAs. At a pH of 5 and higher, the InAlAs etch rate becomes very small while the InGaAs etch rate remains about the same, enabling the selective etching of InGaAs over InAlAs with a selectivity of better than 100 to 1. A typical AlAs stop layer is about 10 monolayers (m.l.) thick (2.73 nm). Stop layers as thin as 3 m.l. can also be used, however, the pH must be increased to at least 6.2 and the selectivity decreases to 25 to 1.

Buffered HF can be used to remove the AlAs stop layer, while it does not etch InGaAlAs to any significant degree.

These selective etchants have enabled us to measure the conductance and mobility of a directly contacted quantum well in a resonant tunneling structure for the first time and have opened up the possibility of fabricating a whole new set of novel quantum devices (see the following section).

9.12 Three-Terminal n-n-n Quantum-Well-Base, Tunnel-Barrier Devices

Sponsors

Belgian American Education Foundation (BAEF)
Feilowship
Joint Services Electronics Program
Contract DAAL03-89-C-0001
National Science Foundation
Grant ECS 90-08485

Project Staff

Thomas P.E. Broekaert, Jurgen Smet, Professor Clifton G. Fonstad, Jr.

We have attained the ellusive goal of making direct electrical contact to a populated conduction band quantum well in a resonant tunneling heterostructure. In a significant breakthrough (see preceeding section), we have recently succeeded in selectively and controllably etching away the layers above the quantum well in an AlAs/InAs/InGaAs resonant tunneling diode. This result is a major advance that opens the way to a whole new class of ultra-high performance electronic, optoelectronic, and photonic devices. We have begun an aggressive program of research utilizing this advance to investigate quantum-well-base, tunnel-barrier (QT) n-n-n transistors, and (see Section 9.15) tunnel-

barrier infrared photodiodes and optotelectronic modulators.

The basis for these devices is the AlAs/InAs/InGaAs double barrier resonant tunneling diode (RTD) structure, which we have used successfully in the past to produce two-terminal RTDs with room temperature peak-to-valley current ratios of 30 to 1, peak current densities in excess of 450kA/cm^2, and characteristics displaying three resonant peaks.

There are at least three unique features of this structure which make it ideally suited for these devices. First, the AlAs tunnel barriers are unusually high relative to the InGaAs injectors and the InAs well, which yields multiple confined well states and sharp quantum structure at room temperature. Second, the InAs well lies below the band edges of the InGaAs injectors so that when it is suitably wide and doped, the first well level will be populated, providing all-important lateral conduction in the plane of the well and the ground-state population necessary for detector and optical modulator applications. Third, the very wide range of materials in these structures has allowed us to develop a selective etch which, in turn, makes electrical contact to the very thin quantum well layer possible.

We are presently developing a fabrication process for QT transistors. Particular attention is being given to the amount and placement of the dopants in the well. Our objective is to simultaneously maximize the lateral sheet conductance while not increasing the scattering experienced by the carriers resonantly tunneling vertically through the structure significantly. Intitial results indicate that moderate levels of carriers introduced using delta doping techniques will be optimal. Overall, the basic details of the fabrication process have been established, and the first devices will be available shortly.

9.13 Self-Consistent Modeling of Biased Quantum-Well-Base, Tunnel-Barrier Structures

Sponsor

Joint Services Electronics Program
Contract DAAL03-89-C-0001

Project Staff

Thomas P.E. Broekaert, Professor Clifton G. Fonstad, Jr.

A numerical model has been developed that solves the Schrodinger equation self-consistently with Poisson's equation for a resonant tunneling structure. The numerical model was implemented as a computer program. The program enables us to calculate the conduction band diagram and the emitter to collector current of a biased resonant tunneling structure with a heavily charged well, as a function of base-emitter and collector-emitter voltage. The goal of this program is to facilitate choice and optimization of device parameters for resonant tunneling structures that are grown by molecular beam epitaxy and processed into resonant tunneling transistors. The most critical parameters that need to be optimized are the well thickness and composition and the doping profile in the well, since they most directly affect the position of the resonant levels, and therefore, any transistor action in the structure.

9.14 Infrared Characterization of InGaAs/AlAs/InP Quantum Well Heterostructures

Sponsors

Harvard University. Division of Applied Physics
National Science Foundation
Grant ECS 90-08485

Project Staff

Lung-Han Peng, Thomas P.E. Broekaert, Professor Clifton G. Fonstad, Jr., in collaboration with R. Victor Jones and Victor Ehrenrich

As a first step to the realization of quantum-well-base, tunnel-barrier (QT) infrared detectors, we have been studying the infrared absorption spectra of InAs/AlAs/InGaAs quantum wells on InP. We have made the first measurements of intersubband absorption in populated pseudomorphic InAs/InGaAs/AlAs quantum wells on InP and demonstrated that very strong absorption can be obtained in this materials system from a single quantum well in a waveguide geometry. Furthermore, we have demonstrated both experimentally and theoretically that TE, as well as TM mode, intersubband absorption can be strong in this system. Finally, we have identified for the first time the "extrinsic" features in the absorption spectra and shown how they can be avoided. These results, applied in concert with recently developed selective etches that allow us to make electrical contact to the quantum well in these structures, open the way to realizing high performance QT optoelectronic devices.

Using a fast Fourier transform infrared spectrometer with a microscope attachment, we have measured the absorption spectra of a variety of samples with the light propagating parallel to the

heterostructure planes. This geometry has important advantages over the more common Brewster angle configuration including longer path length, good optical confinement, excellent polarization purity, and immunity from Fabry-Perot effects. In measurements in which light is guided in the substrate as well as the epilayers, we have measured over 8% intersubband absorption (n = 1 to n = 2) for a single populated quantum well, compared with less than 1% per well typically reported for GaAs. By extrapolation, structures designed to confine the light only to the epilayers are expected to show near total absorption. There is little polarization dependance of the transmission spectra, whereas conventional theory says that only TM polarization should be absorbed. It can be shown, however, that, in a narrow bandgap alloy system, band mixing effects and random potential fluctuation-induced tetragonal distortion (local field) effects relax the polarization selection rules.

Additional features noticed in the absorption spectra have been identified for the first time with multiphonon absorption in the InP substrate and absorption at the interface between the substrate and InGaAs buffer layers. These features can be eliminated by using InAlAs buffer layers and structures in which the light is confined to the epilayers away from the substrate.

Work has now begun on fabricating detector structures and preparations are being made to perform a variety of electrical characterization and optical response measurements on them.

9.15 Damage-Free In-Situ UHV Etching and Cleaning of III-V Heterostructures Using Molecular Beams

Sponsors

AT&T Bell Laboratories Fellowship
DARPA/NCIPT
Subcontract 542383
National Science Foundation
Grant ECS 90-07745

Project Staff

Isako Hoshino, Professor Clifton G. Fonstad, Jr., in collaboration with Professor Sylvia T. Ceyer and Professor Herbert H. Sawin[9]

The development of damage-free ultra-high vacuum (UHV) etching, cleaning, and regrowth techniques compatible with molecular beam epitaxy (MBE) and *ex situ* processing of III-V heterostructures is a major challenge facing device researchers. The ability to selectively pattern, etch, and overgrow quantum heterostructures is crucial to the effective realization of integrated optical circuitry and quantum effect electronic structures. Present techniques to do this involve relatively high energy ion beams (100 eV and above) which cause substantial subsurface damage, much of which is impossible to remove.

As a solution to the problem of process-induced damage, we have begun investigating the use of UHV kinetic molecular beam techniques (widely used to study atomic surface interactions) to etch and clean III-V substrates and heterostructures with a minimum of surface damage and maximum flexibility. Depending on the etchant gas mixture established, it is anticipated that low energy (0.5 to 2 eV) kinetic beams can be used to (1) anisotopically etch-pattern III-V heterostructure wafers with no damage; (2) clean surfaces allowing epitaxial growth on wafers which have been removed from the UHV environment for external processing; and (3) selectively remove masking materials and clean surfaces suitable for subsequent overgrowth.

This program builds on the work of Professor Sylvia T. Ceyer, an expert on using supersonic beams to probe surface reactions and to etch silicon, and that of Professor Herbert H. Sawin, an expert on the design of molecular beam and RF plasma sources and reactors, as well as plasma reaction dynamics. Funding has been obtained to assemble a UHV chamber for kinetic beam processing which will be connected through a transfer mechanism of special design to the present Riber 2300 solid source MBE system. Initial designs for the etcher using a methane-hydrogen gas mixture and a supersonic beam source are currently being investigated.

[9] MIT Department of Chemical Engineering.

9.16 Publications

Published Journal Articles

Bagwell, P.F., T.P.E. Broekaert, T.P. Orlando, and C.G. Fonstad. "Resonant Tunneling Diodes and Transistors with a One, Two, and Three Dimensional Electron Emitter." *J. Appl. Phys.* 68: 4634-4646 (1990).

Broekaert, T.P.E., and C.G. Fonstad. "InGaAs/AlAs Resonant Tunneling Diodes with Peak Current Densities in Excess of 450kA/cm^2." *J. Appl. Phys.* 68: 4310-4312 (1990.)

Burns, G.F., H. Blanck, and C.G. Fonstad. "Low-threshold GaAs/AlGaAs Graded-index Separate-confinement Heterostructure Lasers Grown by Molecular Beam Epitaxy on Oxide-masked Si Substrates." *Appl. Phys. Lett.* 56: 2499-2501 (1990).

Kuo, T.Y., J.E. Cunningham, K W. Goosen, W.Y. Jan, C.G. Fonstad, and F. Ren. "Monolayer Be S-doped Heterostructure Bipolar Transistor - Fabricated Using Doping Slecting Base Contact." *Electron. Lett.* 26: 1187-1188 (1990).

Kuo, T.Y., T.H. Chiu, J.E. Cunningham, K.W. Goosen, C.G. Fonstad, and F. Ren. "Heterostructure Bipolar Transistor Employing Carbon-Doped Base Grown with Trimethyl-Ga and Arsine." *Electron. Lett.* 26: 1260-1262 (1990).

Prasad, S., W. Lee, and C.G. Fonstad. "Reply to 'Comments on Unilateral Gain of Hetrojunction Bipolar Transistors at Microwave Frequences.'" *IEEE Trans. Electron. Dev.* 37: 826 (1990).

Sato, H., J.C. Vlcek, C.G. Fonstad, B. Meskoob, and S. Prasad. "InGaAs/InAlAs/InP Collector - Up Microwave Heterojunction Bipolar Transistors." *Electron Dev. Lett.* 11: 457-459 (1990).

Venkateswsan, V.D., L.J. Cui, M. Li, B.A. Weinstein, K. Elcess, C.G. Fonstad, and C. Mailhoit. "Strain Mapping in (111)- and (100)-InGaAs/GaAs Superlattices." *Appl. Phys. Lett.* 56: 286-288 (1990).

Venkateswasan, V.D., T. Burnett, L.J. Cui, M. Li, B.A. Weinstein, J.M. Kim, C.R. Wie, K. Elcess, C.G. Fonstad, and C. Mailhoit. "Comparison and Spatial Profiling of Strain in [001] and [111] InGaAs/GaAs Superlattices from Raman and X-ray Experiments." *Phys. Rev. B* 42: 3100-3108 (1990).

Journal Articles Accepted for Publication

Vlcek, J.C., and C.G. Fonstad. "Precise Computer Control of the MBE Process - Application of Graded InGaAlAs/InP Alloys." *J. Cryst. Growth.* Forthcoming.

Journal Articles Submitted for Publication

Broekaert, T.P.E., and C.G. Fonstad. "AlAs Etch-Stop Layers for InGaAlAs/InP Heterostructure Devices and Circuits." Submitted to *IEEE Trans. Electron. Dev.*

Peng, L.-H., T.P.E. Broekaert, W-Y. Choi, C.G. Fonstad, and V. Jones. "Defect Activated Infrared Multi-phonon Excitation in Fe-doped Semi-insulating InP." Submitted to *Appl. Phys. Lett.*

Meeting Papers Presented

Blanck, H. "Characterization of GaAs Grown Patterned Si-substrates for Photoelectronic Devices." Fifth New England MBE Workshop, Cambridge, Massachusetts, April 17, 1990.

Broekaert, T.P.E., and C.G. Fonstad. "AlAs Etch-Stop Layers for InGaAs/InP Heterostructure Devices and Circuits." *Technical Digest of the 1990 International Electron Devices Meeting.* Piscataway, New Jersey: IEEE, 1990, pp. 339-342.

Broekaert, T.P.E., P.F. Bagwell, T.P. Orlando, and C.G. Fonstad. "Resonant Tunneling Diodes and Transistors with One, Two, or Three Dimensional Emitter." American Physical Society, Anaheim, California, March 12-16, 1990. Abstract in *Bull. Am. Phys. Soc.* 35: 298 (1990).

Kuo, T.Y., K.W. Goossen, J.E. Cunningham, W.Y. Jan, C.G. Fonstad, and F. Ren. "Monolayer Be d-doped Heterostructure Bipolar Transistor Fabricated using Doping Selective Base Contact." Forty-eighth Annual Device Research Conference, Santa Barbara, California, June 25-27, 1990.

Kuo, T.Y., K.W. Goossen, J.E. Cunningham, C.G. Fonstad, F. Ren, and W. Jan. "Elimination of Emitter-Mesa Etching and Complete Planarization of Heterojunction Bipolar Transistors via Doping Selective Base Contact and Selective Hole Epitaxy." International Confer-

ence on Solid State Devices and Materials, Sendai, Japan, August 23-26, 1990.

Meskoob, B., J.C. Vlcek, H. Sato, S. Prasad, G. Fonstad, and M-K. Vai. "Characterization of InGaAs/InalAs/InP Emitter-Down Heterojunction Bipolar Transistors at Microwave Frequencies." EES of Users's Group Meeting, Dallas, Texas, May 8, 1990.

Ranganathan, R., J. Kaminsky, B.D. McCombe, K. Elcess, and C.G. Fonstad. "Free Electron Laser Studies of the Saturation of Cyclotron Resonance in a <111>-InGaAs/GaAs Strained Layer Superlattice." American Physical Society, Anaheim, California, March 12-16, 1990. Abstract in *Bull. Amer. Phys. Soc.* 35: 346 (1990).

Singer, R.A., and C.G. Fonstad "MBE Growth of InGaAs and InAlAs on (111) B InP." Sixth International Conference on Molecular Beam Epitaxy, San Diego, California, August 27-31, 1990.

Vleck, J.C., and C.G. Fonstad. "Molecular Beams Epitaxial Growth Techniques for Graded-Composition InGaAs/InP Alloys." Conference Proceedings of the Second International Conference on InP and Related Materials (Piscataway, New Jersey: IEEE, 1990), pp. 135-138.

Vlcek, J.C. "Control of Compositional Grading and Abruptness in InGaAlAs Heteroepitaxy." 5th New England MBE Workshop, Cambridge, Massachusetts, April 17, 1990.

Vlcek, J.C., and C.G. Fonstad. "Precise Control of Time-dependent MBE Flux Profiles — Application to InGaAlAs/InP Alloys." Electronic Materials Conference, Santa Barbara, California, June 27-29, 1990.

Vlcek, J.C., and C.G. Fonstad. "Precise Computer Control of the MBE Process — Application to Graded InGaAlAs/InP Alloys." Sixth International Conference on Molecular Beam Epitaxy, San Diego, California, August 27-31, 1990.

Thesis

McCann, P. *Heteroepitaxial Growth of IV-VI Semiconductors on Barium Flouride.* Ph.D. diss. Dept. of Mater. Sci. and Eng., MIT, 1990.

Section 2 Optics and Devices

Chapter 1. Optics and Quantum Electronics

Academic and Research Staff

Professor Hermann A. Haus, Professor Erich P. Ippen, Professor James G. Fujimoto, Professor Peter L. Hagelstein, Professor Peter A. Wolff,[1] Dr. Sunny Auyang, Dr. Santanu Basu, Dr. Jyhpyng Wang

Visiting Scientists and Research Affiliates

Dr. Lucio H. Acioli,[2] Dr. Giuseppe Gabetta[3]

Graduate Students

Keren Bergman, John Paul Braud, Stuart D. Brorson, Claudio Chamon, Jerry C. Chen, Tak K. Cheng, Isaac L. Chuang, David J. Dougherty, James G. Goodberlet, Katherine L. Hall, Michael Hee, David Huang, Charles T. Hultgren, Janice M. Huxley, Joseph M. Jacobson, Sumanth Kaushik, Farzana I. Khatri, Yinchieh Lai, Gadi Lenz, Ling-Yi Liu, John D. Moores, Ann W. Morganthaler, Martin H. Muendel, Kathryn M. Nelson, Janet L. Pan, Lily Y. Pang, Chi-Kuang Sun, Kohichi R. Tamura, Morrison Ulman, David B. Walrod

Undergraduate Students

Michele M. Bierbaum, Patrick Chou, Michael Connell, Boris Golubovic, Peter A. Kner, Gary J. Tarnowski

Technical and Support Staff

Mary C. Aldridge, Donna L. Gale, Cynthia Y. Kopf, Lisbeth N. Lauritzen

1.1 Ultrafast Optics

1.1.1 Picosecond Optical Switching

Sponsors

Joint Services Electronics Program
Contract DAAL03-89-C-0001
National Science Foundation
Grant EET 87-00474
U.S. Air Force - Office of Scientific Research
Contract F49620-88-C-0089

Project Staff

Professor Hermann A. Haus, Professor Erich P. Ippen, Keren Bergman, Farzana I. Khatri, John D. Moores

Our research group has been studying all-optical switching with subpicosecond pulses for several years.[4] We have focused on interferometric switching using the index nonlinearity of optical materials. Lately, we have concentrated on the construction of switches using fiber interferometers because of the close to ideal behavior of optical fibers.[5] Our work is aimed at establishing a "proof of principle," exploring the requirements that must be met by the physical system in order to achieve satisfactory performance. Eventually, when quantum wells or other "engineered" materials of sufficient nonlinearity and with acceptable low linear and two-photon absorption become avail-

---

[1] NEC Research Institute, Princeton, New Jersey.

[2] Dept. de Fisica, Universidade Fed. de Pernambuco, Recife, PE Brazil.

[3] Dip. Electronica, Universita Di Pavia, Pavia, Italy.

[4] A. Lattes, H.A. Haus, F.J. Leonberger, and E.P. Ippen, *IEEE J. Quant. Electron.* QE-19: 1718-1723 (1983); M.J. LaGasse, D. Liu-Wong, J.G. Fujimoto, and H.A. Haus, "Ultrafast Switching with a Single-fiber Interferometer," *Opt. Lett.* 14: 311-313 (1989).

[5] M.J. LaGasse, D. Liu-Wong, J.G. Fujimoto, and H.A. Haus, "Ultrafast Switching with a Single-fiber Interferometer," *Opt. Lett.* 14: 311-313 (1989).

able, the principles demonstrated with the fiber system can be implemented in more practical systems with less "latency."

The fundamental requirement of a practical switch is that the output must be a reasonable replica of the input. By its nature, nonlinear interaction using the Kerr effect (third order nonlinearity), tends to distort the spectrum and pulse shape, the latter due to group velocity dispersion. A working switch must overcome this tendency of pulse distortion. One way to accomplish this is to use soliton-like interactions.[6] If this operating principle is chosen, the interaction region must possess negative dispersion, if the Kerr nonlinearity is positive, and vice versa. The "collisions" of the control pulses and controlled pulses must be soliton collisions or soliton-like so the pulses are not distorted if the system is not strictly a soliton system. Strict soliton collisions require the use of different frequencies for the colliding pulses, but this is sometimes an unacceptable constraint. If the colliding pulses have the same frequency, they must be distinguishable, e.g., by polarization. In general, two orthogonally polarized pulses do not interact in a distortion-free way, but distortion can be minimized if the collision is "weak." In order to achieve large effects, the collisions must be repeated several times.

This operation principle has been chosen for a switch developed in our laboratory that uses a fiber ring reflector interferometer.[7] The collisions of orthogonally polarized pulses, traveling at different velocities due to fiber birefringence, were repeated by splitting the fiber into 11 segments. In each of the segments, one collision occurred, and the effects of the collisions were cumulative. The interaction was distortion-free as anticipated. The operating principle required use of a polarization sensitive coupler. Because the coupler was not performing to specifications, the contrast ratio was not large. Yet the performance was in good agreement with theoretical predictions. The controlling pulses are eliminated by a polarizer. Figure 1 shows the intensity autocorrelation functions of the controlled pulse in the presence (the upper trace) and in the absence (the lower trace) of the controlling pulse. There is no observable distortion of the pulse.

1.1.2 Squeezing in Optical Fibers

Sponsors

Charles S. Draper Laboratory
Contract DL-H-404179
Joint Services Electronics Program
Contract DAAL03-89-C-0001
National Center for Integrated Photonics
National Science Foundation
Grant EET 87-00474

Project Staff

Professor Hermann A. Haus, Professor Erich P. Ippen, Keren Bergman

Squeezing of optical radiation has been pursued by many other laboratories,[8] including Professor Shapiro's group in RLE. Our group started work in this area when a proposal was made to squeeze optical pulses in a fiber ring interferometer,[9] a modification of the all-optical switch which is described in other sections of this report. The use of pulses leads to enhanced nonlinearities. A particularly attractive feature of the proposed scheme is that the pump power used in the squeezing is not wasted, because it is reused as the local oscillator power (at least in principle, if nonreciprocal couplers are used, otherwise a 6 dB loss is incurred).

---

[6] N.J. Doran, K.J. Blow, and D. Wood, *Proc. SPIE* 836: 238-243 (1987); M.N. Islam, E.R. Sunderman, R.H. Stolen, W. Pleibel, and J.R. Simpson, "Soliton Switching in a f1 Nonlinear Loop Mirror," *Opt. Lett.* 14: 811-813 (1989).

[7] J.D. Moores, K. Bergman, H.A. Haus, and E.P. Ippen, "Optical Switching Using Fiber Ring Reflectors," *J. Opt. Soc. Am. B,* forthcoming; J.D. Moores, K. Bergman, H.A. Haus, and E.P. Ippen, "Demonstration of Optical Switching Via Solitary Wave Collisions in a Fiber Ring Reflector," *Opt. Lett.,* forthcoming.

[8] M. Xiao, L. Wu, and H.J. Kimble, "Precision Measurement Beyond the Shot-Noise Limit," *Phys. Rev. Lett.* 53: 278-281 (1987); R.E. Slusher, L.W. Hollberg, B. Yurke, J.C. Mertz, and J.F. Valley, "Observation of Squeezed States Generated by Four-wave Mixing in an Optical Cavity," *Phys. Rev. Lett.* 55: 2409-2412 (1985); R.M. Shelby, M.D. Levenson, S.H. Perlmutter, R.G. DeVoe, and D.F. Walls, "Broad-band Parametric Deamplification of Quantum Noise in an Optical Fiber," *Phys. Rev. Lett.* 57: 691-694 (1986); S. Machida, Y. Yamamoto, and Y. Itaya, "Observation of Amplitude Squeezing in a Constant-current-driven Semiconductor Laser," *Phys. Rev. Lett.* 58: 1000-1004 (1987).

[9] M. Shirasaki, H.A. Haus, and D.L. Wong, "Quantum Theory of the Nonlinear Interferometer," *J. Opt. Soc. Am. B* 6: 82-88 (1989); M. Shirasaki and H.A. Haus, "Squeezing of Pulses in a Nonlinear Interferometer," *J. Opt. Soc. Am. B* 7: 30-34 (1990).

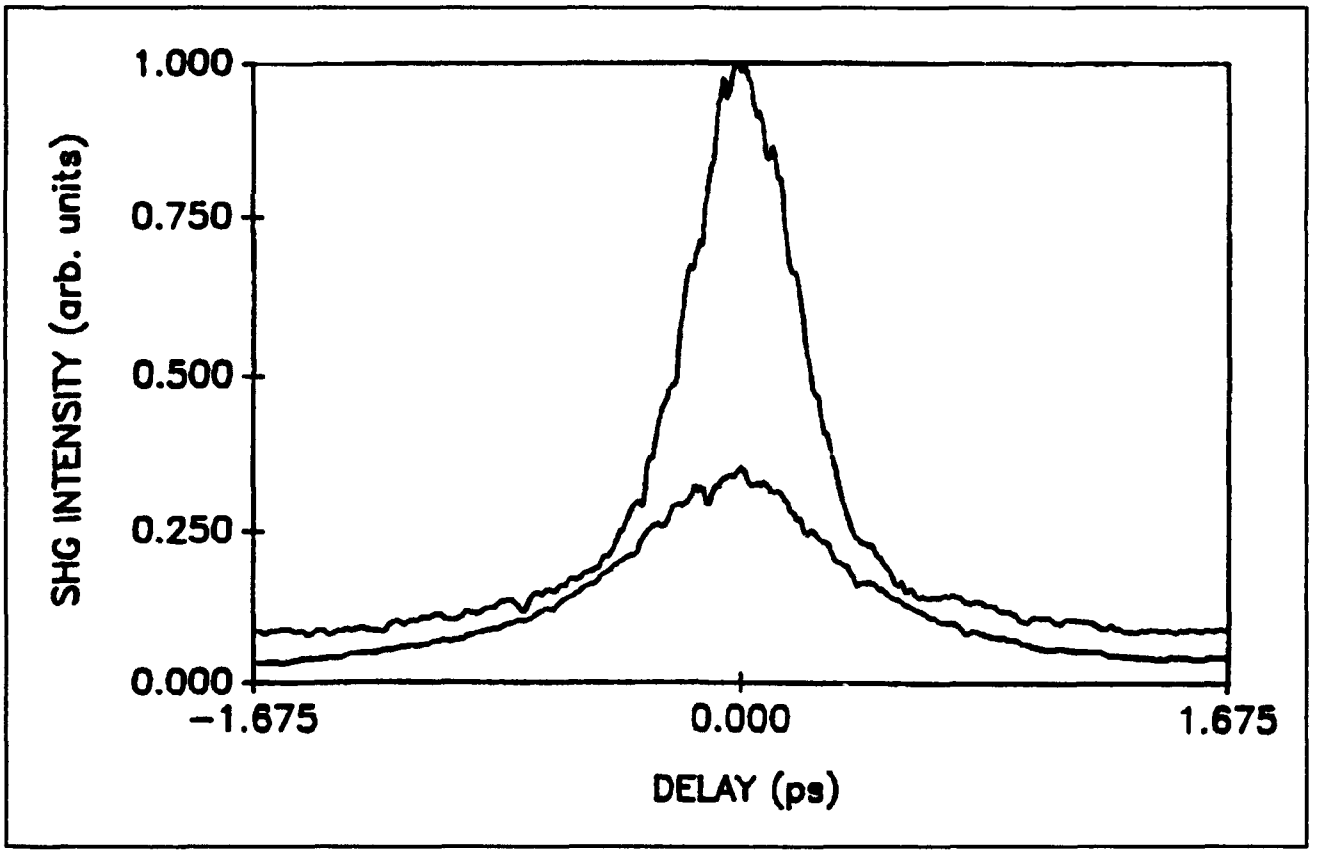

Figure 1.

Experiments using a fiber ring reflector pulse excited by a mode locked Nd:YAG laser operating at 1.3 μ have been gratifyingly successful.[10] Noise reduction greater than 5 dB below the shot noise level in the frequency regime between 40-60 kHz was observed. Figure 2 shows a histogram of noise measurements by the balanced detector. The power of the pump was set at one level and the noise was measured within 2 millisecond intervals. The phase between the squeezed radiation and the local oscillator (the recovered pump pulse) was allowed to drift randomly so that the noise level varied between its minimum and maximum value. The black columns give the shot noise calibration obtained by blocking the squeezed radiation from entering the balanced detector. The reduction below shot noise on the order of 5 db, as well as the enhancement by more than 5 db. The asymmetry is due to the unavoidable variation of squeezing phase across the pump pulse profile.

There are several reasons for the early success of the experiment. First, the threshold of Stimulated Brillouin Scattering is raised significantly by the use of pulses instead of cw excitation so that this source of classical noise is not operative. Similarly, the observation in the low frequency range of 40-60 kHz avoids the effect of Guided Acoustic Brillouin Scattering (GAWBS), which has a higher cutoff frequency. Also, the ring reflector geometry partially suppresses GAWBS at frequencies lower than the transit time of the pulse through the fiber ring. Finally, the modelocked Nd:YAG showed a noise level in the frequency range of the measurement that was only about 25 dB above the shot noise level. The balanced detector could suppress this relatively low "local oscillator" noise.

1.1.3 Quantum Theory of Solitons

Sponsors

Charles S. Draper Laboratory
Contract DL-H-404179
Joint Services Electronics Program
Contract DAAL03-89-C-0001
National Center for Integrated Photonics

[10] K. Bergman and H.A. Haus, "Squeezed Pulse Vacuum from Fiber-ring Interferometer," paper presented at OPTCON90, Boston, Massachusetts, November 4-9, 1990, paper FBB4.

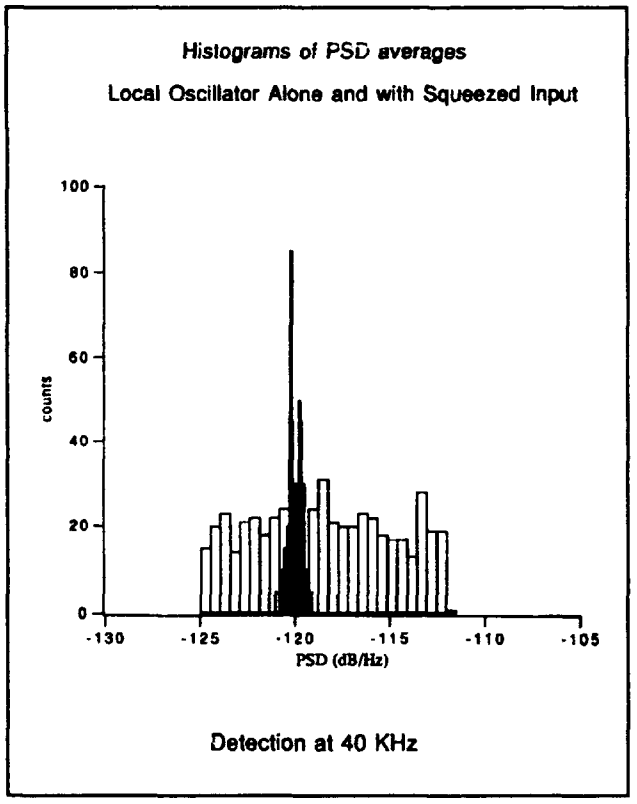

Figure 2.

National Science Foundation
Grant EET 87-00474

Project Staff

Professor Hermann A. Haus, Yinchieh Lai

An understanding of the noise associated with soliton detection necessitates a quantum analysis of solitons, since the shot noise and the reduction below the shot noise level (squeezing), are quantum phenomena. We have pursued this kind of analysis of solitons of the Nonlinear Schrodinger Equation (NLSE), both exactly[11] and approximately.[12] The approximate analysis is based on the linearization of the NLSE and is amenable to simple interpretation. A soliton is found to have both particle and wave properties simultaneously. It is described by noncommuting momentum and position operators, on one hand, and inphase and quadrature operators (or phase and photon number operators) on the other hand. Any one of these operators can be measured with a local oscillator pulse of properly prepared temporal amplitude- and phase-profile. An extended description and analysis will appear in a chapter of the Springer-Verlag series.

1.1.4 Additive Pulse Modelocking

Sponsors

Joint Services Electronics Program
Contract DAAL03-89-C-0001
National Science Foundation
Grant EET 87-00474
U.S. Air Force - Office of Scientific Research
Contract F49620-88-C-0089

Project Staff

Professor Hermann A. Haus, Professor Erich P. Ippen, Professor James G. Fujimoto, Dr. Giuseppe Gabetta, James G. Goodberlet, Katherine L. Hall, Janice M. Huxley, Joseph M. Jacobson, Yinchieh Lai, Kohichi R. Tamura

Additive Pulse Modelocking (APM) is a novel scheme for the production of short pulses, particularly from solid state lasers with long gain-relaxation times.[13] These laser systems cannot be modelocked in a way analogous to the dye laser systems, in which the saturable gain and the saturable loss cooperate in the pulse shaping process.

Thus far, most APM systems employ a coupled cavity system, one cavity containing the laser medium, the auxiliary cavity containing a Kerr medium, generally a fiber. The length of the auxiliary cavity needs to be stabilized by a feedback circuit to maintain the relative phase of the pulses meeting at the coupling mirror between the two cavities.

---

[11] Y. Lai and H.A. Haus, "Quantum Theory of Solitons in Optical Fibers. I. Time-dependent Hartree Approximation," *Phys. Rev. A* 40: 844-853 (1989); Y. Lai and H.A. Haus, "Quantum Theory of Solitons in Optical Fibers. II. Exact Solution," *Phys. Rev. A* 40: 854-866 (1989).

[12] H.A. Haus and Y. Lai, "Quantum Theory of Soliton Squeezing: A Linearized Approach," *J. Opt. Soc. Am. B* 7: 386-388 (1990).

[13] E.P. Ippen, H.A. Haus, and L.Y. Liu, "Additive Pulse Mode Locking," *J. Opt. Soc. Am. B* 9: 1736-1745 (1989).

We have developed the criteria for self-starting of the APM modelocking process.[14] When the process is self-starting, the need for an internal modulator is obviated, not only simplifying the system, but also eliminating the competition between the modulator frequency and the pulse repetition frequency. It is this competition that can render the mode locking process unstable.

We have APM modelocked a flashlamp pumped Nd:YAG laser achieving 6 ps pulses without sacrifice of average power.[15] A diode laser pumped Nd:YAG crystal gave 2 ps modelocked pulses.[16] We have achieved APM action in a Ti:Sapphire laser in a single cavity, analogous to the system demonstrated first by Sibbett et al. Generally, it is necessary to start this system with a moving mirror in an external cavity.

These experimental results have stimulated theoretical work The APM principle applies to any interferometric transformation of nonlinear phase modulation to nonlinear amplitude modulation. The single cavity Ti:Sapphire system operates in this way, the role of the two arms of an interferometer being played by two transverse cavity modes. A theory that considers many possible configurations that produc APM action is currently under investigation.[17]

Modelocking of a Ti:Sapphire system with a saturable absorber in the auxiliary cavity was found to be insensitive to the length of the auxiliary cavity and, therefore, did not require stabilization.[18] The scientists who discovered the phenomenon called it Resonant Pulse Modelocking (RPM).[19] The phenomenon was later explained as a form of self-stabilized Additive Pulse Modelocking. The relative phase at the coupling mirror was shown to be maintained by automatic adjustment of the carrier frequency. This theoretical explanation was confirmed experimentally. While this self-stabilization was shown to work only for absorptive nonlinearities in the auxiliary cavity, the principle is an intriguing one and deserves further investigation to determine whether it could be applied to Kerr nonlinearities as well.

1.1.5 Control of Spontaneous Emission with Semiconductor Microcavities

Sponsors

Joint Services Electronics Program
Contract DAAL03-89-C-0001
U.S. Air Force - Office of Scientific Research
Contract F49620-88-C-0089

Project Staff

Professor Erich P. Ippen, Stuart D. Brorson

Optical microcavities hold technological promise for constructing efficient, high speed semiconductor lasers. One particularly interesting possiblity is the alteration of the spontaneous emission rate of the device by the presence of a cavity. This kind of alteration has previously been observed with atoms by Professor Kleppner's group in RLE, but is more difficult to achieve in a semiconductor device because the broad spontaneous emission bandwidth requires cavity dimensions on the order of a wavelength. To determine the potential feasibility and significance of spontaneous emission alteration in these devices, we have analyzed the radiation modes of oscillating dipoles in planar (one-dimensional confinement and optical-wire (two-dimensional confinement) structures.[20] We found that an idealized planar

---

[14] E.P. Ippen, L.Y. Liu, and H.A. Haus, "Self-starting Condition for Additive-pulse Mode-locked Lasers," *Opt. Lett.* 15: 183-185 (1990).

[15] L.Y. Liu, J.M. Huxley, E.P. Ippen, and H.A. Haus, "Self-starting Additive-pulse Mode Locking of a Nd:YAG Laser," *Opt. Lett.* 15: 553-555 (1990).

[16] J. Goodberlet, J. Jacobson, J.G. Fujimoto, P.A. Schulz, and T.Y. Fan, "Self-starting Additive-pulse Mode-locked Diode-pumped Nd:YAG Laser," *Opt. Lett.* 15: 504-506 (1990).

[17] H.A. Haus, J.G. Fujimoto, and E.P. Ippen, "Structures for Additive Pulse Modelocking," to be submitted.

[18] U. Keller, W. H. Knox, and H. Roskos, "Coupled-cavity Resonant Passive Mode-locked Ti:sapphire Laser," *Opt. Lett.* 15: 1377-1379 (1990).

[19] H.A. Haus, U. Keller, and W. H. Knox, "A Theory of Coupled Cavity Modelocking with a Resonant Nonlinearity," submitted to *J. Opt. Soc. Am. B.*

[20] S.D. Brorson, H.Yokoyama, and E.P. Ippen, "Spontaneous Emission Rate Alteration in Optical Waveguide Structures," *IEEE J. Quant. Electron.* QE-21: 1492 (1990).

metallic mirror cavity can suppress the spontaneous emission by no more than a factor of two with respect to free space. The amount of suppression obtainable with a real dielectric stack will be even less. Theory predicts that much larger effects could be achieved by restricting the dimensionality to that of the optical wire. It has been shown that enhancement of spontaneous emission is more easily observable.[21] With GaAs quantum-wells, monolithically integrated with Fabry-Perot cavities fabricated at NEC, we have observed enhancement of emission by a factor of two and a corresponding reduction in the luminescence lifetime due to cavity effect. Future work on this topic will rely on advances in the fabrication of suitable wire or dot devices or improved resonator structures.

1.1.6 Femtosecond Studies of Superconductors

Sponsors

Joint Services Electronics Program
Contract DAAL03-89-C-0001
U.S. Air Force - Office of Scientific Research
Contract F49620-88-C-0089

Project Staff

Professor Erich P. Ippen, Tak K. Cheng, Stuart D. Brorson

When an ultrashort optical pulse is incident on the surface of a metal, most of its energy is absorbed directly, because of the high electron density, into the free electron gas. The resulting rise in electron temperature produces a dynamic change in reflectivity. Relaxation of this change occurs as the electrons lose energy to the lattice via phonon emission. The rate is governed by the electron-phonon coupling strength. Since the strength of the electron-phonon coupling is an important component in the BCS theory of superconductivity, we were motivated to undertake a systematic study of these dynamics in superconductors. This was done in collaboration with Professor M. Dresselhaus' group. In a series of experiments,[22] we measured λ the relaxation rate, for ten different metals (four superconducting and six not). The agreement between the values obtained and those derived from the literature is strikingly good. The advantages of our method for measuring λ compared with other techniques (e.g., tunneling or heat capacity measurements) are that: (1) it is a direct measurement, (2) it works at room temperature, and (3) it can be applied to nonsuperconducting as well as superconducting samples. In some metals for which the changes in reflectivity were otherwise too small to detect, we have also found that thin overlayers of Cu (which has d-band transitions in the visible) can be used to greatly enhance the experimental reflectivity changes without affecting the inherent relaxation rate. This extends the method to virtually any metal film.

Encouraged by the success of these results, we also performed several preliminary pump-probe reflection and transmission experiments on three high T_c thin films: $YBa_2Cu_3O_{7-x}$, $Bi_2Sr_2CaCu_2O_{8+x}$ and $Bi_2Sr_2Ca_2Cu_3O_{10+y}$.[23] Of course, we do not have a theoretical framework with which to connect our experiments to high T_c superconductivity for these materials yet. Nevertheless, in these preliminary experiments, we have observed strong changes in observed relaxation rates with changing T_c.

1.1.7 Nonlinear Dynamics in Active Semiconductor Devices

Sponsors

Joint Services Electronics Program
Contract DAAL03-89-C-0001
National Center for Integrated Photonics
National Science Foundation
Grant EET 87-00474

---

[21] H. Yokoyama, K. Nishi, T. Anan, H. Yamada, S.D. Brorson, and E.P. Ippen, TITLE? *Appl. Phys. Lett.* 57: 24 (1990).

[22] S.D. Brorson, A. Kazeroonian, J.S. Moodera, D.W. Face, T.K. Cheng, E.P. Ippen, M.S. Dresselhaus, and G. Dresselhaus, "Femtosecond Room-Temperature Measurement of the Electron-Phonon Coupling Constant λ in Metallic Superconductors," *Phys. Rev. Lett.* 64: 2172 (1990).

[23] S.D. Brorson, A. Kazeroonian, D.W. Face, T.K. Cheng, G. L. Doll, M.S. Dresselhaus, G. Dresselhaus, E.P. Ippen, T. Venkatesan, X.D. Wu, and A. Inam, "Femtosecond Thermomodulation Study of High-Tc Superconductors," *Sol. State Commun.* 74: 1305 (1990).

U.S. Air Force - Office of Scientific Research
Contract F49620-88-C-0089

Project Staff

Professor Erich P. Ippen, Katherine L. Hall, Charles T. Hultgren, Yinchieh Lai

Nonlinear optical effects in active waveguides not only influence the generation and propagation of ultrashort pulses in diode lasers, but they can also be applied in all-optical switching. In our laboratory, with 100 fs-duration pulses in the 800-900 nm regime (obtained by fiber compression of synch-pumped dye laser pulses) and with similar pulses in the 1.45-1.65 μm band (from an APM F-center laser), we have performed the first investigations of nonlinear dynamic behavior in both GaAlAs[24] and InGaAsP [25] devices under various excitation conditions. By varying the wavelength of the pump and probe beams, as well as injection current in our diode structures, we have studied interactions in the presence of gain, loss, or nonlinear transparency. In all cases, there is an injected carrier density on the order of $10^{18}/cm^3$, and this makes the nonlinear optical behavior considerably different from what is observed in passive devices or pure materials.

In both GaAlAs and InGaAsP devices, we have discovered a strong nonlinearity due to nonequilibrium between the carrier and lattice temperatures. Heating of the carrier gas with respect to the lattice has a recovery time on the order of 1 ps in GaAlAs and 650 fs in InGaAsP; and, since heating occurs via free electron absorption and no change in carrier number is involved, recovery is complete. This is a particularly important characteristic for all-optical switching applications. Our most recent experiments have yielded preliminary measurements of femtosecond index of refraction dynamics as well as gain changes in GaAlAs. Index changes corresponding to optical Kerr effect and nonequilibrium heating have been observed and are comparable in magnitude to those produced by population changes. During the past year, we have also used a novel means for detecting these nonlinear optical interactions by monitoring changes in diode voltage.[26] By measuring bias voltage as a function of time delay between two optical pulses passing through the diode, we can clearly identify nonlinear optical interactions that utilize active carriers. The time constants observed corroborate those obtained from pump-probe measurements of nonlinear gain.

1.1.8 Impulsive Excitation of Coherent Phonons

Sponsors

Joint Services Electronics Program
Contract DAAL03-89-C-0001
U.S. Air Force - Office of Scientific Research
Contract F49620-88-C-0089

Project Staff

Professor Erich P. Ippen, Tak K. Cheng, Stuart D. Brorson

We have recently reported the first observations of coherent optical phonon excitation in two opaque conducting materials, bismuth and antimony.[27] Previous experiments involving excitation of coherent phonons in transparent materials have relied upon stimulated Raman scattering as the excitation mechanism and have utilized changes in transmission for detection. In our work, we simply observe changes in sample reflectivity following absorption of a femtosecond pulse incident upon the surface. The reflectivity is observed to oscillate at the frequency corresponding to the A_{1g} mode in each case (2.9 THz in Bi and 4.5 THz in Sb), indicating that the modulation varies linearly with phonon amplitude. Both the large amplitudes of the reflectivity changes (greater than 10^{-3}) and the absence of other allowed Raman modes argue that a mechanism other than stimulated Raman scattering is the driving force. The initial phase of the oscillations (cosinusoidal rather than sinusoidal) also imply that an electronic transition is involved. Experiments are in progress to clarify the actual

---

[24] M.P. Kesler and E.P. Ippen, "Subpicosecond Spectral Gain Dynamics in AlGaAs Laser Diodes," *Electron. Lett.* 24: 1102-1104 (1988).

[25] K.L. Hall, J. Mark, E.P. Ippen, and G. Eisenstein, "Femtosecond Gain Dynamics in GaAsP Optical Amplifiers," *Appl. Phys. Lett.* 56: 1740-1742 (1990).

[26] K.L. Hall, E.P. Ippen, and G. Eisenstein, "Bias-lead Monitoring of Ultrafast Nonlinearities in InGaAsP Diode Laser Amplifiers," *Appl. Phys. Lett.* 57: 129-131 (1990).

[27] T.K. Cheng, S.D. Brorson, A.S. Kazeroonian, J.S. Moodera, G. Dresselhaus, M.S. Dresselhaus, and E.P. Ippen, "Impulsive Excitation of Coherent Phonons Observed in Reflection in Bismuth and Antimony," *Appl. Phys. Lett.* 57: 1004-1006 (1990).

mechanism and to use this technique to study electron-phonon interactions. The method opens up the possibility for detailed time-domain studies of phonon dynamics on a whole class of opaque materials.

1.1.9 Observation of Third Order Optical Nonlinearity Due to Intersubband Transitions in AlGaAs/GaAs Superlattices

Sponsors

National Science Foundation
Grant ECS 87-18417
NEC Research Institute

Project Staff

Professor Erich P. Ippen, Professor Peter A. Wolff, Dr. Sunny Auyang, David B. Walrod

Semiconductor growth techniques allow the production of superlattices designed so that the energy subband separations can be matched to a particular laser frequency. As the optical field frequency approaches the intersubband separation, the contribution to the dielectric function from the intersubband transitions grows rapidly. At resonance, the dielectric function can be modulated by as much as 10%. This large effect is primarily due to several factors:

- The very large dipole matrix element ($\approx$ 20Å) for this transition[28] means that each oscillator will provide a substantial contribution to the change in the dielectric.
- The high doping densities possible in semiconductors allow a great number of oscillators per well ($\approx 10^{18}$ cm^{-3}).
- The narrow bandwidths possible in semiconductor superlattices permit a sharp resonance.

This potential for substantial modulations of the dielectric function has led to predictions of large optical nonlinearities when the subband separation matches the frequency of the incident laser radiation.[29] Furthermore, the nonlinearity is expected to have picosecond response times. We observed the modulation of the dielectric by measuring the nondegenerate four-wave signal. The nonlinearity is further enhanced because this process will be triply resonant for small laser difference frequencies. Since this nonlinearity results from the two-dimensional character of the electrons, it is not specific to AlGaAs/GaAs superlattices. Other materials could be used to apply this process to other wavelengths (strained layer) or to match the fundamental bandgap with the subband gap in order to enhance the nonlinearity (HgCdTe/CdTe).

Several AlGaAs/GaAs superlattices were grown to match the subband separation with that produced by a pair of CO_2 lasers. The doping level was chosen to place the Fermi level between the first and second subbands. The absolute value of $\chi^{(3)}$ for these samples was measured at $\Delta\omega$ 3.45 cm^{-1} to be 5x10^{-5} esu. By measuring $\chi^{(3)}$ at a series of difference frequencies, we estimated the intersubband relaxation time to be 3 ps. No saturation was observed for input intensities of up to 200 kW/cm^2.

The optical nonlinear susceptibility of the subband system can be readily calculated if we treat it as a two level system. Using the diagrammatic technique, we can show that

$$\chi^{(3)} = \frac{N e^4 \langle z \rangle^4}{4\hbar^3} \times \left[\frac{1}{(- \omega_2 - \Omega_{gn})} + \frac{1}{(\omega_1 - \Omega_{ng})} \right] \times \frac{1}{(\omega_1 - \omega_2 - \Omega_{nn})} \frac{1}{(2\omega_1 - \omega_2 - \Omega_{ng})} \rho_{gg}^{(0)} \quad (1)$$

where $\langle z \rangle$ is the dipole matrix element, N is the number of electrons and $\Omega_{ng} \equiv \omega_{ng} - i\,\Gamma_{ng}$ and $\Omega_{nn} \equiv i\,\Gamma_{nn}$. Γ_{ng} is the intrasubband rate. This broadening has two different components: impurity scattering and nonparabolicity. We have conducted Hall measurements and found an impurity scattering time of 10^{13} s, which corresponds to a homogeneous broadening of approximately 10 meV. The nonparabolicity is responsible for an inhomogeneous broadening of about 6 meV. Γ_{nn} is the intersubband scattering rate which is essentially the LO-phonon scattering rate. Theoretical

[28] L.C. West and S.J. Eglash, "First Observation of an Extremely Large Dipole Infrared Transition within the Conduction Band of a GaAs Quantum Well," *Appl. Phys. Lett.* 46: 1156 (1985).

[29] S.Y. Yuen, "Fast Relaxing Absorptive Nonlinear Refraction in Superlattices," *App. Phys. Lett.* 43: 813 (1983).

predictions of 1 ps[30] for this time are close to our measured value.

Eq. (1) can be used to generate lineshapes for our samples as well as to predict absolute values for $\chi^{(3)}$. In both cases, we have obtained close agreement between theory and experiment for the values for magnitude and linewidth.[31] Since this process entails a real change in the electron population, the absorption can be very high (4000 cm^{-1}). However, the absorption can be dramatically reduced by detuning the lasers. The lineshapes show that for finite $\Delta\omega$ the maximum absolute value for $\chi^{(3)}$ is not coincident with the absorption peak. By detuning the laser frequency and operating at $\Delta\omega = 3.45\ cm^{-1}$, we can decrease the absorption while keeping the figure of merit ($\chi^{(3)}/\alpha\tau$) constant.

1.1.10 JSEP Publications

Anderson, K.K., M.J. LaGasse, H.A. Haus, and J.G. Fujimoto. "Femtosecond Studies of Nonlinear Optical Switching in GaAs Waveguides Using Time Domain Interferometry." *SPIE 1216: Nonlinear Optical Materials and Devices for Photonic Switching* (1990).

Anderson, K.K., M.J. LaGasse, C.A. Wang, J.G. Fujimoto, and H.A. Haus. "Femtosecond Dynamics of the Nonlinear Index Near the Band Edge in AlGaAs Waveguides." *Appl. Phys. Lett.* 56: 1834-1836 (1990).

Anderson, K.K., M.J. LaGasse, H.A. Haus, and J.G. Fujimoto. "Femtosecond Time Domain Techniques for Characterization of Linear and Nonlinear Optical Properties in GaAs Waveguides." *Mat. Res. Soc. Symp. Proc.* 167 (1990).

Bergman, K., and H.A. Haus. "Squeezing in Fibers with Optical Pulses." Submitted to *Opt. Lett.*

Brorson, S.B., A. Kazeroonian, J.S. Moodera, D.W. Face, T.K. Cheng, E.P. Ippen, M.S. Dresselhaus, and G. Dresselhaus "Femtosecond Room-Temperature Measurement of Electron-Phonon Coupling Constant λ in Metallic Superconductors." *Phys. Rev. Lett.* 64: 2172-2175 (1990).

Brorson, S.D., H. Yokoyama, and E.P. Ippen. "Spontaneous Emission Rate Alteration in Optical Waveguide Structures." *IEEE J. Quant. Electron.* QE-26: 1492 (1990).

Brorson, S.D., A. Kazeroonian, D.W. Face, T.K. Cheng, G.L. Doll, M.S. Dresselhaus, G. Dresselhaus, E.P. Ippen, T. Venkatesan, X.D. Wu, and A. Inam. "Femtosecond Thermomodulation Study of High $-T_c$ Superconductors." *Sol. State. Commun.* 74: 1305-1308 (1990).

Cheng, T.K., S.D. Brorson, A.S. Kazeroonian, J.S. Moodera, G. Dresselhaus, M.S. Dresselhaus, and E.P. Ippen. "Impulsive Excitation of Coherent Phonons Observed in Reflection in Bismuth and Antimony." *Appl. Phys. Lett.* 57: 1004-1006 (1990).

Face, D.W., S.D. Brorson, A. Kazeroonian, J.S. Moodera, T.K. Cheng, G.L. Doll, M.S. Dresselhaus, G. Dresselhaus, E.P. Ippen, T. Venkatesan, X.D. Wu, and A. Inam. "Femtosecond Thermomodulation Studies of Low and High $-T_c$ Superconductors." Paper presented at the *Applied Superconductivity Conference,* Snowmass, Colorado, September 1990.

Hall, K.L., J. Mark, E.P. Ippen, and G. Eisenstein. "Femtosecond Gain Dynamics in InGaAsP Optical Amplifiers." *Appl. Phys. Lett.* 56: 1740-1742 (1990).

Hall, K.L., E.P. Ippen, and G. Eisenstein. "Bias-lead Monitoring of Ultrafast Nonlinearities in InGaAsP Diode Laser Amplifiers." *Appl. Phys. Lett.* 57: 129-131 (1990).

Haus, H.A. "Quantum Noise in Soliton-like Repeater System." *J. Opt. Soc. Am. B* 8 (1991).

Haus, H.A., and W.P. Huang. "Coupled Mode Theory." Invited paper. *IEEE Proc.* Forthcoming.

Haus, H.A., U. Keller, and W.H. Knox. "A Theory of Coupled Cavity Modelocking with a Resonant Nonlinearity." Submitted to *J. Opt. Soc. Am. B.*

Haus, H.A., J.G. Fujimoto, and E.P. Ippen. "Structures for Additive Pulse Modelocking." To be submitted.

---

[30] B.K. Ridley, "Electron Scattering by Confined LO Polar Phonons in a Quantum Well," *Phys. Rev. B* 39: 5282 (1989).

[31] D. Walrod, S.Y. Auyang, P.A. Wolff, M. Sugimoto, "Observation of Third Order Nonlinearity Due to Intrasubband Transitions in AlGaAs/GaAs Superlattices," to be published.

Huxley, J.M., P. Mataloni, R.W. Schoenlein, J.G. Fujimoto, E.P. Ippen, and G.M. Carter. "Femtosecond Excited-state Dynamics of Polydiacetylene." *Appl. Phys. Lett.* 56: 1600-1602 (1990).

Ippen, E.P., L.Y. Liu, and H.A. Haus. "Self-starting Condition for Additive-Pulse Mode-Locked Lasers." *Opt. Lett.* 15: 183-185 (1990).

Kazeroonian, A.S., T.L. Cheng, S.D. Brorson, Q. Li, E.P. Ippen, X.D. Wu, T. Venkatesan, S. Etemad, M.S. Dresselhaus, and G. Dresselhaus. "Probing the Fermi Level of $Y_{1-x}Pr_xBa_2Cu_3O_{(7-\delta)}$ by Femtosecond Spectroscopy." *Sol. State Commun.* Forthcoming.

LaGasse, M.J., K.K. Anderson, C.A. Wang, H.A. Haus, and J.G. Fujimoto. "Femtosecond Measurements of the Nonresonant Nonlinear Index in AlGaAs." *Appl. Phys. Lett.* 56: 417-419 (1990).

Liu, L.Y., J.M. Huxley, E.P. Ippen, and H.A. Haus. "Self-starting Additive-pulse Mode Locking of a Nd: Laser." *Opt. Lett.* 15: 553-555 (1990).

Moores, J.D., K. Bergman, H.A. Haus, and E.P. Ippen. "Optical Switching Using Fiber Ring Reflectors." *J. Opt. Soc. Am. B. Forthcoming.*

Moores, J.D., K. Bergman, H.A. Haus, and E.P. Ippen. "Demonstration of Optical Switching Via Solitary Wave Collisions in a Fiber Ring Reflector." *Opt. Lett.* Forthcoming.

Yokoyama, H., K. Nishi, T. Anan, H. Yamada, S.D. Brorson, and E.P. Ippen. "Enhanced Sponstaneous Emission from GaAs Quantum Wells in Monolithic Microcavities." *Appl. Phys. Lett.* 57: 2814 (1990).

1.2 New Ultrashort Pulse Laser Technology

Sponsors

Joint Services Electronics Program
Contract DAAL03-89-C-0001
National Science Foundation
Grant ECS 85-52701
U.S. Air Force - Office of Scientific Research
Contract F49620-88-C-0089

Project Staff

Professor James G. Fujimoto, Professor Hermann A. Haus, Giuseppe Gabetta, Joseph M. Jacobson, Morrison Ulman

1.2.1 Introduction

Ultrashort pulse laser technology is of primary importance in the study of ultrafast phenomena, to make high speed optical measurements, and in telecommunications applications. The central goals of our research program are the investigation of ultrashort pulse generation, amplification, and measurement techniques, and the development of femtosecond laser technology.

Our investigation of femtosecond technology emphasizes several topics including tunability, high repetition rate amplification, and solid state laser materials. The study of ultrafast phenomena has traditionally been limited by the availability of suitable laser sources. Tunable femtosecond lasers provide a powerful capability for time resolved spectroscopy and are especially important for time domain studies of optoelectronic devices. High peak intensity amplifiers permit the investigation of nonlinear optical effects, while high repetition rate amplifier technology permits high sensitivity measurements using signal averaging techniques. Development of solid state ultrashort pulse laser technology yields significant improvements in performance over conventional dye lasers and is an essential step in developing a compact and low cost ultrashort pulse laser technology for high performance signal processing, measurement, and instrumentation applications.

1.2.2 Ultrashort Pulse Generation in Titanium Sapphire

The $Ti:Al_2O_3$ laser is an important model system for investigating ultrashort pulse generation in solid state lasers. The properties of $Ti:Al_2O_3$ are especially attractive for ultrafast spectroscopy. $Ti:Al_2O_3$ features a tuning range from 700 nm to 1100 nm with room temperature operation, high thermal

conductivity, and high energy storage.[32] The broad gain bandwidth of this material makes it an ideal crystal for the generation and amplification of femtosecond pulses. The tuning range is particularly suited for studies of GaAs and AlGaAs-based opto-electronic devices. In addition, amplification and frequency conversion techniques can be developed to produce tunable ultraviolet pulses for femtosetcond UV spectroscopy. For these reasons, the investigation of ultrashort pulse generation in $Ti:Al_2O_3$ has emerged recently as an active and promising area of research.

Working in collaboration with Professors E.P. Ippen and H.A. Haus in RLE and Dr. P.A. Schulz of MIT Lincoln Laboratory, we have recently developed a new modelocking technique for ultrashort pulse generation in $Ti:Al_2O_3$.[33] This modelocking technique has been termed Additive Pulse Modelocked (APM) because pulse shaping is produced by coherent field addition.[34] Additive Pulse Modelocking in $Ti:Al_2O_3$ is significant because it was the first demonstration of self-starting passive modelocking without the need for active gain or loss modulation. Short pulses can be generated with a significant reduction in cost and complexity over previous approaches.

The APM laser generates short pulses using an external cavity containing a Kerr medium (a single mode optical fiber of appropriate length), which has an intensity dependent index of refraction. The external cavity functions as a nonlinear Fabry Perot with an intensity dependent reflectivity. If the external cavity length is interferometrically controlled relative to the main cavity, it is possible to operate the external cavity as a fast saturable absorber. Pulses as short as 1.4 ps have been generated directly from the $Ti:Al_2O_3$ laser. Using an intracavity prism pair with negative group velocit, dispersion to remove pulse chirp and produce pulse compression resulted in bandwidth limited pulses of 230 fs.[35] Pulses of similar duration can also be achieved by external dispersion compensation by a diffraction grating pair.[36]

During the last year, our research has focused on understanding the starting dynamics of the APM modelocking.[37] Studies of starting dynamics provide an approach for investigating the mechanisms of the pulse formation process. Our investigations demonstrate that the nonlinear external cavity produces pulse shaping by a fast saturable absorber like action. These studies provide important design criteria for optimizing the laser system as well as for generalizing the APM technique to other solid state laser materials.

1.2.3 Additive Pulse Modelocking in Diode Pumped Nd:YAG and Nd:YLF

The objective of this program was to demonstrate the extension of self-starting Additive Pulse Modelocking techniques developed in $Ti:Al_2O_3$ to other solid state laser materials. The diode pumped Nd materials are especially attractive since they can be engineered into a compact and low cost ultrashort pulsed laser technology.

Additive pulse modelocking was studied in Nd:YAG and Nd:YLF.[38] Theoretical studies by E.P. Ippen and H.A. Haus suggest that gain cross section is an important parameter in determining

---

[32] P.F. Moulton, "Spectroscopic and Laser Characteristics of $Ti:Al_2O_3$," *J. Opt. Soc. Am. B* 3: 125-133 (1986).

[33] J. Goodberlet, J. Wang, J.G. Fujimoto, and P.A. Schulz, "Femtosecond Passive Modelocked $Ti:Al_2O_3$ Laser with a Nonlinear External Cavity," *Opt. Lett.* 14: 1125-1127 (1989).

[34] E.P. Ippen, H.A. Haus, and L.Y. Liu, "Additive Pulse Modelocking," *J. Opt. Soc. Am. B* 6: 1736-1745 (1989).

[35] J. Goodberlet, J. Jacobson, G. Gabetta, P.A. Schulz, T.Y. Fan, and J.G. Fujimoto, "Ultrashort Pulse Generation with Additive Pulse Modelocking in Solid States Lasers," OSA Meeting, 1990, paper MB1

[36] J. Goodberlet, J. Jacobson, J. Wang, J.G. Fujimoto, T.Y. Fan, and P.A. Schulz, "Ultrashort Pulse Generation with Additive Pulse Modelocking in Solid State Lasers: $Ti:Al_2O_3$, Diode Pumped Nd:YAG and Nd:YLF," Springer Series in Chemical Physics 53, *Ultrafast Phenomena VII*, eds. C.B. Harris, E.P. Ippen, G.A. Mourou, and A.H. Zewail (New York: Springer-Verlag, 1990).

[37] J. Goodberlet, J. Wang, J.G. Fujimoto, and P.A. Schulz, "Starting Dynamics of Additive Pulse Mode Locking in the $Ti:Al_2O_3$ Laser," *Opt. Lett.* 15: 1300-1302 (1990).

[38] J. Goodberlet, J. Jacobson, J. Wang, J.G. Fujimoto, T.Y. Fan, and P.A. Schulz, "Ultrashort Pulse Generation with Additive Pulse Modelocking in Solid State Lasers: $Ti:Al_2O_3$, Diode Pumped Nd:YAG and Nd:YLF," Springer Series in Chemical Physics 53, *Ultrafast Phenomena VII*, eds. C.B. Harris, E.P. Ippen, G.A. Mourou, and A.H. Zewail (New York: Springer-Verlag, 1990); J. Goodberlet, J. Jacobson, J.G. Fujimoto, P.A. Schulz, and T.Y. Fan, "Self Starting Additive Pulse Modelocked Diode Pumped Nd:YAG Laser," *Opt. Lett.* 15: 504-506 (1990).

whether self-starting APM can be achieved in a given laser.[39] The gain cross sections of Nd:YAG and Nd:YLF are comparable to Ti:Al_2O_3. In addition, these solid state laser materials have absorption peaks which can be pumped by commercially available high power laser diode arrays.

Figure 3 shows a schematic diagram of our Additive Pulse Modelocked diode pumped Nd:YAG and Nd:YLF laser design. Three diode arrays are used as the pump source. The main laser cavity consists of a high reflector, a folding mirror, and an output coupler. The external cavity consists of a beam splitter, an optical fiber, and a retroreflecting mirror. The cavity length is 1.1 m corresponding to a 136 MHz repetition rate. In Nd:YAG, durations of 1.7 ps were obtained with a spectral bandwidth of 0.67 nm.[40] To date, these are the shortest pulses produced directly from an Nd:YAG laser. In Nd:YLF, chirped pulses of 2.0 ps with a bandwidth of 0.8 nm were generated.[41]

These results demonstrate that Additive Pulse Modelocking can be scaled to lower power systems such as diode pumped solid state lasers. Pulse durations are generated which are significantly shorter than possible by previous techniques. Finally, diode pumped solid state lasers can be engineered into a compact and low cost ultrashort pulse technology.

1.2.4 New Modelocking Technology

Recently, ultrashort pulse generation in Ti:Al_2O_3 has become an area of investigation being pursued actively by several research groups. In addition to Additive Pulse Modelocking, a variety of techniques have been explored including active modelocking, passive modelocking with a saturable absorber dye,[42] passive modelocking using a semiconductor saturable absorber in an external cavity,[43] and self modelocking in a single cavity.[44] The result of these studies suggests that it is possible to develop new approaches for ultrashort pulse generation in a variety of solid state laser systems.

One of the key concepts which has emerged is the use of intracavity all-optical switching or modulation to modelock a laser. Solid state lasers permit the generation of high intracavity powers. For pulses in the subpicosecond range, the intracavity intensities can be in excess of ~ 100 KW. This is sufficient to achieve appreciable nonlinear phase shifts in bulk materials such as glass or bulk Ti:Al_2O_3 using the Kerr effect or nonlinear index of refraction.

The problem of modelocking a solid state laser can thus be related to all-optical switching. Furthermore, intracavity pulse compression is possible by incorporating negative group velocity dispersion in the laser cavity and using this in conjunction with nonlinear self phase modulation. Working in collaboration with Professor H.A. Haus and E.P. Ippen, we have developed a closed form analytical theory to predict the operation of modelocked solid state lasers with intracavity self phase modulation and dispersion.[45] Experimental studies using

---

[39] E.P. Ippen, L.Y. Liu, and H.A. Haus, "Self-starting Condition for Additive-pulse Modelocking of an Nd:YAG Laser," *Opt. Lett.* 15: 553 (1990).

[40] J. Goodberlet, J. Jacobson, J.G. Fujimoto, P.A. Schulz, and T.Y. Fan, "Self Starting Additive Pulse Modelocked Diode Pumped Nd:YAG Laser," *Opt. Lett.* 15: 504-506 (1990).

[41] J. Goodberlet, J. Jacobson, J. Wang, J.G. Fujimoto, T.Y. Fan, and P.A. Schulz, "Ultrashort Pulse Generation with Additive Pulse Modelocking in Solid State Lasers: Ti:Al_2O_3, Diode Pumped Nd:YAG and Nd:YLF," Springer Series in Chemical Physics 53, *Ultrafast Phenomena VII*, eds. C.B. Harris, E.P. Ippen, G.A. Mourou, and A.H. Zewail (New York: Springer-Verlag, 1990).

[42] N. Sarukura, Y. Ishida, H. Nakano, and Y. Yamamoto, "CW Passive Mode Locking of a Ti:sapphire Laser," *Appl. Phys. Lett.* 56: 814-815 (1990).

[43] U. Keller, W.H. Knox, and H. Roskos, "Coupled-cavity Resonant Passive Mode-locked Ti:sapphire Laser," *Opt. Lett.* 15: 1377-1379 (1990).

[44] D.E. Spence, P.N. Kean, and W. Sibbett, "60-fsec Pulse Generation from a Self-mode-locked Ti:sapphire Laser," *Opt. Lett.* 16: 42-44 (1991).

[45] H.A. Haus, J.G. Fujimoto, and E.P. Ippen, "Structures for Additive Pulse Modelocking," submitted to *J. Opt. Soc. Am.*

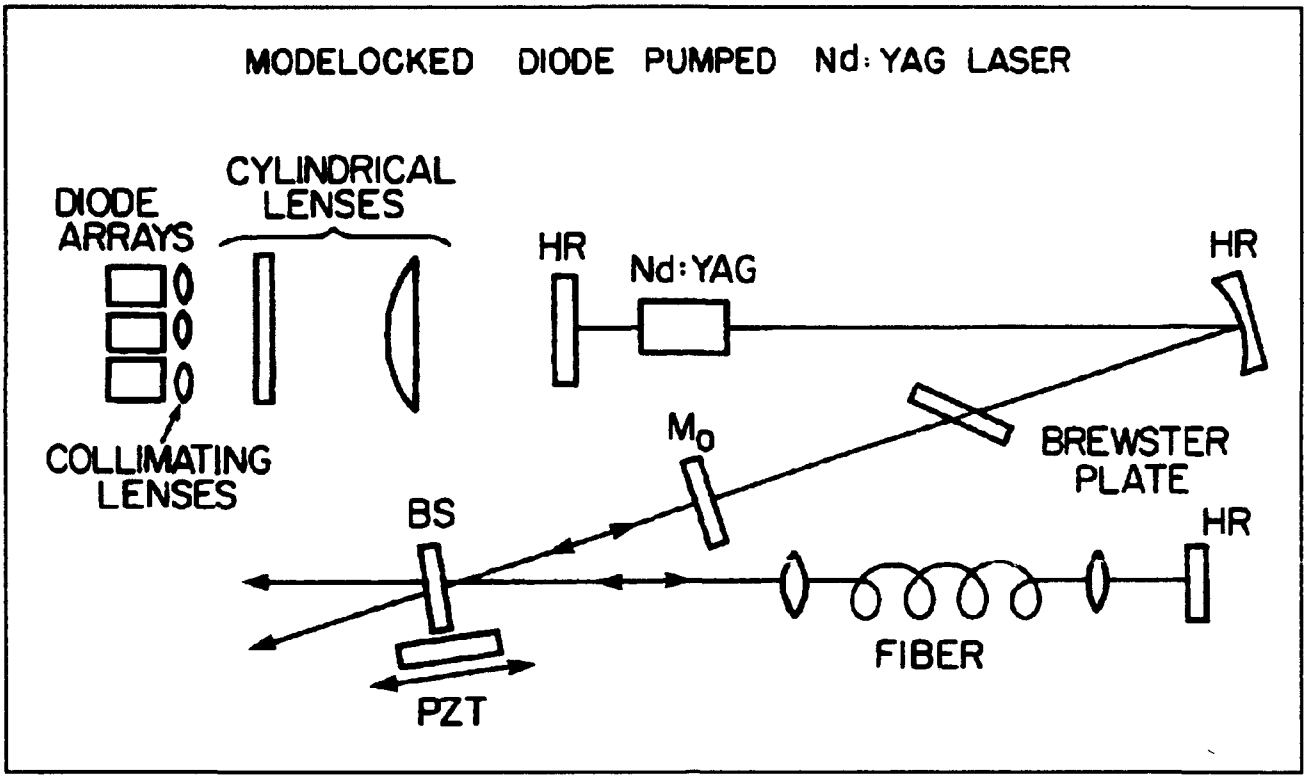

Figure 3. Additive Pulse Modelocked diode pumped Nd:YAG laser. Pulse durations of 1.7 ps were generated using a passive nonlinear external cavity. These are the shortest pulses generated in a YAG laser to date.

different modelocking techniques in Ti:Al_2O_3 are currently in progress.

The objective of our studies is to develop approaches for passive modelocking using different types of nonlinear intracavity all optical modulators. These techniques would represent a significant improvement over current APM which uses optical fibers and requires interferometric cavity length control. If successful, these new modelocking techniques could be applied to a wide range of solid state lasers to generate ultrashort pulses with superior performance and reduced cost compared to previous techniques. The development of low cost laser sources would represent a significant advance for engineering and commercial applications of ultrashort pulse technology and high speed optical measurement.

1.2.5 Multistage High Repetition Rate Femtosecond Amplifiers

Currently, dye laser systems and flowing dye amplifiers are the most widely used technology for ultrashort optical pulse generation. We are continuing our research on dye based systems in order to enhance our experimental facilities for investigating ultrafast phenomena. We have recently completed the development of a multistage, high repetition rate, dye amplifier which may be used for a variety of ultrafast studies in materials and devices.

Our femtosecond pulse laser system is based on a colliding-pulse modelocked ring dye laser (CPM).[46] The CPM generates 35 fs pulses at a wavelength of 630 nm. The advantage of the CPM laser is that it produces extremely short pulse durations. However, since the CPM uses passive modelocking with saturable absorber dyes, the output is not tunable in wavelength. This trade off between short pulse duration and wavelength tunability is typical of ultrafast laser systems, and

[46] J.A. Valdmanis, R.L. Fork, and J.P. Gordon, "Generation of Optical Pulses as Short as 27 Femtoseconds Directly from a Laser Balancing Self-phase Modulation, Group-velocity Dispersion, Saturable Absorption, and Saturable Gain," *Opt. Lett.* 10: 131 (1985).

much of our work focuses on the development of new ultrafast generation techniques to achieve tunable sources.

In order to generate high intensities necessary for studies of nonlinear processes or frequency conversion and pulse compression, the femtosecond pulses generated by our CPM are amplified by a copper vapor laser pumped dye amplifier.[47] The copper vapor laser amplifier operates at 8 kHz repetition rate. The high repetition rate permits the use of lock-in detection and signal averaging to achieve high sensitivity experimental measurements. We have recently completed the development of a novel multistage copper vapor laser pumped amplifier system.[48]

The amplifier system has been designed with modular construction and in a flexible arrangement so it can be configured for amplification, white light continuum generation, or ultrashort pulse compression. The system generates femtosecond pulses with 20-30 μJ pulse energy with pulse durations of 50 fs corresponding to peak intensities in excess of 100 MW.

When an intense ultrashort optical pulse is focused into a material with an intensity dependent index of refraction, self phase modulation effects can be used to broaden the spectrum of the pulse. In the high intensity limit, the spectral broadening becomes very pronounced and a broadband white light continuum is generated with wavelengths ranging from 400 nm to greater than 900 nm.[49] The technique thus provides a source of tunable femtosecond light for experimental studies.

Although continuum generation has been widely used experimentally, the physical origins of the process are not well understood. We are currently investigating the nonlinear frequency modulation and beam propagation effects associated with high peak intensity pulses. These investigations are important because they suggest other techniques for nonlinear frequency generation. In preliminary work, we have observed that the continuum is generated coherently, and that, by using negative group velocity dispersion, it is possible to compress selected wavelength regions of the continuum to less than 20 fs. This represents a powerful new capability for ultrafast spectroscopy.

1.3 Femtosecond Processes in Electronic Materials

Sponsors

Joint Services Electronics Program
Contract DAAL03-89-C-0001
National Science Foundation
Grant ECS 85-52701
U.S. Air Force - Office of Scientific Research
Contract F49620-88-C-0089

Project Staff

Professor James G. Fujimoto, Professor Erich P. Ippen, Dr. Lucio H. Acioli, Morrison Ulman

1.3.1 Studies in Metals and Semiconductors

Advances in high speed electronic and optoelectronic devices require an understanding of the fundamental electronic processes in their constituent materials. The ultimate speed limit for new devices arises from the dynamics of electrons in electronic and optoelectronic materials. Our program focuses on femtosecond studies of electron dynamics in semiconductors and metals. Currently, femtosecond optical measurement techniques are the only methods that allow the direct measurement of ultrafast processes. The temporal resolution of our laser systems is fast enough to resolve the fundamental scattering processes in semiconductors, which occur typically on a 100 fs time scale. In contrast, the electron density in metals is very high so electronic scattering events can occur in 10 fs or less. This is near the limit of the current state-of-the-art femtosecond measurement technology. Our studies of electron dynamics in metals represent some of the first femtosecond experiments performed on these systems.

Working in collaboration with researchers at the General Motors Research Laboratories, we have investigated the dynamics of image potential states

---

[47] W.H. Knox, M.C. Downer, R.L. Fork, and C.V. Shank, "Amplified Femtosecond Optical Pulses and Continuum Generation at 5 kHz Repetition Rate," *Opt. Lett.* 9: 552 (1984).

[48] M. Ulman, R.W. Schoenlein, and J.G. Fujimoto, "Cascade High Repetition Rate Femtosecond Amplifier," paper presented at the Annual Meeting of the Optical Society of America, Orlando, Florida, October 15-20, 1989.

[49] R.L. Fork, C.V. Shank, C. Hirlimann, R. Yen, and W.J. Tomlinson, "Femtosecond White-light Continuum Pulses," *Opt. Lett.* 8: 1 (1983).

in metals.[50] An image potential state occurs in a metal when an electron outside the surface of the metal is bound state to its image charge in the bulk. Electrons in the image potential state form a Rydberg series as a two-dimensional electron gas analogous to quantum well systems in semiconductors. The electrons relax by tunneling from the image potential state back to the bulk states. The investigation of image potential states is thus an important approach to understanding ultrafast electron dynamics in metals.

In order to study femtosecond image potential dynamics, we have developed new measurement techniques which combine photoemission spectroscopy with femtosecond optics. An ultrashort pump pulse is used to prepare the excited state while a delayed pump pulse is used to photoionize the state. The photoemitted electrons are energy analyzed as function of delay between the pump and probe pulses. This permits a transient measurement of photoemssion spectra on the time scale of 10 fs.

Using these techniques, we have performed a comprehensive investigation of the image potential states in Ag. These studies are of interest because they permit us to test theoretical predictions of image potential dynamics. Relaxation dynamics of the n = 1 and n = 2 states on the 100 and 111 surfaces were studied. The dynamics of the image potential state have been measured as a function of time and electron energy. The lifetime of the n = 1 state on Ag(100) was 25 ± 10 fs. To our knowledge, this measurement represents the highest time resolution photoemission measurement to date.[51] Systematic measurements of lifetimes of different states in the Rydberg series on different surfaces have been performed and compared to theoretical descriptions of the image potential dynamics based on tunneling and many particle models.[52]

We are continuing our work on femtosecond carrier dynamics in semiconductors. We have established a collaborative program with condensed matter theorists from the University of Florida.[53] Our objective is to combine state-of-the-art experimental and theoretical techniques to investigate fundamental excited carrier dynamics in technologically relevant compound semiconductors and quantum confined structures. Within this collaborative program, we have begun to develop a comprehensive model for carrier dynamics in the GaAs and AlGaAs semiconductors. This will result in a powerful tool for the prediction of nonequilibrium behavior in a variety of new materials.

Research at MIT focuses on femtosecond experimental studies in GaAs and AlGaAs, while our collaborators at the University of Florida perform theoretical investigations of carrier dynamics using full band structure and ensemble Monte Carlo techniques. The Monte Carlo simulation is used to find the electron and hole distribution functions by developing a correspondence with experimentally measured differential transmission pump probe data. These studies show that it is essential to include collisional broadening during photoexcitation and the effects of hole scattering in the theoretical model.[54] The combination of theoretical and experiment studies provided the first direct evidence for hole redistribution on a femtosecond time scale.

Our work on ultrafast processes in metals and semiconductors provides fundamental information on the ultimate limits of high speed electronic and optoelectronic devices. Many new devices depend on quantum transport effects in semiconductors; femtosecond technology has the highest temporal resolution for investigating these processes in optoelectronic materials.

---

[50] R.W. Schoenlein, J.G. Fujimoto, G.L. Eesley, and T.W. Capehart, "Femtosecond Studies of Image-potential Dynamics in Metals," *Phys. Rev. Lett.* 61: 2596 (1988).

[51] R.W. Schoenlein, J.G. Fujimoto, G.L. Eesley, and T.W. Capehart, "Femtosecond Dynamics of the n = 2 Image-potential State on Ag(100)," *Phys. Rev. B* 41: 5436 (1990).

[52] R.W. Schoenlein, J.G. Fujimoto, G.L. Eesley, and T.W. Capehart, "Femtosecond Relaxation Dynamics of Image-potential States," *Phys. Rev. B,* forthcoming.

[53] D.W. Bailey, C.J. Stanton, K. Hess, M.J. LaGasse, R.W. Schoenlein, and J.G. Fujimoto, "Femtosecond Studies of Intervalley Scattering in GaAs and $Al_xGa_{1-x}As$," *Solid State Electron.* 32:1491 (1989).

[54] D.W. Bailey, C.J. Stanton, and K. Hess, "Numerical Studies of Femtosecond Carrier Dynamics in GaAs," *Phys. Rev. B,* forthcoming; C.J. Stanton, D.W. Bailey, and K. Hess, "Femtosecond Pump, Continuum-probe Nonlinear Absorption in GaAs," *Phys. Rev. Lett.* 65: 231 (1990).

1.3.2 Four Wave Mixing and Information Storage in Photorefractive Crystals

Photorefractive materials such as $BaTiO_3$, SBN, and $LiNbO_3$ present large optical nonlinearities that are attractive for applications in optical devices based on four-wave mixing processes.[55] Although the response times of these crystals are typically in the millisecond range, they provide an important model system for the design of phase conjugation, optical processing, and optical logic techniques. Working in collaboration with investigators from Tufts University, we have performed the first four-wave mixing experiments in $BaTiO_3$ using femtosecond optical pulses.[56]

These investigations explore the factors which determine the temporal broadening of optical signals in four wave mixing. Studies were performed using 40 fs pulse durations from a CPM dye laser. Different phase conjugation geometries were examined including the ring resonator as well as the two beam coupling geometry. A surprising discovery was that temporal signals are influenced only by material dispersion effects and that pulse durations of 40 fs could be preserved in the four wave mixing process. Since four wave mixing in $BaTiO_3$ occurs via the photorefractive effect, these studies determine the transient behavior of scattering from volume index photorefractive gratings.

Four wave mixing in $BaTiO_3$ is a well established approach for encoding image and phase conjugation information. We have extended these concepts and demonstrated the encoding of temporal information using a two beam four wave mixing approach. Our experiments are closely related to femtosecond holography which uses holographic recording to store transient femtosecond images.[57] In our approach, however, the temporal behavior of a signal pulse can be encoded geometrically onto the volume photorefractive grating which is written in the $BaTiO_3$ crystal. Subsequently, this temporal signal can be read out by diffracting as probe pulse from the volume grating. These investigations suggest a new approach for encoding and reconstructing high speed optical information. Extensions of these techniques using acousto-optic modulators or other programmable volume diffraction devices could make possible the generation of programmable optical pulse trains at THz repetition rates.

1.4 Femtosecond Studies of Waveguide Devices

Sponsors

Joint Services Electronics Program
Contract DAAL03-89-C-0001
National Science Foundation
Grant ECS 85-52701
U.S. Air Force - Office of Scientific Research
Contract F49620-88-C-0089

Project Staff

Professor James G. Fujimoto, Professor Hermann A. Haus, Claudio Chamon, Chi-Kuang Sun

1.4.1 Time Domain Interferometry

Investigations of nonresonant nonlinear processes in semiconductors are directly relevant to the development of high-speed all-optical switching devices and the optimization of high speed modulation performance in diode lasers. In particular, the characterization of the nonlinear index of refraction, n_2, and its dynamics is key to the development of such fast devices.[58] Various techniques have been used to measure intensity dependent index changes, such as fringe shift

---

[55] M. Cronin-Golomb, B. Fischer, J.O. White, and A. Yariv, "Theory and Applications of Four-wave Mixing in Photorefractive Media," *IEEE J. Quant. Electron.* QE-20: 12 (1984).

[56] L.H. Acioli, M. Ulman, E.P. Ippen, J.G. Fujimoto, H. Kong, B.S. Chen, and M. Cronin-Golomb, "Femtosecond Two Beam Coupling and Temporal Encoding in Barium Titanate," paper to be presented at CLEO '91, Baltimore, Maryland.

[57] J.A. Valdmanis, H. Chen, E.N. Leith, Y. Chen, J.L. Lopez, "Three Dimensional Imaging with Femtosecond Optical Pulses," *CLEO Technical Digest*, p. 54, paper CTUA1 (1990).

[58] S.W. Koch, N. Peyghambarian, and H.M. Gibbs, "Band-edge Nonlinearities in Direct-gap Semiconductors and Their Application to Optical Bistability and Optical Computing," *J. Appl. Phys.* 63: R1 (1989); G.I. Stegeman, E.M. Wright, N. Finlayson, R. Zanoni, and C.T. Seaton, "Third Order Nonlinear Integrated Optics," *J. Lightwave Tech.* 6: 953 (1988).

interferometry,[59] Mach-Zehnder interferometry,[60] four wave mixing,[61] nonlinear waveguide couplers,[62] and nonlinear Fabry-Perots.[63]

Our group has recently developed a novel technique for performing highly sensitive nonlinear index measurements.[64] This technique is called time division interferometry or TDI and uses a single waveguide with time division multiplexing to perform transient pump probe interferometric measurements of n_2. A pump and time delayed probe pulse are coupled into a waveguide structure. The transient phase shift of the probe pulse produced by the pump is measured by interfering the probe with a time division multiplexed reference pulse. The femtosecond transient behavior of the nonlinear index can be measured by varying the delay between the pump and probe pulses. The TDI technique reduces parasitic contributions from thermal and acoustic effects and achieves a measurement sensitivity of $\lambda/500$ without active length stabilization of the interferometer. Active stabilization increases the sensitivity by over an order of magnitude.

Using this technique, we have performed the first direct measurements of the nonresonant nonlinear index in AlGaAs.[65] We have recently extended these investigations to explore other nonlinear optical waveguide materials. Working in collaboration with investigators at MIT Lincoln Laboratories and Bellcore, we are studying multiple quantum well waveguides and polydiacetylene waveguides.

Many of these new materials have highly anisotropic nonlinear optical properties. In order to address this issue, we have developed variations of our original time division interferometry approach which permit measurement of the different tensor components of the third order nonlinear susceptibility tensor $\chi^{(3)}$ that contribute to the nonlinear index n_2. These studies should permit a comprehensive characterization of the the nonlinear index and its dynamics in a wide range of materials systems.

1.4.2 Time Domain Optoelectronic Diagnostics

In addition to measuring nonlinear properties, it is also possible to develop time domain diagnostics for linear device properties. Since femtosecond pulses have a spatial extent smaller than most waveguide longitudinal dimensions, the impulse response of the waveguide can be measured. The impulse response contains information on linear absorption, group velocity and dispersion and permits a complete characterization of the linear properties of optical guided wave devices.[66]

Nonlinear effects other than the nonlinear index of refraction n_2 can also be studied using time domain techniques. The nonlinear two photon

---

[59] Y.H. Lee, A. Chavez-Pirson, S.W. Koch, H.M. Gibbs, S.H. Park, J. Morhange, A. Jeffrey, N. Peyghambarian, L. Banyai, A.C. Gossard, and W. Wiegmann, "Room-temperature Optical Nonlinearities in GaAs," *Phys. Rev. Lett.* 57: 2446 (1986).

[60] D. Cotter, C.N. Ironside, B.J. Ainslie, and H.P. Girdlestone, "Picosecond Pump-probe Interferometric Measurement of Optical Nonlinearity in Semiconductor-doped Fibers," *Opt. Lett.* 14: 317 (1989).

[61] W.K. Burns and N. Bloembergen, "Third-harmonic Generation in Absorbing Media of Cubic or Isotropic Symmetry," *Phys. Rev. B* 4: 3437 (1971).

[62] P. Li, K. Wa, J.E. Sitch, N.J. Mason, J.S. Roberts, and P.N. Robson, "All Optical Multiple-quantum-well Waveguide Switch," *Electron. Lett.* 21:27 (1985); R. Jin, C.L. Chuang, H.M. Gibbs, S.W. Koch, J.N. Polky, and G.A. Pubanz, "Picosecond All-optical Switching in Single-mode GaAs/AlGaAs Strip-loaded Nonlinear Directional Couplers," *Appl. Phys. Lett.* 53:1791 (1988).

[63] Y.H. Lee, A. Chavez-Pirson, S.W. Koch, H.M. Gibbs, S.H. Park, J. Morhange, A. Jeffrey, N. Peyghambarian, L. Banyai, A.C. Gossard, and W. Wiegmann, "Room-temperature Optical Nonlinearities in GaAs," *Phys. Rev. Lett.* 57: 2446 (1986).

[64] M.J. LaGasse, K.K. Anderson, H.A. Haus, and J.G. Fujimoto, "Femtosecond All-optical Switching in AlGaAs Waveguides Using a Single Arm Interferometer," *Appl. Phys. Lett.* 54: 2068 (1989).

[65] M.J. LaGasse, K.K. Anderson, C.A. Wang, H.A. Haus, and J.G. Fujimoto, "Femtosecond Measurements of the Nonresonant Nonlinear Index in AlGaAs," *Appl. Phys. Lett.* 56: 417 (1990).

[66] K.K. Anderson, J.J. LaGasse, H.A. Haus, and J.G. Fujimoto, "Femtosecond Time Domain Techniques for Characterization of Guided Wave Devices." *Mat. Res. Soc. Symp. Proc.* 167: 51 (1990).

absorption β is an important limiting process for all-optical switching since it produces excited carriers which limit the recovery times of the index nonlinearity.[67] We have performed measurements of β and the associated carrier dynamics for AlGaAs waveguide devices.[68] Coupled with measurements of linear properties and nonlinear index, this constitutes a complete characterization of the waveguide device. This information can be used to calculate the all-optical switching behavior and determine figures of merit for all-optical switching.

With development of new tunable femtosecond laser sources, time domain device diagnostics can become a viable approach for characterizing optoelectronic waveguide devices. The passively modelocked Ti:Al_2O_3 laser is particularly suited for this application since it is a solid state laser which features tunability over the wavelength range from 700 nm to greater than 1000 nm. The improved performance of this laser over existing femtosecond dye lasers will permit us to investigate a broader range of guided wave devices. As described previously, another part of our research program focuses on the development of new femtosecond solid state laser technology. Since low cost, compact femtosecond technology is a major limiting factor in commercial applications, our program concept is to simultaneously address the issues of ultrashort pulse laser develop and applications. Time domain device diagnostics are particularly attractive since they can be applied to investigate processes which cannot be studied using continuous wave techniques.

1.5 Laser Medicine

Sponsors

Medical Free Electron Laser Program
Contract N00014-86-K-0117
National Institutes of Health
Grant 5-RO1-GM35459

Project Staff

Professor James G. Fujimoto, Michael Hee, David Huang, Jyhpyng Wang

1.5.1 Optical Coherent Reflectometry

Optical coherence domain reflectometry (OCDR) is a new optical ranging method that uses short coherence length light sources and interferometric detection to determine the time-of-flight delay of light reflected from a sample.[69] It is the optical analog of ultrasound, but offers higher resolution and noncontact measurement. The coherent detection techniques used in OCDR also offer inherently superior signal to noise ratio compared to other optical ranging methods, including femtosecond ranging techniques we have previously utilized in biological measurements.[70] The high detection sensitivity of OCDR allows us to measure weak backscattered signal from biological systems, not only in the transparent media of the eye, but also in turbid tissues. Additionally, OCDR employs a compact continuous wave laser diode source and can be easily engineered into compact and reliable clinical instruments. We believe that OCDR is a promising technique for many applications in laser microsurgery and medical diagnostics.

Working in collaboration with investigators at the Massachusetts Eye and Ear Infirmary and the Wellman Laboratories of the Massachusetts General Hospital, we have developed an experimental OCDR system to investigate optical

---

[67] K.W. DeLong, K.B. Rochford, and G.I. Stegeman, "Effect of Two-photon Absorption on All-optical Guided-wave Devices," *Appl. Phys. Lett.* 55: 1823 (1989).

[68] K.K. Anderson, M.J. LaGasse, H.A. Haus, and J.G. Fujimoto, "Femtosecond Studies of Nonlinear Optical Switching in GaAs Waveguides Using Time Domain Interferometry," SPIE OE LASE '90, Los Angeles, California, January 14-19, 1990; *Proceedings, Nonlinear Optical Materials and Devices for Photonic Switching* 1216: 2 (1990).

[69] R.C. Youngquist, S. Carr, and D.E.N. Davies, "Optical Coherence Domain Reflectometry: a New Optical Evaluation Technique," *Opt. Lett.* 12: 158 (1987).

[70] D. Stern, W.Z. Lin, C.A. Puliafito, and J.G. Fujimoto, "Femtosecond Optical Ranging of Corneal Incision Depth," *Invest. Ophthamol. Vis. Sci.* 30: 99 (1989).

ranging in biological systems.[71] The system employs a Michelson interferometer with a short coherence length light source (AR coated laser diode at 830 nm) and optical heterodyne detection to achieve a ranging resolution of 10 μm and detection sensitivity of 1 part in 10^{10} (100 dB SNR). The high ranging resolution is obtained because interference fringes are observed only when the two interferometer arms are length matched to within the coherence length of the light source. Noise reduction is achieved by phase modulating the reference arm of the interferometer with a piezoelectrically actuated end mirror at a frequency range at which optical and mechanical noise is low. The light power incident on the biological sample is 7 μW, considerably lower than the safety limit for intraocular applications. This system has been used to demonstrate measurements of both eye structures and turbid tissue samples.

1.5.2 Optical Diagnostics in Ophthalmology

The transparent media of the eye offers unique accessibility to optical diagnostic methods, and we have focused our investigations on applications in the eye that require the high ranging resolution possible with optical coherence domain reflectometry (OCDR). Specifically, we have demonstrated potential applications to corneal measurements in keratorefractive surgeries and retinal measurements which may be useful for the diagnosis of glaucoma and other retinal diseases.

The ability of excimer lasers to remove corneal tissue in submicron increments has led to interest in the use of these lasers for keratorefractive surgeries.[72] In this procedure, the curvature or refractive power of the cornea is altered surgically to achieve refractive correction without the need for external lenses. To exploit the potential for micron-precision ablation control in laser surgery, a precise method for monitoring the excision depth is needed. We have demonstrated in vitro measurements of excimer laser corneal excision depth using OCDR.[73] The corneal thickness in excised and intact areas were determined by the optical delay between reflection peaks at the air/cornea and cornea/aqueous medium boundaries. We have found that OCDR has sufficient sensitivity to detect rough ablated surfaces even in the presence of a precorneal tear film.

Changes in retinal thickness accompany a variety of retinal diseases. In glaucoma, elevated intraocular pressure produces a gradual loss of the retinal nerve fiber layer that may eventually lead to blindness.[74] Currently, there is no reliable diagnostic tool for the in situ evaluation of retinal nerve fiber loss. Changes in visual function and retinal appearance can occur only in late stages in glaucoma and intraocular pressure itself is not a reliable indicator of disease progression.[75] We have demonstrated in vitro measurements of retinal thickness with OCDR. Retinal thickness was determined by the optical delay between reflections at the vitrious medium/retina and retina/choroid boundaries. Potentially, serial measurements of retinal thickness with OCDR is an accurate method for diagnosing the progress of glaucoma and in selecting the proper treatment regimen.

---

[71] D. Huang, J. Wang, C. P. Lin, C. A. Puliafito, and J.G. Fujimoto, "Micron-resolution Ranging of Cornea and Anterior Chamber by Optical Reflectometry," submitted to *Invest. Ophthalmol. Vis. Sci.*

[72] D.S. Aron-Rosa, C.F. Boerner, M. Gross, J.C. Timsit, M. Delacour, and P.E. Bath, "Wound Healing Following Excimer Laser Radial Keratotomy," *J. Cataract Refract. Surg.* 14: 173-179 (1988); J. Marshall, S. Trokel, S. Rothery, and R.R. Krueger, "Photoablative Reprofiling of the Cornea Using an Excimer Laser: Photorefractive Keratectomy," *Lasers Ophthalmol.* 1: 21 (1986).

[73] D. Huang, C.P. Lin, J. Wang, J.G. Fujimoto, and C.A. Puliafito, "High Resolution Measurement of Corneal and Anterior Eye Structure Using Optical Coherence Domain Reflectometry," paper presented at the Association for Research in Vision and Ophthalmology Annual Meeting, Sarasota, Florida, April 1990; *Invest. Ophthal. Vis. Sci.* 31: 244 (1990).

[74] H.A. Quigley and E.M. Addicks, "Quantitative Studies of Retinal Nerve Fiber Layer Defects," *Arch. Ophthalmol.* 100: 807 (1982).

[75] H.A. Quigley, E.M. Addicks and W.R. Green, "Optic Nerve Damage in Human Glaucoma: III Quantitative Correlation of Nerve Fiber Loss and Visual Field Defect in Glaucoma, Ischemic Neuropathy, Papilledema, and Toxic Neuropathy," *Arch. Ophthalmol.* 98: 1564 (1980).

1.5.3 Fiber Optic Integrated Reflectometer

A clinically viable optical reflectometer must be integrated into diagnostic instruments and laser delivery systems and be able to acquire data on the time scale of target motion. We are developing a fiber optic integrated reflectometer in collaboration with Eric Swanson in Group 67 at MIT Lincoln Laboratory. This system will employ modular fiber optic components and a detection scheme capable of high speed data acquisition rate. The system is based on a fiber Michelson interferometer with a superluminescent diode light source (830 nm). Modulation of the interference signal is provided by a combination of piezoelectric fiber length modulation and high speed scanning of the reference arm end mirror. This novel modulation technique allows arbitrary adjustment of signal bandwidth and therefore permits tradeoffs between signal-to-noise ratio and data acquisition rate to be examined. The system has achieved signal-to-noise ratio of 90 dB at a detection bandwidth of 4 kHz. This bandwidth supports scanning data aquisition rate in excess of 1 cm/s, allowing the measurement of thin structures such as cornea and retina without significant motion error. In vitro measurement of cornea thickness has been demonstrated using this system, which will be adapted to a slitlamp biomicroscope for measurements of intraocular structures in vivo.

1.5.4 Variable Pulse Duration Laser

In recent years, laser induced optical breakdown has become an important technique for intraocular surgery.[76] Current clinical systems employ either Q-switched nanosecond pulses or mode-locked picosecond pulse trains. These laser sources generate a single pulse or a pulse train that produces collateral damages through cavitation and shockwave production. This treatment is limited to applications far away from sensitive structures such as the retina and cornea. The use of single picosecond or femtosecond pulses can result in more precise incisions with reduced collateral damage. Shorter pulse duration lowers the threshold energy for optical breakdown and allows the use of less energetic pulses.

We have performed studies of optical breakdown using single 40 ps Nd:YAG laser pulses. Time resolved measurement techniques were used in a comprehensive study of the temporal and spatial dynamics of plasma formation, shock wave, and cavatation processes that accompany optical breakdown.[77] Tissue effects were investigated using corneal endothelium in vitro.[78] Comparison of tissue effects with physical measurements suggests that endothelial cell damage is mediated by shock wave and cavitation precesses while incisions confined to the focal region of the laser beam are produced by the laser-induced plasma. Systematic studies were performed to determine the energy scaling behavior of the tissue effects and to quantify the minimum "safe" distance for clinical photodisruption near sensitive areas. Tissue damage range was found to vary with the cube root of the pulse energy. Picosecond and nanosecond optical breakdown results in comparable damage if the same amount of energy is involved. The minimum damage range of 100 μm was achieved with 8 μJ picosecond pulses.

We have studied corneal excisions generated with nanosecond, picosecond, and femtosecond pulses.[79] Compared with nanosecond pulses, picosecond and femtosecond pulses produced much smoother excision edges and less damage to the adjacent tissue. Pulses shorter than 1 ps produced additional strand-like collateral damage that may be caused by nonlinear processes other than optical breakdown. Because the use of femtosecond pulses is compromised by nonlinear propagation effects, our studies suggest that pulse duration in the 1 to 100 ps range is likely to be optimal for the construction of a precision laser scalpel.

In order to study the optimal pulse duration for a laser scalpel, we have constructed a solid state

---

[76] F. Fankhauser, P. Rousel, J. Steffen, E. Van der Zypen, and A. Cherenkova, "Clinical Studies on the Efficiency of High Power Laser Radiation upon Some Structures of the Anterior Segment of the Eye," *Int. Ophthalmol.* 3: 129-139 (1981).

[77] B. Zysset, J.G. Fujimoto, and T.F. Deutsch, "Time-resolved Measurements of Picosecond Optical Breakdown," *Appl. Phys. B* 48: 139-147 (1989).

[78] B. Zysset, J.G. Fujimoto, C.A. Puliafito, R. Birngruber, and T.F. Deutch, "Picosecond Optical Breakdown: Tissue Effects and Reduction of Collateral Damage," *Lasers Surgery Med.* 9: 193-204 (1989).

[79] D. Stern, R.W. Schoenlein, C.A. Puliafito, E.T. Dobi, R. Birngruber, and J.G. Fujimoto, "Corneal Ablation by Nanosecond, Picosecond, and Femtosecond Lasers at 532 and 625 nm," *Arch. Ophthalmol.* 107: 587-592 (1989).

laser system which features high pulse energy and variable pulse duration. The system consists of a high power modelocked Nd:YLF laser, a pulse stretching/compression stage, and a Nd:Phosphate glass regenerative amplifier.[80] Variable pulse duration is achieved using an optical pulse compression/stretching technique.[81] A pulse train from the modelocked Nd:YLF laser is first sent through a long optical fiber. Frequency dispersion and self-phase modulation in the fiber produce a linear frequency chirp and stretch the laser pulse, which is subsequently amplified and compressed by a grating pair. Varying the distance between the grating pair changes the pulse duration.

This system can produce pulse duration from 100 to 1 ps with energies up to 1 mJ. The variable pulse duration system will permit a wide range of studies in laser tissue interaction as well as photochemical and photobiological reactions.

1.6 The MIT Short-Wavelength Laser Project: A Status Report

Sponsors

Lawrence Livermore National Laboratory
Contract B048704
U.S. Department of Energy
Grant DE-FG02-89-ER14012

Project Staff

Professor Peter L. Hagelstein, Dr. Santanu Basu, Martin H. Muendel, John Paul Braud, Daniel Tauber, Sumanth Kaushik, James G. Goodberlet, Kathryn M. Nelson, Janet L. Pan, Michele M. Bierbaum

1.6.1 Introduction

During the past several years, short-wavelength laser research has advanced to the point where many laboratories around the world have been able to observe stimulated emission in the EUV and soft x-ray regimes. While the use of these lasers in applications is an area of current research, progress has been hindered in most cases by high system cost, low shot rate, and poor beam quality. The resolution of such issues is our principal concern as we seek to develop new EUV lasers.

In this effort, we have chosen to use a Ni-like collisional excitation scheme at low Z; Table 1 lists laser wavelengths and other relevant atomic physics parameters. A solid target will be irradiated by a series of pump pulses,[82] and gain is predicted to appear on the second and following pulses after the plasma is formed. A cavity having a round-trip time equal to the interval between pump pulses would be used to provide feedback synchronous with gain formation.

The experimental facility which we are developing consists of a pump laser system, a target chamber, an automatic target alignment system, and appropriate EUV diagnostics.[83] The pump laser itself is based on a mode-locked, Q-switched Nd:YLF laser which produces a string of 70-100 ps pulses separated by 3.5 ns. Five pulses from this oscillator are amplified in a Nd:glass preamplifier to a total energy of 100 mJ. Final amplification is carried out in a pair of multipass, zig-zag, Nd:glass slabs to produce two beams, each delivering a total of 5 J.

This report describes some of the ongoing and recently completed work associated with this project. Although it will take several months to make our first gain measurements, we have made progress in a number of areas; these are the subjects of the various sections of this report.

---

[80] L. Yan, J.D. Lin, P.T. Ho, C.H. Lee, and G.L. Burdge, "An Active Modelocked Continuous Wave Nd:Phosphate Glass Laser and Regenerative Amplifier," *IEEE J. Quant. Electron.* 24: 418 (1988).

[81] W.J. Tomlinson, R.H. Stolen, and C.V. Shank, "Compresson of Optical Pulses Chirped by Self-phase Modulation in Fiber," *J. Opt. Soc. Am. B* 1: 139 (1984).

[82] P.L. Hagelstein, "Short Wavelength Lasers: Something Old Something New," *Proceedings of the OSA Meeting on Short Wavelength Coherent Radiation: Generation and Applications,* eds. R.W. Falcone and J. Kirz, 1988.

[83] P.L. Hagelstein, J.P. Braud, K. Delin, C. Eugster, S. Kaushik, A. Morganthaler, M.H. Muendel, L. Balents, T. Farkas, T. Hung, and K. Lam, *RLE Progress Report No. 130,* Res. Lab. Electron., MIT, 1988, pp. 48; P.L. Hagelstein, S. Basu, M.H. Muendel, S. Kaushik, D. Tauber, J.P. Braud, and A.W. Morganthaler, *RLE Progress Report No. 132,* Res. Lab. Electron., MIT, 1989, pp. 86; S. Basu, M.H. Muendel et al, "Development of the Tabletop 194 Å Laser in Ni-like Mo," Paper QTuD2, presented at CLEO/IQEC, Anaheim, California, 1990.

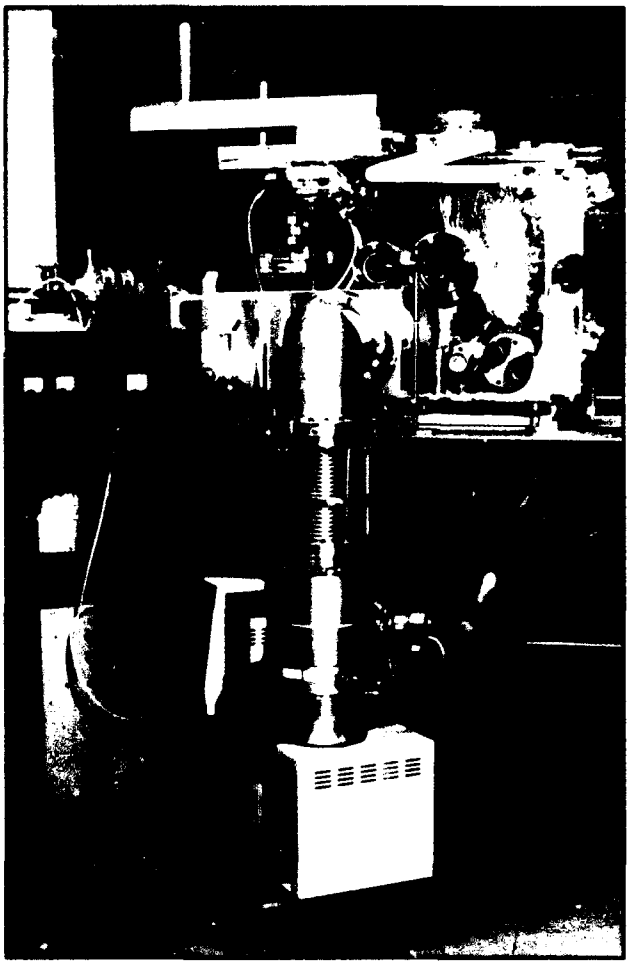

Figure 4. X-ray laser target chamber.

1.6.2 Kinetics of Transiently Pumped Laser Plasmas

Project Staff

Professor Peter L. Hagelstein

In our earlier publication on this approach,[84] we used the numerical simulation tools LASNEX, YODA and XRASER to model the hydrodynamics and laser kinetics. We found that, in contrast to the high-Z systems which have been studied at Lawrence Livermore National Laboratory and elsewhere, low-Z Ni-like systems do not develop significant laser gain under steady-state conditions. The reason is that at low Z, the temperature at which nickel-like ions occur is too low to allow significant excitation of the 4d. Our proposed solution to this problem is to use a low-density transient plasma in which the Ni-like ions are produced at low density and at a temperature matched for 3d-4d electron-collisional excitation. Under these conditions, the Ni-like ions will occur only transiently, since the high temperature will cause the ionization to proceed much further than Ni-like sequence.

The simulations suggested that this approach is basically sound, and we have proceeded to build up an experimental effort to demonstrate the scheme. Further theoretical studies, however, have revealed a very interesting effect: the ion temperature in a plasma pumped by multiple pulses can be very low.[85] During the first pulse, the ions are heated since most of the plasma formation takes place at high density, and the electron-ion coupling times are quite short. After the plasma has expanded and the second pulse arrives, the laser radiation is absorbed at high density, and electron thermal conduction provides a mechanism to heat the electron distribution at low density. At low density the ions couple only weakly to the electrons, and as a result the ion temperature remains quite low; LASNEX calculates an ion temperature of less than 10 eV while the electrons are above 250 eV.

We had not previously appreciated the dramatic disparity in electron and ion temperatures which could be achieved with multiple pulses. This appears to be a new and very interesting regime for x-ray laser physics. Additionally, we note that our earlier estimates of gain in Nd-like ions[86] were low since we had assumed a high value for the ion temperature (ion Doppler broadening dominates the laser line profile). In a plasma pumped by a burst of pulses, if the ion temperature is really below 10 eV, then the Doppler broadening will be reduced by a significant factor (5 or so), and the Nd-like scheme becomes very attractive as a low-intensity means to obtain gain near 100Å and below.

---

[84] P.L. Hagelstein, "Short Wavelength Lasers: Something Old Something New," *Proceedings of the OSA Meeting on Short Wavelength Coherent Radiation: Generation and Applications,* eds. R.W. Falcone and J. Kirz, Cape Cod, Massachusetts, 1988.

[85] S. Kaushik, S. Basu and P. Hagelstein, "Design Studies of the MIT 194 Å Ni-like Mo Laser," CLEO/IQEC '90, Anaheim, California, 1990.

[86] P.L. Hagelstein, "Short Wavelength Lasers: Something Old Something New," *Proceedings of the OSA Meeting on Short Wavelength Coherent Radiation: Generation and Applications,* eds. R.W. Falcone and J. Kirz, 1988.

Z	ΔE(3d-4d)	λ_L(Å)	Ω(3d-4d)	f_L(4p-4d)
32	59	748	0.79	0.29
34	98	468	0.51	0.27
36	143	342	0.37	0.25
38	194	271	0.29	0.23
40	250	224	0.24	0.22
42	311	191	0.20	0.20
44	377	167	0.17	0.19
46	449	148	0.15	0.17

Table 1. Atomic physics parameters for $3d^{10}\,{}^1S_0 - 3d^9 4d^1 S_0$ excitation and 4d-4p laser transitions. The 3d-4d excitation energies are in eV, and the 3d-4d collision strengths are near threshold distorted wave values. Based on new extrapolations, we have revised the estimate of the line in Mo to 191Å. (Second International Conference on X-ray Lasers, York, England, September 1990.)

It may be possible that some of the interesting effects reported by Hara are due to low ion temperature, since his group is working in a very similar regime. Additionally, Boehly has reported positive results from double pulse experiments in Ne-like titanium; it would be interesting to see if the ion temperature is low in these experiments.

We note in closing this section that the use of 2 μm for pumping would result in a higher electron temperature relative to the incident intensity; frequency downconversion of the pump could be done efficiently to produce such radiation.

1.6.3 Nd:Glass Power Amplifier

Project Staff

Martin H. Muendel

Final amplification of the pump laser beam is provided by a pair of zig-zag Nd:glass slab amplifiers operating in parallel.[87] A slab design was chosen in favor of the more traditional rod or disk designs because it offers a much higher repetition rate; this feature occurs because both the cooled surface area is increased and the zig-zag geometry cancels out thermal distortion of the beam to first order. Other groups have built similar slab lasers but have generally run them Q-switched, at very high average power; by contrast, we are operating with short, mode-locked pulses at very high peak powers and are therefore intensity-limited as a result of nonlinear self-focusing in the glass. Our slab is therefore designed to be wider and shorter than others, and it is pumped more strongly (at levels up to 0.4 J/cm^3) so as to minimize the B integral for a given net gain. Vacuum spatial filters, apodizing, and relay imaging are also used to help suppress the self-focusing. The required overall gain of 50-100 requires the use of three passes at a gain of 4-5 per pass; we do this in three geometrically distinct passes angled to overlap within the slab. Because our average power requirements are not stringent, we cool the slabs with air rather than liquid and thus avoid problems with phosphate glass solubility and sealing of the pump cavity.

The first head has been completed and tested. It has demonstrated a single-pass gain of over six with uniformity of better than 10% across the width of the slab and virtually perfect uniformity across the thickness. Experiments have been done with simmering and prepulsing the flashlamps, and improvements in the storage efficiency of up to 15% have been seen as a result; the highest measured storage efficiency was over 4%. A rectangular apodized beam with a fill factor of about 75% was injected into the slab and shown to propagate without significant diffractive degradation, and the apodizer image was relayed through the slab and shown to be largely undistorted. Finally, the behavior of the beam was observed as a function of the slab thermal loading: at the slab's maximum repetition rate of .5 Hz (> 1000 W input power), no beam distortion was observed. Focusability of the beam was found to be better than twice diffraction limited at up to full input power. Following installation of some remaining optical components in the amplifier chain, the system will be ready for full-scale operation.

[87] M.H. Muendel and P.L. Hagelstein, "Short-pulse Glass Slab Amplifier," paper presented at *Lasers '90*, San Diego, California, December 1990; M.H. Muendel and P.L. Hagelstein, "High Repetition Rate, Tabletop X-Ray Lasers," *Proc. OE-Laser '90, SPIE Proc.* 1229: 87 (1990).

Figure 5. Martin Muendel examines the zig-zag amplifier which he built.

1.6.4 EUV Laser Diagnostics

Project Staff

Dr. Santanu Basu, Professor Peter L. Hagelstein

We are developing two primary laser diagnostics. The first instrument, based upon a flat-field Harada grating, will be run in a number of modes: (1) as a time-resolved (fast diode, 1-GHz transient digitizer) single-channel monochromator, (2) as a time-gated (MCP) spectrograph, and (3) as in (2) but with an image-plane slit to check for angular collimation.

The second instrument would be based on our novel high-resolution, single-element holographic toroidal grating, which will be sufficiently stigmatic to provide 2-D imaging capability between 100-300Å, at a resolution of one part in 5000 or higher.[88] Such a grating could be run in any of the three modes described above, as well as in a fourth, spatial-imaging mode.

1.6.5 Whispering-Gallery Cavities for Short Wavelength Lasers

Project Staff

John Paul Braud, Kathryn M. Nelson

Whispering-gallery optics is based on the principle of using a concave surface to deflect light through a large total angle by means of a series of many glancing-incidence reflections. Because whispering-gallery mirrors (WGMs) offer potentially high reflectivities at short wavelength, they have been suggested for use in x-ray laser cavities.[89] Unfortunately, the simplest resonator geometries—those employing cylindrical or spherical mirrors—have cavity modes whose behavior is poorly suited for use with typical x-ray laser amplifiers.

As a beam propagates along the surface of a WGM, its transverse structure evolves in a manner determined by the local curvatures of the surface. This evolution is highly astigmatic, i.e., the beam profile in the direction normal to the surface behaves very differently from that in the direction tangent to the surface. The fact that the normal and tangential structures evolve differently is not necessarily a major issue. The real problem is in the behavior of the normal structure: for mirrors of any reasonble size, a round geometry leads to unacceptably large beam divergence.[90]

---

[88] P.L. Hagelstein, "Design of a Nearly Stigmatic Toroidal Spectrometer," submitted to *Appl. Opt.*

[89] J. Bremer and L. Kaihola, "An X-Ray Resonator Based on Successive Reflections of a Surface Wave," *Appl. Phys. Lett.* 37(4): 360-362 (1980). Erratum: 37(11): 1051 (1980); A.V. Vinogradov, N.A. Konoplev, and A.V. Popov, "Broad-band Mirrors for Vacuum Ultraviolet and Soft X-Ray Radiation," *Sov. Phys. Dokl.* 27(9): 741-742 (1982); A.V. Vinogradov, V.F. Kovalev, I.V. Kozhevnikov, and V.V. Pustovalov, "Diffraction Theory For Grazing Modes in Concave Mirrors and Resonators at X-Ray Wavelengths: II," *Sov. Phys. Tech. Phys.* 30(3): 335-339 (1985).

[90] J.P. Braud and P.L. Hagelstein, "Whispering-Gallery Laser Resonators—Part I: Diffraction of Whispering-Gallery Modes," *IEEE J. Quantum Electron.*, April, 1991, forthcoming.

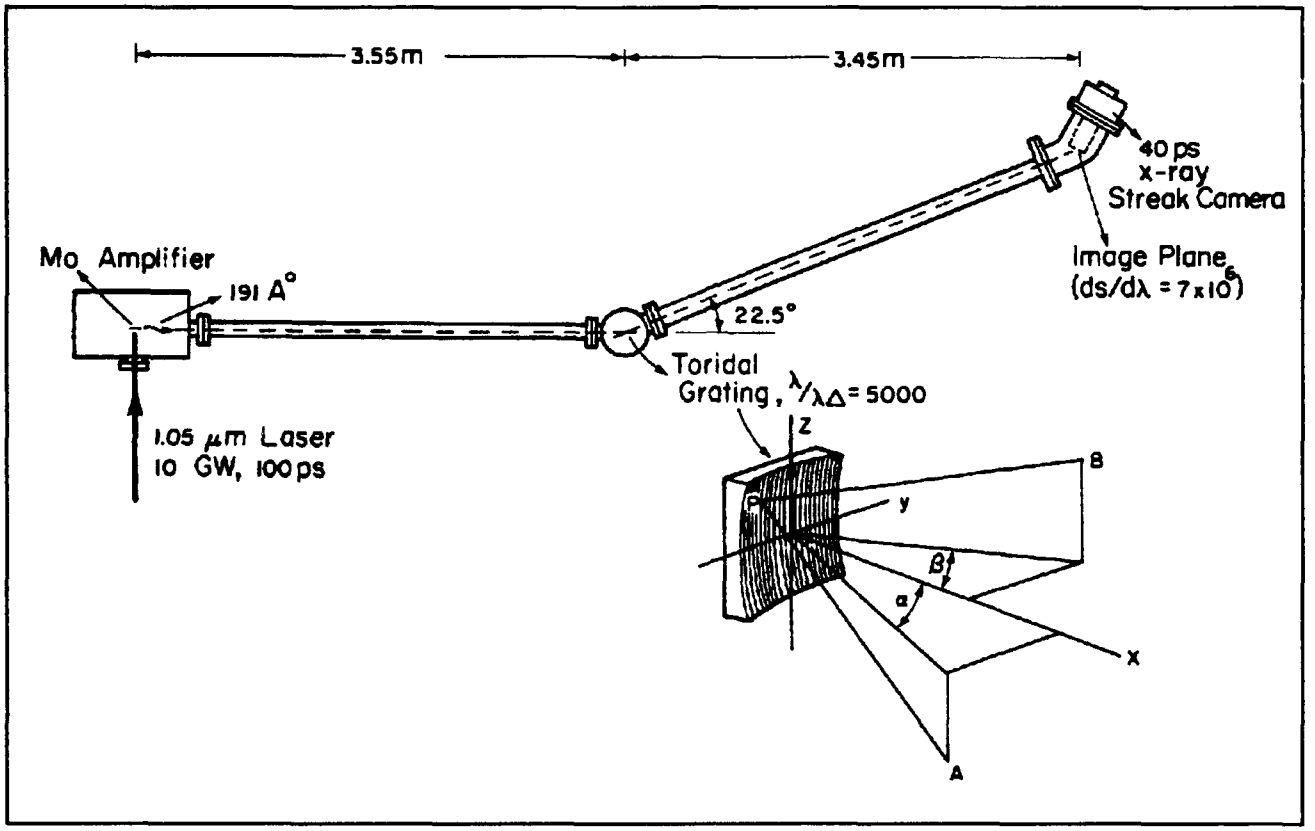

Figure 6. Holographic toroidal grating spectrometer.

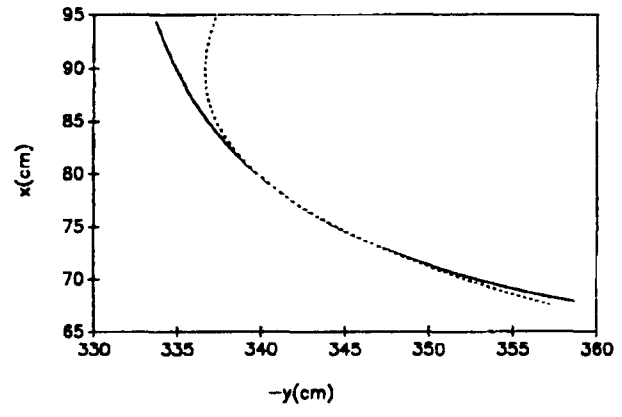

Figure 7. Solutions near image plane for meriodional (solid line) and sagittal (dashed line) imaging.

The beam divergence problem can be ameliorated by using an elongated beam path.[91] Selection of a particular shape for the beam path, however, only partially determines the required mirror shape. At each point along the beam path, the mirror surface looks locally toroidal, with two different curvatures for the directions along the beam and orthogonal to the beam. The desired beam path fixes the curvature along the beam, but the remaining curvature is determined by considerations of how the tangential beam structure should evolve.

[91] J.P. Braud, "Adiabatic Whisper-Gallery Cavities for EUV and Soft X-Ray Laser Cavities," *Proceedings of the International Conference on Lasers '89*, eds. D.G. Harris and T.M. Shay, Society for Optical and Quantum Electronics (McLean, Virginia: STS Press, 1990), pp. 37-39.

The resulting aspheric mirror shapes, although simple to describe in terms of their curvatures, are not at all like those encountered in conventional optics, and their construction appears to present a significant challenge.

As a typical example, we are interested in mirrors for which the "principal" radius of curvature, that along the direction of the beam path, takes the form $R(s) = R_0(1 - s/s^*)^{3/2}$, where s denotes length along the beam path, and where R_0 and s^* are constants; this form appears to be particularly effective in reducing the beam divergence. On the other hand, the evolution of the transverse beam structure is simplest when the the "transverse" radius of curvature Q(s) is chosen so as to keep the product R(s)Q(s) constant; this requires $Q(s) = Q_0(1 - s/s^*)^{-3/2}$. Such a mirror is illustrated in figures 8, 9, and 10.

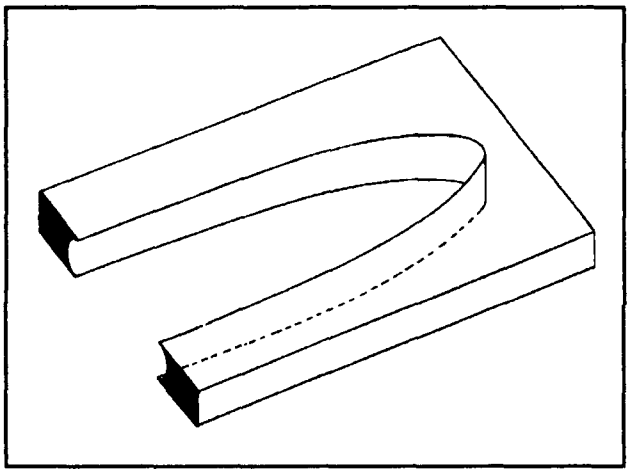

Figure 8. Sketch of the overall shape of a prototypical elongated whispering-gallery mirror.

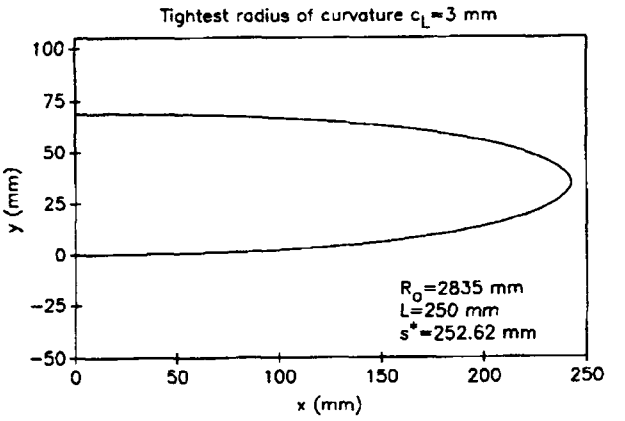

Figure 9. Prototypical elongated whispering-gallery mirror: shape of the beam path, or of the mirror as viewed from above.

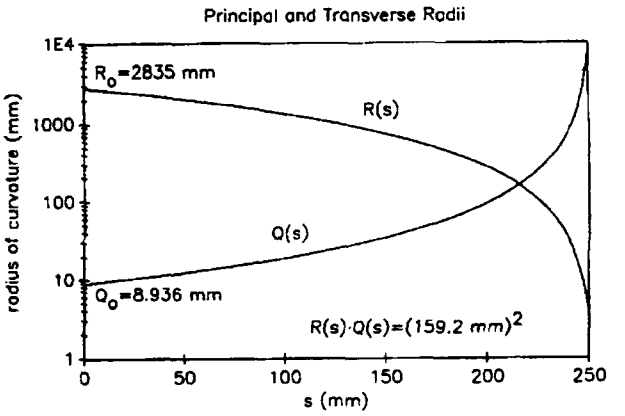

Figure 10. Prototypical elongated whispering-gallery mirror: plots of the radii of curvature. Here s = 0 corresponds to the mirror entrance, and s = 250 mm corresponds to the apex.

1.6.6 Unstable Resonators for EUV Lasers

Project Staff

Dr. Santanu Basu, John Paul Braud, Professor Peter L. Hagelstein

We are investigating the possible implementation of unstable resonators in our Ni-like Mo laser, based on multilayer mirrors[92] and on whispering-gallery mirrors.[93] In the short wavelength region, the unstable geometry has three potential advantages over other resonators. These include: (1) efficient output coupling based on diffraction rather than on transmission, (2) rapid spatial mode formation, and (3) large fractional output coupling.

A 56.3-cm long negative branch confocal strip unstable multilayer mirror resonator has been designed[94] with a magnification of 3.6, which should be capable of producing saturated output in a low divergence beam at 191Å. Fabrication of mirrors will involve growing reflective multi-layers on two concave mirror substrates of radii of curvature 24 cm and 88 cm and cutting out strips of 0.5 mm and 1.8 mm width respectively. The resonator design also makes use of two new features of this laser system: (1) the nearly constant electron density in the gain region parallel to the target surface due to one-sided illumination, and (2) synchronous amplification due to the use of a series of short pulses separated by the cavity round trip time.

1.6.7 Frequency Upconversion of EUV Radiation

Project Staff

Martin H. Muendel, Professor Peter L. Hagelstein

The advent of laser sources in the EUV and soft x-ray regimes suggests the extension of many optical laser techniques and applications to shorter wavelengths. In particular, the prospect of frequency mixing in the EUV is of special interest to our group, both for the production of a bright tunable coherent source for applications as well as for achieving shorter wavelength by means of frequency doubling.

Un-ionized matter is highly absorbing in the EUV. Efficient frequency conversion in the EUV requires low loss, and we have concluded that a low density plasma will probably be most conducive to the mixing process. This conclusion immediately rules out frequency doubling, since parity selection rules cannot be satisfied in isolated ions which are found in such plasmas.

Therefore, our approach is to study four-wave mixing in which two EUV beams are combined with an intense third optical beam to generate harder EUV radiation at roughly twice the frequency of the initial EUV beams.[95] Since it is unlikely that ions can be found with two connected transitions at the same energy (to within a few linewidths), it may not be practical to carry out four-wave mixing experiments with only one EUV laser and one optical laser. Our choice of ion was initially motivated by the hope of developing a scheme in which only a single EUV laser frequency would be required.

We have studied a four-wave mixing process in which a final frequency ω_4 is generated as $\omega_4 = \omega_1 + \omega_2 - \omega_3$, where ω_1 and ω_2 correspond to x-ray laser photons with roughly equal energies, or possibly the same energy, and ω_3 to an optical photon. This difference process is used rather

---

[92] S. Basu and P.L. Hagelstein, "Unstable Resonators for XUV Lasers," Paper CThO6, Conference on Lasers and Electro-Optics, Anaheim, California, 1990.

[93] J.P. Braud, "Whisper-Gallery Mirrors as Unstable Resonators for Short Wavelength Lasers," paper presented at CLEO,IQEC, Anaheim, California, 1990.

[94] S. Basu and P.L. Hagelstein, "Design Analysis of a Short Wavelength Laser in an Unstable Resonator Cavity," *J. Appl. Phys.* 69(4): 1853-1861 (1991).

[95] M.H. Muendel and P.L. Hagelstein, "Four-Wave Frequency Conversion of Coherent Soft X-rays," submitted to *Phys. Rev. A,* 1990; M.H. Muendel and P.L. Hagelstein, "Analysis of a Soft X-ray Frequency Doubler," *Proceedings of the International Conference on LASERS '89,* eds. D.G. Harris and T.M. Shay, 1990; M.H. Muendel, P.L. Hagelstein, and L.B. Da Silva, "Predicted Four-Wave Mixing Rates for Neonlike Yttrium X-Ray Laser Radiation in a Sodiumlike Calcium Plasma," submitted to *Phys. Rev. A,* 1991.

than the straight sum process because in positively dispersive media such as plasmas, only difference processes can be phasematched noncollinearly.

As an example, we have studied conversion in a plasma of Na-like K;[96] and more recently, we have examined conversion of the radiation of a particular x-ray laser (the Ne-like Y laser) at 155Å to yield 78Å using a Na-like Ca plasma.[97] The results indicate that frequency upconversion is somewhat more difficult in the EUV range than in the optical regime since $\chi^{(3)} \sim 1/w^4$ off-resonance; practically speaking, this translates into a more stringent requirement on the degree of resonance than at longer wavelengths. Nevertheless, where resonances can be found, efficient frequency conversion is possible.

As an example, we plot in figure 11 the expected conversion for the Na-like Ca scheme as a function of the optical photon wavelength, assuming that both x-ray photons are at 155Å and that the input laser intensities are 10^{14} W/cm^2. In the neighborhood of the resonance peaks, the conversion is seen to be considerable.

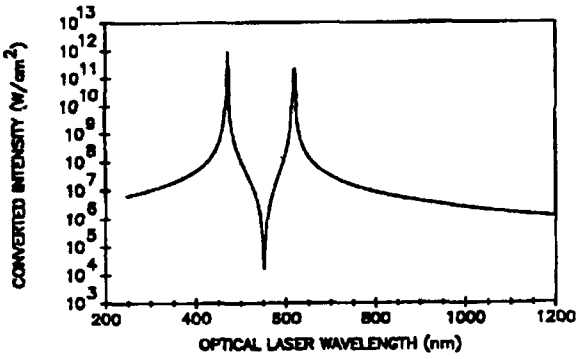

Figure 11. Non-phase-matched conversion as a function of optical laser wavelength, assuming x-ray wavelength 155Å and input intensities of 10^{14} W/cm^2.

1.6.8 X-Ray Detection Based on the MQW Nonlinearity

Project Staff

Dr. Santanu Basu

Great progress has been made during the past several years in the development of quantum well technology for optical nonlinear elements for communications, switching, and computation. In one approach, carriers produced from the absorption of one optical beam are able to alter the optical constants in the vicinity of the exciton absorption peaks, and modulate a second beam which in incident on the MQW structure. We considered the possibility that carriers could also be produced by EUV and x-ray radiation and provide a new x-ray/optical nonlinearity which could serve as the basis for a new class of x-ray detectors.[98]

We initiated a study on x-ray induced nonlinearities in quantum well structures in 1988 and proposed a planar detector scheme and a microetalon scheme for single x-ray photon detection.[98] Since then we have investigated simple designs of quantum well based detectors[99] which can be easily fabricated and can detect a flux of longer-wavelength EUV and soft x-ray radiation incident on the detector.

Once a single x-ray photon is absorbed in the quantum well, carriers are generated by inner-shell photoionization, Auger ionization, followed by collisional ionization. This carrier generation process is estimated to take place within a few picoseconds. The carriers interact with the lattice, losing energy to optical phonons.

The density of electron-hole pairs, N_c generated due to a flux of N_X x-ray photons absorbed in the material may be approximated as $N_c = N_X\eta/h$, where h is the total thickness of the quantum wells and barriers, which is chosen to be equal to the x-ray absorption depth. The average number of e-h pairs created by a single absorbed x-ray photon is $\eta = E_X/E_{eff}$. E_X is the incident x-ray energy, and E_{eff} is the effective bandgap for carrier

[96] M.H. Muendel and P.L. Hagelstein, "Four-Wave Frequency Conversion of Coherent Soft X-rays," submitted to *Phys. Rev. A,* 1990; M.H. Muendel and P.L. Hagelstein, "Analysis of a Soft X-ray Frequency Doubler," *Proceedings of the International Conference on LASERS '89,* eds. D.G. Harris and T.M. Shay, 1990.

[97] M.H. Muendel, P.L. Hagelstein, and L.B. Da Silva, "Predicted Four-Wave Mixing Rates for Neonlike Yttrium X-Ray Laser Radiation in a Sodiumlike Calcium Plasma," submitted to *Phys. Rev. A,* 1991.

[98] C. Eugster and P.L. Hagelstein, "X-ray Detection Using the Quantum Well Exciton Nonlinearity," *IEEE J. Quantum Electron.* QE-26: 75 (1990).

[99] S. Basu, "Possibility of X-ray Detection Using Quantum Wells," *IEEE J. Quantum. Electron.*, forthcoming.

production, which includes the phonon energy and the residual carrier energy and is estimated to be 4.68 eV.

For small carrier densities, the change in optical susceptibility is free of saturation effects, and the total absorption coefficient, $\alpha(E, N_c)$ can be well approximated by a linear function in the electron-hole pair density, N_c. For detection of x-rays, the probe beam will be tuned to near the exciton resonance, and the probe signal will be most affected by the change in the exciton resonace by x-ray generated carriers. We calculate a 1% change in the probe beam in a reflection geometry for an incident flux of 12 x-ray photons per μm^2.

Our analysis showed for the first time that the change in the optical susceptibility is significant enough to construct sensitive time and spatially resolved x-ray detectors. We also investigated a one-dimensional x-ray detector based on Nomarski interference technique. We showed that the time response of a quantum well detector may be diffusion limited to 50 ps by limiting its lateral dimension. Very large area detectors (six inches in diameter) could be made by growing GaAs based quantum wells on Si. Finally, quantum wells may be configured into a two-dimensional array of optical waveguides, in which longer interaction lengths will give rise to higher sensitivity.

1.6.9 Downconversion of 2ω ND:YLF Radiation

Project Staff

James G. Goodberlet, Michele M. Bierbaum

A novel x-ray susceptibility of multiple quantum wells (MQW) has been proposed.[100] In this detection scheme, incident x-ray radiation will locally change the carrier density in a MQW device. This results in a change in the real and imaginary pails of the material's refractive index. The change in optical index is largest at the material's exciton binding energy and can be observed, via phase or amplitude detection schemes, with an optical probe phase which is tuned to the exciton peak.

The proposed MQW x-ray detector requires a tunable probe source. For high temporal resolution, the optical probe should be a source of short pulses, 50 ps, which are produces synchronously with the x-ray emission. This will allow delaying of probe pulses through the x-ray pulses. The optical probe should also have adequate energy for detection purposes.

We have selected an optical parametric amplifier (OPA) as the probe source for an x-ray detector. The OPA has been selected because it meets the above requirements for an optical probe, and also because of its apparent ease of use. Namely, the OPA can be optically pumped with the same source that produces x-rays. The proposed scheme is pictured in figure 12.

For our experiments, x-rays will be generated in a plasma created by a high power, amplified Nd:YLF laser. A portion of the Nd:YLF beam will be frequency doubled to 525 nm which will then pump the OPA. The OPA will down convert the 525 nm to an unused idler frequency and a tunable signal frequency at ~ 850 nm. The 850 nm output will then be used to probe the exciton peak in GaAs multiple quantum wells.

Our strongest requirement is that the OPA have enough conversion efficiency to support adequate

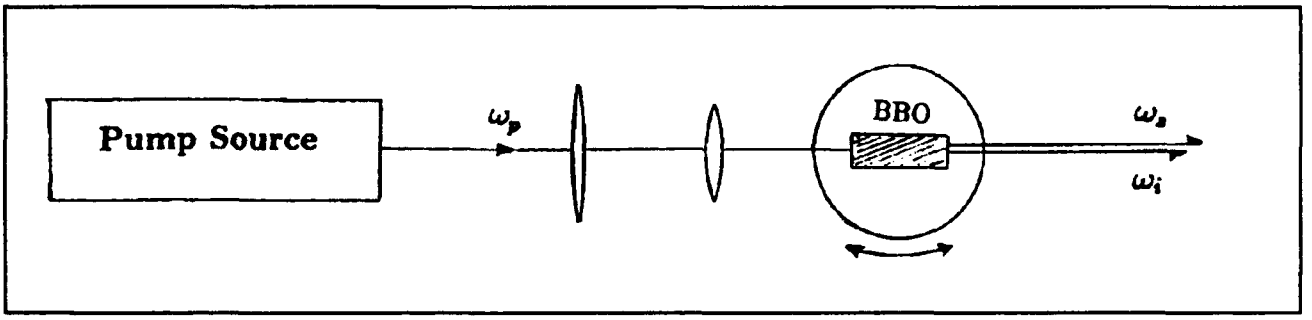

Figure 12. Optical Parametric Amplifier: The pump source provides radiation at ω_p which is focused with a beam reducing telescope into the non-linear crystal BBO. Frequency conversion occurs in the crystal and provides desired signal ω_s and unused idler ω_i outputs.

[100] C. Eugster and P.L. Hagelstein, "X-ray Detection Using the Quantum Well Exciton Nonlinearity," *IEEE J. Quantum Electron.* QE-26: 75 (1990).

probe energy or intensity at the signal wavelength. In the low conversion limit, the exponential single pass gain is proportional to crystal length and the square of the crystal's effective nonlinear coefficient. A review of currently available nonlinear crystals revealed the beta-barium borate (BBO) provides the highest conversion efficiency for our application. Figure 13 shows results of a numerical simulation of OPA conversion in the high gain regime.

The graph shows an optimal conversion length of ~ 20 mm at an pump intensity of 4 GW/cm^2. The graph shows that with proper crystal length and pump intensity, all the input radiation can be converted to signal and idler radiation. The OPA should then provide adequate probe intensity at 850 nm. Preliminary experiments are presently being conducted.

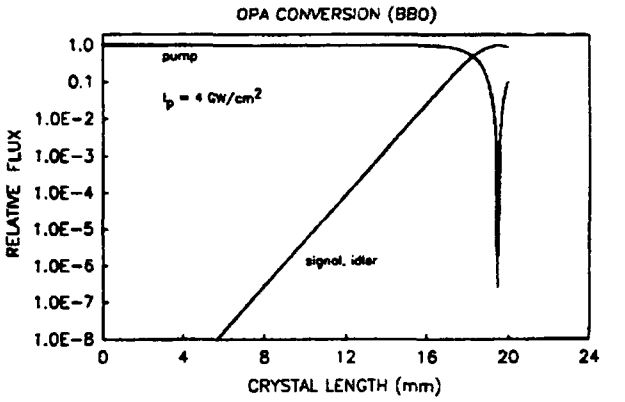

Figure 13. OPA Conversion. Results of numerical simulations in the high gain regime show that an optimal crystal length, or pump intensity, exists for complete conversion of incident pump radiation.

1.7 Generalizing Hydrodynamic Transport in Semiconductor Device Modeling

Sponsor

Columbia University
Contract P0163103

Project Staff

Sumanth Kaushik, Professor Peter L. Hagelstein

The advent of very large scale integrated circuits with submicron features has necessitated the reexamination of semiconductor transport models. The presence of hot electrons, ballistic electrons and large spatial gradients in the carrier concentration (and correspondingly large electrostatic fields) have led to the failure of conventional semiconductor transport models. Two distinct approaches to modeling the physics relevant to transport in submicron devices appear in the literature. The first approach has been to modify the standard drift-diffusion model by including additional moments of the Boltzmann transport equation (BTE). These additional moments (usually energy balance and energy flux equations) when solved together with the standard drift-diffusion equation form what is commonly referred to in the literature as the hydrodynamic model of semiconductor transport. The second approach has been to use Monte Carlo methods to stochastically solve the BTE. The latter approach is generally the most accurate method for solving transport problems in submicron devices. However, stochastic methods are not well suited for boundary value problems and, in addition, the calculations are usually computationally intensive; therefore they are not ideal for design applications.

From the viewpoint of computational complexity, hydrodynamic models are relatively straightforward to implement and are reasonably fast. In addition, boundary conditions appear naturally within the framework of the model. Despite a sizable amount of literature on the application of hydrodynamic models to device modeling, a systematic study of moment expansion methods does not exist. The focus of our research has been the development of a hydrodynamic model of semiconductor transport in which the number of moments retained in the moment expansion is an arbitrary, user supplied parameter. To date, we have adapted an algorithm due to Eddington from the field of radiation transfer to solve an infinite set of moment equations. By constructing a distribution function as an expansion over a large set of basis functions and using the moments to determine the coefficients of expansion, we are seeking an alternative to Monte Carlo methods for physical device modeling applications.

1.8 Hydrodynamic Calculations

Project Staff

Ann W. Morganthaler

An important adjunct to experiments attempting to create a plasma source of coherent x-rays will be the numerical simulation of the behavior of such a plasma. With a sophisticated, non-equilibrium, two-dimensional code which includes calculations of the transition rates between the various species in this plasma, it should be possible to accurately predict plasma temperatures, densities etc., and therefore to predict gain. These hydrodynamic calculations should then greatly aid in optimizing the

shape and composition of the x-ray targets which produce the plasma.

The hydrodynamic codes utilize an implicit Lax-Wendroff-type scheme rather than the usual explicit schemes for which the maximum time step size is severely limited. A fourth-order implicit scheme is being developed, as are codes which include realistic physical modeling rather than the very simple equations of state often used. Electron transport equations will be derived using a series of moment equations, eliminating the need for traditional flux-limited computation. The mesh will ultimately be non-uniform and adaptive, greatly reducing the number of grid points necessary for a realistic calculation. Our goal is to create hydrodynamic models which will give useful design information for the x-ray laser in a minimum amount of computation time.

1.9 Infrared Laser Studies

Project Staff

Janet L. Pan

We are exploring possibilities for new lasers operating in the thermal infrared (2-10 microns). We have investigated the trends in the future of research and applications of coherent radiation product ion in this regime. We have looked at frequency up and down conversion, free electron lasers, gas lasers, and semiconductor and other solid state lasers in this regime.

At present, we are exploring the advantages and limitations of semiconductor quantum dot lasers. At present, the common semiconductor lasers, such as the lead salt or GaSb ones, are limited to low temperature operation because of large Auger recombination rates at these infrared wavelengths. We explored the effects of reduced dimensionality on this Auger rate. Initial calculations indicate that the bound-to-bound Auger rate can be eliminated because of the discrete nature of the energy spectrum in a quantum dot. Practical considerations, such as fabrication tolerances, reduced mometum matrix elements, and the availability of materials with properties that sufficiently emulate a quantum dot, are being considered.

1.10 Approximations to the Single Photon Exchange Interaction

Project Staff

Professor Peter L. Hagelstein, Isaac L. Chuang

Self-energy corrections for highly-stripped and highly charged ions have proven to be difficult to calculate, primarily because of the lack of well-developed systematic methods for evaluating the relevant Feynman diagrams accurately in a nonperturbative scheme. Presently, Lamb shifts for high-Z one-electron systems are calculated using variants of Brown's method which rely heavily on properties of the Dirac-Coulomb Green's function. We have derived an alternative approach based on a generalized partial-wave decomposition which is valid for general potentials (including those for multi-electron atoms).[101] Our approach leads to a numerical technique for obtaining systematic approximations for non-separable matrix elements of the photon exchange operator with full retardation, in terms of a summation of matrix elements of operators which are separable in radial coordinates.

The single photon exchange operator including full retardation in the Feynman Gauge is given by

$$V(\omega; r_1, r_2) = \frac{2}{\pi}[\alpha_1\alpha_2 - 1]\int_0^\infty \frac{1}{\omega + k}\frac{\sin(k|r_1 - r_2|)}{|r_1 - r_2|}\,dk. \quad (1)$$

Low momentum simplification and angular decomposition of this approximation lead directly to the Coulomb interaction (and Breit interaction, in the Coulomb gauge). Unfortunately, direct angular decomposition of this operator does not result in terms which are easily separable into radial and angular coordinates. The use of this operator directly in place of the Coulomb and Breit interaction in atomic physics calculations would lead to a theory in which nonseparable 2-D radial matrix elements would appear.

However, our technique makes this new approach computationally practical. The basic idea is to expand the nonseparable photon exchange operator with full retardation in terms of a series of closely related separable operators. This idea may be summarized by the approximation

[101] P.L. Hagelstein, "On the Partial-Wave Method for Self-Energy Calculations in Non-hydrogenic Ions," *Proceedings of the First International Conference on Coherent Radiation Processes in Strong Fields,* Catholic University, Washington D.C., June 1990.

$$V(\omega; r_1, r_2) \approx \qquad (2)$$

$$\frac{2}{\pi}\sum_i a_i(\omega)[\alpha_1\alpha_2 - 1]\int_0^\infty \frac{k}{b_i^2(\omega)+k^2}\frac{\sin(k|r_1-r_2|)}{|r_1-r_2|}\,dk.$$

The key point of this expansion is that each term in the summation is easily and accurately evaulated in terms of 1-D radial integrals.

Easily accessible numerical algorithms such as ours, which allow the use of the photon exchange operator with full retardation, promise to have a significant impact on atomic physics calculations. Additionally, the new class of algorithms we are developing will allow computations to be done accurately which have historically been deemed impractical.

Currently, we are in the process of systematically quantifying numerical sources of error, in preparation for detailed calculations of self-energy corrections for non-hydrogenic systems, beginning with Li-like, Na-like, and Cu-like systems. Our experience thus far indicates that it may be feasible to maintain 10-digit accuracy throughout our calculations.[102]

1.11 Coherent Neutron Transfer Reactions

Sponsor

U.S. Department of Energy
Grant DE-FG02-89-ER14012

Project Staff

Professor Peter L. Hagelstein

In last year's report, we described the status of coherent fusion theory and the depp reaction scenario. In analyzing this scenario, we have found a new mechanism for resonantly transferring energy between nuclear systems and macroscopic systems.[103] Although not widely appreciated, it appears that standard quantum mechanics predicts the possibility of phonon-induced removal and capture on neutrons from nuclei.

The arguments leading to this conclusion are straightforward; if we consider the coherent transfer of neutrons from deuterium, or the coherent capture of a neutron by proton, then we may describe the transition hamiltonian through

$$\hat{H}_{pd} =$$

$$-\sum_j\int\int\int \hat{\Psi}_n^\dagger(r_1)\hat{\Psi}_p^\dagger(r_2)\mu_j \bullet B(r_j)\hat{\Psi}_d(r_1, r_2)d^3r_1 d^3r_2$$

$$-\sum_j\int\int\int \hat{\Psi}_d^\dagger(r_1, r_2)\mu_j \bullet B(r_j)\hat{\Psi}_n(r_1)\hat{\Psi}_p(r_2)d^3r_1 d^3r_2$$

where the capture or removal is driven by a magnetic dipole transition. The field operators for the protons and deuterons are given by

$$\hat{\Psi}_p(r) = \sum_i\sum_\alpha \hat{b}_{p,\alpha}(i)\phi_p(r-\hat{R}_i)\chi_\alpha^{1/2}$$

and

$$\hat{\Psi}_d(r_1, r_2) = \sum_i\sum_\alpha \hat{b}_{d,\alpha}(i)\phi_d(r_1-\hat{R}_i, r_2-\hat{R}_i)\chi_\alpha^1$$

where $\hat{R}_i$ is a center of mass nucleon position operator which is a function of the lattice mode amplitude operators

$$\hat{R}_i = R_i^o + \sum_m \hat{q}_m u_m(i)$$

Of course the lattice itself differs before and after the transfer by one nucleon, and hence the lattice position operator differs before and after the reaction.

The transition operator is observed to be a highly nonlinear function of the phonon mode amplitudes; if sufficient excitation of a small subset of the phonon modes occurs, then it is possible that the lattice energy can be transferred to and from the nuclear system. One condition that the transition operator produce a large associated matrix element is that the positions of the proton and nucleon within the lattice coincide briefly micro-

---

[102] P.L. Hagelstein, I.L. Chuang, "Approximations to the Single Photon Exchange Interaction with Full Retardation," submitted to *J. Phys. B.*, April 1991.

[103] P.L. Hagelstein, "Coherent Fusion Mechanisms," *Proceedings of the Conference on Anomalous Processes in Deuterated Metals*, Brigham Young University, Salt Lake City, Utah, October 1990; P.L. Hagelstein, "Coherent Neutron Transfer Reactions," submitted to *J. Fusion Tech.* (1991).

scopically to within fermis; this occurs repeatedly for certain lattice motions, and if the process is repeated at enough sites over suffcient vibrational cycles, then a transfer may occur.

This mechanism results in a theory for energy generation in which neutrons are promoted to lattice Bragg states from "donor" nuclei due to coherent lattice excitation; and the coherently captured on "acceptor" nuclei through a reverse version of the coherent process. The mechanism is illustrated in figure 14.

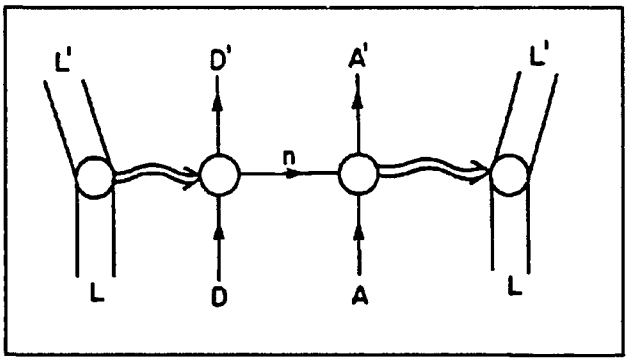

Figure 14. General neutron transfer reaction from donor to acceptor nuclei.

Professor Qing Hu explains the phenomenon of photon-assisted tunneling in superconducting tunnel junctions to graduate students.

Chapter 2. Superconducting Electronic Devices

Academic and Research Staff

Professor Qing Hu, Professor Terry P. Orlando, Dr. John Melngailis, Dr. Ivan V. Zitkovsky

Graduate Students

Partha Saha, Rolf Wyss

Technical and Support Staff

Barbara A. King

2.1 High T_c Superconducting SQUIDs and Mixers

Sponsor

Defense Advanced Research Projects Agency
Contract MDA 972-90-C-0021

Project Staff

Professor Qing Hu, Professor Terry P. Orlando

Many superconducting analog devices have been demonstrated to have higher sensitivities, speed, and frequency limits and lower power dissipation than competing semiconductor devices. Among the superconducting devices, the most successful ones are SQUIDs (Superconducting QUantum Interference Devices) and mixers.

Similar to its optical analog, the Mach-Zehnder interferometer, a SQUID is an interferometer composed of two waves of superconducting electrons. By modulating the relative phases of the two waves using a small magnetic field, a SQUID magnetometer can achieve the sensitivity of a faction of magnetic quantum flux. Superconducting mixers use the high nonlinearity of the current-voltage characteristics of superconducting tunnel junctions to perform high-efficiency mixing. Currently, superconducting mixers have the highest sensitivities which are only limited by Heisenberg's uncertainty principle.

The discovery of superconductors with a superconducting transition temperature higher than liquid nitrogen temperature (high-T_c superconductors) has opened up exciting new possibilities in electronic device technology. The high temperature version of the superconducting devices mentioned above will have a much wider range of applications wherever refrigeration is a problem. However, the benefit of higher operating temperature has posed a new challenge which is not encountered in conventional superconducting devices. The key element for both SQUIDs and mixers is the so-called Josephson junction. This junction is formed by two superconductors weakly coupled together electrically. Heisenberg's uncertainty principle dictates that higher transition temperature will result in a shorter superconducting coherence length. This is the length scale at which superconductivity vanishes at an interfacial boundary. Consequently, high-T_c Josephson junctions require that the weaklink regions are much smaller than those for low T_c devices.

In collaboration with Dr. Melngailis' group, we have invented several novel ways of making high T_c superconducting devices using focused ion beams (FIB). FIBs can be used to either lithographically pattern high-T_c superconducting films or to directly pattern the films or the substrates to form Josephson junctions. Currently, we are optimizing our process to improve the quality of the Josephson junctions.

This work is being performed with the cooperation of the AT&T Bell Laboratories in Murray Hills, New Jersey.

2.2 Millimeter Wave and Infrared Superconducting Receivers

Sponsor

Defense Advanced Research Projects Agency
Contract MDA 972-90-C-0021

Project Staff

Professor Qing Hu

Although there is great potential for applications in remote sensing and communication, millimeter wave and far-infrared frequencies remain one of the most underdeveloped frequency ranges. This is because the millimeter wave and far-infrared frequency range falls between the two other frequency ranges in which conventional

semiconductor devices are usually operated. One is the microwave frequency range, and the other is the near-infrared and optical frequency range. Semiconductor devices which utilize the classical diffusive transport of electrons, such as diodes and transistors, have a high frequency limit. This limit is set by the time it takes for electrons to travel a certain distance. Currently, electron mobility and the smallest feature size which can be fabricated by lithography limit the frequency range to below 100 GHz. It is not likely that this limit can be pushed much higher. Semiconductor devices based on quantum mechanical interband transitions, however, are limited to frequencies higher than those corresponding to the semiconductor energy gap, which is higher than 10 THz for most bulk semiconductors. Therefore, a large gap exists from 100 GHz to 10 THz in which very few devices are available.

The gap energies of conventional superconductors such as Nb are in the range of 100 GHz to 2 THz. This coincidence makes superconducting devices natural candidates for millimeter and submillimeter wave applications. In addition, superconducting devices usually have higher sensitivities and speed and lower power dissipation than semiconductor devices. Two types of superconducting devices are studied in this project: coherent heterodyne receivers and incoherent radiation detectors. The former has potential applications in communication as well as radiation detection, while the latter is usually used for remote sensing.

At millimeter wave frequencies, superconducting radiation detectors have their current responsivity approaching the quantum efficiency $e/\hbar\omega$, that is, a transport of one electron for one incoming photon. Such efficiencies have been achieved only at much higher frequencies by semiconductor photoconductive detectors. Therefore, superconducting radiation detectors may find wide-range applications in remote sensing and far-infrared spectroscopy.

At millimeter and submillimeter wavelengths, the superconducting coherent receivers have their sensitivities limited only by the zero-point fluctuation of vacuum. Such receivers have been used widely in astrophysical studies. More applications are feasible in space-based communication and far-infrared spectroscopy, which requires ultimate sensitivity.

This work is being performed with the cooperation of the MIT Lincoln Laboratory, IBM Corporation's Thomas J. Watson Research Center at Yorktown Heights, New York, and the AT&T Bell Laboratories in Murray Hills, New Jersey.

Section 3 Surfaces and Interfaces

Chapter 1. Statistical Mechanics of Surface Systems and Quantum-Correlated Systems

Academic and Research Staff

Professor A. Nihat Berker

Graduate Students

Daniel P. Aalberts, Alexis Falicov, William C. Hoston, Jr., Roland R. Netz

Technical and Support Staff

Imadiel Ariel

1.1 Introduction

Sponsor

Joint Services Electronics Program
Contract DAAL03-89-C-0001

Our objectives are (1) to produce predictive quantitative properties from first principles for surface systems and systems in which quantum correlations are important, (2) to deduce, using the renormalization-group method of statistical mechanics, broadly relevant properties of condensed matter, and to explore their application to systems of coupled electronic, structural, and magnetic degrees of freedom. In this research, fluctuation dominated — due to finite temperatures, impurities, and/or constrained environments — properties are of paramount interest.

Our recent results, detailed in the following sections, show that both objectives can be achieved. We are in the uniquely fortunate position of having integrated the finite-temperature renormalization-group expertise of our group with the electronic energy calculations of Professor Joannopoulos' group. Thus, microscopic theories can be produced that start with Schroedinger's equation and end with predictions directly observable in the laboratory.

1.2 Finite-Temperature Properties of Vicinal Si(100) Surfaces

In collaboration with Professor J.D. Joannopoulos, we have combined electronic energy calculations and finite-temperature statistical mechanics to study, for the first time, the equilibrium properties of the Si(100) surface. The occurrence of single-layer (SL) or double-layer (DL) steps on these — purposefully — misoriented surfaces has important consequences for the growth of GaAs on Si(100), DL steps not disturbing the epitaxy conditions, while SL steps leading to undesirable antiphase domains. We have predicted, in the variables of temperature and crystal cut angle, a phase boundary between these two regimes, which has been quantitatively confirmed by experiments (figure 1).

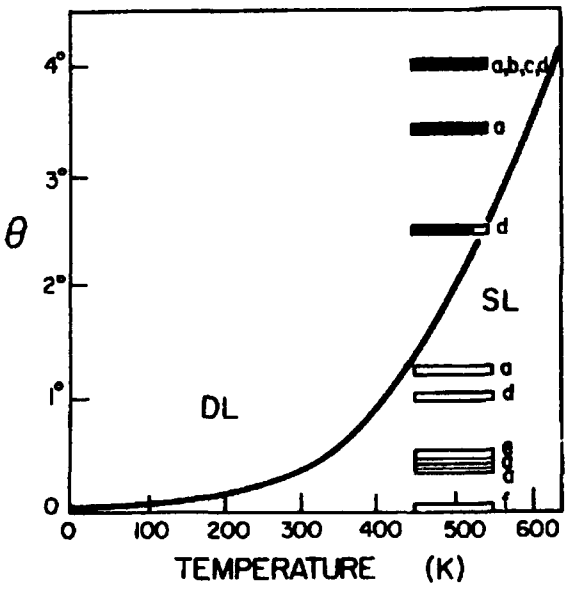

Figure 1. Our calculated phase diagram of vicinal Si(100) in the variables of crystal cut angle and temperature. The solid curve is our theoretically predicted line of first-order phase transitions between the single-layer (SL) and double-layer (DL) stepped surface phases. Open and solid bars represent experimental observations of SL and DL stepped surfaces. The bar at ≈2.5° in fact represents observation of a mixed phase of mostly DL steps!

To conduct this work, we were able to formulate a new Hamiltonian for the temperature-roughened

steps that embodied the accurate electronic calculations of the energies and that was amenable to statistical mechanics calculations. In addition to the phase diagram, which is consistent with new experimental data otherwise unexplained and which brings together into a coherent picture all the existing data on the domain structure of stepped Si(100), we have obtained the free energy, the entropy, as well as the step profiles (figure 2) which are in good agreement with experimental observations. For annealed surfaces, we find that the critical angle at which the transition between SL and DL stepped surfaces occurs is $\approx 2°$, also in agreement with experiment. Before we obtained these results, it was erroneously believed that vicinal Si(100) surfaces have only one equilibrium phase with only DL steps present! Our work has directly and immediately motivated a new set of (confirming) experiments.

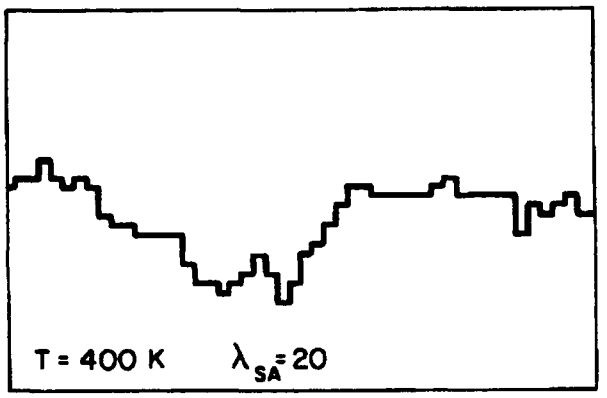

Figure 2. Our calculated step profile on Si(100) at 1 degree misorientation. In our theory, straight steps occur at the horizontal boundaries of the figure. This picture is in remarkable agreement with subsequent observations using scanning tunneling microscopy.

1.3 Impurity-Induced Critical Behavior

Another recent theoretical prediction that we made using the renormalization-group method appears to have general and far-reaching consequences: We discovered that even an infinitesimal amount of randomness in interactions (e.g., distribution of defects), in surface systems, converts first-order phase transitions, characterized by discontinuities, to second-order phase transitions, characterized by infinite response functions. In bulk systems, a (calculable) threshold randomness is needed for this conversion to occur. This general prediction appears to be supported by experiments on doped $KMnF_3$ and by most recent computer simulations.

More specifically, temperature-driven first-order phase transitions that involve a symmetry breaking are converted to second-order phase transitions by the introduction of infinitesimal bond randomness, in spatial dimensions $d \leq 2$ or $d \leq 4$ respectively for systems composed of discrete or continuous microscopic degrees of freedom. Even strongly first-order transitions undergo this conversion to second order! Above these dimensions, this phenomenon still occurs, but requires a threshold amount of bond randomness. For example, under bond randomness, the phase transitions of q-state Potts models, widely encountered in the context of structural and magnetic transitions, are second order for all q in $d \leq 2$. If no symmetry breaking is involved, temperature-driven first-order phase transitions are eliminated under the above conditions. Another consequence of this phenomenon is that bond randomness drastically alters multicritical phase diagrams. For example, tricritical points and critical endpoints are entirely eliminated ($d \leq 2$) or depressed in temperature ($d > 2$ for both discrete and continuous degrees of freedom). These predictions have been confirmed by a renormalization-group calculation. Similarly, bicritical phase diagrams are converted ($d \leq 2$) reentrant-disorder-line or decoupled-tetracritical phase diagrams. These quenched-fluctuation-induced second-order transitions constitute a diametric opposite to the previously known annealed-fluctuation-induced first-order transitions, and point to a multitude of new universality classes of criticality, including many experimentally accessible cases.

This general result should have applications to crystals used as probing devices. These probing crystals are plagued by first-order phase transitions with non-equilibrium hysteresis loops. It would be useful to replace these transitions, via the controlled introduction of randomness (which, we think, could be achieved by crossed laser beams reflected from rough surfaces), by second-order phase transitions with large response functions.

1.4 Monte Carlo Mean-Field Theory and Frustrated Systems in Two and Three Dimensions

We have recently developed a new method of statistical mechanics, merging the effective-field and Monte Carlo approaches. This method brings for the first time to effective-field theory the hard-spin condition, essential to (frustrated) spin systems with competing interactions, and uses much less sampling then Monte Carlo simulation. This method was successfully tested on frustrated Ising magnets in d=2 and 3, in zero and non-zero uniform fields. The phase diagram of the d=2 tri-

angular antiferromagnet was easily obtained with remarkable global quantitative accuracy. The phase diagram of the d=3 stacked triangular antiferromagnet was found to show three ordered phases, in a new finite-field multicritical topology of lines of XY, Ising, and 3-state Potts transitions, accessible to experiments with layered magnets. This result also explains for the first time critical exponents measured at zero field, via crossover phenomena.

Our new method, thus applicable to frustrated system, will be developed towards frustrated quantum spins, which is relevant to high-temperature superconducting systems.

1.5 Quantum Systems

One aim of our research program is to effect the statistical mechanics of quantum mechanical systems. We now report encouraging preliminary results. Progress is achieved by systematically mapping d-dimensional quantum mechanical systems onto (d+1)-dimensional classical systems, but with complicated many-body interactions. Figures 3 and 4 show our calculated results for chains of s=1/2 spins exchange-coupled via their x and y components (known as the XY magnet). Figure 3 shows that our successive approximations to the internal energy systematically and quickly converge to the exact result. Moreover, exact information available to-date on quantum systems is very limited and piecemeal. By contrast, the statistical mechanical solution of the (d+1) dimensional system in our procedure is an entire solution, providing every equilibrium property of the original quantum system. Thus, figure 4 shows the correlation function of the XY chain, for which no information had been available.

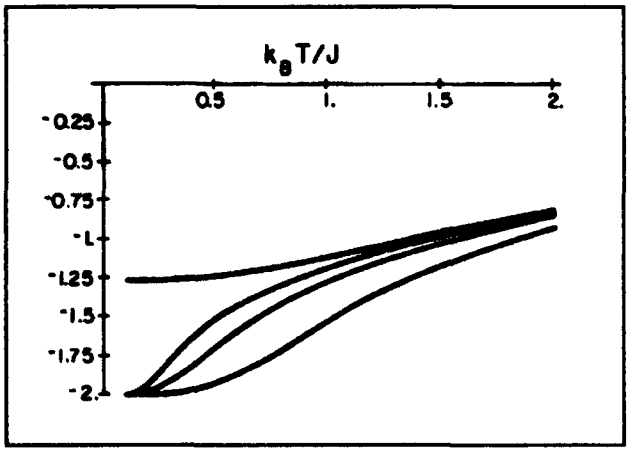

Figure 3. Internal energy of the quantum XY spin chain as a function of temperature. The upper curve is the exact result. The lower curves are our calculations of systematically improved approximations.

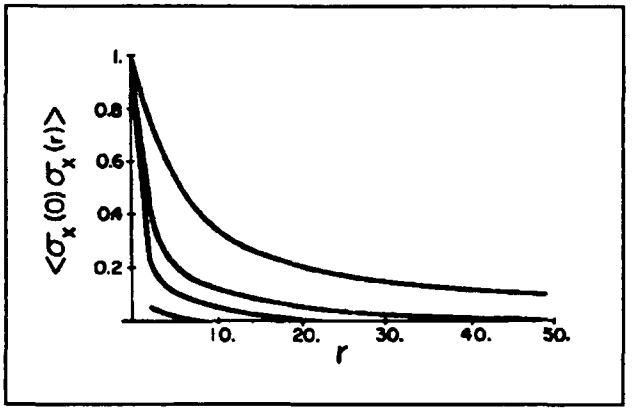

Figure 4. Our calculated correlation functions of the quantum XY spin chain as a function of spin separation. The curves are for temperatures $T = J/k_B$, $2J/k_B$, $3J/k_B$, and $5J/k_B$, where J is the exchange coupling constant. No exact result exists for the correlation function.

We plan to extend our calculations to two-dimensional quantum systems. One system of interest is the d=2 XY magnet, in which the occurrence of a distinctive algebraically ordered phase is controversial. Another system of interest is the d=2 triangular Heisenberg antiferromagnet, which is relevant to high-temperature superconductors. In the latter systems, the interplay of frustration and thermal vacancies is crucial. We believe that our previous work on frustrated triangular systems (Section 4 above) and on thermal vacancies will be helpful. By applying renormalization-group statistical mechanics, we should be able to include even the weak interplanar coupling of the real materials. The subsequent aim of our studies is to include both particle and spin degrees of freedom in considering quantum-mechanical electronic systems.

Publications

Alerhand, O.L., A.N. Berker, J.D. Joannopoulos, D. Vanderbilt, R.J. Hamers, and J.E. Demuth. "Finite-Temperature Phase Diagram of Vicinal Si(100) Surfaces." *Phys. Rev. Lett.* 64 (20): 2406-2409 (1990).

Alerhand, O.L., A.N. Berker, J.D. Joannopoulos, and D. Vanderbilt. "Phase Transitions on Misoriented Si(100) Surfaces." In *20th International Conference on the Physics of Semiconductors.* Eds. E.M. Anastassakis and J.D. Joannopoulos. Singapore: World Scientific, 1990.

Alerhand, O.L. "Equilibrium Properties of Steps on Si(100) Surfaces." Paper to be presented at the General Meeting of the American Physical

Society, Cincinnati, Ohio, March 18-22, 1991. *Bull. Am. Phys.* 36(3): 587 (1991).

Alerhand, O.L., A.N. Berker, J.D. Joannopoulos, D. Vanderbilt, R.J. Hamers, and J.E. Demuth. "Alerhand et al. Reply." *Phys. Rev. Lett.* 66(7): 962 (1991).

Berker, A.N., and K. Hui. "Absence of Temperature-Driven First-Order Phase Transitions in Systems with Random Bonds." In *Science and Technology of Nanostructured Magnetic Materials.* Eds. G.C. Hadjipanayis, G. Prinz, and L. Paretti. New York: Plenum, 1990.

Berker, A.N. "Quenched Fluctuation Induced Second-Order Phase Transitions." Paper to be presented at the General Meeting of the American Physical Society, Cincinnati, Ohio, March 18-22, 1991. *Bull. Am. Phys.* 36(3): 439 (1991).

Berker, A.N. "Harris Criterion for Direct and Orthogonal Quenched Randomness." *Phys. Rev. B* 42(13): 8640-8642 (1990).

Hui, K., and A.N. Berker. "Random-Field Mechanism in Random-Bond Multicritical Systems." *J. Appl. Phys.* 67(9): 5991 (1990).

McKay, S.R., and A.N. Berker. "Magnetization of the d-Dimensional Random-Field Ising Model: An Intermediate Critical Dimension." In *New Trends in Magnetism.* Eds. M.D. Coutinho-Filho and S.M. Rezende. Singapore: World Scientific, 1990.

Netz, R.R., and A.N. Berker. "Monte Carlo Mean-Field Theory and Frustrated Systems in Two and Three Dimensions." *Phys. Rev. Lett.* 66(3): 377-380 (1991).

Netz, R.R. *Frustration in Magnetic, Liquid Crystal, and Surface Systems: Monte Carlo Mean-Field Theory.* S.M. thesis, Dept. of Physics, MIT, 1991.

Chapter 2. Synchrotron X-Ray Studies of Surface Disordering

Academic and Research Staff

Professor Robert J. Birgeneau, Dr. Kenneth I. Blum

Graduate Students

Alan Mak, Do-Young Noh, William J. Nuttall, Monte Ramstad

Technical and Support Staff

Elizabeth M. Salvucci

2.1 Introduction

Sponsor

Joint Services Electronics Program
DAAL03-89-C-0001

In this research program we use modern x-ray scattering techniques to study structures and phase transitions in thin films and on surfaces. We have two principal experimental facilities, one at MIT and the other at the National Synchrotron Light Source at Brookhaven National Laboratory. At MIT, we have four high-resolution computer-controlled x-ray spectrometers using high-intensity, rotating anode x-ray generators. The angular resolution can be made as fine as 1.8 seconds of arc, which enables us to probe the development of order from distances of the order of the x-ray wavelength, ~ 1Å, up to 30,000Å. The sample temperature can be varied between 2 K and 500 K with a relative accuracy of 2×10^{-3} K. At the National Synchrotron Light Source at Brookhaven National Laboratory, in collaboration with IBM, we have three fully instrumented beam lines. Two of these beam lines allow studies with photons varying in energy between 3 and 12 keV; the third has a fixed energy of 17 keV. These facilities make possible high-resolution scattering experiments with a flux of more than three orders of magnitude larger than that of a rotating anode x-ray generator, opening up a new generation of experiments.

Several years ago, as part of this JSEP program, we built an x-ray-compatible, high vacuum single crystal apparatus. This enabled us to use synchrotron radiation to study the structures and transitions occurring at a single surface, and such experiments are now becoming routine. As a result of our recent research, we have determined that a new chamber allowing access to a wider range of reciprocal space is required. In collaboration with Professor Simon G.J. Mochrie, we have designed, and are currently constructing, this second-generation x-ray surface facility.

Our basic scientific objective is to understand the morphologies and microscopic structures of simple semiconductor and metal surfaces at high temperature. Possible phase changes include surface roughening, surface reconstruction, melting, amorphization and dilution. These phenomena are particularly interesting on stepped surfaces, where there may be an interplay between step structures, faceting, reconstruction, and roughening.

2.2 Metal Surface Studies

Previously, we carried out a detailed synchrotron x-ray study of the surface phases and phase transitions of a Au(110) surface. This specific Au(110) crystal had as its stable structure a 1×3 missing-row reconstruction. This corresponds to a periodic array of 4-atom wide (111) microfacets. The transition from this 1×3 structure to a 1×1 structure at 760 K involved a simultaneous deconstruction and roughening.

After further treatment of this same Au crystal we were able to obtain a stable 1×2 phase on the (110) surface. This latter phase is the one most commonly observed in previous experiments. The 1×2 structure corresponds to a periodic array of 3-atom wide (111) microfacets. There are subtle distortions at these faces of the atoms away from their bulk positions. We have performed a synchrotron x-ray scattering study of the thermal disordering of this Au(110) 1×2 reconstructed surface. Observing the temperature dependence of the in-plane superlattice and integral order surface peaks, as well as the $(\ell\ \ell\ 0)$ specular reflectivity,

we find that at Tc = 735 K the 1 × 2 surface undergoes a reversible deconstruction transition characterized by a proliferation of compact anti-phase defects with no measurable change in the density of surface steps. This transition is described by critical exponents close to those characterizing a two-dimensional Ising transition. We also find that by 784 K there has been a significant increase in the density of surface steps of the type associated with surface roughening. This suggests that the Au(110) surface disorders in a two step process, deconstruction followed by roughening, with a difference in the two transition temperatures of less than 50 K. This contrasts with the behavior we previously found for Au(110) 1 × 3 and which has been found recently by Robinson and coworkers[1] in Pt(110).

2.3 Semiconductor Surface Studies

2.3.1 Ge(111)

Currently, experimental information on the morphology of semiconductor surfaces near the bulk melting point is very limited, in spite of its evident importance in many growth processes. The Ge(111) surface has been reported to undergo a phase transition at a crystal temperature of about 1050 K, which is 160 K below the bulk melting temperature Tm (1210 K). The nature of the transition remains controversial.

At room temperature, a c(2 × 8) structure on the Ge(111) surface is stable. Near 573 K, the c(2 × 8) reconstruction converts to a (1 × 1) phase. The (1 × 1) structure may not have an ideally terminated bulk structure; adatoms are believed to be present. At higher temperatures a second structural transition of the Ge(111) surface was first suggested by Lever in 1968.[2] He found that the sticking coefficient of oxygen on Ge(111) dropped precipitously with increasing crystal temperature near 1050 K. McRae and Malic recently studied this reported transition in a Low-Energy Electron Diffraction (LEED) experiment.[3] The intensity of the surface diffraction peaks decreased rapidly near 1050 K saturating at a low but non-zero value. The results were interpreted on the basis of a heuristic model in which the outermost double layer of the Ge(111) consists of incommensurate crystalline islands surrounded by a disordered sea. Electron Energy Loss Spectroscopy done on a Ge(111) single crystal surface, as well as on liquid and amorphous Ge overlayers, suggested that the high temperature disordered Ge(111) surface resembles an amorphous layer more than a liquid layer. Ion scattering indicated that above ~ 1050 K there are local departures of surface atoms from their equilibrium lattice positions.

We have studied the Ge(111) surface using synchrotron x-ray scattering techniques with a glancing angle scattering geometry. Representative scans through the (10) peak at a series of temperatures bracketing 1070 K are shown in figure 1. It is evident that well-defined sharp peaks are observed up to temperatures near bulk melting; significantly, there is no important change in lineshape throughout this temperature range. Similar data are obtained for the (20) peak. The (10) and (20) peak intensities decrease gradually with increasing temperature above ~ 900 K, go through pronounced minima at about 1070 K and then partially recover.

From these data one may exclude all existing models for the surface disordering of Ge(111). We have, however, been able to show that a model involving surface vacancies gives a unique description of our data and is consistent with previous results. Specifically, we hypothesize that near 1000 K, thermally-generated random vacancies in the surface bilayer begin to proliferate. From a quantitative analysis we find that the surface vacancy concentration rises rapidly between ~ 950 K and 1080 K and then saturates; the limiting vacancy concentration is near 50 percent. We are also able to demonstrate that the vacancy concentration decays rapidly to the interior layers.

One important consequence of the high surface vacancy concentration is a dramatic growth in the rate of sublimation. So far there is little quantitative information on sublimation from defected surfaces. We plan to study this problem in more detail in the future.

---

[1] I.K. Robinson, E. Vlieg, and K. Kern. *Phys. Rev. Lett.* 63: 2578 (1989).

[2] R.F. Lever, *Surf. Sci.* 9: 370 (1968).

[3] E.R. McRae and R.A. Malic, *Phys. Rev. Lett.* 58: 1437 (1987); *Phys. Rev. B* 38: 13163 (1988).

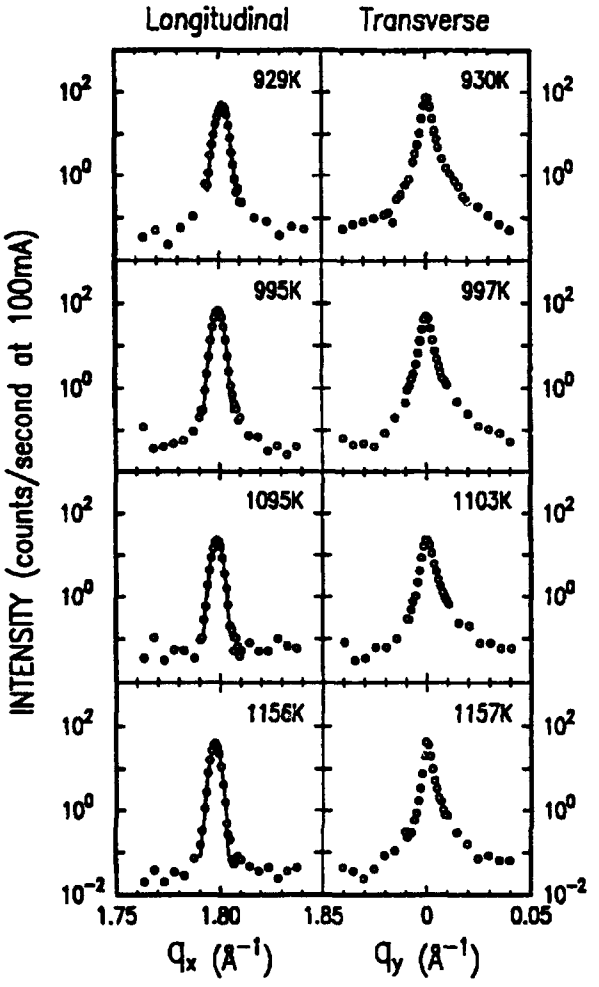

Figure 1. *Longitudinal and transverse scans through* the (10) peak are shown for four different temperatures: 929 K, 995 K, 1095 K, and 1156 K. The central portion of each of the longitudinal scans is fit to a Gaussian curve. All widths fall within ± 10% of the instrumental width of 0.0022Å^{-1} HWHM.

2.4 Stepped Si(111) Surfaces

The behavior of vicinal surfaces (surfaces cut a few degrees away from low index facets) involves essential aspects of surface structures including equilibrium crystal shapes, roughening, faceting, and surface reconstruction. The stability of vicinal surfaces is determined by the shape of the equilibrium crystal surface. By studying a series of vicinal surfaces with various surface normals, one can map out the equilibrium crystal shape. A vicinal surface, when it is stable, forms a structure consistent with low-index terraces separated by steps whose spacing is usually incommensurate with the bulk substrate lattice. As in the case of incommensurate domain wall problems, there can not be true long range order in the structure of the incommensurate steps. This is due to the overwhelming amplitude of the long wavelength thermal fluctuations in two-dimensional systems with continuous symmetry. As a result, an incommensurate stepped surface is rough in an exact sense. A vicinal surface becomes unstable when the free energy of a nearby low index facet is lowered drastically by some mechanism such as reconstruction. One might expect that the lowering of the free energy of a low-index facet would break a vicinal surface into a low-index facet and rough faces with a higher misorientation angle.

We have carried out a preliminary synchrotron x-ray scattering study of a vicinal Si(111) surface misoriented by 3.5° toward the (11$\bar{2}$) direction. At temperatures higher than the 7 × 7- to -1 × 1 transition, we find that the surface is composed of steps with a mean separation of ~ 60Å which are correlated beyond 3000Å. Below the transition, the surface is split into large (> 3000Å) perfectly flat (111) facets together with stepped regions whose misorientation angle increases as temperature is decreased. The transition is first order, indicating that it is induced by the 7 × 7 reconstruction of the (111) facets. We are currently analyzing these data in terms of the equilibrium crystal shape of Silicon. We also have discovered other faceting configurations with higher indices which are presumably stabilized by impurities.

Both future experiments and future theoretical analysis are planned on this important problem.

2.5 Publications

Keane, D.T., P.A. Bancel, G.L. Jordan-Sweet, G.A. Held, A. Mak, and R.J. Birgeneau. "Evidence for Two-Step Disordering of the Au(110) 1 × 2 Reconstructed Surface." *Surface Sci.* Forthcoming.

Mak, A., K. Evans-Lutterodt, K. Blum, D.Y. Noh, J.D. Brock, G.A. Held, and R.J. Birgeneau. "Synchrotron X-ray Diffraction Study of the Disordering of the Ge(111) Surface at High Temperatures." Submitted to *Phys. Rev. Lett.*

Theoretical studies conducted by Professor John D. Joannopoulos have provided many of the first ab-initio calculations for the electronic and geometric structure of solids.

Chapter 3. Semiconductor Surface Studies

Academic and Research Staff

Professor John D. Joannopoulos, Dr. Efthimios Kaxiras, Dr. Oscar L. Alerhand, Dr. Robert D. Meade

Graduate Students

Tomas A. Arias, Kyeongjae Cho, Mark F. Needels, Andrew M. Rappe, Jing Wang

3.1 Introduction

Sponsor

Joint Services Electronics Program
Contract DAAL03-89-C-0001

Understanding the properties of surfaces of solids and the interactions of atoms and molecules with surfaces has been of extreme importance both from technological and academic points of view. The recent advent of ultrahigh vacuum technology has made microscopic studies of well-characterized surface systems possible. The way atoms move to reduce the energy of the surface, the number of layers of atoms involved in this reduction, the electronic and vibrational states that result from this movement, and the final symmetry of the surface layer are all of utmost importance in arriving at a fundamental and microscopic understanding of the nature of clean surfaces, chemisorption processes, and the initial stages of interface formation.

The theoretical problems associated with these systems are quite complex. However, we are currently at the forefront of being able to solve for the properties of real surface systems (rather than simple mathematical models). In particular, we are continuing our goal of calculating the total ground-state energy of a surface system from "first principles," so that we can provide accurate theoretical predictions of surface geometries. Our efforts in this program have concentrated in the areas of surface growth, surface reconstruction geometries, structural phase transitions, and chemisorption.

3.2 Microscopic Model of Heteroepitaxy

Epitaxial growth of dissimilar semiconductor materials holds significant potential for technological applications and has been the subject of major international efforts in recent years. Nevertheless, relatively little theoretical work has been performed to understand the fundamental interactions governing the initial stages of growth and the structure of the first few monolayers in these systems. Of particular interest is the prototypical system involving growth of GaAs on Si(100) substrates. Experimental studies have shown that on slightly miscut (vicinal) Si surfaces GaAs initially grows in an islandlike or three-dimensional mode in the vicinity of *stationary steps*. This is in contrast to both the usual planar or two-dimensional epitaxial mode which proceeds by step motion, as well as the conventional three-dimensional modes driven by strain or absence of wetting. In this work, we have developed a microscopic theoretical model which, for the first time, can explain the fundamental mechanism for this new type of three-dimensional heteroepitaxial growth. The model, supported by total-energy calculations, provides a stage-by-stage description of growth on surface steps, including the driving chemical and rehybridization reactions. It clearly shows the crucial role of double-layer steps (DLS) on the Si surface in initiating the growth of three-dimensional GaAs islands and inhibiting layered epitaxial growth.

The essential physical and chemical concepts which underlie the construction of our model are based on the following observations. First, both Ga and As can form passivated structures with threefold or fourfold coordination. When Ga and As atoms are fourfold coordinated, it is important that they form nearest-neighbor pairs to satisfy charge neutrality requirements. Threefold coordinated Si on the other hand typically has an energetically unfavorable dangling bond. Second, last year we demonstrated that on flat regions of the Si(100) surface a mixed GaAs overlayer phase (formed by switching like-atom bonds to unlike-atom bonds) is energetically favored and inhibits further growth of bulk GaAs along the [100] direction. Thus, there is a strong tendency for mixing at the initial stages which needs to be overcome in any viable model of growth. Finally, idealized growth of GaAs along the [100] direction would lead to physically unacceptable large electric fields due to a net interface charge.

With these ideas in mind, we proceed now to introduce the model of growth. The discussion will follow a realistic sequence of the growth stages as As and Ga atoms are deposited on the Si

surface. We begin with the clean Si surface, which when cut slightly off axis from the (100) orientation, necessarily contains steps. Of the various possible step configurations, we focus on the DLS, which have the appealing feature that they naturally eliminate antiphase domains. Moreover, theoretically it is found that DLS are the lowest-energy steps, and indeed surfaces can be prepared with only these steps present. Theoretical investigations indicate that the lowest-energy configurations for a DLS is as shown in figure 1(a). On this step there is a row of threefold coordinated Si atoms (shown with darker shading) which do not participate in dimer formation. As such, they are more reactive and less stable energetically.

In the usual experimental setup for MBE growth, the ambient pressure of As leads to an As-covered Si surface even before atomic beams are supplied for growth. On the flat regions of the Si substrate the As atoms break the existing Si dimers and form new As dimers. The ensuing threefold coordination of the As atoms and fourfold coordination of the underlying Si atoms is electronically passive and energetically very stable. To obtain the optimal configuration, however, one has to allow for proper bonding of the row of threefold coordinated Si atoms at the steps. We propose that this can be achieved by interchanging these threefold-coordinated Si atoms with As atoms and incorporating the appropriate amounts of As to complete the coverage of the surface. This substitution leads to the novel configuration shown in figure 1(b).

The next step in the growth model consists of depositing Ga on the surface. In the flat regions of the surface, the Ga atoms will break the As-As bonds and form a very low-energy mixed bilayer, with roughly equal amounts of Ga and As atoms in each atomic layer. Thus, growth of zinc-blende GaAs on the flat regions of Si(100) is suppressed.

The new element in the present approach is the influence of the step topology which prevents mixing in the immediate neighborhood of the steps and eventually promotes three-dimensional growth. To see this, first consider the row of Si atoms at the step in which each Si atom is surrounded by three As atoms as shown in figure 1(b). Electronegativity arguments indicate that it is energetically favorable to replace these Si atoms by Ga atoms. The removed Si atoms are allowed to diffuse to bulk positions of lower energy or to equivalent surface sites. The Ga-for-Si substitution creates pairs of fourfold-coordinated Ga and As atoms at the step edge, as shown in figure 1(c). Additional Ga atoms are incorporated between AsPAs bonds on either side of the step. Each Ga atom becomes threefold coordinated,

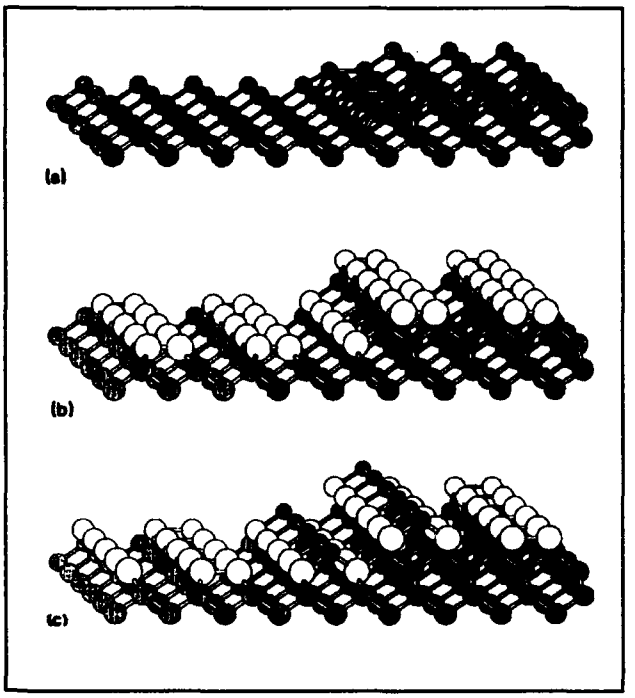

Figure 1. Three stages of growth of GaAs and DLS on Si(100): (a) The clean Si(100) surface with a DLS. The Si dimers on either side of the step are oriented parallel to the step. The threefold coordinated Si atoms at the step (shown by a darker shading) do not participate in dimer formation and should be more reactive. (b) The As-covered configuration. The row of threefold coordinated Si atoms at the step of the clean surface have been substituted by As atoms. The displaced Si atoms (shown by darker shading) are now fourfold coordinated and are bonded to three surface As atoms. (c) The Ga-and-As covered step configuration. Note that adding more Ga atoms on either side of the step would permit mixing which would inhibit (100) growth. Thus, preferred growth proceeds by growing larger and larger overlayers directly on the step along the (211) direction.

bonding to two As and one Ga. The As atoms on either side of the step remain threefold coordinated. Thus, the new structure is again electronically passive. But now, mixing is not energetically favorable to occur in this or any other subsequent overlayer configuration. This is because mixing at the step configuration cannot create more GaAs bonds in place of GaGa or AsAs bonds, which is the driving mechanism for mixing at the terraces. Avoidance of mixing is crucial if the growth of bulklike GaAs is to continue. The structural feature which leads to elimination of mixing is the creation of the Ga-As fourfold-coordinated pairs at the edge of the step. This feature, as a direct consequence of the geometry of the As-covered configuration, is not only intrinsically very stable, but crucial in promoting growth on the step. We emphasize that this is very different from the typical epitaxial growth process where adsorbed

atoms are continuously incorporated at highly reactive propagating steps.

We believe that these results are only the "tip of the iceberg," and we are currently pursuing further studies in this area.

3.3 Finite Temperature Phase Diagram of Vicinal Si(100)

The work described in this section was performed in collaboration with Professor A.N. Berker.

As discussed in the previous section, a vicinal crystal surface is one that is slightly misoriented with respect to a low-index direction and typically consists of terraces of the low-index direction and steps that accommodate the misorientation. Vicinal surfaces can exhibit different structural phases, since steps of different types may be favored depending on temperature T or angle of misorientation θ. Besides their intrinsic interest, stepped surfaces play a central role in important problems in physics and chemistry, including epitaxy, crystal growth, surface chemistry, and catalysis. In this work, we study the equilibrium structure of the vicinal Si(100) surface and calculate its phase diagram as a function of θ and T. This surface has received particular attention largely because it is used as a substrate in the epitaxial growth of GaAs and other III-V compounds and is a prototypical system to study step-flow mechanisms of crystal growth.

The central result of this work challenges a common assumption about the structure of vicinal Si(100). Previous experimental and theoretical work has led to the belief that this surface has only one equilibrium structure, where only biatomic or double-layer (DL) steps are present. We find, however, that for small values of θ, the equilibrium surface is characterized by monatomic or single-layer (SL) steps. These two phases of the surface are separated by a line of first-order transitions. This result has important consequences for the growth of GaAs on Si(100), since DL steps are thought to promote the growth of high-quality GaAs while SL steps may lead to antiphase domains. The equilibrium phase diagram of the surface that is calculated here is consistent with new experimental data that are otherwise unexplained and brings together into a coherent picture all the existing data known to us on the domain structure of vicinal Si(100).

The Si(100) surface reconstructs by forming surface dimers that are arranged in parallel rows. The dimers can be oriented along two possible directions, depending on the plane where the crystal is cut. Thus the surface has two degenerate reconstructed phases; they are related by a 90° rotation, and their surface periodicity is either 2 x 1 or 1 x 2. Consider now a Si(100) surface that is slightly misoriented towards the [011] azimuth by an angle θ; the resulting steps are then oriented either parallel or perpendicular to the surface dimers. The surface misorientation can be accommodated by SL or DL steps, leading to surfaces that are not only different in the height of the steps and the width of the terraces, but also in their basic lattice structure (see figure 2). The SL stepped surface has a two-sublattice structure with terraces of both 2 x 1 and 1 x 2 periodicity, while on the DL stepped surface all the terraces have the same orientation and is a so-called primitive surface.

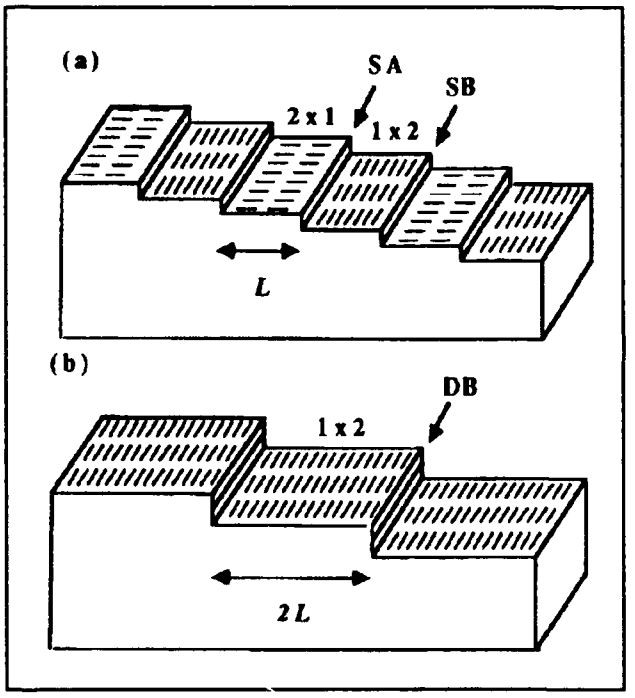

Figure 2. Schematic representation of the (a) single-layer and (b) double-layer step structures of a vicinal Si(100) surface. The surface misorientation θ is related to the terrace width L by $\tan(\theta) = z_{SL}/L$, where $z_{SL} = 1.36$Å is the height of a single-layer step.

Compared with these previous studies, there are two new elements that are incorporated into this work. The first is a strain relaxation that occurs when the terraces alternate orientation and their surface stress tensor is anisotropic. The second is the effect of thermal fluctuations or roughening of the surface steps.

First, let us consider the energy difference E between the SL and the DL stepped Si(100) surfaces at T = 0. Finite-temperature effects will be added later. There are two contributions to E:

1. *Step energies.* There are two types of SL steps and also two types of DL steps on Si(100). On a vicinal SL stepped surface, terraces of 2 x 1 and 1 x 2 orientation as well as both types of SL steps alternate down the surface (see figure 2(a)). A step of type SA connects a higher 2 x 1 terrace with a lower 1 x 2 terrace, and a step of type SB connects a higher 1 x 2 terrace with a lower 2 x 1 terrace. The bonding topology of these steps is different. For SA steps, the dimers on the upper terrace are perpendicular to the step edge, and for SB steps they are parallel. Our calculations show that $\lambda_{SB} \gg \lambda_{SA}$, where λ_{SA} and λ_{SB} are the energies (per unit length) of SA and SB steps, respectively. On a DL stepped surface all the terraces have the same orientation, and only one type of DL step is required (see figure 2(b)). Our calculations show that $\lambda_{DB} \ll \lambda_{DA}$.

2. *Strain relaxation energy.* From elasticity theory we have proved that a crystal surface with degenerate phases and anisotropic surface stress tensor can lower its energy with respect to a uniform one-domain surface by forming an ordered domain configuration. The reduction in energy comes from a long-range elastic or strain relaxation in the semi-infinite medium that is driven by the difference in surface stress of the domains. Our calculations show that the surface stress tensor of Si(100) is anisotropic: The surface is under tensile stress σ_1 parallel to the surface dimers and under compressive stress σ_2 in the perpendicular surface direction. Thus the formation of 2 x 1 and 1 x 2 domains on Si(100) is energetically favored.

The energy difference between the SL and the DL stepped configurations of a vicinal Si(100) surface with misorientation θ is thus

$$E(L) = L^{-1}[(\lambda_{SA} + \lambda_{SB} - \lambda_{DB})/2 - \lambda_\sigma \ln(L/\pi a)] \quad (1)$$

The step-energy difference in eq. (1) is calculated to be $\lambda_{SA} + \lambda_{SB} - \lambda_{DB} = 110$ meV/a, favoring the DL stepped surface. For sufficiently large values of L, however, E_{strain} stabilizes the SL stepped surface. The condition E(L) = 0 defines a first-order phase transition at

$$L_c = \pi a e^{(\lambda_{SA} + \lambda_{SB} - \lambda_{DB})/2\lambda\sigma}. \quad (2)$$

At this point the energy gained by strain relaxation is equal to the energy cost of introducing SL steps instead of the lower-energy DL steps. The SL stepped surface has lower energy for $L > Lc$ (or $\theta < \theta_c$), and the DL stepped surface has lower energy for $L > Lc$ (or $\theta < \theta_c$). For a geometry of striped domains as in figure 2 and $\sigma_1 - \sigma_2 = 1.0$ eV/a^2, the parameter in E_{strain} is $\lambda_\sigma = 11.5$ meV/a. Using this number in eq. (2) yields $Lc \approx 1500$Å, or equivalently $\theta_c \approx 0.05°$. Such a small value of θ_c implies that the SL steps would most probably never be observed on an equilibrium stepped surface. This result, however, holds only for T = 0.

At T > 0 fluctuations must be taken into account. For the temperatures of interest here ($T \ll T_{melting}$), the most relevant thermal fluctuations are the formation of kinks along the steps and their associated roughening. At T = 0 the steps occur as straight lines, but at finite temperatures they meander about the T = 0 direction. To obtain a detailed description of the step roughening, a series of scanning tunneling microscope (STM) images of the Si(100) surface were generated. A typical image of a SL stepped surface is shown in figure 3. We note that the *high-energy* SB steps undergo large fluctuations, while the *low-energy* SA steps remain relatively straight.

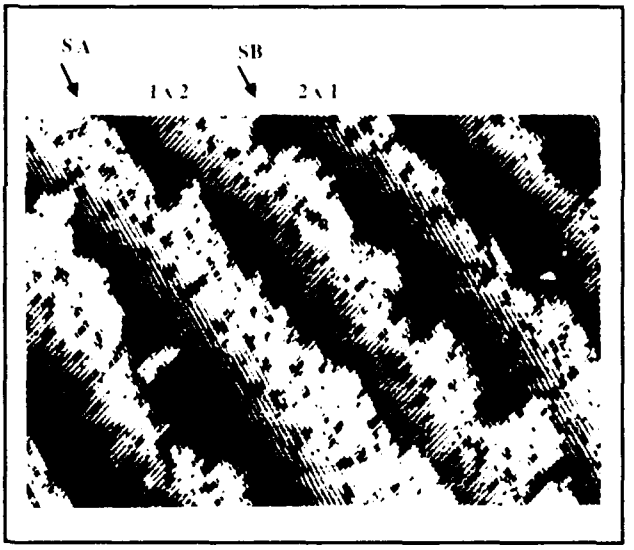

Figure 3. STM image of a single-layer stepped Si(100) surface tilted towards [011] by ~ 0.4°. The terraces alternate in orientation and are separated by alternating SA and SB steps. A small misorientation towards [01$\bar{1}$] is also present, and thus the steps are not perfectly aligned with respect to the surface dimers.

A simple model Hamiltonian was used to study the statistical mechanics of the surface steps. The energy associated with the fluctuations of a step is taken to be

$$H = \sum_i (\lambda_\perp | h_i - h_{i-1} | + \kappa h_i^2), \quad (3)$$

where h_i is the position of the step with respect to its T = 0 line at the point i along this line (in

units of a dimer length). h_i represents the fluctuations, in the profile of a step in units of surface dimers and can take positive or negative integer values. The first term in H is the energy cost associated with the increase in the length of the step in the direction perpendicular to the T = 0 line. λ is the energy per unit length of a step segment in this direction. The quadratic energy term in H has its origin in the strain relaxation energy E_{strain} of eq. (1). E_{strain} has its minimum for a surface with equally spaced steps. In the presence of fluctuations this perfect periodicity is broken, with an associated cost in strain energy. This leads to the quadratic term in h_i, which is derived from the equilibrium equations of the surface. The spring constant κ of eq. (3) is related to the stress parameter $\kappa = \lambda_\sigma(\pi a)^2/8L^2 = 14.2(a/L)^2$ meV/a. Note that $\kappa \sim 1/L^2$, and thus fluctuations are more strongly inhibited as the width of the terraces decreases.

The partition function Z_H associated with eq. (3) can now be calculated using the transfer-matrix method, where

$$< h \mid e^{\kappa h^2/2\kappa_B T} e^{\lambda_\perp \mid h-h' \mid} \mid \tfrac{1}{2} k_B T\, e^{kh'^2 2k_B T} \mid h' > \quad (4)$$

is the transfer matrix associated with H. The free-energy difference F(L,T) between SL and DL can then be readily obtained. F(L,T) has the same form as E(L), except that λ_{SB} is replaced as

$$\lambda_{SB} \rightarrow \lambda_{SB} - (k_B T)^{-1} \ln Z_H.$$

The condition for the phase transition is

$$F(L_c, T) = 0. \quad (5)$$

The results of these calculations are shown in figure 4. This is the phase diagram of vicinal Si(100) in the θ - T plane. The first-order phase-transition line $\theta_c(T)$ is determined by the equation $F(L_c, T) = 0$. The equilibrium phases above and below the $\theta_c(T)$ line are the DL and the SL stepped configurations, respectively. To test this prediction, a series of STM scans of the Si(100) surface were analyzed by correlating the presence of SL and DL steps with the misorientation angle. The results of this analysis are summarized in figure 4, where a typical STM image of a DL stepped configuration is shown in the inset.

The data in figure 4 also include other available experimental results where the surface has been annealed at high temperatures for long times to assure that kinetic constraints have been eliminated. The measured structure at room temperature, however, is not at equilibrium. Rather, it reflects the equilibrium structure at some higher, freezing-in temperature. From different experiments on epitaxial growth, this freezing-in temperature is estimated to lie between 450 and 550 K (note that only mass transport *along* the steps is required in the fluctuations of the steps, but not mass transport across the terraces). The agreement between theory and experiment is satisfactory. The theory predicts that for annealed surfaces the transition between the S1 and DL stepped surfaces is in the range $\theta_c \approx 1.2°$-$2.5°$. The experimental data place upper and lower bounds of $1° \lesssim \theta_c \lesssim 3.5°$. Moreover, the experiment that reports a mixed phase at $\theta \sim 2.5°$ may be evidence, via a coexistence region, of a first-order transition. The data point at $\theta \approx 0°$, which originally was reported as a primitive surface, has most recently been found to be unstable to the formation of 2 x 1 and 1 x 2 domains.

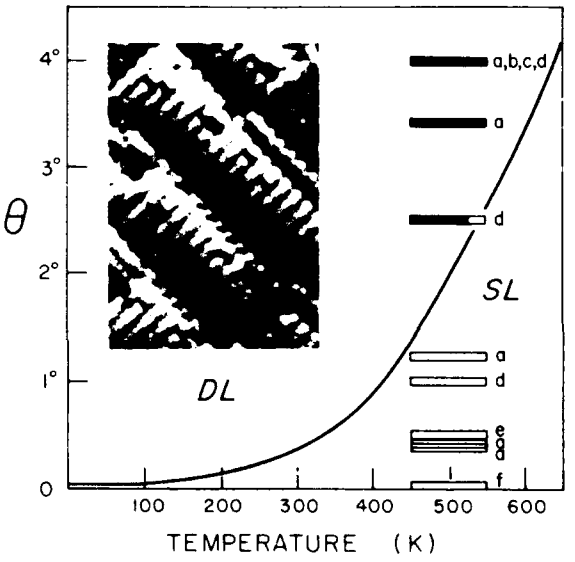

Figure 4. Phase diagram of vicinal Si(100). The solid curve is the theoretically predicted line of first-order transitions between the single-layer (SL) and double-layer (DB) stepped configurations. At T = 0, $\theta_c = 0.05°$. Open and solid bars represent experimental observations of SL and DL stepped surfaces, respectively. The bar at $\sim 2.5°$ represents observations of a mixed phase with mostly DL steps. The horizontal range of the data is an estimate of the temperature where fluctuations of the steps are frozen. Inset: STM image of DL stepped Si(100) surface with $\theta \approx 3.5°$.

Publications

Alerhand, O., A.N. Berker, J.D. Joannopoulos, D. Vanderbilt, R.J. Hamers, and J.E. Demuth. "Finite Temperature Phase Diagram of Vicinal Si(100) Surfaces." *Phys. Rev. Lett.* 64: 2406 (1990).

Alerhand O., A.N. Berker, J. Joannopoulos, and D.

Vanderbilt. "Phase Transitions on Misoriented S(100) Surfaces." *Proc. 20th Int. Conf. Phys. Semi.* 2181 (1990).

Alerhand O., E. Kaxiras, J. Joannopoulos, and G. Turner. "Kinetics and Growth Channels in GaAs Epitaxy on Si(100)." *Proc. 20th Int. Conf. Phys. Semi.* 284 (1990).

Kaxiras E., O. Alerhand, J.D. Joannopoulos, and T. Turner. "Microscopic Theory of GaAs Growth on Si(100) Vicinal Surfaces." *Proc. El. Chem. Soc. Can.* (1990).

Kaxiras E., O, Alerhand, J. Joannopoulos, and G. Turner. "Thermodynamic and Kinetic Aspects of GaAs Growth on Si(100)." *Proc. 5th Int. Conf. Phys. Herakleion.* (1990).

Rappa, A., K. Rabe, E. Kaxiras, and J.D. Joannopoulos. "Optimized Pseudopotentials." *Phys. Rev. Rapid Comm.* B41: 1227 (1990).

Wang J., M. Needels, and J. Joannopoulos. "Surface and Fracture Energies in GaAs." *Xie Xide Festschrift.* Teaneck, NJ: World Scientific Pub., 1991.

Chapter 4. Single Electron Transistors

Academic and Research Staff

Professor Marc A. Kastner,[1] Professor Henry I. Smith, Professor Dimitri A. Antoniadis, Paul McEuen

Visiting Scientists and Research Affiliates

Shalom Wind[2]

Graduate Students

Ethan D. Foxman, Udi E. Meirav

Technical and Support Staff

Angela R. Odoardi

4.1 Project Description

Sponsors

Joint Services Electronics Program
Contract DAAL03-89-C-0001
National Science Foundation
Grant ECS 88-13250

Two years ago we discovered, completely *unexpectedly, new behavior* in very small Si MOSFETs. Whereas conventional transistors turn from the off state to the on state only once as the gate voltage increases, these small transistors turn on and off periodically, in some cases as many as one hundred times. We have since learned how to control the period of these oscillations in GaAs field effect devices and have shown that a nm-size transistor turns on and off once for every electron added to it. Because of this, we call this kind of device a Single Electron Transistor. Having established that each cycle corresponds to the addition of one electron, the period in gate voltage provides a very precise measure of the capacitance of our devices. Because it is very small, $\sim 10^{-16}$ F, such transistors may eventually find application in ultrasensitive charge detection. Different applications utilizing the multistate characteristics of the devices can be imagined. Unfortunately, so far the single electron behavior has only been observed below about 1 K. Whether this behavior can be observed at higher temperatures in the future depends on the details of the mechanism that causes it. Our objective is, therefore, to better understand that mechanism.

Our initial discovery was made[3] with inversion layers in Si which were about 30 nm wide and several mm long. These were dual gate MOSFETs with a narrow slot, ~ 600 nm wide, in the lower gate, fashioned with x-ray lithography. This lower gate was made of refractory metals allowing a high temperature anneal after all unconventional lithography was complete. In the end, these devices were the narrowest transistors ever made, but while most previous narrow devices had low mobility, these had mobilities comparable to wide devices. The successful fabrication of these ultranarrow devices was the result of a close collaboration between H.I. Smith, D.A. Antoniadis, M.A. Kastner and their students.

Soon after these devices were first fabricated, it was discovered that their conductance oscillated periodically as a function of the density of electrons in the conducting channel, proportional to the gate voltage, V_g. An example of this distinctive behavior is shown in figure 1.

---

[1] Donner Professor of Physics

[2] IBM Thomas J. Watson Research Center, Yorktown Heights, New York.

[3] J.H.F. Scott-Thomas, S.B. Field, M.A. Kastner, H.I. Smith, and D. A. Antoniadis, "Conductance Oscillations Periodic in the Density of a One-Dimensional Electron Gas." *Phys. Rev. Lett.* 62: 583 (1989); S.B. Field, M.A. Kastner, U. Meirav, J.H.F. Scott-Thomas, D.A. Antoniadis, H.I. Smith, and S.J. Wind. "Conductance Oscillations Periodic in the Density of One-Dimensional Electron Gases." Phys. Rev. B 42: 3523 (1990).

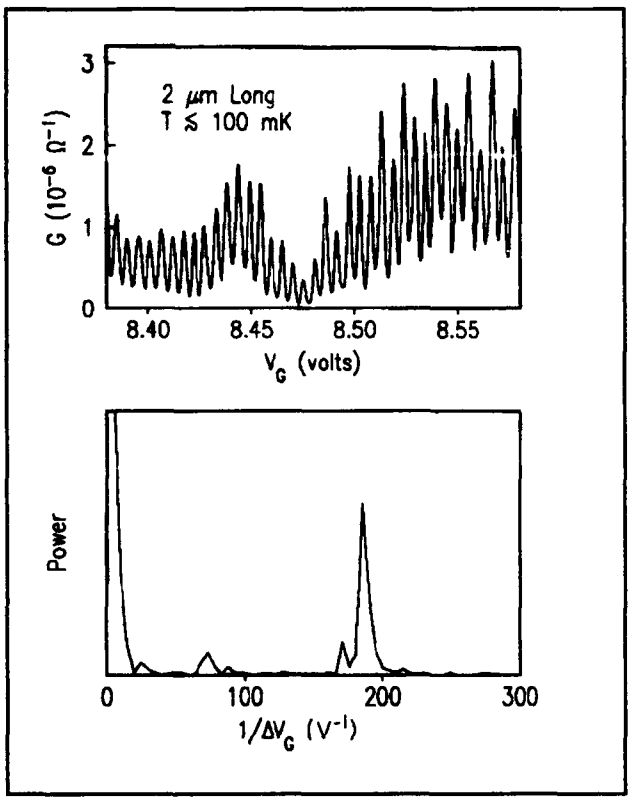

Figure 1.

The foremost problem posed by our discovery was to find out what determined the period of the conductance oscillations. We soon discovered that the period varied at random from device to device, indicating that it was determined by the random spacing of interface charges that happened to fall over the conducting channel. This suggested that potential barriers resulting from the interface charges were isolating a segment of the channel and that the conductance underwent one cycle every time the same number of electrons was added to the isolated segment. To prove this, and to ascertain what that number of electrons was, new devices had to be made.

The first step was to produce devices close in their operation to a MOSFET but in GaAs where the influence of interface charges is much weaker.[4] This was accomplished through a remarkably successful collaboration with M. Heiblum of IBM. The new structure was created by growing AlGaAs on a conductive substrate, followed by a layer of undoped GaAs. The electron density at the GaAs/AlGaAs interface, inverted from the usual configuration was varied by applying a voltage to the substrate. Heiblum was able to grow such inverted heterojunctions with mobilities of $\sim$ 500,000 cm^2/V-s.

Next, the conducting channel is defined by depositing a metal gate on top of the GaAs, and a gap is patterned in the gate by electron beam lithography. Because a depletion region is created under the gate, the electrons accumulate only under the gap. In order to emulate the effect of two charged impurities, two constrictions are patterned in the gap, as illustrated in figure 2. The electron beam lithography was done at IBM with the help of S. Wind.

Devices of the kind depicted in figure 2 worked exactly as we hoped they would.[5] Periodic oscillations of the conductance were seen again, but now they were controlled: The period was the same for different devices with the same spacing between constrictions and was larger when the spacing was shorter, which is consistent with the idea that the same number of electrons is added for one period in all devices. This is illustrated in figure 3. Calculations of the capacitance of such devices are only consistent with each period corresponding to one electron added per oscillation.

This is an amazing result: Figure 3 shows that for the shortest structures the conductance consists of periodic, narrow, well-separated resonances. The conductance rises and falls by a factor $\sim$ 100 with a variation of gate voltage that corresponds to only $\sim$ 1/10 of an electron.

[4] U. Meirav, M.A. Kastner, M. Heiblum, and S.J. Wind, "One-Dimensional Electron Gas in GaAs: Periodic Conductance Oscillations as a Function of Density," *Phys. Rev. B (Rapid Comm.)* 40: 5871(1989).

[5] U. Meirav and S. J. Wind, "Single Electron Charging and Periodic Conductance Resonances in GaAs Nanostructures," *Phys. Rev. Lett.* 65: 771(1990).

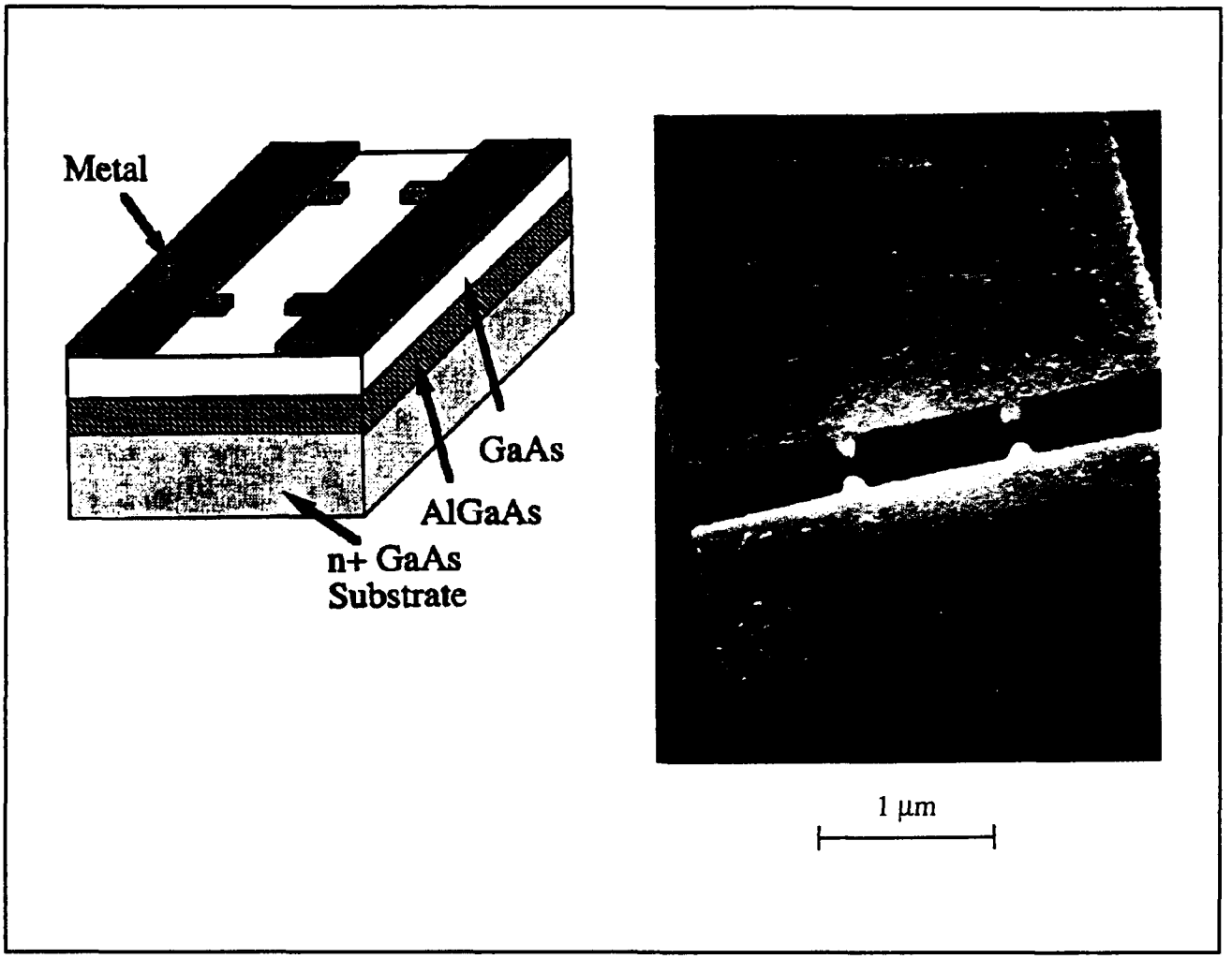

Figure 2.

We are not yet sure what causes the Single Electron Transistor to work the way it does. The conductance appears to result from resonant tunneling, but the nature of the states that are resonant is still unclear. Patrick Lee and his collaborators believe that the states arise from single particle quantum states (the Fabry-Perot states induced by the two barriers, the same as expected for any "quantum dot"), but that the energies of the levels are dominated by the Coulomb interaction between the electrons in the isolated segment. Van Houten and Beenakker argued that the Coulomb interaction alone could explain the phenomena we see, and that the effect was the same as the Coulomb blockade recently popularized by Likharev. Some of our measurements suggest, however, that electron-electron correlation, in addition to the simple Coulomb interaction, may be important.

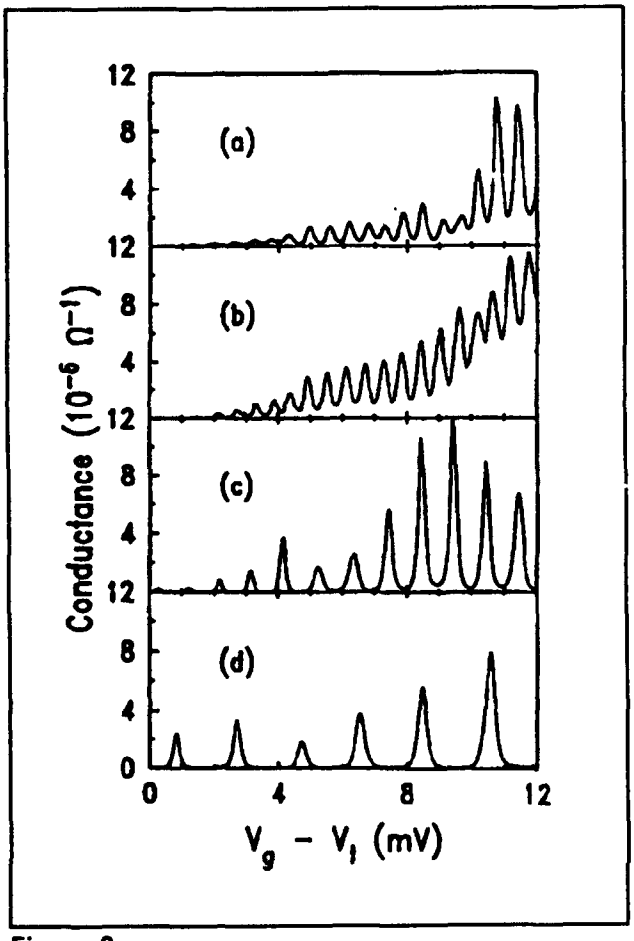
12
8
4
(a)
12
8
4
(b)
12
8
4
(c)
12
8
4
(d)
0
Conductance (10^{-6} Ω^{-1})
0
4
8
12
$V_g - V_t$ (mV)

Figure 3.

Chapter 5. Coulomb Blockade in Narrow MOSFETs

Academic and Research Staff

Professor Patrick A. Lee, Dr. Yigal Meir, Dr. Ned S. Wingreen

Graduate Student

Jari M. Kinaret

Technical and Support Staff

Imadiel Ariel

5.1 Project Description

Sponsor

Joint Services Electronics Program
Contract DAAL03-89-C-0001

We are investigating the conductance through a quantum dot where the discrete nature of the electron charge on the dot and the Coulomb energy U associated with the addition or removal of a charge dominate the physics. This theoretical work is inspired by the experimental work of Professor Kastner's group, which discovered periodic structures in the conductance as a function of gate voltage in a narrow MOSFET structure with two constrictions. These constrictions create a quantum dot through which the electron must tunnel. There are two energy scales in the problem: (1) the energy spacing $\Delta\varepsilon$ between energy levels in the quantum dot which we estimate to be $\Delta\varepsilon \approx 0.1$ meV for a 50 nm x 1 μm quantum dot in GaAs and (2) The Coulomb interaction energy between electrons U which is approximately equal to the capacitive charging energy of the quantum dot e^2/C where C is the capacitance and we estimate $e^2 2/C \approx 1$ meV, so that $U \gg \Delta\varepsilon$. Under these conditions, an electron must overcome the Coulomb energy in order to tunnel, a phenomenon known as the Coulomb blockade.

We treat a model consisting of two ideal leads coupled to a site with n energy levels and a Coulomb interaction energy U every time an extra electron is added to the site. This model is reminiscent of the Anderson model of magnetic impurities, in which electrons of either up or down spin (n = 2) can occupy a site, and there is an on-site repulsion U for double occupation. The present problem is richer because the Fermi level in the right and left ideal leads can be separately adjusted.

Earlier we had examined the low temperature limit of this model,[1] and we found important correlation between the electron state on the quantum dot and the electrons in the lead when the temperature T is less than T_K, the Kondo temperature. However, in most cases T_K is very low, and we have recently developed a formalism to describe the high temperature limit[2] when $T \gg T_K$. We note that $\Delta\varepsilon$ can be comparable to kT, and there are interesting changes in the lineshape of the conductance peaks as kT goes from $kT \ll \Delta\varepsilon$ to $kT \gg \Delta\varepsilon$. For $kT \ll \Delta\varepsilon$, the lineshape is a Lorentzian broadened by the derivative of the Fermi function. As kT is increased through $\Delta\varepsilon$, this is no longer the case, and we find that the peak height can increase or decrease with temperature, depending on the way the levels couple to the leads. This feature, which was observed experimentally, has been a puzzle for some time.

According to our theory, the observed temperature dependence is explained by simultaneous transport through multiple levels whose coupling to the leads increases rapidly with energy near the top of the tunnel barriers. Our theory gives a satisfactory account of the temperature dependence of the periodic structure in conductance, thus providing strong support for the validity of the Coulomb blockade model.

---

[1] T.-K. Ng and P.A. Lee, "On Site Coulomb Repulsion and Resonant Tunnelling," *Phys. Rev. Lett.* 61:1768 (1988).

[2] Y. Meir, N. Wingreen, and P. Lee, "Transport Through a Strongly Interacting Electron System: Theory of Periodic Conductance Oscillations," submitted to *Phys. Rev. Lett.*

5.1.1 Publications

Kinaret, J., and P.A. Lee. "Exchange Interaction in a Quantum Wire in a Strong Magnetic Field." *Phys. Rev. B* 42(18): 768-773 (1990).

Kinaret, J., and P.A. Lee. "Conductance of a Disordered Narrow Wire in a Strong Magnetic Field." *Phys. Rev. B.* Forthcoming.

Meir, Y., N. Wingreen, and P.A. Lee. "Transport Through a Strongly Interacting Electron System: Theory of Periodic Conductance Oscillations." Submitted to *Phys. Rev. Lett.*

Professor Patrick A. Lee's recent work is focused on the effect of Coulomb repulsion on the tunneling probability through a quantum dot.

Chapter 6. Epitaxy and Step Structures on Semiconductor Surfaces

Academic and Research Staff

Professor Simon G.J. Mochrie

Graduate Students

Douglas L. Abernathy

6.1 Project Description

Sponsor

Joint Services Electronics Program
Contract DAAL03-89-C-0001

Under JSEP sponsorship, we have completed a comprehensive x-ray scattering study of the clean Pt(001) surface between 300 and 2000 K. We initiated work on this surface because it is relatively inert and detailed measurements are straightforward. However, the behavior of the Pt(001) surface has proven to be so rich that we decided a comprehensive study was mandated. Specifically, within the context of this single surface, we have obtained results that are important for understanding orientational epitaxy and associated two-dimensional phase transformations and for demonstrating that surface strain is the origin of surface reconstruction for certain metal surfaces.[1] Most recently, we have conducted a detailed study of the diffuse scattering in a high temperature disordered phase of this surface.

Below 1820 K, the Pt(001) surface layer exhibits a hexagonal atomic arrangement despite the planes of square symmetry which lie immediately beneath. However, above 1820 K our experiments on the Pt(001) surface reveal that there is no scattering at wave vectors associated with the hexagonal reconstruction. To elucidate the nature of the surface in this temperature range, we have performed measurements of the specular x-ray reflectivity at temperatures both above and below 1820 K. Such measurements are sensitive to the surface morphology, in particular, to surface steps and their distribution. Simply stated, if the surface is atomically flat, the x rays are reflected only at an angle of reflection equal to their angle of incidence. On the other hand, for a surface that is not ideally flat, there is a distribution of reflected angles representative of the surface roughness. It is remarkable that the roughness of a solid surface in equilibrium is expected to result from capillary modes, just as for a liquid surface. Microscopically, the capillary modes in question are fluctuations in the location of atomic steps and islands on the surface.[2]

Above 1820 K, we indeed find that the distribution of reflected x rays is characteristic of a rough interface, which supports capillary modes. Our observations are important for several reasons. First, they demonstrate for the first time that close-packed surfaces, in this case, fcc(001), may become rough at temperatures below the bulk melting point. Second, detailed analysis of the distribution of reflected x rays, as the angle of incidence is varied, provide the most compelling evidence to date that the character of the roughness is as expected. Specifically, at a given value of the momentum transfer normal to the surface (Q_z), one expects the distribution of x rays scattered away from the specular direction to be given by[3]

$$I_s \sim Q_x^{-2+\eta},$$

where Q_x is the deviation in wave vector from the specular condition (i.e., $Q_x = 0$). The exponent $\eta = k_B T Q_z^2/2\pi\phi$, where ϕ is the surface stiffness.

---

1 R.J. Needs, "Calculations of the Surface Stress Tensor at Aluminum (111) and (110) Surfaces," *Phys. Rev. Lett.* 58: 53 (1987).

2 J.D. Weeks, "The Roughening Transition," in *Ordering in Strongly Fluctuating Condensed Matter Systems* (New York: Plenum, 1980).

3 B.M. Ocko and S.G.J. Mochrie, "Facetting of the Cu(110) Surface: X-ray Fresnel Reflectivity," *Phys. Rev. B* 38: 7378 (1988).

Our results confirm, for the first time, the scaling of η with Q_z^2. Representative experimental profiles and the associated best fit model line shapes are shown in figure 1.

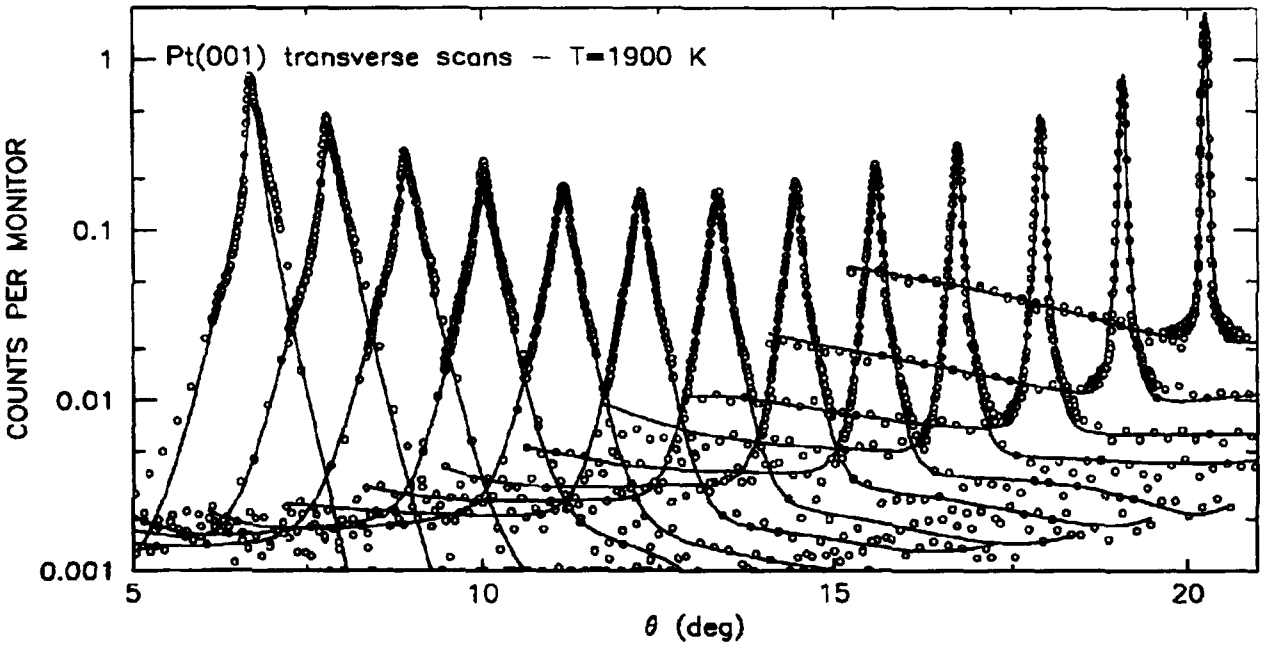

Figure 1. Scans across the x-ray specular reflectivity of the Pt(001) surface at different values of $Q_z = 4K \sin \Theta/\lambda$ for T = 1900 K. The solid lines show the best fit to the form discussed in the text. The fits confirm the expected scaling of η with Q_z^2.

Part II Applied Physics

Section 1 Atomic, Molecular and Optical Physics

Chapter 1. Quantum Optics and Photonics

Academic and Research Staff

Professor Shaoul Ezekiel

Visiting Scientists and Research Affiliates

Dr. Philip R. Hemmer, John D. Kierstead, Dr. Elias Snitzer,[1] Dr. Mara G. Prentiss[2]

Graduate Students

M. Selim Shahriar, Stephen P. Smith, Farhad Zarinetchi, John J. Donoghue

Technical and Support Staff

Margaret M. McCabe

1.1 Applications of Stimulated Brillouin Fiber Lasers

Sponsor

Charles S. Draper Laboratory
Contract DL-H-418468

Brillouin scattering,[3] i.e., spontaneous Brillouin scattering, is the scattering of an incident field, the pump, by thermal acoustic waves in the medium, or, fiber, in our case. Of interest here is the scattering by acoustic waves propagating along the fiber. Since forward scattering by such acoustic waves does not generate a frequency shifted beam, it has no interest for us. However, backscattering by such acoustic waves will generate a beam that is doppler shifted by $2 f_p v_a/c_m$ from the pump, where f_p is the frequency of the pump, v_a is the acoustic velocity in the fiber, and c_m is the speed of light in the fiber medium. The peak amplitude of the backscattered wave, frequency f_B, is derived from that acoustic wave that satisfies the Bragg condition, i.e., $2\lambda_a = \lambda_{Bm}$, where λ_a is the wavelength of that acoustic wave, and λ_{Bm} is the wavelength of the backscattered wave in the medium. In other words, the frequency of this acoustic wave is $f_a = v_a/\lambda_a = v_a/(\lambda_{Bm}/2)$. The backscattered beam will interfere with the pump beam to form a traveling wave at the difference frequency f_a that propagates along the pump direction. This traveling wave will induce an acoustic wave (via the electro-striction effect in quartz) that propagates along the pump direction and enhances that particular thermal acoustic wave that satisfied the Bragg condition.

With increasing pump intensity, the intensity of the acoustic wave increases, and consequently the intensity of the backscattered beam, i.e., the Brillouin beam, will increase. The growth or the amplification of the Brillouin beam with pump intensity is stimulated Brillouin scattering.[3] The downshift of the Brillouin beam from the pump is therefore $2 f_p v_a/c_m$ and the width of the stimulated Brillouin scattering is determined by the damping of the acoustic waves, i.e., phonon relaxation, in the medium.[4] For a quartz fiber at a λ of 1 micron, the downshift is about 15 GHz and the bandwidth of the SBS is about 25 MHz.

The following describes the operation of the SBS laser.[5]

---

[1] Professor, Rutgers University, New Brunswick, New Jersey.

[2] Professor, Harvard University, Cambridge, Massachusetts.

[3] R.Y. Chiao, C.H. Townes, and B.P. Stoicheff, *Phys. Rev. Lett.* 12: 592 (1964).

[4] D. Heiman, D.S. Hamilton, and R.W. Hellwarth, *Phys. Rev. B* 19: 6583 (1979).

[5] K.O. Hill, B.S. Kawasaki, and D.C. Johnson, *Appl. Opt. Lett.* 28: 608 (1976); D.R. Ponikvar, and S. Ezekiel, *Opt. Lett.* 6: 398 (1981); L.F. Stokes, M. Chodorow, and H.J. Shaw, *Opt. Lett.* 7: 509 (1982).

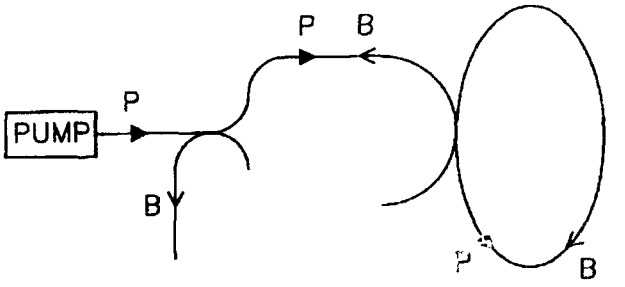

Figure 1. Brillouin laser output.

Figure 1 shows the pump propagating in a fiber ring resonator. If the pump frequency is held at the center of a cavity resonance, the pump intensity inside the resonator is enhanced. The resulting SBS which propagates along the opposite direction of the pump will also be enhanced when there is a cavity resonance within the SBS bandwidth. If the SBS gain in the resonator is greater than the loss, we get SBS lasing as denoted by B in figure 1. Threshold pump power for SBS lasing can be very low, 35 μW, which we recently achieved.[6] The frequency of the SBS laser is therefore determined primarily by the acoustic velocity in the fiber, and the spectral width of the SBS laser can be very narrow,[7] around 1 kHz, since the fiber cavity is a relatively quiet cavity. In this way, the SBS laser linewidth can be much narrower than the pump spectral width.[7] However, if the pump spectral width does not lie well within the passive linewidth of the cavity, we get pump intensity fluctuations within the resonator which will broaden out the SBS laser spectral width.

By constructing two similar Brillouin lasers and subjecting one of them to a disturbance such as temperature, pressure, acoustics, magnetic field, etc., then the beat between the two lasers will give a very sensitive measure in digital form of the applied disturbance.

Since the linewidth of the Brillouin laser can be much narrower than that of the pump laser, the Brillouin laser concept can also be used as a means of reducing the jitter of a laser, especially high frequency jitter, without the need for sophisticated wideband feedback loops.[7]

There are many applications of the two Brillouin lasers that share the same fiber cavity but have either common or independent pumps. Because cavity fluctuations are common to both lasers in this case, the relative jitter between the two lasers is very small. Measuring this relative frequency jitter by simply beating the outputs of two Brillouin lasers that share the same cavity, we found the width of the beat to be limited by the 30 Hz instrumental linewidth of our spectrum analyzer.[7]

Applications of the common cavity Brillouin lasers include:

- fiberoptic ring laser gyroscope, where the output is inherently digital, similar to the HeNe ring laser gyroscope;[6]
- magnetic field sensor with a digital readout;
- tunable, narrow linewidth, high frequency sources in the microwave to millimeter-wave range;[7]
- the generation of high frequency, amplitude modulated laser beams for use in sensitive absolute distance and ranging measurements;[7]
- wideband frequency shifting without the need for wideband modulators;
- the generation of two laser sources with correlated frequency jitter for use in high resolution two-photon interactions for the development of atomic clocks, precision two-photon spectroscopic studies and fast flow laser doppler velocimeters (LDV);[7]
- finally, a distributed spectroscopic sensor based on two-photon interaction using exposed sections of fiber, where the pump photon is pulsed and the probe photon is CW.

[6] F. Zarintechi, S.P. Smith, and S. Ezekiel, *Opt. Lett.* 16: 229 (1991).

[7] S.P. Smith, F. Zarintechi, and S. Ezekiel, *Opt. Lett.* 16: 393 (1991).

1.2 Stimulated Brillouin Fiber Laser Gyroscope

Sponsor

Charles S. Draper Laboratory
Contract DL-H-418468

We present recent developments in a new type of fiberoptic gyroscope[8] based on two counterpropagating stimulated Brillouin lasers[9] sharing the same single mode fiber ring resonator. In the presence of inertial rotation normal to the plane of the resonator, a difference frequency is automatically generated between the counterpropagating Brillouin lasers which is proportional to the rotation, as predicted by the Sagnac effect.[10] The operation of such a gyro is very similar to that of the bulkoptic ring laser gyro (RLG) that is based on two counterpropagating He-Ne lasers that share the same ring resonator.[11] Unlike the passive interferometric fiber gyro,[12] the Brillouin fiber gyro does not require external means for the measurement of nonreciprocal phase shifts induced by the rotation.

Figure 2 shows a simplified schematic diagram of the Brillouin fiber laser gyroscope. Light from a 2 mW single frequency He-Ne pump laser at 1.15 micrometers is split into two beams, P1 and P2, and these beams are frequency shifted by acousto-optic (A/O) modulators before they are coupled along opposite directions of a fiber ring resonator. The fiber resonator is made from a 25 m long single mode fiber wrapped around a cylindrical drum 7.5 cm in diameter. The finesse of the resonator is 250 and the linewidth is 30 kHz. In order to achieve the lowest Brillouin threshold, the polarizations of the input beams are matched into an eigen polarization of the resonator, and the frequency of pump P1 is held at the center of the cavity resonance by a servo loop. When the pump intensities were increased above 60 microwatts, we observed Brillouin lasing, B1 and B2, along directions opposite to those of P1 and P2, that were downshifted by 15 GHz from the pump as expected for the stimulated Brillouin[9] effect at this wavelength. B1 and B2 are combined by beam splitter BS1 and directed to detector D1, after passing through a Fabry-Perot cavity acting as a filter to block out the pump.

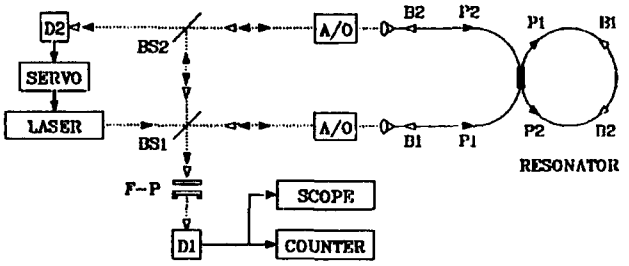

Figure 2.

Figure 3a shows the 3 kHz sinusoidal beatnote between B1 and B2 when a constant rotation of 4 degrees/second is applied to the set up. The magnitude of this beatnote is consistent with that predicted by the Sagnac effect for this configuration and varies linearly with rotation. However, at low rotation rates, the corresponding beatnote becomes highly nonlinear, as shown in figure 3b, and disappears altogether when operating close to zero rotation. This undesirable behavior at low rotation rates, caused by the coupling of the Brillouin lasers through backscattering within the fiber resonator, is called the "lock-in" effect and has been studied extensively in bulkoptic ring laser gyros.

---

[8] S.P. Smith, F. Zarintechi, and S. Ezekiel, "Fiberoptic Ring Laser Gyroscope," *Proceedings of OFS '89,* Paris, France, 1989.

[9] P.J. Thomas, H.M. van Driel, and G.I.A. Stegeman, "Possibility of Using an Optical Fiber Brillouin Ring Laser for Inertial Sensing," *Appl. Opt.* 19: 1906 (1980); K.O. Hill, B.S. Kawasaki, and D.C. Johnson, "Cw Brillouin Laser," *Appl. Phys. Lett.* 28: 608 (1976); D.R. Ponikvar and S. Ezekiel, "Stabilized Single-frequency Stimulated Brillouin Fiber Ring Laser," *Opt. Lett.* 6: 398 (1981); L.F. Stokes, M. Chodorow, and H.J. Shaw, "All Fiber Stimulated Brillouin Ring Laser with Submilliwatt Pump Threshold," *Opt. Lett.* 7: 509 (1982); P. Bayvel and I.P. Giles, "Evaluation of Performance Parameters of Single Mode All Fiber Brillouin Ring Lasers," *Opt. Lett.* 14: 581 (1989).

[10] A.H. Rosenthal, "Regenerative Circulatory Multiple-beam Interferometry for the Study of Light-propagation Effects," *J. Opt. Soc. Am.* 52: 1143 (1962).

[11] W.M. Macek and D.T.M. Davis, Jr., "Rotation Rate Sensing with Traveling Wave Ring Laser," *Appl. Phys. Lett.* 2: 67 (1963).

[12] V. Vali and L.W. Shorthill, "Fiber Ring Interferometer," *Appl. Opt.* 15: 1099 (1976).

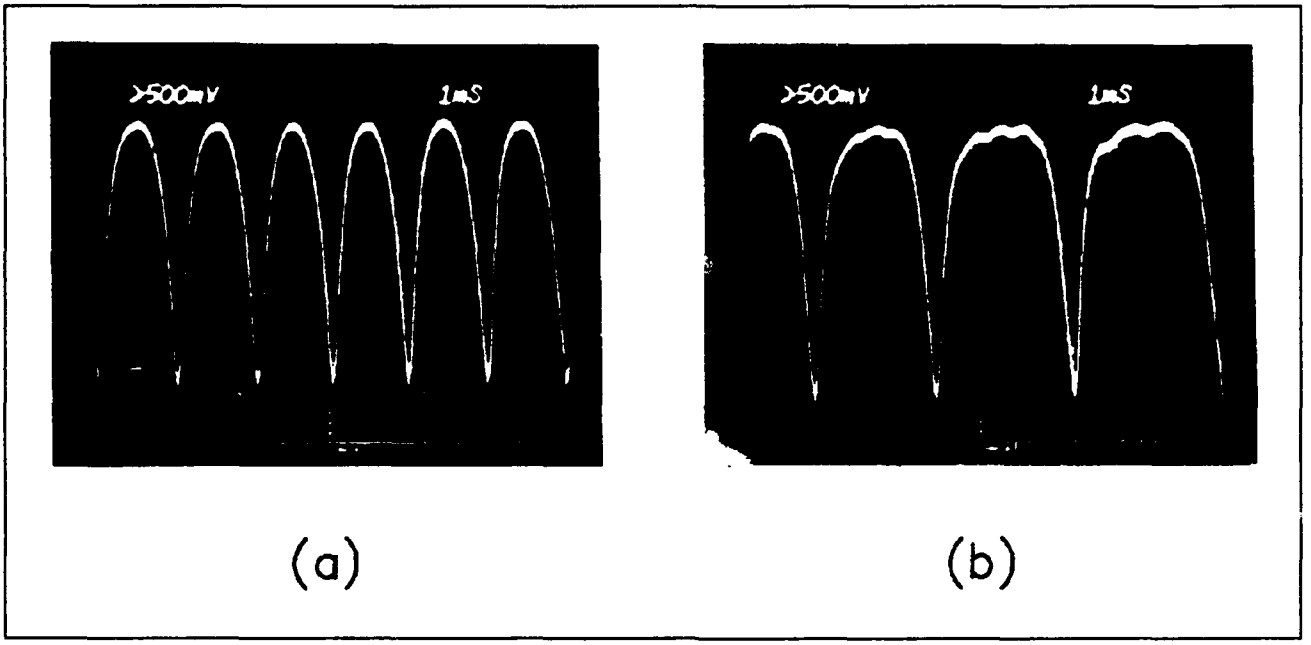

Figure 3.

Figure 4a shows the variation of the Brillouin beatnote, measured by a frequency-to-voltage converter, as a function of an applied sinusoidal rotation, shown in figure 4b, having a peak angular deviation of 5 degrees and a period of 12 seconds. As shown in figure 4a, the Brillouin beat note varies linearly with rotation rate and exhibits a peak beat frequency of 2 kHz for a peak rate of 2.5 degrees/second. However, at low rotation rates, as mentioned above, the beat goes to zero, demonstrating a "lock-in" range of about 1 kHz. To record the direction of the angular motion in figure 4a, a 5 kHz frequency difference was applied to the acousto-optic shifters in figure 2 to generate a bias of 5 kHz. The main advantage of the Brillouin gyro is that it puts an output frequency in response to an applied rotation, without the need for a complicated measurement system.

The data presented here is still preliminary; there are a number of issues that influence performance that have yet to be investigated. For example, a suitable means must be found to overcome the "lock-in" effect. In addition, error sources due to fiber birefringence, back scattering, optical Kerr effect, etc., must be studied. Finally a convenient pump source, preferably a solid state laser such as a semiconductor laser or fiber laser, needs to be identified.

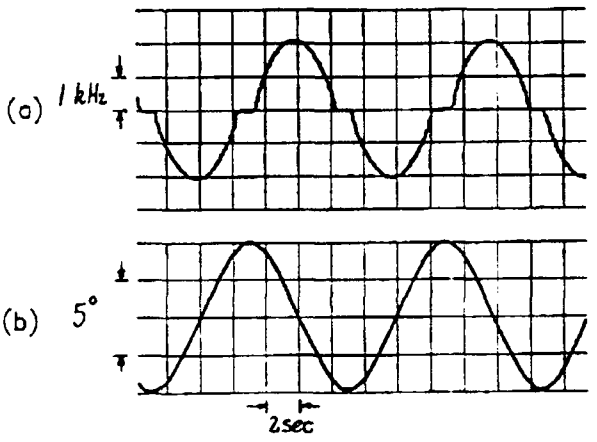

Figure 4.

1.3 Structures Much Shorter and Longer Than Optical Wavelengths Predicted in the Force on a Three-Level System

Sponsor

U.S. Air Force - Electronic Systems Division
Contract F19628-89-K-0030

Recently, a three-level atom in the Λ configuration has been employed to cool atoms in one dimension to the lowest temperature yet achieved. In addition, recent calculations have indicated that structures observed in trapped atoms may be due to interactions with such a system. We have calculated the force on this kind of system excited by Raman resonant bichromatic standing wave light fields in the limit when optical pumping into the trapped state is important.[13] For simplicity, we have considered stationary atoms first. The influence of the non-absorbing trapped state leads to very different predictions for the optical forces than in the case of two level atoms or three level atoms in the Λ configuration. In particular, large stimulated forces can be produced which vary on distance scales both much longer and much shorter than the optical wavelength. Our results differ significantly from those derived in other theoretical treatments[14] which ignore optical pumping into the trapped state.

The appropriate atomic level diagram is shown in figure 5. The basis state transformation is given by:[15]

$$\begin{bmatrix} |-> \\ |+> \\ |e> \end{bmatrix} = \begin{bmatrix} \cos\theta & -\sin\theta & 0 \\ \sin\theta & \cos\theta & 0 \\ 0 & 0 & 1 \end{bmatrix} \begin{bmatrix} |a> \\ |b> \\ |c> \end{bmatrix}$$

where θ is defined by the following Rabi frequency expressions:

$$\Omega_1 = \sqrt{2}\,\Omega \sin\theta = \Omega_0 \sin(kx),$$

$$\Omega_2 = \sqrt{2}\,\Omega \cos\theta = \Omega_0 \sin(kx + \Psi), \text{ and}$$

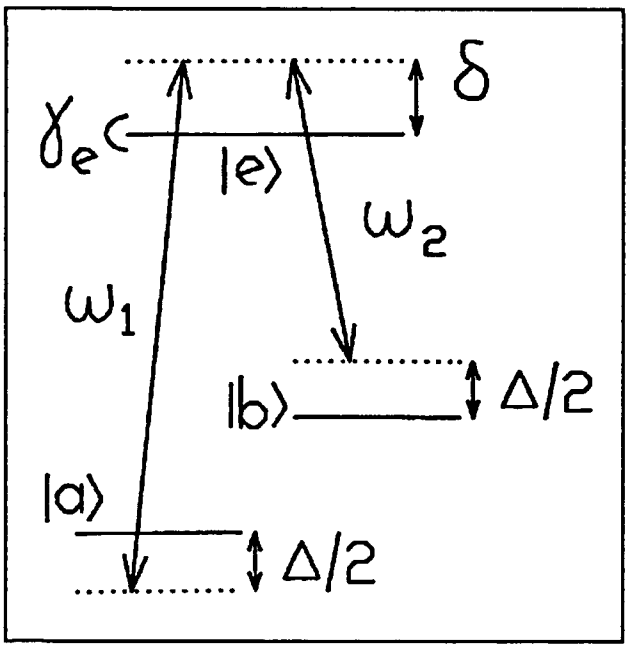

Figure 5. Schematic diagram of a three-level system in the Ω configuration.

$$\sqrt{2}\,\Omega = \sqrt{|\Omega_1|^2 + |\Omega_2|^2}$$

Here, Ψ varies on the scale of the beatlength, which is assumed negligible on the optical wavelength scale.

For zero difference detuning $\Delta \neq 0$, the $|->$ state is coupled to the $|+>$ state and both states experience a force. We find that this force is proportional to Δ and can be separated into a component associated with the $|+>$ state and a component associated with the $|->$ state. The $|+>$ state component averages to zero over an optical wavelength while the $|->$ state component can have a substantial non-zero average value. An example of this is shown in figure 6 for the $\delta = 0$ case where the $|+>$ state force is zero. This rectified component of the force (dashed line in figure 6) is periodic over half the beat wavelength as shown in figure 7. It is important to note that the force also displays features which are much narrower than an optical wavelength (see figure 6). Further calculations are needed to determine the implications of these narrow structures.

---

[13] M.S. Shahriar, P.R. Hemmer, N.P. Bigelow, and M.G. Prentiss, *Proceedings of the Quantum Electronics and Laser Science Conference*, Baltimore, Maryland, 1991.

[14] J. Javanainen, *Phys. Rev. Lett.* 64: 519 (1990).

[15] H.R. Gray, R.M. Whitley, and C.R. Stroud, Jr., *Opt. Lett.* 3: 218 (1978).

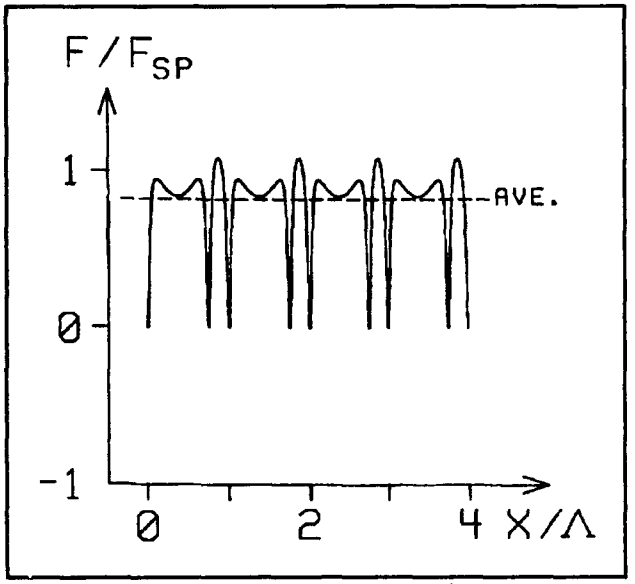

Figure 6. Stimulated force on the $|->$ state, for $\delta = 0, 2\Delta = \Omega_0 = 4\gamma_0, \Psi = \pi/4$. Dashed line is average (rectified) force.

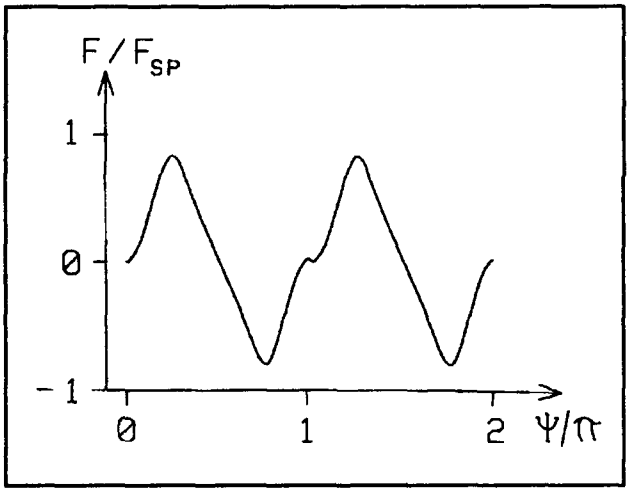

Figure 7. Rectified force, averaged over an optical wavelength, plotted as a function of Ψ, over one beat wavelength, for $\delta = 0, 2\Delta = \Omega_0 = 4\gamma_0$.

1.4 Phase-Locked, Closed-Loop Three-Wave Mixing Demonstrated in Atomic Sodium via Excitation of Microwave Dressed States With Optical Frequencies

Sponsor

U.S. Air Force - Electronic Systems Division
Contract F19628-89-K-0030

It is well known[16] that a laser excited Raman interaction causes atoms to be optically pumped into a non-absorbing dressed state called the trapped state. In atomic sodium, the trapped state consists of a linear combination of hyperfine levels having a microwave frequency separation. We have demonstrated that in the presence of a resonant microwave field, the Raman trapped state translates into one or the other microwave spin-locked (dressed) state under appropriate experimental conditions.[17] Analogously, we have shown that a microwave field can also be used to excite the optical Raman trapped state.

Figure 8a shows a three-level atomic system in the Λ configuration where ω_1 and ω_2 are the frequencies of the optical fields and ω_3 is the frequency of the microwave field. Here it is assumed that states 1 and 3 are long lived, but state 2 is short lived with a decay rate of γ_2. The Raman trapped state has the form[16]

$$|1> |n_1 + 1> |n_2> \exp(i(k_1 z_1 - k_2 z_2)) -$$

$$|3> |n_1> |n_2 + 1>,$$

where equal Rabi frequencies have been assumed. Here, $|1>$ and $|3>$ are the bare-atom states, and $|n_1> |n_2>$ is a field state with n_1 photons at frequency ω_1 and n_2 photons at ω_2. In addition, $(k_i z_i)$ represents the phase of the field at frequency ω_i, and the phase factor of the field at ω_2 has been factored out. Similarly, the high- and low- energy dressed states of the ground sublevel microwave transition[18] are

[16] H.R. Gray, R.M. Whitley, and C.R. Stroud, Jr., *Opt. Lett.* 3: 218 (1978); G. Alzetta, A. Gozzini, L. Moi, and G. Orriols, *Nuovo Cimento 36B: 5 (1976).*

[17] M.S. Shahriar and P.R. Hemmer, *Phys. Rev. Lett.* 65: 1277 (1985).

[18] S.R. Hartmann and E.L. Hahn, *Phys. Rev.* 128: 2042 (1962); Y.S. Bai, A.G. Yodh, and T.W. Mossberg, *Phys. Rev. Lett.* 55: 1277 (1985).

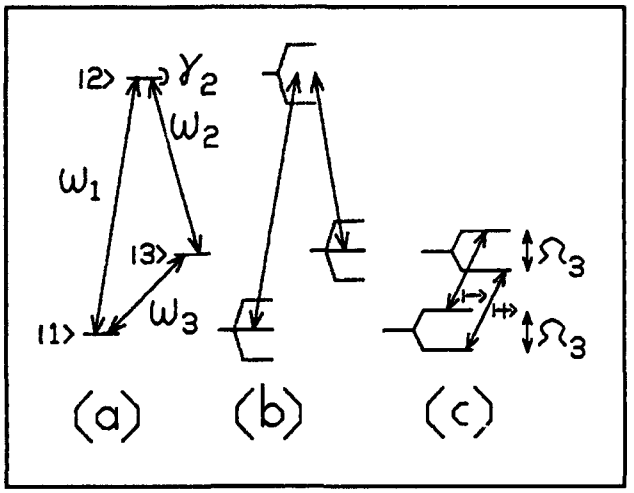

Figure 8.

$$|1> |n_3 + 1> \exp(i(k_3 z_3)) - |3> |n_3>$$

and

$$|1> |n_3 + 1> \exp(i(k_3 z_3)) + |3> |n_3>$$

respectively.

To help clarify the physics involved, consider a step-wise process wherein the optical Raman interaction and the microwave interaction are separated in time. First, the optical Raman interaction puts the atoms into the trapped state as illustrated in figure 8b. Next, the laser fields are turned off and a microwave field is turned on. In general, two microwave dressed states are possible as shown by the energy level diagram of figure 8c. To determine into which microwave eigenstate the Raman trapped state evolves, it is necessary to know the relative phase of the microwave and the double optical (Raman) fields. This relative phase is given by

$$\phi = [(k_1 z_1 - k_2 z_2) - k_3 z_3],$$

where it is assumed that all three states are in phase at

$$z_1 = z_2 = z_3 = 0.$$

When the laser difference frequency is exactly in (or out of) phase with the microwave frequency, i.e., $\phi = 0$ (or $\phi = \pi$), the Raman trapped state translates directly into the high (or low) energy microwave dressed state. For any other value of the relative phase ϕ, a linear combination of microwave dressed states results. In such a case, Rabi spin flips occur (>) (largest for $\phi = \pi/2$), partially destroying the original dressed state. To detect the degree of microwave interaction, the microwave field can be turned off, and the Raman interaction can be turned back on. Population lost from the trapped state would then appear as an increase in optical absorption.

Experimentally, the three-step process can be realized using a separated field excitation scheme in an atomic beam. The experimental setup we used is illustrated schematically in figure 9. To minimize the effects of laser jitter,[19] the field at frequency ω_2 is generated from that at ω_1 by using an acousto-optic modulator (A/O). The microwave field is generated by detecting and amplifying the beat between the two optical fields using a 2 GHz avalanche photodiode (APD). This ensures that the microwave and the double optical fields are phase locked. The relative phase ϕ between the microwave and laser difference frequencies is controlled with an optical delay line consisting of a translating corner cube (as shown in figure 9).

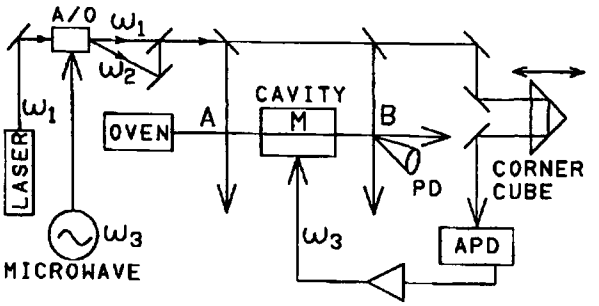

Figure 9.

First, Raman excitation in zone A pumps the atoms into the trapped state. Then, these atoms interact with a microwave field, zone M. The Raman probing interaction in zone B measures the degree of the microwave interaction by detecting any loss of the trapped state population, via the fluorescence detecting photodiode (PD). The pathlengths to zones A and B are set so that the optical difference frequencies in zones A and B are in phase.

Figure 10a shows the Raman-Ramsey fringes observed in zone B when the laser difference is scanned, for zero microwave power. Figure 10b shows the fluorescence observed, with the laser

[19] N.F. Ramsey, *Molecular Beams* (London: Oxford University Press, 1956); J.E. Thomas, P. R. Hemmer, S. Ezekiel, C.C. Leiby, Jr., R.H. Picard, and C.R. Willis, *Phys. Rev. Lett.* 48: 867 (1981).

difference frequency held exactly on resonance (fluorescence minimum), but the microwave power scanned. Here, the microwave field is exactly in phase with the optical difference frequency, i.e., $\phi = 0$. As can be seen, the microwave field has no effect, since in this case the optical Raman trapped state translates into a pure microwave spin-locked eigenstate. Figure 10c shows the case of $\phi = \pi/2$, as the microwave power is scanned again with the laser difference frequency held on resonance. Here, the fluorescence depends strongly on microwave power, undergoing large oscillations caused by Rabi spin flips, indicating that a microwave eigenstate is no longer excited. The damping with increasing microwave power in figure 10c is caused by velocity averaging effects. Comparison with the theoretical plots of figures 10d, 10e, and 10f show good agreement.

We also performed the complimentary experiment in which a microwave field is used to excite the optical Raman trapped state. This involves replacing the first Raman zone in figure 9 by an optical pumping zone (not shown), which effectively puts all the atoms into state $|3>$ before entering the microwave cavity. For a microwave power corresponding to a $\pi/2$ pulse, the resulting state is

$$(-i|1>|n_3>\exp(-ik_3z) + |3>|n_3 - 1>)$$

This can be made to correspond to a Raman trapped state if the relative phase ϕ between the microwave and the laser difference frequency is $\pi/2$.

Experimental evidence of microwave excitation of an optical Raman trapped state appears in figure 11. Figure 11a shows the zone B fluorescence obtained by scanning the laser difference frequency with a microwave power corresponding to a $\pi/2$ pulse and a relative phase of $\phi = \pi/2$. As can be seen, Ramsey fringes are obtained which closely resemble those in figure 10a, even though only one Raman excitation zone is present. Thus, an optical Raman trapped state has been excited by the microwave field. For completeness, figure 11b shows the zone B fluorescence obtained with the microwaves turned off. As expected, no Ramsey fringes are seen in this case.

Extension of these results to a single zone excitation scheme (where both microwave and optical Raman fields are present simultaneously) is also of interest because of the possibility of exciting a three photon trapped state. This would occur for a relative Raman and microwave phases of $\phi = 0$ or π. For other values of ϕ, all dressed states are partially optically absorbing, where the steady state absorption depends on ϕ. For a properly chosen configuration, the position dependence of the relative phase ϕ would result in a grating being produced, which would diffract both optical and microwave fields. Numerous applications of this effect can be imagined if the microwave transition is replaced by a mm-wave or far infrared transition. For example, real time mm-wave beam steering can be performed wherein the mm-wave could be deflected by the optical beams. It should also be possible to perform real time holographic far infrared to visible image conversion.

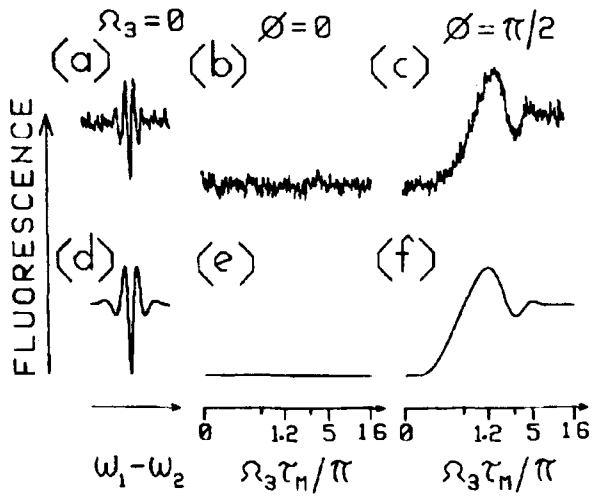

Figure 10.

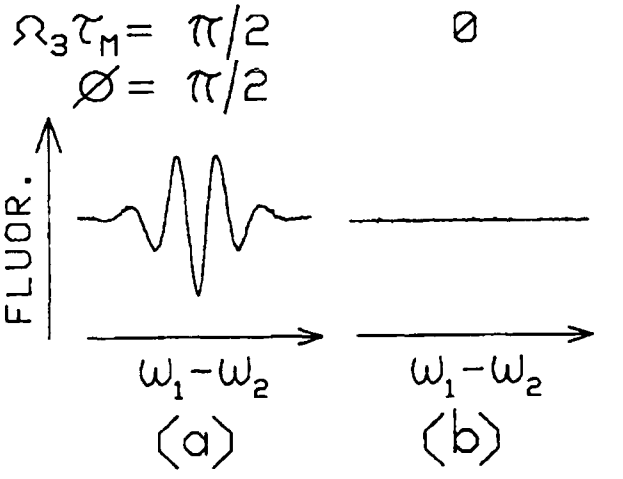

Figure 11.

Chapter 2. Basic Atomic Physics

Academic and Research Staff

Professor Daniel Kleppner, Professor David E. Pritchard, Dr. Chun-Ho Iu, Dr. Wolfgang Ketterle, Dr. Min Xiao

Visiting Scientist and Research Affiliates

Dr. Tomaz Catunda, Dr. Theodore W. Ducas,[1] Dr. Alex Martin

Graduate Students

Kevin R. Boyce, Pin P. Chang, Eric A. Cornell, Michael W. Courtney, Kendall Davis, Frank DiFilippo, Christopher R. Ekstrom, Troy Hammond, Kristian P. Helmerson, Jeff Holley, Hong Jiao, Michael A. Joffe, David W. Keith, Robert Lutwak, Vasant Natarajan, Bruce G. Oldaker, Scott Paine

Undergraduate Students

Charles Freeman, John Gachora, Matthew Marjanovic, David Mitchell, Quentin Turchette

Technical and Support Staff

Carol Costa

2.1 The Diamagnetic Rydberg Atom

Sponsors

National Science Foundation
Grant PHY 89-19381
U.S. Navy - Office of Naval Research
Grant N00014-90-J-1322

Project Staff

Dr. Chun-Ho Iu, Michael W. Courtney, Dr. Tomaz Catunda, Hong Jiao, Professor Daniel Kleppner

A highly excited hydrogen atom in a strong magnetic field, the so-called "diamagnetic hydrogen atom," is among the simplest nonseparable systems in quantum mechanics. Understanding it can provide a key to the more general aspects of nonseparable systems. The problem is also attracting attention in the context of nonlinear dynamics because its classical behavior displays a transition from orderly to disorderly motion as the energy is increased in a fixed magnetic field. One can study the quantum structure of the system in this regime both theoretically and experimentally. Thus, the diamagnetic hydrogen atom provides an ideal testing ground for studying the relation between quantum structure and disorderly classical motion, a subject sometimes called "quantum chaos."

We have developed techniques for carrying out high resolution laser spectroscopy on the lithium atom in a strong magnetic field. (As we shall demonstrate, the differences between lithium and hydrogen are essentially negligible.)

The experiment uses a lithium atomic beam which is excited by two c.w. lasers. The first laser excites the atoms from the 2S state to the 3S state by a two-photon transition and the second laser excites the atoms to Rydberg states. The excited atoms are detected by electric field ionization. We typically operate in magnetic fields near 6T. We can determine the energy within 10^{-3} cm^{-1}, and the magnetic field within 5 gauss.

The Hamiltonian for the diamagnetic hydrogen atom, in atomic units, is

$$H = \frac{p^2}{2} - \frac{1}{r} + \frac{1}{2} L_z B + \frac{1}{8} B^2 \rho^2, \qquad (1)$$

There are no general solutions to this problem, and perturbation theory is not applicable in the positive energy regime. Our experimental results[2] have

[1] Department of Physics, Wellesley College, Wellesley, Massachusetts.

[2] C. Iu, G.R. Welch, M.M. Kash, L. Hsu, and D. Kleppner, *Phys. Rev. Lett.* 63: 1133 (1989).

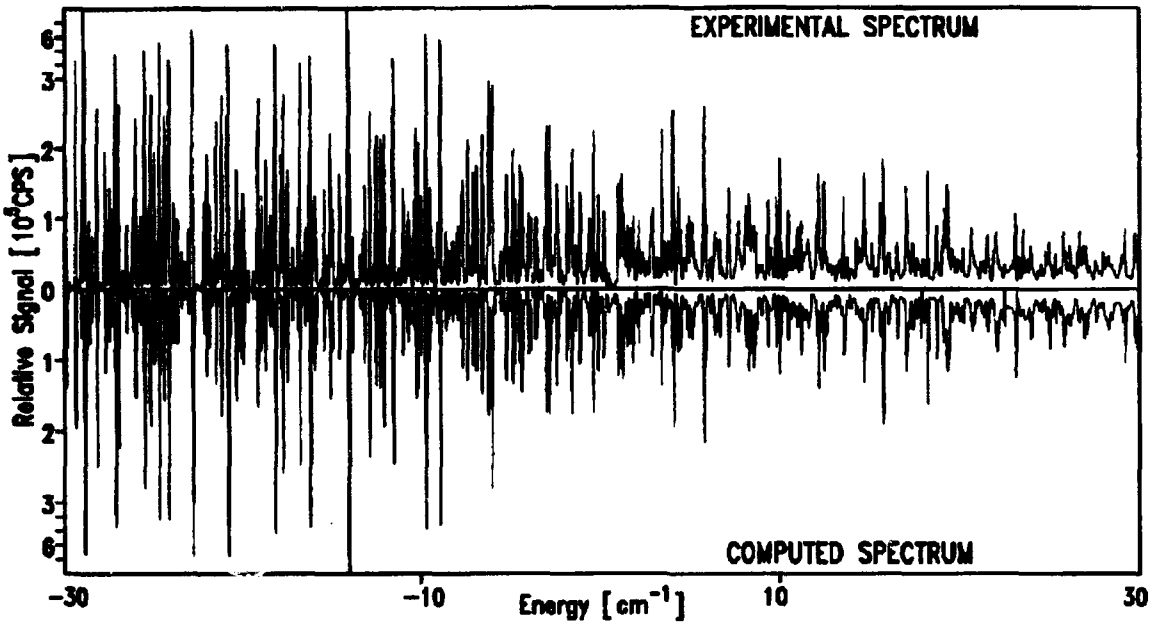

Figure 1. Comparison between the experimental spectrum of lithium at B = 6.113 T ($L_z = 0$, odd parity) with the calculated spectrum of hydrogen, from reference 1.

helped to stimulate theoretical advances, and these two efforts have now been joined to provide a comparison of experiment and theory at an unprecedented level of detail. Figure 1 displays a high resolution spectrum of lithium in a field of 6 tesla in an energy range near the ionization limit, a region that until recently was essentially unexplored. The results of a recent theoretical calculation by Delande and Gay[3] are displayed for comparison. They employ the complex coordinate-rotation method and a matrix diagonalization using a Sturmian-type basis. Figure 2 shows a detailed comparison between our experiment and their calculation near 7 cm^{-1} at 6.131 T. This is well above the ionization limit in this field, 2.81 cm^{-1}. The agreement is, for all present purposes, perfect.

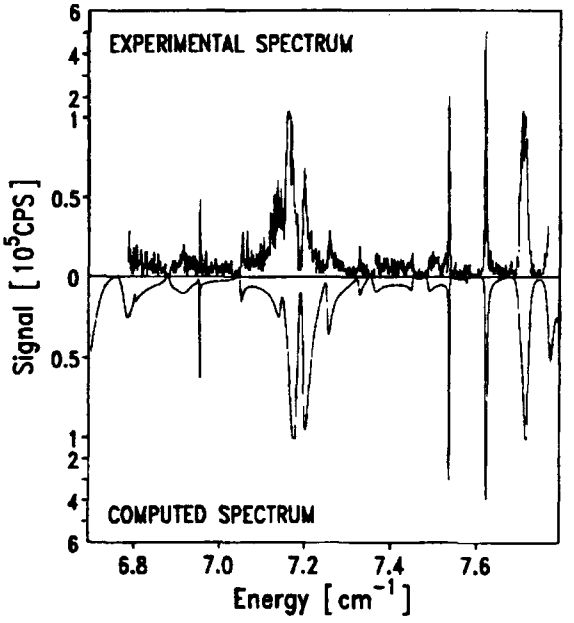

Figure 2. Detailed comparison of experiment and theory, from reference 1.

[3] D. Delande, A. Bommier, and J.C. Gay, *Phys. Rev. Lett.* 66: 141 (1991); C. Iu, G.R. Welch, M.M. Kash, D. Kleppner, D. Delande, and J.C. Gay, *Phys. Rev. Lett.* 66: 145 (1991).

This result represents a twofold achievement. By confirming the validity of the calculation, our experiment has opened the way to the use of calculational methods for studying the atom-field system in broad regimes. Thus, we have a powerful new tool for studying the system. Furthermore, the agreement between theory and experiment confirms the reliability of the experiment. It assures, for instance, that lithium is a suitable test atom for the diamagnetic hydrogen problem and that potentially worrisome experimental effects, for instance the effects of small stray electric fields, are not, in fact, important.

In addition to our experimental work, we have been investigating the theoretical energy level structure in a bound state regime where numerical calculations are relatively straight forward. The goal of this effort is to shed light on the origin of periodic structures in the spectrum that we have discovered in the positive energy regime.[2] We have carried out calculations for energy levels below $-35\ cm^{-1}$ from 0 to 6 tesla using an IBM RT computer. The calculations were carried out by diagonalizing 1,241 λ type bases.[4] The results of the calculation were verified by experiment at a field of 6T. A typical result is shown in figure 3.

The important physical features revealed in figure 3 are these. In the low field region the principal quantum number n is "good," though the angular quantum number l is destroyed by the magnetic field. The levels follow quadratic trajectories in the field that are governed by an approximate sym-

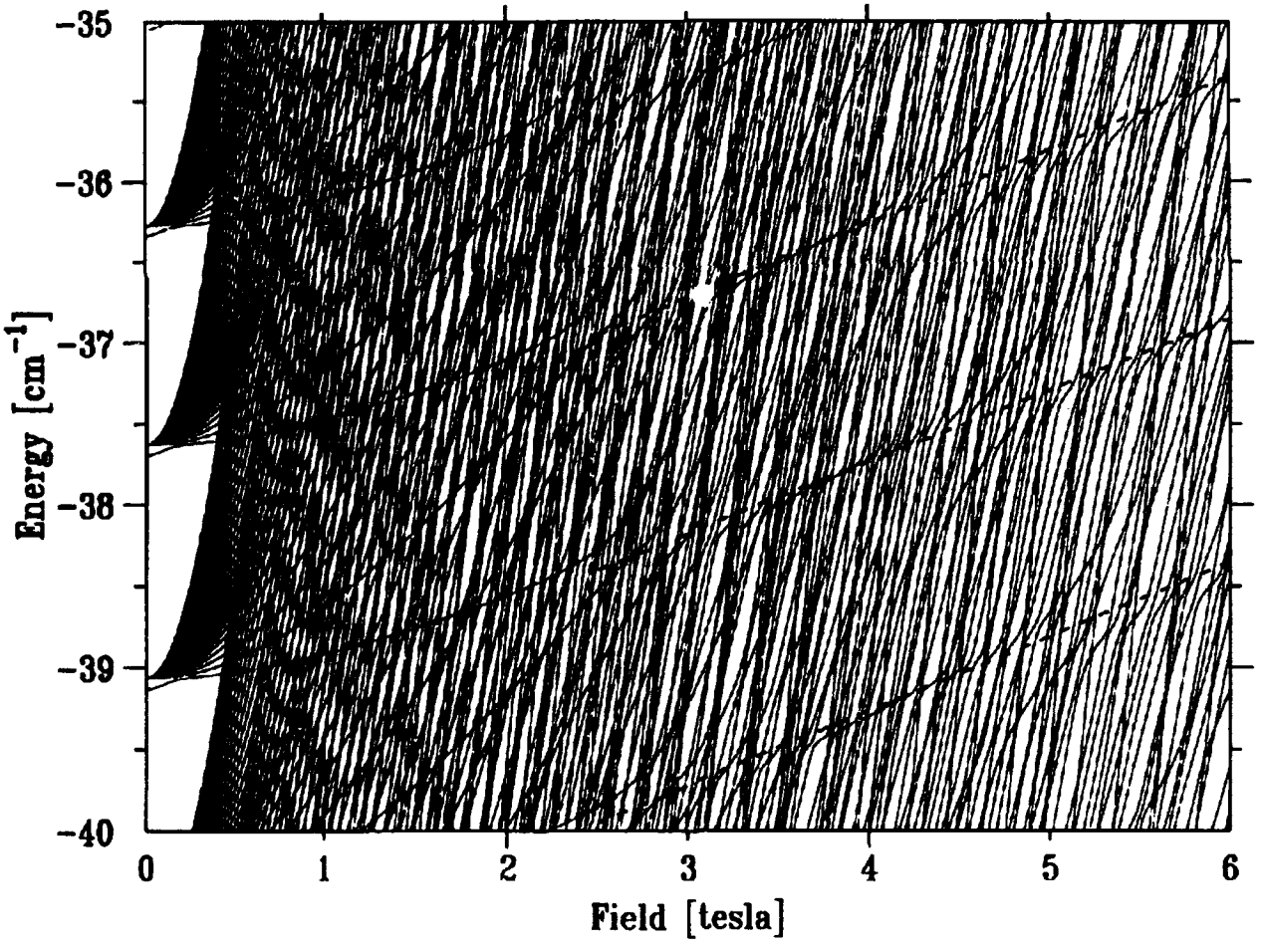

Figure 3. Diamagnetic structure of lithium from 0 to 6 T.

[4] C. Iu, Ph.D. diss. Dept. of Physics, MIT, 1990.

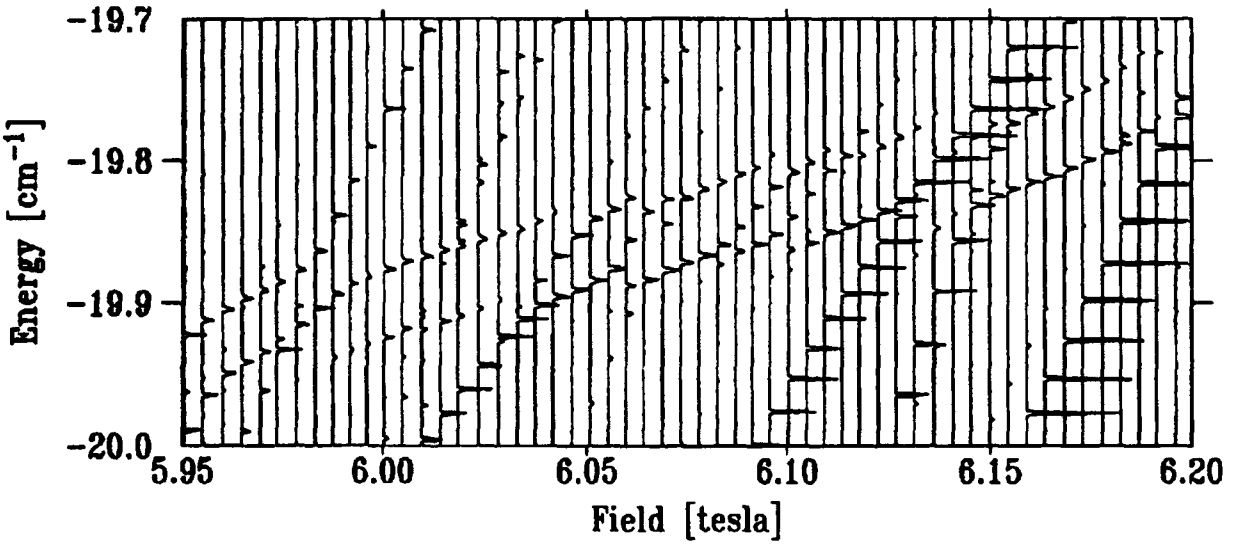

Figure 4. One-dimensional Stark splitting near 6 T, n = 70. The electric field is approximately 80 mV/cm.

metry, the λ symmetry.[5] As the field is increased, levels from different n-manifolds begin to interact and the levels start to repel each other. One expects that as the field is increased the level interactions would become so strong that the λ symmetry would be completely destroyed. However, in figure 3, we can see the levels reconstitute themselves after passing through a region of strong level repulsion, as manifested by a structure of successive narrowly avoided crossings. At large field, these levels form approximately parallel structures with spacings equal to a sequence of Rydberg levels. (Dashed lines are drawn along these lines to help their identification.) These levels appear to correspond to the Rydberg series of the lowest Landau level near the ionization limit seen in reference 1, except that they lie at much lower energy.

In addition to the study of level structure, we have studied the Stark splitting of the one-dimensional hydrogen atom that is created by magnetic confinement of the electron transverse to the magnetic field. Figure 4 shows an example of the Stark splitting. The levels correspond to the Rydberg level of n = 70. The electric field was about 80 mV/cm. The predicted Stark splitting is 0.050 cm^{-1}, and the measured splitting from figure 4 is 0.047 cm^{-1}. This observation of the one-dimensional Stark splitting further confirms the regular behavior of the quantum system.

Publications

Iu, C., G.R. Welch, M.M. Kash, D. Kleppner, D. Delande, and J.C. Gay. "The Diamagnetic Rydberg Atom: Confrontation of Calculated and Observed Spectra." *Phys. Rev. Lett.* 66: 145 (1991).

Kleppner, D., C. Iu, and G.R. Welch. "Positive Energy Spectroscopy of the Diamagnetic Lithium System." *Comments At. and Mol. Phys.* 25: 301 (1991).

Thesis

Iu, C. *Energy Level Structure of Atoms in Magnetic Fields.* Ph. D. diss. Dept. of Physics, MIT, 1990.

[5] D. Delande and J.C. Gay, *Comment At. Mol. Phys.* 19: 35 (1986).

2.2 Millimeter-Wave Frequency Measurement of the Rydberg Constant

Sponsors

Joint Services Electronics Program
Contract DAAL03-89-C-0001
National Science Foundation
Grant PHY 89-19381

Project Staff

Pin P. Chang, Scott Paine, Robert Lutwak, Professor Daniel Kleppner

The Rydberg constant R_∞ determines the wavelengths of the spectrum of hydrogen. More fundamentally, it relates the atomic and practical length scales. It is among the most accurately known fundamental constants: Recent experiments have determined R_∞ to nearly one part in 10^{10} using optical spectroscopy.[6] These measurements are approaching the practical limits of optical wavelength metrology. Future progress will have to come from frequency measurements, making use of the modern definition of length in terms of time intervals and a defined speed of light c.

We are attempting to advance the precision of R_∞ by measuring it in frequency units. The specific quantity we are measuring is cR_∞, which might be called the "Rydberg frequency." Our approach is based on millimeter wave spectroscopy on transitions between adjacent Rydberg states of hydrogen, around n = 30. Because the frequency of millimeter wave radiation can be measured to the full precision of modern atomic clocks, the experiment is not limited by metrological standards.

The goals of our experiment are three-fold: First is the reevaluation of R_∞ itself. Second is the measurement of the Lamb shift. Our measurements involve high angular momentum states for which the Lamb shift is extremely small. A comparison of our results with optical measurements can yield an improved value of the Lamb shift. Third is the precise frequency calibration of the spectrum of hydrogen in order to provide independent confirmation of the accuracy of optical frequency metrology as this technique starts to advance.

Our experiment works as follows. Hydrogen or deuterium in an atomic beam is excited by two-photon absorption to the state n = 29, m = 0. A crossed electric and magnetic field scheme[7] then transfers the atoms to the longer-lived n = 29, |m| = 28 "circular" state. The atoms then pass into an interaction region where a resonance transition takes place on the $n = 29 \rightarrow n = 30$ transition. The atoms interact with the millimeter wave radiation at two locations in a Ramsey separated oscillatory fields geometry. Finally, the atoms are state-analyzed in a selective electric field ionization detector capable of differentiating between the n = 29 and n = 30 circular states. The resonance signal is obtained by counting the atoms in each state as the millimeter wave frequency is tuned across the $n = 29 \rightarrow n = 30$ transition.

Figure 5 illustrates the main features of the atomic beam apparatus. Atomic hydrogen is produced by dissociating H_2 in a radio frequency discharge. To minimize the frequency width of the resonance transition, the interaction time is prolonged by cooling the atomic beam. This is accomplished by flowing the hydrogen through an aluminum thermalizing channel whose temperature can be as low as 10K. The atoms are excited optically in a crossed electric and magnetic field region. The magnetic field is produced by permanent magnets. The electric field is produced by an arrangement of strip electrodes that allows the field magnitude and direction to be switched in order to boost the atoms to the circular state. A pulsed electric field ionization detector is available to monitor the excited atoms shortly after they are produced during laser setup and tuning.

The interaction region is designed to allow application of a carefully controlled electric field which defines the quantization axis for the Rydberg states. It is shielded both electrically and magnetically and cooled by a liquid helium flow system to reduce the effects of blackbody radiation.

The final detectors employ a spatially-resolved electric field ionization method. Here, the atoms enter a region of increasing electric field (1kV/cm–2kV/cm) produced by a ramped field plate. The two detectors are spaced such that the n = 30 atoms, which ionize in lower field, are picked up in the first detector, and n = 29 are picked up in the second. A quadrupole mass analyzer at the far end of the apparatus is used to

---

[6] M.G. Boshier et al., *Phys. Rev. A* 40: 6169 (1989); P. Zhao et al., *Phys. Rev.* A 39: 2888 (1989); F. Biraben et al., *Phys. Rev. Lett.* 62: 621 (1989).

[7] D. Delande and J. C. Gay, *Europhys. Lett.* 5: 303 (1988).

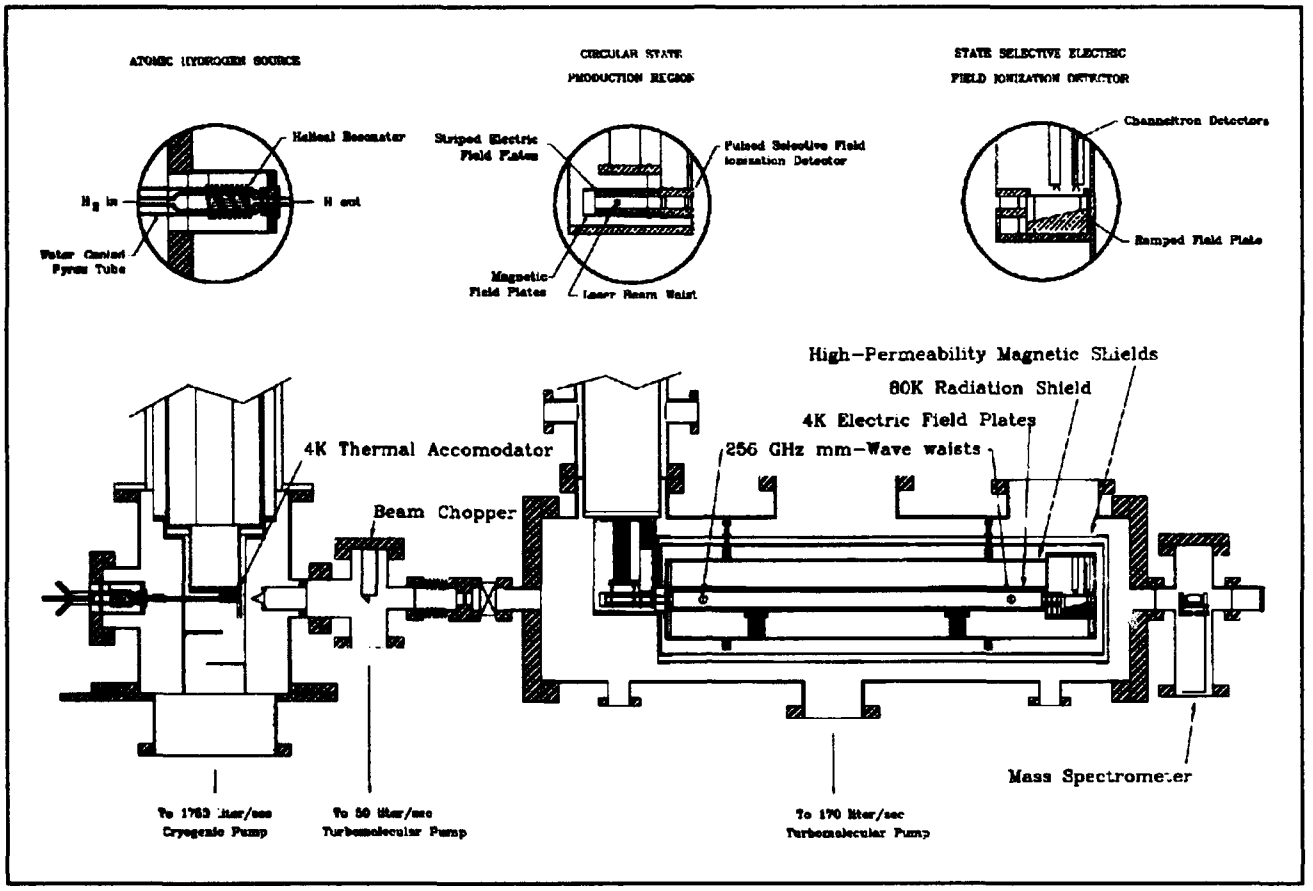

Figure 5. Schematic of the atomic beam apparatus. Insets detail the dissociation, production, and detection of circular states of atomic hydrogen.

monitor the intensity and dissociation fraction of the atomic beam.

A schematic of the laser system is shown in figure 6. Two independent systems produce tunable UV light near 365 nm by sum frequency mixing the fundamental output of a pulsed Nd:YAG laser with tunable yellow dye lasers pumped by the second harmonic of the YAG. One of the UV beams is frequency tripled in Kr gas to produce 121 nm light to drive the $1s \rightarrow 2p$ transition; the second UV beam drives the $2p \rightarrow n = 29$ transition. The dye lasers (figure 7) are required to have narrow spectral linewidth and are thus designed to operate in a single longitudinal mode. A feedback system[8] keeps the laser cavity mode centered on the frequency band selected by the grating and tuning mirror.

The millimeter wave optical system is shown in figure 8. Its function is to place two beam waists of appropriate size with adjustable power, polarization, and relative phase on the atomic beam.

The apparatus is substantially complete. Improvements are now under way, and we expect to commence millimeter wave spectroscopy shortly.

[8] Raymond et al., *Opt. Lett.* 14: 1116 (1989).

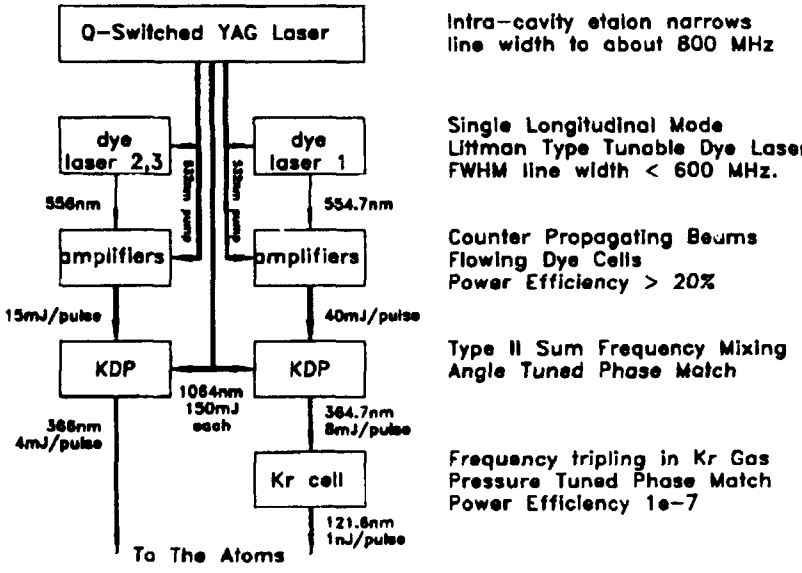

Figure 6. Schematic of the optical system employed in exciting Rydberg states of atomic hydrogen.

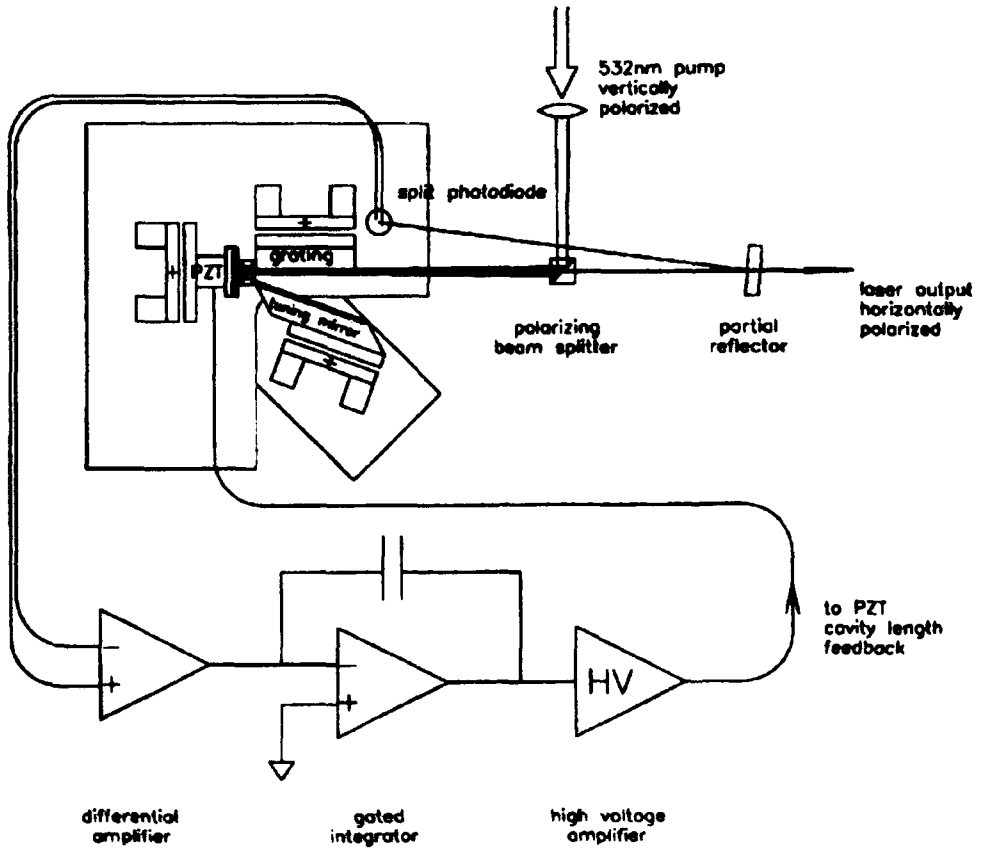

Figure 7. Detail of pulsed tunable dye laser. Laser operates in a single longitudinal cavity mode for narrow line width.

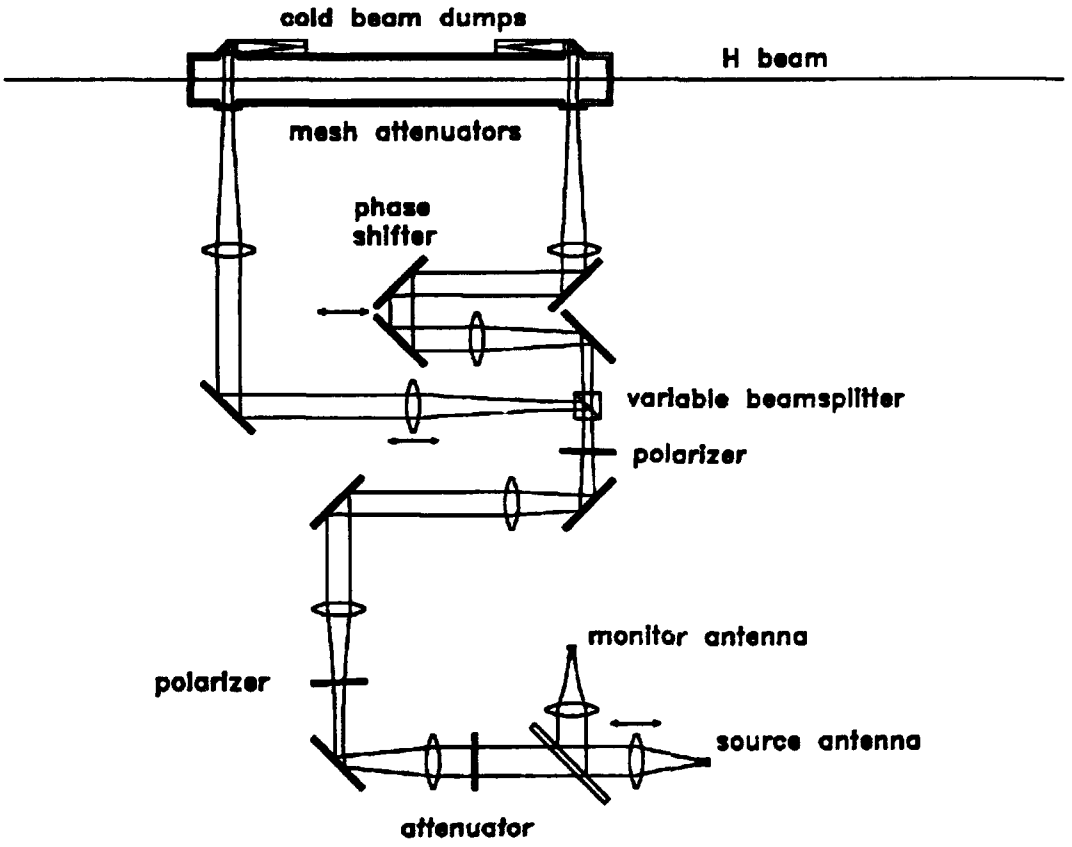

Figure 8. Layout of quasi-optical system for the 256 GHz mm-wave radiation.

2.3 Precision Mass Spectroscopy of Ions

Sponsors

Joint Services Electronics Program
Contract DAAL03-89-C-0001
National Science Foundation
Grant PHY 86-05893

Project Staff

Kevin R. Boyce, Eric A. Cornell, Vasant Natarajan, Professor David E. Pritchard

In 1990 we initiated a program to substantially improve our precision mass measurement experiment. These improvements should allow us to reach a precision of about 10^{-11} in our mass measurements of individual atomic and molecular ions, the next step toward our ultimate goal of a few parts in 10^{12}. This capability will allow us to do a variety of experiments which address issues in both fundamental and applied physics, including:

1. The $^3H^+ - {}^3He^+$ mass difference, important in ongoing experiments to determine the electron neutrino rest mass;
2. Determination of excitation and binding energies of atomic and molecular ions by weighing the small decrease in energy, $\Delta m = E_{bind}/c^2$;
3. Determination of Avogadro's number N_A, by weighing γ-rays—its accurate determination would permit the replacement of the "artifact" mass standard by an atomic mass standard; and
4. Improvement of many traditional applications of mass spectroscopy by orders of magnitude improvement in both accuracy and sensitivity.

Our experimental approach is to measure ion cyclotron resonance on a single molecular or atomic ion in a Penning trap, a highly uniform magnetic field with axial confinement provided by weaker electric fields. We monitor the ion's oscillation along the magnetic field lines by detecting the currents induced in the trap electrodes. Working with only a single ion is essential because

space charge from other ions leads to undesired frequency shifts. This work in trapping and precision resonance draws on techniques developed by Hans Dehmelt at the University of Washington and Norman Ramsey at Harvard, for which they shared in the 1989 Nobel Prize.

We have developed techniques for driving, cooling, and measuring the frequencies of all three normal modes of Penning trap motion. Thus we can manipulate the ion position reproducibly to within 30 microns of the center of the trap, correcting for electrostatic shifts in the cyclotron frequency to great accuracy. We use a π-pulse method to coherently swap the phase and action of the cyclotron with the axial modes.[9] Therefore, although we detect only the axial motion directly, we can determine cyclotron frequency by measuring the phase accumulated in the cyclotron motion in a known time interval (figure 9).

In the past year we have built an entirely new Penning trap and detector, including a higher-Q resonant circuit and quieter RF SQUID; all of which should improve our signal to noise ratio by a factor of two. We have also replaced the DC electric field supply, added provisions for rapidly cycling between two ion species, and added a pressure regulator to the liquid helium bath of our superconducting magnet to help stabilize the field.

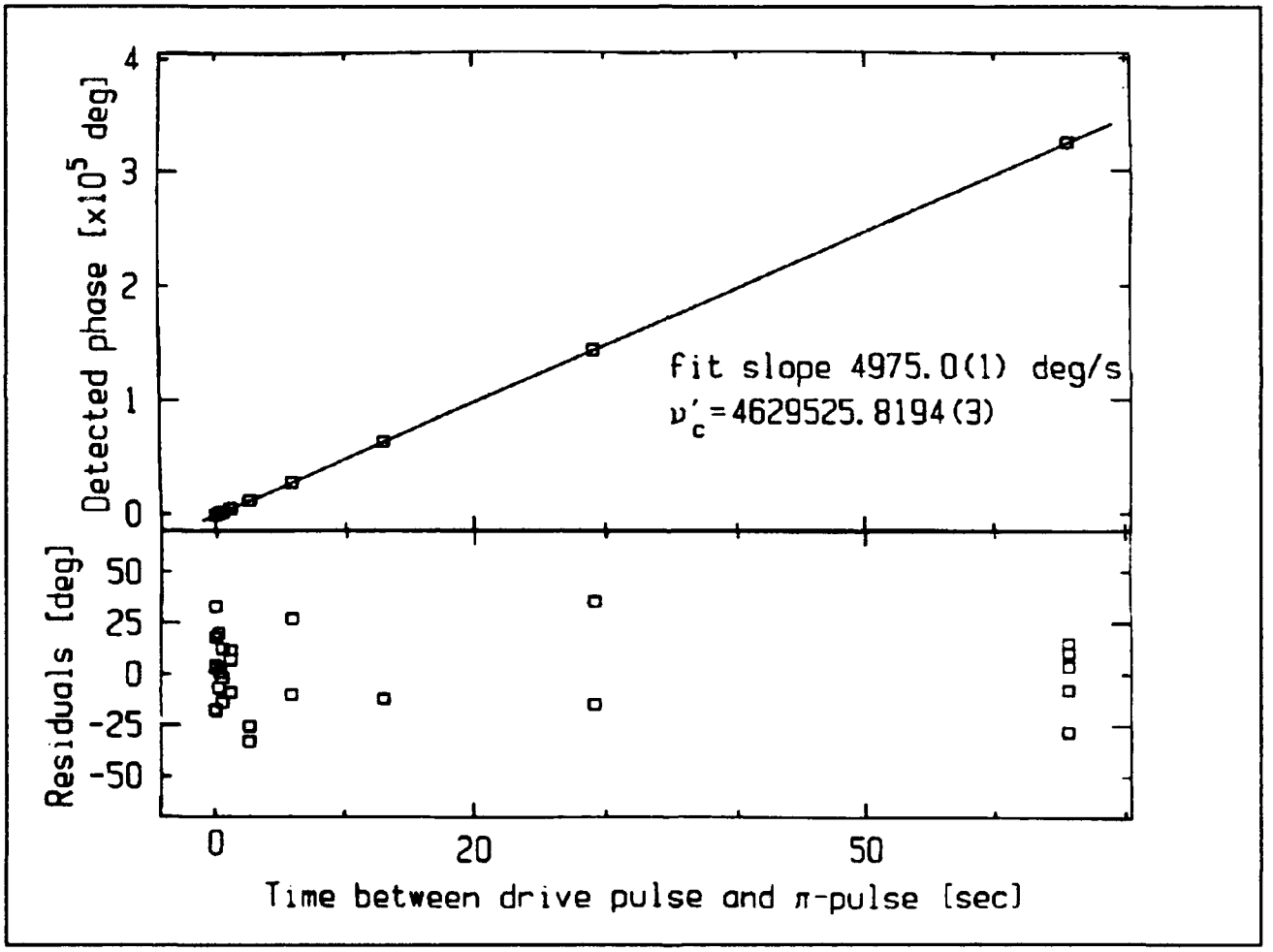

Figure 9. For each plotted point, we perform the following experiment: The initially cold ion is pulsed into a cyclotron orbit of known initial phase, and then allowed to evolve "in the dark" for an indicated amount of time, t. Then a pulse is applied which exchanges cyclotron and axial motions, bringing the ion's cyclotron action and phase into the axial mode. As the ion's axial motion rings down, its phase is detected. The appropriate multiple of 360° is added, and a line is fitted to the points. The slope of the line is the frequency difference between the frequency generator and the trap cyclotron frequency.

[9] E.A. Cornell, R.M. Weisskoff et al., *Phys. Rev. A* 41: 312 (1990).

In addition, we are building ion optics and an external ion source to allow us to make the ions in a discharge at room temperature and then load them into the trap. This will eliminate the problem of residual neutral gas in the trap when using volatile species such as hydrogen and helium.

We also performed a mass "comparison" between N_2^+ and itself, to check for any unsuspected effects of loading new ions.[10] The results, shown in figure 10, indicate that any systematic shifts due to our ion-loading process are below the uncertainty of our previous measurement of $N_2^+ - CO(< 4 \times 10^{-10})$.

With all the improvements to the system, we foresee being able to resolve the existing 10 eV discrepancy between measurements of $m(^3H) - m(^3He)$ in the next year. In addition, we plan to demonstrate a classical squeezing technique which should reduce the thermal fluctuations of our measurement by a factor of three to five. After that, we should continue development of techniques to measure two ions of different mass simultaneously. The two-ion technique in combination with the various improvements made over the last year will lead to precision in the range of 10^{-11}.

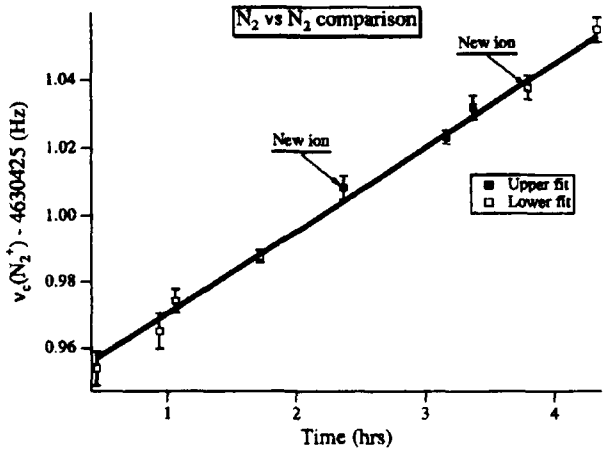

Figure 10. We loaded the same type of ion three times and measured the cyclotron frequency. The lines are a single fit to three parameters: slope, intercept, and splitting. The lower line is the fit for the open squares (ions numbers 1 and 3), and the upper line is the fit for the filled squares (ion number 2). The error bar for the splitting (not shown) is 1.8 mHz (compared to 1.1 mHz splitting). The slope is due to the trap moving in the linear magnetic field gradient as the liquid nitrogen boils off.

Publications

Cornell, E.A., R.M. Weisskoff, K.R. Boyce, and D.E. Pritchard. "Mode Coupling a Penning Trap: π Pulses and a Classical Avoided Crossing." *Phys. Rev. A.* 41: 312 (1990).

Cornell, E.A. *Mass Spectroscopy Using Single Ion Cyclotron Resonance.* Ph.D. diss., Dept. of Physics, MIT, 1990.

2.4 Atom Interferometry

Sponsors

Joint Services Electronics Program
Contract DAAL03-89-C-0001
U.S. Army Research Office
Contract DAAL03-89-K-0082
U.S. Navy - Office of Naval Research
Grant N00014-89-J-1207

Project Staff

Christopher R. Ekstrom, David W. Keith, Quentin Turchette, Professor David E. Pritchard

Using fabricated transmission gratings as optical elements for matter waves, we are constructing an atom interferometer which will physically separate atom waves before recombining them. Atom interferometers will be useful in studies of atomic properties, tests of basic quantum physics, for metrology, as a rotation sensor, and perhaps ultimately as devices to make ultra-small structures using atom holograms.

During 1990 our atom interferometer evolved from a rough and ready state to an essentially complete device. Major effort was spent on a new detector and on developing procedures to increase detector sensitivity, source modifications which have given about ten times the previous signal with more reliability, a computer data acquisition and analysis system and appropriate software, rebuilding components to reduce the vibrational noise level, and a simulation program to calculate the expected interference pattern and signal. We also worked in collaboration with the MIT Submicron Structures Laboratory to produce atom gratings with higher transmission, better dimensional stability, and less distortion. We tried several times to observe atom fringes, but were frustrated by grating problems each time. The improvements in signal to noise

[10] E.A. Cornell, *Mass Spectroscopy Using Single Ion Cyclotron Resonance,* Ph.D. diss., Dept. of Physics, MIT, 1990.

and grating transmission resulted in much better atom diffraction patterns (see figure 11).

Our interferometer consists of three 0.2 μm-period diffraction gratings equally spaced ~0.65 m apart in our atomic beam machine. The maximum separation of the atom waves will be ~60 μm. The first two gratings separate and redirect the atomic beam forming a standing wave interference pattern in the atomic flux at the third grating, which acts like a mask to sample this pattern. Figure 12 shows the design of the interferometer.

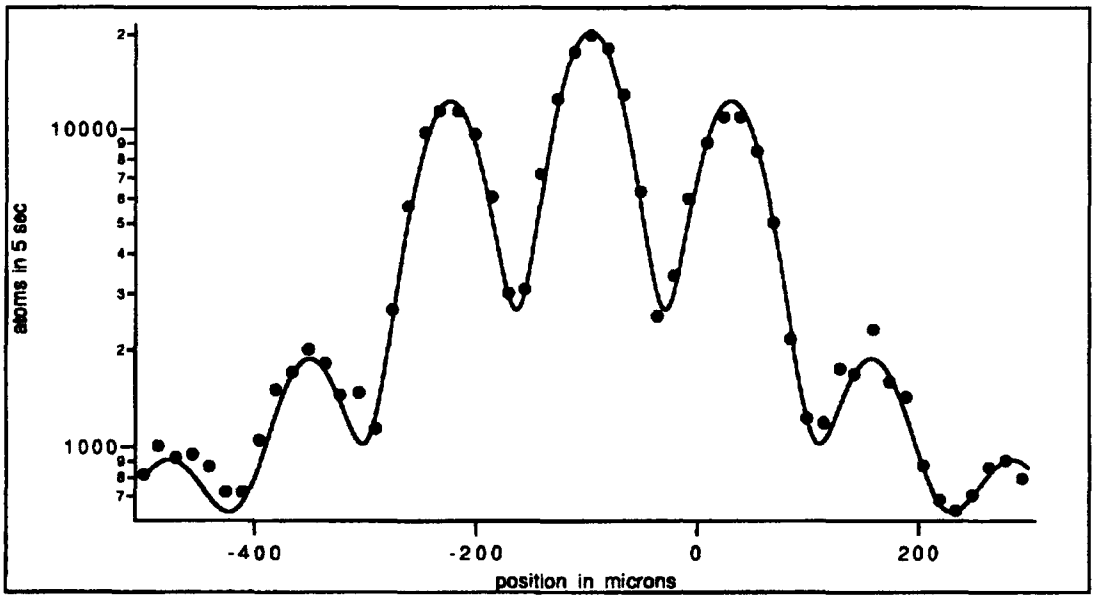

Figure 11. Diffraction of atoms from fabricated grating.

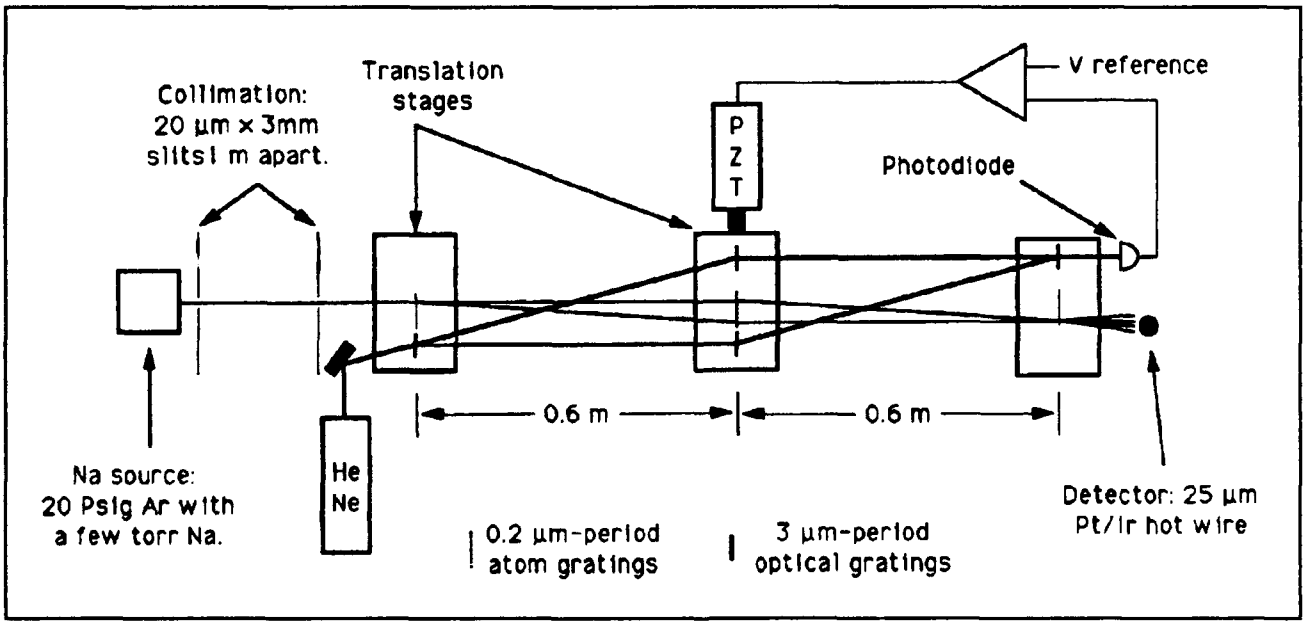

Figure 12. Our current atom interferometer with laser interferometer stabilization system (not to scale).

The mechanical vibrations of our machine present a principal technical obstacle because they might blur the interference pattern. There are two types of required limits on vibrations. First, the three gratings must move relative to each other by less than ~1/4 period (50 nm) during the time the

final grating samples the intensity at a given position. Thus, the rms amplitude of relative vibrations integrated over all frequencies greater than the reciprocal of the detector integration time must be less than ~50 nm. The second requirement is related to the motion of the gratings due to acceleration of, or rotation about, the center of mass of the grating system during the 1.3 ms it takes for the atoms to traverse the interferometer. This means that below ~900 Hz the rms acceleration must be less than $10^{-2}ms^{-2}$ and the rms angular velocity must be held below 10^{-4} radians per second.

Because each grating/slit assembly in the interferometer is in neither the near nor the far field of the others, it is not possible to derive an analytic expression for the interference signal. We have advanced the state-of-the-art of interferometer calculations by devising a way to cast the multiple grating problem as a convolution problem, enabling us to use Fast Fourier Transforms. A ten-minute run on a CRAY computer can simulate the interferometer with an incoherent source possessing the actual velocity profile. Figure 13 shows the results of a typical calculation.

These numerical simulations have allowed us to investigate several important issues in interferometer design. We have investigated the rate at which fringe contrast degrades with mis-spacing of the three gratings and due to the spread of initial velocities (and corresponding change of deBroglie wavelengths) in the source beam. We have also examined the possibilities of constructing interferometers with varying degrees of beam collimation, and we plan to study the effects of source coherence (the collimator does not really have a blackbody source behind it).

When we have successfully demonstrated this interferometer, our first experimental objective is to make improved measurements of the polarizability of sodium and the Aharonov-Casher effect.

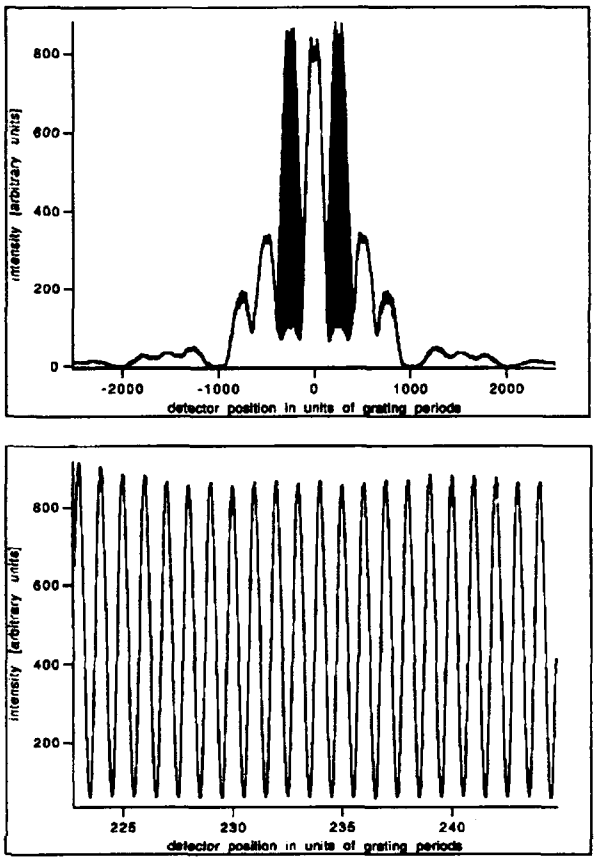

Figure 13. (Top) Predicted intensity distribution at position of third grating. Atoms diffracted by different routes wind up in the major bumps shown. When different routes diffract into the same bumps, interference results, which appears as solid black. (Bottom) Detail of intensity on right side of first order bump (the one used in our interferometer). The interference pattern has the period of one grating period—hence the total transmitted intensity is a periodic function of the third grating's position.

Publications

Keith, D.W. and D.E. Pritchard. "Atom Optics." *New Frontiers in Quantum Electrodynamics and Quantum Optics.* Ed. A.O. Barut. New York: Plenum Press, 1990.

Oldaker, B.G., P.J. Martin, P.L. Gould, M. Xiao, and D.E. Pritchard. "Experimental Study of Sub-Poissonian Statistics in the Transfer of Momentum from Light to Atoms." *Phys. Rev. Lett.* 65: 1555 (1990).

Oldaker, B.G. *Multi-Photon Momentum Transfer from Light to Atoms.* Ph.D. diss. Dept. of Physics, MIT, 1990.

Pritchard, D.E. "Atom Optics." *Yearbook of Science and Technology.* New York: McGraw-Hill, 1990.

2.5 Cooling and Trapping Neutral Atoms

Sponsor

U.S. Navy - Office of Naval Research
Grant N00014-90-J-1642

Project Staff

Kristian P. Helmerson, Michael A. Joffe, Dr. Wolfgang Ketterle, Professor David E. Pritchard

Our current objective is to produce an intense slow atom beam and trap it in a magnetic trap. The atoms will be trapped by the forces of an inhomogeneous magnetic field on the magnetic moment of the atom. We have in mind several schemes capable of cooling the atoms to microkelvin temperatures, which will greatly increase the density in the bottom of the trap.

Dense samples of atoms cooled to microkelvin temperatures promise to open up new and exciting areas of physics. The lower interaction rate of the atoms due to their reduced thermal motion, together with the possibility of indefinitely long interaction times, make samples of trapped atoms ideal for high resolution spectroscopy and for use as atomic frequency standards.[11] High density samples of ultra-cold atoms will also make it possible to study interatomic collisions in a new regime characterized by a long deBroglie wavelength, the importance of weak forces, and collision durations which are longer than radiative lifetimes so that absorption, stimulated and spontaneous radiative transitions take place *during* a collision. This opens the possibility of controling the outcome of collisions by weak laser irradiation. High density samples of atoms at low temperature atoms are also well suited in the search for quantum collective phenomena such as Bose-Einstein condensation, and a predicted increase or decrease of the radiative decay in a dense gas of Bose and Fermi particles respectively.[12]

In 1990 we have made progress in our development of a continuous source of slow atoms which will be used for the study of cold collisions and to load future magnetic traps. In addition, we have completed the modeling of rf and optical absorption spectra of cold atoms in a magnetic trap.

2.5.1 Slow Atom Source

We are working on a simple, intense, continuous source of slow atoms that separates the atoms from the laser light used to slow them. Separating the atoms is a crucial requirement for further experiments because the atoms are perturbed by the intense light used to slow them. There are several promising schemes for achieving these goals, and we have successfully demonstrated the first steps in two of these schemes.

One technique uses a continuous "Zeeman slower"—a spatially varying magnetic field used to compensate the changing Doppler shifts of the atoms in the slowing process.[13] Our present setup is very compact, 25 cm in length, and slows atoms with thermal velocities below 600 meters/second. By recording the Doppler profile with a second probe laser, we have observed a high flux of slow atoms with velocities of 100 to 200 meters/second. We are now designing a new magnetic field configuration which should allow us to achieve considerably smaller final velocities.

The second step in this scheme for a slow atom source is the separation of the cold atoms from the counterpropagating slowing laser beam. This will be done by using light pressure forces from the side. The deflecting laser must have two frequencies to circumvent optical pumping to hyperfine levels not excited by the laser. Furthermore, the laser frequencies have to be chirped to achieve large deflection angles, because of the changing Doppler shift of the deflected atoms. The setup for generating the frequency chirped light has been built and tested and consists of electro-optical and acousto-optical modulators and various rf generators.

Our second approach toward an intense slow atomic beam is based on our spontaneous light

---

[11] D.E. Pritchard, "Trapping and Cooling Neutral Atoms," in *Electronic and Atomic Collisions*, eds. D.C. Lorents, W.E. Meyerhof, and J.R. Peterson (New York: Elsevier B.V., 1986).

[12] K. Helmerson, M. Xiao, and D. Pritchard, "Radiative Decay of Densely Confined Atoms," International Quantum Electronics Conference, Anaheim, California, May 21-25, 1990.

[13] J.V. Prodan, W.D. Phillips, and H. Metcalf, "Laser Production of a Very Slow Monoenergetic Atomic Beam," *Phys. Rev. Lett.* 49: 1148 (1982).

force trap.[14] Slow atoms are collected from the thermal Maxwell-Boltzman distribution and are cooled in the intersection volume of six laser beams. A weak magnetic quadrupole field of 10 Gauss per cm induces an imbalance in the scattering forces from the six laser beams, resulting in restoring forces. About 10^6 atoms were captured from sodium vapor at a pressure of 10^{-9} Torr and trapped for about one second. We are now trying to increase the number of trapped atoms and to extract them from the trap, either by imbalance in the intensities of counterpropagating laser beams or by frequency modulation techniques.

2.5.2 Magnetic Trap for Neutral Atoms

In the last year we have performed numerical simulations to extract quantitative details form rf and optical spectra obtained in our pioneering experiments on sodium atoms in a superconducting magnetic trap. For the first time, absorption and rf spectra were obtained for trapped atoms.[15] Our models allow us to derive the density and energy distribution of trapped atoms, thus making spectroscopy a powerful technique to characterize samples of magnetically trapped atoms in future experiments.

In addition to spectroscopy, we have demonstrated Doppler cooling of the magnetically confined atoms. Since Doppler cooling was applied in only one dimension, we had to take into account the coupling of all the motions inside the trap to describe quantitatively the time dependence of the cooling process. Our analysis of the absorption spectra obtained from Doppler cooled atoms (figure 14) shows that we were able to cool the thermal motion of the trapped atoms to a few millikelvin.

Publications

Bagnato, V.S., G.P. Lafyatis, A. Martin, K. Helmerson, J. Landry, and D.E. Pritchard. "Laser Deceleration and Velocity Bunching of a Neutral Sodium Beam." *J. Opt. Soc. Amer.* 6: 2171 (1989).

Helmerson, K., M. Xiao, and D. Pritchard. "Radiative Decay of Densely Confined Atoms." International Quantum Electronics Conference, Anaheim, California, May 21-25, 1990.

[14] E.L. Raab, M. Prentiss, A. Cable, S. Chu and D.E. Pritchard, "Trapping of Neutral Sodium Atoms with Radiation Pressure," *Phys. Rev. Lett.* 59: 2631-2634 (1987).

[15] V.S. Bagnato, G.P. Lafyatis, A.G. Marti~ E.L. Raab, R.N. Ahmad-Bitar, and D.E. Pritchard, "Continuous Stopping and Trapping of Neutral Atoms," *Phys. Rev. Lett.* 58: 2194-2197 (1987); A.G. Martin, K. Helmerson, V.S. Bagnato, G.P. Lafyatis, and D.E. Pritchard, "rf Spectroscopy of Trapped Neutral Atoms," *Phys. Rev. Lett.* 61: 2431-2434 (1988).

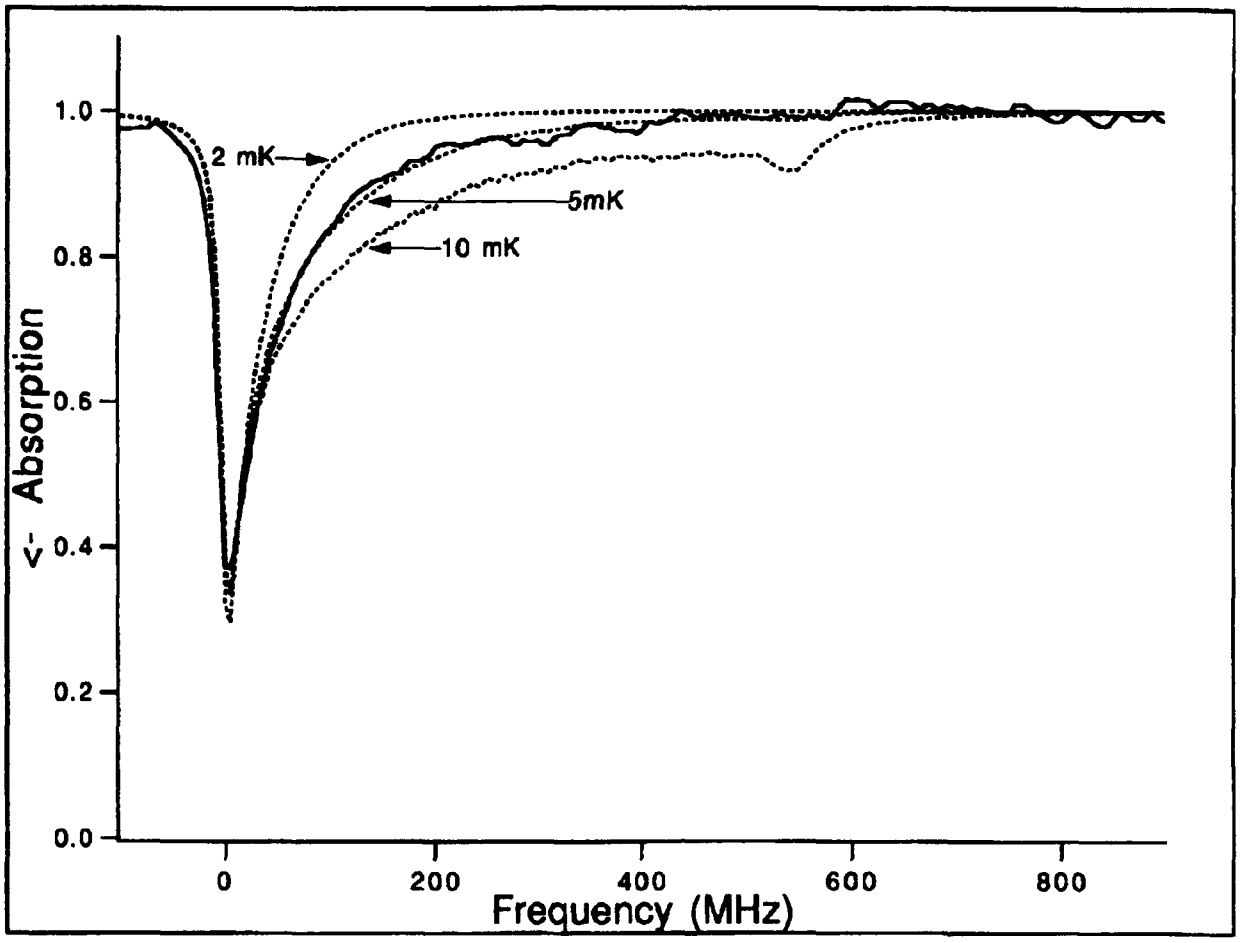

Figure 14. Absorption spectrum of Doppler cooled atoms and calculated lineshapes for temperatures of 2.5, 5.0 and 10 mK.

Chapter 3. Small Angle X-Ray and Neutron Scattering — Its Application to Supramolecular Solutions

Academic and Research Staff

Professor Sow-Hsin Chen

Visiting Scientists and Research Affiliates

Gian P. Felcher,[1] Pierandrea Lo Nostro,[2] Dr. Jacques Rouch,[3] Dr. Nadia Stubicar,[4] Dr. Piero Tartaglia,[5] Dr. Xiu-Bing Wei

Graduate Students

Bruce L. Carvalho, Szu-Li Chang, Xuan-Hui Guo, Xiao-Lin Zhou

Undergraduate Students

Simphiwe Duma, Sucharita Sahu

3.1 A New Inversion Algorithm for Obtaining Density Profiles of Thin Films From X-Ray and Neutron Reflectivity Data

Sponsor

Argonne National Laboratory

Project Staff

Xiao-Lin Zhou, Gian P. Felcher, Professor Sow-Hsin Chen

Specular reflectivity spectroscopy has been developed in recent years to probe the one-dimensional scattering length density profile of molecular and magnetic thin films. To exploit this technique, a few x-ray and neutron reflectometers have been constructed and successfully operated. These spectrometers have the merit that data collection is simple and and automatic. However, the data inversion process remains a practical challenge. On one hand, there is no closed-form expression for the reflection coefficient as a functional of the sample profile. On the other hand, there exists no standard way to do inversion, namely, to compute the sample profile straight forwardly from the reflectivity data. Another complication of the situation is that the reflectometers in use at present only measure the squared amplitude of the reflection coefficient but not its phase. All this adds to the difficulty of developing a practical data inversion algorithm.

To develop an inversion scheme, successful attempts have been made to derive a mathematical relationship between the reflection coefficient and the sample profile. Then an iterative inversion procedure based on such a relationship has been devised. Preliminary computations using simulated reflection data have shown that this procedure can invert the data to reproduce the sample profile. More work is underway to investigate the extra measures necessary to make the algorithm effective on actual experimental data which contain error bars. To make this inversion scheme systematic and versatile, a variety of physical samples are to be used to test it. It is expected that this scheme can be applied to other wave propagation situations such as acoustic and elec-

---

[1] Argonne National Laboratory, Argonne, Illinois.

[2] Department of Physical Chemistry, University of Florence, Italy.

[3] Physics Department, University of Bordeaux, France.

[4] Laboratory of Physical Chemistry, University of Zagreb, Yugoslavia.

[5] Physics Department, University of Rome, Italy.

tromagnetic probing of layered structures of a wide range of scales.

3.2 Interlayer Diffusion in Langmuir-Blodgett Films

Sponsor

U.S. Department of Energy
DE-FG01-90ER45429

Project Staff

Bruce L. Carvalho, Professor Sow-Hsin Chen

The Langmuir-Blodgett film deposition technique has been recently used to fabricate a variety of dense electronic and nonlinear optic devices on a single crystal silicon surface. Interdiffusion of polymer or surfactant molecules between multilayers in Langmuir-Blodgett films is therefore an important technological problem because it directly relates to the stability of such films as a function of temperature and age.

We have recently studied the interdiffusion of surfactant molecules using the neutron specular reflection technique. This is a new technique which allows one to obtain the refractive index profile, normal to the surface, with a spatial resolution of 15 A. Because the refractive index can be easily related to molecular composition, this technique is seen as a powerful tool in understanding the structure of thin films. It should also be noted that since deuterated and protonated molecules have a different refractive index for neutrons, one can label an interface within a Langmuir-Blodgett film and it is precisely this kind of labeling that we have used to observe the self-diffusion of surfactant molecules.

An example of our neutron reflection measurement is shown in figure 1. For this measurement, we constructed a film that consisted of silicon then five layers of deuterated cadmium arachidate then four layers of protonated cadmium arachidate. This film was designed to emphasize the thickness of the deuterated layers and the sharpness of the deuterated-protonated interface. Figure 1 shows three neutron reflectivity measurements; the squares correspond to the as-made film; the crosses correspond to the same film after it was heated to 95°C for one hour; and the diamonds correspond to the same film after it was heated for another nine hours at 95°C. The as-made film shows interference fringes which are characteristic of the five deuterated layers and the initially sharp deuterated-protonated interface. The subsequent heatings show not only a decrease in reflectivity but also the introduction of another period for the interference fringes. Both observations indicate that the deuterated-protonated interface has broadened substantially. We are presently formulating a model to account for this broadening. We have also begun to use the synchrotron x-ray reflectivity technique to study these same films. While the neutron reflection measurement is sensitive to the composition profile of hydrocarbons, the x-ray reflectivity technique is mainly sensitive to the cadmium ion concentration profile through the film's thickness.

3.3 Structure of a Protein/SDS Complex in Low Ionic Strength Solution Studied by Small Angle Neutron Scattering

Sponsor

National Science Foundation

Project Staff

Xuan-Hui Guo, Professor Sow-Hsin Chen

During the past few years we have studied the structure of bovine serum albumin (BSA)/sodium dodecylsulfate (SDS) complexes in solutions by small angle neutron scattering (SANS). We concluded that BSA/SDS complexes in high ionic strength solution were flexible polymer-like objects. This view has led us to discover the polymer-like phase separation phenomenon of BSA/SDS complexes in solution.

However, there are still some uncertainties on the structure of protein/SDS complexes in low ionic strength solutions. This case has practical interest because the conventional SDS polyacrylamide gel electrophoresis measurements are all carried out in low ionic strength solutions (I = 0.2 M). The structure determination in this case would contribute significantly to the understanding of the gel electrophoresis.

We used perdeuterated SDS molecules to carry out SANS measurements. The solvent is a mixture 40% D_2O and 60% H_2O in which the contrast between proteins and solvent is matched, namely, only the perdeutrated SDS molecules can be seen in the SANS measurements. We systematically measured the SANS intensity distribution for the complexes in solution under different protein concentrations and ionic strength (I = .1 M, .2 M). It was found that the intensities for $Q < 0.03Å^{-1}$ were considerably depressed due to the charge repulsion between complexes in solution. However, the intensities for $Q > 0.03Å^{-1}$ are not affected by ionic strength and can be scaled into one curve after normalizing by the concentrations. We therefore concentrate mainly on the analyses

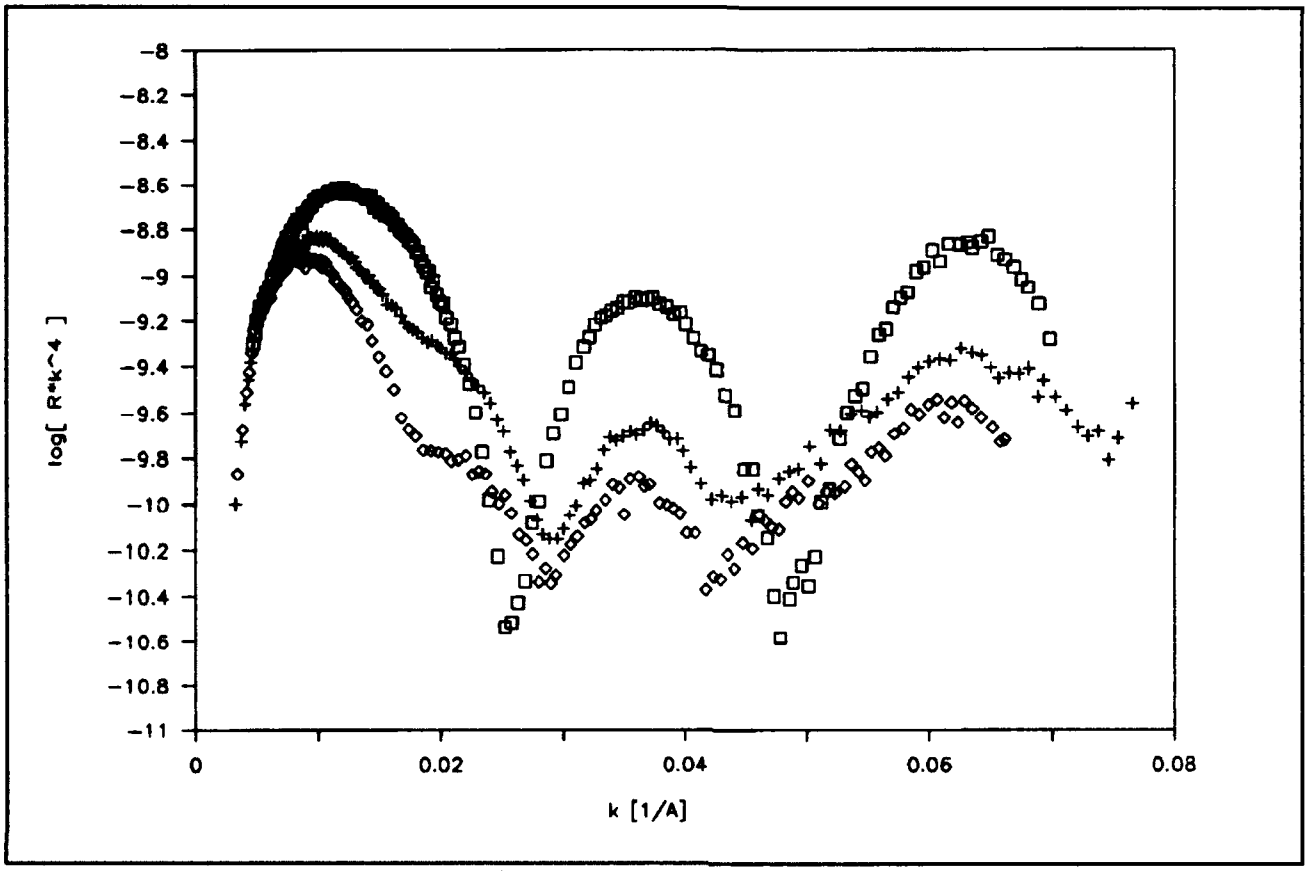

Figure 1. The logarithm of reflectivity * k^4 is plotted as a function of k, the incident neutron momentum for the as-made film (squares); T=95°C, 1 hour (crosses) and T=95°C, 10 hours (diamonds).

of the intensity distributions for $Q > 0.03Å^{-1}$, to critically test all the proposed models.

We have compared SANS data with curves calculated based on all the proposed structural models. It was found that only one model is able to describe SANS data satisfactorily. That is the model in which the bound SDS molecules form micelle-like clusters, and the clusters are assumed to be correlated for portions of the flexible polypeptide chain, namely a Gaussian chain with an excluded volume effect. In figure 2 we show the comparison between SANS data and the calculated curves. The excluded volume exponent is found to be 2/3, close to the Flory exponent 3/5. From these careful measurements and analyses, we are confident that the structure of the complex in low ionic strength solution is also a polymer-like object. This conclusion, coming from SANS data analyses, further supports that the reptation mechanism, which we proposed earlier, is responsible for the protein separation in the process of protein-SDS polyacrylamide gel electrophoresis.

3.4 Isotope Effect in Phase Separation of a Lipid/Water Micellar System

Sponsor

University of Florence, Italy

Project Staff

Pierandrea Lo Nostro, Nadia Stubicar, Professor Sow-Hsin Chen

We have found that the upper consolute temperature of the dioctanoyl-phosphatidylcholine (diC_8-PC)/water system has a substantial isotope effect. The consolute temperature of diC_8-PC/H_2O system is 318 K, while that of diC_8-PC/D_2O is 332 K, with a difference of 14 K. The complete binodal curves for R (= D_2O/H_2O v/v) ranging from 1.00, 0.66, 0.50, 0.33, to 0.00 have been determined. The consolute temperature scales linearly with R.

It is known that a fraction of hydrogen bonding in D_2O is higher than in H_2O at the same temperature in the vicinity of the room temperature. Therefore, the hydrophobic effect of diC_8-PC in D_2O is

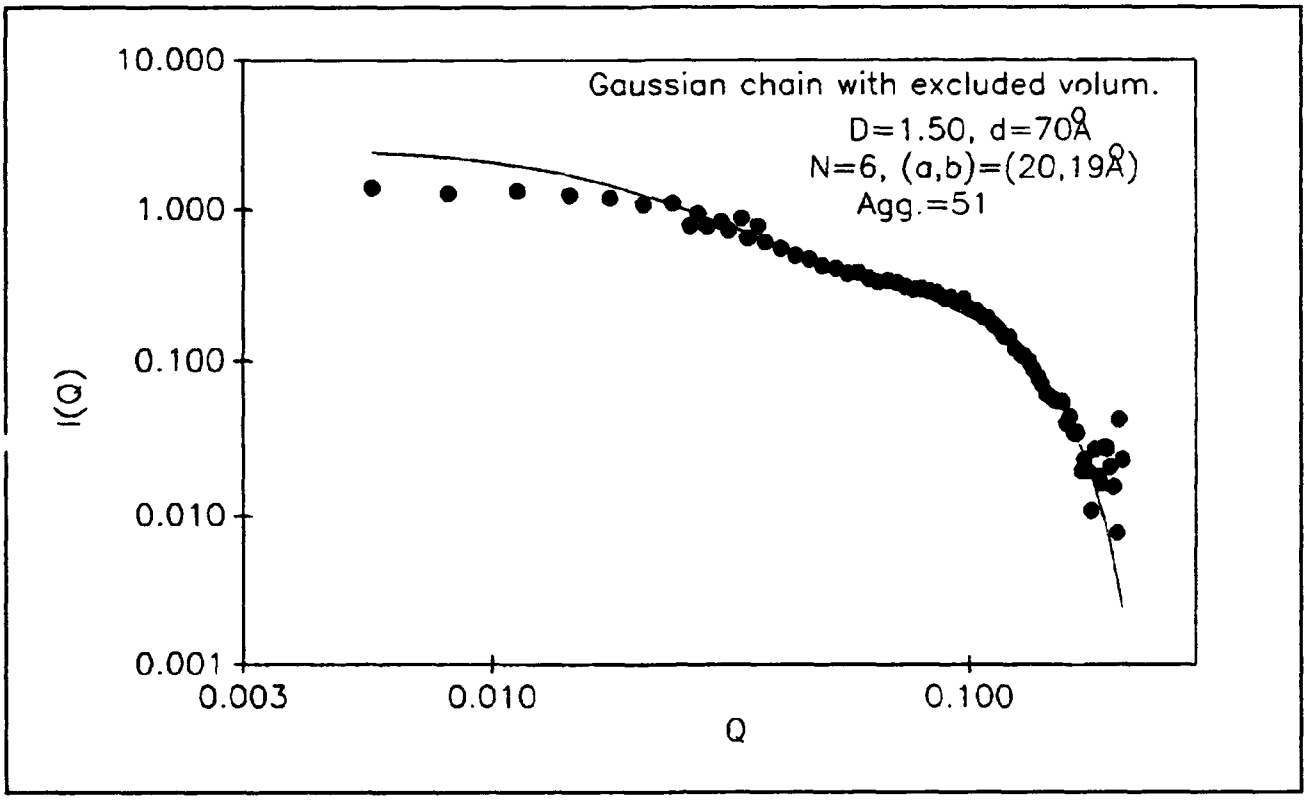

Figure 2. Comparison of the SANS intensity distribution with the calculated curve using a model in which the bound SDS molecules form micelle-like clusters and the clusters are correlated by portions of the flexible polypeptide chain, namely assumed to be a Gaussian chain with an excluded volume effect.

expected to be higher than in H_2O; this explains the observed temperature effect on phase separation.

We have measured the light-scattering intensities as a function of the molar fraction of lecithin in the solution and found that it is peaked at the critical molar fraction which is 0.0008 for diC_8-PC/D_2O/H_2O (R = 0.50) and 0.0010 for R = 1.

3.5 Measurement and Interpretation of Counterion Distribution Around Cylindrical Polyelectrolytes

Sponsor

Exxon Fellowship

Project Staff

Szu-Li Chang, Professor Sow-Hsin Chen

Counterion distributions around rod-like polyelectrolytes in solution are measured directly using small angle x-ray scattering (SAXS). Two systems are studied: cylindrical micelles formed by a comb-shaped copolymer poly-(1-octadecene-co-maleic anhydride) (PODMA), neutralized by CsOH, in aqueous solution; and 500Å persistence length DNA fragments in aqueous solution having Na^+ or Cs^+ as counterions respectively. A new method of SAXS data analysis is developed. Poisson-Boltzmann (P-B) equation in the cell model is used to compute the counterion distributions. Comparison of SAXS data for the PODMA case with the theory shows that the P-B solution overestimates the charge accumulation on the micellar surface due to the very high linear charge density parameter ξ (=33) of the micelle, while for the case of CsDNA, one needs to assume considerable amount of counterions present in the major and minor grooves of the double helices. Figure 3a shows the scattering length density profile for a single PODMA micelle enclosed in a cell of radius R=201Å. This is a sample containing 1wt% PODMA in aqueous solution fully neutralized by CsOH. Figure 3b shows a comparison of SAXS data with the theoretical calculation of the scattering intensity distribution in absolute scale. The dotted line gives the micelle's only contribution, which is seen to be negligibly small. The counterion's only contribution is shown by the dashed line, which is a much larger contribution. The solid line is due to a coherent sum of the

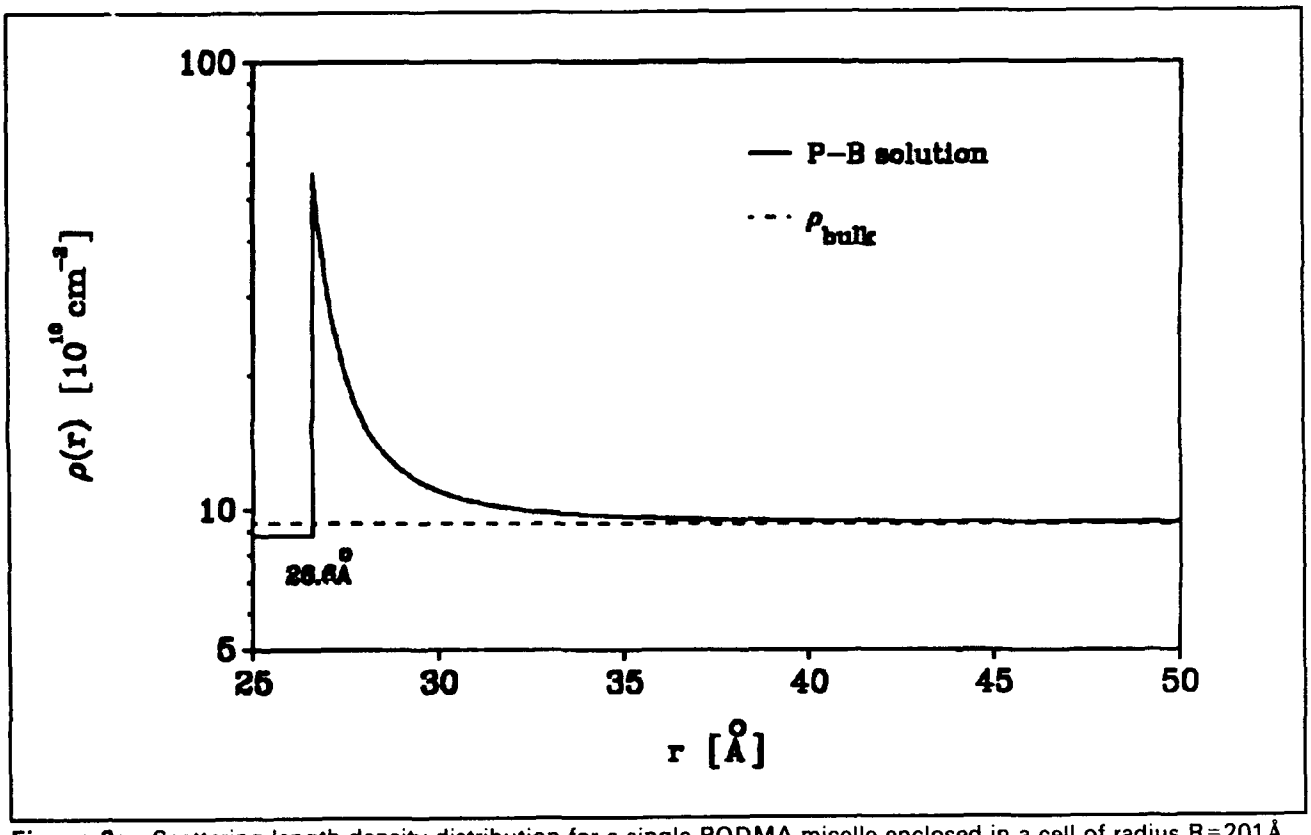

Figure 3a. Scattering length density distribution for a single PODMA micelle enclosed in a cell of radius R=201Å.

above two contributions which is the quantity to be compared with experimental data. In the small Q region, the agreement of the theory with the experiment is quantitative, including the correct prediction of the dip in the curve due to the discontinuity of the scattering length density at the micellar surface.

3.6 Aggregation Behavior and Phase Transition of Semifluorinated n-Alkanes in Hydrocarbons and Fluorocarbons

Sponsor

University of Florence, Italy

Project Staff

Pierandrea Lo Nostro, Professor Sow-Hsin Chen

Amphiphilic molecules contain a polar head group (hydrophilic part) and one or more aliphatic chains which constitute the hydrophobic part, so that, when they are dissolved in an aqueous medium, they can produce several kinds of aggregates, such as micelles, vesicles, discs and cylinders. Usually the polarities of the hydrophilic and the hydrophobic parts are very different. In fact the head group can be either ionic or non-ionic but it is always highly polar, whereas the hydrophobic part is commonly consisting of $-CH_2-$ groups which are apolar. Therefore, an amphiphile can produce aggregates in water solutions only if the difference in polarity of the two parts of the molecule is considerably large.

The syntheses of molecules like $F(CF_2)_m(CH_2)_nH$ and $F(CF_2)_m(CH_2)_n(CF_2)_pF$ (or shortly F_mH_n and $F_mH_nF_p$ respectively) are relatively recent; "m" and "n" can vary between 2 and 20. In this case the polarity of the two chains, the fluorocarbon chain and the hydrocarbon one, are very close, therefore we cannot use water to distinguish them. On the other hand, a fluorinated solvent or a hydrocarbon can interact differently with them. A few years ago, the formation of *star micelles* in fluorocarbons was reported for the first time for these kind of compounds. In fact the molecules aggregate in such a way that the fluorinated chains face the solvent, whereas the hydrogenated parts collapse together and form the core of the micelle. Conversely, in a hydrogenated solvent, the hydrocarbon chain will face the solvent and the fluorinated chain will constitute the inner part.

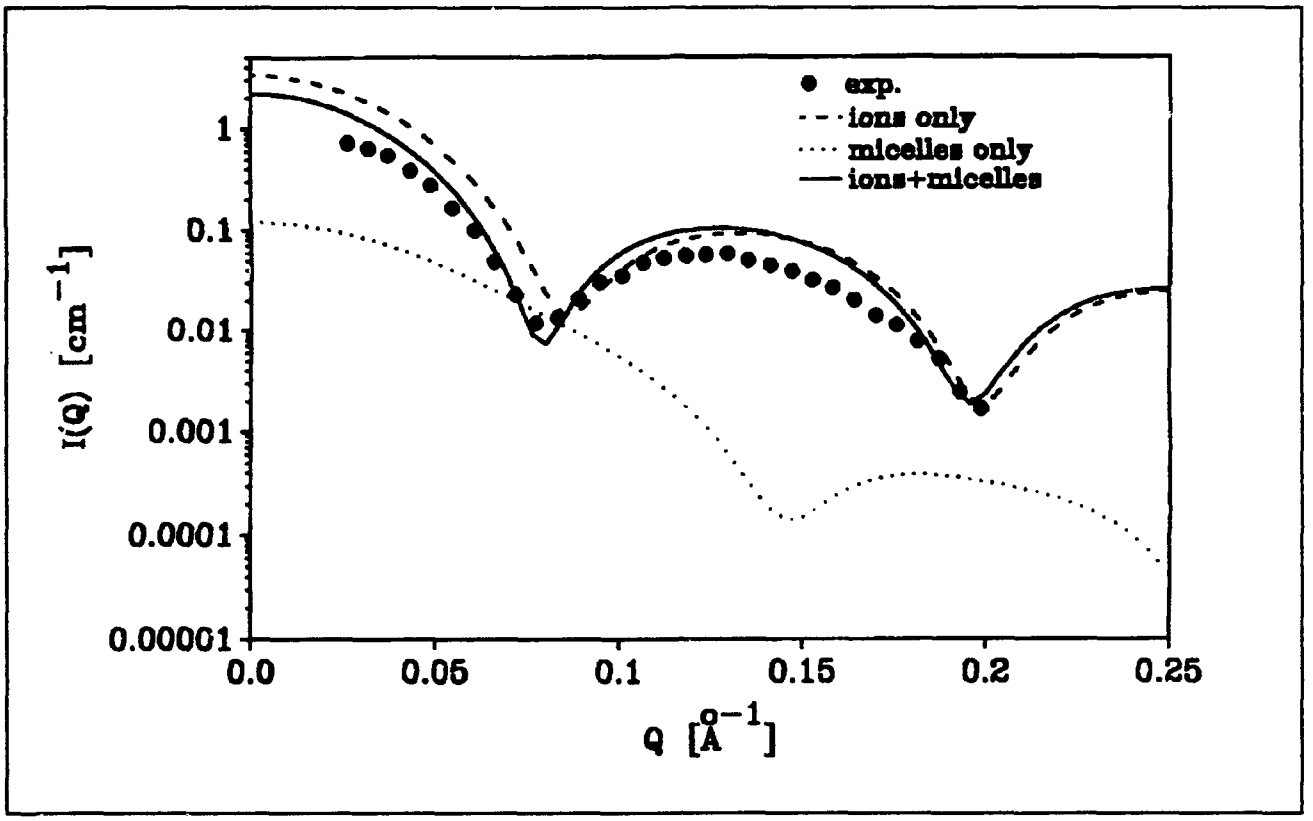

Figure 3b. The comparison of the experimental and calculated SAXS intensities for 1wt% PODMA in aqueous solution fully neutralized by CsOH.

We synthesized three different chemicals:

$$[a] = F_{10}H_8$$

$$[b] = F_8H_{10}$$

$$[c] = F_8H_{16}$$

in two steps:

$$F(CF_2)_mI + CH_2CH = (CH_2)_{n-2}H + AIBN =$$

$$F(CF_2)_mCH_2CHI(CH_2)_{n-2}H$$

This is a radical reaction initiated by AIBN (azo-bis(isobutyro-nitrile)). The intermediate then reacts with zinc and gaseous hydrogen chloride to give the semifluorinated n-alkane:

$$F(CF_2)_mCH_2CHI(CH_2)_{n-2}H + Zn/HCl = F_mH_n$$

Through light-scattering measurements we investigated the formation of aggregates: compounds [a] and [b] did not produce any aggregate in perfluorohexane, perfluorooctane and n-octane; [c] gave large micelles in perfluorooctane above 40°C, with CMC = 5.4% at 51°C.

Compound [c] also showed an interesting phase transition in perfluorooctane and n-octane. In fact, at low temperatures it forms a white gel that melts at higher temperatures to give a transparent liquid. This phase transition occurs between 25° and 40°C for concentration of F_8H_{16} between 2.5% and 20% in perfluorooctane. In n-octane the phase transition occurs at much lower temperatures, below 0°C.

3.7 Light Scattering From Dense Percolating Microemulsions

Sponsor

National Science Foundation
Grant INT 87-5085

Project Staff

Dr. Piero Tartaglia, Dr. Jacques Rouch, Professor Sow-Hsin Chen

The theory of static and dynamic light scattering from a system of dense, surfactant coated water droplets dispersed in oil, forming polydisperse fractal percolation clusters, is formulated. The scattering intensity shows the characteristic $q^{-D(3-\tau)}$ behavior at large q, and the density-density time correlation function, while initially decaying exponentially, evolves continuously into a stretched exponential asymptotically with a characteristic exponent $\beta = D/(D+1)$. A set of static and dynamic light scattering measurements of the AOT-water-decane microemulsions are analyzed to substantiate the predicted behavior. The theory, applicable for microemulsions near the percolation threshold, bears striking resemblance to the well-known static and dynamic fluctuation theory near the consolute point of binary mixture of liquids. Both theories share a common feature: the scaled intensity and linewidth can be expressed in terms of universal functions of the single scaling variable $x = q\xi$.

Publications

Bratko, D., D. Wang, and S.H. Chen. "Spatial Correlations in Aqueous Protein Solutions." *Chem. Phys. Lett.* 163: 239-245 (1990).

Cametti, C., P. Codastefano, P. Tartaglia, J. Rouch, and S.H. Chen. "Theory and Experiment of Electrical Conductivity and Percolation Locus in Water-in-oil Microemulsions." *Phys. Rev. Lett.* 64: 1461-1464 (1990).

Cametti, C., P. Codastefano, G. D'Arrigo, P. Tartaglia, J. Rouch, and S.H. Chen. "Viscoelastic Behavior of Dense Microemulsions." *Phys. Rev. A* 42: 3421-3426 (1990).

Chang, S.L., S.H. Chen, R.L. Rill, and J.S. Lin. "Measurements of Monovalent and Divalent Counterion Distributions Around Persistence Length DNA Fragments in Solution." *J. Phys. Chem.* 94: 8025-8028 (1990).

Chen, S.H., S.L. Chang, and R. Strey. "Structural Evolution within the One-Phase Region of a Three-Component Microemulsion System Water - n-decane - sodium-bisethylhexyl-sulfosuccinate (AOT)." *J. Chem. Phys.* 93: 1907-1918 (1990).

Chen, S.H., S.L. Chang, and R. Strey. "On the Interpretation of Scattering Peaks from Bicontinuous Microemulsions." *Progr. Colloid. Polym. Sci.* 81: 30-35 (1990)

Guo, X.H., N.M. Zhao, S.H. Chen, and J. Teixeira. "Small Angle Neutron Scattering Study of the Structure of Protein-Detergent Complexes." *Biopolymers* 29: 335-346 (1990).

Guo, X.H., and S.H. Chen. "Observation of Polymer-like Phase Separation of Protein-Surfactant Complexes in Solution." *Phys. Rev Lett.* 64: 1979-1982 (1990).

Guo, X.H., and S.H. Chen. "Reptation Mechanism in Protein-SDS Polyacrylamide Gel Electrophoresis." *Phys. Rev. Lett.* 64: 2579-2582 (1990).

Guo, X.H., and S.H. Chen. "The Structure and Thermodynamics of Protein-SDS Complexes in Solution and the Mechanism of Their Transports in Gel Electrophoresis Process." *Chem. Phys.* 149: 129-139 (1990).

Kreuger, S., S.H. Chen, J. Hofrichter, and R. Nossal. "Small Angle Neutron Scattering Studies of HbA in Concentrated Solutions." *Biophys. J.* 58: 745-757 (1990).

Lin, T.L., S.H. Chen, N.E. Gabriel, and M.F. Roberts. "SANS Study of Triglyceride Solubilization by Lecithin Micelles: A Direct Observation of Rod-to-Sphere Transition." *J. Phys. Chem.* 94: 855-862 (1990).

Lin, T.L., M.Y. Tseng, S.H. Chen, and M.F. Roberts. "Temperature Dependence of the Growth of Diheptanoylphosphatidylcholine Micelles Studied by Small-Angle Neutron Scattering." *J. Phys. Chem.* 94: 7239-7243 (1990).

Section 2 Plasma Physics

Chapter 1 Plasma Dynamics

Chapter 1. Plasma Dynamics

Academic and Research Staff

Professor George Bekefi, Professor Abraham Bers, Professor Bruno Coppi, Professor Miklos Porkolab, Professor Jonathan S. Wurtele, Dr. Shien-Chi Chen, Dr. Ronald C. Englade, Ivan Mastovsky, Dr. Stefano Migliuolo, Dr. Abhay K. Ram, Dr. Linda E. Sugiyama

Visiting Scientists and Research Affiliates

Dr. Jean-Loup Delcroix,[1] Paolo Detragiache,[2] Dr. Lazar Friedland,[3] Dr. Vladimir Fuchs,[4] Dr. Eli Jerby,[5] Dr. Chaim Leibovitch,[6] Dr. Marco Nassi,[7] Dr. Leonid E. Zakharov[8]

Graduate Students

Riccardo Betti, Carson C. Chow, Jeffrey A. Colborn, Manoel E. Conde, Christian E. de Graff, Anthony C. DiRienzo, Darin Ernst, Mark Jablonski, Kenneth C. Kupfer, Michael C. Moldoveanu, Jared P. Squire, Richard E. Stoner, Jesus Noel Villasenor

Undergraduate Students

Daniel P. Aalberts, Salvatore DiCecca

Technical and Support Staff

Felicia G. Brady, Laura B. Doughty, Edward W. Fitzgerald, Catherine Lorusso

1.1 Relativistic Electron Beams

Sponsors

Lawrence Livermore National Laboratory
Subcontract 6264005
National Science Foundation
Grants ECS 84-13173 and ECS 85-14517
U.S. Air Force - Office of Scientific Research
Contract AFOSR 89-0082-A
U.S. Army - Harry Diamond Laboratories
Contract DAAL02-86-C-0050
U.S. Navy - Office of Naval Research
Contract N00014-87-K-2001

Project Staff

Professor George Bekefi, Professor Jonathan S. Wurtele, Daniel P. Aalberts, Dr. Shien-Chi Chen, Manoel E. Conde, Christian E. de Graff, Salvatore DiCecca, Anthony C. DiRienzo, Dr. Eli Jerby, Dr. Chaim Leibovitch, Ivan Mastovsky, Richard E. Stoner

---

[1] Professor, University of Paris, Orsay, and Ecole Supérieure d'Electricité, France.

[2] University of Turin, Torino, Italy.

[3] Professor, Hebrew University of Jerusalem, Israel.

[4] Centre Canadien de Fusion Magnétique (CCFM), Quebec, Canada.

[5] Tel Aviv University, Tel Aviv, Israel.

[6] Rafael Laboratory, Haifa, Israel.

[7] Politecnico di Milano, Milan, Italy.

[8] Kurchatov Institute of Atomic Energy, Moscow, U.S.S.R.

1.1.1 A Planar Electromagnet Microwiggler for Free Electron Lasers

Short-period (1-10 mm) wigglers for free electron laser (FEL) applications have been a subject of considerable interest.[9] The use of this kind of microwiggler permits higher frequency radiation to be generated with a device which is more compact than one employing wigglers of standard lengths (typically 3-10 cm).

Reduced length scales imply that fabrication imperfections become increasingly more serious. Field amplitude tunability, as a means of compensating for the resulting random field errors, becomes a particularly important attribute for a microwiggler design. Field amplitude tunability also has a general usefulness for applications like field tapering for FEL efficiency enhancement. The use of electromagnets permits such tunability; moreover, a planar geometry wiggler readily lends itself to a tunable configuration because it can be made of discrete electromagnets.

We have constructed a four period microwiggler prototype with a period of 10.2 mm and gap of 5.1 mm consisting of 16 wire coil electromagnets wound on laminated Microsil (silicon iron) cores. Each core consists of seven laminations of dimensions 1.27 x 3.81 x 0.356 cm. Figure 1 illustrates the geometry. The test piece has a tunable amplitude with the current delivered to each half-period, adjustable by means of a precision potentiometer. Each coil consists of 50 turns of 32 AWG copper wire (0.0202 cm diameter) and has a resistance of 2.4 Ω. The coils are connnected in parallel, and the wiggler is energized by a simple pulser circuit consisting of an air core inductor (L = 1.3 mH) and a bank of six 1500 μF capacitors connected in parallel. The resulting waveform is an underdamped sine wave. The pulser is fired by an SCR which commutates off at the first zero crossing of the current. Hence, the wiggler is energized by a single positive current pulse. The full period of the underdamped waveform is about 22 ms.

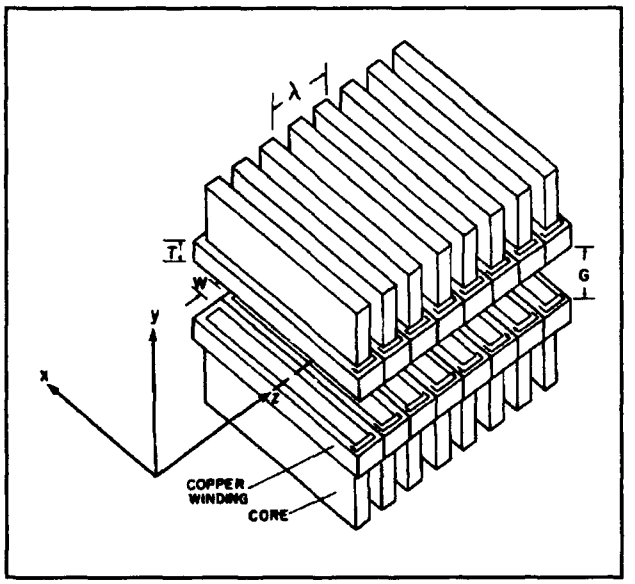

Figure 1. Geometry of the microwiggler test piece. The coordinate axes as well as definitions of design parameters are shown. The arrows inscribed on the copper windings indicate the direction of current flow.

[9] S.C. Chen, G. Bekefi, S. DiCecca, and A.C. Wang, *Nucl. Instrum. Methods* A285: 290 (1989); J.H. Booske et al., *J. Appl. Phys.* 64: 6 (1988) and references therein; R.M. White, *App. Phys. Lett.* 46: 194 (1985); G. Ramian, L. Elias, and J. Kimel, *Nucl. Instrum. Methods* A250: 125 (1986); B.G. Danly et al., *IEEE J. Quantum Electron.* QE 23: 103 (1987); S.C. Chen, G. Bekefi, S. DiCecca, and R. Temkin, *Appl. Phys. Lett.* 46: 1299 (1989).

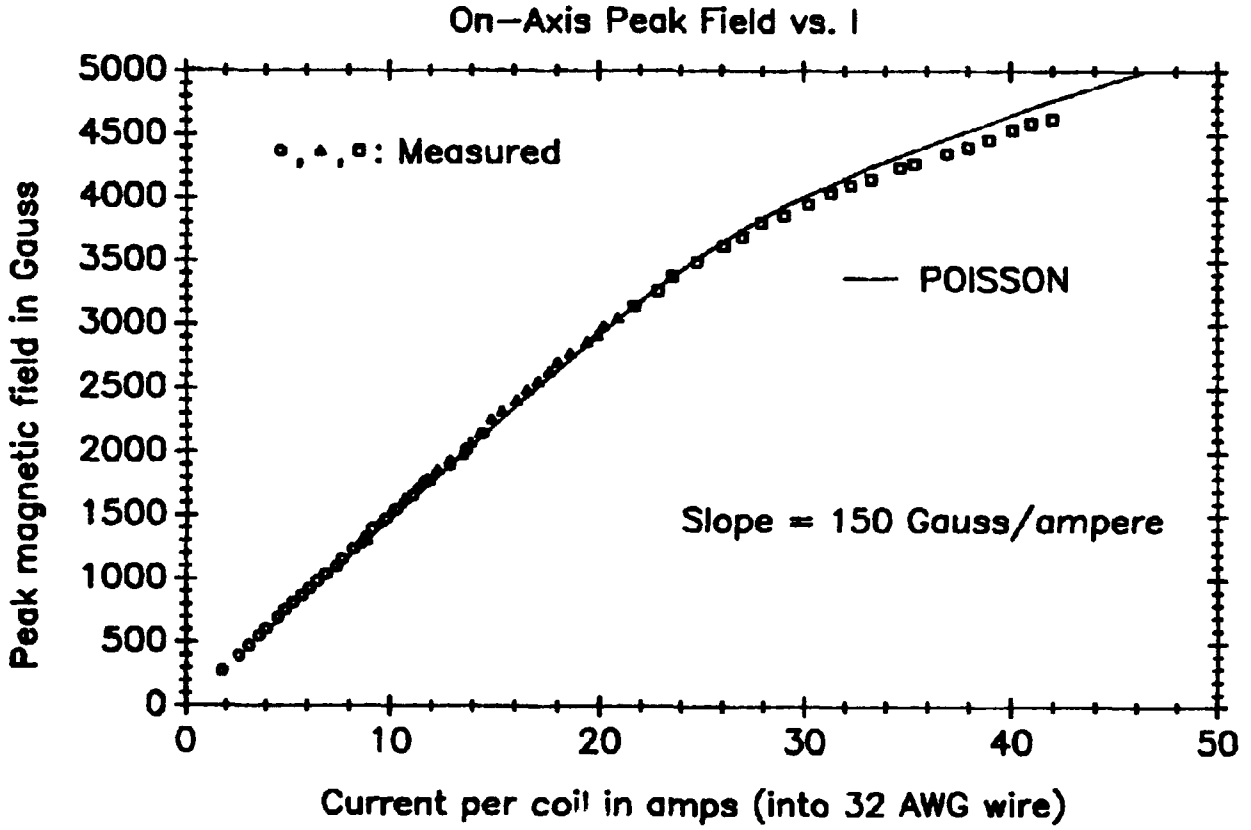

Figure 2. Wiggler field amplitude as a function of current density. Measured data and Poisson calculations are shown.

The wiggler field amplitude as a function of the input current density was measured and is shown plotted in figure 2. The results of a Poisson simulation match the data quite well. This is partly fortuitous, since we made no effort to model the permeability of our particular material. The probe was located at a peak near the central part of the wiggler; the input current was measured using a Rogowski coil, and the field was measured by means of a Hall probe gaussmeter, using a specially designed miniature probing tip. The current values shown are those borne by the 32 AWG wire. A current of 20 A corresponds to a current density of 6.24×10^4 A/cm^2.

Note that B as a function of I is quite linear to about 3.2 kG. The 3-kG linear field regime of our design extends further than those of ferro core designs reported previously. Figure 3 shows a Poisson-generated flux map of our prototype in its linear regime. The regions of highest flux density in the cores occur inside the windings, which are thus purposely displaced toward the polefaces relative to the center of the cores. The closer to the polefaces the highest flux density region occurs, the higher will be the fields at the polefaces (and on the wiggler axis) when the cores saturate. The windings do not extend along the entire ferro core since, in this kind of configuration, the highest flux density occurs at the center of the cores, well back from the polefaces, leading to the onset of saturation at relatively low field levels.

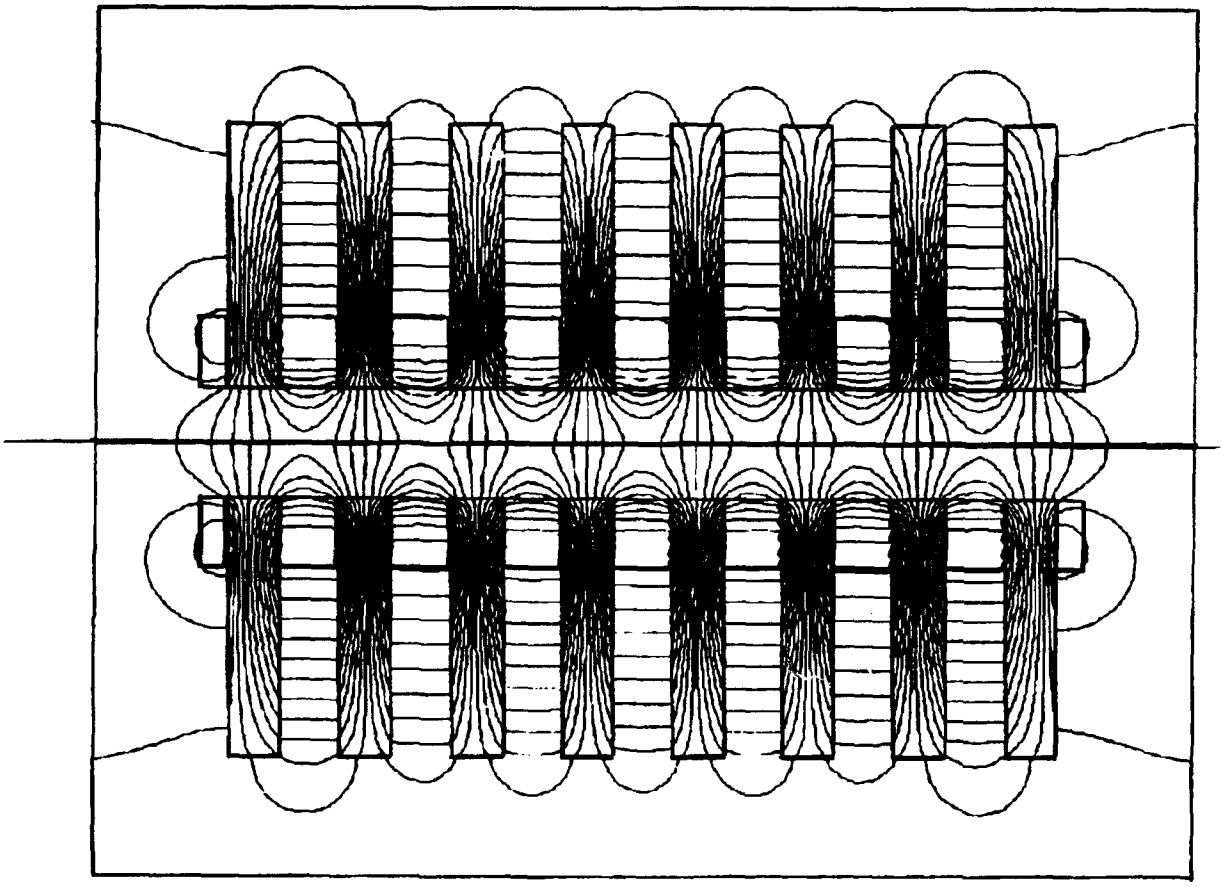

Figure 3. Poisson-generated equipotential map for the MIT prototype. The field map shown corresponds to the linear B/H regime.

Figure 4 shows the prototype's measured, untuned, on axis magnetic field profile. Poisson calculations of the peak fields are also shown. There is very little higher harmonic content in the field. This is mainly due to the large gap to period ratio: The field at a given point on the wiggler axis is the sum of contributions from many half period elements. The wiggler end effects are quite small due to the favorable symmetry of the current density about the central plane perpendicular to the wiggler (z) axis. In the absence of tuning, we observe random field amplitude errors in the prototype of $\pm 4\%$; this is a reasonable value, considering the very simple methods used in its construction.

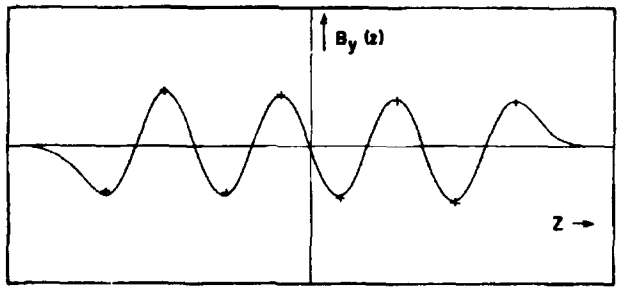

Figure 4. Measured wiggler field profile taken along the wiggler axis without tuning. The continuous curve is the measured data. Poisson calculated values for the peaks are shown as crosses.

Random field errors as well as undesired systematic finite wiggler effects are sharply reduced by tuning. The results of profile tuning experiments are shown in figure 5. Figure 5(a) is a plot of the prototype's on axis magnetic field tuned to a constant amplitude profile. Random field errors are 0.4% rms, with a maximum deviation from the constant amplitude of 0.6%. Amplitude tuning has therefore reduced random field errors by an order of magnitude. Minor improvements in the tuning regimen should permit further reduction of random field errors, perhaps to the level of 0.2% rms. Figure 5(b) is a measured profile demonstrating the capability of adiabatic field up-taper for improved e beam coupling into the wiggler. The magnet was deenergized with about 0.5 A per coil (for a total of 8.0 A) during the tuning and profile measurements.

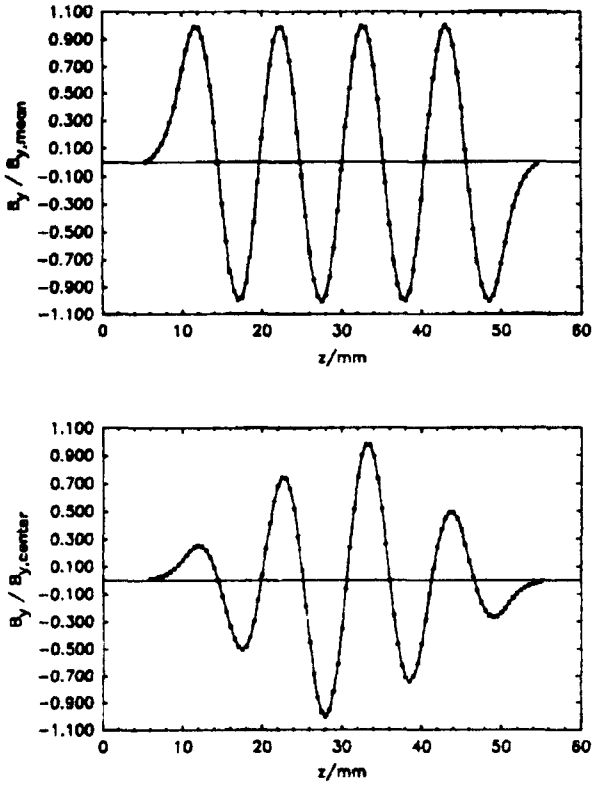

Figures 5a and 5b. Measured wiggler field profiles taken along the wiggler axis with tuning. A constant amplitude profile is shown in 5a (above). The amplitude is constant to 0.4 π rms with a maximum deviation of 0.6 π. A "linear ramp" profile is shown in 5b (below) which demonstrates the capability for adiabatic up taper for wiggler e-beam matching.

Figure 6 is a plot of the measured wiggler field profile across the gap, along a line from poleface center to poleface center. The data are again well matched by the Poisson code and also well represented by a hyperbolic cosine curve, in agreement with expectations. The distance over which measurements could be taken was restricted by the Hall probe hitting the polefaces.

The testing of the four-period prototype has ended and construction of a 70-period system has begun. During the summer of 1991, it will be moved to the Brookhaven National Laboratory in a MIT/BNL research collaboration. Our microwiggler will be installed in a new 50 MeV RF Linac under construction at BNL. Output peak power of ~ 10 MW at a wavelength of 532 nm is expected (see table I and figure 7).

MIT/BNL Microwiggler FEL Collaboration

- e-beam (BNL):
  - 0.3 mm radius, $\Delta\gamma/\gamma < .001$
  - Normalized emittance, 6 mm-mrad
  - 50 A, 6 psec micropulses, 100 per 1 μ sec macropulse, at 50 MV
  - SLAC-style RF linac with photocathode
- Wiggler (MIT):
  - 8.8 mm period, 70 periods, each half-period tunable.
  - 4.4 mm gap, planar geometry.
  - Uniform axial field profile, ends tapered for zero displacement and steering.
  - Operating magnetic field level $\geq$ 5 kG.
  - Tunable to accuracy of $\leq$ 0.5%.
- Output radiation:
  - 532 nm
  - 100 MW intracavity power, 10 outcoupling: 10 MW peak output

Table 1.

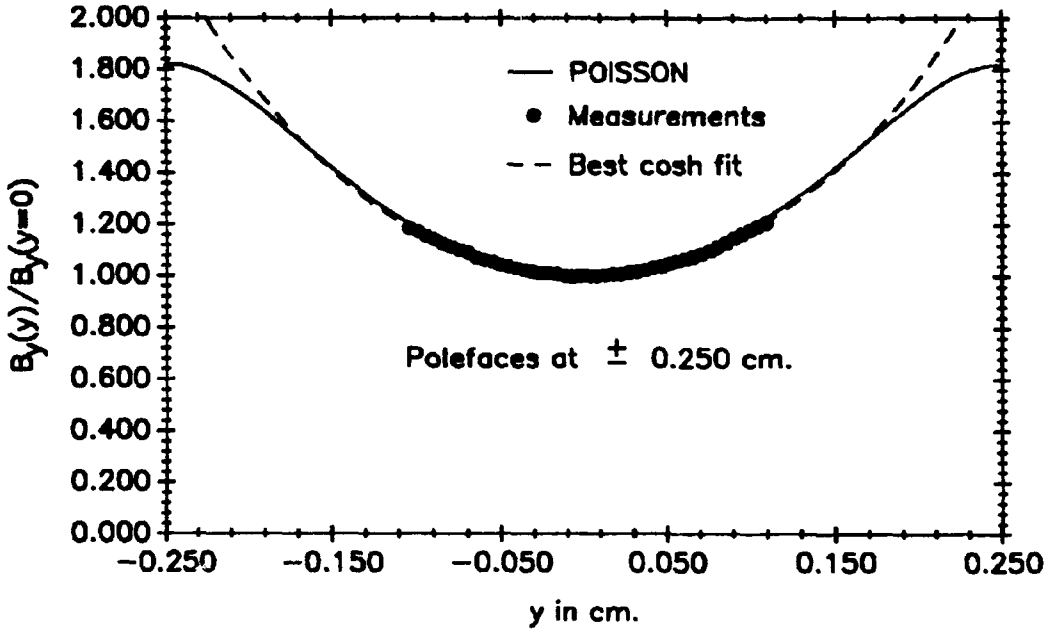

Figure 6. Measured wiggler field profile taken across the wigglergap from poleface center to poleface center. The data is normalized to the value of the filed at the gap center. A Poisson calculation of the filed profile is shown as well as the hyperbolic cosine function that best fits the data.

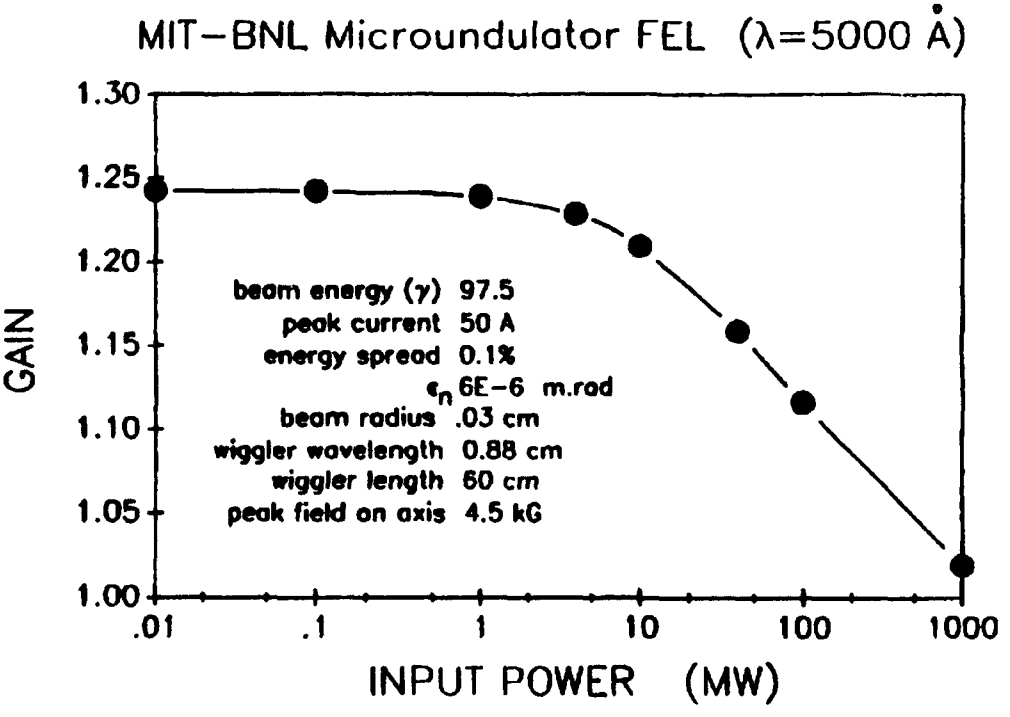

Figure 7.

1.2 Plasma Wave Interactions — RF Heating and Current Generation

Project Staff

Professor Abraham Bers, Dr. Abhay K. Ram, Dr. Jean-Loup Delcroix, Dr. Vladimir Fuchs, Dr. Lazar Friedland, Carson C. Chow, Mark Jablonski, Kenneth C. Kupfer, Michael C. Moldoveanu

1.2.1 Introduction

The research work of this group is concerned with studies on the electrodynamics of plasmas. Particular attention is directed toward understanding the nonlinear dynamics of plasmas driven by high-frequency electromagnetic fields (as in RF heating and current drive of magnetically confined plasmas, or in laser-plasma interactions). This entails extending dynamical chaos studies to infinite dimensional systems of continua. In particular, such nonlinear dynamics can lead to *spatio-temporal chaos* which we have undertaken to study in the generic nonlinear interaction of three wavepackets. Our studies also continue on the generation and propagation of unstable radiations from laser-plasma interactions and anisotropic electron distributions in space and astrophysical plasmas.

1.2.2 Spatio-Temporal Chaos in the Nonlinear Three-Wave Interaction

Sponsors

Lawrence Livermore National Laboratory
Subcontract B108472
National Science Foundation
Grant ECS 88-22475
U.S. Department of Energy
Contract DE-FG02-91-ER-54109

We have examined the large system, longtime behavior of the nonlinear three-wave interaction describing the saturation of an unstable wave by coupling to two damped waves. We observe spatio-temporal chaos involving coherent structures that are characterized by temporal and spatial scales.

The term spatio-temporal chaos has been used to describe a spatially extended system where coherent structures or spatial patterns exhibit chaotic dynamics. This is contrasted with fully developed turbulence where there is a cascade to finer and finer scales. The Kuramoto-Sivashinsky (KS) equation describing the propagation of flame fronts has been used as one of the paradigms for spatial chaos in one dimension and has been studied in great detail.[10] In that system, a stable periodic pattern becomes chaotic as the length of the system increases. The chaotic state is characterized by a finite spatial correlation length and a power law scaling for low frequencies.

The nonlinear three-wave interaction in its various forms has applications to plasma physics, nonlinear optics, and hydrodynamics. In its conservative form, the space-time evolution of this nonlinear interaction is integrable by inverse scattering and exhibits the generation and interchange of solitons by the three wavepackets.[11] We consider one form of these equations, the three wave decay instability, to describe the saturation of a linearly unstable parent wave by nonlinear coupling to two damped daughter waves. We have found that this three wave decay instability possesses coherent structures that interact chaotically. The conservative form of the system has soliton solutions and the coherent structures are remnants of these solitons. We refer to these objects as quasi-solitons. They are of finite spatial extent but they damp as they propagate, and they do not preserve their form after collisions as solitons would. For space-time scales larger than those that characterize these structures, there is no coherence. For very long wavelengths, there is incoherence as occurring in the KS equation.

Researchers have previously looked at the dynamics of the three wave decay instability for evolution in time only (i.e., with imposed spatially uniform amplitudes).[12] They have observed subharmonic cascades to chaos and intermittency depending on the ratio of the damping rate of the daughter waves to the growth rate of the parent wave. They also found that a small amount of temporal dephasing or frequency mismatch is required to saturate the instability. We find for

---

[10] P.C. Hohenberg and B.I. Shraiman, *Physica* 37D: 109 (1989).

[11] A. Bers, D.J. Kaup, and A.H. Reiman, *Phys. Rev. Lett.* 37: 182 (1976); D.J. Kaup, A. Reiman, and A. Bers, *Rev. Mod. Phys.* 51: 915 (1979); and references therein.

[12] J.-M. Wersinger, J.M. Finn, and E. Ott, *Phys. Fluids* 23: 1142 (1980); C. Meunier, M.N. Bussac, and G. Laval, *Physica* 4D: 236 (1982).

spatio-temporal evolution, that a cutoff for high wavenumbers in the unstable growth in the form of diffusion is necessary to saturate the instability. Temporal dephasing produces no noticeable effect in the results. We also find that spatio-temporal chaos can occur for arbitrarily small growths of the parent wave. All that is required is that the system size be large enough to accommodate more than one quasi-soliton. We do not find routes to chaos traditionally ascribed to low dimensional systems.

1.2.3 Quasiperiodicity in Stimulated Brillouin Scattering

Sponsors

Lawrence Livermore National Laboratory
Subcontract B108472
National Science Foundation
Grant ECS 88-22475

The dynamics of stimulated Brillouin scattering (SBS) has captured considerable interest recently, both in laser plasma interactions and in optical fibers. A recent experiment has demonstrated evidence of complex temporal evolution of SBS in an optical fiber without external feedback.[13] To understand this, we have considered a simple model of SBS in a finite sized, homogeneous medium with the inclusion of very small temporal dephasing and shown the occurrence of quasiperiodicity and propagating spatial patterns. The model involves three interacting waves without any external feedback. Previous theoretical analyses of SBS without temporal dephasing have found limit-cycle behavior and chaos, but with more complicated models involving more than one pump beam[14] or with external optical feedback[15] (e.g., reflection at the boundaries). In our three-wave model with dephasing, we observe broad band temporal behavior but no transition to chaos defined by a positive Lyapunov exponent. The dephasing may be externally imposed on the pump. However, we find that the amount of dephasing required to exhibit the observed behavior is so small that it may occur merely from the inherent temporal variations of the system. These results indicate that nonlinear SBS may be intrinsically unsteady, so any long time modeling requires a full dynamical analysis.

1.2.4 Bandwidth of Scattered Radiation in Laser-Plasma Interactions

Sponsor

Lawrence Livermore National Laboratory
Subcontract B108472

Using three-dimensional space-time analysis of the evolution of linear instabilities, we have shown that both stimulated Raman scattering (SRS) and stimulated Brillouin scattering (SBS) have a finite bandwidth regardless of whether the instability is convective or absolute. We have calculated the bandwidth for typical laser-plasma experiments and find that it has a strong dependence on the scattering angle. The SBS bandwidth increases as the ion sound speed is increased, while the SRS bandwidth decreases when the density of the region where the instability is generated is increased.

Both SBS and SRS are three-wave parametric instabilities produced by the interaction of an incident laser field with a plasma wave.[16] One of the characteristics observed in laser-plasma experiments has been the bandwidth associated with the scattered light of the two processes. Recent advances in streak-camera diagnostics of the scattered light in laser plasma experiments give a measurement of the emitted bandwidth.[17] Although this bandwidth may be strongly affected by the nonlinear saturation characteristics of these instabilities, a first step in understanding the observed bandwidth (particularly at early times) can be based upon the linear theory of evolution of these instabilities.

---

[13] R. Harrison, J. Uppal, A. Johnstone, and J. Moloney, *Phys. Rev. Lett.* 65: 167 (1990).

[14] A. Gaeta, M. Skeldon, R. Boyd, and P. Narum, *J. Opt. Soc. Am. B* 6: 1709 (1989).

[15] C. Randall and J. Albritton, *Phys. Rev. Lett.* 52: 1887 (1984); K. Sauer and K. Baumgartel, *Phys. Rev. Lett.* 52: 1001 (1984); R. Blaha, E. Laedke, A. Rubenchik and K. Spatschek, *Europhys. Lett.* 7: 237 (1988).

[16] W.L. Kruer, *The Physics of Laser-Plasma Interactions* (Reading, MA: Addison-Wesley Publishing Co., 1988); A. Bers, "Linear Waves and Instabilities," in *Plasma Physics—Les Houches 1972* (London: Gordon and Breach, 1975).

[17] R.P. Drake, P.E. Young, E.A. Williams, K. Estabrook, W.L. Kruer, B.F. Lasinski, C.B. Darrow, H.A. Baldis, and T.W. Johnston, *Phys. Fluids* 31: 1795 (1988), and references therein.

Previous linear instability analyses of the bandwidth were based upon the complex frequency solutions of the (SRS/SBS) dispersion relations for real wave-vectors; the bandwidth was then taken as the range of real frequencies associated with temporal growth.[18] However, such analyses are not sufficient to describe the space-time evolution of the instabilities; this requires a Green's function and pinch-point analysis that properly describes the evolution of the instability as a growing pulse in space-time.[19] Such an analysis for the evolution of these instabilities has been carried out in three spatial dimensions and time.[20] Based upon the same type of Green's function analysis, we find that the scattered light emanating from a local density in the plasma has a substantial bandwidth (ranging up to 10's of Å for SBS, and up to 100's of Å for SRS), as is frequently observed; we also find that the bandwidth varies strongly with the direction of observation. By contrast, the usual analysis of the dispersion relation predicts much narrower (by one to two orders of magnitude) bandwidths. We find that the bandwidth is finite regardless of whether the nature of the instability is absolute or convective[21] and is a natural consequence of the space-time evolution of the SRS and the SBS. The bandwidth is a function of the viewing angle; it is a maximum in the forward direction.

1.2.5 Absolute Versus Convective Instabilities in Space Plasmas

Sponsor

National Aeronautics and Space Administration
Grant NAGW-2048

Laboratory, Space, and Astrophysical plasmas are rich sources of electromagnetic radiation which have intensities above the thermal levels of emission. There are two generic ways of generating this radiation. The first is due to some internal sources of free energy which excite, from noise, an instability inside the plasma. This occurs, for instance, due to spatial gradients or anisotropies inherent in the plasma. The second way that the plasma acts as a source of electromagnetic radiation is by stimulated scattering of some of the externally incident electromagnetic waves. This may happen when the incident waves couple nonlinearly to some normal modes of the plasma and unstably drive, from noise, the scattered radiation from inside the plasma. In either case, the instability evolves in the free energy source region, leading, eventually, to electromagnetic radiation propagating out of the plasma.

An aspect of the radiation that is observed and measured by a detector or a probe, which is located in the source region or far away from it, is the intensity of the emission as a function of either the frequency or the wavelength of the emission. In order to understand the emission one needs to know about the onset of the instability that leads to the observed emission; the propagation in space and time of the instability through the source region and beyond; and, finally, the evolution toward the saturated nonlinear state which is eventually observed.

The linear evolution and propagation of instabilities in a homogeneous medium is studied by well-known techniques.[22] We have used these to study the propagation of cyclotron maser type of instabilities. Such instabilities are believed to be a source of some types of observed planetary, solar and stellar emissions, and, in particular, of auroral kilometric radiation.[23]

We have considered a highly anisotropic, ring-like, electron distribution function in a uniform, background magnetic field and studied the space-time evolution of instabilities propagating along the

---

[18] J.F. Drake, P.K. Kaw, Y.C. Lee, G. Schmidt, C.S. Liu, and M.N. Rosenbluth, *Phys. Fluids* 17: 778 (1974); K. Nishikawa, *J. Phys. Soc. Japan* 24: 916 (1968).

[19] A. Bers, *Handbook of Plasma Physics,* eds. M.N. Rosenbluth and R.Z. Sagdeev (Amsterdam: North-Holland, 1983), vol. 1, chap. 3.2.

[20] F.W. Chambers, Ph.D. diss., Dept. of Phys., MIT, 1975.

[21] A. Bers, "Linear Waves and Instabilities," in *Plasma Physics Les Houches 1972* (London: Gordon and Breach, 1975); A. Bers, *Handbook of Plasma Physics,* eds. M.N. Rosenbluth and R.Z. Sagdeev (Amsterdam: North Holland, 1983), vol. 1, chap. 3.2.

[22] A. Bers, *Handbook of Plasma Physics,* eds. M.N. Rosenbluth and R.Z. Sagdeev (Amsterdam: North-Holland, 1983), vol. 1, chap. 3.2.

[23] D.B. Melrose, *Astrophys. J.* 207: 651 (1976); C.S. Wu and L.C. Lee, *Astrophys. J.* 230: 621 (1979).

magnetic field.[24] The relativistic Vlasov dispersion relation shows three branches: one corresponding to a whistler mode (with a phase velocity less than the speed of light); an electromagnetic mode (with phase velocity greater than the speed of light); and a negative energy mode. The coupling of the negative energy mode to the whistler mode or the electromagnetic mode leads to the whistler instability or the relativistic instability, respectively.

The pinch-point instability analysis[25] in the laboratory frame shows that there are three pinch points with two of them corresponding to the whistler instability and one to the relativistic instability. The whistler instability, while it has a larger growth rate than the relativistic instability, can be stabilized by a finite thermal spread along the magnetic field.[26] The relativistic instability is not affected by such thermal effects since its phase velocity is greater than the speed of light. For ring distributions with no drift along the magnetic field, both instabilities are absolute and characterized by a narrow bandwidth. For sufficiently high drift velocities along the magnetic field, both instabilities are convective and characterized by a broad bandwidth of frequencies. Thus, there is a distinct observational difference between absolute and convective instabilities. The emission corresponding to an absolute instability will have a narrow frequency spectrum while a convective instability will correspond to a broadband emission.

We have also done a pinch-point analysis for electromagnetic instabilities propagating across a magnetic field that are generated by a ring distribution function of electrons. We have studied those instabilities with phase velocities greater than the speed of light and, thus, are not affected by cyclotron resonance damping. Furthermore, we have restricted ourselves to the case of low-densities (which is an appropriate limit for the conditions that exist in the source regions of the auroral kilometric radiation). Instabilities are found to be generated near the electron cyclotron frequency and its harmonics. We observe an interesting space-time behavior of these instabilities as a function of density. For very small densities, the instability near the fundamental electron cyclotron frequency is an absolute instability, while the instabilities at the harmonics are convective instabilities. As the density is increased, the instability at the second harmonic also becomes an absolute instability. For further increases in density, the instability at the fundamental cyclotron frequency becomes convective, while the instability at the second harmonic remains as an absolute instability. Hence, we have harmonic generation from a completely linear theory. These results should be important in explaining the observed emission at harmonics of the electron cyclotron frequencies in the auroral regions.[27]

1.2.6 Fast Electron Transport during Lower-Hybrid Current Drive

Sponsors

National Science Foundation
Grant ECS 88-22475
U.S. Department of Energy
Contract DE-FG02-91-ER-54109

We have carried out a study of electron transport driven by externally imposed wave fields during lower-hybrid current drive. When the plasma dissipation is weak, the ray paths of the waves can make several toroidal transits and suffer numerous radial reflections during which time the poloidal mode numbers of the rays upshift until the fields are Landau damped.[28] In this case, one may assume that there exists in the plasma a random phase ensemble of waves with a broad distribution

[24] V.V. Zhelezniakov, *Izv. Vys. Voch. Zaved. Radiofiz.* 2: 14 (1959); A. Bers, J.K. Hoag, and E.A. Robertson, *Quart. Prog. Rep.* 77: 149-152, 78: 105-110, 79: 107-112, Res. Lab. of Electron., MIT, 1965; A.K. Ram, G. Francis, and A. Bers, "Relativistic Electromagnetic Instabilities Near Electron Cyclotron Frequency and Harmonics," *Proceedings of the Fourth International Workshop on Electron Cyclotron Emission and Electron Cyclotron Resonance Heating*, Ufficio Edizioni Scientifiche, Frascati, Rome, Italy, 1984; Report PFC/CP-84-5, Plasma Fusion Ctr., MIT, 1984.

[25] A. Bers, *Handbook of Plasma Physics*, eds. M.N. Rosenbluth and R.Z. Sagdeev (Amsterdam: North-Holland, 1983), vol. 1, chap. 3.2.

[26] E.A. Robertson and A. Bers, *Quart. Prog. Rep.* 79: 107-112, Res. Lab. of Electron., MIT, 1965.

[27] R.F. Benson, *J. Geophys. Res.* 90: 2753 (1985).

[28] P.T. Bonoli and R.C. Englade, *Phys. Fluids* 29: 2937 (1986).

of both poloidal and toroidal mode numbers;[29] radial electron transport is induced by the poloidal component of the wave fields via the guiding center $E \times B$ drift of electrons in resonance with the wave fields. The transport is studied via a quasilinear-Fokker-Planck equation which includes resonant $E \times B$ diffusion. Two types of radial flows are obtained: (1) a convective flow driven by an asymmetric poloidal wave spectrum, and (2) a collisionless diffusive flow proportional to the width of the poloidal spectrum. The convective flow is outward when the poloidal spectrum is upshifted to fill the spectral gap. Upperbounds are put on both the radial convection velocity and diffusion coefficient by assuming that the upshifted poloidal mode numbers dominate the toroidal mode numbers in determining the resonance condition. Based solely on these estimates, the outward convection would be important in determining the fast electron confinement time. Specific cases were studied by toroidal ray tracing to determine the spectrum inside the plasma and the resulting convection and diffusion coefficients. Simulations of Alcator C and JT60 show that the radial convection velocity has a broad maximum of nearly 1 m/sec and is independent of the amplitude of fields. In both cases, the radial diffusion is found to be highly localized near the magnetic axis. For JT60, the peak of the diffusion can be quite large, nearly 1 m^2/sec.

1.2.7 Publications

Bers, A., V. Fuchs, and C.C. Chow. "Single-Pass Absorption in Ion-Cyclotron Heating." *Bull. Amer. Phys. Soc.* 35: 2047 (1990).

Chow, C.C., A.K. Ram, and A. Bers. "Spatio-Temporal Chaos and Quasiperiodicity in the Nonlinear Three Wave Interaction." *Bull. Amer. Phys. Soc.* 35: 2006 (1990).

Chow, C.C., V. Fuchs, and A. Bers. "Reflection at the Resonance Layer of the Fast Alfvén Wave in Ion Cyclotron Heating." *Phys. Fluids B* 2: 2185 (1990).

Chow, C.C., A. Bers, and A.K. Ram. "Bandwidth of Scattered Radiation in Laser-Plasma Interactions." Paper presented at the 20th Annual Anomalous Absorption Conference, Traverse City, Michigan, July 9-13, 1990.

Chow, C.C., A.K. Ram, and A. Bers. "Bandwidth of Scattered Radiation in Laser-Plasma Interactions." Report PFC/JA-90-24. Plasma Fusion Ctr., MIT, 1990.

Chow, C.C., V. Fuchs, and A. Bers. "The Dispersion Relation for D^3(He) Ion-Cyclotron Resonance Heating." *Phys. Fluids B* 2: 1089 (1990).

Chow, C., V. Fuchs, and A. Bers. "Reflection at the Resonance Layer of the Fast Alfvén Wave in Ion Cyclotron Heating." Report PFC/JA-90 2. Plasma Fusion Ctr., MIT, 1990.

Kupfer, K., A. Bers, and A.K. Ram. "Stochastic Electron Transport Induced by Lower-Hybrid Current Drive Wave Fields." *Bull. Amer. Phys. Soc.* 35: 1984-5 (1990).

Kupfer, K., A. Bers, and A.K. Ram. "Guiding Center Stochasticity and Transport Induced by Electrostatic Waves." Report PFC/JA-90-22. Plasma Fusion Ctr., MIT, 1990.

Kupfer, K., A. Bers, and A.K. Ram. "Guiding Center Stochasticity in a Tokamak." *Proceedings of the International Sherwood Theory Meeting*, Williamsburg, Virginia, April 23-25, 1990.

Kupfer, K., A. Bers, and A.K. Ram. "Guiding Center Stochasticity and Transport Induced by Electrostatic Waves." *Proceedings of the Topical Conference on Research Trends in Nonlinear and Relativistic Effects in Plasmas*, La Jolla Institute, La Jolla, California, February 5-8, 1990.

Ram, A.K., and A. Bers. "Propagation and Damping of Mode Converted Ion-Bernstein Waves in Toroidal Plasmas." *Phys. Fluids B*, April 1991.

Ram, A.K., and A. Bers. "Absolute Versus Convective Analysis of Instabilities in Space Plasmas." Report PFC/JA-91-2. Plasma Fusion Ctr., MIT, 1991.

Ram, A.K., and A. Bers. "Absolute Versus Convective Analysis of Instabilities in Space Plasmas." Paper presented at the 1990 Cambridge Workshop on Theoretical Geoplasma Physics, in *Physics of Space Plasmas* (1990), forthcoming; *SPI Conference Proceedings and Reprint Series*, Number 10. Eds. T. Chang, G.

[29] D. Moreau, J.M. Rax, and A. Samain, *Plasma Phys. and Contr. Fusion* 31: 1895 (1989).

B. Crew, and J. R. Jasperse. Cambridge, MA: Scientific Publishers, 1991.

Ram, A.K., and A. Bers. "Space-Time Analysis of Electromagnetic Instabilities with Application to Auroral Kilometric Radiation." *EOS Trans. Amer. Geophys. Union* 71(43): 1532 (1990)

Ram, A.K., C.C. Chow, and A. Bers. "Bandwidth of Scattered Radiation in Laser-Plasma Interactions." *Bull. Amer. Phys. Soc.* 35: 2126 (1990).

Ram, A.K., and A. Bers. "Propagation and Damping of Mode Converted Ion-Bernstein Waves in Toroidal Plasmas." Report PFC/JA-90-20. Plasma Fusion Ctr., MIT, 1990.

Ram, A.K., and A. Bers. "Propagation of Ion-Bernstein Waves in Toroidal Plasmas." *Proceedings of the International Sherwood Theory Meeting,* Williamsburg, Virginia, April 23-25, 1990.

1.3 Physics of Thermonuclear Plasmas

Sponsor

U.S. Department of Energy
Contract DE-AC02-ET-51013

Project Staff

Professor Bruno Coppi, Dr. Ronald C. Englade, Dr. Stefano Migliuolo, Dr. Marco Nassi, Dr. Linda E. Sugiyama, Dr. Leonid E. Zakharov, Riccardo Betti, Paolo Detragiache, Darin Ernst

The main theme of this program is the theoretical study of magnetically confined plasmas in regimes of thermonuclear interest. A variety of physical regimes that fall in this category characterize both present-day experiments on toroidal plasmas (e.g., Alcator, TFTR, JET) as well as future experiments that will contain ignited plasmas. These will either involve first generation fuels, namely a deuterium-tritium mixture (Ignitor, CIT), or more advanced fuels such as deuterium-deuterium or deuterium-helium mixtures (Candor). A coordinated effort of collaboration between the design group of the U.S. compact ignition experiment, CIT, and that of the European experiment, Ignitor, has been set up with our participation. At MIT, the Alcator C-MOD experiment that combines the favorable features of an elongated plasma cross section with a high magnetic field is under construction. These features, which are also being planned for CIT and Ignitor, were originally proposed for a machine called Megator, designed by us in the early 1970s.

Presently, our research program follows two major avenues. First, the basic physical processes of thermonuclear plasmas (equilibrium, stability, transport, etc.) are being studied as they apply to existing or near-term future systems. In this effort we closely collaborate with our experimental colleagues, as well as theorists from other research groups (e.g., Joint European Undertaking (J.E.T), Princeton, Columbia). This work also involves time-dependent simulations of plasma discharges in the planned D-T burning Ignitor experiment, with particular attention being focused on the evolution of spatial profiles of plasma current and temperature. Collaboration with our colleagues at the Italian laboratories of E.N.E.A. (Energia Nucleare e Energie Alternative), as well as in-house code development by young scientists "on loan" from Italy, plays a major role in this endeavor. Second, we explore advanced regimes of thermonuclear burning, including those employing low neutron yield fuels (^{3}D-He, and "catalyzed" D-D). We consider both the design of machines that will contain these very high temperature plasmas as well as the physics that govern their behavior.

We present below some of the salient results on work completed or presently being worked on by members of our research group.

1.3.1 Symmetries and Global Transport Equations

We formulate[30] constraints that apply to the current density profile in a high temperature toroidal plasma and introduce an effective thermal force and electron viscosity term in the current density equation. Correspondingly, the electron thermal energy equation acquires new terms. A matrix equation that relates the electron thermal energy transport to that of the current density is derived. The symmetry properties of this matrix are identified and used to prescribe realistic conditions on the electron temperature and current density profiles.[30]

These profiles are relevant to high temperature regimes. In fact, in these regimes the presence of a population of magnetically trapped electrons affects the plasma resistivity so that it causes a

[30] B. Coppi and F. Pegoraro, submitted to *Phys. Fluids* (1991).

current density distribution with a cusp-like profile[31] near the magnetic axis for the observed (canonical)[32] electron temperature profiles, when a simple Ohm's law is adopted to relate the current to the electric field.

The product of our theory that involves coupling of the transport of the electron thermal energy and of the current density is a "profile equation," which relates the two equilibrium profiles to the resistivity and a new thermal-viscous transport coefficient. The equation is of the singular, nonlinear, integrodifferential type.

We have solved this equation numerically for five resistivity models:[33]

1. An oversimplified neoclassical model with $\nu_{*e} \equiv 0$
2. A more realistic neoclassical model that includes particle detrapping $\nu_{*e} \neq 0$
3. A simplified neoclassical model giving qualitatively identical results to (b).
4. A model obtained from a transport code combined with the neoclassical theory near the magnetic axis.
5. A model obtained from JET experimental data.

In all cases we find current profiles that are well-behaved near the magnetic axis, resolving the problem of the cusp-like profiles previously predicted by neoclassical resistivity and Ohm's law. In addition, the resulting electron temperature profile is found to be insensitive to the size of the thermal-viscous diffusion coefficient, in agreement with the principle of profile consistency.

Finally, we have solved the profile equation analytically and studied the mathematical properties of its solutions.[33] This work will form the basis for use of this model in transport codes.

1.3.2 Combined Transport and Ray Tracing Studies of ECRF Heating in CIT

We have continued our productive collaboration with Dr. Miklos Porkolab, task leader for the assessment of electron cyclotron radiofrequency (ECRF) heating prospects in the proposed Compact Ignition Tokamak (CIT). Moving beyond an approach[34] which modeled power deposition results obtained from a stand-alone ray tracing package as input to a 1 1/2D equilibrium and transport calculation, we have succeeded in developing a large combined code in which the ECRF ray propagation and absorption, the MHD equilibrium calculation, and the plasma heat transport are treated self-consistently.[35] The ECRF package is a variation of the TORAY[36] toroidal ray tracing code, valid in both the Doppler and relativistic regimes. The values along a ray trajectory of the temperature, density, magnetic field components, and the derivatives of these quantities in a Cartesian coordinate system that are required inputs to TORAY have been obtained by a modification of the BALDUR 1 1/2 D equilibrium package described by Coppi and Pegoraro.[37] This modification makes extensive use of a procedure originally developed to track a chord through the nested flux surface geometry of a toroidal device.[38] We have used the combined code to simulate start up scenarios for CIT in which the ECRF frequency and injection angle are chosen to maintain either centralized or

---

[31] B. Coppi and L. Sugiyama, *Comm. Plasma Phys. Cont. Fusion* 10: 43 (1986).

[32] B. Coppi, *Comm. Plasma Phys. Cont. Fusion* 5: 261 (1980).

[33] D. Ernst, Report PTP-90/12, Res. Lab. of Electron., MIT, 1990.

[34] M. Porkolab, P. Bonoli, R. Englade et al., Sixteenth European Conference on Controlled Fusion and Plasma Physics, Venice, 1989.

[35] P. Bonoli, R. Englade, M. Porkolab, et al., Seventeenth European Conference on Controlled Fusion and Plasma Physics, Amsterdam, 1990; R. Englade, P. Bonoli, M. Porkolab et al., *Bull. Am. Phys. Soc.* 35: 2142 (1990).

[36] A. Kritz et al., *Proceedings of the Third International Symposium on Heating in Toroidal Plasmas*, Brussels, 1982, Vol. II, p. 707.

[37] B. Coppi and F. Pegoraro, submitted to *Phys. Fluids* (1991).

[38] S. Attenburger, W. Houlberg, and S. Hirshman, *J. Comput. Phys.* 72: 435 (1987).

off-axis heating for the most recent machine parameters.[39]

1.3.3 Fixed Boundary Transport Code Simulation of DT Ignition

Detailed numerical analyses of the approach to ignition in proposed high field, tight aspect ratio toroidal experiments such as the Ignitor and CIT have been performed with a 1 1/2D fixed boundary equilibrium-transport code. These investigations have, for the most part, involved start-up scenarios for the latest design of the Ignitor device with maximum current and field of 12MA and 13T respectively. In one series of runs, the electron thermal transport was assumed to consist of a term of either the Coppi-Mazzucato-Grüber or Intor type dominant in the ohmic regime, with an additional contribution depending on the ratio of fusion (and auxiliary) heating to ohmic heating, the global poloidal beta, and the local electron density whose magnitude was determined by bench-marking with existing NBI experimental results. The ion thermal transport was taken to be twice that of the "non-ohmic" electron contribution plus neoclassical diffusivity. Particle transport was assumed to consist of an outward diffusion and an inward convection, with both terms proportional to the anomalous electron thermal diffusivity. Centrally peaked source terms with magnitudes determined by the desired rate of density ramping were used to simulate multiple pellet fueling. Electrical resistivity was assumed to be of the Spitzer type corrected for the effects of trapped particles, and sawtooth phenomena were simulated by periodic flattening of the particle density and temperature spatial profiles within a mixing radius defined by conservation of helical flux. Finally, the code allowed for arbitrary time variation of the toroidal plasma current, vacuum toroidal field, and the shape and location of the outer plasma boundary.

Two D-T start-up scenarios have been investigated in detail with the code as described above. In the first, the current was ramped linearly from 1MA to 12MA, the field from 9T to 13T, and the central electron (and ion) density from 7×10^{19} m^{-3} to 7×10^{20} m^{-3}, all in 3 seconds. The plasma was assumed to have its full size throughout, however, resulting in a pronounced skin current and a non-monotonic q profile everywhere above unity. In addition, the rise of the central temperatures and thus significant fusion heating was relatively slow due to the poor current penetration. In the second scenario, the plasma boundary was expanded non-linearly so as to maintain a relatively constant value of q_{edge} during ramp. This approach resulted in good current penetration and rapid heating, but with the region of $q < 1$ occupying less than 10% of the plasma volume throughout the run. In this situation, even quite rapid sawteeth (100 msec) had only a small effect on the plasma energy balance, and ignition was achieved one second after the end of the ramp phase.

The effects of varying the thermal transport coefficients have also been studied. In particular, it was found that increasing the magnitudes of the "non-ohmic" electron and ion coefficients by a factor of three did not prevent ignition if the central density at the end of the ramp was allowed to be 1.2×10^{20} m^{-3}. In another series of runs, the electron thermal transport was taken to be the sum of a CMG term and a term expressed as

$$\chi_e^{LG}\left(\frac{P_\alpha}{P_\alpha + P_{OH}}\right)^{1.5}$$

where $\kappa a^2/\chi_e^{LG}$ scales like the Läckner-Gottardi global confinement time and where χ_e^{LG} has a magnitude that is adjusted to agree with TFTR beam results and increases radially in an ad hoc manner. As before, the thermal transport was taken to consist of a neoclassical contribution plus twice the "non-ohmic" χ_e. Assuming $Z_{eff} = 1.5$ due to carbon impurity, and a central electron density of 1.0×10^{20} m^{-3} at the end of the ramp phase ($t = 3.0$ sec), we find that Ignitor attains $Q = 5$ at $t = 3.9$ sec. True ignition is not reached but at $t = 6.0$ sec; the fusion alpha power is 31 MW. A somewhat higher density allows ignition to be attained.

1.3.4 Plasma Dynamics Simulation by the TSC Code

We are carrying out an investigation of the dynamics of the plasma discharge, starting with the current ramp-up phase, in a typical high field deuterium-tritium ignition experiment, using the TSC[40] code. This is the first free boundary simulation of ignition, and the first study of the effects of a realistic current ramp on ignition (after initial

[39] R. Englade, P. Bonoli, M. Porkolab et al., *Bull. Am. Phys. Soc.* 35: 2142 (1990).

[40] S.C. Jardin, N. Pomphrey, and J. DeLucia, *J. Comp. Phys.* 66: 481 (1986).

studies by Houlberg).[41] The Tokamak Simulation Code, developed at PPPL, models the transport time evolution, positional stability, and control properties of non-circular, free boundary axisymmetric tokamaks.[42] It provides a time dependent, nonlinear description of the axisymmetric MHD and transport behavior of the plasma in two spatial dimensions. This problem is very complex, due to the disparate time scales of diffusion-like and wave-like phenomena and to the anisotropy introduced by the magnetic field. A self-consistent solution is obtained by solving the plasma momentum and field evolution equations on a two-dimensional X-Z grid, and the plasma energy and particle evolution equations in a one dimensional coordinate system which evolves with the plasma magnetic surfaces.[43] The TSC code takes into account the plasma interaction with a set of poloidal conductors that model the passive structure of the plasma chamber as well as with the active poloidal field coils. These conductors obey electromagnetic circuit equations with active feedback systems included. For the ignition studies, the toroidal magnetic field is presented as a function of time. Preliminary results[14] on the ignition plasma performance using the Coppi-Tang transport model[45] as well as a study on the Volt-second requirements throughout the discharge have been presented.[46] More recently, we have modified the transport model by assuming that the anomalous electron heat flux can be described by a modified form of the Coppi-Mazzucato-Grüber thermal diffusivity, which can reproduce ohmic and L- or H-mode experimental results in the auxiliary heating regimes or by a diffusion coefficient based on the ubiquitous mode.[47] We have shown[48] that the current ramp phase of the discharge contributes substantially to the ohmic heating to ignition in a high field device, since the ohmic heating increases linearly with time if the density is ramped simultaneously, even up to ignition temperatures. Due to its spatial distribution off-axis, the ohmic heating can remain relatively large in the interval between the end of the ramp and ignition.

The stability of the plasma to instabilities associated with magnetic reconnection can also be improved by controlling the current ramp. First, it was found relatively easy to keep the radius of the $q = 1$ surface small or nonexistent during the current ramp-up, so that it reached significant size only when the central temperature reached values of around 5 keV or higher. Then kinetic effects would be expected to help stabilize $m^0 = 1$ modes associated with the sawtooth crash.[49] Modest amounts of auxiliary heating (4 MW ICRH) could keep $q > 1$ until ignition. Ramping down the current can prevent large $q = 1$ surfaces without severely compromising ignition, except in marginal cases. The edge q_ψ of the plasma can be maintained between integral values during the ramp, $3 < q_{\psi a} < 4$, to avoid triggering serious edge instabilities associated with broad current profiles. Development of interior hollow current density profiles were shown to be closely related to violation of the JET stability diagram in $(l_i - q_{\psi a})$ space, if the current evolved under a purely neoclassical resistivity.

The evolution of the plasma and current density proved to be sensitive to values of the temperature in the outer region of the plasma. The spatial and temporal variation of the thermal transport also must be considered. There is a range of allowable energy confinement levels that permits ohmic ignition without serious problems with nonmonotonic current density profiles and large $q = 1$ surfaces. This range is under investigation.

---

[41] W. Houlberg, *Nucl. Fusion* 27: 1009 (1987).

[42] S.C. Jardin et al., *Nucl. Fusion* 27: 569 (1987); B.J. Merril and S.C. Jardin, *J. Nucl. Mat.* 145-147:881 (1987).

[43] S.C. Jardin, in *Multiple Time Scales,* eds. J.U. Brackbill and B.I. Cohen (San Diego, California: Academic Press, 1985).

[44] M. Nassi, S.C. Jardin, N. Pomphrey, *Bull. Am. Phys. Soc.* 34: 1974 (1989).

[45] W.M. Tang, *Nucl. Fusion* 26: 1605 (1986).

[46] M. Nassi, Report PTP-90/1, Res. Lab. of Electron., MIT, 1990.

[47] B. Coppi, *Comm. Plasma Phys. Controlled Fusion* 12: 319 (1989).

[48] L. Sugiyama and M. Nassi, Report PTP-90/8, Res. Lab. of Electron., MIT, 1990.

[49] B. Coppi, P. Detragiache, S. Migliuolo, F. Pegoraro, and F. Porcelli, *Phys. Rev. Lett.* 63: 2733 (1989).

1.3.5 Momentum Transport Processes and Collective Modes

Many tokamak experiments[50] have shown that during neutral beam coinjection (NBI), the imparted angular momentum diffuses away from the magnetic axis with a radial diffusivity $\chi_\phi \approx 30$ to 100 times greater than the known collisional theory predicts.[51] Correspondingly, when the neutral beam is turned off, the slowing down time is 30 to 100 times shorter than the collisional time $a^2/(\nu_{ii}\rho_i^2)$. In addition, it is well-documented that the experimental radial diffusivities of toroidal momentum (χ_ϕ) and ion thermal energy (χ_i) scale almost identically with the minor radius of the plasma column.[52] As one might expect, χ_i often exceeds its neoclassical estimate.

The experimental conditions are characterized by a poloidal flow strongly damped at a rate $\tau_p^{-1} \sim V_{fi}^2/(a^2\nu_{ii})$, rapid even on the anomalous transport timescale. Therefore, the remaining flow is predominantly toroidal, and can easily be shown to be constant on magnetic flux surfaces.[51] Consequently, we seek a collisionless transport theory to explain the observed radial diffusion of toroidal momentum across the magnetic field. Fluctuations traveling in both the electron and the ion diamagnetic directions have been observed, and the shape of the associated spectrum is independent of the toroidal flow velocity while acquiring a Doppler shift. This suggests anomalous transport by modes of the electron-drift type. The theory should predict the scaling $\chi_\phi \sim \chi_i$ and be consistent with observed profile shapes as well.

A report[53] has been written describing two collective modes of the electron-drift type[54] driven unstable by the large ion flow velocity shear induced by NBI. The modes described are consistent with the above conditions. One mode requires large flow velocities in addition to shear, while the other, weaker instability does not require such high flow velocities but relies on the existence of a parallel ion viscosity. Recent experimental conditions in TFTR[55] are right for the excitation of this weaker instability. Both instabilities are shown to produce momentum diffusivities χ_ϕ greatly exceeding the neoclassical result.

Following this work, we have obtained scaling laws for χ_ϕ employing the neoclassical parallel viscosity. In addition, we have compiled scalings for χ_ϕ for other "anomalous viscosity" theories in a form convenient for comparison with experimental data obtained from interpretation codes. To this end, transport equations describing the radial diffusion of toroidal momentum have been derived for axisymmetric systems, and a method for extracting χ_ϕ from experimental radial profile data has been developed.

Hospitality extended to one of us (Darin Ernst) by our colleagues at the J.E.T., the Joint European Undertaking, during the summer of 1990 has been particularly beneficial in this work. With the assistance of the theory group there, we have compiled an experimental database consisting of 365 radial profiles. We expect this data, together with the methods described above, to aid greatly in our effort to connect theory and experiment in this problem.

1.3.6 The Ellipticity Induced Alfvén Eigenmodes

During the past several years there has been increasing interest in the problem of energetic particle-Alfvén wave interactions. These interactions can drive instabilities that may play an important role in (1) the observation of fishbone oscillations in existing tokamaks[56] and (2) the possible enhanced loss of alpha particles in future

---

[50] S.D. Scott et al., *Phys. Rev. Lett.* 64: 531 (1990); S.D. Scott et al., *Plasma Physics and Controlled Nuclear Fusion Research 1988*, Paper I.A.E.A.-CN-50/E-3-5 (Vienna: I.A.E.A., 1989).

[51] J.W. Connor, S.C. Cowley, R.J. Hastie and L.R. Pan, *Plasma Phys. and Cont. Fusion* 29: 919 (1987).

[52] S.D. Scott et al., *Phys. Rev. Lett.* 64: 531 (1990).

[53] B. Coppi, Report PTP 89/2, Res. Lab. of Electron., MIT, 1989.

[54] B. Coppi, M.N. Rosenbluth and R.Z. Sagdeev, *Phys. Fluids* 10: 582 (1967).

[55] S.D. Scott et al., *Plasma Physics and Controlled Nuclear Fusion Research 1988*, Paper I.A.E.A.-CN-50/E-3-5 (Vienna: I.A.E.A., 1989).

[56] J.D. Strachan, B. Grek, W. Heidbrink, D. Johnson, S.M. Kaye, H.W. Kugel, B. LeBlanc, and K. McGuire, *Nucl. Fusion* 25: 863 (1985).

ignited devices such as CIT and ITER.[57] Specifically, in the latter case it has been shown that MHD Alfvén waves whose frequency ω_A is lower than the alpha diamagnetic frequency $\omega_{*\alpha}$ can be driven unstable by resonant particle interactions. Within this class of instabilities, the current view is that toroidally induced Alfvén eigenmodes (TAE)[58] may pose the most serious threat. The TAE instabilities have global structure and a real frequency that lies in a narrow gap in the continuum caused by toroidal mode coupling. Hence, they are sometimes called "gap modes."

We have shown that noncircularity as well as toroidicity can lead to the existence of gap modes.[59] We have focused attention on ellipticity as this may be the most important effect in tokamaks. In particular, since many tokamaks have a finite elongation ($\kappa - 1 \sim 1$) as compared to a small toroidicity ($\varepsilon << 1$), the elliptically induced Alfvén eigenmode (EAE) that we found, may indeed be a more robust and potentially dangerous mode than the TAE. A summary of the properties of the EAE mode is given below.

1. The most macroscopic and thus potentially dangerous EAE in a tokamak couples the m = 1, n = 1, and m = 3, n = 1 "cylindrical" eigenmodes.
2. The region of strong coupling (i.e., the gap) occurs at the radius r_0 corresponding to $q(r_0) \equiv 2$.
3. The real frequency of the mode is approximately $\omega_0 = v_A(r_0)/R_0 q(r_0)$. The actual eigenfrequency is shifted slightly from ω_0. In principle, the shift can be positive or negative.
4. For the sake of analytic simplicity the ellipticity is ordered small: $\kappa - 1 \sim \varepsilon^{1/2}$. Since our results show that $\Delta\omega/\omega_0 \sim \kappa - 1$, the implication is that finite ellipticity leads to finite frequency shift. Similarly, the width of the coupling layer scales $\Delta r/r_0 \sim \kappa - 1$ indicating a region of finite extent.

The EAE as well as the TAE can be excited by resonance with circulating alpha particles.[60] The drift kinetic theory of these modes indicate that growth or damping depends upon a competition between the alpha particle driver, electron Landau damping and continuum damping. Both the TAE and EAE need further investigation to determine the extent of their detrimental effect on alpha particle confinement in ignited tokamaks.

1.3.7 $M^0 = 1$ Internal Modes in High Temperature Regimes

As present experiments (e.g., JET) reach the multi-keV regime of plasma temperatures, models for the stability of $m^0 = 1$ internal modes must be improved to account for kinetic effects due to ions and electrons. In these regimes, as well as in those relevant to planned ignition experiments such as Ignitor, standard two-fluid theory[61] is inadequate: the Larmor radius of the plasma ions, $\rho_i \equiv \sqrt{2T_i m_i}\, c/eB$, becomes a finite fraction of the scaled radius of the singular surface, $\varepsilon_\eta^{1/3} r_0$. Here r_0 is the radius where $q(r) = rB_\zeta/RB_\theta = 1$ and $\varepsilon_\eta = \eta c^2 \tau_H / 4\pi r_0^2$ is a measure of the electrical resistivity. As a consequence, finite Larmor radius (FLR) effects must be taken into account. These effects are known[62] to be destabilizing in that they establish a minimum value for the thickness of the singular layer about $r = r_0$, where reconnection can occur: $\delta/r_0 = \max(\rho_i/r_0, \lambda_H)$ where λ_H is the ideal MHD stability parameter. Also, in regimes where $\lambda_H < \rho_i/r_0$, FLR acts to raise the mode frequency, thereby lessening the stabilizing effect of finite diamagnetic ion frequency (ω_{*i}).

---

[57] D.J. Sigmar, C.T. Hsu, R. White, and C.Z. Cheng, I.A.E.A. Technical Committee Meeting on *Alpha Particles/Confinement and Heating*, Kiev, USSR, October 1989.

[58] C.Z. Cheng and M.S. Chance, *Phys. Fluids* 29: 3659 (1986); G.Y. Fu and J.W. Van Dam, *Phys. Fluids* B1: 1949 (1989); J.W Van Dam, G.Y. Fu, and C.Z. Cheng, *Fus. Tech.* 18: 461 (1990).

[59] R. Betti and J.P. Freidberg, *Elliptically Induced Alfvén Eigenmodes,* Report PFC/JA-91-1, Plasma Fusion Ctr., MIT, 1991.

[60] C.Z. Cheng and M.S. Chance, *Phys. Fluids* 29: 3659 (1986); G.Y. Fu and J.W. Van Dam, *Phys. Fluids* B1: 1949 (1989); J.W. Van Dam, G.Y. Fu, and C.Z. Cheng, *Fus. Tech.* 18: 461 (1990).

[61] G. Ara, B. Basu, B. Coppi, G. Laval, M.N. Rosenbluth, and B.V. Waddell, *N.Y. Ann. Phys.* 112: 443 (1978).

[62] F. Pegoraro, F. Porcelli, and T.J. Schep, *Phys. Fluids* B1: 364 (1989).

We have generalized[63] the kinetic model of Pegoraro et al.[62] including the stabilizing effects of ion viscosity through a particle and momentum conserving Krook collision operator. For low values of FLR and ion viscosity effects (i.e., compared to λ_H and in the regime where the ideal mode is stable, $\lambda_H < \omega_{*i}\,\tau_H/2$), the normalized eigenfrequency of the internal $m^0 = 1$ resistive kink, $\lambda = -i\omega\tau_H$ becomes:

$$\lambda = i\,\frac{\lambda_H^2}{\lambda_i} + \frac{5\varepsilon_\eta}{2\lambda_i^2} - \frac{\rho_i^2\lambda_\nu}{4\lambda_H^2}\left[\frac{\lambda_i^2\lambda_\nu^2 + 3\lambda_H^4}{(\lambda_i\lambda_\nu + \lambda_H^2)^2} - \frac{3}{4}\right] +$$

$$\frac{i\rho_i^2}{4\lambda_i}\left[\frac{3}{4} - \frac{\lambda_i^2\lambda_\nu^2}{(\lambda_i\lambda_\nu + \lambda_H^2)^2}\right]^2$$

which clearly shows the stabilization to the FLR enhanced resistive mode when $\lambda_\nu \equiv \nu_i\tau_H$ is large enough to overcome the effect of finite electrical resistivity, e.g., $\lambda_\nu \geq 40\varepsilon_\eta(\lambda_H/\rho_i\lambda_i)^2$ when $\lambda_H^2 \ll \lambda_i\lambda_\nu$.

We are continuing this study by numerically exploring regions in parameter space (e.g., $\lambda_H \to 0$ and/or $\rho_i/\varepsilon_\eta^{1/3}\, r_0 > 1$) where analytic perturbation techniques are inappropriate. In particular, we find that the growth rate of resistive $m^0 = 1$ modes is a non-monotonic function of the effective FLR parameter $\hat{\rho} \equiv \rho_i/\varepsilon_\eta^{1/3} r_0$. For $\hat{\rho} \leq 1$, the mode actually becomes less unstable. Hence, the results of two-fluid theory (which formally holds for $\hat{\rho} \ll 1$) can be applied (with caution) to the entire regime $0 \leq \hat{\rho} \leq 1$. In this manner, we are able to accurately predict regimes in which ignition experiments (e.g., Ignitor) will be able to operate without incurring sawtooth crashes, e.g., for central electron temperatures exceeding 5 keV.

1.3.8 On Temperature Gradient Instabilities and Radial Electric Fields

The improved level of confinement found in the Tokamak H-mode has been attributed, among others, to the presence of shear in the equilibrium poloidal velocity produced by a radial electric field.[64] Since it is by now generally accepted that ion temperature gradient instabilities have a deleterious affect on energy confinement, we have studied the effects of dV_E/dr on the linear theory of those modes.[65] The simplest magnetic field geometry was assumed (shearless slab) and the following results were obtained.

1. First order effects (proportional to dV_E/dr) come into play by modifying the effective FLR of the mode: $k_\perp^2\rho_i^2 \to k_\perp^2\rho_i^2/(1 + V'_E/\Omega)$ where $V'_E \equiv dV_e/dr$. This shift effects long ($k_\perp\rho_i < 1$) and short wavelength modes in opposite fashion, causing (for a given sign of V'_E) one to become more unstable (at fixed $\eta_i = d\ln T_i/d\ln n$) while the other becomes more stable.
2. Second order effects (proportional to $V''_E = d^2V_E/dr^2$) also cause a shift in effective FLR. More importantly, however, they produce a secular term to the particles unperturbed orbit ($\propto tV''_EV_\perp^2/4\Omega^2$). This term was known long ago[66] as the FLR correction to the EXB drift. This term has a definite effect on the stability properties of all ion temperature gradient modes: for $V''_E < 0$ the value of η_i at marginal stability is increased and (above marginal stability) the most unstable mode moves to shorter perpendicular wavelengths and has a lower growth rate.

---

[63] S. Migliuolo, *Nucl. Fusion* 31: 365 (1991).

[64] See, e.g., H. Biglari et al., in *Plasma Physics and Controlled Nuclear Fusion Research*, Paper IAEA-CN-53/D-3-5-2, 1990.

[65] S. Migliuolo and A.K. Sen, *Phys. Fluids* B2: 3047 (1990).

[66] T.E. Stringer and G. Schmidt, *Plasma Phys.* 9: 53 (1967).

1.4 Versator II Plasma Research Program

Sponsor

U.S. Department of Energy
Contract DE-AC02-78-ET-51013

Project Staff

Professor Miklos Porkolab, Jeffrey A. Colborn, Jared P. Squire, Jesus Noel Villasenor, Edward W. Fitzgerald

Versator II is a small scale tokamak facility (major radius R = 40 cm., minor radius a = 13 cm.) with modest plasma parameters (magnetic field $B_0 \lesssim 1.3$ Tesla, density $n_e \sim 3 \times 10^{13}$ cm^{-3}, and plasma current $I_p \sim 10$-80 kA) which is used for fundamental studies of the interaction of electromagnetic waves with a fully ionized, nearly collisionless plasma. For this purpose, we use several high power (~ 100 kW) microwave sources to launch waves at frequencies near the electron-gyro frequency (f $\sim$ 28-35 GHz) and the lower hybrid (ion-plasma) frequency (f = 800 MHz or 2.45 GHz). In the section below, we describe three different experimental projects which were carried out in the past year.

1.4.1 Electron Cyclotron Resonance Heating Experiments

The purpose of the Electron-Cyclotron-Resonance-Heating (ECRH) on Versator II is to better understand the physical mechanisms of toroidal plasma formation and confinement by ECRH. In addition, ECRH is combined with lower-hybrid current drive (LHCD) for aiding in the efficiency of startup of a tokamak plasma. Finally, theory predicts improved current drive efficiency with LHCD in the steady state mode of tokamak operation. In addition to its scientific interest, better understanding of these mechanisms may enable the construction of improved steady state fusion power plants.

The main hardware used for these experiments are the radiofrequency (RF) power systems including sources, transmission lines, and antennas. These include a 100 kW, 40 ms, 2.45 GHz LHCD system; a 150 kW, 50 ms, 800 GHz LHCD system; and a 220 kW, 75 ms, 28 GHz ECRH system. Diagnostics include an electron cyclotron radiation transmission receiver, arrays of hard X-ray detectors, a movable interferometer, probes, and ultraviolet and microwave radiation detectors. Emphasis is being placed on diagnosing the electron distribution function.

In earlier years, a 35 GHz NRL-manufactured gyrotron was used as the ECRH power source. This gyrotron was limited to pulse lengths of less than 3 ms, so only short pulse experiments could be performed. After considerable effort was expended to improve its performance, this gyrotron was replaced in the Fall 1990 with a Varian 28 GHz gyrotron. This tube is rated for 75 ms pulses and has since operated reliably on Versator-II with pulse lengths up to 20 ms, and is limited only by the power supply. This new gyrotron has enabled our rapid progress, and the experimental program described above is now underway.

Recent experiments have focused on hard x-ray and EC radiation diagnosis of startup plasmas and ECRH-formed plasmas. For example, recent startup plasmas have been formed by 5 ms of ECRH at 50 kW, followed by 25 ms of 2.45 GHz LHCD and a small loop voltage. The plasma density rose to about 7×10^{12} cm^{-3}, and the plasma current rose to 16 kA. These parameters are similar to those of typical conventional discharges on Versator-II. The electron distribution has been diagnosed during the early ramp-up, late ramp-up, and fully developed stages of these discharges. These results, combined with observations from experiments scheduled for the next six months, should increase our understanding of the mechanism of current-generation by rf power in tokamaks, particularly when ECRH and LHCD are combined.

1.4.2 800 MHZ Fast Wave Current Drive Experiments

These experiments are aimed at finding ways to improve rf current drive efficiency in tokamak plasmas. While in past experiments the so-called "slow" lower hybrid wave was used successfully to drive toroidal plasma currents,[67] theory predicts improved efficiency if "fast" lower hybrid waves are used instead.[68] To launch such waves, a novel launcher was developed and manufactured with industrial help (figure 8). The antenna is composed of dielectric loaded waveguides (using the ceramic TiO_2, $\varepsilon = 80$) arrayed along the toroidal direction of the tokamak, and the relative phasing

[67] M. Porkolab et al., *Phys. Rev. Lett.* 53: 450 (1984).

[68] K. Teilhaber, A. Bers, *Nucl. Fusion* 20: 547 (1980).

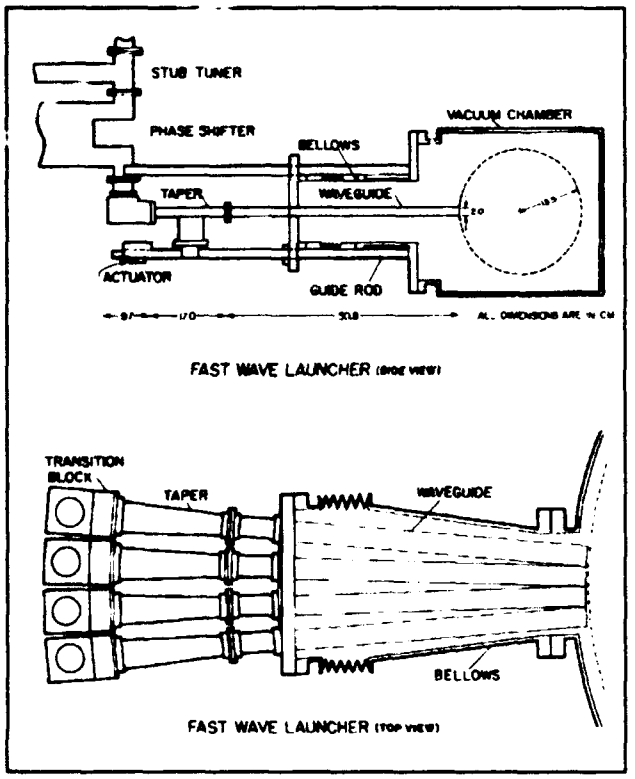

Figure 8. Top and side view of the fast wave antenna.

between adjacent waveguides can be adjusted to launch power at suitable angles (e.g., 90 degrees). Our eventual goal in this experiment is to couple sufficient high power from the antenna to drive current in the plasma and to study the physics of wave particle interaction. In addition, the fast waves will be launched in conjunction with 2.45 GHz slow lower hybrid waves to improve fast wave absorption.

In the past year, we have continued studies on antenna-plasma coupling at low power at 800 MHz. Previously, we had shown that the coupling between our antenna and the plasma is poor (~ 85-90 % reflectivity). This is in agreement with theoretical predictions[68] and code simulations,[69] and may be attributed to the high dielectric constant of the waveguides which leads to a high impedance mismatch at the waveguide-plasma interface. We had also found that to couple significant amounts of power, high edge plasma densities $\sim 2\text{-}3 \times 10^{12}\,\mathrm{cm}^{-3}$ are required. These conditions are difficult to achieve in normal Versator II operations, especially at low average densities ($\bar{n}_e \lesssim 5 \times 10^{12}\,\mathrm{cm}^{-3}$), where the current drive efficiency would be high.

We have decided to optimize coupling by retuning the antenna using a phase shifter and stub tuner assembly to match out the impedance mismatch at the interface. This method is used successfully to match ICRF antennas on tokamaks. To accomplish this, components of the antenna had to be redesigned to allow tuning over a range of VSWRs expected for antenna plasma coupling. In particular, the junction between the rectangular waveguide section and the (air) coax waveguide section was found to be highly reflective (VSWR ~ 3.5-4.0). A new design was employed to reduce this mismatch. Our measurements show improved performance (VSWR ~ 1.1) at the junction. We have also motorized the tuning assemblies (e.g., the tuning stubs and phase shifters) in order to provide remote control and allow for tuning adjustments between shots.

We have done a preliminary retuning at moderate edge conditions ($\sim 5 \times 10^{11}\,\mathrm{cm}^{-3}$), and this has resulted in a marked decrease in the total antenna reflectivity to values as low as 35-45% for 60 degree relative phasing. Our current efforts are aimed at optimizing good coupling at 90 degree phasing, which is the usual setting for current drive experiments. We will commence high power operations in 1991.

1.4.3 High Beta-Poloidal Experiments with Advanced Diagnostics

The purpose of this project is (1) to measure the distribution of fast electrons during rf current drive experiments, and (2) to study the equilibrium and stability of high beta poloidal plasmas in the Versator II tokamak. In these plasmas, the entire plasma current and most of the plasma pressure is supplied by highly energetic electrons created by launched lower-hybrid plasma waves.[70] We plan to map the spatial and velocity distributions of these fast current carrying electrons. With this information we can calculate realistic plasma current and pressure distributions. Along with other basic plasma parameters, we can then test theoretical predictions regarding the stability of these plasmas. Specifically, we would like to determine if these equilibria are in or near what is called the

[69] R. Pinsker, R. Duvall, C. Fortgang, P. Colestock, *Nucl. Fusion* 26: 7 (1986).

[70] S.C. Luckhardt et al., *Phys. Rev. Lett.*, 62: 1508 (1989).

second stability regime.[71] In addition, we wish to determine the possible presence of MHD instabilities, such as ballooning modes.

To accomplish this goal, we have developed an array of hard x-ray (10-500 kev) spectrometers as well as an array of magnetic pickup loops. With the x-ray detectors we look at plasma bremsstrahlung emission from the collision of the energetic electrons with the plasma ions. We can exploit the fact that bremsstrahlung emission becomes asymmetric with respect to the direction of the electron motion at high energies. This would tell us if an asymmetric electron velocity distribution has evolved during rf current drive experiments. We do this by looking at the x-ray emissions at various angles to the toroidal magnetic field. For the spatial distribution we can look at the emissions at different plasma radii (see figure 9). We can then unfold this data to obtain the distribution of the energetic electrons. We also have an array of magnetic pickup loops inside the tokamak vacuum chamber near the plasma to measure magnetic fluctuations. This gives us some information about the stability of the plasma by observing oscillations in the external magnetic field induced by the currents in the plasma.

In the past year, we have obtained x-ray profile data from emission perpendicular to the toroidal magnetic field as a function of the tokamak major radius. We first did this using a single movable detector, and, more recently (this past year), we used a newly completed array of detectors. The array can take time integrated x-ray energy spectra and energy integrated time dependent data simultaneously on all detectors. We have been using it to acquire data from high poloidal beta plasmas as well as rf plasma startup experiments. We have observed outward shifts in major radius of the x-ray emission profiles corresponding to high poloidal beta, but we also see a large emission of x-rays toward the inside of the plasma major radius.

We have also recently installed an array of ten toroidally spaced magnetic pickup loops for monitoring the fluctuations in the poloidal magnetic field. We also used this during high poloidal beta experiments. No coherent fluctuations have been observed during high beta poloidal equilibria, but some transient oscillations were seen in the phase between low and high beta poloidal.

In 1991, we plan to extend our database of perpendicular profile data of x-ray emissions and analyze the data to model current profiles. Finally, we are presently installing an array of x-ray detectors for observing emissions at various angles to the toroidal magnetic field. This array will obtain energy spectra for modeling the electron velocity distribution. In addition, this array will be movable to obtain a clearer picture of the spatial dependence of the distribution of fast electrons.

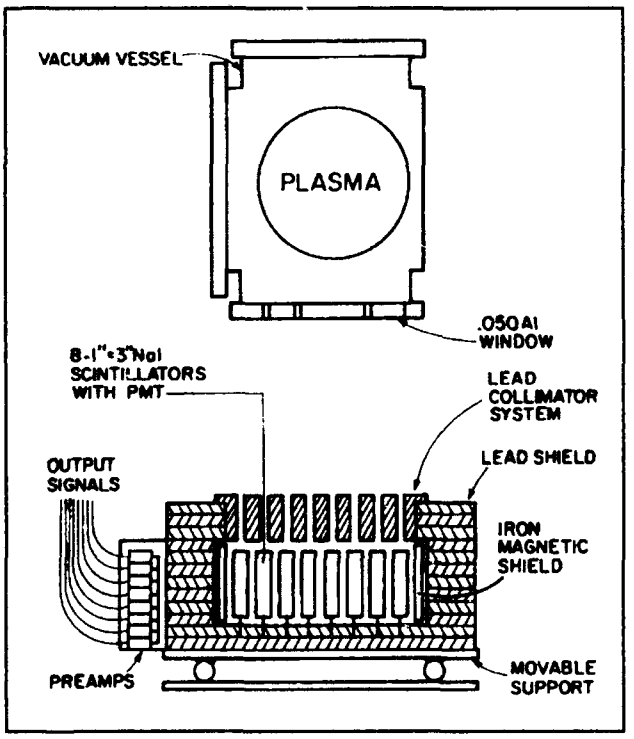

Figure 9. Drawing of the perpendicular viewing radial array of x-ray detectors.

[71] B. Coppi, A. Ferreira, J.W-K. Mark, and J.J. Ramos, *Nucl. Fusion* 19: 715 (1979).

Section 3 Electromagnetics

Chapter 1. Electromagnetic Wave Theory and Applications

Academic and Research Staff

Professor Jin Au Kong, Dr. Sami M. Ali, Dr. Robert T. Shin, Dr. Ying-Ching E. Yang, Ramon F. Herrara, Barbara A. Roman

Visiting Scientists and Research Affiliates

Qizheng Gu,[1] Dr. Tarek M. Habashy,[2] Dr. Arthur K. Jordan,[3] Dr. Kevin O'Neill,[4] Dr. Soon Y. Poh,[5] Dr. Tsuneki Yamasaki[6]

Graduate Students

Khurram K. Afridi, David V. Arnold, Robert G. Atkins, Judy Chen, Nelson C. Chu, Hsiu C. Han, Chih-Chien Hsu, Gregory T. Huang, Jean-Fu Kiang, Cheung-Wei Lam, Gloria W. Lau, Check-Fu Lee, Hongsing Lee Kevin Li, Victor Liau, Harold H. Lim, Son V. Nghiem, David M. Sheen, M. Ali Tassoudji, Michael J. Tsuk, Ann N. Tulintseff, Murat E. Veysoglu, Li-Fang Wang, Jiqing Xia, Herng A. Yueh

Undergraduate Students

Daniel J. Chung, Diana Wong

Technical and Support Staff

Margery E. Brothers, Kit-Wah F. Lai, Sarah L. Larson, Anh Lieu, Wei Ming-yu Lin

1.1 Electromagnetic Waves in Multilayer Media

Sponsors

Joint Services Electronics Program
Contract DAAL03-89-C-0001
National Science Foundation
Grant ECS 86-20029
Schlumberger-Doll Research
U.S. Army Research Office
Contract DAAL03 88-K-0057
U.S. Navy - Office of Naval Research
Contract N00014-90-J-1002

Project Staff

Professor Jin Au Kong, Dr. Sami M. Ali, Dr. Tarek M. Habashy, Robert G. Atkins, Qizheng Gu, Hsiu C. Han, Cheung-Wei Lam, Check-Fu Lee, Son V. Nghiem, David M. Sheen, Michael J. Tsuk, Ann N. Tulintseff, Jiqing Xia, Herng A. Yeuh

Cylindrical microstrip antennas find many applications in high-speed aircraft and spacecraft because of their conformity with the aerodynamical structure of such vehicles. Recently, there has been some progress in the theoretical study of this kind of antenna. The radiation from the wraparound cylindrical microstrip element was computed using a magnetic wall cavity model. More recently, the radiation from the wraparound, and the rectangular patches was computed by assuming an electric surface current distribution on the microstrip

---

[1] Shanghai Research Institute of Mechanical and Electrical Engineering, Shanghai, China.

[2] Schlumberger-Doll Research, Ridgefield, Connecticut.

[3] U.S. Navy, Office of Naval Research, Arlington, Virginia.

[4] Civil and Geotechnical Engineering, Department of the Army, Hanover, New Hampshire.

[5] Digital Equipment Corporation, Andover, Massachusetts.

[6] Department of Electrical Engineering, College of Science and Technology, Nihon University, Tokyo, Japan.

patch. The excitation problem of realizing such a current distribution was not addressed in these investigations. Furthermore, the input impedance for the cylindrical microstrip antennas was not reported.

We addressed the more realistic problem of the radiation from a cylindrical microstrip antenna excited by a probe.[7] Both the cylindrical-rectangular and the wraparound elements are discussed. The current distribution on the patch is rigorously formulated using a cylindrically stratified medium approach. A set of vector integral equations is derived which governs the current distribution on the patch. This set of equations is then solved using a moment method in which the patch current is expanded in terms of a complete set of basis functions that can take into account the edge singularity condition. The input impedance together with the radiation pattern are derived both exactly and in the small substrate thickness limit where a single mode approximation is employed.

Frequency domain analytical work with complicated microstrip circuits has generally been done using planar circuit concepts in which the substrate is assumed to be thin enough that propagation can be considered in two dimensions by surrounding the microstrip with magnetic walls. Fringing fields are accounted for by using either static or dynamic effective dimensions and permittivities. Limitations of these methods are that fringing, coupling, and radiation must all be handled empirically since they are not allowed for in the model. Also, the accuracy is questionable when the substrate becomes thick relative to the width of the microstrip. To fully account for these effects, it is necessary to use a full-wave solution.

Finite difference time domain methods have recently been used to effectively calculate the frequency dependent characteristics of microstrip discontinuities. Analysis of the fundamental discontinuities is of great importance since more complicated circuits can be realized by interconnecting microstrip lines with these discontinuities and using transmission line and network theory. Some circuits, however, such as patch antennas, may not be realized in this way. Additionally, if the discontinuities are too close to each other the use of network concepts will not be accurate due to the interaction of evanescent waves. To accurately analyze these types of structures it is necessary to simulate the entire structure in one computation. The finite difference time domain (FDTD) method shows great promise in its flexibility to handle a variety of circuit configurations. An additional benefit of the time domain analysis is that a broadband pulse may be used as the excitation and the frequency domain parameters may be calculated over the entire frequency range of interest by Fourier Transform of the transient results.

The frequency dependent scattering parameters are calculated for several printed microstrip circuits, specifically, a line-fed rectangular patch antenna, a low pass filter, and a rectangular branch line coupler.[8] These circuits represent resonant microstrip structures on an open substrate, hence, radiation effects can be significant, especially for the microstrip antenna. Calculated results are presented and compared with experimental measurements.

Finite difference techniques have been applied to analyze various electromagnetic problems in both frequency and time domains. Examples of these applications include scattering and radiation, microwave and millimeter wave circuits, and hyperthermia. Besides the widespread applications, the latest research efforts have been directed at achieving more accurate discretization schemes, improving absorbing boundary conditions for open region problems, and efficient implementations on supercomputers. We investigated three topics relevant to the finite difference technique: absorbing boundary conditions, spatial discretization, and time domain model of dispersive materials.

The absorbing boundary conditions on circular and elliptical boundaries are investigated.[9] The absorbing boundary conditions are crucial for open region problems such as scattering and radiation. The absorbing boundary conditions are used to simulate the unbounded space, and hence, provide

---

[7] T.M. Habashy, S.M. Ali, and J.A. Kong, "Input Impedance Parameters and Radiation Pattern of Cylinderical-Rectangular and Wraparound Microstrip Antennas," *IEEE Trans. Antennas Propag.* 38(5): 722-731 (1990).

[8] D.M. Sheen, S.M. Ali, M.D. Abouzahra, and J.A. Kong, "Application of the Three Dimensional Finite Difference Time-Domain Method to the Analysis of the Planar Microstrip Circuits," *IEEE Trans. Microwave Theory Tech.* 38(7): 849-857 (1990).

[9] C.F. Lee, R.T. Shin, and J.A. Kong, "Fine Difference Method for Electromagnetic Scattering Problems," In *Progress In Electromagnetics Research,* ed. J.A Kong (New York: Elsevier, 1990), Vol. 4, Ch. 11, pp. 373-442; C.F. Lee, R.T. Shin, J.A. Kong, and B.J. McCartin, "Absorbing Boundary Condions on Circular and Elliptic Boundaries," *J. Electromag. Waves Appl.* 4(10): 945-962 (1990).

finite computational domain for open region problems. The size of the computational domain is directly related to the absorbability of the absorbing boundary condition. The absorbing boundary condition is derived by factorizing the wave equation using pseudo-differential operator technique. The factorization scheme presented by Engquist and Majda is modified to derive absorbing boundary conditions for circular and elliptical boundaries. In the case of circular boundary, the modified factorization scheme yields results equivalent to that of Bayliss and Turkel. In the case of elliptical boundary, the absorbing boundary condition is derived and numerically demonstrated to be efficient in reducing the size of the computational domain for elongated scatterers.

FD-TD scheme on triangular grids is discussed. The discretization scheme is crucial in geometrical modeling, treating dielectric/magnetic materials, and efficient implementation. The discretization scheme is based on the combination of the finite difference and control region approximations. The flexibility of the triangular grid is utilized to provide accurate geometrical modeling. It is demonstrated that the FD-TD technique on triangular grid provides more accurate target modeling capability than the traditional FD-TD technique of the rectangular grid.

An efficient FD-TD algorithm for treating frequency dispersive material is presented. Accurate and efficient time domain model of dispersive materials is very important in time domain analysis. Accurate time domain results cannot be obtained unless the dispersive nature of the material is properly modeled. The traditional model of the dispersive characteristic is based on the time domain convolution integral which requires large memory and long computation time. A more recent model is based on the exponential approximation of the time domain response of the material. In this section, we model the dispersive characteristics using ordinary time differential equations and provide an efficient discretization scheme.

For microwave integrated circuit applications, the characteristics of interconnects have been investigated for propagation modes, time response, crosstalk, coupling, delay, etc. In these analyses, it is assumed that quasi-TEM modes are guided along the multiconductor transmission line. To perform the quasi-TEM analysis, the capacitance matrix for the multiconductor transmission line has to be obtained first. Both the spectral and the spatial domain methods have been proposed to calculate the capacitance matrix. In the spectral domain methods, two side walls are used to enclose the whole transmission line structure, and the thickness of the strip lines has not been considered. In using the spatial domain method, the structure has to be truncated to a finite extent to make the numerical implementation feasible. However, the infinite extent of the structure was incorporated, but only a two-layer medium was considered.

A quasi-TEM analysis of coupled lossy microstrip lines of finite strip thickness embedded in different layers of a lossy isotropic stratified medium is presented.[10] First, a spectral domain scalar Green's function in a lossy isotropic stratified medium is derived. Based on the scalar Green's function, a set of coupled integral equations is obtained for the charge distribution on the strip surfaces. The method of moments is then applied where pulse basis functions and a point-matching scheme is used to solve numerically the set of integral equations for the charge distribution, and hence the capacitance matrix. The duality between the electrostatic problem and the magnetostatic one is applied to calculate the inductance matrix. The conductance matrix is obtained by using the duality between the electrostatic problem and the current field problem. A perturbation method is used to calculate the resistance matrix. Finally, a transmission line analysis is derived to obtain the transfer matrix for the multiconductor line, which significantly reduces the effort in treating the load and the source conditions. Transient responses are obtained by using the Fourier transform. The results for two coupled lines are presented.

A full modal analysis is used to study the dispersion characteristics of microstrip lines periodically loaded with crossing strips in a stratified uniaxially anisotropic medium.[11] Dyadic Green's functions in the spectral domain for the multilayered medium in conjunction with the vector Fourier transform (VFT) are used to formulate a coupled set of vector integral equations for the current distribution on the signal line and the crossing strips. Galerkin's procedure is applied to derive the eigenvalue equation for the propagation constant. The effect of anisotropy for both open

---

[10] J.F. Kiang, S.M. Ali, and J.A. Kong, "Modelling of Lossy Microstrip Lines with Fine Thickness," *Progress In Electromagnetics Research,* ed. J.A. Kong (New York: Elsevier, 1990), Vol. 4, Ch. 3, pp. 85-117.

[11] C.W. Lam, S.M. Ali, and J.A. Kong, "The Propagation Characteristics of Signal Lines with Crossing Strips in Multilayered Anisotropic Media," *J. Electromag. Waves Appl.* 4(10): 1005-1021 (1990).

and shielded structures on the stopband properties is investigated.

The excitation of the earth-ionosphere waveguide by point dipoles at satellite heights was studied by Einaudi and Wait. In their formulation, the ionosphere was crudely modeled as a single D-layer, moreover the geomagnetic field was assumed to be vertical, thus rendering the validity of the model to polar regions. Then, a more general analysis was performed where the geomagnetic field was assumed to be arbitrarily-oriented and the earth to be curved along the direction of propagation. However, the ionosphere was assumed to be a semi-infinite homogeneous medium and the results presented in these papers were limited to a frequency of 75 Hz. Furthermore, in these papers an indirect scheme was employed to formulate the response of point dipole sources: the case of line quadrupole sources was first considered, and then at the end of the development, the results were converted to apply to a point source.

We presented a rigorous approach to the problem of radiation of electric or magnetic sources in a stratified arbitrary magnetized linear plasma.[12] The fields are obtained in terms of dyadic Green's functions of electric or magnetic type represented in the spectral domain. First, the dyadic Green's function for an unbounded arbitrary magnetized linear plasma is derived. The formulation is considerably simplified by using the kDB system of coordinates in conjunction with the Fourier transform. This leads to compact and explicit expressions for the dyadic Green's functions. The distributional singular behavior of the various dyadic Green's functions in the source region is investigated and taken into account by extracting the delta function singularities. Finally, the dyadic Green's function in any arbitrary layer is obtained in terms of appropriately defined global upward and downward reflection and transmission matrices. The field expressions for an arbitrary distribution of sources or linear antennas can be obtained by performing a convolution integral over the volume of the antenna weighted by the current density on the antenna.

The study of electromagnetic radiation from sources in the ionospheric plasmas has received much attention in the research on the satellite-borne antennas. For many years, special attention has been given to the radiation in the very low frequency (VLF) band due to its applications in the down-link communication systems. The far field pattern of a VLF phased array located in a magnetized plasma is studied.[13] The general principles of antenna array design in the anisotropic media are discussed. Special attention is drawn to the two-dimension planar array allowed to rotate with respect to an axis perpendicular to the plane of the array, and the main beam of which is kept in the same direction as that of the geomagnetic field line during the rotation. The applicability of the principle of pattern multiplication as well as the effects of different types of radiating elements for different k-surface geometries are investigated.

An inversion algorithm based on a recently developed inversion method referred to as the Renormalized Source-Type Integral Equation approach is presented.[14] The objective of this method is to overcome some of the limitations and difficulties of the iterative Born technique. It recasts the inversion, which is nonlinear in nature, in terms of the solution of a set of linear equations; however, the final inversion equation is still nonlinear. The derived inversion equation is an exact equation which sums up the iterative Neuman (or Born) series in a closed form and; thus, is a valid representation even in the case where the Born series diverges; hence, the name Renormalized Source-Type Integral Equation Approach.

There has been considerable interest in the theoretical study of scattering from chiral media. Chiral medium characterized by biisotropic constitutive relation is a special case of the bianisotropic medium whose electromagnetic properties have been extensively studied by Kong. Periodic gratings have been the object of extensive research through the years because of its many applications in distributed feedback laser, integrated optics, acousto-optics, quantum electronics, and holography. For the analysis of wave diffraction by periodic surface grating, methods including the method of moments and extended boundary condition method are rigorous and in general compu-

---

[12] T.M. Habashy, S.M. Ali, J.A. Kong, and M.D. Grossi, "Dyadic Green's Functions in a Planar Stratified, Arbrarily Magnetized Linear Plasma," *Radio Sci.*, forthcoming.

[13] C.H. Han, J.A. Kong, T.M. Habashy, and M.D. Grossi, "Principles of VLF Antenna Array Design in Magnetized Plasmas," URSI National Radio Science Meeting, Boulder, Colorado, January 3-5, 1990.

[14] T.M. Habashy, M. Moldoveanu, and J.A. Kong, "Inversion of Permtivy and Conductivy Profiles Employing Transverse-Magnetic Polarized Monochromatic Data," SPIE 1990 International Symposium on Optical and Optoelectronic Applied Science and Engineering, San Diego, California, July 8-13, 1990.

tationally efficient. For the analysis of periodic slanted dielectric gratings, a coupled-wave method has been developed.

The coupled-wave theory is generalized to analyze the diffraction of waves by chiral gratings for arbitrary angle of incidence and polarizations.[15] Numerical results are illustrated for the Stokes parameters of diffracted Floquet modes versus the thickness of chiral gratings with various chiralities. Both horizontal and vertical incidences are considered for illustration. The diffracted waves from chiral gratings are in general elliptically polarized; and at some particular instances, it is possible for chiral gratings to convert a linearly polarized incident field into two nearly circularly polarized Floquet modes propagating in different directions.

The integral equation method has been used to solve for the dispersion relation of the rectangular dielectric waveguide.[16] This method incorporates the continuous spectrum, and hence the radiation loss is taken into account. However, no results concerning practical single and coupled dielectric strip waveguides were presented; and the leakage phenomenon was not investigated. We derived an integral equation formulation using the dyadic Green's function to solve for the dispersion relation of single and coupled dielectric strip waveguides. A method to predict the leakage is presented, and the leakage properties are investigated. The integral equation formulation for an arbitrary number of inhomogeneous dielectric strips is derived and Galerkin's method is used to obtain the matrix eigenvalue equations. Numerical results and discussions are presented.

A microstrip antenna consisting of two circular microstrip disks in a stacked configuration driven by coaxial probe excitation is considered.[50] The two different stacked configurations are investigated. A rigorous analysis of the two stacked circular disks in a layered medium is performed using a dyadic Green's function formulation. Using the vector Hankel transform, the mixed boundary value problem is reduced to a set of coupled vector integral equations and solved by employing Galerkin's method in the spectral domain. The current distribution on each disk is expanded in terms of two sets of basis functions. The first set of basis functions used are the complete set of transverse magnetic (TM) and transverse electric (TE) modes of a cylindrical resonant cavity with magnetic side walls. The second set of basis functions used employ Chebyshev polynomials and enforce the current edge condition. An additional term in the current expansion is taken to account for the singular nature of the current on the disk in the vicinity of the probe and to ensure continuity of current at the junction. This term, the "attachment mode," is taken to be the disk current of magnetic cavity under a uniform cylindrical current excitation. It is shown here explicitly that continuity of the current at the probe/disk junction must be enforced to rigorously include the probe self-impedance. The convergence of the results is investigated and ensured by using a proper number of basis functions. The input impedance of the stacked microstrip antenna is calculated for different configurations of substrate parameters and disk radii. Disk current distributions and radiation patterns are also presented. Finally, the results are compared with experimental data and shown to be in good agreement.

With the ever increasing speed and density of modern integrated circuits, the need for electromagnetic wave analysis of phenomena such as the propagation of transient signals, especially the distortion of signal pulses, becomes crucial. One of the most important causes of pulse distortion is the frequency dependence of conductor loss, which is caused by the "skin effect," and which can be incorporated into the circuit models for transmission lines as frequency-dependent resistance and inductance per unit length. Efficient and accurate algorithms for calculating these parameters are increasingly important.

A new hybrid cross-section finite element/coupled integral equation method is presented,[17] which is both efficient and flexible in regards to the kinds of configurations which can be handled. An interpolation between the results of these two methods gives very good results over the entire frequency range, even when few basis functions are used. For low frequencies, we use a cross-section finite element method with triangular basis functions. For high frequencies, a coupled surface integral equation technique is used. For the intermediate frequency range, where the conductors are on the order of skin depth, we found it very

---

[15] S.H. Yueh and J.A. Kong, "Analysis of Diffraction from Chiral Gratings," *J. Electromag. Waves Appl.*, forthcoming.

[16] J.F. Kiang, S.M. Ali, and J.A. Kong, "Integral Equation Solution to the Guidance and Leakage Properties of Coupled Dielectric Strip Waveguides," *IEEE Trans. Microwave Theory Tech.* 38(2): 193-203 (1990).

[17] M.J. Tsuk and J.A. Kong, "A Hybrid Method for the Calculation of the Resistance and Inductance of Transmission Lines with Arbrary Cross-Sections," submitted to *IEEE Trans. Microwave Theory Tech.*

efficient to interpolate between the results of the cross-section and surface methods.

1.2 Remote Sensing of Earth Terrain

Sponsor

National Aeronautics and Space Administration
Grant NAGW-1617

Project Staff

Professor Jin Au Kong, David V. Arnold, Robert G. Atkins, Nelson C. Chu, Harold H. Lim, Son V. Nghiem, Dr. Robert T. Shin, Herng A. Yueh

Accurate calibration of polarimetric radar systems is essential for the polarimetric remote sensing of earth terrain. A polarimetric calibration algorithm using three arbitrary in-scene reflectors is developed.[18] The transmitting and receiving ports of the polarimetric radar are modeled by two unknown polarization transfer matrices. These unknown matrices are determined using the measured scattering matrices from the calibration targets. A Polarization-Basis Transformation technique is introduced to convert the scattering matrices of the calibration targets into one of the six sets of targets with simpler scattering matrices. Then, the solution to the original problem can be expressed in terms of the solution obtained using the simpler scattering matrices. The uniqueness of polarimetric calibration using three targets is addressed for all possible combinations of calibration targets. The effect of misalignment of the calibration targets and the sensitivity of the polarimetric calibration algorithm to the noise are illustrated by investigating several sets of calibration targets in detail.

Classification of earth terrain within an image is one of the many important applications of polarimetric data. A systematic classification procedure will place the classification process on a more quantitative level and reduce the amount of photo-interpretation necessary. Both the supervised and unsupervised classification techniques are applied to San Francisco Bay and Traverse City Synthetic Aperture Radar (SAR) images, supplied by the Jet Propulsion Laboratory.[19] For supervised classification processing, the Bayes technique is used to classify fully polarimetric and normalized polarimetric SAR data. Simpler polarimetric discriminates, such as the absolute and normalized magnitude response of the individual receiver channel returns, in addition to the phase difference between the receiver channels, are also considered. An unsupervised technique, based on comparing general properties of the Stokes parameters of the scattered wave to that of simple scattering models, is also discussed . It is shown that supervised classification yields the best overall performance when accurate classifier training data are used, whereas unsupervised classification is applicable when training data are not available.

Classification or identification of radar targets from measurements of their radar signatures continues to be an area of considerable interest and active research. In the past, a variety of classification algorithms have been proposed, and these techniques have yielded varied levels of effectiveness in differing applications. One novel group of classification techniques which overcome the limitations of the conventional ones, and which has recently received considerable attention, is a set of methods based on the use of neural networks. The application of neural networks to the problem of target classification from high range resolution profiles is considered.[20] The effectiveness of the neural network classifier is demonstrated using synthetically generated range profiles of two groups of geometries, produced using RCS prediction techniques. For both groups, the neural network approach is compared with the conventional techniques of profile matching, and Euclidean and Mahalanobis distance classifiers. In addition, the performance of both conventional and neural network classifiers in the presence of additive noise and alignment uncertainty is explored. Finally, a comparison of the computational and storage requirements of each approach is presented.

---

[18] S.H. Yueh, J.A. Kong, and R.T. Shin, "Calibration of Polarimetric Radars using In-Scene Reflectors," In *Progress In Electromagnetic Research,* ed. J.A. Kong (New York: Elsevier, 1990), Vol. 3, Ch. 9, pp. 451-510; S.H. Yueh, J.A. Kong, and R.T. Shin, "Calibration of Polarimetric Radars Using In-Scene Reflectors," Tenth International Geoscience and Remote Sensing Symposium (IGARSS'90), College Park, Maryland, May 20-24, 1990.

[19] J.A. Kong, S.H. Yueh, H.H. Lim, R.T. Shin, and J.J. van Zyl, "Classification and Maximum Contrast of Earth Terrain Using Polarimetric Synthetic Aperture Radar Images," In *Progress In Electromagnetics Research,* ed. J.A. Kong (New York: Elsevier, 1990), Vol. 3, Ch. 6, pp. 327-370.

[20] R.G. Atkins, R.T. Shin, and J.A. Kong. "A Neural Net Method for High Range Resolution Target Classification," In *Progress In Electromagnetics Research,* ed. J.A. Kong. (New York: Elsevier, 1990), Vol. 4, Ch. 7, pp. 255-292.

Besides classifying earth terrain into different classes, there is also considerable interest in determining the optimal polarizations that maximize contrast between two scattering classes in polarimetric radar images. Contrast enhancement is a processing technique which modifies the input data structure so that either the human observer, computer, or other hardware devices can extract certain information from the processed data more readily after the change. We employed a Lagrange multiplier method which determines the transmitting and receiving polarization state which produces maximum contrast, or separation in the average intensity, between the two scattering classes.[21] To realize this objective, the contrast ratio is maximized, i.e., the maximum contrast ratio is computed in order to obtain the optimal linear weighting vector or optimal polarimetric matched filter. Processing polarimetric synthetic aperture radar (SAR) images with this filter performs a polarization synthesis on the data which yields maximum contrast between classes.

Polarimetric terrain backscatter data observed with satellite and airborne synthetic aperture radars (SAR) have demonstrated potential applications in geologic mapping and terrain cover classification. In previous publications on this subject, Gaussian statistics have been frequently assumed for the radar return signals to build the Bayes terrain classifier. However, abundant experimental evidence shows that terrain radar clutter is non-Gaussian, i.e., non-Rayleigh in amplitude distribution. An n-dimensional anisotropic random walk model is used to derive the zero-mean multivariate K-distribution for polarimetric data.[22] Anisotropy refers to the fact that the polarimetric covariance matrix is not proportional to an identity matrix. In order to apply the K-distribution to the normalized polarimetric classifier problem, the probability density function (PDF) of the normalized K-distributed vector is derived and discussed. Finally, four sets of experimental data, obtained from MIT Lincoln Laboratory, the Jet Propulsion Laboratory (JPL), and the German Aerospace Research Establishment (DLR) of the Federal Republic of Germany, are compared with the K-distribution to lend support to the above model. As compared with C-, L- and P-band polarimetric SAR image simultaneously measured by the Jet Propulsion Laboratory (JPL) on Mt. Shasta, it is found that α appears to decrease from C- to P-band for both the forest and burned areas.

In remote sensing, the encountered geophysical media such as agricultural canopy, forest, snow, or ice are inhomogeneous and contain scatterers in a random manner. Furthermore, weather conditions such as fog, mist, or snow cover can interfere with the electromagnetic observation of the remotely sensed media. In the modeling of such media accounting for the weather effects, a multilayer random medium model has been developed.[23] The scattering effects of the random media are described by three-dimensional correlation functions with variances and correlation lengths corresponding to the fluctuation strengths and the physical geometry of the inhomogeneities, respectively. With proper consideration of the dyadic Green's function and its singularities, the strong fluctuation theory is used to calculate the effective permittivities which account for the modification of the wave speed and attenuation in the presence of the scatterers. The distorted Born approximation is then applied to obtain the correlations of the scattered fields. From the correlation of the scattered field, calculated are the scattering coefficients for polarimetric radar observation or brightness temperature in passive radiometer applications.

The layered random medium model is used to investigate the fully polarimetric scattering of elec-

---

[21] J.A. Kong, S.H. Yueh, H.H. Lim, R.T. Shin, and J.J. van Zyl, "Classification and Maximum Contrast of Earth Terrain Using Polarimetric Synthetic Aperture Radar Images," In *Progress In Electromagnetics Research,* ed. J.A. Kong (New York: Elsevier, 1990), Vol. 3, Ch. 6, pp. 327-370.

[22] S.H. Yueh, J.A. Kong, R.T. Shin, and H.A. Zebker, "Statistical Modelling for Polarimetric Remote Sensing of Earth Terrain," Tenth International Geoscience and Remote Sensing Symposium (IGARSS'90), College Park, Maryland, May 20-24, 1990; S.H. Yueh, J.A. Kong, J.K. Jao, R.T. Shin, H.A. Zebker, T. Le Toan, and H. Öttl, "K-distribution and Polarimetric Terrain Radar Clutter," In *Progress In Electromagnetics Research,* ed. J.A. Kong. (New York: Elsevier, 1990), Vol. 3, Ch. 4, pp. 237-275; H.A. Yueh, J.A. Kong, R.T. Shin, H.A. Zebker, and T. Le Toan, "K-distribution and Multi-Frequency Polarimetric Terrain Radar Clutter," *J. Electromag. Waves Appl.,* forthcoming.

[23] S.V. Nghiem, J.A. Kong, and T. Le Toan, "Electromagnetic Wave Modeling for Remote Sensing," International Conference on Directions in Electromagnetic Wave Modeling, New York, October 22-24, 1990; S.V. Nghiem, M. Borgeaud, J.A. Kong, and R.T. Shin, "Polarimetric Remote Sensing of Geophysical Media with Layer Random Medium Model," In *Progress In Electromagnetics Research,* ed. J.A. Kong (New York: Elsevier, 1990), Vol. 3, Ch. 1, pp. 1-73.

tromagnetic waves from vegetation.[24] The vegetation canopy is modeled as an anisotropic random medium containing nonspherical scatterers with preferred alignment. The underlying medium is considered as a homogeneous half space. For a vegetation canopy with low attenuation, the boundary between the vegetation and the underlying medium can give rise to significant coherent effects. The model is used to interpret the measured data for vegetation field such as rice, wheat, or soybean over water or soil. The temporal variation of σ_{hh} and σ_{vv} of the X-band SAR data of rice fields shows a wide range of responses at different growth stages. From the data of wheat, recognizable changes of the angular and polarization behaviour of the backscattering coefficients are observed at X-band before and after the heading of the wheat. For soybean, the data collected during the growing season show similar results for both *h*- and *v*-polarizations. The observed effects on backscattering coefficients of the vegetation structural and moisture conditions at different growth stages can be explained by analyzing the different interaction processes pointed out by the model.

Strong permittivity fluctuation theory is used to solve the problem of scattering from a medium composed of completely randomly oriented scatterers under the low frequency limit.[25] Gaussian statistics are not assumed for the renormalized scattering sources. The effective permittivity is obtained under the low frequency limit and the result is shown to be isotropic due to no preferred direction in the orientation of the scatterers. Numerical results of the effective permittivity are illustrated for oblate and prolate spheroidal scatterers and compared with the results for spherical scatterers. The results derived are shown to be consistent with the discrete scatterer theory. The effective permittivity of random medium embedded with nonspherical scatterers shows a higher imaginary part than that of a spherical scatterer case with equal correlation volume. Under the distorted Born approximation, the polarimetric covariance matrix for the backscattered electric field is calculated for the half-space randomly oriented scatterers. The nonspherical geometry of the scatterers shows significant effects on the cross-polarized backscattering returns σ_{hv} and the correlation coefficient ρ between HH and VV returns. The polarimetric backscattering coefficients can provide useful information in distinguishing the geometry of scatterers.

As an electromagnetic wave propagates through a random scattering medium, such as a forest, its energy is attenuated and random phase fluctuations are induced. The magnitude of the random phase fluctuations induced is important in estimating how well a Synthetic Aperture Radar (SAR) can image objects within the scattering medium. The two-layer random medium model, consisting of a scattering layer between free space and ground, is used to calculate the variance of the phase fluctuations induced between a transmitter located above the random medium and a receiver located below the random medium.[26] The effective permittivity of the random medium is first calculated using the strong fluctuation theory, which accounts for large permittivity fluctuations of the scatterers. The distorted Born approximation is used to calculate the first-order scattered field. A perturbation series for the phase of the received field is then introduced and the variance of the phase fluctuations is solved to first order in the permittivity fluctuations. The variance of the phase fluctuations is also calculated assuming that the transmitter and receiver are in the paraxial limit of the random medium, which allows an analytic solution to be obtained. The effects studied are the dependence of the variance of the phase fluctuations on receiver location in lossy and lossless regions, medium thickness, correlation length and fractional volume of scatterers, depolarization of the incident wave, ground layer permittivity, angle of incidence, and polarization.

In the interpretation of active and passive microwave remote sensing data from earth terrain, the random medium model has been shown to be quite successful. In the random medium model, a correlation function is used to describe the random permittivity fluctuations with associated mean and variance. We calculated the correlation function for a random collection of discrete scatterers imbedded in a background medium of constant permittivity. Correlation functions are first calculated for the simple cases of the uniform distribution of scatterers and the uniform distribution with

[24] S.V. Nghiem, J.A. Kong, and T. Le Toan, "Application of Layered Random Medium Model to Polarimetric Remote Sensing of Vegetation," URSI International Commission F meeting, Hyannis, Massachusetts, May 16-18, 1990.

[25] H.A. Yueh, R.T. Shin, and J.A. Kong, "Scattering from Randomly Oriented Scatterers with Strong Permittivity Fluctuations," *J. Electromag. Waves Appl. 4(10): 983-1004 (1990).*

[26] N.C. Chu, J.A. Kong, H.A. Yueh, S.V. Nghiem, J.G. Fleischman, S. Ayasli, and R.T. Shin, "Variance of Phase Fluctuations of Waves Propagation through a Random Medium," *J. Electromag. Waves Appl.*, forthcoming.

the hole correction. Then, the correlation function for a more realistic case is obtained using the Percus-Yevik pair distribution function. Once the correlation function is obtained, the strong fluctuation theory is used to calculate the effective permittivities. Then, the distorted Born approximation is used to calculate the backscattering coefficients from a halfspace configuration. The theoretical results are illustrated by comparing the effective permittivities and the backscattering coefficients with the results obtained with the discrete scatterer theory.[27]

The concept of polarimetry in active remote sensing is extended to passive remote sensing. The potential use of the third and fourth Stokes parameters U and V, which play an important role in polarimetric active remote sensing, is demonstrated for passive remote sensing. It is shown that, by the use of the reciprocity principle, the polarimetric parameters of passive remote sensing can be obtained through the solution of the associated direct scattering problem. These ideas are applied to study polarimetric passive remote sensing of periodic surfaces.[28] The solution of the direct scattering problem is obtained by an integral equation formulation which involves evaluation of periodic Green's functions and normal derivative of those on the surface. The study has shown that the brightness temperature of the Stokes parameter *U* can be significant in passive remote sensing. Values as high as 50 K are observed for certain configurations.

Tower-based measurements of sea-state bias were made using a 14 GHz scatterometer (Ku-Bands) and a collocated IR wave gauge during SAXON-CLT. The measured bias was found to be an increasing fraction of the significant wave height with increasing wind speed. The measurements are consistent with a two-scale model of the EM scattering from the ocean surface. The implications of the measurements for the improvement of sea-state bias algorithms are discussed. Results of a more recent series of tower-based measurements in the Gulf of Mexico at both Ku and C bands are presented.[29]

1.2.1 Remote Sensing of Sea Ice

Sponsor

U.S. Navy - Office of Naval Research
Grant N00014-89-J-1107

Project Staff

Professor Jin Au Kong, Dr. Robert T. Shin, Son V. Nghiem

In remote sensing, the encountered geophysical media such as agricultural canopy, forest, snow, or ice are inhomogeneous and contain scatterers in a random manner. Furthermore, weather conditions such as fog, mist, or snow cover can intervene the electromagnetic observation of the remotely sensed media. In the modeling of such media accounting for the weather effects, a multi-layer random medium model has been developed.[30] The scattering effects of the random media are described by three-dimensional correlation functions with variances and correlation lengths corresponding to the fluctuation strengths and the physical geometry of the inhomogeneities, respectively. With proper consideration of the dyadic Green's function and its singularities, the strong fluctuation theory is used to calculate the effective permittivities which account for the modification of the wave speed and attenuation in the presence of the scatterers. The distorted Born approximation is then applied to obtain the correlations of the scattered fields. From the correlation of the scattered field, calculated are the complete set of scattering coefficients for polarimetric radar observation or

---

[27] H.H. Lim, S.H. Yueh, R.T. Shin, and J.A. Kong, "Correlation Function for a Random Collection of Discrete Scatterers," Tenth International Geoscience and Remote Sensing Symposium (IGARSS'90), College Park, Maryland, May 20-24, 1990.

[28] M.E. Veysoglu, H.A. Yueh, R.T. Shin and J.A. Kong, "Polarimetric Passive Remote Sensing of Periodic Surfaces," *J. Electromag. Waves Appl.* 5(3): 267-280 (1991).

[29] W.K. Melville, J.A. Kong, R.H. Stewart, W.C. Keller, D. Arnold, A.T. Jessup, and E. Lamarre, "Measurements of Sea-State Bias at Ku and C Bands," URSI International Commission F meeting, Hyannis, Massachusetts, May 16-18, 1990; W.K. Melville, D.V. Arnold, J.A. Kong, A.T. Jessup, E. Lamarre, R.H. Stewart, and W.C. Keller, "Measurements of EM Bias at Ku and C Bands," OCEANS'90, Washington, D.C., September 24-26, 1990.

[30] S.V. Nghiem, J.A. Kong, and T. Le Toan, "Electromagnetic Wave Modeling for Remote Sensing," International Conference on Directions in Electromagnetic Wave Modeling, New York, October 22-24, 1990; S.V. Nghiem, M. Borgeaud, J.A. Kong, and R.T. Shin, "Polarimetric Remote Sensing of Geophysical Media with Layer Random Medium Model," In *Progress In Electromagnetics Research,* ed. J.A. Kong (New York: Elsevier, 1990), Vol. 3, Ch. 1, pp. 1-73.

brightness temperature in passive radiometer applications.

Fully polarimetric scattering of electromagnetic waves from snow and sea ice is studied with a layered random medium model and applied to interpret experimental data obtained under laboratory controlled conditions.[31] There is considerable interest in identifying and classifying ice types by using polarimetric scattering data. Due to differences in structure and composition, ice of different types such as frazil, first-year, or multiyear can have different polarimetric scattering behaviors. To study the polarimetric response of sea ice, the layered random medium model is used.[32] In this model, the sea-ice layer is described as an anisotropic random medium composed of a host medium with randomly embedded inhomogeneities, such as elongated brine inclusions, which can have preferred orientation direction. The underlying sea-water layer is considered as a homogenous half space. The scattering effect of the inhomogeneities in the sea ice are characterized by three-dimensional correlation function with variance and correlation lengths respectively corresponding to the fluctuation strength and the physical geometry of the scatterers. The effective permittivity of the sea ice is calculated with the strong fluctuation theory and the polarimetric backscattering coefficients are obtained under the distorted Born approximation. The distinction on the characteristics of different ice types are investigated with the conventional backscattering coefficients and the complex correlation coefficient ρ between σ_{hh} and σ_{vv}. The correlation coefficient ρ contains additional information on the sea-ice structure and can be useful in the identification of the ice types. By relating to the covariance matrices, the model is used to explain the polarization signatures of different ice types. In the case of snow-covered sea ice, the snow layer is modeled as an isotropic random medium and the obtained solution accounts for the effect of snow cover on polarimetric scattering properties of sea ice.

To explain polarimetric scattering from the experimentally simulated bare sea ice, the two-layer configuration is used to model sea-ice layer over sea water. The distinction on the characteristics of the media are investigated with the conventional backscattering coefficients and the complex correlation coefficient ρ between σ_{hh} and σ_{vv}. For ice-type identification, the measured covariance matrices are studied with the model to infer the physical characteristics pertaining to the different ice types. The three-layer configuration is then used to investigate the effects on fully polarimetric radar returns from snow covered sea ice.

Accurate calibration of polarimetric radar systems is essential for the polarimetric remote sensing of earth terrain. A polarimetric calibration algorithm using three arbitrary in-scene reflectors is developed.[33] The transmitting and receiving ports of the polarimetric radar are modeled by two unknown polarization transfer matrices. These unknown matrices are determined using the measured scattering matrices from the calibration targets. A Polarization-Basis Transformation technique is introduced to convert the scattering matrices of the calibration targets into one of the six sets of targets with simpler scattering matrices. Then, the solution to the original problem can be expressed in terms of the solution obtained using the simpler scattering matrices. The uniqueness of polarimetric calibration using three targets is addressed for all possible combinations of calibration targets. The effect of misalignment of the calibration targets and the sensitivity of the polarimetric calibration algorithm to the noise are illustrated by investigating several sets of calibration targets in detail.

Strong permittivity fluctuation theory is used to solve the problem of scattering from a medium composed of completely randomly oriented scat-

[31] S.V. Nghiem, J.A. Kong, R.T. Shin, H.A. Yueh, and R. Onstott, "Theoretical Models and Experimental Measurements for Polarimetric Remote Sensing of Snow and Sea Ice," URSI International Commission F meeting, Hyannis, Massachusetts, May 16-18, 1990.

[32] S.V. Nghiem, J.A. Kong, and R.T. Shin, "Study of Polarimetric Response of Sea Ice with Layered Random Medium Model," Tenth International Geoscience & Remote Sensing Symposium (IGARSS'90), College Park, Maryland, May 20-24, 1990.

[33] S.H. Yueh, J.A. Kong, and R.T. Shin, "Calibration of Polarimetric Radars using In-Scene Reflectors," In *Progress In Electromagnetic Research*, ed. J.A. Kong (New York: Elsevier, 1990), Vol. 3, Ch. 9, pp. 451-510; S.H. Yueh, J.A. Kong, and R.T. Shin, "Calibration of Polarimetric Radars Using In-Scene Reflectors," Tenth International Geoscience and Remote Sensing Symposium (IGARSS'90), College Park, Maryland, May 20-24, 1990.

terers under the low frequency limit.[34] Gaussian statistics is not assumed for the renormalized scattering sources. The effective permittivity is obtained under the low frequency limit and the result is shown to be isotropic due to no preferred direction in the orientation of the scatterers. Numerical results of the effective permittivity are illustrated for oblate and prolate spheroidal scatterers and compared with the results for spherical scatterers. The results derived are shown to be consistent with the discrete scatterer theory. The effective permittivity of random medium embedded with nonspherical scatterers shows a higher imaginary part than that of spherical scatterer case with equal correlation volume. Under the distorted Born approximation, the polarimetric covariance matrix for the backscattered electric field is calculated for the half-space randomly oriented scatterers. The nonspherical geometry of the scatterers shows significant effects on the cross-polarized backscattering returns σ_{hv} and the correlation coefficient ρ between HH and VV returns. The polarimetric backscattering coefficients can provide useful information in distinguishing the geometry of scatterers.

In the interpretation of active and passive microwave remote sensing data from earth terrain, the random medium model has been shown to be quite successful. In the random medium model, a correlation function is used to describe the random permittivity fluctuations with associated mean and variance. In the past, the correlation functions used were either assumed to be of certain form or calculated from cross sectional pictures of scattering media. We calculated the correlation function for a random collection of discrete scatterers imbedded in a background medium of constant permittivity. Correlation functions are first calculated for the simple cases of the uniform distribution of scatterers and the uniform distribution with the hole correction. Then, the correlation function for a more realistic case is obtained using the Percus-Yevik pair distribution function. Once the correlation function is obtained, the strong fluctuation theory is used to calculate the effective permittivities. Then, the distorted Born approximation is used to calculate the backscattering coefficients from a halfspace configuration. The theoretical results are illustrated by comparing the effective permittivities and the backscattering coefficients with the results obtained with the discrete scatterer theory.[35]

1.3 SAR Image Interpretation and Simulation

Sponsors

National Aeronautics and Space Administration
Grant NAGW-1272 and Agreement 958461
U.S. Army - Corps of Engineers
Contract DACA39-87-K-0022

Project Staff

Professor Jin Au Kong, Dr. Robert T. Shin, Dr. Ying-Ching E. Yang, Hsiu C. Han, M. Ali Tassoudji, Herng A. Yeuh

Classification or identification of radar targets from measurements of their radar signatures continues to be an area of considerable interest and active research. In the past, a variety of classification algorithms have been proposed, and these techniques have yielded varied levels of effectiveness in differing applications. One novel group of classification techniques which overcome the limitations of the conventional ones, and which has recently received considerable attention, is a set of methods based on the use of neural networks. As classifiers, neural networks have shown greater flexibility than conventional algorithms, adapting themselves more easily to distributions possessing a high degree of complexity, and have found application in diverse problems such as speech recognition and multisensor fusion. Presented a set of sample feature vectors during the training process, the neural network tries to selectively and automatically choose those characteristics of the feature vector which lead to the greatest separability between classes. The application of neural networks to the problem of target classification from high range resolution profiles is considered.[36] The effectiveness of the neural network classifier is demonstrated using synthetically generated range profiles of two groups of geometries,

---

[34] H.A. Yueh, R.T. Shin, and J.A. Kong, "Scattering from Randomly Oriented Scatterers with Strong Permittivity Fluctuations," *J. Electromag. Waves Appl. 4(10): 983-1004 (1990).*

[35] H.H. Lim, S.H. Yueh, R.T. Shin, and J.A. Kong, "Correlation Function for a Random Collection of Discrete Scatterers," Tenth International Geoscience and Remote Sensing Symposium (IGARSS'90), College Park, Maryland, May 20-24, 1990.

[36] Atkins, R.G., R.T. Shin, and J.A. Kong. "A Neural Net Method for High Range Resolution Target Classification," In *Progress In Electromagnetics Research*, ed. J.A. Kong. (New York: Elsevier, 1990), Vol. 4, Ch. 7, pp. 255-292.

produced using RCS prediction techniques. For both groups, the neural network approach is compared with the conventional techniques of profile matching, and Euclidean and Mahalanobis distance classifiers. In addition, the performance of both conventional and neural network classifiers in the presence of additive noise and alignment uncertainty is explored. Finally, a comparison of the computational and storage requirements of each approach is presented.

Besides classifying earth terrain into different classes, there is also considerable interest in determining the optimal polarizations that maximize contrast between two scattering classes in polarimetric radar images. Contrast enhancement is a processing technique which modifies the input data structure so that either the human observer, computer, or other hardware devices can extract certain information from the processed data more readily after the change. The polarimetric properties of the radar returns are utilized to enhance the contrast between two scattering classes. It is assumed a priori that complete statistical knowledge of the two scattering classes or types exists and the polarimetric signals backscattered from the two scattering classes are independent. The processing requirement is then to determine the optimal transmitting and receiving polarization state which will maximize the separation of the average power returns between the two classes. Applying such a technique to radar imagery allows for better discrimination of the two classes.[37]

An n-dimensional anisotropic random walk model is used to derive the zero-mean multivariate K-distribution for polarimetric data.[38] Anisotropy refers to the fact that the polarimetric covariance matrix is not proportional to an identity matrix. The polarimetric amplitude data are normalized by the square root of the illuminated area so that the measured covariances of the polarimetric data are in terms of scattering cross section per unit area. The polarimetric covariance matrix is shown to be directly related to that of a single scatterer. The result is then generalized to the nonzero-mean multivariate K-distribution. There are two ways to introduce nonzero mean into the K-distribution. The directional bias random walk model will lead to a generalized K-distribution, and the homodyned approach will result in a homodyned K-distribution. We applied both approaches in deriving the nonzero mean K-distribution and discussed the corresponding scattering processes. In order to apply the K-distribution to the normalized polarimetric classifier problem, the probability density function (PDF) of the normalized K-distributed vector is derived and discussed. Finally, four sets of experimental data, obtained from MIT Lincoln Laboratory, the Jet Propulsion Laboratory (JPL), and the German Aerospace Research Establishment (DLR) of the Federal Republic of Germany, are compared with the K-distribution to lend support to the above model. As compared with C-, L- and P-band polarimetric SAR image simultaneously measured by the Jet Propulsion Laboratory (JPL) on Mt. Shasta, it is found that α appears to decrease from C- to P-band for both the forest and burned areas.

In remote sensing, the encountered geophysical media such as agricultural canopy, forest, snow, or ice are inhomogeneous and contain scatterers in a random manner. Furthermore, weather conditions such as fog, mist, or snow cover can intervene the electromagnetic observation of the remotely sensed media. In the modeling of such media accounting for the weather effects, a multi-layer random medium model has been developed.[39] The scattering effects of the random media are described by three-dimensional correlation functions with variances and correlation lengths corresponding to the fluctuation strengths and the physical geometry of the inhomogeneities, respectively. With proper consideration of the dyadic Green's function and its singularities, the strong

---

[37] J.A. Kong, S.H. Yueh, H.H. Lim, R.T. Shin, and J.J. van Zyl, "Classification and Maximum Contrast of Earth Terrain Using Polarimetric Synthetic Aperture Radar Images," In *Progress In Electromagnetics Research,* ed. J.A. Kong (New York: Elsevier, 1990), Vol. 3, Ch. 6, pp. 327-370.

[38] S.H. Yueh, J.A. Kong, R.T. Shin, and H.A. Zebker, "Statistical Modelling for Polarimetric Remote Sensing of Earth Terrain," Tenth International Geoscience and Remote Sensing Symposium (IGARSS'90), College Park, Maryland, May 20-24, 1990; S.H. Yueh, J.A. Kong, J.K. Jao, R.T. Shin, H.A. Zebker, T. Le Toan, and H. Ottl, "K-distribution and Polarimetric Terrain Radar Clutter," In *Progress In Electromagnetics Research,* ed. J.A. Kong. (New York: Elsevier, 1990), Vol. 3, Ch. 4, pp. 237-275; H.A. Yueh, J.A. Kong, R.T. Shin, H.A. Zebker, and T. Le Toan, "K-distribution and Multi-Frequency Polarimetric Terrain Radar Clutter," *J. Electromag. Waves Appl.,* forthcoming.

[39] S.V. Nghiem, J.A. Kong, and T. Le Toan, "Electromagnetic Wave Modeling for Remote Sensing," International Conference on Directions in Electromagnetic Wave Modeling, New York, October 22-24, 1990; S.V. Nghiem, M. Borgeaud, J.A. Kong, and R.T. Shin, "Polarimetric Remote Sensing of Geophysical Media with Layer Random Medium Model," In *Progress In Electromagnetics Research,* ed. J.A. Kong (New York: Elsevier, 1990), Vol. 3, Ch. 1, pp. 1-73.

fluctuation theory is used to calculate the effective permittivities which account for the modification of the wave speed and attenuation in the presence of the scatterers. The distorted Born approximation is then applied to obtain the correlations of the scattered fields. From the correlation of the scattered field, the complete set of scattering coefficients for polarimetric radar observation or brightness temperature in passive radiometer applications are calculated.

Fully polarimetric scattering of electromagnetic waves from snow and sea ice is studied with a layered random medium model and applied to interpret experimental data obtained under laboratory controlled conditions.[40]

Strong permittivity fluctuation theory is used to solve the problem of scattering from a medium composed of completely randomly oriented scatterers under the low frequency limit.[41] Gaussian statistics is not assumed for the renormalized scattering sources. The effective permittivity is obtained under the low frequency limit and the result is shown to be isotropic due to no preferred direction in the orientation of the scatterers. Numerical results of the effective permittivity are illustrated for oblate and prolate spheroidal scatterers and compared with the results for spherical scatterers. The results derived are shown to be consistent with the discrete scatterer theory. Under the distorted Born approximation, the polarimetric covariance matrix for the backscattered electric field is calculated for the half-space randomly oriented scatterers. The nonspherical geometry of the scatterers shows significant effects on the cross-polarized backscattering returns σ_{hv} and the correlation coefficient ρ between HH and VV returns. The polarimetric backscattering coefficients can provide useful information in distinguishing the geometry of scatterers.

The layered random medium model is used to investigate the fully polarimetric scattering of electromagnetic waves from vegetation.[42] The vegetation canopy is modeled as an anisotropic random medium containing nonspherical scatterers with preferred alignment. The underlying medium is considered as a homogeneous half space. The scattering effect of the vegetation canopy are characterized by three-dimensional correlation functions with variances and correlation lengths respectively corresponding to the fluctuation strengths and the physical geometries of the scatterers.

The model is used to interpret the measured data for fields of vegetation such as rice, wheat, or soybean over water or soil. The temporal variation of σ_{hh} and σ_{vv} of the X-band SAR data of rice fields shows a wide range of responses at different growth stages. From the data of wheat, recognizable changes of the angular and polarization behaviour of the backscattering coefficients are observed at X-band before and after the heading of the wheat. For soybean, the data collected during the growing season shows similar results for both *h*- and *v*-polarizations. The observed effects on backscattering coefficients of the vegetation structural and moisture conditions at different growth stages can be explained by analyzing the different interaction processes pointed out by the model.

In the interpretation of active and passive microwave remote sensing data from earth terrain, the random medium model has been shown to be quite successful. In the random medium model, a correlation function is used to describe the random permittivity fluctuations with associated mean and variance. In the past, the correlation functions used were either assumed to be of certain form or calculated from cross-sectional pictures of scattering media. We calculated the correlation function for a random collection of discrete scatterers imbedded in a background medium of constant permittivity. Correlation functions are first calculated for the simple cases of the uniform distribution of scatterers and the uniform distribution with the hole correction. Then, the correlation function for a more realistic case is obtained using the Percus-Yevik pair distribution function. Once the correlation function is obtained, the strong fluctuation theory is used to calculate the effective permittivities. Then, the distorted Born approximation is used to calculate the backscattering coefficients from a halfspace configuration. The theoretical results are illustrated by comparing the effective permittivities and the backscattering coef-

---

[40] S.V. Nghiem, J.A. Kong, R.T. Shin, H.A. Yueh, and R. Onstott, "Theoretical Models and Experimental Measurements for Polarimetric Remote Sensing of Snow and Sea Ice," URSI International Commission F meeting, Hyannis, Massachusetts, May 16-18, 1990.

[41] H.A. Yueh, R.T. Shin, and J.A. Kong, "Scattering from Randomly Oriented Scatterers with Strong Permittivity Fluctuations," *J. Electromag. Waves Appl. 4(10): 983-1004 (1990).*

[42] S.V. Nghiem, J.A. Kong, and T. Le Toan, "Application of Layered Random Medium Model to Polarimetric Remote Sensing of Vegetation," URSI International Commission F meeting, Hyannis, Massachusetts, May 16-18, 1990.

ficients with the results obtained with the discrete scatterer theory.[43]

As an electromagnetic wave propagates through a random scattering medium, such as a forest, its energy is attenuated and random phase fluctuations are induced. The magnitude of the random phase fluctuations induced is important in estimating how well a Synthetic Aperture Radar (SAR) can image objects within the scattering medium. The two-layer random medium model, consisting of a scattering layer between free space and ground, is used to calculate the variance of the phase fluctuations induced between a transmitter located above the random medium and a receiver located below the random medium.[26] The scattering properties of the random medium are characterized by a correlation function of the random permittivity fluctuations. The effective permittivity of the random medium is first calculated using the strong fluctuation theory, which accounts for large permittivity fluctuations of the scatterers. The distorted Born approximation is used to calculate the first-order scattered field. A perturbation series for the phase of the received field is then introduced and the variance of the phase fluctuations is solved to first order in the permittivity fiuctuations. The variance of the phase fluctuations is also calculated assuming that the transmitter and receiver are in the paraxial limit of the random medium, which allows an analytic solution to be obtained. The effects studied are the dependence of the variance of the phase fluctuations on receiver location in lossy and lossless regions, medium thickness, correlation length and fractional volume of scatterers, depolarization of the incident wave, ground layer permittivity, angle of incidence, and polarization.

Classification of earth terrain within an image is one of the many important applications of polarimetric data. Both the supervised and unsupervised classification techniques are applied to San Francisco Bay and Traverse City Synthetic Aperture Radar (SAR) images, supplied by the Jet Propulsion Laboratory.[44] These images were collected at L-band (1.225 GHz) with near range along the upper part of the image. There are 896 pixels in the range and 4096 pixels in the azimuth with approximately 10 m by 3 m resolution per pixel. For supervised classification processing, the Bayes technique is used to classify fully polarimetric and normalized polarimetric SAR data. An unsupervised technique, based on comparing general properties of the Stokes parameters of the scattered wave to that of simple scattering models, is also discussed. It is shown that supervised classification yields the best overall performance when accurate classifier training data are used, whereas unsupervised classification is applicable when training data are not available.

1.4 Microwave and Millimeter Wave Integrated Circuits

Sponsors

U.S. Air Force - Electronic Systems Division
Contract F19628-88-K-0013
U.S. Navy - Office of Naval Research
Grant N00014-89-J-1019

Project Staff

Professor Jin Au Kong, Dr. Sami M. Ali, Dr. Tarek M. Habashy, Cheung-Wei Lam, Check-Fu Lee, David M. Sheen, Michael J. Tsuk, Ann N. Tulintseff, Jiqing Xia

Frequency domain analytical work with complicated microstrip circuits has generally been done using planar circuit concepts in which the substrate is assumed to be thin enough that propagation can be considered in two dimensions by surrounding the microstrip with magnetic walls. Fringing fields are accounted for by using either static or dynamic effective dimensions and permittivities. Limitations of these methods are that fringing, coupling, and radiation must all be handled empirically since they are not allowed for in the model. Also, the accuracy is questionable when the substrate becomes thick relative to the width of the microstrip. To fully account for these effects, it is necessary to use a full-wave solution.

Finite difference time domain methods have recently been used to effectively calculate the frequency dependent characteristics of microstrip discontinuities. Analysis of the fundamental discontinuities is of great importance since more complicated circuits can be realized by intercon-

[43] H.H. Lim, S.H. Yueh, R.T. Shin, and J.A. Kong, "Correlation Function for a Random Collection of Discrete Scatterers," Tenth International Geoscience and Remote Sensing Symposium (IGARSS'90), College Park, Maryland, May 20-24, 1990.

[44] J.A. Kong, S.H. Yueh, H.H. Lim, R.T. Shin, and J.J. van Zyl, "Classification and Maximum Contrast of Earth Terrain Using Polarimetric Synthetic Aperture Radar Images," In *Progress In Electromagnetics Research*, ed. J.A. Kong (New York: Elsevier, 1990), Vol. 3, Ch. 6, pp. 327-370.

necting microstrip lines with these discontinuities and using transmission line and network theory. Some circuits, however, such as patch antennas, may not be realized in this way. Additionally, if the discontinuities are too close to each other the use of network concepts will not be accurate due to the interaction of evanescent waves. To accurately analyze these types of structures it is necessary to simulate the entire structure in one computation. The finite difference time domain (FDTD) method shows great promise in its flexibility to handle a variety of circuit configurations. An additional benefit of the time domain analysis is that a broadband pulse may be used as the excitation and the frequency domain parameters may be calculated over the entire frequency range of interest by Fourier Transform of the transient results.

The frequency dependent scattering parameters are calculated for several printed microstrip circuits, specifically, a line-fed rectangular patch antenna, a low pass filter, and a rectangular branch line coupler.[45] These circuits represent resonant microstrip structures on an open substrate, hence, radiation effects can be significant, especially for the microstrip antenna. Calculated results are presented and compared with experimental measurements.

For microwave integrated circuit applications, the characteristics of interconnects have been investigated for propagation modes, time response, crosstalk, coupling, delay, etc. In these analyses, it is assumed that quasi-TEM modes are guided along the multiconductor transmission line. To perform the quasi-TEM analysis, the capacitance matrix for the multiconductor transmission line has to be obtained first. Both the spectral and the spatial domain methods have been proposed to calculate the capacitance matrix. In the spectral domain methods, two side walls are used to enclose the whole transmission line structure, and the thickness of the strip lines has not been considered. In using the spatial domain method, the structure has to be truncated to a finite extent to make the numerical implementation feasible. However, the infinite extent of the structure was incorporated, but only a two-layer medium was considered.

A quasi-TEM analysis of coupled lossy microstrip lines of finite strip thickness embedded in different layers of a lossy isotropic stratified medium is presented.[46] First, a spectral domain scalar Green's function in a lossy isotropic stratified medium is derived. Based on the scalar Green's function, a set of coupled integral equations is obtained for the charge distribution on the strip surfaces. The method of moments is then applied where pulse basis functions and a point-matching scheme is used to solve numerically the set of integral equations for the charge distribution, and hence the capacitance matrix. The duality between the electrostatic problem and the magnetostatic one is applied to calculate the inductance matrix. The conductance matrix is obtained by using the duality between the electrostatic problem and the current field problem. A perturbation method is used to calculate the resistance matrix. Finally, a transmission line analysis is derived to obtain the transfer matrix for multiconductor line, which significantly reduces the effort in treating the load and the source conditions. Transient responses are obtained by using the Fourier transform. The results for two coupled lines are presented.

A full modal analysis is used to study the dispersion characteristics of microstrip lines periodically loaded with crossing strips in a stratified uniaxially anisotropic medium.[47] Dyadic Green's functions in the spectral domain for the multilayered medium in conjunction with the vector Fourier transform (VFT) are used to formulate a coupled set of vector integral equations for the current distribution on the signal line and the crossing strips. Galerkin's procedure is applied to derive the eigenvalue equation for the propagation constant. The effect of anisotropy for both open and shielded structures on the stopband properties is investigated.

The excitation of the earth-ionosphere waveguide by point dipoles at satellite heights was studied by Einaudi and Wait. In their formulation, the ionosphere was crudely modeled as a single D-layer, moreover the geomagnetic field was assumed to be vertical, thus rendering the validity of the model to polar regions. Then, a more general analysis was performed where the

---

[45] D.M. Sheen, S.M. Ali, M.D. Abouzahra, and J.A. Kong, "Application of the Three Dimensional Finite Difference Time-Domain Method to the Analysis of the Planar Microstrip Circuits," *IEEE Trans. Microwave Theory Tech.* 38(7): 849-857 (1990).

[46] J.F. Kiang, S.M. Ali, and J.A. Kong, "Modelling of Lossy Microstrip Lines with Fine Thickness," *Progress In Electromagnetics Research*, ed. J.A. Kong (New York: Elsevier, 1990), Vol. 4, Ch. 3, pp. 85-117.

[47] C.W. Lam, S.M. Ali, and J.A. Kong, "The Propagation Characteristics of Signal Lines with Crossing Strips in Multilayered Anisotropic Media," *J. Electromag. Waves Appl.* 4(10): 1005-1021 (1990).

geomagnetic field was assumed to be arbitrarily-oriented and the earth to be curved along the direction of propagation. However, the ionosphere was assumed to be a semi-infinite homogeneous medium and the results presented in these papers were limited to a frequency of 75 Hz. Furthermore, in these papers, an indirect scheme was employed to formulate the response of point dipole sources: the case of line quadrupole sources was first considered and then at the end of the development, the results were converted to apply to a point source.

We presented a rigorous approach to the problem of radiation of electric or magnetic sources in a stratified arbitrary magnetized linear plasma.[12] The fields are obtained in terms of dyadic Green's functions of electric or magnetic type represented in the spectral domain. First, the dyadic Green's function for an unbounded arbitrary magnetized linear plasma is derived. The formulation is considerably simplified by using the kDB system of coordinates in conjunction with the Fourier transform. This leads to compact and explicit expressions for the dyadic Green's functions. The distributional singular behavior of the various dyadic Green's functions in the source region is investigated and taken into account by extracting the delta function singularities. Finally, the dyadic Green's function in any arbitrary layer is obtained in terms of appropriately defined global upward and downward reflection and transmission matrices. The field expressions for an arbitrary distribution of sources or linear antennas can be obtained by performing a convolution integral over the volume of the antenna weighted by the current density on the antenna.

The integral equation method has been used to solve for the dispersion relation of the rectangular dielectric waveguide.[48] This method incorporates the continuous spectrum, and hence the radiation loss is taken into account. However, no results concerning practical single and coupled dielectric strip waveguides were presented; and the leakage phenomenon was not investigated. We derived an integral equation formulation using the dyadic Green's function to solve for the dispersion relation of single and coupled dielectric strip waveguides. A method to predict the leakage is presented, and the leakage properties are investigated. The integral equation formulation for an arbitrary number of inhomogeneous dielectric strips is derived and Galerkin's method is used to obtain the matrix eigenvalue equations. Numerical results and discussions are presented.

Cylindrical microstrip antennas have many applications in high-speed aircraft and spacecraft because of their conformity with the aerodynamical structure of such vehicles. Recently, there has been some progress in the theoretical study of this kinds of antenna. The radiation from the wraparound cylindrical microstrip element was computed using a magnetic wall cavity model. More recently, the radiation from the wraparound and the rectangular patches was computed by assuming an electric surface current distribution on the microstrip patch. The excitation problem of realizing such a current distribution was not addressed in these investigations. Furthermore, the input impedance for the cylindrical microstrip antennas was not reported.

We addressed the more realistic problem of the radiation from a cylindrical microstrip antenna excited by a probe.[49] Both the cylindrical-rectangular and the wraparound elements are discussed. The current distribution on the patch is rigorously formulated using a cylindrically stratified medium approach. A set of vector integral equations is derived which governs the current distribution on the patch. This set of equations is then solved using a moment method in which the patch current is expanded in terms of a complete set of basis functions that can take into account the edge singularity condition. The input impedance together with the radiation pattern are derived both exactly and in the small substrate thickness limit where a single mode approximation is employed.

A microstrip antenna consisting of two circular microstrip disks in a stacked configuration driven by coaxial probe excitation is considered.[50] The two different stacked configurations are investigated. A rigorous analysis of the two stacked circular disks in a layered medium is performed using a dyadic Green's function formulation. Using the vector Hankel transform, the mixed boundary value problem is reduced to a set of coupled vector integral equations and solved by employing Galerkin's

---

[48] J.F. Kiang, S.M. Ali, and J.A. Kong, "Integral Equation Solution to the Guidance and Leakage Properties of Coupled Dielectric Strip Waveguides," *IEEE Trans. Microwave Theory Tech.* 38(2): 193-203 (1990).

[49] T.M. Habashy, S.M. Ali, and J.A. Kong, "Input Impedance Parameters and Radiation Pattern of Cylinderical-Rectangular and Wraparound Microstrip Antennas," *IEEE Trans. Antennas Propag.* 38(5): 722-731 (1990).

[50] A.N. Tulintseff, S.M. Ali, and J.A. Kong, "Input Impedance of a Probe-Fed Stacked Circular Microstrip Antenna," *IEEE Trans. Antennas Propag.*, forthcoming.

method in the spectral domain. The current distribution on each disk is expanded in terms of two sets of basis functions. The first set of basis functions used is the complete set of transverse magnetic (TM) and transverse electric (TE) modes of a cylindrical resonant cavity with magnetic side walls. The second set of basis functions used employ Chebyshev polynomials and enforce the current edge condition. An additional term in the current expansion is taken to account for the singular nature of the current on the disk in the vicinity of the probe and to ensure continuity of current at the junction. This term, the "attachment mode," is taken to be the disk current of magnetic cavity under a uniform cylindrical current excitation. It is shown here explicitly that continuity of the current at the probe/disk junction must be enforced to rigorously include the probe self-impedance. The convergence of the results is investigated and ensured by using a proper number of basis functions. The input impedance of the stacked microstrip antenna is calculated for different configurations of substrate parameters and disk radii. Disk current distributions and radiation patterns are also presented. Finally, the results are compared with experimental data and shown to be in good agreement.

The study of electromagnetic radiation from sources in the ionospheric plasmas has received much attention in the research on the satellite-borne antennas. For many years, special attention has been given to the radiation in the very low frequency (VLF) band due to its applications in the down-link communication systems. Intensive efforts had been placed on the investigation on the single element radiations by many authors, both theoretically and experimentally. However, limited by its low radiation efficiency, the utility of a practically sized single VLF radiator could depend upon the focusing effects characterized by the inflection points on the k-surface associated with the medium. In recent years, the construction of a large space-based antenna array has been made feasible by the progress of spacecraft technology. With a properly phased large VLF linear or planar array, a narrow beam width and consequently the high directivity can then be achieved.

The far field pattern of a VLF phased array located in a magnetized plasma is studied. The general principles of antenna array design in the anisotropic media are discussed.[51] Special attention is drawn to the two-dimension planar array allowed to rotate with respect to an axis perpendicular to the plane of the array, and the main beam of which is kept in the same direction as that of the geomagnetic field line during the rotation. The applicability of the principle of pattern multiplication as well as the effects of different types of radiating elements for different k-surface geometries are investigated.

There has been considerable interest in the theoretical study of scattering from chiral media. Chiral medium characterized by biisotropic constitutive relation is a special case of the bianisotropic medium whose electromagnetic properties have been extensively studied by Kong. Periodic gratings have been the object of extensive research through the years because of their many applications in distributed feedback lasers, integrated optics, acousto-optics, quantum electronics, and holography. For the analysis of wave diffraction by periodic surface grating, methods, including the method of moments and extended boundary condition method, are rigorous and in general computationally efficient. For the analysis of periodic slanted dielectric gratings, a coupled-wave method has been developed.

The coupled-wave theory is generalized to analyze the diffraction of waves by chiral gratings for arbitrary angle of incidence and polarizations.[52] Numerical results are illustrated for the Stokes parameters of diffracted Floquet modes versus the thickness of chiral gratings with various chiralities. Both horizontal and vertical incidences are considered for illustration. The diffracted waves from chiral gratings are in general elliptically polarized; and at some particular instances, it is possible for chiral gratings to convert a linearly polarized incident field into two nearly circularly polarized Floquet modes propagating in different directions.

1.5 High-Speed Integrated Circuit Interconnects

Sponsors

Digital Equipment Corporation
IBM Corporation

---

[51] C.H. Han, J.A. Kong, T.M. Habashy, and M.D. Grossi, "Principles of VLF Antenna Array Design in Magnetized Plasmas," URSI National Radio Science Meeting, Boulder, Colorado, January 3-5, 1990.

[52] S.H. Yueh and J.A. Kong, "Analysis of Diffraction from Chiral Gratings," *J. Electromag. Waves Appl.*, forthcoming.

Project Staff

Professor Jin Au Kong, Dr. Sami M. Ali, Dr. Tarek M. Habashy

We presented, a new hybrid cross-section finite element/coupled integral equationbreak method,[53] which is both efficient and flexible in regards to the kinds of configurations which can be handled. The technique is a combination of a cross-section finite element method, which is best for high frequencies. An interpolation between the results of these two methods gives very good results over the entire frequency range, even when few basis functions are used.

For low frequencies, we use a cross-section finite element method. Our method is based on the Weeks method, but with two major modifications. First, we use triangular patches, rather than the rectangular patched used by Weeks; secondly we do not change the distribution of patches with frequency. It is shown that both of these improvements, along with the fact that we do not use the cross-section method for high frequencies, greatly increase the efficiency of the method.

As frequency increases, the need to keep the uniform current approximation valid in the patches requires either the addition of many more patches as the skin depth decreases, or a redistribution of the existing patches to the surface, where the current is. However, changing the distribution of patches makes it necessary to recalculate the resistance and inductance matrice of the patches, thus increasing the computation time. Since we use a surface integral equation method for high frequencies, we do not change the distribution of the triangular patches for the cross-section method as we increase the frequency.

For high frequencies, we use a coupled surface integral equation technique. Under the quasi-TEM assumption, the frequency-dependent resistance and inductance result from the power dissipation and magnetic stored energy, which can be calculated by solving a magnetoquasistatic problem, with the vector potential satisfying Laplace's equation in the region outside all the conductors. The resistance and inductance are usually given by integrals of these field quantities over the cross-sections of the wires, but by using some vector identities it is possible to convert these expressions to integrals only over the surfaces of the wires. These expressions contain only the current at the surface of each conductor, the derivative of that current normal to the surface and constants of the vector potential. A coupled integral equation is then derived to relate these quantities through Laplace's equation and its Green's function outside the conductors and the diffusion equation and its Green's function inside the conductors. The method of moments with pulse basis functions is used to solve the integral equations. This method differs from previous work in that the calculation of resistance and inductance is based on power dissipation and stored magnetic energy, rather than on impedance ratios. It will therefore be more easily extended to structures where non-TEM propagation can occur.

For the intermediate frequency range, where the conductors are on the order of skin depth, we found it very efficient to interpolate between the results of the cross-section and surface methods. The interpolation function was based on the average size of the conductors, measured in skin depths, and was of the form $1/(1 + 0.16a^2/\delta^4)$, where it is the average cross-section of the conductors, and δ is the skin depth.

1.6 ILS/MLS Frequency Management Assessment

Sponsor

U.S. Department of Transportation
Contract DTRS-57-88-C-00078

Project Staff

Professor Jin Au Kong, Dr. Robert T. Shin, Dr. Ying-Ching E. Yang, Qizheng Gu, John W. Barrett, Daniel J. Chung, Ramon F. Herrara, Chih-Chien Hsu, Gregory T. Huang, K. Mustafa, Barbara A. Roman, M. Ali Tassoudji, Murat E. Veysoglu, Li-Fang Wang, Diana Wong

The Instrument Landing System (ILS) for airport runway was developed during World War II and was standardized by the end of the war. It is a low-approach guidance system to aid pilots in landing the aircraft when weather is bad and visibility is poor. ILS is currently used worldwide as the standard precision approach guidance system. It consists of three basic components: a localizer to line the airplane up with the runway, a glideslope for vertical glide path control, and marker beacons for homing and position determination. To improve the range accuracy, Distance Measurement Equipment (DME) is often used as a replacement for the marker beacon in newer ILS.

[53] M.J. Tsuk and J.A. Kong, "A Hybrid Method for the Calculation of the Resistance and Inductance of Transmission Lines with Arbrary Cross-Sections," submitted to *IEEE Trans. Microwave Theory Tech.*

The localizer transmitter is installed approximately 1000 feet from the end of the runway. The glide slope transmitter is located on a line perpendicular to the runway centerline at the point where airplanes touch down.

The ILS localizer operates in the band 108.00 to 112.00 MHz using only those frequencies where the digit in the tenths-of-a-megahertz position is odd. Prior to the late 1970s, there were 20 channels allocated for localizer at 100 kHz spacing (108.1 MHz, 108.3 MHz, etc.). However, with the rapid increase of air traffic, 20 ILS localizer channels were insufficient to meet the demand. In order to solve this problem, the separation between localizer channels was reduced to 50 kHz from 100 kHz. Although the number of channels allocated for the localizer was thus increased to 40 (108.1 MHz, 108.15 MHz, 108.3 MHz, 108.35 MHz, etc.), not all new channel frequencies are assigned because some older localizer receivers designed in accordance with RTCA DO-131 (100 KHz channel spacing) are still in use today and may not operate properly in the environment in which the separation between localizer channels is 50 kHz.

Microwave landing system (MLS) was developed to overcome some of the problems and limitations associated with the instrument landing system (ILS). In order to install ILS, flat terrain over an extended area is required since glideslope antennas use ground reflection to generate desired radiation patterns. Furthermore, clearance requirement around an ILS site is very stringent to avoid guidance error caused by multipath interference. MLS overcomes these limitations by using much higher frequencies (5030 MHz - 5090 MHz) so that very narrow beams can be formed from antennas of reasonable sizes. The narrow beams can avoid most structures near the airport and flat terrain is not required in front of the vertical guidance part of MLS. Current ILS also confines arriving aircrafts to a single straight approach path. The long straight approach paths could create some traffic problems in multiairport environments. Since MLS allows curved approach paths, the aircrafts are allowed to make shorter direct approaches. This is very desirable for fuel conservation and noise reduction. Another advantage is that the number of channels available for MLS is five times that for ILS. There are 200 channels allocated for MLS in the band between 5030 MHz and 5090 MHz. This allows installation of more MLS facilities in areas of heavy air traffic without interference problems. The MLS currently being deployed is called a time-reference scanning-beam (TRSB) system.

In view of the ILS frequency congestion problems that metropolitan areas throughout the continental United States are facing and for future planning with MLS growth, the objectives of this project are to utilize specially developed computer simulation tools named EMSALS (Electromagnetic Simulations Applied to Landing Systems) for both ILS and MLS to:

1. predict channel capacities of ILS and MLS in congested metropolitan areas, such as New York, Chicago, Los Angeles and Dallas/Fort Worth as well as in any other geographical area,
2. perform quantitative analyses of in-band (aviation band) and out-of-band electromagnetic interferences, and
3. make quantitative assessments of electromagnetic interferences within the ILS/MLS service volume.

Based upon the above requirements, we established methodology for implementing the simulation software from theoretical studies of electromagnetic interference phenomena. In brief, we first locate potential interference sources and use electromagnetic propagation model to compute the desired and interfering signal strengths. Then interference analysis based upon safety standard, which is developed from the receiver model, is performed. Finally, interference analysis results for various locations are combined to make channel capacity assessment. Accordingly, the following tasks have been carried out:

1. identification of radiation sources, including in-band and out-of-band sources,
2. development of propagation models, to be used to calculate the interference level,
3. development of receiver models, to determine the quantitative effect of interference signals,
4. verification and validation of models through testing and checking against existing data,
5. development of graphical user interface which allows for interactive retrieval of quantitative information on assessment.

In this project, we have utilized computer simulation tool EMSALS to analyze the frequency congestion and electromagnetic interference problems for the continental United States, with emphasis in ten mutually-disjointed complex metropolitan areas. Each of them is formed by drawing 100-nmi circles around a few central locations. The central locations of different areas are typically more than 200 nmi away, so they can be considered to be independent for interference assessment. These areas are:

1. New York-Philadelphia-D.C.
2. Chicago
3. Miami-Tampa-Orlando
4. Dallas-Ft. Worth-Houston
5. Los Angeles-San Diego
6. San Francisco
7. Denver
8. Detroit
9. Memphis-Nashville-Atlanta
10. St. Louis-Kansas City

The results of computer simulation across the ten regions predict significant shortfall in ILS channel capacity. For example, ILS substantially fails to meet the precision landing runway requirements in the New York-Philadelphia-DC area. The limitation of ILS spectrum is best illustrated by the fact that as frequency assignment priorities are changed, the number of available channels for specific regions in a large geographical area will vary because assigning more frequencies in one region can seriously reduce the channel availability in nearby regions. In other areas such as Denver and Chicago, we demonstrated that the limited ILS channel capacity could potentially impede the expansion plans.

1.7 Superconducting Electronics

Sponsor

Defence Advanced Research Projects Agency
Contract MDA972-90-C-0021

Project Staff

Professor Jin Au Kong, Dr. Sami M. Ali, Hongsing Lee, David M. Sheen

The calculation of the electrical parameters of superconducting transmission lines is very important not only for design of circuitry and devices, but also for the characterization of the superconductors. Currently, there is considerable effort directed at microwave-frequency characterization of both high-T_c and low-T_c superconducting thin films. The microwave measurements can determine the fundamental physical properties of these films, such as penetration depth, intrinsic surface resistance or the real part of the conductivity, as well as other parameters such as critical temperature, critical current density, critical magnetic field strength, etc. To enable measurement at microwave frequencies, these films are often fabricated into stripline or microstrip resonators. The resonant frequencies and the associated quality factors are readily measured as a function of temperature. To accurately infer the fundamental physical properties from these measurements requires accurate calculation of the current distribution, resistance, and inductance of the stripline.

We presented a method for the calculation of the current distribution, resistance, and inductance, as functions of the penetration depth for a superconducting strip transmission line.[54] Unlike the previous work, resistance will be considered in the formulation as well as inductance. The inductance calculation is then used to determine the penetration depth at zero temperature, $\lambda(0)$, for *Nb*, *NbN*, and $YBa_2Cu_3O_{7-x}$ superconducting thin films from the measured temperature dependence of the resonant frequency of a stripline resonator. The calculations are also used to convert measured temperature dependence of the stripline resonator Q to the intrinsic surface resistance as a function of temperature for the *Nb* resonator. Agreement between the intrinsic surface resistance of *Nb* determined in this way and the BCS theory calculation is shown.

Among the most promising applications of high-T_c superconductors in computers is in passive elements, such as interconnects, signal transmission lines, or board level wiring. The signal delay in a computing system can be reduced by increasing the density of circuits. The finer dimensions of the interconnecting lines can cause unacceptable signal losses in normal metals due to resistive attenuation. However, superconductors offer lower attenuation and signal distortion.

Approximate theoretical analyses and experiments have been performed to study the propagation characteristics of high-T_c superconducting planar transmission lines. However, no rigorous analysis of the wave propagation in the superconducting microstrip lines has been performed. A full-wave analysis has only been applied to the special case when the film thickness is thin compared to the penetration depth of the superconductor and thus surface impedance boundary condition can be used. Also, in the previous studies, no information

[54] D.M. Sheen, S.M. Ali, D.E. Oates, R.S. Whers, and J.A. Kong, "Current Distribution, Resistance, and Inductance for Superconducting Strip Transmission Lines," *IEEE Trans. Appl. Superconductivity,* forthcoming.

on the current distribution in the strips has been presented.

We are investigating a hybrid-mode analysis of superconducting planar transmission lines with finite film thickness.[55] Two different geometries are considered: the microstrip and the coplanar strips. The cross sections of the strips are assumed to be rectangular. Using the dyadic Green's function, the problem is formulated in terms of a set of integral equations. Galerkin's method is then used to solve the integral equations for the dispersion relation. The propagation and attenuation constants are obtained as function of frequency for different physical and geometrical parameters of the superconducting lines. The current density distribution in the strips is calculated for various penetration depths and film thicknesses.

1.8 Publications and Conference Papers

Atkins, R.G., R.T. Shin, and J.A. Kong. "A Neural Net Method for High Range Resolution Target Classification." In *Progress In Electromagnetics Research.* Ed. J.A. Kong. New York: Elsevier, 1990, Vol. 4, Ch. 7, pp. 255-292.

Chu, N.C., J.A. Kong, H.A. Yueh, S.V. Nghiem, J.G. Fleischman, S. Ayasli, and R.T. Shin. "Variance of Phase Fluctuations of Waves Propagation through a Random Medium." *J. Electromag. Waves Appl.* Forthcoming.

Chu, N.C., J.A. Kong, H.A. Yueh, S.V. Nghiem, J.G. Fleischman, S. Ayasli, and R.T. Shin. "Variance of Phase Fluctuations of Waves Propagating through a Random Medium." *J. Electromag. Waves Appl.* June 1990.

Habashy, T.M., S.M. Ali, and J.A. Kong. "Input Impedance Parameters and Radiation Pattern of Cylinderical-Rectangular and Wraparound Microstrip Antennas." *IEEE Trans. Antennas Propag.* 38(5): 722-731 (1990).

Habashy, T.M., M. Moldoveanu, and J.A. Kong. "Inversion of Permittivity and Conductivity Profiles Employing Transverse-Magnetic Polarized Monochromatic Data." SPIE 1990 International Symposium on Optical and Optoelectronic Applied Science and Engineering, San Diego, California, July 8-13, 1990.

Habashy, T.M., S.M. Ali, J.A. Kong, and M.D. Grossi. "Dyadic Green's Functions in a Planar Stratified, Arbitrarily Magnetized Linear Plasma." *Radio Sci.* Forthcoming.

Habashy, T.M., M. Moldoveanu, and J.A. Kong. "Inversion of Permittivity and Conductivity Profiles Employing Transverse-Magnetic Polarized Monochromatic Data." SPIE 1990 International Symposium on Optical and Optoelectronic Applied Science and Engineering, San Diego, California, July 8-13, 1990.

Han, C.H., J.A. Kong, T.M. Habashy, and M.D. Grossi. "Principles of VLF Antenna Array Design in Magnetized Plasmas." URSI National Radio Science Meeting, Boulder, Colorado, January 3-5, 1990.

Han, C.H., J.A. Kong, T.M. Habashy, and M.D. Grossi. "Principles of VLF Antenna Array Design in Magnetized Plasmas." URSI National Radio Science Meeting, Boulder, Colorado, January 3-5, 1990.

Kiang, J.F., S.M. Ali, and J.A. Kong, "Modelling of Lossy Microstrip Lines with Fine Thickness," In *Progress In Electromagnetics Research.* Ed. J.A. Kong. New York: Elsevier, 1990, Vol. 4, Ch. 3, pp. 85-117.

Kiang, J.F., S.M. Ali, and J.A. Kong. "Integral Equation Solution to the Guidance and Leakage Properties of Coupled Dielectric Strip Waveguides." *IEEE Trans. Microwave Theory Tech.* 38(2): 193-203 (1990).

Kong, J.A., S.H. Yueh, H.H. Lim, R.T. Shin, and J.J. van Zyl. "Classification and Maximum Contrast of Earth Terrain Using Polarimetric Synthetic Aperture Radar Images." In *Progress in Electromagnetics Research.* Ed. J.A. Kong. New York: Elsevier, 1990, Vol. 3, Ch. 6, pp. 327-370.

Lam, C.W., S.M. Ali, and J.A. Kong. "The Propagation Characteristics of Signal Lines with Crossing Strips in Multilayered Anisotropic Media." *J. Electromag. Waves Appl.* 4(10): 1005-1021 (1990).

Lee, C.F., R.T. Shin, J.A. Kong, and B.J. McCartin. "Absorbing Boundary Condions on Circular and Elliptic Boundaries." *J. Electromag. Waves Appl.* 4(10): 945-962 (1990).

[55] H. Lee, S.M. Ali, and J.A. Kong, "Hybrid-Mode Analysis of High-Tc Superconducting Planar Transmission Lines," submitted to Progress In Electromagnetics Research Symposium, Cambridge, Massachusetts, July 1-5, 1991.

Lee, H., S.M. Ali, and J.A. Kong. "Hybrid-Mode Analysis of High-T_c Superconducting Planar Transmission Lines." Submitted to the Progress In Electromagnetics Research Symposium, Cambridge, Massachusetts, July 1-5, 1991.

Lee, C.F., R.T. Shin, and J.A. Kong. "Fine Difference Method for Electromagnetic Scattering Problems," In *Progress In Electromagnetics Research*. Ed. J.A. Kong. New York: Elsevier, 1990, Vol. 4, Ch. 11, pp. 373-442.

Lim, H.H., S.H. Yueh, R.T. Shin, and J.A. Kong. "Correlation Function for a Random Collection of Discrete Scatterers." Tenth International Geoscience and Remote Sensing Symposium (IGARSS'90), College Park, Maryland, May 20-24, 1990.

Melville, W.K., D.V. Arnold, J.A. Kong, A.T. Jessup, E. Lamarre, R.H. Stewart, and W.C. Keller. "Measurements of EM Bias at Ku and C Bands." OCEANS'90, Washington, D.C., September 24-26, 1990.

Melville, W.K., J.A. Kong, R.H. Stewart, W.C. Keller, D. Arnold, A.T. Jessup, and E. Lamarre. "Measurements of Sea-State Bias at Ku and C Bands." URSI International Commission F meeting, Hyannis, Massachusetts, May 16-18, 1990.

Nghiem, S.V., M. Borgeaud, J.A. Kong, and R.T. Shin. "Polarimetric Remote Sensing of Geophysical Media with Layer Random Medium Model." In *Progress In Electromagnetics Research*. Ed. J.A. Kong. New York: Elsevier, 1990, Vol. 1, Ch. 3, pp. 1-73.

Nghiem, S.V., J.A. Kong, and T. Le Toan. "Electromagnetic Wave Modeling for Remote Sensing." International Conference on Directions in Electromagnetic Wave Modeling, New York, October 22-24, 1990.

Nghiem, S.V., M. Borgeaud, J.A. Kong, and R.T. Shin. "Polarimetric Remote Sensing of Geophysical Media with Layer Random Medium Model." Progress In Electromagnetics Research. Ed. J.A. Kong. New York: Elsevier, 1990, Vol. 3 Ch. 1, pp. 1-73.

Nghiem, S.V., J.A. Kong, R.T. Shin, H.A. Yueh, and R. Onstott. "Theoretical Models and Experimental Measurements for Polarimetric Remote Sensing of Snow and Sea Ice." URSI International Commission F meeting, Hyannis, Massachusetts, May 16-18, 1990.

Nghiem, S.V., J.A. Kong, and R.T. Shin. "Study of Polarimetric Response of Sea Ice with Layered Random Medium Model." Tenth International Geoscience and Remote Sensing Symposium (IGARSS'90), College Park, Maryland, May 20-24, 1990.

Nghiem, S.V., J.A. Kong, and T. Le Toan. "Application of Layered Random Medium Model to Polarimetric Remote Sensing of Vegetation." URSI International Commission F meeting, Hyannis, Massachusetts, May 16-18, 1990.

Sheen, D.M., S.M. Ali, M.D. Abouzahra, and J.A. Kong. "Application of the Three Dimensional Fine Difference Time-Domain Method to the Analysis of Planar Microstrip Circuits." *IEEE Trans. Microwave Theory Tech.* 38(7): 849-857, (1990).

Tsuk, M.J., and J.A. Kong. "A Hybrid Method for the Calculation of the Resistance and Inductance of Transmission Lines with Arbrary Cross-Sections." Submitted to *IEEE Trans. Microwave Theory Tech.*

Tulintseff, A.N., S.M. Ali, and J.A. Kong, "Input Impedance of a Probe-Fed Stacked Circular Microstrip Antenna." *IEEE Trans. Antennas Propag.* Forthcoming.

Veysoglu, M.E., H.A. Yueh, R.T. Shin and J.A. Kong. "Polarimetric Passive Remote Sensing of Periodic Surfaces." *J. Electromag. Waves Appl.* 5(3): 267-280 (1991).

Yueh, S.H., and J.A. Kong. "Analysis of Diffraction from Chiral Gratings." *J. Electromag. Waves Appl.* Forthcoming.

Yueh, S.H., J.A. Kong, and R.T. Shin. "Calibration of Polarimetric Radars Using In-Scene Reflectors." In *Progress In Electromagnetic Research*. Ed. J.A. Kong. New York: Elsevier, 1990, Vol. 3, Ch. 9, pp. 451-510.

Yueh, S.H., J.A. Kong, and R.T. Shin. "Calibration of Polarimetric Radars Using In-Scene Reflectors." Tenth International Geoscience and Remote Sensing Symposium (IGARSS'90), College Park, Maryland, May 20-24, 1990.

Yueh, S.H., J.A. Kong, R.T. Shin, and H.A. Zebker. "Statistical Modelling for Polarimetric Remote Sensing of Earth Terrain." Tenth International Geoscience and Remote Sensing Symposium (IGARSS'90), College Park, Maryland, May 20-24, 1990.

Yueh, S.H., J.A. Kong, J.K. Jao, R.T. Shin, H.A. Zebker, T. Le Toan, and H. Öttl. "K-distribution

and Polarimetric Terrain Radar Clutter," In *Progress In Electromagnetics Research*. Ed. J.A. Kong. New York: Elsevier, 1990, Vol. 3, Ch. 4, pp. 237-275.

Yueh, H.A., J.A. Kong, R.T. Shin, H.A. Zebker, and T. Le Toan. "K-distribution and Multi-Frequency Polarimetric Terrain Radar Clutter." *J. Electromag. Waves Appl.* Forthcoming.

Yueh, H.A., R.T. Shin, and J.A. Kong, "Scattering from Randomly Oriented Scatterers with Strong Permittivity Fluctuations." *J. Electromag. Waves Appl.* 4(10): 983-1004 (1990).

Section 4 Radio Astronomy

Chapter 1. Radio Astronomy

Academic and Research Staff

Professor Bernard F. Burke, Professor David H. Staelin, Professor Jacqueline N. Hewitt, Dr. Philip W. Rosenkranz, John W. Barrett

Visiting Scientists and Research Affiliates

Dr. Michael Shao[1]

Graduate Students

Ashraf S. Alkhairy, Pierino G. Bonanni, William J. Chiarchiaro, Kevin G. Christian, Samuel R. Conner, John T. Delisle, Stephen S. Eikenberry, John D. Ellithorpe, André B. Fletcher, Mark R. Griffith, Michael B. Heflin, Lori K. Herold, Joseph Lehár, Darren L. Leigh, Howard R. Stuart

Undergraduate Students

Gregory S. Adams, Joseph V. Kaliszewski, Michael Petro, Jo-Ana Quirch

Technical and Support Staff

Wendy E. Hunter, Clare F. Smith

1.1 Galactic and Extragalatic Research

Sponsor

National Science Foundation
Grant AST 88-19848

Project Staff

Professor Bernard F. Burke, John W. Barrett, Samuel R. Conner, André B. Fletcher, Mark R. Griffith, Michael B. Heflin, Joseph Lehár, Lori K. Herold, Gregory S. Adams, Joseph V. Kaliszewski

1.1.1 Completion of the MG Survey

During the 1980s, the Radio Astronomy group was engaged in a survey of radio sources in the northern sky, using the 300-foot transit radio telescope of the National Radio Astronomy Observatory (NRAO), with its 7-feed, 14-channel radiometer. The first two sections of the MIT Green Bank catalog were published in earlier years; sections III and IV have been published in the current year. The northern sky has now been covered completely between the declinations −0.5 and +39.15, and up to +50.98 declination from right ascensions 15.5–2.5. The survey containing over 10,000 new radio sources, terminated with the collapse of the 300-foot Green Bank telescope in November 1988. Fortunately, a successor survey will start, taking up the slack. This survey, the Parkes-MIT-NRAO (PMN) Survey, uses the Parkes 210-foot telescope in Australia (see section 1.1.5 for details).

1.1.2 The MIT VLA Gravitational Lens Search

The radio astronomy group at MIT has completed a VLA search for gravitational lenses at 6 cm,[2] using as a source list the MGI 5 Ghz radio survey[3] down to 100 mJy. This sample of 4000 sources, extending between 0 and 20 degrees in declination, has produced three established lens systems:

---

[1] Jet Propulsion Laboratory, California Institute of Technology.

[2] J. Hewitt, Ph.D. diss., MIT, 1986.

[3] Lawrence et al., *Astrophys. J. Suppl.* 61:105 (1986).

2016+112,[4] MG1131+0456,[5] and MG1654+1346.[6] Three more candidates, MG0414+0534, 0023+171, and MG1045+1735 need further work, but are very likely to be gravitationally lensed. There may be more lensed systems in the MGI sample, and about 200 more promising sources are being pursued optically.

We are currently continuing the search using 4000 additional sources drawn from the MGII and MGIII 5 GHz radio surveys,[7] which cover 20 to 40 degrees in declination. The observations are being carried out at 3.6 cm for improved angular resolution and to take advantage of the sensitive X band receivers at the VLA. Kochanek and Lawrence[8] point out that most multiply imaged compact sources have image separations of less than 0.5 arcseconds and suggest that many more gravitational lenses might be discovered with higher resolution searches.

The first part of this survey, which has been completed, consists of a complete sample of about 360 radio sources in a narrow strip ($\alpha = 8^h \rightarrow 18^h$, $\delta = 28° \rightarrow 32°$), to a limiting flux of 50 mJy. VLA maps were made for each source, followed by Palomar plate identifications, using the Minnesota Automated Plate Scanner, which found counterparts for about half the sources. CCD images have been made for about 40 of the most interesting sources using the 1.3 m McGraw-Hill telescope at Kitt Peak. The most promising candidate for lensing from this first sample is 0956+300, which is discussed below. There also are 18 compact double sources with a separation of less than 1 arcsecond. They have predominantly steep spectra and about half of them have faint optical identifications ($m_R \approx 21$) on the CCD images. Two of them have flat spectra and stand out as promising candidates for multiply imaged quasar cores, although the double structure could not be discerned in the CCD images. These close compact doubles might also be ordinary double lobed radio galaxies, in which case they represent either a very distant sample, or a population of intrinsically small radio galaxies.

The number of available sources will increase as the 3.6 cm VLA survey continues. We have since observed another 1000 sources, which are currently being reduced at MIT, and we expect to obtain another 48 hours of observations this summer during the coming A configuration.

1.1.3 The Close Pair of Quasars 0956+300

One of the most interesting sources to result from the 3.6 cm VLA search for gravitational lenses so far is 0956+300,[9] which consists of a pair of quasars separated by only 8 arcseconds which are at different redshifts. Both have radio emission at 40 mJy and 4 mJy (8.4 GHz) and have 19th magnitude blue optical counterparts. Their spectra were measured using the 200-inch Palomar telescope by Dr. D.P. Schneider (Institute for Advanced Study). Strong emission lines have been found in both cases, though the brighter quasar, A, has a redshift of 2.1, while the fainter, B, has a redshift of 2.8. At 1.4 GHz, both quasars have extended lobes in addition to a compact core, although the southern quasar appears to be one-sided.

Due to the close separation of the two quasars, B is certainly magnified by A. If B has a second lobe, it would probably fall in the region behind A, and there is some likelihood of multiple imaging or the formation of a "ring" or "arc," due to the distortion of the extended lobe. Since the lobes have a steep spectrum, we expect that their structure will be most evident at low frequencies, and there is indeed a peculiar northward extension from the A quasar at 1.4 GHz. If this is a distorted image of a second radio lobe associated with the B quasar, it would be even more evident at lower frequencies. This would be the first case of a quasar as the lensing object as well as the most distant gravitational lens yet observed and would provide a direct constraint on the mass distribution of the A quasar.

---

[4] Lawrence et al., *Sci.* 223: 46 (1984).

[5] Hewitt et al., *Nature* 333: 537 (1988).

[6] Langston et al., *Astron. J.* 97: 1283 (1989).

[7] Langston et al., *Astrophys. J. Suppl.* 72: 621 (1989); Griffith et al., *Astrophys. J. Suppl.* 74: 129 (1990).

[8] *Astron. J.* 99: 1700 (1990).

[9] Lehár et al., in preparation.

1.1.4 A New Measurement of the Hubble Constant

The gravitational lens effect manifests itself as a splitting of a quasar image into multiple images. A foreground mass, such as a galaxy or a cluster of galaxies, deflects the radiation from the quasar by the action of its gravitational field. The observed image is displaced from the location of the true image and may appear as several images in various locations around the deflecting mass. We have been studying the lens system 0957+561 intensively for the past ten years, using the VLA at 6-cm wavelength. There are two principal images designated A and B (A being the brightest and the northernmost). Quasars generally fluctuate in intensity, both at optical and radio wavelengths, but the ray paths across the universe have different lengths for these two images. The background quasar is at a redshift of 1.4, and the foreground lens (a composite of a cluster and a massive galaxy) is at a redshift 0.36. Model calculations have shown that a difference of about 1.4 years should be observed in the fluctuations of the two images. The flux curves of the two images constructed from the VLA data are presented in figure 1. The best fit time delay, illustrated by the delayed and superimposed plot in figure 2, is 1.4 $\pm$ 0.1 years (513 $\pm$ 40 days, A leading), and the magnification ratio (B/A) is 0.697 $\pm$ .003.

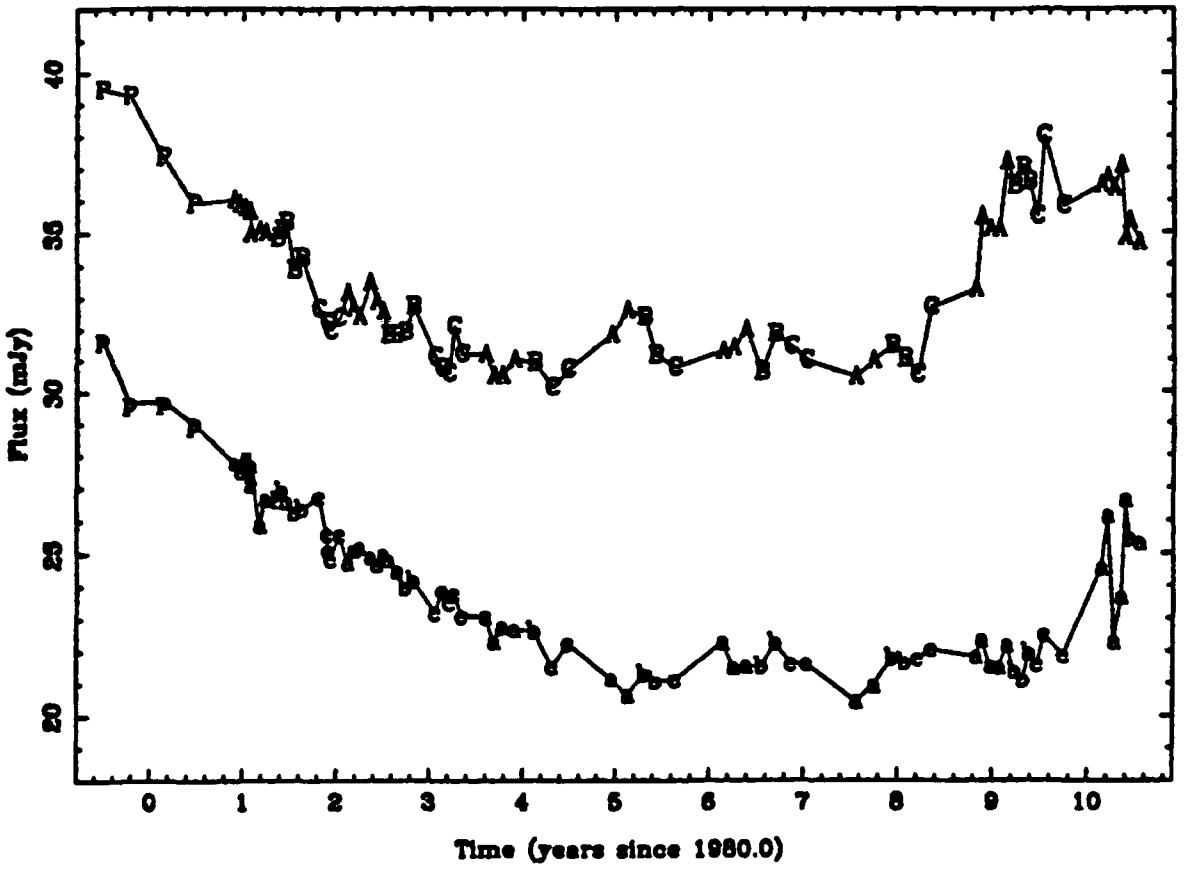

Figure 1. 0957+561 VLA quasar image light curves.

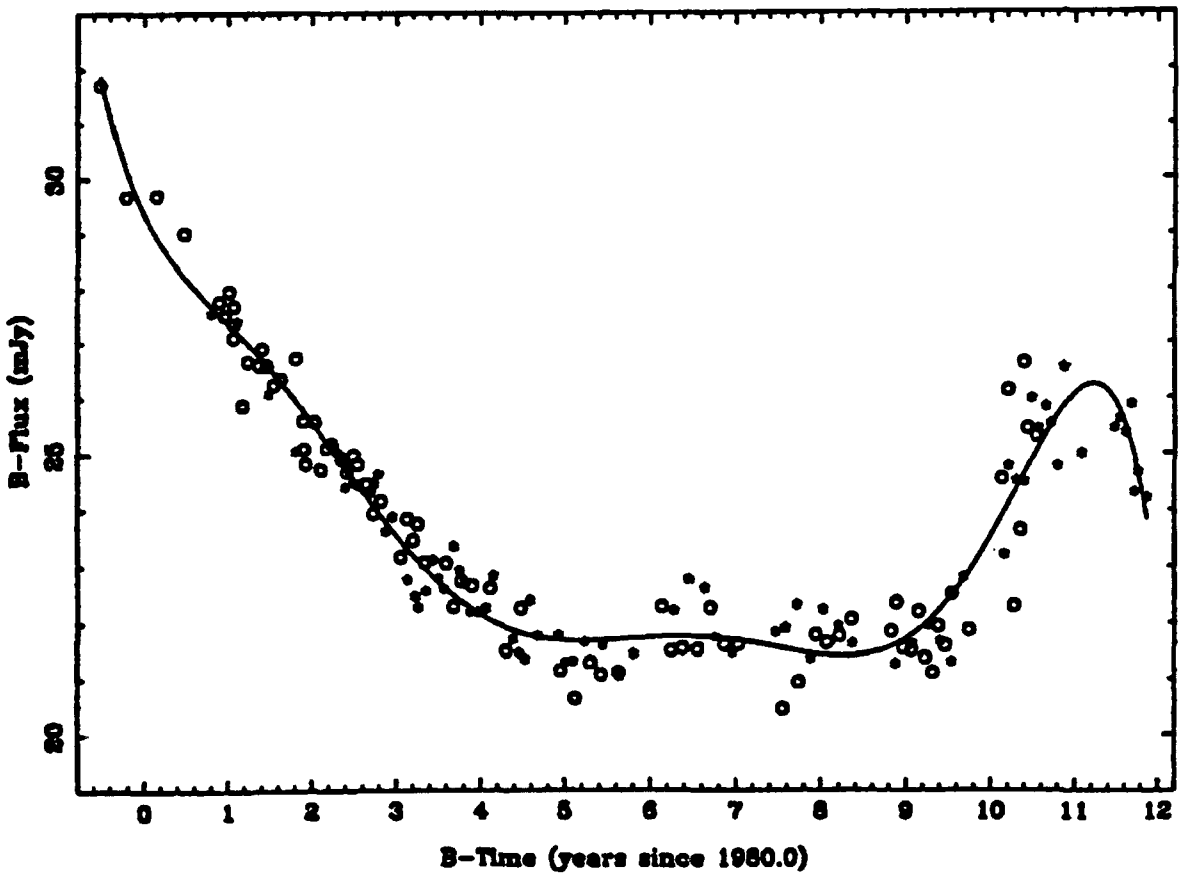

Figure 2. Best fit 7th order polynomial and shifted VLA data.

The time delay can be used to make a model dependent estimate of Hubble's constant. Using the model of Falco, Gorenstein and Shapiro, in combination with recent estimates of the velocity dispersion in the principal lensing galaxy G1, we find that $H_0 = 46 \pm 14$ [42 ± 14] kms^{-1} Mpc^{-1} for $\Omega = 0$ [$\Omega = 1$]. The presence of dark matter in G1 can strongly affect the interpretation of optical velocity dispersions. A reasonable model for a massive dark halo in G1 increases H_0 to 90 [84] kms^{-1} Mpc^{-1}. Since this technique relies on angular size distances, it is free of the uncertainties of traditional methods which use standard candles. This estimate, however, is strongly affected by the mass distributions in the lensing system, which is as yet poorly known. It appears that the information in the radio image has not been fully utilized and efforts are under way to place more stringent conditions on the nature of the lens.

This work is being done in collaboration with Professor Jacqueline N. Hewitt.

1.1.5 The Parkes-MIT-NRAO (PMN) Survey

The Parkes-MIT-NRAO (PMN) Survey was carried out at the Parkes 210-foot telescope in Australia, using the multichannel NRAO 6 cm receiver that had been used for the earlier MG Surveys. The collaborators include Bob Duncan and Ron Ekers (AT/CSIRO), Professor Bernard Burke and Mark R. Griffith (MIT), Ann Burgess (University of Sydney), Phil Randall, Mark Suters, Bill Zealey (University of Wollongong), Graeme White (University of Western Sydney, Neapean), Alan Vaughan (Maquarie University), Ann Savage (Anglo-Australian Observatory), and Dave Jauncey (Australian National University).

Observations were taken during the month of June 1990 and for three weeks in October 1990. The entire southern sky from the south celestial pole to +9 degrees declination was surveyed. An indication of the increase in knowledge is illustrated in figure 3. On the left are plotted the radio sources known to exist in the southern sky from −36 degrees to the south celestial pole. A preliminary

map of the new sources discovered in the same region is shown on the right side. The survey has increased by nearly a factor of ten the known number of radio sources in the Southern Hemisphere.

Detailed reduction of the data is expected to take most of 1991. The collaboration will continue, using the new Australia telescope to determine accurate radio positions and to determine source structure. This data will have many uses, although our immediate interest is to discover new examples of gravitational lenses in the Southern Hemisphere.

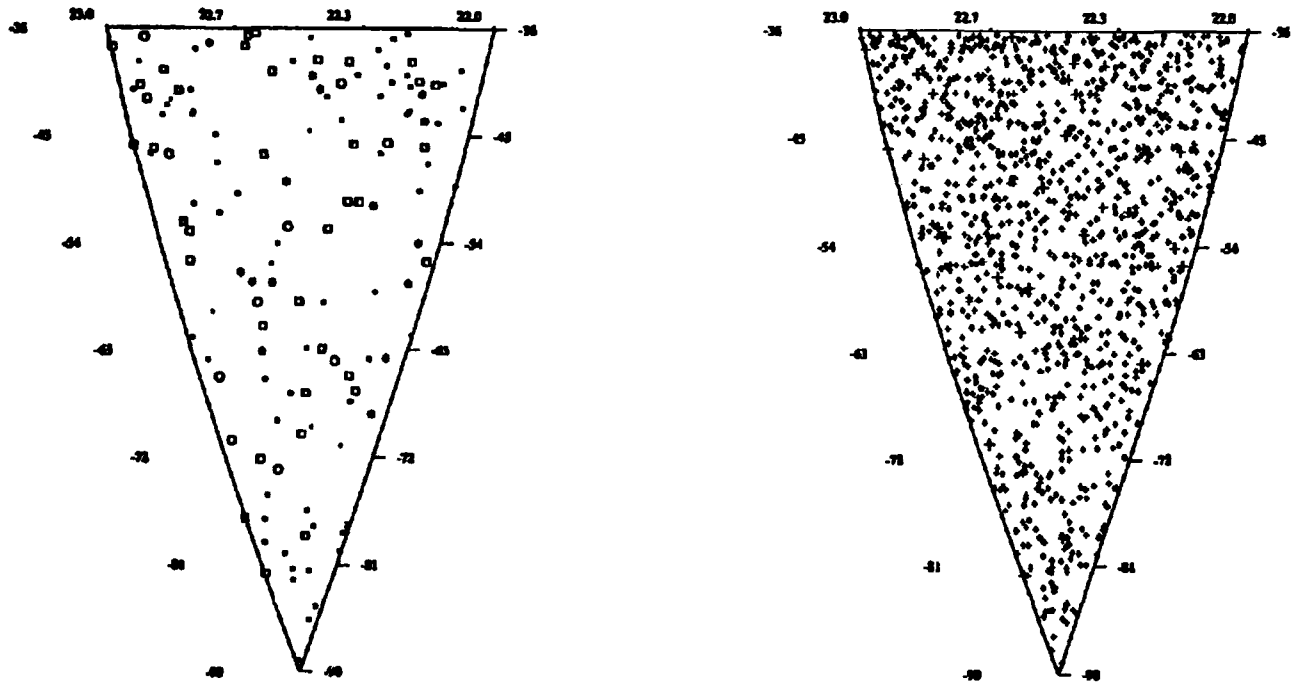

Figure 3.

1.2 Radio Interferometry of Nearby dMe Stars

Sponsor

National Aeronautics and Space Administration
Goddard Space Flight Center
Grant NAGW-2310

Project Staff

Professor Jacqueline N. Hewitt, John D. Ellithorpe

dMe stars are dwarf M stars that show evidence of surface activity. For some time, they have been known to flare strongly at optical and radio wavelengths and, more recently, it has been demonstrated that many dMe stars exhibit low level quiescent emission that is detectable in Very Long Baseline Interferometry (VLBI). The detection of dMe stars on VLBI baselines makes possible the measurement of the position of these stars with high precision, and the astrometric detection of planetary companions may be feasible. We are currently investigating the nature of the radio emission, and we have identified extragalactic radio sources suitable as positional references for the stars AD Leo, EV Lac, and YZ CMi. Last June we carried out first-epoch VLBI astrometric measurements, using a VLBI array composed of telescopes in the United States, Spain and Germany. The analysis of the data is in progress.

This work is being done in collaboration with colleagues at Haystack Observatory, the Jet Propulsion Laboratory, and the Bureau des Longitudes (France).

1.3 Tiros-N Satellite Microwave Sounder

Sponsor

SM Systems and Research, Inc.

Project Staff

Professor David H. Staelin, Dr. Philip W. Rosenkranz

This effort involves scientific support of the Advanced Microwave Sounding Unit (AMSU) scheduled for launch on polar-orbiting weather satellites in the mid 1990s. Support of this passive microwave spectrometer program emphasizes atmospheric transmittance spectra, retrieval methods, and instrumentation issues.

Knowledge of the surface microwave emissivity at the AMSU observing wavelengths is important for accurate interpretation of the data. An approach using window channels to estimate it accurately was developed. This involves use of a multistate emissivity model to structure the estimation process.

A manuscript concerning estimation of atmospheric humidity profiles was prepared and submitted for publication.[10] Improved methods for estimating precipitation rates using AMSU data are also being developed.

1.4 Non-Thermal Radio Emission from the Jovian Planets

Sponsor

National Aeronautics and Space Administration
Goddard Space Flight Center
Grant NAG 5-537

Project Staff

Professor David H. Staelin, Stephen S. Eikenberry

The Planetary Radio Astronomy (PRA) experiment on the Voyager-2 spacecraft observed radio emission from five planets in 198 channels distributed over the band from 1.2 kHz to 40.5 MHz.

During August 1989, Voyager 2 encountered Neptune. Initial studies of emission with high spectral resolution reveal frequency structures that evolve in a manner reminiscent of emission seen on the other three Jovian planets. One interesting feature is the presence of a slowly drifting spectral region of little or no emission, bounded on both sides by emission that varies relatively smoothly with time and frequency. These frequencies of reduced emission correspond to radii where several Neptunian satellites are located, but this association could be coincidental.

1.5 High-Resolution Passive Microwave Imaging of Atmospheric Structure

Sponsor

National Aeronautics and Space Administration
Goddard Space Flight Center
Grant NAG 5-10

Project Staff

Professor David H. Staelin, Dr. Philip W. Rosenkranz, John W. Barrett, Pierino G. Bonanni, William J. Chiarchiaro

Additional scientific results obtained from passive microwave observations of clear air and storms by the MIT imaging microwave spectrometer on the NASA ER-2 high-altitude aircraft were published. One paper described the instrument (MTS), which employed eight double-sideband channels centered around the 118.75-GHz O_2 resonance. This paper also summarized the results from 32 aircraft flights during the 1986 wintertime Genesis of Atlantic Lows Experiment (GALE) and the summertime COoperative Huntsville Meteorological EXperiment (COHMEX).[11] A nadir-viewing single-beam 53.6-GHz radiometer and a video camera made simultaneous co-located observations.

Comparison of the 118-GHz COHMEX spectral data with theoretical predictions of microwave emission spectra yielded good agreement, within 10%, over the opaque mature centers of cells despite the approximations made. Liquid and frozen hydrometers were modeled as spherical Marshall-Palmer and Sekhon-Srivastava distributed Mie scattering polydispersions, respectively, with Henyey-Greenstein phase functions. Comparisons over the partially transparent anvil regions of the precipitation cells were highly sensitive to the assumed mean ice particle size. The retrieval of cell water densities was facilitated by observations at both 53 and 118 GHz, where the

[10] C.C. Kuo, P.W. Rosenkranz, and D.H. Staelin, "Statistical Iterative Scheme for Estimating Atmospheric Relative Humidity Profiles," submitted for publication.

[11] A.J. Gasiewski, J. Barrett, P.G. Bonanni, and D.H. Staelin, "Aircraft Based Radiometric Imaging of Tropospheric Profiles and Precipitation Using the 118.75 GHz Oxygen Resonance," *J. App. Meteor.* 29: 620-632 (1990).

transmittances are similar but the sensitivities to hydrometeors are different; again the assumed mean ice particle size was a source of discrepancy.[12]

In preparation for aircraft flight experiments in 1991, further improvements are being made to the MTS 53.6-GHz radiometer. In addition, a 16-channel 2-bit autocorrelation unit was constructed for observations of Zeeman-split oxygen lines and was tested in the laboratory. The ability of such ground-based observations of Zeeman-split lines to yield estimates of atmospheric temperatures near 50-km altitude was analyzed further and presented.[13]

1.6 Characterization of Dolphin Whistles

Project Staff

Professor David H. Staelin, Kevin G. Christian

Dolphin communication is characterized by sequences of repetitive whistles resembling birdsong. This project involves substantial compression of these signals followed by development of methods for organizing these compressed signals in a database so as to facilitate rapid identification of repetitious song elements. One anticipated result of this research is improved understanding of how various songs are created and evolve in dolphin communities. The results of this research should also lead to signal analysis tools useful for acoustic diagnosis of machinery and other devices.

This year a dolphin song database was assembled and methods for song compression were developed. One problem involves the requirement that similar whistles be coded similarly, despite uncertainties in the initiation and termination times of the whistles due to fading. One promising approach is to code segments internal to the song, where these segments are bounded by inflection points in pitch.

1.7 Rapid Precision Net-Form Manufacturing

Sponsor

Leaders for Manufacturing Program

Project Staff

Professor David H. Staelin, Ashraf S. Alkhairy, John T. Delisle, Darren L. Leigh, Howard R. Stuart

This project has three interrelated elements: (1) development of methods and apparatus for measuring the shape of arbitrary three-dimensional objects with sub-mil accuracy, (2) development of methods and apparatus for forming such objects in metal, ceramics, or plastics rapidly with sub-mil precision, and (3) development of new methods for adaptive experimental design that could facilitate process characterization and help achieve desired levels of precision by iteration of elements (1) and (2).

Most of the work has involved development of a 4-axis stage with a scannable volume of ~ 20 cubic inches; its open loop accuracy is better than 25 microns. A 512^2 pixel CCD camera has been linked to a telescope with an adjustable field of view down to 1-mm^2, and to a computer capable of receiving up to 30 frames per second. Holographically generated illumination patterns provide the signal which permits object shape to be measured at high data rates. Initial tests yielded measurements of surface position with $\sim 12\ \mu$m rms accuracies.

Work on improved methods for parameter design and for materials forming are still in the formative stages. Preliminary analyses of new methods for experiment and parameter design are encouraging, however, and are expected to be more general and to perform better than methods now commonly used.

---

[12] A.J. Gasiewski and D.H. Staelin, "Numerical Modeling of Passive Microwave O_2 Observations over Precipitation," *Radio Sci.* 25: 217-235 (1990).

[13] P.W. Rosenkranz, "Oxygen Line Emission as a Measure of Temperature in the Upper Stratosphere and Mesosphere," *Proceedings of the Tenth Annual International Geoscience and Remote Sensing Symposium,* College Park, Maryland, May 20-24, 1990, pp. 1185-1188.

1.8 Earth Observing System: Advanced Microwave Sounding Unit

Sponsor

National Aeronautics and Space Administration
Goddard Space Flight Center
Grant NAS 5-30791

Project Staff

Professor David H. Staelin, Dr. Philip W. Rosenkranz

A copy of the Advanced Microwave Sounding Unit (AMSU) will provide the microwave-band observing capability for the Atmospheric Infrared Sounder (AIRS); these instruments will operate together on the proposed Earth Observing System Platform A, a polar-orbiting platform to be launched late in this decade. AMSU and AIRS will infer atmospheric profiles of temperature and humidity and also numerous other geophysical parameters characterizing clouds and the terrestrial surface. Our effort in support of this project will develop algorithms for temperature and humidity profiles, precipitation, sea ice and land snow cover, and other parameters.

Part III Systems and Signals

Section 1 Digital Signal Processing

Section 1 Digital Signal Processing

Chapter 1. Digital Signal Processing Research Program

Academic and Research Staff

Professor Alan V. Oppenheim, Professor Arthur B. Baggeroer, Professor Charles S. Burrus,[1] Professor Bruce R. Musicus, Giovanni Aliberti

Visiting Scientists and Research Affiliates

Dr. Meir Feder,[2] Dr. John L. Spiesberger,[3] Dr. Makoto Tabei,[4] Dr. Ehud Weinstein[5]

Graduate Students

Paul E. Beckmann, John R. Buck, Daniel T. Cobra, James W. Fleming, Steven H. Isabelle, Jacek Jachner, Anthony C. Kam, James M. Njeru, G.N. Srinivasa Prasanna, James C. Preisig, Michael D. Richard, Stephen F. Scherock, Andrew C. Singer. Taylen J. Wong, Gregory W. Wornell, Kambiz C. Zangi

Technical and Support Staff

Deborah A. Gage, Giampiero Sciutto

1.1 Introduction

The research of the Digital Signal Processing Group is directed at the development of new algorithms and their applications in a variety of areas. In addition to specific projects being carried out on campus, there is close interaction with Lincoln Laboratory and the Woods Hole Oceanographic Institution. We are involved primarily in the application areas of speech, image, and underwater acoustic signal processing. In addition to algorithm development and applications, there are a number of projects directed at issues of algorithm implementation. Also affecting our research direction is the recognition that while, historically, signal processing has principally emphasized numerical techniques, it will increasingly exploit a combination of numerical and symbolic processing, a direction that we refer to as knowledge-based signal processing.

1.2 A True Maximum Likelihood Method for Directional Wave Spectra Estimation and Matched-field Source Localization

Sponsor

U.S. Navy - Office of Naval Research
Contract N00014-90-J-1544

Project Staff

Professor Arthur B. Baggeroer

Most methods of estimating directional spectra involve a step wherein the cross spectral covariance of the signal field over the array elements must be estimated. When the arrays are large and the data sparse, this estimate is singular or poorly conditioned. Several methods of mitigating this, including diagonal loading, eigenvalue

---

[1] Director, Department of Electrical Engineering, Rice University, Houston, Texas.

[2] Department of Electrical Engineering, Systems Division, Faculty of Engineering, Tel-Aviv University, Israel.

[3] Department of Applied Ocean Sciences and Engineering, Woods Hole Oceanographic Institution, Woods Hole, Massachusetts.

[4] Tokyo Institute of Technology, Yokohama, Japan.

[5] Department of Electrical Engineering, Systems Division, Faculty of Engineering, Tel-Aviv University, Israel; adjunct scientist, Department of Applied Ocean Sciences and Engineering, Woods Hole Oceanographic Institution, Woods Hole, Massachusetts.

thresholding, and subspaces have been traditionally used to circumvent these singularities. The fundamental problem is that an arbitrary covariance matrix has many more degrees of freedom than the data can constrain. A new algorithm is introduced that starts directly from the data to form an estimate of the covariance matrix that is constrained by the wave equation describing the propagation of the directional signals. It is found that a "true" maximum likelihood estimate (not a minimum variance, distortionless filter in the guise of maximum likelihood) can be specified and an iterative algorithm for implementing it can be derived. The results are similar in structure to those derived by Snyder and Miller[6] for estimating power densities by imposing a Toeplitz constraint. The algorithm can be extended to matched-field processing for localizing-independent sources. One of the advantages is that *a priori* information about the sources can be used in estimating their distribution.

These findings were reported at the 120th Meeting of the Acoustical Society of America, San Diego, California, November 26-30, 1990.

1.3 Performance Bounds on the Passive Localization of a Moving Source for Ocean Acoustics

Sponsor

U.S. Navy - Office of Naval Research
Contract N00014-90-J-1544

Project Staff

Professor Arthur B. Baggeroer, Hee Chun Song[7]

Matched-field processing (MFP), presently used for locating a point acoustic source in the ocean using a vertical array, is extended to treat a moving source problem. The extension involves both temporally nonstationary and spatially inhomogeneous structure of the sound field generated by a time-harmonic point source moving uniformly in a stratified oceanic waveguide. Using normal mode description of the sound field, the focus was on the effect of source motion on MFP. An optimum receiver based on maximum likelihood method was developed in the presence of spatially and temporally white noise. The generalized ambiguity function (GAF) was used to analyze problems of accuracy, ambiguity, and resolution. The principal result is the demonstration that a moving source problem can be treated as a stationary source problem if the source travel distance (uncompensated speed times time window) is less than half the wavelength of trapped modes. Also, a closed-form expression for the optimum potential resolution is derived based on the Cramer-Rao bound. The lower bound provides physical insight into how each mode contributes to the localization process and can be easily evaluated for a wide range of source positions in any sound channel using sound channel eigenfunctions, eigenvalues, and the number of modes involved. Simulations of GAF and the bounds for Arctic environment illustrate the coupling of ocean environment to the localization performance.

These findings were reported at the 120th Meeting of the Acoustical Society of America, San Diego, California, November 26-30, 1990.

1.4 Fault-Tolerant Algorithms and Architectures for Digital Signal Processing

Sponsors

Charles S. Draper Laboratory
Contract DL-H-404158
Rockwell Corporation
Doctoral Fellowship
U.S. Navy - Office of Naval Research
Grant N00014-89-J-1489

Project Staff

Professor Bruce R. Musicus, Professor Alan V. Oppenheim, Paul E. Beckmann

In many digital signal processing applications, there is a high cost of failure so that continuous error-free operation is required. Traditionally, this problem has been solved through the use of Modular Redundancy in which several copies of the system operate in parallel, and their outputs are compared with voter circuitry. Modular redundancy is a very general technique which can be applied to any system. However, this technique does not take advantage of the details of a specific problem and thus requires substantial amounts of overhead. (100% for single error detection, 200% for single error correction.)

---

[6] D.L. Snyder and M.L. Miller, *Proc. IEEE* 75: 892-907 (1987).

[7] MIT Department of Ocean Engineering.

Recently, an alternative method of protecting signal processing operations called Algorithm Based Fault Tolerance (ABFT) has emerged.[8] ABFT combines the design of algorithms, architectures, and fault-tolerant systems, and results in more reliable, less costly systems. The regularity of operations in DSP algorithms is exploited, and in some applications, single fault correction may be achieved with only 30%-40% overhead.

Applications of ABFT thus far examined have all been linear systems, and the data encoding and fault detection/correction techniques can be described using standard linear error correcting codes. In this research, we apply other encoding methods such as oversampling and cyclical error correcting codes. By using other encoding methods, we hope to protect a wider range of signal processing operations. Substantial progress has already been made, and ABFT has been successfully applied to two new operations: A/D conversion and convolution. Another goal of this research is to unify ABFT techniques into a general theory covering both linear and nonlinear systems.

1.5 Fault-Tolerant Round Robin A/D Converter System

Sponsors

Charles S. Draper Laboratory
Contract DL-H-404158
Rockwell Corporation
Doctoral Fellowship
U.S. Navy - Office of Naval Research
Grant N00014-89-J-1489

Project Staff

Paul E. Beckmann, Professor Bruce R. Musicus

We describe a robust A/D converter system which requires much less hardware overhead than traditional modular redundancy approaches. A modest amount of oversampling is used to generate information which can be exploited to achieve fault tolerance. A generalized likelihood ratio test is used to detect the most likely failure and also to estimate the optimum signal reconstruction. The error detection and correction algorithm reduces to a simple form and requires only a slight amount of hardware overhead. We present a derivation of the algorithm followed by simulation results for both ideal and optimized FIR processing.

Publication

Beckmann, P.E., and B.R. Musicus. *Fault-Tolerant Round Robin A/D Converter.* RLE TR-561. Res. Lab. of Electron., MIT, 1990.

1.6 Implementation and Evaluation of a Dual-Sensor Time-Adaptive EM Algorithm

Sponsor

U.S. Navy - Office of Naval Research
Grants N00014-89-J-1489 and
N00014-90-J-1109

Project Staff

Professor Alan V. Oppenheim, Dr. Ehud Weinstein, John R. Buck

Signal enhancement seeks to remove or reduce some corrupting signal or noise from a desired signal. Typical desired signals include speech or sonar. This work focuses on the implementation and the evaluation of a newly-formulated adaptive, time-domain, sequential implementation of the EM algorithm for two sensors. The algorithm assumes that the primary sensor receives the desired signal with Gaussian noise coupled in through a finite-impulse response filter. The secondary sensor receives noise with some filtered version of the desired signal. By iterating between a Kalman filter which estimates the signal and noise including the just-received data, and a maximum-likelihood parameter estimate, the algorithm converges to the uncorrupted signal while estimating the coefficients of the coupling filters.

Initial simulations indicate this sequential time-domain implementation performs comparably with Feder's block-processing frequency-domain implementation for the same problem. In addition, this implementation takes advantage of structural properties of the Kalman filter to minimize computation at each time step.

Future work will include implementing and examining a new formulation of the parameter estimation based on explicit calculation of the gradient, which should further reduce computational requirements significantly from the current maximum-likelihood parameter estimation. We also plan to examine the performance of the algorithm on more demanding "real-world" noise

[8] J.A. Abraham, "Fault-tolerance Techniques for Highly Parallel Signal Processing Architectures," *SPIE Highly Parallel Signal Processing Architectures* 614: 49-65 (1986).

sources, such as airplane noise, as opposed to white Gaussian noise.

1.7 Estimation and Correction of Geometric Distortions in Side-Scan Sonar Images

Sponsors

The Federative Republic of Brazil Scholarship
Lockheed Sanders, Inc.
National Science Foundation
Grant MIP 87-14969
U.S. Navy - Office of Naval Research
Grant N00014-89-J-1489

Project Staff

Professor Alan V. Oppenheim, Daniel T. Cobra

This research introduces a new procedure for the enhancement of acoustic images of the bottom of the sea produced by side-scan sonar. Specifically, it addresses the problem of estimating and correcting geometric distortions frequently observed in such images as a consequence of motion instabilities of the sonar array. This procedure estimates the geometric distortions from the image itself without requiring any navigational or attitude measurements. A mathematical model for the distortions is derived from the geometry of the problem and is applied to estimates of the local degree of geometric distortion obtained by cross-correlating segments of adjacent lines of the image. The model parameters are then recursively estimated through deterministic least-squares estimation. An alternative approach based on adaptive Kalman filtering is also proposed, providing a natural framework in which *a priori* information about the array dynamics may be easily incorporated. The estimates of the parameters of the distortion model are used to rectify the image, and may also be used for estimating the attitude parameters of the array. A simulation is employed to evaluate the effectiveness of this technique, and examples of its application to high-resolution side-scan sonar images are provided.

1.7.1 Publication

Cobra, Daniel T. *Estimation and Correction of Geometric Distortions in Side-Scan Sonar Images.* RLE TR-556. Res. Lab. of Electron., MIT, 1990.

1.8 Signal Processing Applications of Chaotic Dynamical Systems

Sponsors

AT&T Bell Laboratories Doctoral Program
U.S. Navy - Office of Naval Research
Grant N00014-89-J-1489

Project Staff

Professor Alan V. Oppenheim, Steven H. Isabelle

Unlike linear time invariant systems which display only simple periodic or fixed point behavior under zero input, nonlinear dynamical systems display a much broader range of behavior. The realization that this complex behavior may result from even very simple nonlinear difference or differential equations has caused much excitement in the physics community. Chaotic dynamics, it is speculated, may provide a simple explanation for complicated phenomena observed in nature, such as turbulence in fluid flow and the erratic orbits of the planets. Chaos has also caused excitement in the signal processing community where it may provide a rich new set of tools for signal analysis and modeling.

In moving from linear to nonlinear signal models, entirely new classes of signal processing problems may be addressed. The goal of this research is to explore applications of nonlinear systems operating in the regime of chaotic behavior to problems of signal description. One fundamental issue to be addressed is determining when these models are appropriate. To resolve this issue, we are currently exploring techniques of detecting chaotic behavior in observed signals.

1.9 High-Resolution Direction Finding for Multidimensional Scenarios

Sponsors

Bell Northern Research Ltd.
U.S. Navy - Office of Naval Research
Grant N00014-89-J-1489

Project Staff

Professor Alan V. Oppenheim, Jacek Jachner

There has been considerable interest recently in High-Resolution Techniques for direction finding

(DF) and for time series analysis. Recent results[9] have improved understanding of High-Resolution direction finding techniques in the following areas:

1. Beamformer design for Beamspace approaches
2. Analytical expressions for the threshold SNR at which algorithms can resolve closely-spaced sources
3. Cramer-Rao lower bounds on the variances of unbiased estimators of direction
4. Covariance matrix eigenstructure for closely-spaced sources.

The results are applicable to far-field planar scenarios in which the location of each source is specified by a single angular parameter.

In practice, common applications of DF techniques to non-planar far-field and near-field problems are multidimensional in nature, requiring estimation of a vector of parameters. For example, two angular parameters are necessary in 3-D far-field problems (e.g., azimuth, elevation). Extension of 1-D approaches to multi-D is not always direct, as several high-resolution techniques, including MinNorm and minimum dimension Beamspace algorithms, fail to uniquely locate sources for multi-dimensional scenarios. This research explores the multidimensional Direction Finding problem, and extends recent 1-D results to multi-D scenarios.

1.10 Signal Processing for Ocean Acoustic Tomography

Sponsor

U.S. Navy - Office of Naval Research
Grant N00014-89-J-1489

Project Staff

Professor Alan V. Oppenheim, Dr. John L. Spiesberger, James M. Njeru

This work involves the signal processing techniques used to develop a thermal map of a 1000 km-long section of the ocean through Ocean Acoustic Tomography. Acoustic tomography is a technique in which travel time measurements over large distances in the ocean are used to infer ocean properties such as temperature and tidal motion. Large-scale (> 500 km) fluctuations of temperature in the ocean are important in determining weather, climate, ocean circulation, and the distribution of marine organisms. The temperature spectrum over horizontal distances exceeding 500 km is usually obtained from point measurements. Point measurements contain both large-scale and smaller-scale (meso and fine) spectral components. And, often, they are not obtained simultaneously in time. Tomographic measurements of large-scale signals, however, are both virtually instantaneous and integral, attenuating signals from the smaller scales.[10]

More specifically, pulse compression of the maximal length sequence signals, wide band Doppler correction to account for source-receiver motion, cross-correlation and coherent averaging to increase signal to noise ratio will be performed. To initialize the problem, multipath identification will be done using ray theory. Finally, a Kalman filter will be used to tomographically invert for the temperature profile. Using a 900 m-long vertical acoustic array, this is the first experiment in which acoustic time fronts have been observed at long range. We expect the number and the diversity of multipaths to yield high resolution.

1.11 Structure Driven Multiprocessor Compilation of DSP and Linear Algebra Problems

Sponsors

Defense Advanced Research Projects Agency
Contract N00014-87-K-0825
IBM Corporation
Sloan Foundation

---

[9] H.B. Lee and M.S. Wengrovitz, "Resolution Threshold of Beamspace Music for Two Closely Spaced Emitters," *IEEE Trans. ASSP* 38(9): 1545-1559 (1990);. H.B. Lee and M.S. Wengrovitz, "Beamformer Preprocessing for Enhanced Resolution by the MUSIC Algorithm," *IEEE Trans. ASSP*, forthcoming; H.B. Lee, "The Cramer-Rao Bound on Frequency Estimates of Signals Closely Spaced in Frequency," *IEEE Trans. ASSP*, forthcoming; H.B. Lee, "Eigenvalues and Eigenvectors of Covariance Matrices for Signals Closely Spaced in Frequency," submitted to *IEEE Trans. ASSP*.

[10] J.L. Spiesberger, "Basin-Scale Tomography: A New Tool for Studying Weather and Climate," *J. Geophys. Res.*, forthcoming.

U.S. Navy - Office of Naval Research
Grant N00014-89-J-1489

Project Staff

Professor Bruce R. Musicus, Professor Anant Agarwal,[11] G.N. Srinivasa Prasanna

In this thesis,[12] we explore issues related to the automatic compilation of linear algebra and digital signal processing problems onto multiprocessors. The highly regular structure, the high computation, and the data-independent control of these problems makes them ideally suited for automatic compilation onto multiprocessors. In this research, shared memory multiprocessors like the MIT Alewife Machine[13] are targeted.

Most algorithms in signal processing and inner loops of linear algebra algorithms can be expressed in terms of expressions composed of matrix operators. The matrix operator dataflowgraphs have regular data and control flow, and regular communication structure. The nodes of the matrix expression dataflowgraph are matrix operators themselves (macro-nodes). The matrix expression dataflowgraph (also called a macro dataflowgraph), in general, exhibits little structure, but has data-independent control.

The basic compilation paradigm explored in the research is to exploit the structure in the dataflowgraphs of such numeric problems. These numeric problems can be conveniently represented as compositions of basic matrix operators. If good compilations for the basic matrix operators are known, and good techniques to compose these operator algorithms are used, then a good compilation for the numeric problem can be derived. The strategy will be fast if each of the two steps is fast. This is a hierarchical compilation strategy.

This thesis has two major parts. First, it shows that it is possible to analyze and derive good algorithms for the basic matrix operators, thus deriving a parallel operator library. Second, it shows that one can quickly compose these library routines to get good algorithms for the complete matrix expression. This yields a speedy hierarchical compilation strategy for such structured problems.

Specifically, we demonstrate how the structure present in matrix operator data flowgraphs can be used to derive close to optimal routines for them. Our techniques can be used to develop a parallel library of routines for these operators.

We have developed theoretical insights into effectively composing matrix operator algorithms to yield algorithms for the matrix expression. These insights have been obtained by viewing scheduling from the perspective of optimal control theory. Minimal time scheduling strategies can be identified with time optimal control strategies. Under certain conditions, the scheduling problem is equivalent to shortest path and flow problems. The approach has been used to derive simple heuristics for composing matrix operator algorithms to form algorithms for the expression.

We have implemented these ideas in the form of a prototype compiler producing Multilisp code from a matrix expression in Lisp-like syntax. Timings statistics on the MIT Alewife Machine[13] have been obtained that, in general, verify our ideas.

1.12 Robust Non-planewave Array Processor Development Using Minmax Design Criteria

Sponsor

U.S. Navy - Office of Naval Research
Grant N00014-89-J-1489

Project Staff

Professor Alan V. Oppenheim, James C. Preisig

Underwater acoustic array processors often must operate in environments whose characteristics are not completely specified at the time of design of the processor. These unknown characteristics may be characteristics of (1) the signal which the processor is attempting to receive, (2) the interfering signals which it also receives, (3) the environment in which the signal propagates, or (4) the array geometry.

---

[11] MIT Department of Electrical Engineering and Computer Science.

[12] G.N.S. Prasanna, *Structure Driven Scheduling of Linear Algebra and Digital Signal Processing Problems*, Ph.D. diss. proposal, Dept. of Electr. Eng. and Comput. Sci., MIT, 1988; M.M. Covell, *Representation and Manipulation of Signal Processing Knowledge and Expressions*, Ph.D. diss. proposal, Dept. of Electr. Eng. and Comput. Sci., MIT, 1987; C.S. Myers, *Signal Representation for Symbolic and Numerical Processing*, Ph.D. diss., Dept. of Electr. Eng. and Comput. Sci., MIT, 1986.

[13] A. Agarwal, "Overview of the Alewife Project," Alewife Systems Memo, Lab. for Comput. Sci., MIT, 1990.

This research focuses on developing efficient array processors which are robust with respect to these kinds of uncertainties. For some applications, such as far-field beamforming in a known homogeneous propagation environment, there are established efficient algorithms for developing minmax beamformers which are robust with respect to the location of interfering signal sources. Unfortunately, many underwater acoustic array processing problems require detection and filtering or estimation of parameters, that, associated with signals propagating through inhomogeneous media, are poorly modeled as propagating planewaves. Novel formulations have been proposed for some of these problems, the solutions of which are optimal array processors with respect to minmax design criteria and which are robust with respect to specified uncertainties. Mathematically, these problems are posed as complex Chebyshev approximation problems on multidimensional spaces. The available algorithms to solve these problems are inefficient and limit the practical applicability of the resulting array processors. Efficient methods of finding optimal and near-optimal solutions to these problems are being explored, and the salient characteristics and the performance capabilities of the resulting array processors are being investigated.

1.13 Shadowing and Noise Reduction in Chaotic Systems

Sponsors

U.S. Air Force - Office of Scientific Research
Fellowship and Grant AFOSR-91-0034
U.S. Navy - Office of Naval Research
Grant N00014-89-J-1489

Project Staff

Professor Alan V. Oppenheim, Michael D. Richard

Chaotic systems are nonlinear dynamical systems characterized by extreme sensitivity to initial conditions. A signal generated by a chaotic system may appear random, despite its having been generated by a low-order, deterministic dynamical system. Both random and chaotic signals lack long-term predictability; but, in contrast to truly random signals, chaotic signals exhibit short-term predictability. Evidence of chaotic behavior has been reported in many diverse disciplines, including physics, biology, engineering, and economics.

An interesting research question arises when simulating a chaotic orbit by iterating a set of difference equations. Specifically, how quickly does the simulated orbit deviate from the actual orbit with the same initial conditions, because of noise induced by round-off errors and finite precision arithmetic – so-called dynamical noise—at each iteration? Also, does an actual orbit, perhaps with different initial conditions, stay close to or shadow the simulated orbit? A related question that arises when measuring a chaotic signal is whether or not knowledge that the signal is chaotic can be exploited to reduce noise due to measurement errors—so-called observational noise.

This research is (1) exploring techniques to reduce noise, both dynamical and observational, in chaotic systems and (2) establishing the utility of these techniques to typical noise-reduction problems in signal processing. An iterative technique for noise reduction, which was proposed in the literature, was implemented and is being studied. This technique was derived from a mathematical proof of the Shadowing Lemma which established the existence of actual, shadowing orbits to noisy, simulated orbits for a certain class of non-chaotic dynamical systems. The use of an Estimate-Maximize (EM) algorithm for noise reduction is also being considered. Finally, the value of various noise reduction techniques in improving the short-term predictability of chaotic signals will be ascertained.

1.14 Causal Filters with Negative Group Delay

Sponsors

National Science Foundation
Graduate Fellowship
U.S. Navy - Office of Naval Research
Grant N00014-89-J-1489

Project Staff

Professor Alan V. Oppenheim, Stephen F. Scherock

Traditional prediction schemes often assume an input signal with a fixed (ARMA) model. The performance of such schemes degrades as the input signal deviates from the model. In particular, a fixed linear predictor performs poorly when the characteristics of the signal vary with time (as would the output of a frequency-hopping transmitter). This research investigates the designs of those filters which have a negative group delay characteristic over a desired frequency range. Since negative group delay corresponds to (positive) time advance, one might initially think that all filters of this type were noncausal and therefore unrealizable in real time. In fact, causal filters with negative group delay can be realized. Such filters could provide a new framework for predicting a

signal that is only known to lie within a certain band.

Currently, the scope of the research is restricted to discrete time FIR filters. Several design algorithms have been successfully implemented, and new error measures have been developed to judge the quality of the filters. The current algorithms are fast and direct (not iterative), but are impractical for large filters. Future work will explore new algorithms, and algorithms for FIR filters.

1.15 Signal Prediction Based on Nonlinear and Chaotic System Models

Sponsors

Lockheed Sanders, Inc.
U.S. Navy - Office of Naval Research
Grant N00014-89-J-1489

Project Staff

Professor Alan V. Oppenheim, Gregory W. Wornell, Andrew C. Singer

A standard assumption made in signal processing is that an observed signal is the product of a linear, time-invariant system. Signals of this class have a rich history for which the mathematics is tractable, and many techniques have been explored. Based on this assumption, many linear methods of signal prediction and smoothing are used in applications, such as speech and image coding, and forecasting. However, many signals of interest arise from physical processes that are inherently nonlinear. Consequently, nonlinear dynamical system models may be much better suited to these phenomena.

Recently, the subject of nonlinear dynamics in general and chaotic dynamics in particular has attracted increasing attention in the research literature. A number of new paradigms for signal modeling have emerged. While initial attention had focused on the study of the richness of behavior and properties of these systems, there is now considerable interest in problems associated with modeling data based on this class of systems and in addressing problems of signal processing for these systems. We are presently considering a number of problems based on the preliminary work of Farmer, Casdagli, Abarbanel, and others which address problems of prediction and smoothing based on a state space framework.

1.16 Signal Enhancement Using Single and Multisensor Measurements

Sponsors

Lockheed Sanders, Inc.
U.S. Navy - Office of Naval Research
Grants N00014-89-J-1489 and N00014-90-J-1109

Project Staff

Professor Alan V. Oppenheim, Dr. Meir Feder, Dr. Ehud Weinstein

A time-domain approach to signal enhancement based on single and multiple sensor measurements is developed. The procedure is based on the iterative Estimate-Maximize (EM) algorithm for maximum likelihood estimation. On each iteration, in the M step of the algorithm, parameter values are estimated based on the signal estimates obtained in the E step of the prior iteration. The E step is then applied using these parameter estimates to obtain a refined estimate of the signal. In our formulation, the E step is implemented in the time domain using a Kalman smoother. This enables us to avoid many of the computational and conceptual difficulties with prior frequency domain formulations. Furthermore, the time domain formulation leads naturally to a time-adaptive algorithm by replacing the Kalman smoother with a Kalman filter. In place of successive iterations on each data block, the algorithm proceeds sequentially through the data with exponential weighting applied to permit the algorithm to adapt to changes in the structure of the data. A particularly efficient implementation of the time-adaptive algorithm is formulated for both the single- and the two-sensor cases by exploiting the structure of the Kalman filtering equations. In addition, an approach to avoiding matrix inversions in the modified M step is proposed based on gradient search techniques.

Publication

Weinstein, E., A.V. Oppenheim, and M. Feder. *Signal Ehancement Using Single and Multi-Sensor Measurements*. RLE TR-560, Res. Lab. of Electron., MIT, 1990.

1.17 Synthesis, Analysis, and Processing of Fractal Signals

Sponsors

Canada, Natural Science and Engineering Research Council Scholarship
U.S. Air Force - Office of Scientific Research Grant AFOSR-91-0034
U.S. Navy - Office of Naval Research Grant N00014-89-J-1489

Project Staff

Professor Alan V. Oppenheim, Gregory W. Wornell

Recently, we have developed a novel and highly useful framework for addressing a broad class of signal processing problems involving fractal signals and systems. This framework is based upon an efficient wavelet-based expansion for the 1/f family of fractal processes in terms of uncorrelated coefficients.[14] Since 1/f processes are inherently well-suited for modeling a wide range of natural and manmade phenomena, there are many potentially important applications of this work.

Subsequent work has focused on exploiting this framework in the solution of some rather general signal processing problems involving these processes. For example, in Wornell and Oppenheim,[15] we consider the problem of parameter estimation and signal estimation (smoothing) for fractal signals embedded in white noise. The whitening and discretization achieved by the wavelet representation leads to a highly tractable analysis and computationally efficient algorithms.

Continuing this work, we have been studying the related problems of prediction and interpolation of fractal processes. We have also considered the extension of this work to more general classes of fractal processes.

Additional work has addressed a number of general detection problems involving signals in fractal backgrounds. Here we consider both coherent and incoherent detection scenarios. This work has provided a foundation for our more recent work in developing signaling strategies for communication over fractal channels[16] and in designing signals for low probability of detection in fractal backgrounds.

1.18 Active Noise Cancellation

Sponsors

Texas Instruments, Inc.
U.S. Navy - Office of Naval Research Grant N00014-89-J-1489

Project Staff

Professor Alan V. Oppenheim, Kambiz C. Zangi

Unwanted acoustic noise is a by-product of many industrial processes and systems. With active noise cancellation (ANC), one introduces secondary noise sources to generate an acoustic field that interferes destructively with the unwanted noise to eliminate it. Examples of unwanted noise include: machinery, aircraft cabin, and fan noise.

Traditional active noise cancellation systems assume that the statistical characteristic of the primary noise is known *a priori*. Furthermore, almost all of the existing systems use two microphones, and, as a result, suffer from an acoustic feedback between the cancelling speaker and the input microphone.[17]

We are currently studying an active noise cancellation system which uses only one microphone and therefore has no feedback problem. In addition, we are looking at various algorithms to adapt the system to the time-variations of the primary noise source. To this end, we have been able to use the estimate maximizing algorithm to find the maximum likelihood estimate of the time-varying noise statistics.[18]

---

[14] G.W. Wornell, "A Karhunen-Loeve-like Expansion for 1/f Processes via Wavelets," *IEEE Trans. Info. Theory* IT-36: 859-861 (1990).

[15] G.W. Wornell and A.V. Oppenheim, "Estimation of Fractal Signals from Noisy Measurements Using Wavelets," *IEEE Trans. SP*, forthcoming.

[16] G.W. Wornell, "Communication over Fractal Channels," *Proc. ICASSP* (1991), forthcoming.

[17] L.J. Eriksson, M.C. Allie, and C.D. Bremigan, "Active Noise Control Using Adaptive Digital Signal Processing," *Proc. ICASSP* 1988, pp. 2594-2597.

[18] M. Feder, A. Oppenheim, and E. Weinstein, "Methods for Noise Cancellation Based on the EM Algorithm," *Proc. ICASSP* 1987, pp. 201-204.

A problem of immediate interest is to develop similar algorithms with faster rates of convergence. We are also working on algorithms with better computational efficiency.[19]

Professor Alan V. Oppenheim with his graduate students. From left, Daniel T. Cobra, Professor Oppenheim, Tae H. Joo, Michele M. Covell, and Gregory W. Wornell.

[19] E. Weinstein, A. Oppenheim, and M. Feder, *Signal Enhancement Using Single and Multi-Sensor Measurements*, RLE TR-560. Res. Lab. of Electron., MIT, 1990.

Chapter 2. Speech Processing Research Program

Academic and Research Staff

Professor Jae S. Lim, Giampiero Sciutto

Graduate Students

Michael S. Brandstein, Shiufun Cheung, John C. Hardwick, Katherine S. Wang, Chang Dong Yoo

Technical and Support Staff

Debra L. Harring, Cynthia LeBlanc

2.1 Introduction

The objective of this research program is to develop methods for solving important speech communication problems. Current research topics in progress include development of a new speech model and algorithms to (1) enhance speech degraded by background noise and (2) modify the time scale of speech. We are also investigating methods for displaying spectrograms more efficiently.

2.2 Development of a 1.5 Kbps Speech Vocoder

Sponsor

National Science Foundation Fellowship

Project Staff

Michael S. Brandstein, Professor Jae S. Lim

The recently developed Multi-Band Excitation Speech Model has been shown to accurately reproduce a wide range of speech signals without many of the limitations inherent in existing speech model based systems.[1] The robustness of this model makes it particularly applicable to low bit rate, high quality speech vocoders. Griffin and Lim first described a 9.6 Kbps speech coder based on this model.[2] Later work resulted in a 4.8 Kbps speech coding system.[3] Both of these systems are capable of high quality speech reproduction in both low and high SNR conditions.

The purpose of this research was to explore methods for using the new speech model at the 1.5 Kbps rate. Results indicated that a substantial amount of redundancy exists between the model parameters. Research focused on exploiting redundancies to quantize these parameters more efficiently. Attempts were also made to simplify the existing model without significantly reducing speech quality.

This research was completed in June 1990.

2.3 A New Method for Representing Speech Spectrograms

Sponsors

National Science Foundation
Grant MIP 87-14969
U.S. Navy - Office of Naval Research
Contract N00014-89-J-1489

Project Staff

Shiufun Cheung, Professor Jae S. Lim

The spectrogram, which is a two-dimensional time-frequency display of a one-dimensional signal, is used extensively in speech research. Existing spectrograms are generally divided into

---

[1] D.W. Griffin and J.S. Lim, "A New Model-Based Speech Analysis/Synthesis System," *IEEE International Conference on Acoustic, Speech and Signal Processing,* Tampa, Florida, March 26-29, 1985, pp. 513-516.

[2] D.W. Griffin and J.S. Lim, "A High Quality 9.6 Kbps Speech Coding System," *IEEE International Conference on Acoustic, Speech and Signal Processing,* Tokyo, Japan, April 8-11, 1986.

[3] J.C. Hardwick, "A 4.8 Kbps Multi-Band Excitation Speech Coder," S.M. thesis, Dept. of Electr. Eng. and Comput. Sci., MIT, 1988.

two types, wideband spectrograms and narrowband spectrograms, according to the bandwidth of the analysis filters used to generate them. Due to the different characteristics of the two types of spectrograms, they are employed for different purposes. The wideband spectrogram is valued for its quick temporal response and is used for word boundary location and formant tracking. On the other hand, the narrowband spectrogram, with its high frequency resolution, is primarily used for measuring the pitch frequency.

Various attempts have been made to improve the spectrographic display. Past efforts include the development of neural spectrograms which use critical bandwidth analysis filters in the imitation of the human auditory system and the development of better time-frequency distributions such as the Wigner distribution.

In this research, we propose a different approach. The spectrogram is viewed as a two-dimensional digital image instead of a transformed one-dimensional speech signal. Image processing techniques are used to create an improved spectrogram which preserves the desirable visual features of the wideband and narrowband spectrograms. This transforms a speech processing problem into an image processing problem.

At this point, we have developed a simple but effective method for combining the two types of spectrograms. In this method, each pixel of the combined spectrogram is the geometric mean of corresponding pixel values of the two original spectrograms. Apart from the geometric-mean merge, we are also experimenting with the use of color and other merge algorithms. Initial results are promising.

2.4 A Dual Excitation Speech Model

Sponsors

U.S. Air Force - Electronic Systems Division
Contract F19628-89-K-0041
U.S. Navy - Office of Naval Research
Contract N00014-89-J-1489

Project Staff

John C. Hardwick, Professor Jae S. Lim

One class of speech analysis/synthesis system (vocoder) which has been extensively studied and used in practice is based on an underlying model of speech. Even though traditional vocoders have been quite successful in synthesizing intelligible speech, they have not been successful in synthesizing high quality speech. The Multi-Band Excitation (MBE) speech model, introduced by Griffin, improves the quality of vocoder speech through the use of a series of frequency dependent voiced/unvoiced decisions. The MBE speech model, however, still results in a loss of quality when compared with the original speech. This degradation is caused in part by the voiced/unvoiced decision process. A large number of frequency regions contain a substantial amount of both voiced and unvoiced energy. If a region of this type is declared voiced, then a tonal or hollow quality is added to the synthesized speech. Similarly, if the region is declared unvoiced, then additional noise occurs in the synthesized speech. As the signal-to-noise ratio decreases, the classification of speech as either voiced or unvoiced becomes more difficult, and, consequently, the degradation is increased.

A new speech model has been proposed in response to the aforementioned problems. This model is referred to as the Dual Excitation (DE) speech model, due to its dual excitation and filter structure. The DE speech model is a generalization of most previous speech models, and, with the proper selection of the model parameters, it reduces to either the MBE speech model or to a variety of more traditional speech models.

Current research is examining the use of this speech model for speech enhancement, time scale modification and bandwidth compression. Additional areas of study include further refinements to the model and improvements in the estimation algorithms.

2.5 Speech Enhancement Techniques for the Dual Excitation Vocoder Model

Sponsors

National Science Foundation Fellowship
U.S. Air Force - Electronic Systems Division
Contract F19628-89-K-0041
U.S. Navy - Office of Naval Research
Contract N00014-89-J-1489

Project Staff

Katherine S. Wang, Professor Jae S. Lim

We explored some conventional methods for speech enhancement in the presence of additive

white noise[4] in a new framework where the voiced estimation provided by the MBE model[5] allowed us to perform noise reduction separately on voiced and unvoiced components.

Conventional methods which take advantage of the periodic structure of voiced speech include comb filtering and adaptive noise cancellation. A technique based on short-time spectral amplitude estimation obtains the minimum mean-square-error, linear estimator of the speech signal by non-causal Wiener filtering, which we could approximate by an adaptive Wiener filtering technique. Speech enhancement can also be model based, for example, by using classical estimation theory applied to an all pole model of speech. We drew from some of these conventional techniques to create a speech enhancement system customized to the traits of the Multi-Band Excitation (MBE) Vocoder and, subsequently, to the Dual Excitation Model.[6] The noiselike characteristics of unvoiced speech and the harmonic structure of voiced speech suggest that noise reduction can most effectively be done on speech that has been separated into the two components, rather than attempting to categorize the frequency band as purely voiced and unvoiced.

The recently developed Multi-Band Excitation (MBE) Speech Model has been shown to accurately reproduce a wide range of speech signals without many of the limitations inherent in existing speech model based systems.

This research was completed in August 1990.

2.6 Nonlinear and Statistical Approach to Speech Synthesis

Sponsor

U.S. Navy - Office of Naval Research
Contract N00014-89-J-1489

Project Staff

Chang Dong Yoo, Professor Jae S. Lim

Numerous speech models have been proposed, and most of these models have been incorporated with some variation into the basic speech production model where a linear time invariant system is excited by periodic or random pulses depending on voiced/unvoiced decision. But studies have indicated that speech production is a nonlinear process and that for some sounds such as the voiced fricatives, it is difficult to make a hard voiced/unvoiced decision. Discrepancy between actual speech production and production from the linear model system might stem from the Teager paradigm, considering the vocal tract operation from the air flow point of view.

For higher quality speech synthesis, we need to derive either an enhanced speech production model incorporating more of the nonlinear effects of speech production or a speech synthesis method totally divorced from the mechanism of speech production such as the hidden Mardov modeling of speech production.

In this research, various nonlinear and statistical aspects of speech characteristics are being studied to derive a more efficient method of speech analysis/synthesis.

---

[4] J.S. Lim and A.V. Oppenheim, "Enhancement and Bandwidth Compression of Noisy Speech," *IEEE Proc.* 67 (12): 1586-1604 (1979); J.S. Lim, ed. *Speech Enhancement* (Englewood Cliffs, N.J.: Prentice Hall, 1983).

[5] D.W. Griffin and J.S. Lim, "A New Model-Based Speech Analysis/Synthesis System," *IEEE International Conference on Acoustics, Speech and Signal Processing,* Tampa, Florida, March 26-29, 1985, pp. 513-516.

[6] John Hardwick, Ph.D. research, MIT.

Professor Jae S. Lim (standing) and graduate student Matthew M. Bace demonstrate a new method that was recently developed to reduce channel degradation in the National Television Standards Committee system.

Chapter 3. Advanced Television Research Program

Academic and Research Staff

Professor Jae S. Lim, Professor William F. Schreiber

Graduate Students

John G. Apostolopoulos, Babak Ayazifar, Matthew M. Bace, David M. Baylon, Warren H. Chou, Ibrahim A. Hajjahmad, David D. Kuo, Peter A. Monta, Aradhana Narula, Julien J. Nicolas, Julien Piot, Ashok C. Popat, Paul X. Shen, Lon E. Sunshine, Adam S. Tom

Technical and Support Staff

Debra L. Harring, Cynthia LeBlanc

3.1 Introduction

The present television system was designed nearly 35 years ago. Since then, there have been significant developments in technology which are highly relevant to the television industries. For example, advances in the very large scale integration (VLSI) technology and signal processing theories make it feasible to incorporate frame-store memory and sophisticated signal processing capabilities in a television receiver at a reasonable cost. To exploit this new techology in developing future television systems, Japan and Europe established large laboratories funded by government or industry-wide consortia. The lack of this type of organization in the United States was considered detrimental to the broadcasting and equipment manufacturing industries, and, in 1983, the Advanced Television Research Program (ATRP) was established at MIT by a consortium of U.S. companies.

Currently, consortium members include ABC, Ampex, General Instrument, Kodak, Motorola, NBC, NBC Affiliates, PBS, Tektronix, and Zenith.

The major objectives of the ATRP are:

1. To develop the theoretical and empirical basis for the improvement of existing television systems, as well as the design of future television systems;
2. To educate students through television-related research and development and to motovate them to undertake careers in television-related industries;
3. To facilitate continuing education of scientists and engineers already working in the industry;
4. To establish a resource center to which problems and proposals can be brought for discussion and detailed study; and
5. To transfer the technology developed from this program to the sponsoring companies.

The research areas of the program include (1) the design of channel-compatible advanced television (ATV) system, (2) receiver-compatible ATV system and digital ATV system, and (3) development of transcoding methods. Significant advances have already been made in some of these research areas. A channel-compatible ATV system has been designed and is scheduled to be tested in 1991 by the FCC for possible adoption as the U.S. HDTV standard for terrestrial broadcasting.

3.2 ATRP Facilities

The ATRP Laboratory's computer facilities are currently based on a network of seven Sun-4 workstations. There are approximately 13.8 GB of disk space, distributed among the various machines. Attached to one Sun-4 is a DATARAM Wide Word Storage system with 320 MB of RAM. The high speed interface to the Wide Word system drives a three-dimensional interpolator that was constructed by graduate students in the Lab. The three-dimensional interpolator has the ability to perform separable spatio-temporal interpolation. The output of the interpolator feeds a custom-built data concentrator which drives a Sony 2k by 2k monitor, running at 60 frames/second.

In addition to displaying high resolution real time sequences, the ATRP facilities include a 512 x 512 Rastertek frame buffer and an NTSC encoder. The Rastertek distributes static images to nearly a dozen monitors around the Lab and offices. The NTSC encoder allows image sequences to be recorded onto either three-quarter inch or VHS videotape. For hard copy output, the Lab uses an Autokon 8400 graphics printer for generating high resolution black and white images directly onto photographic paper.

Other peripherals include an Exabyte 8 mm tape drive, capable of storing 2.3 GB on an 8 mm cassette, a 16-bit digital audio interface with two channels and sampling rates to 48 kHz per channel, and an "audio workstation" with power amplifier, speakers, CD player, tape deck, etc.

For preparing presentations, the ATRP facilities also include a Macintosh SE30 microcomputer, a Mac IIx, and an Apple LaserWriter.

To support the growing computation needs of the group, several additional Sun-4 workstations will be installed in the near future. They will have 24-bit color displays, local disk storage, and DSP boards to assist with computation-intensive image processing. Some of the existing machines may also be supplemented with such DSP boards.

A fast network (FDDI) is under consideration to augment the current 10 Mbps Ethernet. The new network would enable much faster data transfer to display devices such as the Dataram and support large NFS transfers more easily.

3.3 Coding of the Motion Compensated Residual for an All-Digital HDTV System

Sponsor

Advanced Television Research Program

Project Staff

John Apostolopoulos, Professor Jae S. Lim

An All-Digital High Definition Television system is being developed at MIT to transmit higher quality video and audio information in the same channel bandwidth as today's conventional television. To achieve this goal, the system must eliminate redundant information which exists because of the high correlation inherent to video and audio. For normal television broadcasts, the image from one frame to the next is very similar. In order to reduce this redundancy in the temporal direction, we implement a motion estimation/motion compensation algorithm in the transmitter and the receiver. This algorithm generates motion vectors which are used by the receiver to predict the next frame from the current frame. The transmitter will transmit these motion vectors as well as the error between the predicted and the actual next frame. The receiver will apply these motion vectors to create the predicted next frame, and add to it the prediction error to produce the next displayed frame. The prediction error, or residual, as it is commonly called, also contains much redundancy which can be reduced by further coding. The purpose of this work is to find the optimal method to code this motion compensated residual to achieve the "best" image quality at the receiver.

Methods for coding the residual that will be analyzed include the blocked DCT and various QMF subband filtering schemes. The primary performance criteria for comparing the various methods are (1) visual image quality and (2) the mean square error between the image at the receiver and the original image. Other issues to be considered include the effects of energy compaction of the residual, quantization of the coefficients and pixel-adaptive selection of the transmitted coefficients.

3.4 Motion-Compensated Vertico-Temporal and Spatial Interpolation

Sponsor

Advanced Television Research Program

Project Staff

Babak Ayazifar, Professor Jae S. Lim

In this project, we examine the application of a motion-estimation algorithm to the field and line-rate conversion issues which exist in the process of converting video signals from the European to the Amercian standards and vice-versa.

Topics explored are simultaneous temporal and vertical interpolation of image sequences and strictly spatial interpolation of individual frames (e.g., line and column doubling) using a novel generalized form of the well known "spatio-temporal" constraint equation-based motion estimation algorithms.

3.5 Receiver-Compatible Adaptive Modulation for Television

Sponsors

National Science Foundation
Grant MIP 87-14969
National Science Foundation Fellowship

Project Staff

Matthew M. Bace, Professor Jae S. Lim

There have been numerous proposals for developing methods to improve upon the quality of the current NTSC television picture. Most of these proposals have concentrated on methods that increase either the spatial or the temporal resolution of the television picture. While these proposals promise significant improvements in picture quality, the fact remains that until an effective scheme for combatting channel noise has been introduced, these improvements can not be fully realized. Degradations such as random noise ("snow"), echo, and intersymbol interference (channel crosstalk) are still the greatest barriers to high-quality television.

This research developed a receiver-compatible scheme to reduce the effects of channel imperfections on the received television picture. In particular, the method of adaptive modulation was employed in an attempt to make more efficient use of the currently underutilized bandwidth and dynamic range of the NTSC signal. By concentrating more power in the higher spatial frequencies and using digital modulation to send additional information in the vertical and horizontal blanking periods, the existing television signal can be altered so that it is more robust in the presence of high frequency disturbances. Furthermore, it is possible to adjust the parameters of this scheme so that the modulated signal may be received intelligibly even on a standard receiver (although an improved receiver will be required to realize the full benefits of adaptive modulation).

Before we concluded which adaptive modulation scheme was optimal, many details were considered. Among the parameters which may be varied were: the control over the adaptation and compression factors; the form of the input low-pass filters; the interpolation scheme to be used at both the transmitter and receiver; and the encoding of the digital data. These parameters were adjusted to optimize the performance of the modulation scheme with repect to two fundamental performance criteria: the degree to which the channel degradations are removed when the signal is received on an improved receiver, and the degree to which the signal is distorted when received on a standard receiver.

This research was completed in June 1990.

3.6 Adaptive Amplitude Modulation for Transform Coefficients

Sponsor

Advanced Television Research Program

Project Staff

David M. Baylon, Professor Jae S. Lim

Adaptive amplitude modulation/demodulation (AM/DM) has been shown to be an effective noise reduction technique. However, the adaptation factors must be transmitted as side information. It is important to minimize the required side information in systems that have limited transmission bandwidth. This research focused on representing the adaptation factors by a few parameters exploiting properties of the signal in the transform (frequency) domain.

Previous investigations of adaptive amplitude modulation have been based upon time domain methods. Specifically, in two-dimensional subband filtering, an image is decomposed into a set of spatial frequency subbands that are adaptively modulated. Similarities among subbands are exploited in reducing the number of adaptation factors to about one-sixth the number of data points. Nevertheless, further reduction in the amount of side information is desirable.

This research took a different approach to reducing the amount of side information by adaptively modulating the transform of the signal. Transform coefficients of typical images tend to decrease in energy away from DC. By exploiting this property, the transform coefficients and the adaptation factors can be modeled with a few parameters (for example, an exponential model). Consequently, the amount of side information can be significantly reduced compared with the amount required by previous approaches.

Research focused on determining the best way to model the adaptation factors with a few parameters in systems that are bandwidth and peak power constrained. Performance criteria of the various AM/DM schemes included signal-to-noise ratios and overall image quality. Among the many ways of obtaining the coefficients (such as using subband filtering or the lapped orthogonal transformation (LOT)), the discrete cosine transformation (DCT) was used because of its many desirable properties, including coefficient uncorrelation, energy compaction, and efficient computation using the fast Fourier transform (FFT). Issues that were addressed included choosing the appropriate block size and determining the best AM/DM

method with an adaptive coefficient selection scheme (such as used in image coding systems). Both two-dimensional images and three-dimensional video were studied.

This research was completed in June 1990.

3.7 Transform Coding for High Definition Television

Sponsor

Advanced Television Research Program

Project Staff

Ibrahim A. Hajjahmad, Professor Jae S. Lim

Field of image coding is usefully applied in many areas. For instance, one of the most prominent of these areas is compressing channel bandwidth for image transmission systems; this is helpful for applications in HDTV, video conferencing, and facsimile. Another important area is reducing storage requirements for tasks such as digital video recording.

Image coding can be divided into a number of classes, depending on which aspects of the image are being coded. In the transform image coder,[1] an image is transformed from the spatial domain to a different domain more suitable for coding. Then, the transform coefficients are quantized and coded. When received, the coded coefficients are decoded and then inverse transformed to obtain the reconstructed image.

To perform transform coding, one must select an appropriate transform. In particular, the Discrete Cosine Transform (DCT) is very useful because of two important properties.[2] The first is the energy compaction property, which states that a large amount of energy is concentrated in a small fraction of the transform coefficients (typically the low frequency components). Because of this property, only a small fraction of the transform coefficients need to be coded, while little is sacrificed in terms of quality and intelligibility of the coded images. The second property is the correlation reduction property in which the high correlation among pixels intensities in the spatial domain is reduced. In effect, the redundant spatial information is not coded.

Current research is investigating the use of the DCT for bandwidth compression. In addition, new adaptive techniques for quantization and bit allocation are being studied to further reduce the bit rate without sacrificing image quality or intelligibility.

3.8 Adaptive Spatio-temporal Filtering

Sponsors

Advanced Television Research Program
Kodak Fellowship

Project Staff

David D. Kuo, Professor Jae S. Lim

The current NTSC television standard specifies a frame rate of 60 fields/second throughout the transmission chain. This frame rate was chosen to minimize the visibility of annoying flicker at the display. However, to eliminate flicker, only the display must operate at the high frame rate; there is no need to constrain the channel to 60 frames/second. It is widely accepted that there exists a great deal of correlation between neighboring frames of an image sequence. As such, a high frame rate through the channel seems bandwidth inefficient.

One way to take advantage of the correlation between neighboring frames is to transmit only a temporally subsampled version of the original sequence and to rely on the receiver to recover the inbetween frames. However, prior work along these lines suggested that the receiver must have more information than simply the subsampled frames. This research focused on using motion vectors as part of the image sequence representation.

There were three main areas of focus in this research. First, it considered the use of adaptive spatio-temporal prefiltering as a means of reducing the aliasing that arises from temporal subsampling. Secondly, the characteristics of the motion vectors were explored. Finally, our research considered how to use multiple frames of data to improve the motion estimation process.

This research was completed in June 1990.

---

[1] J.S. Lim, *Two-Dimensional Signal and Image Processing* (Englewood Cliffs, N.J.: Prentice Hall, 1990); R.J. Clarke, *Transform Coding of Images* (London: Academic Press, 1985).

[2] N. Ahmed, T. Natarajan, and K.R. Rao, "Discrete Cosine Transform," *IEEE Trans. Comput.* C-23: 90-93 (1974).

3.9 Signal Processing for Advanced Television Systems

Sponsor

Advanced Television Research Program

Project Staff

Peter A. Monta, Professor Jae S. Lim

Digital signal processing (DSP) will play a large role in future advanced television systems. Source coding to reduce the channel capacity necessary to transmit a television signal and display processing such as spatial and temporal interpolation are its major applications. Present-day television standards will also benefit significantly from signal processing designed to remove transmission and display artifacts. This research will focus on algorithms and signal models designed to enhance current standards (both compatibly and with some degree of cooperative processing at both transmitter and receiver) and to improve proposed HDTV systems.

Given a receiver with a high-quality display and significant computation and memory, the American television standard, NTSC, can be improved in a number of ways. Interlace artifacts, such as line visibility and flicker, can be removed by converting the signal to a progressive format prior to display. Color cross-effects can be greatly reduced with accurate color demodulators implemented with DSP. If the original source material is film, an advanced receiver can recover a much improved image by exploiting structure in the film-NTSC transcoding process; such an algorithm has been implemented and tested.

Similar ideas apply to HDTV systems. For example, film will be a major source material well into the next century, and HDTV source coders should recognize film as a special case, trading off the inherent reduced temporal bandwidth for better spatial resolution. The MIT Channel Compatible (MIT-CC) HDTV system will adapt to film in this way.

3.10 MIT Channel Compatible System

Sponsor

Advanced Television Research Program

Project Staff

Julien J. Nicolas, Professor Jae S. Lim

The MIT Channel Compatible system was developed by ATRP over the course of the last three years as a new high-efficiency alternative to existing television systems and as a candidate for the FCC/ATTC competition. Key features of this system include (1) decomposition of the signal into a set of spatio-temporal frequency subbands, (2) a hybrid analog/digital representation of the signal for both source and channel coding; and (3) use of a technique called adaptive modulation to reduce the effects of the channel noise and other impairments in the areas where they are most noticeable.

Recent investigations have been aimed at finding efficient ways of representing the hybrid information and especially at reducing the amount of digital data required by this system. In the MIT-CC system, digital data is used to represent the lowest spatio-temporal subbands to code the location of the largest subband coefficients and the adaptive modulation coefficients. New methods to reduce selection information are being studied currently. These methods will be used in conjunction with effective adaptive modulation techniques previously developed and a hybrid digital/analog transmission scheme to meet the bandwidth constraints for terrestrial broadcasting and to optimize the information transfer in a large portion of the service area.

Future work will involve comparing the spatio-temporal subband decomposition approach with techniques based on coding the motion-compensated prediction errors, as is commonly done in digital systems. This research is aimed at gaining a better understanding of the advantages and limitations of the different types of signal representations pertaining to motion picture coding.

3.11 Subband Coding for Channel-Compatible Transmission Of High-Definition Television

Sponsor

Advanced Television Research Program

Project Staff

Ashok C. Popat, Professor William F. Schreiber

In recent years, subband coding has received considerable attention from the image coding community as a simple and effective means of efficiently

representing image and image-sequence data.[3] A three-dimensional (horizontal, verticle, and temporal) subband coding technique has been proposed by the Advanced Television Research Program at MIT for application to a 6-MHz channel-compatible high-definition television (HDTV) distribution system.[4] Although preliminary "proof-of-principal" tests have demonstrated that the technique is effective, these tests have also shown that considerable improvement could be achieved by adjusting various parameters in the system (such as the degree of data compression; the number of subbands in each dimension; the type and length of the subband analysis/synthesis filters; and the means of selecting subband pixels to be retained and transmitted). A high degree of interdependency among many of the system parameters has been observed; this interdependency has complicated the process of identifying the particular combination of parameters that is best suited to the present application. In particular, the strong interdependency seems to eliminate the possibility of finding the best choice for each parameter separately. A major objective of our research is to search through the vast parameters separately by judicious choice of parameters for computer simulation and by objective and subjective evaluation of the simulation results.

One of the more critical set of system parameters is the set of coefficients used in the subband analysis/synthesis filter banks. A novel approach to designing such filters based on time-domain numerical search has been developed; the approach is fairly general and has resulted in critically-sampled filter banks that are extremely well-suited to image coding applications.[5]

A seemingly basic principle of image subband/transform coding has emerged from the present study. In particular, it is evident that the best choice for the length of the analysis/synthesis filters depends only slightly on the number of subbands and depends more strongly on the spatial extent over which the image can be well-modeled as stationary. Thus, the nonstationarity of images inevitably leads to an uncertainty-principle based tradeoff in the selection of the number of subbands and lengths of filters.

We found that it is extremely important that the allocation of channel capacity was allowed to be spatially varying; that is, it is essential to be able to increase the number and/or fidelity of samples used in representing action regions of the image at the expense of more poorly representing inactive regions. A fixed-rate, practicable means of exploiting this principle was devised.

This research was completed in March 1990.

3.12 Hybrid Analog/Digital Representation of Analog Signals

Sponsor

Advanced Television Research Program

Project Staff

Lon E. Sunshine, Professor Jae S. Lim

Transform coding has been shown to be an effective way to represent images, allowing for a significant amount of data-compression while still enabling high-quality reproduction of the original picture. One result of the transform coding of images is that at a given signal-to-noise ratio, the (spatially) low-frequency components are much more sensitive to additive noise than the high-frequency components.

In the MIT-CC television system, we must employ a noise reduction technique which is sufficient to eliminate the effects of additive noise in the low frequencies. We have chosen to do this is by representing these analog (continuous-amplitude) coefficients by a hybrid analog/digital signal. This representation consists of a new analog value plus a discrete-valued piece of side information. The advantage of using this hybrid format is that we can reduce the noise added to a particular coefficient by at least 6 dB for each bit used in the side information.

---

[3] J.W. Woods and S.D. Oneil, "Subband Coding of Images," *IEEE Trans. ASSP* 34: 1278-1288 (1986); H. Gharavy and A. Tabatabai, "Subband Coding of Monochrome and Color Images," *IEEE Trans. Circuits Syst.* 35: 207-214 (1988).

[4] W.F. Schreiber, et al., *Channel-Compatible 6-MHzHDTV Distribution Systems,* CIPG Technical Report ATRP-T-79, MIT, January 1988.

[5] A.C. Popat, "Time-Domain Numerical Design of Critically Sampled Filter Banks," presentation viewgraphs, Advanced Television Research Program, MIT, October 1988; A.C. Popat, "A Note of QMF Design," unpublished memo, Advanced Television Research Program, MIT, December 1988.

This research considers the task of determining the "best" hybrid representation for an image. Here, "best" is characterized by a tradeoff between sufficient noise reduction, simplicity in implementation, and minimization of necessary side information.

3.13 Channel Equalization and Interference Reduction Using Adaptive Amplitude Modulation and Scrambling

Sponsor

Advanced Television Research Program

Project Staff

Adam S. Tom, Professor William F. Schreiber

Terrestrial broadcast channels and cable channels are imperfect. Random noise, multipath (ghosts), adjacent and co-channel interference, and an imperfect frequency response degrade these transmission channels so that the quality of the signal at the receiver is significantly below that at the transmitter. In order to appreciate the increased resolution of high definition images, a means of reducing the degradation due to channel defects needs to be employed. Conventional methods of channel equalization use adaptive filters. These methods are limited by convergence time, length of filters, and computational complexity. We are doing research on a new method of channel equalization and interference reduction based upon the ideas of adaptive amplitude modulation and pseudo-random scanning (scrambling). This new method is not bound by the above limitations; however, it is limited by the energy of the channel degradations produced.

Adaptive modulation is a noise reduction technique. It is applied only to the high frequency components of the signal. Prior to transmission, a set of adaptation factors are multiplied with the input signal. The net effect of this is to raise the amplitude of the signal according to the strength of the signal. At the receiver, the signal is divided by these same adaptation factors. In this manner, the random noise added in the channel is reduced by a factor equal to the adaptation factor. The noise is reduced more in the blank areas relative to the busy areas.

Scrambling is a technique to reduce the effects of multipath, adjacent and co-channel interference, and an imperfect frequency response. Prior to transmission, the input sequence is pseudo-randomly scanned; thus, in essence scrambling the signal so that it appears as random noise. This scrambled signal is transmitted through the channel, and the reverse of the scrambling is performed at the receiver. Consequently, any degradations in the channel are themselves scrambled at the receiver and, thus, have the appearance of pseudo-random noise in the decoded signal while the desired signal remains sharp and in full bandwidth.

Since the resultant signal in the receiver now has a noisy appearance, we apply the noise reduction technique of adaptive modulation to the input signal. In our scheme we first apply adaptive modulation to the input signal and then scrambling. The coded signal is transmitted through the imperfect channel and decoded at the receiver. The decoding consists of doing the reverse of the scrambling and then the reverse of the adaptive modulation. Scrambling causes any channel degradations to have a noiselike appearance, and Adaptive Modulation reduces the appearance of this pseudo-random noise. In this manner the degradations to a transmitted signal are reduced, and the channel is equalized.

This research was completed in June 1990.

Professor Donald E. Troxel has made significant contributions to image processing research in RLE. His primary focus is now in the area of computer-aided fabrication of integrated circuits.

Chapter 4. Computer-Aided Fabrication System Structure

Academic and Research Staff

Professor Donald E. Troxel, Michael B. McIlrath, Wilberto Martinez

Graduate Students

Michael L. Heytens, Abbas Kashani, Weng-Yew Ko

Technical and Support Staff

Francis M. Doughty

4.1 CAFE—The MIT Computer Aided Fabrication Environment

Sponsor

Defense Advanced Research Projects Agency
Contract MDA 972 88-K-0008

4.1.1 Research Goals and Objectives

CAFE (Computer-Aided Fabrication Environment) is a software system being developed at MIT for use in the fabrication of integrated circuits and microstructures. CAFE is distinguished by its use in all phases of process design, development, planning, and manufacturing of integrated circuit wafers. While still being actively developed, CAFE presently provides day-to-day support to research and production facilities at MIT with both flexible and standard product capabilities. CAFE provides a platform for work in several active research areas, including "technology" (process and device) computer aided design (TCAD), process modeling, manufacturing quality control, and scheduling.

4.1.2 Architecture

The CAFE architecture is a computer integrated manufacturing (CIM) framework for the deployment and integration of IC circuit and process design and manufacturing software. The CAFE infrastructure consists of supporting components such as the operating system or database that are independent of the application domain (IC fabrication). The integration architecture includes the conceptual schema and models used to represent the IC manufacturing domain in CAFE, and the user and programmatic interfaces to the various applications. Two important CAFE applications relate process simulation and actual wafer fabrication to the very same process flow representation.

4.1.3 Infrastructure

An early and deliberate design decision was to use an object oriented data model, including the development of an explicit schema to organize the data storage. A high degree of modularity was realized because we have developed a schema which consists of small groups of related objects. Our database schema is based on GESTALT, an object oriented, extensible data model. GESTALT is a layer of abstraction which provides a mapping of user defined objects onto existing database systems (e.g., a relational DBMS) and shields application programs from the details of the underlying database. The programming interface, supported for C and Common Lisp, includes a set of operators for accessing and manipulating persistent data.

Ease of use of any large software system requires a coherent user interface. We have developed FABFORM, a highly programmable and flexible textual interface generator supporting an event model of user interaction. A primary motivation for development of this common user interface was to simplify user training. It also has been proven to have other benefits which simplify the generation of application programs and development tools.

A most important part of creating a set of application modules is the creation or modification of the schema, i.e., the objects used to store information relevant to the application. Incremental changes to the schema are easily made by running a schema modification program which also uses a FABFORM user interface. The addition of new schema objects or the addition of attributes to existing objects rarely impacts existing programs.

A crucial architectural principle of CAFE is the requirement of programmatic, as well as user, interfaces to all application modules. Programmatic interfaces to application modules are necessary in order to integrate existing software into future, higher level applications.

A second important design decision was to concentrate on the development of a manufacturing process flow representation (PFR) that could be accessed and manipulated by computer programs, as well as by design and production engineers. Applications implementing fabrication, simulation, analysis, real time process control, scheduling, and planning all access and derive information from the same representation of the process. The PFR provides an extensible framework for knowledge about process steps, including instructions to operators and equipment, scheduling requirements, changes effected to the wafer product, and physical process model parameters.

4.1.4 Applications

In the following we briefly describe two important CAFE applications, integrated circuit fabrication and process simulation. The fabrication of wafers with a process represented as a PFR involves several steps. A suitable PFR for the specific process must be created and installed. Wafer lots must be created and associated with this specific PFR. These lots must then be "started" to create a task data structure which is isomorphic to the hierarchical structure of the PFR.

At this point, actual machine operations can be scheduled and reservations made for both machines and operators. Finally, the machine operations can be performed, instructions given to the operator and machines, and data collected from the operator or machine and entered into the database.

Process simulation is a critical function at several points in the life cycle of a manufacturing process flow, from early design, documentation, and optimization through to diagnosis and support of the process. We are using the PFR as a mechanism for achieving tight coupling between process design and fabrication. Process development takes place by incrementally generating a PFR for the process. Design may proceed on various levels, including change in wafer state, physical treatment, or machine settings. Process advisors aid the task of treatment level synthesis by providing analytic model based estimates for the initial choice of process parameters. A simulation manager helps the process designer to perform simulations by automatically generating input for target simulators from the PFR. Changes to the PFR are analyzed and resimulations are required only for the affected parts of the process. Simulation results can be interpreted by calculation of layer thicknesses, sheet resistances, threshold voltages, or plots of diffusion profiles.

Current work involves the implementation of hierarchical scheduling, real time process control using the PFR, and integration of a mechanical TCAD system using the PFR.

Publications

Kashani, A. *A Reservation-based Scheduler.* S.M. thesis. Dept. of Electr. Eng. and Comput. Sci., MIT, 1990.

McIlrath, M.B., D.E. Troxel, D.S. Boning, M.L. Heytens, and P. Penfield. "CAFE - The MIT Computer Aided Fabrication Environment." *Proceedings Ninth IEEE/CHMT International Electronics Manufacturing Technology Symposium,* 1990.

McIlrath, M.B. and D.S. Boning. "Integrating Semiconductor Process Design and Manufacture Using a Unified Process Flow Representation." *Proceedings Rensselaer's Second International Conference on Computer Integrated Manufacturing,* Troy, New York, May 21-23, 1990.

Troxel, D. and M. McIlrath. "The MIT PFR - Application to Fabrication." Paper presented at the SRC/DARPA CIM-IC Workshop, San Francisco, California, August 14-17, 1990.

Troxel, D. "CAFE - The MIT Computer Aided Fabrication Environment." *MTL Microsystems Research Review,* MIT, November 27, 1990.

Chapter 5. Optical Propagation and Communication

Academic and Research Staff

Professor Jeffrey H. Shapiro, Dr. Robert H. Rediker, Dr. Ngai C. Wong

Graduate Students

D. Shane Barwick, Bradley T. Binder, Donald E. Bossi, Christopher J. Corcoran, Thomas J. Green, Jr., Suzanne D. Lau, Dicky Lee, Kin-Wai Leong, Robert E. Mentle, Brian K. Pheiffer, Scott R. Shepard, Ke-Xun Sun, Peter T. Yu

Undergraduate Student

Bing Wang

Technical and Support Staff

Barbara A. King

5.1 Introduction

The central theme of our programs has been to advance the understanding of optical and quasi-optical communication, radar, and sensing systems. Broadly speaking, this has entailed: (1) developing system-analytic models for important optical propagation, detection, and communication scenarios; (2) using these models to derive the fundamental limits on system performance; and (3) identifying, and establishing through experimentation the feasibility of, techniques and devices which can be used to approach these performance limits.

5.2 Squeezed States of Light

Sponsors

Maryland Procurement Office
Contract MDA 904-90-C-5070
National Science Foundation
Grant ECS 87-18970

Project Staff

Professor Jeffrey H. Shapiro, Dr. Ngai C. Wong, Kin-Wai Leong, Scott R. Shepard, Ke-Xun Sun, Bing Wang

The squeezed states of light are minimum uncertainty states for the quadrature components of the electromagnetic field which possess an asymmetric noise distribution between the two quadratures. The standard minimum uncertainty state that appears in quantum optics is the Glauber coherent state; it has an equal noise division between the two quadratures and is the quantum analog of the classical electromagnetic wave. Squeezed states are nonclassical and are of interest because their asymmetric noise division can lead to lower noise in photodetection measurements than that achievable with coherent states of the same energy. These noise reductions have been shown, theoretically, to afford significant benefits in interferometric precision measurements and novel guided-wave optical communication devices. We have pursued a vigorous program of experimental and theoretical research on squeezed-state and related nonclassical light.

5.2.1 Experiments

We have two principal experiments for the generation of nonclassical light: a forward four-wave mixer, and an optical parametric oscillator (OPO). The forward four-wave mixer is a simple, single-beam configuration using atomic sodium vapor. Our best results in an initial series of measurements show approximately 60 percent inferred quadrature-noise squeezing, at our overall measurement efficiency of approximately 40 percent. More importantly, these experiments have identified differential pump-probe self-focusing as the major limiting factor in achieving optimal squeezing in atomic vapor four-wave mixing

pumped by a Gaussian beam.[1] We have been improving both the vacuum setup and the detection electronics of our four-wave mixer, preparatory to a new series of measurements aimed at circumventing the self-focusing regime via use of higher Fresnel-number pump profiles.

In our OPO experiment, we are trying a different approach to nonclassical light. The parametric downconversion process, which is involved automatically creates pairs of perfectly correlated photons, one at the signal wavelength and one at the idler wavelength, as a result of absorption of one pump photon. This correlation provides a directly detectable nonclassical signature—perfect intensity correlation between the photocurrents produced by detectors viewing the signal and idler beams separately—and can be adapted, through feedback or feedforward schemes, to produce squeezed light. We have the first type-I phase matched OPO to show this nonclassical correlation. Our MgO doped $LiNbO_3$ system has yielded approximately 50 percent observed noise reduction in the differenced photocurrents from the signal and idler detectors.[2] This initial setup—a three-element cavity—has since been replaced by a simpler, two-element arrangement with vastly superior mechanical stability. We are presently working on a more compact, more stable version of the Mach-Zehnder interferometer used to separate the signal and idler beams produced by the OPO.

5.2.2 Theory

Our theoretical work on nonclassical light has addressed issues relevant to our squeezed-state generation experiments involving four-wave mixing[3] and optical parametric oscillation.[4] The former has examined the broad range of effects affecting choice of an optimal operating point for four-wave mixing squeezed state generation, e.g., spontaneous emission, Doppler broadening, Gaussian-beam profile, etc. The latter has provided a linearized quantum theory for OPO signal-idler correlation, demonstrating the extreme sensitivity of the low-frequency differenced photocurrent spectrum to pump excess noise when there is an intracavity loss mismatch between the signal and idler beams. This sensitivity has led us to propose that a sub-shot-noise intracavity absorption spectrometer could be built by modulating the OPO pump beam.

In addition to these squeezed-state generation theories, we have been continuing our fundamental attack on the ultimate limits of quantum phase measurement. Here we have made substantial inroads in understanding the properties of the Susskind-Glogower (SG) phase measurement—the maximum-likelihood measurement of a single-mode field's quantum phase. Several new classes of nonclassical states related to this measurement have been identified and analyzed, and a deep analogy between number-phase wavefunction representations and causal discrete-time waveforms has been explored.[5] Work is continuing on ways to realize the SG measurement, and on the multimode phase measurement problem.

5.2.3 Publications

Ho, S.T., P. Kumar, and J.H. Shapiro. "Quantum Theory of Nondegenerate Multiwave Mixing III. Application to Single-Beam Squeezing." *J. Opt. Soc. Am. B* 8(1): 37-57 (1991).

Ho, S.T., N.C. Wong, and J.H. Shapiro. "Single-Beam Squeezed State Generation in Sodium Vapor and its Self-Focusing Limitations." Submitted to *Opt. Lett.*

Ho, S.T., N.C. Wong, and J.H. Shapiro. "Self-Focusing Limitations on Squeezed State Generation in Two-level Media." In *Coherence and Quantum Optics VI.* Eds. L. Mandel, E. Wolf, and J.H. Eberly. New York: Plenum, 1990.

---

[1] S.T. Ho, N.C. Wong, and J.H. Shapiro, "Single-Beam Squeezed State Generation in Sodium Vapor and its Self-Focusing Limitations," submitted to *Opt. Lett.*

[2] K.W. Leong, N.C. Wong, and J.H. Shapiro, "Nonclassical Intensity Correlation from a Type-I Phase-Matched Optical Parametric Oscillator," *Opt. Lett.* 15(19): 1058-1060 (1990).

[3] S.T. Ho, P. Kumar, and J.H. Shapiro, "Quantum Theory of Nondegenerate Multiwave Mixing III. Application to Single-Beam Squeezing," *J. Opt. Soc. Am. B* 8(1): 37-57 (1991).

[4] N.C. Wong, K.W. Leong, and J.H. Shapiro, "Quantum Correlation and Absorption Spectroscopy in an Optical Parametric Oscillator in the Presence of Pump Noise," *Opt. Lett.* 15(6): 891-893 (1990).

[5] J.H. Shapiro and S.R. Shepard, "Quantum Phase Measurement: A System Theory Perspective," *Phys. Rev. A*, forthcoming.

Leong, K.W., N.C. Wong, and J.H. Shapiro. "Nonclassical Intensity Correlation from a Type-I Phase-Matched Optical Parametric Oscillator." *Opt. Lett.* 15(19): 1058-1060 (1990).

Leong, K.W. *Intensity Quantum Noise Reduction with an Above-Threshold Optical Parametric Oscillator.* Ph.D. diss., Dept. of Electr. Eng. and Comput. Sci., MIT, 1990.

Shapiro, J.H., and S.R. Shepard. "Quantum Phase Measurement: A System Theory Perspective." *Phys. Rev. A.* 43(7): 3795-3818 (1991).

Shapiro, J.H., S.R. Shepard, and N.C. Wong. "A New Number-Phase Uncertainty Principle." In *Coherence and Quantum Optics VI.* Eds. L. Mandel, E. Wolf, and J.H. Eberly. New York: Plenum, 1990.

Shapiro, J.H., S.R. Shepard, and N.C. Wong. "Coherent Phase States and Squeezed Phase States." In *Coherence and Quantum Optics VI.* Eds. L. Mandel, E. Wolf, and J.H. Eberly. New York: Plenum, 1990.

Shapiro, J.H., S.R. Shepard, and N.C. Wong. "Fourier Theory, Uncertainty Relations, and Quantum Phase." Paper presented at 17th International Conference on Quantum Electronics, Anaheim, California, May 21-25, 1990.

Shapiro, J.H., S.R. Shepard, and N.C. Wong. "Fourier Theory, Number-Ket Causality, and Rational Phase States." Paper presented at Nonlinear Optics '90, Kauai, Hawaii, July 16-19, 1990.

Shapiro, J.H. "Going Through a Quantum Phase." Paper presented at the 1990 United States – Japan Seminar on Quantum Electronic Manipulation of Atoms and Fields, Kyoto, Japan, September 3-7, 1990.

Wong, N.C., K.W. Leong, and J.H. Shapiro. "Quantum Correlation and Absorption Spectroscopy in an Optical Parametric Oscillator in the Presence of Pump Noise." *Opt. Lett.* 15(6): 891-893 (1990).

Wong, N.C., K.W. Leong, and J.H. Shapiro. "Nonclassical Intensity Correlation from a Type I Phase Matched Optical Parametric Oscillator." Paper presented at 17th International Conference on Quantum Electronics, Anahein., California, May 21-25, 1990.

Wong, N.C., K.W. Leong, and J.H. Shapiro. "Quantum Correlation and Absorption Spectroscopy in an Optical Parametric Oscillator." Paper presented at the Annual Meeting of the Optical Society of America, Boston, Massachusetts, November 4-9, 1990.

5.3 Optical Frequency Division

Sponsors

National Institute of Standards and Technology
Grant 60-NANBOD-1052
U.S. Army Research Office
Grant DAAL03-90-G-0128

Project Staff

Dr. Ngai C. Wong, Dicky Lee

An optical parametric oscillator (OPO) converts with high efficiency an input pump, of frequency ν_p, into two intense, coherent subharmonic outputs, a signal (ν_1) and an idler (ν_2), whose frequencies are tunable and whose linewidths are essentially limited by the input pump linewidth. Energy conservation requires that

$$\nu_p = \nu_1 + \nu_2. \tag{1}$$

By phase-locking the output difference frequency

$$\delta = \nu_1 - \nu_2 \tag{2}$$

relative to a microwave, millimeter wave or even infrared reference source, the output frequencies are precisely determined:

$$\nu_{1,2} = \nu_p \pm \delta, \tag{3}$$

and the OPO functions as an optical frequency divider.[6] OPO-dividers can be operated in series or in parallel to measure, compare, and synthesize frequencies from optical to microwave, with high precision and resolution. This new technique of optical frequency division will be important in areas of precision measurements, optical frequency standards, and coherent optical communications.

To demonstrate the feasibility of optical frequency division, we use a 2-element OPO using a type-II

[6] N.C. Wong, "Optical Frequency Division using an Optical Parametric Oscillator," *Opt. Lett.* 15(20): 1129-1131 (1990).

KTP crystal. We have obtained stable cw single-mode operation of our KTP-OPO near its frequency degeneracy, $\nu_1 \simeq \nu_2$. Angle tuning of the crystal permits the output frequency separation δ to be set anywhere within 1 THz of degeneracy. We have made direct frequency measurement of the subharmonic output difference frequency δ up to 26 GHz, limited only by the photodetector frequency response and available microwave electronics. Continuous tuning of about 0.5 GHz around the set point is obtained through temperature tuning of the crystal and a piezoelectrically controlled cavity length servo.

We have therefore successfully demonstrated the first tunable optical frequency divider using a KTP-OPO with excellent tuning characteristics—any frequency separation within 1 THz of frequency degeneracy can be obtained by angle and temperature tuning of the crystal. We are in the process of: (1) stabilizing the pump laser frequency to reduce the beatnote jitter; and (2) extending the beat frequency measurement beyond 26 GHz.

5.3.1 Publications

Wong, N.C. "Optical Frequency Division Using an Optical Parametric Oscillator." *Opt. Lett.* 15(20): 1129-1131 (1990).

Wong, N.C. "Optical Frequency Measurement and Synthesis Using Optical Parametric Oscillators." Paper presented at the Annual Meeting of the Optical Society of America, Boston, Massachusetts, November 4-9, 1990.

5.4 Laser Radar System Theory

Sponsor

U.S. Army Research Office
Contract DAAL03-87-K-0117

Project Staff

Professor Jeffrey H. Shapiro, Bradley T. Binder, Thomas J. Green, Jr., Robert E. Mentle

Coherent laser radars represent a true translation to the optical frequency band of conventional microwave radar concepts. Due to the enormous wavelength disparity between microwaves and light, laser systems offer vastly superior space, angle, range, and velocity resolution when compared to their microwave counterparts. However, the resolution benefits associated with the shortness of laser wavelengths are accompanied by the penalties of this wavelength region: the ill effects of atmospheric optical wave propagation in turbulent or turbid conditions and the speckle patterns resulting from target roughness on wavelength scales. The ensuing trade-off between resolution advantages and propagation/speckle disadvantages makes it likely that laser radars will fill new application niches, rather than supplant existing microwave systems.

We have been working to quantify the preceding issues through development and experimental validation of a laser radar system theory. Our work includes a collaborative arrangement with the Opto-Radar Systems Group of MIT Lincoln Laboratory, under which the experimental portions of the research are carried out with measurements from their CO_2 laser radar test beds.

5.4.1 Multipixel Detection Theory

We have been developing the appropriate target-detection theory for multipixel, multidimensional laser radar imagers, including those systems which augment their active-sensor channels with a forward-looking infrared (FLIR) passive channel. Our development of generalized likelihood-ratio tests (GLRTs) and associated receiver operating characteristics (ROCs) for this problem has addressed the realistic case of detecting a spatially-resolved, speckle target embedded in a spatially-resolved, speckle background. The target, if present, has unknown azimuth, elevation, range, and reflectivity. The background reflectivity is also unknown. Results of theory, computer simulation, and experiments have supported and quantified the intuitive notion that additional sensor dimensionality significantly improves detection performance.[7] This work applied to 2-D pulsed imagers, i.e., the range information was limited to resolution cells broader than target depth, and assumed that a background range-profile was known. We are now deriving the corresponding 3-D pulsed imager results—here fine-range information is used to resolve targets in depth—and using the estimation-maximization algorithm to obtain maximum-likelihood background range estimates.

[7] S.M. Hannon and J.H. Shapiro, "Active-Passive Detection of Multipixel Targets," *Proc. SPIE* 1222: 2-23 (1990).

5.4.2 Multipixel Laser Radar Target Tracking

The preceding target detection work is a multipixel multidimensional single-frame theory. Once a laser radar has detected a target, it will usually need to track that target. Here we have a multipixel multidimensional multiframe task. We had previously established the basic theory for such tracking problems in an upward-looking, i.e., a background-free, scenario. During the past year, this generalized Kalman-filter approach has been converted to the downward-looking case, viz. background is now included.[8] Furthermore, this new work has used analysis plus computer simulation to understand the loss-of-lock that can occur in track-while-image operation.

5.4.3 Laser Radar Tomographic Imaging

Through collaboration with the Lasar Radar Measurements Group of MIT Lincoln Laboratory, we have begun an investigation of the effects of target speckle on tomographic laser radar imaging. Initial work has focused on determining the impulse-response description for Doppler-time-intensity operation. Our results suggest that use of additional target projections suppress speckle in back-projection and filtered-backprojection imaging, without drastically affecting image resolution.[9]

5.4.4 Publications

Green, T.J., Jr., J.H. Shapiro, and M.M. Menon. "Target Detection Performance Using 3-D Laser Radar Images." Accepted for presentation at Society of Photo-Optical Instrumentation Engineers OE '91, Orlando, Florida, April 1-5, 1991.

Hannon, S.M., and J.H. Shapiro. "Active-Passive Detection of Multipixel Targets." *Proc. SPIE* 1222: 2-23 (1990).

Mentle, R.E. *Laser Radar Performance Theory for Track-While-Image Operation.* S.M. thesis, Dept. of Electr. Eng. and Comput. Sci., MIT, 1990.

Mentle, R.E., and J.H. Shapiro. "Track-While-Image in the Presence of Background." Accepted for presentation at Society of Photo-Optical Instrumentation Engineers OE '91, Orlando, Florida, April 1-5, 1991.

5.5 Fiber-Coupled External-Cavity Semiconductor High Power Laser

Sponsor

U.S. Navy - Office of Naval Research
Grant N00014-89-J-1163

Project Staff

Dr. Robert H. Rediker, Christopher J. Corcoran, D. Shane Barwick

During 1989, we achieved the milestone of five semiconductor gain elements (lasers with one facet AR coated) fiber-coupled into the external cavity and operating as a coherent ensemble. This year we have quantified the properties of the ensemble external-cavity operation. The cavity output has been shown to be in a single spectral line with a linewidth less than the instrumental resolution (7.5 MHz) of the Fabry-Perot spectrum analyzer used. The phase at the fiber input to the cavity has been changed by stretching each fiber as required using piezoelectric transducers. When the optical path lengths of all of the fibers were initially adjusted to give maximum output power and then the length of one of the fibers changed, the output power decreased and then increased in sequence as the output wavelength changed. This is in theoretical agreement with the inputs from all the fibers being initially in phase and then as the length of one fiber is changed seeking new wavelengths for in-phase operation. With the input phases to the cavity randomized by suitable adjustments of fiber lengths, the output is generally multimode, and the power is about two-thirds of the maximum above and relatively insensitive to change in the length of one of the fibers. Further quantitative experiments and associated theory will be performed in 1991 towards understanding the physics of ensemble external-cavity operation.

---

[8] R.E. Mentle, *Laser Radar Performance Theory for Track-While-Image Operation*, S.M. thesis, Dept. of Electr. Eng. and Comput. Sci., MIT, 1990.

[9] B.T. Binder, *Laser Radar Tomography: The Effects of Speckle*, Ph.D. diss. proposal, Dept. of Electr. Eng. and Comput. Sci., MIT, 1990.

Publications

Corcoran, C., and R.H. Rediker. "Operation of Five Discrete Diode Lasers as a Coherent Ensemble by Fiber-Coupling into an External Cavity." *Technical Digest Series* 7: 552-554 (1990). Washington, D.C.: Optical Society of America, 1990.

Corcoran, C.J., and R.H. Rediker. "Operation of Five Individual Diode Lasers as a Coherent Ensemble by Fiber Coupling into an External Cavity." Submitted to *Appl. Phys. Lett.*

Schloss, R.P., K.A. Rauschenbach, and R.H. Rediker. "Operation of a Coherent Ensemble of Five Diode Lasers in an External Cavity." *IEEE J. Quantum Electron.* Forthcoming.

5.6 Analog Processing of Optical Wavefronts Using Integrated Guided-Wave Optics

Sponsor

U.S. Air Force - Office of Scientific Research
Contracts F49620-87-C-0043 and F49620-90-C-0036

Project Staff

Dr. Robert H. Rediker, Donald E. Bossi, Suzanne D. Lau, Brian K. Pheiffer

This program, initiated in March 1987 and renewed in June 1990, explores fundamental issues associated with optical wavefront corrections using integrated guided-wave optical devices in GaAlAs. Device fabrication and optimization are being performed at Lincoln Laboratory while results are being evaluated at RLE.

Two tasks have continued to be emphasized during 1990. The first has been the development of an adiabatic antenna (an antenna that remains single-mode and loses no energy out of this mode) with an antenna pattern in which almost all of the energy is in a highly-directional central lobe. The second task that is being addressed is the measurement of the wavefront phase. This task includes the development of heterostructure waveguides, bends and Y-junctions and phase modulators. These optical components must be consistent with the eventual goal of integration with electronic components on the same chip.

Reduced-confinement GaAlAs slab-waveguide antennas have been fabricated by using an improved MBE growth technique to produce longitudinal variations in the refractive index and thickness of a waveguide film. This technique utilizes the fact that, for substrate surface temperatures above 650°C, the sticking coefficient of Ga on GaAs decreases with increasing temperature, while, below 650°C, this sticking coefficient is essentially independent of temperature. By using both growth-temperature regimes and applying graded heating to the substrate wafer throughout the growth process, the entire reduced-confinement antenna is now produced in a single MBE run without breaking vacuum. The experimentally-determined beam divergences for both the guide and the antennas are in excellent agreement with those predicted from the width and Al composition of both these structures. Forty percent reduction in the beam divergence due to the antenna has been measured.

In wavefront sensing and correction, it is envisioned that 10^3–10^4 basic modules would be used. In integrated optics, as in integrated circuits, it is important to relax the requirements on individual components and require that the operation of the integrated optics (circuits) be independent of significant component variations. The wavefront is sensed by interferometers between the multiplicity of through waveguides with the arms of the interferometers evanescently coupled to adjacent waveguides. The input powers to the interferometer arms will not be equal as a result of (1) the input power to the waveguide array being nonuniform and (2) unequal coupling by the evanescent couplers. A small-amplitude phase dither is applied to the interferometer arms, and the phase tilt between the adjacent through waveguides is determined, independent of power inequality, by the ratio of the amplitudes of the fundamental and second harmonic terms. The voltage from the interferometer output is fed back to an electrode on the through waveguide to set the desired tilt.

A proof-of-concept AlGaAs Mach-Zehnder experimental interferometer system has been designed and built to validate the phase measurement and correction. In this system, there are four p-n junction phase modulators, two on each arm of the interferometer. The sinusoidal dither voltage is applied to one electrode, a voltage V_ϕ to vary the phase in one arm applied to a second electrode, and the feedback voltage used to maintain a zero phase difference between the output of the two arms applied to a third electrode. The fourth electrode can be forward biased to investigate amplitude as well as phase change.

Publications

Bossi, D.E., W.D. Goodhue, M.C. Finn, K. Rauschenbach, J.W. Bales, and R.H. Rediker. "Reduced-Confinement Antennas for GaAlAs Integrated Optical Waveguides." *Appl. Phys. Lett.* 56 (5): 420-422 (1990).

Bossi, D.E., W.D. Goodhue, M.C. Finn, K. Rauschenbach, and R.H. Rediker. "Fabrication and Enhanced Performance of Reduced-Confinement GaAlAs Tapered-Waveguide Antennas." *Technical Digest Series* 5: 41-42 (1990). Washington, D.C.: Optical Society of America, 1990.

Bossi, D.E. *Reduced-Confinement GaAlAs Tapered Waveguide Antennas.* Ph.D. diss., Dept. of Electr. Eng. and Comput. Sci., MIT, 1990.

Bossi, D.E., W.D. Goodhue, L.M. Johnson, and R.H. Rediker. "Reduced-Confinement GaA1As Tapered Waveguide Antennas for Enhanced Far-Field Beam Directionality." *IEEE J. Quantum Electron.* Forthcoming.

Goodhue, W.D., D.E. Bossi, M.C. Finn, J.W. Bales, and R.H. Rediker. "Reduced-Confinement GaAlAs Tapered-Waveguide Antenna Grown by Molecular-Beam Epitaxy." *J. Vac. Sci. Technol.* B8 (2): 349-351 (1990).

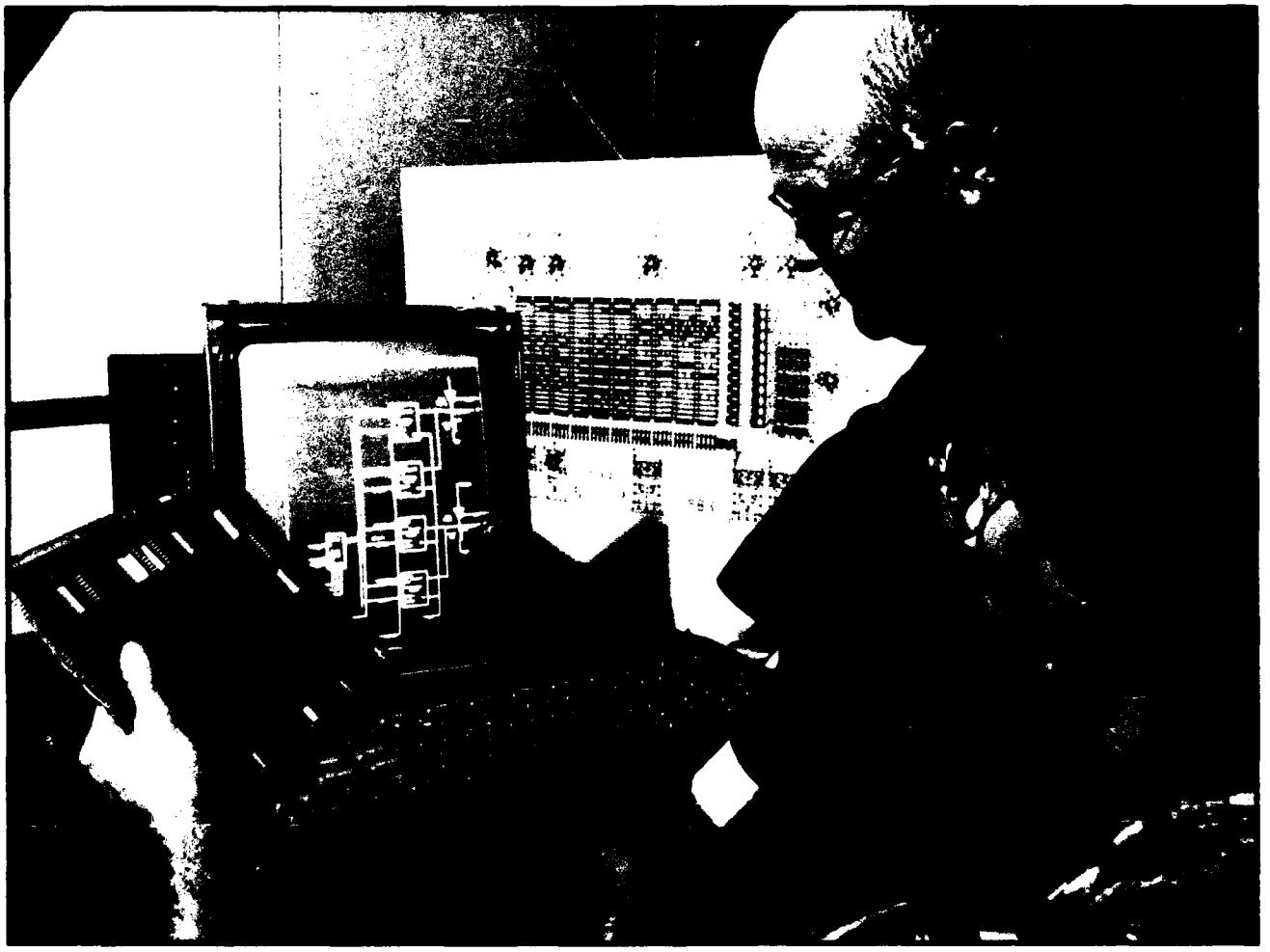

From left, Professor Jonathan Allen, Director of the Research Laboratory of Electronics, and graduate student Larry D. Seiler are inspecting the design of a system for high-speed design rule checking which uses four custom integrated circuits in a novel architecture.

Chapter 6. Custom Integrated Circuits

Academic and Research Staff

Professor Jonathan Allen, Professor John L. Wyatt, Jr., Professor Srinivas Devadas, Professor Jacob White

Visiting Scientists and Research Affiliates

James H. Kukula[1]

Graduate Students

Robert C. Armstrong, Donald G. Baltus, Cyrus S. Bamji, Curtis S. Chen, Steven J. Decker, Ibrahim M. Elfadel, Marina Frants, Juha M. Hakkarainen, Craig L. Keast, Songmin Kim, Kevin Lam, Steven B. Leeb, Jennifer A. Lloyd, Andrew Lumsdaine, Ignacio S. McQuirk, Keith S. Nabors, Joel Phillips, Khalid Rahmat, Mark W. Reichelt, Mark N. Seidel, Amelia H. Shen, Luis M. Silveira, David L. Standley, Ricardo Telichevesky, Christopher B. Umminger, Filip Van Aelten, Woodward Yang, Paul C. Yu

Technical and Support Staff

Dorothy A. Fleischer, Susan E. Nelson

6.1 Custom Integrated Circuits

Sponsors

Analog Devices, Inc.
IBM Corporation

Project Staff

Professor Jonathan Allen, Robert C. Armstrong, Donald G. Baltus, Cyrus S. Bamji, Mark W. Reichelt, Filip Van Aelten

The overall goal of VLSI CAD research is to provide the means to produce custom integrated circuits correctly, quickly, and economically. Traditionally, correctness is checked at several representational levels, such as layout (via design rule checking) and circuit and logic (both via simulation). The techniques for checking correctness are usually local to the particular representational level involved. While these techniques are important components of the design testing, they do not attempt to provide alignment and consistency checks between the different representational levels and an input behavioral specification. In addition, they do not characterize the set of possible designs at each representational level corresponding to the initial functional specification while ranging over a variety of performance levels. For this reason, there is an increasing need to provide CAD tools that can serve as the framework for design exploration, providing the desired performance together with consistently aligned representations at all levels.

In this research group, we are studying a variety of research topics with an emphasis on performance-directed synthesis of custom VLSI designs. An overview of the viewpoint that motivates these projects has recently been provided in a major survey paper[2] in which the need for coordinating the design optimization process over the several levels of representation is emphasized. Since design exploration is so central to the production of high-performance designs, emphasis is placed on how performance can be characterized at the several levels of representation and how overall optimal performance can be achieved in an integrated way. In addition to the basic issues of circuit optimization, architectures for digital signal processing have been studied because of the highly parallel nature of the algorithms involved and the need for a very high level of real-time performance in these systems. We have increased our emphasis on developing the means for formally specifying designs that facilitate performance-directed design exploration as well as efficient verification of correctness of the coordinated set of design-level representations. All of these studies are taking on an increasingly theoretical approach, signifying the transition of digital system design from an art to a science.

---

[1] IBM Corporation.

[2] J. Allen, "Performance-Directed Synthesis of VLSI Systems," *Proc. IEEE* 78(2): 336-355 (1990).

In previous work, techniques were developed to automatically transfer a netlist of an MOS circuit (either NMOS or CMOS in any circuit style) to a highly efficient, compacted layout. Providing algorithmic control over this important transformation is essential in overall design optimization. This procedure has been used as a "back end" for technology mapping processes, and the corresponding program has been very successful in benchmark tests.[3]

Given this assurance of the generation of high-quality layout for circuit netlist specification, attention is now being turned to performance exploration at the architectural level, with a focus on digital signal processing applications which are highly parallel. In this research, architectures that repeatedly use a small set of circuit cells in a regular array are being emphasized, such as systolic arrays. While these arrays, which utilize nearest neighbor communication, have been successfully used for a wide variety of signal processing tasks, it is of interest to explore more relaxed models where communication is allowed to extend beyond nearest neighbors to a larger local area. This extension admits a wider class of architectures and invites a more comprehensive level of design exploration where architectural flexibility is traded off against more complex, local delay models. Formal techniques for specifying these signal processing tasks at a behavioral level have been introduced, and means for mapping the algorithm onto multiple index spaces have been devised, together with the means to explore these mappings. An affine delay model has been introduced to quantify communication delay, and an overall integer linear programming approach has been used to optimize the overall design on a timing performance basis. In addition, branch and bound techniques have been used to prune the possibly large search space to a smaller and more manageable set of alternatives that can be quickly assessed. In this way, global optimization is being directly addressed through the linking of architectural exploration and delay models in the context of a large but restricted design space. Since these circuit models are well characterized, the previously developed techniques for automatic conversion between circuit netlist representation and layout provides an overall means for simultaneous optimization across all representational levels, from layout through circuit, to logic, and architecture. This investigation aims to provide one of the first instances of overall global optimization across all representational levels, avoiding premature local optimization at any single level of representation.

There is increasing interest in extending circuit design and optimization techniques to the device level by refining the device models, and also by simulating them directly rather than using approximate average device model parameters in a circuit simulator. While the device-level equations can be solved directly to provide the needed accuracy, their solution is generally found to be too time-consuming on conventional architectures. Accordingly, Reichelt has been studying techniques for the parallelization of transient two-dimensional simulation of MOS devices using waveform relaxation techniques.[4] Uniform convergence of the waveform relaxation algorithm in this application has been demonstrated, and speedups between five and eleven times have been found using these new algorithms. These techniques have recently been implemented on three-dimensional parallel architectures in a way that exploits the inherent parallelism of the waveform relaxation techniques.

In earlier work, Bamji demonstrated how context-free grammars could be used to formally represent large classes of circuit netlists, such as ratioed NMOS designs, static CMOS designs, and precharge/evaluate circuit designs.[5] He also represented the class of all layouts as a regular structure grammar and showed how to verify the correctness of the resulting layout using parsing techniques. This formalism has essentially provided a new technique for hierarchical design rule verification using a cell library through formal characterization of the interactions of cell templates.[6] Design rule verification is achieved by covering the layout with these templates, which are defined in terms of graphs, and all operations are performed in the graph domain. The verification procedure is incremental, and because the number of cell instances is usually much smaller than the number of mask geometries, it is much faster than

---

[3] D.G. Baltus and J. Allen, "SOLO: A Generator of Efficient Layouts from Optimized MOS Circuit Schematics," Proceedings of the 25th Design Automation Conference, June 1988.

[4] M. Reichelt, J. White, and J. Allen, "Waveform Relaxation for Transient Two-Dimensional Simulation of MOS Devices," *IEEE Trans. Comput-Aided Des.*, forthcoming.

[5] C.S. Bamji and J. Allen, "GRASP: A Grammar-based Schematic Parser," Proceedings of the 26th Design Automation Conference, June 1989.

[6] C.S. Bamji and J. Allen, "GLOVE: A Graphic-based Layout Verifier," forthcoming.

techniques that directly manipulate mask geometries. A current emphasis is on the automatic discovery of cells from nonhierarchical layout. Through these means we expect to derive design hierarchy automatically, and hence, suggest new cells for a library. The graph-based template techniques are similar to those previously used in a regular structure generator,[7] which has proved to be a convenient method for the elaboration of layout corresponding to higher level architectural connectivity.

In earlier studies, Van Aelten showed how to perform the verification of circuit properties based on a grammar-based schematic parser developed by Bamji. These formal techniques are now being extended to the verification of relations between synchronous machines. Since the machines may be implemented in many different ways, it is important to be able to transform representations of these machines into alternate forms that can be directly compared. Using a new set of primitive relations between string functions, an arbitrarily long sequence of behavioral transformations can be compressed into a single, composite relation that is guaranteed to correctly represent the given sequence of primitive transformations.[8] In this way, it is possible to use these composite transformations to verify the behavioral specification against the resultant logic implementation with one automata equivalence check, using any one of several available methods. In this way, a computationally expensive verification technique is reduced to a much simpler verification task.

We continue to focus on issues of design database and framework specification. It is increasingly recognized that a design database is the central component of an overall design system, along with a variety of specialized CAD algorithms that utilize one consistently maintained overall design representation. Nevertheless, maintenance of this database so that all levels of representational view are consistent with one another and are hence projections of one (and only one) underlying design is an exceedingly difficult problem. One single representational formalization has recently been introduced by Armstrong, and it is expected to support all levels of representation currently utilized or anticipated.[9] By setting up a series of explicit correspondences between representational levels, consistency can readily be verified and maintained in the face of design modifications at any of the several different representational levels. This automatic consistency maintenance is highly desirable in any design system, and can be readily coupled to performance exploration strategies at levels where a change at a higher level of abstraction gives rise to many possible lower level representations, as in the transition from a circuit specification to layout. A preliminary version of this procedure has now been implemented, and is being tested over a substantial variety of cases.

With the advent of a new emphasis on central databases and their connections to specialized CAD algorithms, there is new concern for the study of integrated, cooperative CAD computing environments involving both workstations and mainframes. A proposal has been developed for the study of coordinated workstation, mainframe, and large disk system environments that are interconnected in a flexible way using fiberoptic switching. In this way, large, high-performance disk systems are flexibly coupled between both mainframe servers and high-performance workstations, and a means is provided to explore the optimal distribution of tasks over such a distributed framework. This environment also provides a structure in which distributed parallel algorithms can run in a coherent way within an overall environment that supports other specialized nonparallel CAD algorithms.

6.2 The MIT Vision Chip Project: Analog VLSI Systems for Fast Image Acquisition and Early Vision Processing

Sponsors

National Science Foundation/Defense Advanced Research Projects Agency
Grant MIP 88-14612

Project Staff

Professor John L. Wyatt, Jr., Professor Berthold K.P. Horn, Professor Hae-Seung Lee, Professor

---

[7] C.S. Bamji, C.E. Hanck, and J. Allen, "A Design-by-Example Regular Structure Generator," Proceedings of the 22nd Design Automation Conference, June 1985, pp. 16-22.

[8] F. Van Aelten, J. Allen, and S. Devadas, "Verification of Relations between Synchronous Machines," 1991 MCNC Logic Synthesis Workshop, forthcoming.

[9] R.C. Armstrong, *A Formal Approach to Incremental Consistency Maintenance in Multirepresentation VLSI Databases*, Ph.D. diss. proposal, Dept. of Electr. Eng. and Comput. Sci., MIT, 1987.

Tomaso Poggio, Professor Charles G. Sodini, Professor Jacob White, Steven J. Decker, Ibrahim M. Elfadel, Juha M. Hakkarainen, Craig L. Keast, Ignacio S. McQuirk, Mark N. Seidel, David L. Standley, Christopher B. Umminger, Woodward Yang, Paul C. Yu

6.2.1 Introduction

In real-time machine vision, the sheer volume of image data to be acquired, managed and processed leads to communications bottlenecks between imagers, memory, and processors and also to very high computational demands. Our group is designing experimental analog/VLSI systems to overcome these problems. The work is presently concentrated entirely on early vision tasks, i.e., tasks that occur early in the signal flow path of a machine vision system. Designs of chips for certain tasks in velocity estimation, image moment calculations, depth from stereo, and edge detection are currently underway or have been completed.

This project began in September 1988, and the faculty involved are Professors Berthold K.P. Hae-Seung Lee, Tomaso Poggio, Charles G. Sodini, Jacob White, and John L. Wyatt, Jr., who is the principal investigator. This work was inspired by Professor Carver Mead's pioneering efforts at the California Institute of Techology, although our project methods and goals are different from Mead's.

The goal of this project is to design and build prototype early vision systems that are remarkably low-power, small, and fast. The typical system will perform one or more computation-intensive image-processing tasks at hundreds to thousands of frames per second using only tens to hundreds of milliwatts. The entire system with lens, imager, power supply and support circuitry could fit inside a cigar box.

In this project, we are exploring the various types of analog processing for early vision. There is no single design strategy, but each design has many of the following features:

- sensors and processing circuitry integrated on a single chip,
- parallel computation,
- analog circuits for high speed, small area and low power,
- selection of tasks and algorithms requiring low to moderate precision (roughly equivalent to 6-8 bit fixed point precision in a digital machine),
- special emphasis on computations that map naturally to physical processes in silicon, e.g., to relaxation processes or to resistive grids,
- emphasis on charge-domain processing, e.g., CCD and switched-capacitor impiementations, for maximal layout density and compatibility with CCD sensors,
- sufficiently fast processing that no long-term storage circuitry is required, and
- careful matching of algorithms, architecture, circuitry and (often custom) fabrication for maximum performance.

The advantages of this analog design approach to early vision hardware are (1) high speed (both in the sense of high throughput and low latency), (2) low power, and (3) small size and weight. High throughput can be important in high speed inspection processes, e.g., for printed materials or PC boards. Low latency is very important for closed loop systems because delays are destabilizing. Relevant examples might include vehicle navigation and robot arm guidance. Low power together with small size and weight are important for airborne and space applications. And finally, small systems tend to be affordable.

These advantages are achieved at a cost. One problem is that a high degree of care and expertise is required for high performance analog design. Another is that performance and functionality of analog integrated circuits is critically dependent on exact fabrication process parameters. For these reasons, the first design of an analog chip, even by an experienced designer, often does not work, so that repeated efforts are required.

Another problem is that there is a large amount of labor and frequent delays involved in custom fabrication on campus. Finally, analog systems have little flexibility compared with their digital counterparts. Thus analog design, often coupled with custom fabrication, is only appropriate when extremely high performance is required.

Chips are fabricated through MOSIS whenever possible. Chips requiring special processing are fabricated on campus at MIT's Microsystems Technology Laboratories where Craig Keast and Professor Charles Sodini have developed a special CMOS/CCD fabrication process for vision applications.

Sections 1.1.2 and 1.1.3 describe chips that have been designed and tested by doctoral students David Standley and Woodward Yang.

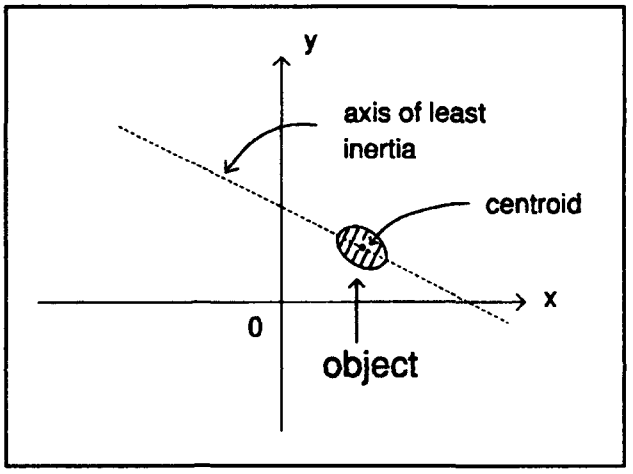

Figure 1. Example of object centroid and axis of least inertia.

6.2.2 Fast Imager and Processor Chip for Object Position and Orientation

This analog VLSI chip finds the position and orientation of an object's image against a dark background. The algorithm is based on finding the first and second moments of the object intensity. These moments allow the centroid (an indicator of position) and the axis of least inertia (an indicator of orientation) to be computed; see figure 1. If I(x,y) is the intensity as a function of position, and we (initially) assume that I(x, y) = 0 outside the object, then the required quantities are given by

$$\int\int I(x, y)h(x, y)dA$$

for all of the following h:

$$h(x, y) = 1, x, y, xy, x^2 - y^2$$

(x^2 and y^2 are not needed separately). All of the weighting functions h are harmonic; i.e., the Laplacian vanishes identically:

$$\Delta h(x, y) \equiv 0.$$

This observation is a key to a scheme proposed by Horn, in which an analog computer based on a resistive sheet (or resistor grid) can be constructed, in principle. In the implementation described here, an N x N array of discrete intensity data is reduced to a set of 4N quantities by a 2-D resistor grid and is subsequently reduced to a set of just eight quantities by 1-D resistor lines, all in a continuous-time, asynchronous fashion – no clocking required. The eight outputs can be digitized, and the centroid and orientation can be found using simple expressions. While resistive sheets have been used in earlier systems to compute position, none have been previously used to perform the orientation task, which requires computing second moments.

Figure 2 shows the resistor grid and its associated array of photoreceptor cells, which are uniformly spaced and occupy most of the chip area. The object image is focused onto the surface of the chip, inside the array. Each photoreceptor cell contains a phototransistor and processing circuitry; it converts the incident light intensity into a current that is injected into the grid. Thresholding is available to remove a dim (yet nonzero) scene background, so it does not interfere with the calculation. If the intensity I at a particular cell is below an adjustable threshold value I_{th}, then no current is injected. If $I > I_{th}$, then the output current, which is analogous to the gray-level weighting at that location, is proportional to $I - I_{th}$. The result is a continuous, piecewise-linear response characteristic. The array size is 29 x 29; intentional image blurring over a few elements gives substantially increased resolution.

The perimeter of the grid is held at a constant voltage by the current buffers in figure 2; this ensures proper operation of the grid as a "data reduction" computer. The buffer outputs are simply copies of the currents flowing into them from the grid; the buffers are needed to isolate the grid from the effects of other circuitry. Figure 3, which shows the complete architecture of the chip, indicates how the (copied) grid currents are fed into resistor lines on the perimeter, how the ends of these lines are connected, and where the eight output currents exit the chip near the corners. These currents are measured by external circuitry (which also holds the ends of the lines at ground potential). In this setup, there are two lines on each side: one uniform and one quadratic line. These calculate weighted sums of the grid currents, where the weighting is (respectively) a linear or square-law function of the position along the line. The buffer outputs are steered either to the uniform or quadratic lines, so that four outputs are available at a time; i.e., multiplexing is required here (but is not necessary in general).

Working chips have been fabricated using the MOSIS service. The die size is 7.9 mm x 9.2 mm, and the imaging array is a 5.5 mm square. Accuracy is dependent on the object. For moderately sized and sufficiently elongated objects, e.g. a diamond of diagonal dimensions 25 by 50 on a (normalized) 100 by 100 image field, orientation is typically determined to within $\pm 2°$. The speed is 5000 frames per second, and power consumption is typically 30 mW.

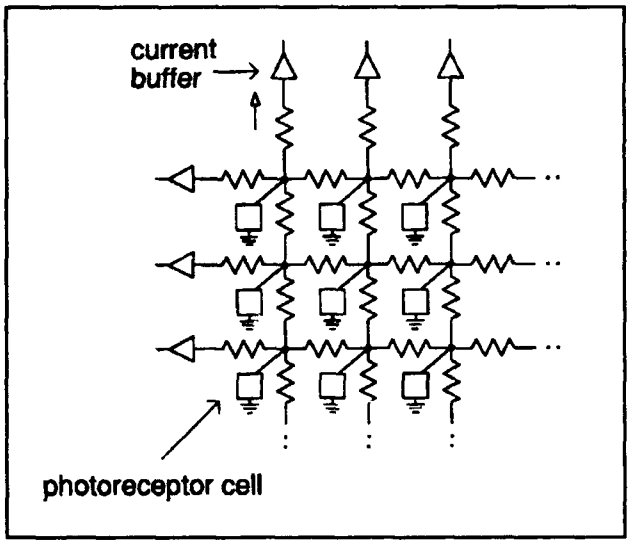

Figure 2. Resistor grid and photoreceptor cell array.

6.2.3 Integrated CCD Imager and Processors for Edge Detection

Parallel, Pipelined Architecture

Many image processing algorithms and machine vision tasks consist of calculations or operations performed on spatially localized neighborhoods. Therefore, the highly parallel nature of these algorithms can be effectively exploited if they are performed directly on the imaging device before the parallel structure of the data is disrupted by serial data output.

For a typical CCD imaging array, the parallel, pipelined architecture (see figure 4) provides a balance of computation speed, internal clock rate, internal storage, and I/O bandwidth without degrading the imager fill-factor (sensitivity). As columns of image data are clocked from left to right in parallel, local interactions between neighboring column elements are directly computed by the processor elements. As row values are sequentially clocked through the processor, local interactions between neighboring row elements are similarly performed by utilizing delay elements. This architecture is able to efficiently implement linear convolutions that are separable and recursively defined. This architecture is also suitable for certain types of nonlinear filtering operations that perform image segmentation, a basic machine vision task.

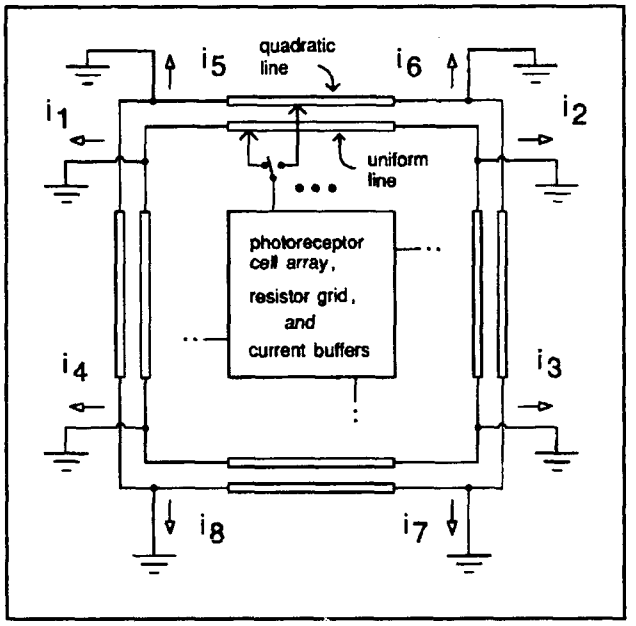

Figure 3. Main chip architecture.

CCD Processors for Edge Detection

A full fill-factor CCD (64 x 64) imager with an integrated, analog CCD signal processor for edge detection was implemented using standard 4 μm, CCD/NMOS technology. By combining simple charge-domain, analog circuitry in a parallel, pipelined architecture, the prototype image processor was capable of performing a simple edge detection algorithm at 1000 frames/second. Furthermore, this signal processing capability was achieved with only a 15% increase in area, without any additional fabrication steps, decreasing the fill-factor of the CCD imager, or a significant increase in power dissipation.

While there are many edge detection algorithms, the LoG (Laplacian of Gaussian) of the image was chosen for its ease of implementation. The Laplacian is a rotationally symmetric, scalar operator. The zero-crossings of the Laplacian correspond to maxima in the image gradient which are interpreted as object edges. The Gaussian acts as a low-pass image filter that reduces the effects of noise in the image and has several desirable properties such as (1) rotational symmetry, (2) separability into 1-D convolutions within row and column elements, and (3) approximation by a binomial distribution which is recursively defined. The Gaussian (actually, binomial) convolver on this chip is a parallel, pipelined version of a CCD architecture developed first by Sage and Lattes at MIT Lincoln Laboratories.

In addition to image sensing, CCDs are also capable of performing simple analog charge-domain computations such as charge packet split-

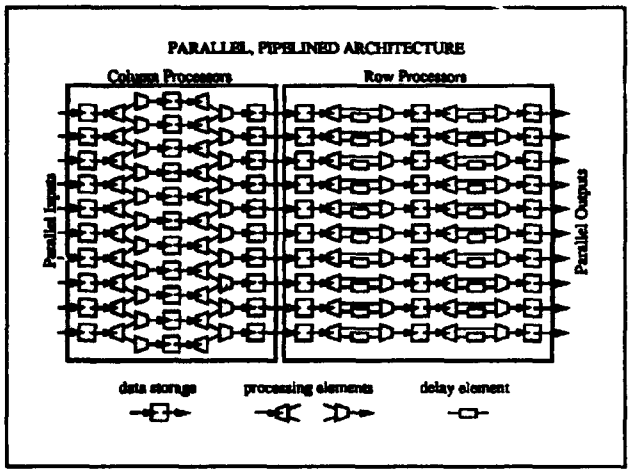

Figure 4. The parallel, pipelined architecture for high throughput image processing. The entire image is transferred through the column and row processors as a pipelined sequence of column vectors of image pixels. The column processors compute local interactions between neighboring column pixels in parallel. The row processors pipeline the computation of local interactions between neighboring row pixels by using additional delay elements.

ting, charge packet summation, charge packet subtraction, and delay. By combining the CCD structures for charge packet splitting and charge packet summation, a 1-D binomial convolution within parallel column elements can be directly implemented as shown in figure 5. With the addition of a delay element, a 1-D binomial convolution within sequential row elements can be implemented as shown in figure 6.

Similarly, CCD structures for charge packet splitting, charge packet summation, charge packet subtration and delay elements can be combined as shown in figure 7 to perform a Laplacian convolution. Thus, the LoG processor can be simply realized by cascading the CCD structures for Laplacian convolution, 1-D binomial convolution within column elements, and 1-D binomial convolution within row elements. Notice that the parallel, pipelined architecture allows efficient integration with a CCD imager, as a column of image data can be directly clocked out of a CCD imager into the LoG processor. Furthermore, the parallel, pipelined architecture can be extended to the implementation of other linear and nonlinear image filters by proper modification of the processing elements. This prototype device demonstrates the feasibility and computational power of integrating CCD signal processors with CCD imaging arrays for real-time image processing.

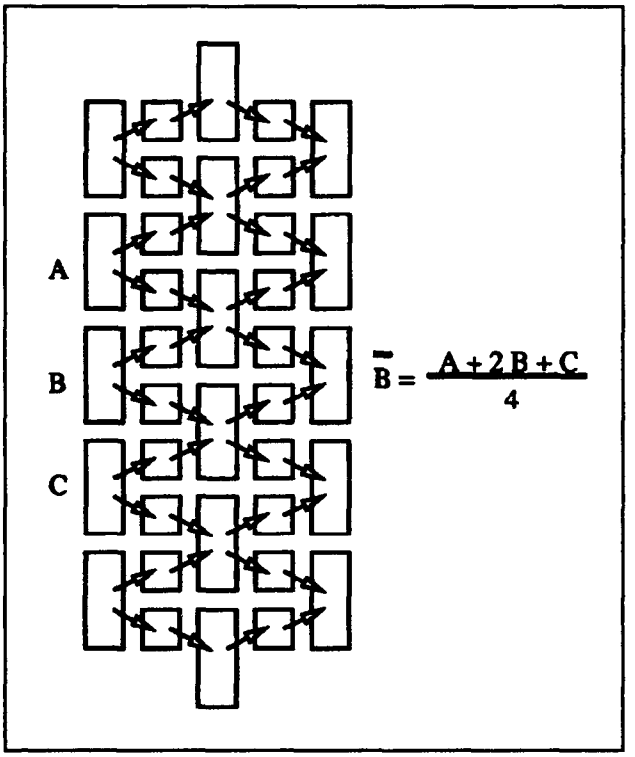

Figure 5. CCD structure for 1-D binomial convolution within column elements. As the column elements are clocked in parallel from left to right, the analog charge packets are split into halves. Subsequently, the halved charge packets are summed in parallel to compute the average of neighboring column elements. Repeated operations with cascaded structures increase the order and extent of the 1-D binomial distribution within column elements.

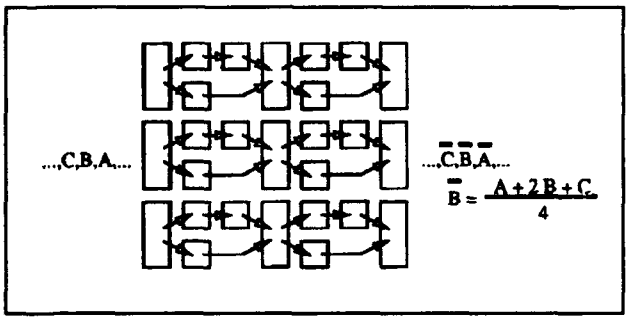

Figure 6. CCD structure for 1-D binomial convolution within row elements. As row elements are clocked from left to right, the analog charge packet is split into halves. Half of the charge packet is delayed, and the other half of the charge packet is summed with the half of the preceding charge packet to compute the average of sequential row elements. Repeated operations with cascaded structures increase the order and extent of the 1-D binomial distribution within row elements.

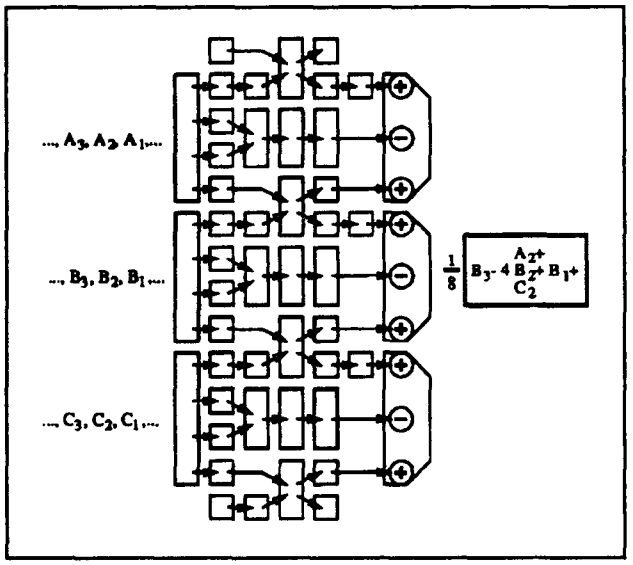

Figure 7. CCD structure for Laplacian convolution. As image data are clocked from left to right, the charge packets are split, delayed, summed, and subtracted to compute the discrete convolution approximating the Laplacian computation.

6.2.4 Overall Project Scope

Listed below are the individual efforts that are underway or have been completed in this project. The single-chip systems are chips with imagers for input that produce highly processed, low-bandwidth output that can be readily handled by conventional digital systems. David Standley's chip in section 1.1.3. is an example. The "modular vision system component chips" may or may not have imagers on board. They produce high bandwidth output such as filtered images or depth maps that require specialized processing hardware for high speed operation.

Single-Chip Systems

CMOS Image Moment Chip (completed)
CCD/CMOS Focus of Expansion Chip (in progress)

Modular Vision System Component Chips

CCD/CMOS Analog Convolver (completed)
CCD/CMOS Image Smoothing and Segmentation Chip (in progress)
CCD/CMOS Stereo Chip (in progress)
Switched-Capacitor Surface Reconstruction Chip (in progress)

Technology Development

CCD/CMOS Fabrication Process (completed)
Switched-Capacitor Resistive Grids (completed)
CMOS Image Segmentation Circuits (in progress)

Theory

Stability of Active Resistive-Grid Systems (completed)
Texture and Halftoning Using Markov Random Fields (in progress)
Switched-Capacitor Network Settling Time (in progress)
Least-Squares Camera Calibration Method (in progress)

Simulation

Parallel Simulator for Large Arrays of Analog Cells (in progress)

Publications

Elfadel, I., and R. Picard. "Miscibility Matrices Explain the Behavior of Grayscale Textures Generated by Gibbs Random Fields." *SPIE Proceedings on Intelligent Robots and Computer Vision IX,* OE/Boston '90, Boston, Massachusetts, November 4-9, 1990.

Keast, C.L., and C.G. Sodini. "A CCD/CMOS Process for Integrated Image Acquisition and Early Vision Signal Processing." *Proceedings SPIE Charge-Coupled Devices and Solid State Sensors,* Santa Clara, California, February 1990, pp. 152-161.

Lumsdaine, A., J.L. Wyatt, Jr., and I.M. Elfadel. "Nonlinear Analog Networks for Image Smoothing and Segmentation." *J. VLSI Sig. Process.* Forthcoming.

Lumsdaine, A., J. Wyatt, and I. Elfadel. "Nonlinear Analog Networks for Image Smoothing and Segmentation." *Proceedings of the IEEE International Symposium on Circuits and Systems,* New Orleans, Louisiana, May 1990, pp. 987-991.

Sarpeshkar, R., J.L. Wyatt, Jr., N.C. Lu, and P.D. Gerber, "Mismatch Sensitivity of a Simultaneously Latched CMOS Sense Amplifier." *IEEE J. Solid-State Circuits.* Forthcoming.

Standley, D. "Stability in a Class of Resistive Grid Networks Containing Active Device Realizations of Nonlinear Resistors." *Proceedings of the IEEE International Symposium on Circuits and Systems,* New Orleans, Louisiana, May 1990, pp. 1474-1477.

Umminger, C.B., and C.G. Sodini. "Switched Capacitor Networks for Monolithic Image Processing Systems." Submitted to *IEEE J. Solid-State Circuits.*

Wyatt, J.L., Jr., and M. Ilic. "Time-Domain Reactive Power Concepts for Nonlinear, Nonsinusoidal or Nonperiodic Networks." *Proceedings of the IEEE International Symposium on Circuits and Systems,* New Orleans, Louisiana, May 1990, pp. 387-390.

Wyatt, J., D. Standley, and B. Horn. "Local Computation of Useful Global Quantities Using Linear Resistive-Grid Networks." Poster session, Conference on Neural Networks for Computing, Snowbird, Utah, April, 1990.

Yang, W., and A.M. Chiang. "A Full Fill-Factor CCD Imager with Integrated Signal Processors." *Proceedings of the ISSCC,* San Francisco, California, February 1990, pp. 218-219.

Patents

Decker, S., H.-S. Lee, and J.L. Wyatt, Jr. "Resistive Fuse Circuits for Image Segmentation and Smoothing." Submitted to U.S. Patent Office 12/14/90, receipt no. 628-340.

Standley, D., and B.K.P. Horn. "Analog VLSI Chip for Object Position and Orientation." Submitted to U.S. Patent Office 9/28/90, receipt no. 591,145.

Theses

Umminger, C.B. *Switched Capacitor Networks for Machine Vision.* S.M. thesis. Department of Electrical Eng. and Comput. Sci. MIT, 1990.

Yang, W. *The Architecture and Design of CCD Processors for Computer Vision.* Ph.D. diss. Dept. of Electr. Eng. and Comput. Sci. MIT, 1990.

6.3 Techniques for Logic Synthesis, Verification and Testing

Sponsors

Analog Devices Career Development Assistant Professorship
U.S. Navy - Office of Naval Research Contract N0014-87-K-0825

Project Staff

Professor Srinivas Devadas, James H. Kukula, Curtis S. Chen, Marina Frants, Kevin Lam, Amelia H. Shen, Filip Van Aelten

6.3.1 Introduction

In order to design and build large-scale computers that achieve and sustain high performance, it is essential to carefully consider reliability issues. Although these issues have several aspects, our focus here is on the important problem of detecting failures in a computer's VLSI components which are caused by errors in the design specification, implementation or manufacturing processes.

Design verification involves ensuring that the specification of a design is correct prior to carrying out its implementation. Implementation verification ensures that the manual design or automatic synthesis process is correct, i.e., checking that the mask-level descriptions obtained correctly implement the specification. Manufacture testing involves checking the complex fabrication process for correctness, i.e., checking that there are no manufacturing defects on the integrated circuit. It should be noted that the three verification mechanisms described above deal not only with verifying the functionality of the integrated circuit but also with its performance.

In the Custom Integrated Circuits Group at MIT, we are attempting to develop synthesis, specification and verification mechanisms that are versatile as well as efficient. More importantly, we are developing strategies that address reliability issues in the many steps of the complex VLSI design process, and this involves varied levels of design abstraction from behavioral specifications to mask-level layout. Because many aspects of reliability cannot be investigated by focusing on a single level of design abstraction, such a complete program is essential when addressing reliability.

In the following sections, we elaborate on our current work in developing CAD algorithms and tools for highly reliable VLSI circuits and on our plans for the future. Included in the description is our research in the development of provably correct behavioral transformations with applications to design and implementation verification, synthesis of testable VLSI circuits in the area of manufacture test, and the development of a framework for logic synthesis, verification and testing.

In Sections 6.3.2 through 6.3.4, we describe work categorized largely by the mathematical and algorithmic techniques used in each problem domain.

6.3.2 Design Verification

Introduction

The specifications for a large VLSI circuit are typically expressed in a high-level language by a computer architect or VLSI designer. Then the architect uses high-level simulators to check whether the exact functionality of the circuit has been captured in the design. Unfortunately, an exhaustive simulation that can guarantee correctness is possible only for the smallest circuits. Ideally, the architect would like to formally verify and guarantee that the specifications are correct, so that, if they are implemented and fabricated without error, a functionally-correct IC will result.

Several errors may occur in the manual process of design specification. For example, in a recent personal computer (PC) product by a major company, a particular number which was supposed to be squared was multipled by two instead. This was tracked to an error in the specification. The specification had been rigorously (but obviously not exhaustively) simulated. Protocol chips are typically small compared to general-purpose μ processors, but experience has shown that they are particularly prone to deadlock errors, due to incorrect specifications.

While we believe that formal verification methods will never replace simulation, they can augment simulation-based correctness checking in design verification. Verification methods could uncover specification errors without simulating huge numbers of test cases or using exorbitant amounts of CPU time. We have recently begun work in the area of design verification, specifically in the areas of temporal-logic-based model checking and protocol verification.

Temporal Logic Model Checking

Model checking, a design verification method developed initially by Clarke et al. at CMU,[10] (1) specifies a property that the design should satisfy as a formula in computation-tree logic (CTL) and (2) verifies a design specification against the CTL formula using a model checker.

The model checking approach suffers from several drawbacks. First, the designer has to specify manually the properties that the specification is supposed to satisfy. This can become a tedious and error-prone task for complex properties and large designs. Second, not all useful properties can be specified in CTL. More expressive logics have been devised, but the complexity of model checking increases for such logics. Third, model checking entails the traversal of the entire state space of the design specification, which can be huge. The last mentioned problem is called state explosion.

We have developed strategies to efficiently traverse the state space of a given design specification (or implementation) using a mixed depth-first/breadth-first strategy (c.f. "Sequential Logic Verification" on page 276) as opposed to previous traversal algorithms.[11] This traversal method is more complex to implement than the traversal methods proposed in the past, and model checking under this approach requires substantial modifications to retain efficiency. We will develop a new model checking algorithm based on our traversal algorithm. We believe that this new algorithm will be applicable to larger circuits than previous approaches have been.

Protocol Verification by Symbolic Analysis

One problem with most current approaches to design verification is that they do not scale well with problem size. For instance, model checking using currently available traversal algorithms for an 8-bit circuit will typically take significantly more time than for a 4-bit version of the same circuit, even though the property to be checked for is independent of bit-width.

Symbolic analysis can alleviate the scalability problem. For instance, checking a protocol corresponding to interdependent processes and interacting sets of timers for correctness involves checking to ensure that deadlock does not occur. More simply stated, control does not remain indefinitely in a particular loop. One way we can analyze the loop is to traverse the entire state space represented by the loop, but this approach has the same drawbacks mentioned above. A symbolic analysis can result in a significantly faster judgment regarding the nature of the loop. The

[10] E.M. Clarke and O. Grumberg, "Research on Automatic Verification of Finite State Concurrent Systems," *Ann. Rev. Comput. Sci.* 2: 269-290 (1987).

[11] A. Ghosh, S. Devadas, and A.R. Newton, "Verification of Interacting Sequential Circuits," paper presented at the 27th Design Automation Conference, Orlando, Florida, June 1990, pp. 213-219.

existence or non-existence of exit conditions can be determined easily.

We are attempting to classify protocols based on their amenability to symbolic analysis. We have found that the state space corresponding to loops in a common class of protocols can be simply specified using a linear system of equations. This implies that the reachability analysis of such protocols can be accomplished in polynomial time. A traversal method that depends on the bit-width could take exponential time for these circuits. We are currently trying to generalize our method to handle a larger class of protocols.

6.3.3 Implementation Verification

Introduction

During the design process, increasingly sophisticated optimization tools that modify a design to improve its area, performance or power dissipation characteristics are applied simultaneously or in sequence at various levels of design abstractions. Beginning from a behavioral specification, we typically move through register-transfer level representations, symbolic finite state machine representations, logic-level representations and transistor-level representations all the way to mask-level layout.

In order to ensure a working IC, each step of the design process above has to be checked for correctness. A viewpoint might be that we can check the transformations applied by the CAD tools for correctness once, and all the designs produced by the CAD system will be "correct by construction." Verifying the correctness of transformations in a synthesis system is absolutely necessary, but our experience has found that it is equally essential to provide an independent verification mechanism. For example, in logic synthesis systems all logic optimization steps are typically verified, formally or informally, to be correct, but experience has shown that it is necessary to supply *post facto* verification procedures to independently verify the results of the application of logic transformations on a particular example. Similarly, while behavioral transformations may have been proved correct, the correctness of their realization in a particular software system is not presently amenable to proof, and, as a result, the final product of their application in synthesizing a circuit also requires independent verification.

Timing Verification

It is important to determine efficiently and accurately the critical path delay of a VLSI circuit so that the clock period can be chosen to be greater than the critical delay. Overestimating the critical path can lead to an unnecessarily slow design, while underestimating the critical path has dangerous reliability implications.

Determining the critical path of a combinational circuit is complicated because a combinational circuit may have false paths, i.e., paths that are never sensitized during normal system operation. Therefore, simply picking the longest path in the circuit as the critical path can result in gross overestimations of critical delay.

Viability has been proposed by McGeer and Brayton as a robust and correct criterion for determining the critical path delay of a combinational circuit. Currently, algorithms that determine the longest viable path in a circuit require large amounts of CPU time on medium-large circuits. We are investigating more efficient means of determining the longest viable path in a given network. In particular, we see a connection between determining the longest viable path and generating a test for a particular multiple stuck-at fault in the circuit.

Circuit-Level Verification

Logic net-lists can be implemented in a variety of circuit-level methodologies. Static or dynamic circuits in CMOS or nMOS may be used. In the case of dynamic circuits, a wide range of clocking methodologies serve as design alternatives. Different methodologies impose differing sets of restrictions on the topology and interconnection of the circuit blocks. Violations of these circuit design rules can go undetected during simulation. It is important that one checks for schematic-level correctness under the chosen design methodology.

Recent work by Bamji and Allen[12] formalized the process of verifying that a circuit-level schematic obeys a particular design methodology. Circuit correctness was tied to a rigorous set of context-free grammar composition rules. These rules define how a small set of module symbols may be combined for circuits adhering to the design methodology. Schematic net-lists are represented by graphs, and composition rules are defined as graph

[12] C. Bamji and J. Allen, "GRASP: A Grammar-Based Schematic Parser," in *Proceedings of the 26th Design Automation Conference*, June 1990, pp. 448-453.

transformations similar to grammatical productions. Starting with a circuit net-list, a hierarchical parse tree that can demonstrate the well-formedness of the circuit is constructed. Since the procedure is hierarchical and incremental, it operates one or two orders of magnitude faster than previous approaches.

A drawback to the above approach is that it can handle only circuit design methodologies which can be specified under context-free grammar rules. While context-free grammars can be used to specify a variety of circuit design methodologies (e.g., a 2-phase CMOS clocking methodology), complex special-case rules typically cannot be specified. We are currently investigating the use of higher-level grammars under a similar mechanism which will allow for the verification of more complex circuit design methodologies.

Sequential Logic Verification

It is necessary to verify the equivalence of combinational or sequential circuits described at the logic level to check that a logic design step or a logic optimization system has not introduced errors into the design.

Recently, there has been considerable progress in the area of sequential logic verification. Two broad classes of approaches can be identified — approaches that use reduced, ordered Binary Decision Diagrams as their base representation to perform a breadth-first traversal of the State Transition Graph (STG) of a FSM[13] and approaches that use cube representations to perform a depth-first traversal of the STG.[14] The former approach performs significantly better than the latter on datapath-like FSMs whose STGs are highly connected, while the latter outperforms the former on counter-like FSMs where there are long chains of states.

We have developed a depth-first traversal technique for sequential machines that enables the traversal of counter FSMs in O(n) steps, where n is the number of bits in the counter. Our depth-first geometric chaining is based on it traversing geometrically increasing (or decreasing) chains of states and edges in the STG in any given set of steps. Other STG traversal approaches require 2^n steps, since only one state can be traversed in each step. We believe that a synergistic combination of depth-first geometric chaining and previously proposed breadth-first approaches offers an efficient traversal technique for a broad class of circuits that include both datapath and control portions. We will implement and investigate the applicability of this mixed depth-first/breadth-first strategy on real-life circuits.

Behavioral Verification

As described above, equivalence checking between two finite-state automata or two combinational logic circuits is precisely defined and supported by a body of theoretical work. The major issue in the use of these algorithms is CPU efficiency. In contrast, verifying that a logic-level description correctly implements a behavioral specification is considerably less developed. One major hindrance toward a precise notion of behavioral verification has been that parallel, serial or pipelined implementations of the same behavioral description can be implemented in finite-state automata with different input/output behaviors.[15]

In recent work,[16] we used nondeterminism to model the degree of freedom that is afforded by parallelism in a behavioral description that also contains complex control. Given some assumptions, we showed how the set of finite automata derivable from a behavioral description under all possible schedules of operations can be represented compactly as an input-programmed automaton (p-Automaton). The above method allows for extending the use of finite-state automata equivalence-checking algorithms to the problem of behavioral verification.

---

[13] O. Coudert, C. Berthet, and J.C. Madre, "Verification of Sequential Machines Using Boolean Functional Vectors," In IMEC-IFIP International Workshop on Applied Formal Methods for Correct VLSI Design, November 1989, pp. 111-128.

[14] S. Devadas, H-K. T. Ma, and A.R. Newton, "On the Verification of Sequential Machines at Differing Levels of Abstraction," in *IEEE Trans. Comput.-Aided Des.* 7: 713 (June 1988); A. Ghosh, S. Devadas, and A.R. Newton, "Verification of Interacting Sequential Circuits," paper presented at the 27th Design Automation Conference, Orlando, Florida, June 1990, pp. 213-219.

[15] M.C. McFarland and A.C. Parker, "An Abstract Model of Behavior for Hardware Descriptions," in *IEEE Trans. Comput.* C-32: 621 (1983).

[16] S. Devadas and K. Keutzer, "An Automata-Theoretic Approach to Behavioral Equivalence," in *Proceedings of the International Conference on Computer Aided Design,* November 1990.

We are in the process of extending the above approach to handle a richer set of behavioral transformations including pipelining and complex don't care conditions specified at a behavioral level. We believe that the use of p-Automata represents a general method to verify behavior against implementation.

6.3.4 Manufacture Test and VLSI Synthesis for Testability

Introduction

Once a chip has been fabricated, it is essential to check that no manufacturing defects have been introduced during the fabrication process. Manufacturing defects are modeled at different levels of design abstraction, and these fault models are used as a base for generating test vectors for a given design.

Fault models associated with defects that alter logical functionality are called logical fault models. For example, the most commonly used and the simplest logical fault model is the single stuck-at fault model, where a single wire in the IC is tied to a constant logical "1" or "0." Enhanced logical fault models like the multiple stuck-at fault model and the bridging fault model are more comprehensive, i.e., test vectors generated under these fault models typically detect a larger fraction of possible manufacturing defects. Deriving the test vectors under these fault models is considerably more difficult. For instance, given k wires in a circuit, there are only 2k single stuck-at faults, but $3^k - 1$ multiple stuck-at faults (multifaults), an astronomical number even for small circuits. However, for some applications reliability considerations are paramount, and it may be necessary to obtain as comprehensive a test set as possible.

Just checking the logical functionality of a fabricated circuit is not enough, its performance has to be verified as well. Manufacturing defects can degrade performance without altering logical functionality. Temporal or dynamic fault models like the gate delay fault model, transistor stuck-open fault model, and the path delay fault model have been proposed to model manufacturing defects that alter the performance characteristics of a circuit. As with the more comprehensive logical fault models, test generation under these dynamic fault models is considerably more difficult than under the simplistic single stuck-at fault model.

Most circuits being designed today are not testable for dynamic faults, and testing for multifaults and bridging faults requires exorbitant amounts of CPU time. Also, post-design testability measures cannot, in general, increase the testability of the circuit under these fault models. Our solution to this problem is to completely integrate testability considerations into an automatic design process, i.e., synthesize the circuit to be highly or fully testable under any given fault model.

VLSI circuits are typically sequential, and the problem of generating tests for sequential circuits is more difficult than that for combinational circuits, under any given fault model. While techniques such as scan design can transform a sequential test problem into a simpler one of combinational test generation, these techniques have not found widespread use due to reasons stemming from the design constraints, and the area and performance penalties associated with scan methods. Our research in testing also targets test generation under stuck-at and delay fault models for non-scan VLSI circuits, and synthesis for sequential testability.

Combinational Logic Synthesis for Testability Under Enhanced Fault Models

Combinational logic synthesis and optimization is a well-understood problem. The traditional cost functions used in synthesis have been layout area and circuit performance. Researchers have only recently begun to investigate the effect of logic transformations on the single and multiple stuck-at fault testability of a circuit[17] We are working on deriving algebraic and Boolean transformations for logic circuits to improve testability (and remove redundancy) with minimal or no impact on area and performance. Methods for implicit/test generation, i.e., obtaining test vectors to detect stuck-at faults as a by-product of the optimization steps, will be investigated. These methods are potentially much more efficient than explicit test generation algorithms, especially for multiple stuck-at faults.

---

[17] G.D. Hachtel, R.M. Jacoby, K. Keutzer, and C.R. Morrison, "On the Relationship Between Area Optimization and Multifault Testability of Multilevel Logic," paper published in the International Conference on Computer-Aided Design, November 1989, 422-425, (extended version submitted to *IEEE Trans. Comput.-Aided Des.*); S. Devadas and K. Keutzer, "Necessary and Sufficient Conditions for Robust Delay-Fault Testability of Logic Circuits," in the *Proceedings of the Sixth MIT Conference on Advanced Research on VLSI* (Cambridge: MIT Press, 1990).

Physical defects in ICs can degrade performance without affecting logic functionality. It is important to ensure that a given IC satisfies its timing specifications — This requires performing a delay fault test. This is especially important for aggressive design methodologies that push processing technology to the utmost. We have done some recent work on the synthesis of delay-fault testable combinational circuits. Certain classes of large circuits can be synthesized for complete robust path-delay-fault testability (which is the most comprehensive fault model devised thus far) with small area and performance penalties.[18] The primary drawbacks of current techniques are that non-flattenable random logic circuits, those that cannot be reduced to sum-of-products form, cannot be synthesized efficiently. We are currently improving upon the available synthesis techniques through the use of Binary Decision Diagrams as our base representation. Multiplexor-based networks, derived from replacing the nodes of Binary Decision Diagrams by 2-input multiplexors, have very interesting testability properties. Exploiting these properties can lead to an efficient synthesis-for-test strategy.

We are also investigating dynamic compaction techniques for test sets during synthesis. Compaction techniques tailored toward multiple stuck-at faults and delay faults are being developed. For instance, we believe that complete multiple stuck-at-fault test sets can be generated for random logic blocks that are only two to four times the size of the single-fault test set. Nonrobust delay test methodologies are not as comprehensive as robust delay test methodologies but offer scope for smaller test vector sets.

Sequential Logic Synthesis for Testability Under Enhanced Fault Models

VLSI circuits are typically sequential. A popular method of reducing the complexity of sequential test generation has involved the use of scan design methodologies (e.g., LSSD). Sequential test generation[19] and sequential logic synthesis for testability techniques that ensure non-scan single-stuck-at fault testability[20] have been, and will continue to be, a subject of investigation at MIT and elsewhere.

We are now looking toward the synthesis of sequential circuits for delay-fault testability. It is well known that arbitrary vector pairs cannot be applied to a sequential circuit under a standard-scan design methodology. This means that even if the combinational logic of a sequential circuit is made fully robustly delay-fault testable, it may not be fully testable under a standard-scan design implementation. An enhanced scan flip-flop that can store two bits of state is required. This "triple-latch" flip-flop increases the area of the circuit.

We have made preliminary investigations into the synthesis of non-scan sequential circuits for gate-delay-fault testability[21] These initial approaches were limited to circuits of small size. Several avenues are being explored in current research. First, we are developing techniques that ensure fully robustly gate-delay-fault testable chips under a standard-scan design methodology. Second, we are exploring the use of partial enhanced-scan and standard-scan design methods to improve the robust delay-fault testability of sequential circuits. Third, we are investigating the use of partial standard-scan and non-scan design. Our goal is to eventually obtain non-scan circuits that are completely robustly gate-delay-fault testable, with negligible area/performance penalties.

---

[18] S. Devadas and K. Keutzer, "Design of Integrated Circuits Fully Testable for Delay Faults and Multifaults," In *Proceedings of the International Test Conference,* October 1990, pp. 284-293; S. Devadas and K. Keutzer, "Synthesis and Optimization Procedures for Delay-Fault Testable Combinational Logic," paper presented at the 27th Design Automation Conference, Orlando, Florida, June 1990.

[19] A. Ghosh, S. Devadas, and A. R. Newton, "Test Generation and Verification of Highly Sequential Circuits," In *Proceedings of the International Conference on Computer-Aided Design,* November 1989, pp. 362-365.

[20] S. Devadas and K. Keutzer, "A Unified Approach to the Synthesis of Fully Testable Sequential Machines," *IEEE Trans. Comput.-Aided Des.,* 10(1): 39-50 (1991); S. Devadas and H-K. T. Ma, "Easily Testable PLA-based Finite State Machines," *IEEE Trans. on Comput.-Aided Des.,* 9(5): 614-611 (1990).

[21] S. Devadas," Delay Test Generation for Synchronous Sequential Circuits," in *Proceedings of the International Test Conference* (Washington, D.C.: August 1989), pp. 144-152.

Publications

Ashar, P., S. Devadas, and A.R. Newton. "Testability-Driven Decomposition of Large Finite State Machines." *Proceedings of International Conference on Computer Design: VLSI in Computers and Processors,* Boston, Massachusetts, September 1990.

Ashar, P., S. Devadas, and A.R. Newton. "Optimum and Heuristic Algorithms for A Formulation of Finite State Machine Decomposition." *IEEE Trans. Comput.-Aided Des.* 10(3): 296-310 (1991).

Ashar, P., A. Ghosh, S. Devadas, and K. Keutzer. "Implicit State Transition Graphs: Applications to Sequential Logic Synthesis and Test." *Proceedings of the International Conference on Computer-Aided Design,* Santa Clara, California, November 1990.

Ashar, P., S. Devadas, and A. Ghosh. "Boolean Satisfiability and Equivalence Checking Using General Binary Decision Diagrams." International Conference on Computer Design: VLSI in Computers and Processors, Cambridge, Massachusetts, October 1991.

Ashar, P., S. Devadas, and K. Keutzer. "Testability Properties of Multilevel Logic Networks Derived From Binary Decision Diagrams." *Proceedings of the Conference on Advanced Research in VLSI,* Santa Cruz, California, March 1991.

Ashar, P., S. Devadas, and A.R. Newton. "Irredundant Interacting Sequential Machines Via Optimal Logic Synthesis." *IEEE Trans. Comput.-Aided Des.* 10(3): 311-325 (1991).

Bryan, M.J., S. Devadas, and K. Keutzer. "Testability-Preserving Circuit Transformations." *Proceedings of the International Conference on Computer-Aided Design,* Santa Clara, California, November 1990.

Bryan, M.J., S. Devadas, and K. Keutzer. "Analysis and Design of Regular Structures for Robust Dynamic Fault Testability." IEEE International Symposium on Circuits and Systems, Singapore, June 1991.

Bryan, M.J., S. Devadas, and K. Keutzer, "Analysis and Design of Regular Structures for Robust Dynamic Fault Testability." *Inter. J. Comput.-Aided VLSI Des.* Forthcoming

Cheng, K-T., S. Devadas, and K. Keutzer. "Robust Delay-Fault Test Generation and Synthesis for Testability Under a Standard Scan Methodology." 28th Design Automation Conference, San Francisco, California, June 1991.

Devadas, S. "Delay Test Generation for Sychronous Sequential Circuits." *Inter. J. Comput.-Aided VLSI Des.* Forthcoming.

Devadas, S. "Optimization of Interacting Finite State Machines Using Sequential Don't Cares." *IEEE Trans. Comput.-Aided Des.* Forthcoming.

Devadas, S. "Optimal Layout Via Boolean Satisfiability." *Inter. J. Comput.-Aided VLSI Des.* 2(2): 251-262 (1990).

Devadas, S. "Optimization of Interacting Finite State Machines Using Sequential Don't Cares." *IEEE Trans. Comput.-Aided Des.* Forthcoming.

Devadas, S., and H-K. T. Ma. "Easily Testable PLA-based Finite State Machines." *IEEE Trans. Comput.-Aided Des.* 9(5): 614-611 (1990).

Devadas, S., and K. Keutzer. "A Unified Approach to the Synthesis of Fully Testable Sequential Machines." *IEEE Trans. Comput.-Aided Des.* 10(1): 39-50 (1991).

Devadas, S., and K. Keutzer. "Synthesis of Robust Delay-Fault Testable Circuits: Practice." *IEEE Trans. Comput.-Aided Des.* Forthcoming.

Devadas, S., and K. Keutzer. "Synthesis of Robust Delay-Fault Testable Circuits: Theory." *IEEE Trans. Comput.-Aided Des.* Forthcoming.

Devadas, S., and K. Keutzer. "An Automata-Theoretic Approach to Behavioral Equivalence." *Proceedings of the International Conference on Computer-Aided Design,* Santa Clara, California, November 1990.

Devadas, S., K. Keutzer, and A. Ghosh. "Recent Progress in VLSI Synthesis for Testability." *Proceedings of the VLSI Test Symposium,* Atlantic City, April 1991.

Devadas, S., and K. Keutzer. "Design of Integrated Circuits Fully Testable for Delay Faults and Multifaults." *Proceedings of the International Test Conference,* Washington, D.C., September 1990.

Devadas, S., and A.R. Newton. "Exact Algorithms for Output Encoding, State Assignment and Four-Level Boolean Minimization." *IEEE Trans. Comput.-Aided Des.* 10(1): 13-27 (1991).

Devadas, S., and K. Keutzer. "An Automata-Theoretic Approach to Behaviorial

Equivalence." *Intern. J. Comput.-Aided VLSI Des.* Forthcoming.

Devadas, S., K. Keutzer, and J.K. White. "Estimation of Power Dissipation in CMOS Combinational Circuits Using Boolean Function Manipulation." *IEEE Trans. Comput.-Aided Des.* Forthcoming.

Devadas, S., K. Keutzer, and S. Malik. "A Synthesis-Based Approach to Test Generation and Compaction for Multifaults." 28th Design Automation Conference, San Francisco, California, June 1991.

Devadas, S., K. Keutzer, and A.S. Krishnakumar. "Design Verification and Reachability Analysis Using Algebraic Manipulation." International Conference on Computer Design: VLSI in Computers and Processors, Cambridge, Massachusetts, October 1991.

Ghosh, A., S. Devadas, and A.R. Newton. "Heuristic Minimization of Boolean Relations Using Testing Techniques." *Proceedings of International Conference on Computer Design: VLSI in Computers and Processors,* Boston, Massachusetts, September 1990.

Ghosh, A., and S. Devadas. "Implicit Depth-First Transversal of Sequential Machines." IEEE International Symposium on Circuits and Systems, Singapore, June 1991.

Ghosh, A., S. Devadas, and A.R. Newton. "Test Generation and Verification of Highly Sequential Circuits." *IEEE Trans. Comput.-Aided Des.* Forthcoming.

Ghosh, A., S. Devadas, and A.R. Newton. "Synthesis for Sequential Logic Testability using Register-Transfer Level Descriptions." *Proceedings of the International Test Conference,* Washington, D.C., September 1990.

6.4 Mixed Circuit/Device Simulation

Sponsors

IBM Corporation
U.S. Navy - Office of Naval Research
Contract N00014-87-K-0825

Project Staff

Mark W. Reichelt, Professor Jacob White, Professor Jonathan Allen

For critical applications, the four-terminal lumped models for MOS devices used in programs like SPICE are not sufficiently accurate. Also, it is difficult to relate circuit performance to process changes using lumped models. Sufficiently accurate transient simulations can be performed if, instead of using a lumped model for each transistor, some of the transistor terminal currents and charges are computed by numerically solving the drift-diffusion based partial differential equation approximation for electron transport in the device. However, simulating a circuit with even a few of the transistors treated by solving the drift-diffusion equations is very computationally expensive because the accurate solution of the transport equations of an MOS device requires a two-dimensional mesh with more than a thousand points.

One approach to accelerating this kind of mixed device and circuit simulation is to use waveform relaxation to perform the transient simulation, not only at the circuit level, but also inside the devices being simulated with a drift-diffusion description. In the present investigation, the WR algorithm is being applied to the sparsely-connected system of algebraic and ordinary differential equations in time generated by standard spatial discretization of the drift-diffusion equations that describe MOS devices. Several theoretical results about the uniformity of WR convergence for the semiconductor problem have been proved,[22] and we have also completed experiments using waveform relaxation to perform transient two-dimensional simulation of MOS devices. Speed and accuracy comparisons between standard direct methods and red/black overrelaxed waveform-relaxation-Newton indicate that for the experiments examined, calculated terminal currents match well between the methods, and our overrelaxed waveform-relaxation-Newton

[22] M. Reichelt, J. White, J. Allen and F. Odeh, "Waveform Relaxation Applied to Transient Device Simulation," *Proceedings of the International Symposium on Circuits and Systems,* Espoo, Finland, June 1988, pp. 1647-1650.

method was five to eleven times faster.[23] Currently, efforts are underway to develop the WORDS program (Waveform OverRelaxation Device Simulator) into a more robust code, with adaptive SOR parameterization; Poisson-only, or one or two carrier simulation options; and improved physical modeling. All physical models were verified by comparison and agreement with the industry-standard device simulator PISCES. Finally, a parallel version of WORDS was written for the iPSC/2 parallel architecture, demonstrating a speedup factor of 15.5 on 16 processors.

6.5 Simulation Algorithms for Clocked Analog Circuits

Sponsors

AT&T
Analog Devices
Digital Equipment Corporation
IBM Corporation
National Science Foundation
Grant MIP 88-58764
U.S. Navy - Office of Naval Research
Contract N00014-87-K-0825

Project Staff

Steven B. Leeb, Luis M. Silveira, Professor Jacob White

A challenging problem in the area of analog circuits is the simulation of clocked analog circuits like switching filters, switching power supplies, and phase-locked loops. These circuits are computationally expensive to simulate using conventional techniques because these kinds of circuits are all clocked at a frequency whose period is orders of magnitude smaller than the time interval of interest to the designer. To construct such a long time solution, a program like SPICE or ASTAP must calculate the behavior of the circuit for many high frequency clock cycles. The basic approach to simulating these circuits more efficiently is to exploit only the property that the behavior of such a circuit in a given high frequency clock cycle is similar, but not identical to, the behavior in the preceding and following cycles. Therefore, by accurately computing the solution over a few selected cycles, an accurate long time solution can be constructed.

Simulating clocked analog systems is an old problem, but this novel approach has led to a very efficient algorithm for the distortion analysis of switched-capacitor filters. The idea is based on simulating selected cycles of the high-frequency clock accurately with a standard discretization method and pasting together the selected cycles by computing the low frequency behavior with a truncated Fourier series. If carefully constructed, the nonlinear system that must be solved for the Fourier coefficients is almost linear and can be solved rapidly with Newton's method.[24] Transient behavior, important for switching power supply designers, has also been accelerated using similar techniques.[25] In particular, the "envelope" of the high-frequency clock can be followed by accurately computing the circuit behavior over occasional cycles.

6.6 Parallel Simulation Algorithms for Analog Array Signal Processors

Sponsors

National Science Foundation
Grant MIP 88-58764
U.S. Navy - Office of Naval Research
Contract N00014-87-K-0825

Project Staff

Andrew Lumsdaine, Luis M. Silveira, Professor John L. Wyatt, Jr., Professor Jacob White

The "vision circuits" form a class of circuits which, for the most part, cannot be simulated with traditional programs. These circuits are necessarily very large and must be simulated exactly at an analog level (i.e., one cannot perform simulations at a switch or gate level as is commonly done with very large digital circuits). Typical analog circuit simulators can not handle vision circuits simply

---

[23] M. Reichelt, J. White, and J. Allen, "Waveform Relaxation for Transient Simulation of Two-Dimensional MOS Devices," *Proceedings of the International Conference on Computer-Aided Design*, Santa Clara, California, October 1989, pp. 412-415.

[24] K. Kundert, J. White, and A. Sangiovanni-Vincentelli, "A Mixed Frequency-Time Approach for Distortion Analysis of Switching Filter Circuits," *IEEE J. Solid-State Circ.* 24(2): 443-451(1989).

[25] J. White and S. Leeb, "An Envelope-Following Approach to Switching Power Converter Simulation," *IEEE Trans. Power Electron.*

because of their immense size, since the computation time for these simulators grows super-linearly with the size of the circuit. However, because these circuits are somewhat similar to certain discretized partial differential equations, one can exploit their special characteristics to obtain efficient simulation techniques.

Over the last past year, we have completed the development of CMVSIM, a program for circuit-level simulation of grid-based analog signal processing arrays which uses a massively parallel processor. CMVSIM uses: (1) the trapezoidal rule to discretize the differential equations that describe the analog array behavior, (2) Newton's method to solve the nonlinear equations generated at each time-step, and (3) a block conjugate-gradient squared algorithm to solve the linear equations generated by Newton's method. Excellent parallel performance is achieved through the use of a novel, but very natural, mapping of the circuit data onto the massively parallel architecture. The mapping takes advantage of the underlying computer architecture and the structure of the analog array problem. Experimental results demonstrate that a full-size Connection Machine can provide a 1400 times speedup over a SUN-4/280 workstation.[26]

6.7 Numerical Simulation of Short Channel MOS Devices

Sponsors

Analog Devices
U.S. Navy - Office of Naval Research
Contract N00014-87-K-0825.

Project Staff

Jennifer A. Lloyd, Joel Phillips, Khalid Rahmat, Professor Dimitri A. Antoniadis, Professor Jacob White

The model which is used in conventional device simulation programs is based on the drift-diffusion model of electron transport and does not accurately predict the field distribution near the drain in small geometry devices. This prediction is of particular importance for predicting oxide breakdown due to penetration by "hot" electrons. There are two approaches for more accurately computing the electric fields in MOS devices: one is based on adding an energy equation to the drift-diffusion model and the second is based on particle or Monte-Carlo simulations.

In the first approach, an energy balance equation is solved along with the drift-diffusion equations so that the electron temperatures are computed accurately. This combined system is numerically less tame than the standard approach and must be solved carefully. The most serious problem was that with the physically correct mobility model, which utilizes the electron temperature, our simulator did not converge if the mesh spacing was not fine enough; this problem was especially acute in the region under the drain junction. The problem was inherent in the method used to discretize the energy balance equation. With a new discretization strategy, this problem was solved, and the simulator now converges even when a very coarse mesh is used.

Besides including the electron temperature dependence, the mobility model used in the simulator has been made more physically realistic by including the effects of the vertical gate field. To tune some of the empirical parameters in the simulator, extensive comparisons with data from fabricated devices, including some with very short channels (0.16 um), were done. The simulator predicts the current to about 10-12 percent accuracy. The largest errors occur in deep saturation. This also leads to inaccuracies in the conductance in the deep saturation region.

Also, a simple method for estimating the substrate current has been implemented. The scheme assumes that the substrate current is proportional to the number of electrons above a threshold energy. With a fixed choice of this energy threshold, good agreement has been achieved with measured data except for low gate biases and high drain voltages.

In the area of Monte Carlo device simulation, we are focusing on transient calculations with self-consistent electric fields. Specifically, we are trying to apply the recently developed implicit particle methods. To apply these implicit particle methods to semiconductors, we are decomposing the field calculation into three parts: one due to charged particles, a second due to dopant ions, and a third due to boundaries. This allows the calculation of the electric field acting on every charged particle in the system to be performed rapidly and accurately. In particular, this allows the use of the fast multipole algorithm for the

[26] L.M. Silveira, A. Lumsdaine, and J. White, "Massively Parallel Simulation of Grid-based Analog Circuits," *Proceedings of the International Conference on Computer-Aided Design*, Santa Clara, California, October 1990; A. Lumsdaine, L. Silveira, and J. White, "CVSim Users Guide," in preparation.

particle-particle interactions. Currently, we have rewritten a Silicon Monte Carlo code from the National Center for Computational Electronics to use ensemble Monte Carlo methods and are now including the electric field calculations.[27]

6.8 Efficient 3-D Capacitance Extraction Algorithms

Sponsors

IBM Corporation
National Science Foundation
Grant MIP 88-58764
U.S. Navy - Office of Naval Research
Contract N00014-87-K-0825.

Project Staff

Keith S. Nabors, Songmin Kim, Professor Jacob White

We have developed a fast algorithm for computing the capacitance of a complicated 3-D geometry of ideal conductors in a uniform dielectric and have implemented the algorithm in the program FASTCAP. This method is an acceleration of the boundary-element technique for solving the integral equation associated with the multiconductor capacitance extraction problem. Boundary-element methods become slow when a large number of elements are used because they lead to dense matrix problems which are typically solved with some form of Gaussian elimination. This implies that the computation grows as n^3, where n is the number of panels or tiles needed to accurately discretize the conductor surface charges. Our new algorithm, which is a generalized conjugate residual iterative algorithm with a multipole approximation to compute the iterates, reduces the complexity so that accurate multiconductor capacitance calculations grow nearly as nm where m is the number of conductors.[28]

Our most recent work has been to develop an adaptive multipole algorithm, and establish a link between the FASTCAP program and the MIT Micro-Electrical-Mechanical CAD (MEMCAD) system, by using the MEMCAD system to draft and compute the capacitance of a realistic geometry. Our future work in this subject will be to include dielectric interfaces and then to turn our attention to developing a multipole algorithm to accelerate the calculation of inductances.

6.9 Parallel Numerical Algorithms

Sponsor

U.S. Navy - Office of Naval Research
Contract N00014-87-K-0825.

Project Staff

Andrew Lumsdaine, Mark W. Reichelt, Luis M. Silveira, Ricardo Telichevesky, Professor Jacob White

We are trying to develop parallel algorithms for circuit and device simulation that are effective on either massively parallel machines like the Connection Machine or on hypercube machines like the Intel hypercube. In the sections above we described our work on parallel device simulation using waveform relaxation and on parallel simulation algorithms for analog arrays. In addition, we are also trying to understand some fundamental problems of the interaction between architecture and certain numerical algorithms.

For example, the direct solution of circuit simulation matrices is particularly difficult to parallelize, in part because methods like parallel nested dissection are ineffective due to the difficulty of finding good separators. For that reason, general sparse matrix techniques are being studied. In particular, the interaction between sparse matrix data structures, computer memory structure, and multiprocessor communication is being investigated (with Professor W. Dally). The most interesting results from simulations so far is that communication throughput, and not latency, is more crucial to final performance.

Explicit integration methods avoid matrix solution and are, therefore, also interesting algorithms to use on parallel processors. For this reason, we investigated some of properties of the recently developed explicit exponentially-fit integration algorithms. We considered the multivariate test problem $x = -Ax$ where $A \in \mathcal{R}^{n \times n}$ and is assumed to be connectedly diagonally-dominant with posi-

---

[27] J. Lloyd, J. Phillips, and J. White, "A Boundary-Element/Multipole Algorithm for Self-Consistent Field Calculations in Monte-Carlo Simulation," *Proceedings of Workshop on Numerical Modeling of Processes and Devices for Integrated Circuits*, NUPAD III, Honolulu, Hawaii, June 1990, pp. 81-82.

[28] K. Nabors and J. White, "FastCap: A Multipole-Accelerated 3-D Capacitance Extraction Program," *IEEE Trans. Comput.-Aided Des.*, forthcoming; K. Nabors, S. Kim, and J. White, "FastCap Users Guide," in preparation.

tive diagonals, because this models the equations resulting from the way MOS circuits are treated in timing simulation programs. We showed that for these problems the CINNAMON exponentially-fit algorithm is A-stable and gave an example where the algorithm in XPSim is unstable. A semi-implicit version of the XPSim algorithm was derived and shown to be A-stable. Examination of examples demonstrate that neither the stabilized XPSim algorithm nor the CINNAMON algorithm produces satisfactory results for very large timesteps. This is also the case for the semi-implicit algorithms as used in the MOTIS timing simulator. The effect of ordering on the accuracy and stability of the integration methods was also examined, and it was shown that ordering always enhances accuracy, although not significantly for large timesteps, and that the XPSim algorithm can be made more stable with a carefully chosen ordering.[29]

6.10 Integrated Circuit Reliability

Sponsors

Digital Equipment Corporation
U.S. Navy - Office of Naval Research
Contract N00014-87-K-0825

Project Staff

Kevin Lam, Professor Srinivas Devadas, Professor Jacob White

The high transistor density now possible with CMOS integrated circuits has made peak power dissipation and peak current density important design considerations. However, peak quantities in a logic circuit are usually a function of the input vector or vector sequence applied. This makes accurate estimation of peak quantities extremely difficult, since the number of input sequences that have to be simulated in order to find the sequence that produces the peak is *exponential* in the number of inputs to the circuit. By using simplified models of power and current dissipation, peak quantities, like power or current density, can be related to maximizing gate output activity and weighted to account for differing load capacitances or transistor sizes. Transformations can then be derived that convert a logic description of a circuit into a multiple-output Boolean function of the input vector or vector sequence, where each output of the Boolean function is associated with a logic gate output transition. It then follows that to find the input or input sequence that maximizes the quantity of interest, a *weighted max-satisfiability* problem must be solved. For the problem of estimating peak power dissipation, algorithms for constructing the Boolean function for dynamic CMOS circuits, as well as for static CMOS, which take into account dissipation due to glitching, have been derived and exact and approximate algorithms for solving the associated weighted max-satisfiability problem have been developed.[30]

[29] H. Neto, L. Silveira, J. White, and L. Vidigal, "On Exponential Fitting for Circuit Simulation," *Proceedings of the International Symposium on Circuits and Systems*, New Orleans, 1990, pp. 514-518.

[30] S. Devadas, K. Keutzer, and J. White, "Estimation of Power Dissipation in CMOS Combinational Circuits," *Proceedings of the Custom Integrated Circuits Conference*, Boston, 1990, pp. 19.7.1-19.7.6.

Part IV Language, Speech and Hearing

Section 1 Speech Communication

Chapter 1. Speech Communication

Academic and Research Staff

Professor Kenneth N. Stevens, Professor Jonathan Allen, Professor Morris Halle, Professor Samuel J. Keyser, Dr. Corine A. Bickley, Dr. Suzanne E. Boyce, Dr. Carol Y. Espy-Wilson, Dr. Marie K. Huffman, Dr. Michel T. Jackson, Dr. Melanie L. Matthies, Dr. Joseph S. Perkell, Dr. Mark A. Randolph, Dr. Stefanie R. Shattuck-Hufnagel, Dr. Mario A. Svirsky, Dr. Victor W. Zue

Visiting Scientists and Research Affiliates

Giulia Arman-Nassi,[1] Dr. Richard S. Goldhor,[2] Dr. Robert E. Hillman,[3] Dr. Jeannette D. Hoit,[4] Eva B. Holmberg,[5] Dr. Tetsuo Ichikawa,[6] Dr. Harlan L. Lane,[7] Dr. John L. Locke,[8] Dr. John I. Makhoul,[9] Dr. Carol C. Ringo,[10] Dr. Noriko Suzuki,[11] Jane W. Webster[12]

Graduate Students

Abeer A. Alwan, Marilyn Y. Chen, Helen M. Hanson, Andrew W. Howitt, Caroline B. Huang, Lorin F. Wilde

Undergraduate Students

Anita Rajan, Lorraine Sandford, Veena Trehan, Monnica Williams

Technical and Support Staff

Ann F. Forestell, Seth M. Hall, D. Keith North, Arlene Wint

1.1 Introduction

Sponsors

C.J. Lebel Fellowship
Dennis Klatt Memorial Fund
Digital Equipment Corporation

---

[1] Milan Research Consortium, Milan, Italy.

[2] Audiofile, Inc., Lexington, Massachusetts.

[3] Boston University, Boston, Massachusetts.

[4] Department of Speech and Hearing Sciences, University of Arizona, Tucson, Arizona.

[5] MIT and Department of Speech Disorders, Boston University, Boston, Massachusetts.

[6] Tokushima University, Tokushima, Japan.

[7] Department of Psychology, Northeastern University, Boston, Massachusetts.

[8] Massachusetts General Hospital, Boston, Massachusetts.

[9] Bolt Beranek and Newman, Inc., Cambridge, Massachusetts.

[10] University of New Hampshire, Durham, New Hampshire.

[11] First Department of Oral Surgery, School of Dentistry, Showa University, Tokyo, Japan.

[12] Massachusetts Eye and Ear Infirmary, Boston, Massachusetts.

National Institutes of Health
Grants T32 DC00005, 5-R01 DC00075, F32 DC00015, S15 NS28048, R01 NS21183,[13] P01 NS23734,[14] and 1-R01 DC00776
National Science Foundation
Grants IRI 88-05680[13] and IRI 89-10561

The overall objective of our research in speech communication is to gain an understanding of the processes whereby (1) a speaker transforms a discrete linguistic representation of an utterance into an acoustic signal, and (2) a listener decodes the acoustic signal to retrieve the linguistic representation. The research includes development of models for speech production, speech perception, and lexical access, as well as studies of impaired speech communication.

1.2 Models, Theory, and Data in Speech Physiology

1.2.1 Comments on Speech Production Models

A paper on speech production models has been prepared for the 12th International Congress of Phonetic Sciences (Aix-en-Provence, France, August 1991). The paper discusses modeling which covers the entire transformation from a linguistic-like input to a sound output. Such modeling can make two kinds of contribution to our understanding of speech production: (1) forcing theories of speech production to be stated explicitly and (2) serving as an organizing framework for a focused program of experimentation. As an example, a "task dynamic" production model is cited. The model incorporates underlying phonological primitives that consist of "abstract articulatory gestures." Initial efforts have been made to use the model in interpreting experimental data. Several issues that arise in such modeling are discussed: the validity of the underlying theory, incorporating realistic simulations of peripheral constraints, accounting for timing, difficulties in using models to evaluate experimental data, and the use of neural networks. Suggestions for an alternative modeling approach center around the need to include the influence of speech acoustics and perceptual mechanisms on strategies of speech production.

1.2.2 Models for Articulatory Instantiation of Feature Values

Data from previous studies of speech movements have been used as a basis for several theoretical papers focusing on models for the articulatory instantiation of particular distinctive feature values. Two of the papers (prepared in collaboration with colleagues from Haskins Laboratories) address models of coarticulation for the features +/- ROUND and +/- NASAL. In both papers, we review conflicting reports in the literature on the extent of anticipatory coarticulation and present evidence to suggest that these conflicts can be resolved by assuming that segments not normally associated with a rounding or nasalization feature show stable articulatory patterns associated with those features. In one of the papers, we point out that these patterns may have been previously interpreted as anticipatory coarticulation of rounding or nasality. We further argue that timing and suprasegmental variables can be used to show that this is the case and that the coproduction model of coarticulation can best explain the data. In the other paper, we use similar data to argue against the "targets and (interpolated) connections" model proposed by Keating. In a third paper on this general topic, coarticulatory patterns of rounding in Turkish and English are compared and evidence is given to show that their modes of articulatory organization may be different.

1.2.3 Modeling Midsagittal Tongue Shapes

Two projects on articulatory modeling are in progress. The first is concerned with the construction of a quantitative, cross-linguistic articulatory model of vowel production, based in cineradiographic data from Akan, Arabic, Chinese, and French. Programs for displaying, processing, and partially automating the process of taking measurements from cineradiographic data have been developed for the purpose of gathering data for this work. The second project is concerned with quantitatively testing the generalizability of this model to similar data gathered from speakers of English, Icelandic, Spanish, and Swedish.

Future work will focus on the degree to which this model generalizes from vowel production to consonant production. Velar and uvular consonants, which, like vowels, are articulated primarily with

[13] Under subcontract to Boston University.

[14] Under subcontract to Massachusetts General Hospital.

the tongue body, should be able to be generated by the model with no additional parameters; it is an open question whether or not the same will be true of other consonants such as pharyngeals and palatals, it almost certainly will not be true of coronals.

1.3 Speech Synthesis

Research on speech synthesis has concentrated for the most part on developing improved procedures for the synthesis of consonant-vowel and vowel-consonant syllables. With the expanded capabilities of the KLSYN88 synthesizer developed by Dennis Klatt, it is possible to synthesize utterances that simulate in a more natural way the processes involved in human speech production. The details of these procedures are based on theoretical and acoustical studies of the production of various classes of speech sounds, so that the manipulation of the synthesis parameters is in accord with the mechanical, aerodynamic, and acoustic constraints inherent in natural speech production.

For example, using the improved glottal source, including appropriately shaped aspiration noise, procedures for synthesizing the transitions in source characteristics between vowels and voiceless consonants and for synthesizing voicing in obstruent consonants have been specified. Methods for manipulating the frequencies of a pole-zero pair in the cascade branch of the synthesizer have led to the synthesis of nasal, lateral, and retroflex consonants with spectral and temporal characteristics that match closely the characteristics of naturally-produced syllables. The synthesis work is leading to an inventory of synthetic consonant-vowel and vowel-consonant syllables with precisely specified acoustic characteristics. These syllables will be used for testing the phonetic discrimination and identification capabilities of an aphasic population that is being studied by colleagues at Massachusetts General Hospital.

An additional facet of the synthesis research is the development of ways of characterizing different male and female voices by manipulating the synthesizer parameters, particularly the waveform of the glottal source, including the noise component of this waveform. We have found informally that it is possible to reproduce the spectral properties of a variety of different male and female voices by adjustment of these parameters.

1.4 Speech Production of Cochlear Implant Patients

1.4.1 Longitudinal Changes in Vowel Acoustics in Cochlear Implant Patients

Acoustic parameters were measured for vowels spoken in /hVd/ context by three postlingually-deafened cochlear implant recipients. Two female subjects became deaf in adulthood; the male subject, in childhood. Longitudinal recordings were made before and at intervals following processor activation. The measured parameters included formant frequencies, *F0*, *SPL*, duration and amplitude difference between the first two harmonic peaks in the log magnitude spectrum (*H1* - *H2*). A number of changes were observed from pre- to post-implant with inter-subject differences. The male subject showed changes in *F1*, vowel durations and *F0*. These changes were consistent with one another; however, they were not necessarily in the direction of normalcy. On the other hand, the female subjects showed changes in *F2*, vowel durations, *F0* and *SPL* which were in the direction of normal values and, for some parameters, tended to enhance phonemic contrasts. For all three subjects, *H1* - *H2* changed in a direction which was consistent with previously-made flow measurements. Similar data from additional subjects are currently being analyzed.

1.4.2 Effects on Vowel Production and Speech Breathing of Interrupting Stimulation from the Speech Processor of a Cochlear Prosthesis

We have completed a study on the short-term changes in speech breathing and speech acoustics caused by 24 hours of processor deactivation and by brief periods of processor activation and deactivation during a single experimental session in cochlear implant users. We measured the same acoustic parameters employed in the above-described longitudinal study of vowel production and the same physiological parameters used in a longitudinal study of changes in speech breathing.

We found significant and asymmetric effects of turning the processor on and off for a number of speech parameters. Parameter changes induced by short-term changes in the state of the processor were consistent with longitudinal changes for two of the three subjects. Most changes were in the direction of enhancing phonetic contrasts when

the processor was on. Although each subject behaved differently, within a subject the pattern of changes across vowels was generally consistent. Certain parameters, such as breathiness and airflow proved to be closely coupled in their changes, as in the longitudinal studies. (This coupling occurred even in the subject whose responses to processor activation where inconsistent with the long-term changes obtained in the longitudinal study.) The greater responsiveness of speech parameters to the onset of processor activation than to its offset supports the hypothesis that auditory stimulation has a "calibrational" role in speech production, retuning pre-existing articulatory routines. Many of the findings thus far implicate control of the larynx as a major focus of recalibration, but other speech production parameters need to be analyzed. As suggested by certain findings about parameter relations in the longitudinal study, we expect that as we progress in our understanding of those relations, we will be able to give a principled account of many of the apparent differences we observed among these initial subjects.

1.4.3 Methods for Longitudinal Measures of Speech Nasality in Cochlear Implant Patients

We have been examining the validity of longitudinal measures of nasality in cochlear implant patients, based on acoustic spectra, sound levels and outputs of nasal and throat accelerometers. Speech materials consist of isolated utterances and reading passages. Preliminary observations indicate the following: The ratio of RMS values of nasal and throat accelerometer outputs (a technique used in published experiments) may be influenced by: (1) variation in the relative levels of the two signals during the recommended calibration maneuver, i.e., production of a sustained /m/; and (2) substantial changes in SPL that accompany onset of "auditory" stimulation from a cochlear prosthesis. These observations raise uncertainty about using the throat accelerometer output as a reference and the sensitivity of this kind of measure to longitudinal changes in nasality across experimental sessions. In addition, measures of harmonic and formant amplitudes from acoustic spectra may be confounded by changes in coupling to tracheal resonances that also accompany the activation of the prosthesis. These observations and additional measures and calibration strategies are being explored further.

1.5 Phonatory Function Associated with Misuse of the Vocal Mechanism

1.5.1 Vocal Nodules in Females

In this study, we used our methods for obtaining measurements from the inverse filtered glottal waveform, electroglottographic signal (EGG), and average transglottal pressure and glottal airflow to compare phonatory function for a group of twelve female bilateral vocal-fold nodules patients with a control group of age-matched normal females. Statistical analysis of the data involved analysis of variance (ANOVA) and analysis of covariance (ANCOVA with SPL the covariate) procedures to test for significant differences between the groups. Standard and regressed Z scores were also used to compare measurements for individual nodules subjects with the normal group.

The largest number of significant differences between the nodules and normal group were found for the loud voice condition, with normal voice having the second largest number of significant differences and soft voice the smallest number of differences. A majority of the significant differences between nodules and normal subjects were associated with higher SPL used by the nodules group. Increased SPL in the nodules group was accompanied, most notably, by increases in parameters. These are believed to reflect greater potential for vocal-fold trauma (i.e., increased transglottal pressure, AC (modulated) glottal flow, peak glottal flow and maximum rate of glottal flow declination) due to high vocal-fold closure velocities and collision forces. In addition, an examination of individual Z-score profiles revealed that three of the twelve nodules patients displayed instances in which SPL was within normal limits, but AC flow and/or maximum flow declination rate was abnormally high. In addition, there were four nodules patients who displayed instances in which SPL, AC flow and maximum flow declination rate were all abnormally high, but AC flow and/or maximum flow declination rate was proportionally higher than the SPL.

In summary, the results suggest that for most female nodules patients, abnormalities in vocal function are primarily associated with use of excessive loudness. Thus, for patients who fit this profile, simply reducing loudness through direct facilitation and/or vocal hygiene training may represent appropriate treatment. However, there appears to be a smaller proportion of female nodules patients whose abnormalities in vocal function are not completely accounted for by excessive loudness. These patients may be dis-

playing an underlying "pattern" of vocal hyperfunction which could require additional therapeutic procedures to ameliorate.

1.5.2 Speech Respiration Associated with Vocal Hyperfunction: a Pilot Study

This pilot study compared respiratory function in an adult female nodules patient with a sex, age and body-type matched normal control. Inductance plethysmography (a Respitrace) was used to obtain a variety of speech and non-speech respiratory measures at normal and "loud" vocal intensity.

The non-speech respiratory performance of both subjects was within normal limits. The matched control also displayed normal values for measures of speech respiration. In contrast, the subject with vocal-fold nodules showed clear evidence of deviant speech respiration during oral reading such as abnormally low inspiratory volumes, with the majority of expiratory limbs for speech being initiated at levels within the quiet tidal volume range. During loud reading, the nodules patient initiated speech at lung volumes that were equal to or less than those used at normal loudness. This result is quite unlike normal speakers who tend to inhale to higher lung volumes in preparation for louder utterances. The nodules patient also displayed consistent, marked encroachment into the expiratory reserve volume during reading at normal loudness, with even further encroachment during loud reading. This pattern is deviant from normal speakers who tend to terminate utterances close to the functional residual capacity. Taken together, the results for the nodules subject reflect reduced efficiency of speech respiratory function. This patient produced alveolar pressures required for speech by expending greater expiratory muscular effort, instead of inhaling like normal speakers to larger lung volumes, thereby taking advantage of greater natural recoil forces to assist in generating required pressures. The nodules patient also tended to stop at inappropriate (non-juncture) points within sentences to inhale and evidenced loss of substantial volumes of air prior to the initiation of phonation.

Thus, the results indicate that abnormalities in speech respiration can occur in a patient with a hyperfunctionally-related voice disorder (nodules). This finding will be pursued in future studies of additional patients.

1.5.3 Comparisons Between Inter- and Intra-speaker Variation in Aerodynamic and Acoustic Parameters of Voice Production

In this study, intraspeaker variation of non-invasive aerodynamic and acoustic measurements of voice production was examined across three recordings for three normal female and three normal male speakers. Data from one recording for each of fifteen females and fifteen males served as normative references. The following measurements were made for productions of sequences of the syllable /pæ/ in soft, normal and loud voice and low and high pitch: the inverse filtered airflow waveform average transglottal air pressure and glottal airflow, and the amplitude difference between the two first harmonics of the acoustic spectrum. Linear regression analyses between individual values of SPL and each of the other parameters were performed for data pooled across the three recordings. In addition, comparisons between the individual subjects and the reference groups were performed using Z-score analysis.

Preliminary results showed that a small amount of SPL variation could be accompanied by large variation in other parameters. For some parameters (e.g., maximum flow declination rate and AC flow), both inter- and intra-speaker variation were significantly related to SPL. For such parameters the effects of SPL can be removed statistically, and comparisons between individual subjects and group data can readily be made. For other parameters, which showed large inter-speaker variation not significantly related SPL, intra-speaker variation for individual subjects could be orderly related to SPL (e.g., for DC flow offset). For such parameters, data from several baseline recordings can be useful to establish to what extent parameters—for which both inter- and intra-speaker variation was large and not significantly related to SPL (e.g., average flow)—were considered less useful as indices of abnormal vocal function. These data suggest that in order to quantify normal variation, both inter- and intra-speaker variation should be considered.

1.6 Studies of Acoustics and Perception of Speech Sounds

1.6.1 Vowels

Previous reports have described an acoustic study of vowels in which the effects of consonantal context, lexical stress, and speech style were compared using the same database of utterances. That study, which had been extended, was completed during the past year and included perceptual experiments in which listeners identified vowels excised from the utterances in the database. The completed data compilation verifies that consonant context affects the vowel midpoints more than lexical stress and speech style. The direction and magnitude of the formant frequency shifts were consistent with findings of previous studies. The liquid and glide contexts, /w/, /r/, and /l/, lowered the *F*2 frequency of front vowels, especially lax front vowels, on the order of one Bark relative to the *F*2 frequencies when the same vowels are adjacent to stop consonants. Shifts for *F*1 tended to be smaller than shifts in *F*2, even on a Bark scale, and were less consistent across speakers.

The formant frequency midpoints and durations of vowels carrying primary stress were shown to differ only slightly on average from those vowels carrying secondary stress, if the other factors were held constant. Vowels in speech read continuously also differed only slightly on the average from vowels in spontaneous speech.

In general, the data show that variations in vowel midpoint formant frequencies, durations, and trajectory shapes are correlated with the perception of the vowel by human listeners. For example, /ɛ/ tokens which have *F*1 - *F*2 midpoint values typical of /ʌ/ tend to be identified as /ʌ/, and /e/ tokens which are short and lack a /y/ offglide, typical characteristics of lax vowels, tend to be misidentified as lax vowels.

Aspects of the trajectories which are important for characterizing the vowel were sought. The trajectory was used to derive a representation of the vowel by one point per formant, a modified "midpoint." Performance by a Gaussian classifier was the criterion used to evaluate different representations of the vowels. If the effect of perceptual overshoot for *F*2 and perceptual averaging for *F*1 was simulated, and the resulting modified midpoint was used as an input for the classifier, performance was somewhat better than if the durational midpoints were used as input. However, the best performance was achieved if the raw data—the quarter-point, midpoint, and three-quarter point of the trajectory and the duration—were used as input to the classifier. The improved performance with the raw data over the modified midpoints shows that not all of the significant aspects of the trajectory have been captured in a one-point representation. It may be that a new one-point representation could be found which would result in as high performance as the raw data. Alternatively, it may be necessary to use more than a modified midpoint to fully characterize a vowel.

Of all the representations used as input to the statistical classifier, the raw data also result in the best agreement of the classifier with the human performance. If the classifier is also allowed to train and test on vowels in stop and liquid-glide contexts separately, agreement with the listeners' responses (and performance in the conventional sense, i.e., agreement with the transcriber's phonemic labels) improves further. The improvement due to separating the contexts suggests that humans perform vowel identification in a context-dependent manner.

1.6.2 Analysis and Modeling of Stop and Affricate Consonants

We have been developing models for the production of various types of stop consonants including voiceless aspirated stops, voiced stops, affricates, and prenasal stops. In all of these models, estimates are made of the changes in cross-sectional area of the airways as the various articulators (glottis, velopharyngeal opening, supraglottal constriction, pharyngeal expansion or contraction) are manipulated to produce the different classes of consonants. From these estimates, aerodynamic parameters such as flows and pressures are calculated, and the time course of different acoustic sources at the glottis and near the supraglottal constriction are then determined. The modification of the sources by the vocal-tract transfer function is included to obtain predictions of the spectral changes in the radiated sound for different phases of the consonant production. The predictions are then compared with acoustic measurements of utterances produced by several speakers. In some cases where there are discrepancies between the acoustic data and the predictions, revised estimates of the model parameters are made. This process leads to reasonable agreement between the acoustic measurements and the predictions and provides a way of estimating the time course of the articulatory changes from the acoustic data.

In the case of voiceless aspirated stop consonants, the model includes a glottal spreading maneuver and manipulation of the pharyngeal walls to inhibit expansion of the vocal-tract volume during the

consonantal closure interval. The model generates a quantitative description of the sequence of acoustic events following the consonantal release: an initial transient, an interval of frication noise (at the supraglottal constriction), an interval of aspiration noise (at the glottis), a time in which there is breathy vocal-fold vibration, and, finally, modal vocal-fold vibration. For a voiced stop consonant, active pharyngeal volume expansion is included in the model, and the increase in intraoral pressure is thereby delayed.

The model for the production of the affricate /č/ in English specifies four components: (1) an initial release phase for the tongue tip, (2) a relatively slow downward movement of the tip (30-50 ms), (3) a steady palato-alveolar fricative portion, and (4) a release of the fricative portion into the vowel. From the model it is possible to calculate the amplitude, spectrum, and time course of the components of the sound resulting from these movements, as well as the airflow. The acoustic and aerodynamic predictions are on the range observed in actual productions of affricates. In the initial 30-50 ms there is a brief transient (1-2 ms), followed by a gradually rising noise amplitude, with a spectral prominence corresponding to the acoustic cavity in front of the tongue tip. During the later fricative phase, there is acoustic coupling to the palatal channel, leading to a second major prominence in the spectrum. The single prominence in the initial phases and the two prominences in the later frication spectrum achieve amplitudes that are comparable to or greater than the corresponding spectral prominences in the adjacent vowel. The sequence of acoustic events cannot be described simply a /t/ followed by /š/ or as a /š/ with an abrupt onset, but is unique to the affricate.

1.6.3 Fricative Consonants: Modeling, Acoustics, and Perception

We have continued our modeling studies of the production of fricative consonants with an analysis of the aerodynamic and acoustic processes involved in the production of these consonants and have completed an investigation of the voicing distinction for fricatives. The fricative studies reported previously have been extended to include quantitative estimates of the amplitudes and locations of turbulence noise sources at the glottis and at the supraglottal constriction for various places of articulation. Reasonable agreement has been obtained between acoustic characteristics of fricatives in intervocalic position. The acoustic and perceptual studies of voicing in fricatives (in collaboration with Sheila Blumstein of Brown University) have led to a delineation of the roles of the extent of formant transitions and the presence of glottal vibration at the edges of the obstruent interval in determining the voicing status of intervocalic fricatives. Data have also been obtained for fricative sequences with mixed voicing (e.g., the /zf/ sequence in **his form**), and have shown the predominant role of regressive voicing assimilation relative to progressive assimilation.

1.6.4 Acoustic Properties of Devoiced Semivowels

When the semivowels /w,y,r,l/ occur in clusters with unvoiced consonants, they are sometimes at least partially devoiced so that much of the information about their features is in the devoiced region. While the acoustic characteristics of the semivowels which are manifest as sonorants are fairly well understood, little research has been conducted on those semivowels which are fricated. In this acoustic study, we recorded groups of words such as "keen," "clean," "queen," and "cream" at a slow and fast rate by two speakers, one male and one female. We are investigating the spectral characteristics of the word-initial consonants and consonant clusters to determine the attributes in this region which signal the presence of a semivowel and the attributes which distinguish among the devoiced semivowels. So far, our findings suggest that the spectral characteristics of the consonant clusters can change considerably over time due to the presence of the semivowel. Data are being collected to quantify changes in the spectral characteristics within the consonant cluster from an initial frication burst to noise generated at the constriction for the semivowel to voicing as the semivowel constriction is released. For example, one notable time-varying property of the [sw] cluster in "sweet" is the change from a rising spectral snape where the main concentration of energy is between 4-5 kHz (at the beginning of the frication noise) to a falling spectral shape where the main concentration of energy is between 1-2 kHz (towards the end of the frication noise), as the place of noise generation shifts from a postdental to a velar location.

1.6.5 Spreading of Retroflexion in American English

In this acoustic study we investigated the factors which influence the spreading of retroflexion from a postvocalic /r/ into the preceding vowel, /ɑ/, in American English. We consider the acoustic correlate for the feature "retroflex" to be a low third formant (*F*3) which is close in frequency to the second formant (*F*2). Minimal pair words with initial and final obstruent consonants were recorded by six speakers at a slow and a fast

speaking rate. Several basic *F*3 trajectories could be observed during the /ɑr/ region, depending upon the timing of the minimum in the *F*3 trajectory in relation to the beginning and ending of the sonorant region. Given the same word said by different speakers at different speaking rates, the minimum in the *F*3 trajectory can occur at the beginning, in the middle and at the end of the sonorant region. In addition, *F*3 can remain fairly flat at a low frequency throughout the sonorant region. We believe that this variability in the *F*3 trajectory can be explained by several factors. First, there is a certain basic *F*3 trajectory needed to articulate a postvocalic /r/: a downward movement from the *F*3 frequency in the previous sound and an upward movement to either a neutral position or the *F*3 position for the following sound. The *F*3 slopes on either side of the minimum will depend upon the context. Second, only a portion of this full *F*3 trajectory may be observable during the sonorant region. How much and what portion of the *F*3 trajectory can be observed will depend upon the duration of the sonorant region and on how early the speaker starts to produce the /r/. The anticipation of /r/ as well as the duration of the sonorant region appear to depend on speaking rate, consonantal context and speaker differences. Further analysis is planned to determine more accurately the minimum time needed to execute the articulation of /r/.

1.6.6 Studies of Unstressed Syllables

We have begun an investigation of the acoustic properties of the vowels and consonants in unstressed syllables in utterances produced with different speech styles. The aim of this study is to determine the kinds of reductions that can occur in unstressed syllables and to attempt to establish what aspects of the syllables are retained in spite of the reductions. As a first step in this project, we are examining vowels and consonants in unstressed syllables in which the consonants preceding and following the vowel are both voiceless (as in **support**, cla**ssical**, **pot**ato). These are situations in which the vowel can become devoiced, but in which some remnant of the vowel remains in voiceless form, or in which temporal properties of the surrounding segments signal the presence of the syllable.

When there is severe reduction of the vowel, the presence of the unstressed syllable appears to be signaled in various ways: (1) the vowel is devoiced, but there is an interval in which the presence of a more open vocal-tract configuration between the consonants is signaled by aspiration noise; (2) in a word like **support**, when the vowel is devoiced, the frication (and possibly aspiration) noise within the initial /s/ shows an increased amplitude toward the end of the consonant, indicating that the consonant is being released into a more open vocal-tract configuration or that the consonant itself is more open toward the end of its duration; (3) properties of the adjacent consonant (such as aspiration in /p/ in **support** or in /k/ in **classical**) indicate that the consonant sequence could not have arisen unless an unstressed vowel were inserted between the consonants. These properties have been observed in a preliminary study, and a larger database of utterances is being prepared to conduct a more detailed investigation.

1.6.7 Nasalization in English

Nasalization is one of the sound properties, or features, languages use to distinguish words. Understanding the acoustic consequences of nasalization is therefore necessary for understanding how nasal sounds pattern in natural languages, and also for developing models of speech acoustics for use in speech synthesis and recognition. We have been investigating the important spectral consequences of nasalization using analysis of natural speech, and we have carried out perception experiments using both natural and synthetic speech. One set of perceptual experiments investigated how readily listeners can use nasalization on a (natural) vowel to guess the nasality of a following consonant (bead vs. bean). Our results indicate that English speakers notice nasality on a vowel more readily when the experimental task focuses their attention on it. This observation may be because they are not expecting nasalization on vowels, since in English vowels are nasalized only incidentally, before a nasal consonant, rather than being nasalized contrastively, as in French. One of the most consistent spectral effects of nasalization is damping of the first formant. Our analyses of natural speech items indicate that *F*1 prominence decreases with increasing opening of the velopharyngeal port. Perceptual experiments with synthetic speech indicate that even in the absence of other spectral cues to nasalization, a decrease in *F*1 prominence increases the likelihood that a vowel will be heard as nasal. This effect is stronger when *F*1 prominence decreases over the course of the vowel, rather than remaining static, suggesting that a decrease in *F*1 prominence over time is an essential part of the spectral pattern which is heard as nasal. However, it could also be simply due to the fact that time-varying synthetic items sound more natural to the listener than do static items. To choose between these alternative explanations, we plan to run similar experiments with listeners whose native language has contrastively nasalized vowels, in which the spectral cues to nasalization change little over the

course of the vowel. A somewhat less consistent spectral effect of nasalization is the presence of a visible zero in the spectral valley between *F*1 and *F*2. Our perceptual studies with natural speech items suggest that the zero can be an important factor in determining when a vowel is heard as nasal. One may infer from this result that a measure of relative spectral balance in the region between *F*1 and *F*2 may correlate well with independent indications of perceived nasality. This measure is currently under development. The results of this research, along with work reported previously, should lead to an improved understanding of the use of nasalization in natural speech.

1.6.8 Modeling Speech Perception in Noise: A Case Study of Prevocalic Stop Consonants

The present study is part of an attempt to model speech perception in noise by integrating knowledge of the acoustic cues for phonetic distinctions with theories of auditory masking. The methodology in the study is twofold: (1) modeling speech perception in noise based on results of auditory-masking theory and (2) evaluating the theoretical predictions by conducting a series of perceptual experiments in which particular acoustic attributes that contribute to several specific phonetic distinctions are selectively masked. The model predicts the level and spectrum of the masker needed to mask out important acoustic attributes in the speech signal and predicts listeners' responses to noisy speech signals.

We have been focusing on the importance of the *F*2 trajectory in signaling the place of articulation for the consonants /b,d/ in /CV/ syllables with the vowels /ɑ/ and /ɛ/ In the /Cɑ/ context, the *F*2 trajectory from /d/ to the vowel falls, whereas the *F*2 trajectory in /bɑ/ syllables rises into the vowel and is less extensive than the /dɑ/ trajectory. The reverse is true for /Cɛ/ syllables: the *F*2 trajectory is less extensive for /dɛ/ than it is for /bɛ/, i.e., there is almost no transition in *F*2 from the consonant to the vowel in /dɛ/.

Two perceptual experiments using synthetic /CV/ syllables were conducted. /C/ was either /b/ or /d/; the first set of experiments used the vowel /ɑ/, and the second set used the vowel /bɛ/. The synthetic pairs (/bɑ, dɑ/) and (/bɛ/, /dɛ/). were identical except for differences in the *F*2 trajectories (as described above). The utterances were degraded by adding various levels of white noise, and were presented to subjects in identification tests. Results show that for /Cɑ/ stimuli with most of the *F*2 transition masked—yielding to the perception of an almost "flat" trajectory— the listeners label the /dɑ/ stimuli as /bɑ/. The reverse is true for /Cɛ/ syllables: when most of the *F*2 transition is masked leaving a flat trajectory appropriate for /dɛ/, the listeners label the /bɛ/ stimuli as /dɛ/. These results indicate that the shape of the *F*2 trajectory is crucial in signaling the place of articulation for these consonants in noise. Results also show that the thresholds where confusion in place of articulation occur can be estimated successfully from masking theory.

In future experiments we will examine listeners' responses to speech signals degraded by shaped noise, rather than white noise, in addition to using a larger set of consonants.

1.7 Speech Production Planning

Our work in speech planning continued the analysis of patterns in segmental speech errors, which provide evidence for models of the phonological planning process. For example, when two target segments in an utterance exchange, as in "pat fig" for "fat pig," they usually share position in both their words and stressed syllables. Since this constraint is widespread, it suggests that one or both of these larger units plays a role in the segmental planning process. In a series of elicitation experiments, we contrasted stimuli like "parade fad" (where /p/ and /f/ share word position but not stress) and "repeat fad" (where /p/ and /f/ share stress but not word position) with "ripple fad" (where /p/ and /f/ share neither word position nor stress). Results show that word position induces the largest number of errors, stress the next-largest, and pairs of segments that share neither positional factor participate in almost no errors. We conclude that both word structure and syllable stress must be incorporated into models of the representation that speakers use for phonological planning.

We are further pursuing the issue of position constraints on segmental errors and their implications for processing representations by examining an earlier finding that word-final segments participate in more errors when speakers produce lists of words (leap note nap lute), and fewer errors when those words occur in grammatically well-formed phrases (From the leap of the note to the nap of the lute) or in spontaneous speech. One possible account of this observation is that the planning of a more complex syntactic structure somehow protects word-final segments; another is that the presence of intervening words provides the protection, and a third possibility is that the more complex prosodic planning of longer grammatical phrases is

responsible. We are comparing the error patterns in short word lists (e.g., lame run ram Len) with sentences of similar length (Len's ram runs lame), and with longer sentences (But if Len has a ram it can run if it's lame) similar to the phrase condition in the earlier experiments. If syntactic structure alone is the factor that changes the proportion of final-segment errors, then short sentences should be as effective as longer sentences in eliciting the difference.

In a second line of investigation, we are asking how complex prosody affects the process of phonological planning. Our initial experiments determined that speakers using reiterant speech to imitate target sentences (i.e., using repeated instances of the syllable /ma/ to reproduce the prosody of the original) showed that it is more difficult to imitate metrically irregular sentences like "He told us it was too hot to work" than metrically regular sentences like "It was hot so we swam in the pool." Difficulty is measured by whether the number of syllables in the reiterant imitation matches that of the target sentence and by the speaker's estimate of whether the imitation was hard, medium or easy). If prosodic planning and segmental planning interact, then prosodically irregular utterances with normal segment structure should elicit more segmental errors in normally-produced utterances as well. We are currently investigating this possibility.

Finally, in collaboration with Mari Ostendorf of Boston University and Patti Price of the Stanford Research Institute, we have investigated a third issue in production planning: the role of prosodic information (prominence, duration, etc.) in signaling aspects of both the structure and the meaning of utterances. In a study of seven types of syntactic ambiguity, using trained FM-radio speakers, we confirmed earlier (but not unanimous) findings showing that listeners can select the meaning intended by the speaker reliably for some but not all types of bracketing ambiguity. Phonological and acoustic analyses showed that speakers signal these distinctions in part by placement of the boundaries of prosodic constituents and that these boundaries are indicated by such prosodic cues as boundary tones and duration lengthening in the pre-boundary syllable.

1.8 Models Relating Phonetics, Phonology, and Lexical Access

In recent years phonologists have proposed that the features that characterize the segments in the representation of an utterance in memory should be organized in a hierarchical fashion. A geometrical tree-like arrangement for depicting phonological segments has emerged from this proposal. We have been examining whether phonetic considerations might play a role in the development of these new approaches to lexical representation of utterances. Our efforts in this direction are following two different paths: (1) a theoretical path that is attempting to modify or restructure the feature hierarchy derived from phonological considerations, and (2) a more practical path in which we are examining how a lexicon based on these principles might be implemented and how it might be accessed from acoustic data.

Theoretical considerations have led to a separation of features into two classes: (1) articulator-free features that specify the kind of constriction that is formed in the vocal tract, and (2) articulator-bound features indicating what articulators are to be manipulated. The articulator-bound features for a given segment can, in turn, be placed into two categories: (1) features specifying which articulator is implementing the articulator-free feature, and (2) features specifying additional secondary articulators that create a distinctive modulation of the sound pattern. The articulator-free features are manifested in the sound stream as landmarks with distinctive acoustic properties. The articulator-bound features for a given segment are represented in the sound in the vicinity of these landmarks. Details of the feature hierarchy that emerges from this view will appear in papers that are in press or in preparation.

Implementation of a lexicon based on this hierarchical arrangement is beginning, and we are planning the development of a system for automatic extraction of acoustic properties that identify some of the articulator-free and articulator-bound features in running speech.

1.9 Other Research Relating to Special Populations

1.9.1 Breathiness in the Speech of Hearing-impaired Children

One of the more prevalent speech abnormalities in the speech of the hearing-impaired that contributes to reduced intelligibility is excessive breathiness. According to a past study of normal speakers done by D. H. Klatt and L. C. Klatt, *H*1 - *H*2 and aspiration noise are highly correlated to breathiness judgments. (*H*1 and *H*2 are the amplitudes of the first two harmonics, in dB, of the spectrum of a vowel.) A study was done to analyze quantitatively the middle of the vowel of hearing-impaired children and a few normal-hearing children. Acoustic parameters *F*0 (fundamental frequency), *H*1 - *H*2, aspiration noise, and spectral tilt were examined in relation to the vowel perceptual judgments on breathiness done by two experienced phoneticians exposed to the vowel in a word or phrase context. The correlation coefficients were unexpectedly low for all of the acoustic parameters. Also, according to the judges, nasality often accompanied breathiness in the vowels of the hearing-impaired and it was difficult to distinguish the two. To lessen the effect of nasality on breathiness judgments, only vowels with low nasality judgments were analyzed. Although the correlation improved, the change was not large.

The main difference between the study and that of Klatt and Klatt was that the judgments in the Klatt study were done on isolated vowels. Another study was conducted to examine the effect of adjacent segments on breathiness perceptual judgments by presenting to the listeners vowels that were both isolated and imbedded in a word. According to the preliminary study, a large difference was observed in the judgments of imbedded vowels in certain words: more breathiness was detected in the vowel when it was in a word context than when it was isolated. However, more experiments and examination of acoustic events near consonant-vowel boundaries must be done.

Another characteristic of breathiness is the introduction of extra pole-zero pairs due to tracheal coupling. Analysis-by-synthesis was done using KLSYN88 developed by Dennis Klatt. An extra pole-zero pair was often observed around 2 kHz for hearing-impaired speakers but not for normal speakers. However, there was low correlation between prominence of the extra peak and breathiness judgments, suggesting that it may not be possible to use prominence of extra peaks to quantify breathiness. Synthesis was also done in which the extra pole-zero pair was removed. In some cases, the breathiness perceptual judgments were lower than the vowels synthesized with the pole-zero pair, although in most cases there was not much difference.

1.9.2 Speech Planning Capabilities in Children

A project at Emerson College is studying the processes of speech encoding in children both with and without language impairment. One component of that project involves collaboration with our Speech Communications group at RLE. The purpose of this research is to examine the two populations for differences in ability to encode phonological information and translate it into a motor program. We have designed a test of children's word repetition skills that will give insight into their speech planning capabilities, and this test is being run on the two populations of children.

1.9.3 Training the /r/-/l/ Distinction for Japanese Speakers

For adult second-language learners, certain phoneme contrasts are particularly difficult to master. A classic example is the difficulty native Japanese speakers have with the English /r/-/l/ distinction. Even when these speakers learn to produce /r/ and /l/ correctly, their ability to perceive the distinction is sometimes at chance.

In conjunction with the Athena second language learning project, we developed a computer-aided training program to assist in teaching the /r/-/l/ perceptual distinction. The basis of the training is the use of multiple natural tokens and the ability to randomly select tokens and to obtain feedback after presentation. While training was slow, it was effective for a majority of subjects. Many reached 100 percent correct identification when tested after 30-50 sessions.

As another component of this project, a fast spectrograph display was developed as an aid to teaching production of /r/ and /l/.

1.10 Facilities

1.10.1 Articulatory Movement Transduction

Development and testing of our system for Electro-Magnetic Midsagittal Articulometry has been completed. The final stages of this effort included: revising the electronics to eliminate two sources of transduction error, development of a more efficient transducer calibration method and construction of an apparatus to implement the method, improvement of transducer connecting wire to overcome insulation failures, updating and elaboration of signal processing software, development of a new computer program to display and extract synchronous data from articulatory and acoustic signals, and running a variety of tests to validate system performance. These tests indicate that performance is now acceptably close to its theoretical limit. Two trial experiments have been run with subjects. Those experiments have resulted in several important improvements to experimental methods, including techniques for attaching transducers to subjects and presenting utterance materials. Preparations have been made to run experiments on "motor equivalence" and anticipatory coarticulation.

1.10.2 Computer Facilities

Work is in progress on a program for displaying spectrograms on our workstation screens, to increase the efficiency of certain kinds of acoustic analyses. A RISC-based compute server has been integrated into our network of workstations. Among other functions, it will perform compute-intensive calculations (such as for spectrogram generation) at ten times the rate currently possible on our VAXStations. The WAVES acoustic analysis package has been installed on the RISC workstation for future use in work on lexical access.

1.11 Publications

Journal Articles and Published Papers

Butzburger, J., M. Ostendorf, P.J. Price, and S. Shattuck-Hufnagel. "Isolated Word Intonation Recognition Using Hidden Markov Models." *Proc. ICASSP* 90, pp. 773-776 (1990).

Boyce, S.E. "Coarticulatory Organization for Lip Rounding in Turkish and English." *J. Acoust. Soc. Am.* 88: 2584-2595 (1990).

Boyce, S.E., R.A. Krakow, F. Bell-Berti, and C.E. Gelfer. "Converging Sources of Evidence for Dissecting Articulatory Movements into Core Gestures." *J. Phonetics* 18: 173-188 (1990).

Hillman, R.E., E.B. Holmberg, J.S. Perkell, M. Walsh, and C. Vaughn. "Phonatory Function Associated with Hyperfunctionally Related Vocal Fold Lesions." *J. Voice* 4: 52-63 (1990).

Klatt, D.H, and L.C. Klatt. "Analysis, Synthesis, and Perception of Voice Quality Variations Among Female and Male Talkers." *J. Acoustic. Soc. Am.* 87: 820-857 (1990).

Manuel, S.Y. "The Role of Contrast in Limiting Vowel-to-Vowel Coarticulation in Different Languages." *J. Acoustic. Soc. Am.* 83: 1286-1298 (1990).

Perkell, J.S. "Testing Theories of Speech Production, Implications of Some Detailed Analyses of Variable Articulatory Data." In *Speech Production and Speech Modeling.* Eds. W.J. Hardcastle and A. Marchal. Boston: Kluwer Academic Publishers, 1990, pp. 263-288.

Stevens, K.N., and C.A. Bickley. "Higher-level Control Parameters for a Formant Synthesizer." *Proceedings of the First International Conference on Speech Synthesis,* Autrans, France, 1990, pp. 63-66.

Veilleux N., M. Ostendorf, S. Shattuck-Hufnagel, and P.J. Price. "Markov Modeling of Prosodic Phrases." *Proc. ICASSP* 90, pp. 777-780 (1990).

Wodicka, G.R., K.N. Stevens, H.L. Golub, and D.C. Shannon. "Spectral Characteristics of Sound Transmission in the Human Respiratory System." *IEEE Trans. Biomed. Eng.* 37(12): 1130-1134 (1990).

Papers Submitted for Publication

Bickley, C.A. "Vocal-fold Vibration in a Computer Model of a Larynx." Submitted to *Proceedings of the Vocal Fold Physiology Conference,* Stockholm, Sweden, 1989. New York: Raven Press.

Halle, M., and K.N. Stevens. "The Postalveolar Fricatives of Polish." Submitted to *Osamu Fujimura Festschrift.*

Halle, M., and K.N. Stevens. "Knowledge of Language and the Sounds of Speech." Submitted to *Proceedings of the Symposium on Music, Language, Speech and Brain,* Stockholm, Sweden.

Huang, C.B. "Effects of Context, Stress, and Speech Style on American Vowels." Submitted to *ICSLP'90,* Kobe, Japan.

Lane, H., J.S. Perkell, M. Svirsky, and J. Webster. "Changes in Speech Breathing Following Cochlear Implant in Postlingually Deafened Adults." Submitted to *J. Speech Hear. Res.*.

Perkell, J.S., and M.H. Cohen. "Token-to-token Variation of Tongue-body Vowel Targets: the Effect of Context." Submitted to *Osamu Fujimura Festschrift.*

Perkell, J.S., E.B. Holmberg, and R.E. Hillman. "A System for Signal Processing and Data Extraction from Aerodynamic, Acoustic and Electroglottographic Signals in the Study of Voice Production." Submitted to *J. Acoust. Soc. Am.*

Perkell, J.S., and M.L. Matthies. "Temporal Measures of Labial Coarticulation for the Vowel /u/." Submitted to *J. Acoust. Soc. Am.*

Shattuck-Hufnagel, S. "The Role of Word and Syllable Structure in Phonological Encoding in English." Submitted to *Cognition* (special issue).

Stevens, K.N. "Some Factors Influencing the Precision Required for Articulatory Targets: Comments on Keating's Paper." *Papers in Laboratory Phonology I.* Eds. J.C. Kingston and M.E. Beckman. Cambridge: Cambridge University Press.

Stevens, K.N. "Vocal-fold Vibration for Obstruent Consonants." *Proc. of the Vocal Fold Physiology Conference,* Stockholm, Sweden. New York: Raven Press.

Stevens, K.N., and C.A. Bickley. "Constraints among Parameters Simplify Control of Klatt Formant Synthesizer." Submitted to *J. Phonetics.*

Section 2 Sensory Communication

Chapter 1 Sensory Communication

Chapter 1. Sensory Communication

Academic and Research Staff

Dr. Joan M. Besing, Professor Louis D. Braida, Lorraine A. Delhorne, Nathaniel I. Durlach, Dr. Donald K. Eddington, Dr. Kenneth W. Grant, Professor Richard M. Held, Dr. Xiao Dong Pang, Dr. William M. Rabinowitz, Dr. Christine M. Rankovic, Dr. Charlotte M. Reed, Dr. Mandayam A. Srinivasan, Timothy J. Stellmach, Dr. Rosalie M. Uchanski, Dr. Victor W. Zue, Dr. Patrick M. Zurek

Visiting Scientists and Research Affiliates

Dr. Richard L. Freyman, Dr. Janet D. Koehnke, Dr. Jack Kotik, Dr. Neil A. Macmillan, Dr. Karen L. Payton, Dr. Patrick M. Peterson, Dr. Bruce Schneider

Graduate Students

Santosh Ananthraman, Jyh-Shing Chen, Paul Duchnowski, Kiran Dandekar, Joseph A. Frisbie, Eric Fuchs, Julie E. Greenberg, Yoshiko Ito, Zoher Karu, Wolfgang G. Knecht, Gregory R. Martin, Matthew H. Power, Michael T. Richey, Barbara Shinn-Cunningham, Robert Stadler, Hong Z. Tan

Undergraduate Students

Michael Aponte, Susan E. Bach, Younes Borki, Swaroop Gantela, Andrew H. Grant, Darby A. Hailes, John Hedgcock, Mary Hou, Michael H. Lim, Manilo Lopez, Sandra Y. Ma, Quintin T. Ndibongo, Prashun Patel, Charles Reisman, Rebecca J. Renn, Alexander P. Rigopulos, Sumeet Sandhu, Lynore Taylor, Derrick Yim

Technical and Support Staff

Kai P. Chen, Ann K. Dix, Paula M. Ferguson, Seth M. Hall, Eleanora M. Luongo, Michael T. Tuyo

1.1 Introduction

The Sensory Communication Group is conducting research on (1) the auditory and tactual senses, (2) speech-reception aids (both auditory and tactual) for individuals who are hearing-impaired or deaf, and (3) human-machine interfaces for teleoperator and virtual-environment systems (involving the visual as well as the auditory and tactual senses). Within the domain of hearing aids, research is being conducted on systems that bypass the outer and middle ear and directly stimulate the auditory nerve electrically (cochlear prostheses), as well as on systems that stimulate the system acoustically. The research on taction is focused not only on speech reception for the totally deaf, but also on the ability of the human hand to sense and manipulate the environment. Within the domain of human-machine interfaces, topics of special interest concern the development of principles for mapping the human sensorimotor system into non-anthropomorphic slave mechanisms (or the equivalent in virtual space) and the ability of the human sensorimotor system to adapt to alterations of normal sensorimotor loops caused by the presence of the interface.

1.2 Hearing Aid Research

Sponsor

National Institutes of Health
Grant 5 R01 DC00117

Project Staff

Dr. Joan M. Besing, Professor Louis D. Braida, Lorraine A. Delhorne, Nathaniel I. Durlach, Dr. Kenneth W. Grant, Dr. Christine M. Rankovic, Dr. Charlotte M. Reed, Dr. Rosalie M. Uchanski, Dr. Victor W. Zue, Dr. Patrick M. Zurek

This research is directed toward the development of improved hearing aids for people suffering from hearing impairments that cannot be treated medically. Since the major problem for most people with impaired hearing is a degraded ability to understand speech, and since medical treatments are available for abnormalities of the outer and middle ear, the work is directed towards aids that better match speech signals to residual auditory function in people with impairments central to the middle ear. More specifically, the research is directed at improving speech reception for people with sensorineural impairments. The work performed during the past year can be divided into

four project areas: linear amplification, speech token variability, prediction of speech intelligibility, and aids to speechreading.

1.2.1 Linear Amplification

This research has focused on (1) theoretical analysis of suggested prescriptive methods for fitting frequency-gain characteristics to individual listeners, (2) investigation of the reduction in speech intelligibility associated with strong high frequency emphasis,[1] and (3) the use of adaptive frequency-gain characteristics to combat the effects of background interference on target speech intelligibility.[2] Current research on adaptive frequency-gain characteristics includes both experimental intelligibility studies to determine the potential benefits of adaptive systems and development of real-time signal-processing for implementing such systems.

1.2.2 Speech Token Variability

Performance in intelligibility tests for speech segments depends on the set of segments to be identified and the characteristics of the talker. It also depends, however, on the number and variability of the speech tokens chosen to represent a given segment. (The use of a single token for each segment leads to the use of artifacts as perceptual cues and results in artificially high performance.) In order to predict performance on such tests, it is necessary to model the effects of token variability. With this goal in mind, we are (1) measuring the physical variability of tokens,[3] (2) determining the perceptual effects of this variability on intelligibility for both normal and impaired listeners,[4] and (3) developing a model that relates the perceptual effects to the acoustic characteristics of the stimuli.

1.2.3 Prediction of Speech Intelligibility

This project involves the development of computational methods for predicting the intelligibility of speech subjected to a waveform degradation. Our work in this area during the past grant year has consisted of three components: (1) completion of preliminary experiments using a two-talker database (to determine the feasibility of our approach); (2) establishing the amount of speech data required for our base set of experiments (based on theoretical considerations for information transfer); and (3) completion of the first portion of these base experiments.

1.2.4 Aids to Speechreading

Our study of aids to speechreading has focused on (1) developing a theoretical understanding of the effects of speechreading supplements and (2) evaluating the training requirements involved in teaching Cornett's manual Cued Speech system to listeners with normal hearing. The theoretical work exploits two related models of speech segment confusions: a model that describes confusions in terms of a multidimensional Thurstonian decision model[5] and a model that specifies the relation between the decision space for multimodal (e.g., audiovisual) presentation conditions and the constituent unimodal spaces.[6] Our results on the training of Cued Speech reception suggest that the relatively small amount of training required to achieve high levels of performance on isolated speech segments is a poor indicator of training requirements for sentence reception.

---

[1] C.M. Rankovic and P.M. Zurek, "Rollover with High-Frequency Emphasis," *J. Acoust. Soc. Am.* 87: S87 (1990).

[2] C.M. Rankovic, R.L. Freyman, and P.M. Zurek, "Potential Benefits of Varying the Frequency-Gain Characteristic for Speech Reception in Noise," submitted to *J. Acoust. Soc. Am.*

[3] L. Taylor, *Token Variability of Intra-Speaker Speech: Fricative Consonant Sounds.* S.B. thesis, Dept. of Electr. Eng. and Comput. Sci., MIT, 1990.

[4] K.M. Millier, *Intelligibility of Vowels Represented by Multiple Intra-Speaker Tokens,* S.B. thesis, Dept. of Electr. Eng. and Comput. Sci., MIT, 1990.

[5] L.D. Braida, "Development of a Model for Multidimensional Identification Experiments," *J. Acoust. Soc. Am.* 84: S142(A) 1988.

[6] L.D. Braida, "Crossmodal Integration in the Identification of Consonant Segments," *Quart. J. Exper. Psych.*, forthcoming: L.D. Braida, "Two Types of Audiovisual Integration for the Identification of Speech Segments," *J. Acoust. Soc. Am.* 88: S82 (1990).

1.3 Multimicrophone Hearing Aids

Sponsor

National Institutes of Health
Grant 2 R01 DC00270

Project Staff

Nathaniel I. Durlach, Dr. Xiao Dong Pang, Dr. William M. Rabinowitz, Dr. Patrick M. Zurek

The long-term goal of this research is the development of sensory aids that improve the ability of hearing-impaired listeners to function in complex acoustic environments. The more immediate goal is to determine the benefits that can be achieved for monaural listening through the use of microphone arrays that sample the acoustic field at more than one point in space. Since the reception of speech is the most important problem for the hearing impaired, the target signal of primary interest is speech.

To enhance monaural speech reception, we envision a microphone array that resolves the incoming signals into simultaneous directional channels, followed by a coding operation that transforms these resolved signals in such a way that resolution is preserved at the perceptual level after the signals are summed for presentation to a single ear.[7] Such a system would permit the monaural listener (like the normal binaural listener) to monitor all directions simultaneously, to detect and localize in the same operation, and to focus on a single direction. Our initial work on the microphone array is directed toward the creation of a single directional channel containing the target signal (assumed to arise from a target source straight ahead of the listener) and the reduction of interference from sources directionally distinct from the target source. Parallel processing of array outputs to achieve simultaneous multiple directional channels will be considered only after further progress on the coding problem has been achieved.

During the past year, work has focused on acoustic measurements for fixed-array design, adaptive beamforming (analysis of an adaptive noise canceller and construction of a real-time system), and experimental studies of natural spatial coding.

1.3.1 Acoustic Measurements for Fixed-Array Design

We have completed measurements on a set of transfer functions from many source angles within the upper hemisphere to 10 microphone locations situated along the frame of eyeglasses worn by KEMAR wihin our anechoic chamber. Two arrays of particular interest are an array that encompasses much of the eyeglass span and a second one that is substantially smaller (a few cm span), situated either broadside along the eyeglass front or endfire along the temple. We have also begun to employ analytic formulations of diffraction and scattering for interpreting the acoustic data and for predicting the performance of optimum processors.

1.3.2 Adaptive Beamforming: Analysis of the Adaptive Noise Canceller

The adaptive beamforming algorithm that has been the focus of much of our work, the Griffiths-Jim beamformer,[8] can be viewed as a simple preprocessor operating in conjunction with an adaptive noise canceller (ANC), which was described by Widrow et al.[9] Two of the problems encountered with this beamforming system are associated with, and can be described more simply in terms of, the ANC. The first problem is known as misadjustment and is due to fluctuations in the adaptive filter's weights. The second problem comes from leakage of the target signal into the reference channel, which is ideally free of target for best estimation of the jammer. Both problems increase in severity with input target-to-jammer power ratio. Our previously-proposed modifications of the Griffiths-Jim beamformer were ad hoc attempts to address these problems.[10] In order to gain a more

---

[7] N.I. Durlach, R.C. Corbett, M.V. McConnell, W.M. Rabinowitz, P.M. Peterson, and P.M. Zurek, "Multimicrophone Monaural Hearing Aids," RESNA 10th Annual Conference, San Jose, California, 1987.

[8] L.J. Griffiths and C.W. Jim, "An Alternative Approach to Linearly Constrained Adaptive Beamforming," *IEEE Trans. Antennas Propag.* AP-30: 27-34 (1982).

[9] B. Widrow, J.R. Glover, Jr., J.M. McCool, J. Kaunitz, C.S. Williams, R.H. Hearn, J.R. Zeidler, E. Dong, Jr., and R.C. Goodlin, "Adaptive noise cancelling: Principles and Applications," *Proc. IEEE* 63: 1692-1716 (1975).

[10] J.E. Greenberg, *A Real-time Adaptive-beamforming Hearing Aid,* S.M. thesis, Dept. of Electr. Eng. and Comput.

complete understanding of the limitations of the ANC, we are now attempting to derive analytic expressions for system performance.

1.3.3 Adaptive Beamforming: A Head-Worn Real-Time System

We are continuing development of a battery-powered, body-worn audio processor based on a Motorola DSP56001 chip. Functionally, the unit accepts two microphone inputs and provides a single output. The hardware is general-purpose, and the device can be programmed to perform a wide variey of algorithms requiring one or two input signals. To date, it has been programmed to implement the modified Griffiths-Jim beamformer as well as a simple algorithm that automatically selects the microphone signal estimated to have less noise (due to head shadow).

1.3.4 Spatial Coding: Natural References

Our work on spatial coding[11] is aimed at developing transformations of multiple source signals (which we expect eventually to be able to extract with microphone arrays) to render these signals maximally intelligible when summed for monaural presentation. As background for this work we have measured the extent to which natural coding systems—monaural and binaural hearing—keep spatially-separate sources perceptually separate. Specifically, using two or three sources, we have measured the intelligibility of each source serving as the target in the presence of the others as interference. The results, averaged over source configurations, show an advantage of about 10 dB for binaural over monaural listening to two sources. As expected, this binaural advantage is reduced by introducing a second jammer.

1.4 Cochlear Prostheses

Sponsor

National Institutes of Health
Grant 1 P01 DC00361[12]

Project Staff

Professor Louis D. Braida, Lorraine A. Delhorne, Dr. Donald K. Eddington, Dr. William M. Rabinowitz, Dr. Charlotte M. Reed

The overall goal of this research project is to determine and understand the potential and limitations of cochlear prostheses and to develop improved prostheses. Residual sensorineural hearing is measured prior to implantation in connection with subject selection and to provide baseline data for later comparison. Following implantation, auditory performance is evaluated by studying psychophysical performance, discrimination of speech elements, and comprehension of speech and the acoustic environment. Attempts are made to identify and measure central processing abilities that are relevant to speech-reception performance with an implant and that may help explain the large intersubject variations observed. Also, for comparison purposes, speech-reception tests are performed using a promising multichannel tactile vocoder. To minimize differential learning effects in the comparison, these tests are restricted to discrimination of speech segments. Further research focuses on alternative speech-processing schemes to achieve improved implant performance. This research capitalizes on analytic results from other parts of our research and the direct accessibility of the implanted electrode array (via a percutaneous plug). During the past year, work has focused on evaluation of overall performance, the effects of background noise, and alternative speech processing.

1.4.1 Overall Performance

This work is concerned with documenting implantees' speech-reception abilities at a variety of different levels and establishing relationships among different tests. At present, about twenty subjects have participated in our program and about eight have completed most of our routine evaluations. Some preliminary observations which

Sci., MIT, 1989; J.E. Greenberg, P.M. Zurek, and P.M. Peterson, "Reducing the Effects of Target Misalignment in an Adaptive Beamformer for Hearing Aids," *J. Acoust. Soc. Amer.* 85: S26 (1989).

[11] C.R.Corbett, *Filtering Competing Messages to Enhance Mutual Intelligibility,* S.M. thesis, Dept. of Electr. Eng. and Comput. Sci., MIT, 1986.

[12] Subcontract from Massachusetts Eye and Ear Infirmary. Dr. Joseph B. Nadel, M.D., Principal Investigator.

appear interesting are the following: Auditory word recognition with the IEEE/Harvard sentences correlates highly with auditory performance on the NU-6 monosyllabic word test (R = 0.98). Speech-segment discrimination tests reveal some subjects with relatively good performance who (on the basis of other tests) derive little communicative benefit from their implant; these subjects may be particularly good candidates for specialized aural rehabilitation. Finally, measures of speech-segment identification performance, in contrast to discrimination performance, relate directly to overall measures of communicative benefit.

1.4.2 Effects of Background Noise

Everyday communication often occurs in the presence of background noise. During this past year we began studies on the effects of background noise on speech reception with the Richards (Symbion) implant system. In comparison to normal-hearing subjects tested under the same conditions, the implantees appear about 15 dB more sensitive to noise for both consonant and vowel identification. Analyses are presently underway to examine the dependencies of particular consonant and vowel features on speech-to-noise ratios.

1.4.3 Alternative Speech and Processing

Collaboration with Blake Wilson and his associates at the Research Triangle Institute (RTI) has continued. Best perceptual results have been obtained with a "supersampler" scheme consisting of interleaved-pulse stimulation that is updated over the six channels at a rate of 1600 Hz. Substantial improvements over previous results (obtained with the normal processor which employs simultaneous multichannel stimulation) have been demonstrated for both monosyllabic word recognition and sentence reception.[13]

1.5 Binaural Hearing

Sponsor

National Institutes of Health
Grant 2 R01 DC00100[14]

Project Staff

Nathaniel I. Durlach, Dr. Patrick M. Zurek

The long-term goal of this program is (1) to develop an integrated, quantitative theory of binaural interaction that is consistent with psychophysical and physiological data on normal and impaired auditory systems and (2) to apply our results to the diagnosis and treatment of hearing impairments.

Research in this area (performed under a subcontract from Boston University) has focused on lateralization phenomena. One series of studies has explored the effect of onset cues for long-duration sounds. It has been found that the degree to which onset information dominates lateralization depends not only on the strength and consistency of the lateralization information in the ongoing stimulus, but also on the extent to which the ongoing stimulus appears to constitute a single "auditory object." Thus, for example, the onset's control of lateralization can be greatly reduced by introducing into the continuing signal an abrupt change in amplitude (an increase as well as a decrease).

Work on the precedence effect with pairs of binaural noise bursts has shown that there is a large variation in the strength of the effect across noise tokens (some tokens even show a reverse precedence effect). Efforts are now being made to determine the stimulus variables (such as phase spectrum, cross-spectral magnitude, etc.) that are responsible for these phenomena.

We have also completed an analysis of the probability distributions of interaural cues in simple binaural detection stimuli.[15] This report presents derivations of these distributions in calculable form, as well as a summary of the dependence of variance on signal-to-noise ratio.

---

[13] B.S. Wilson, C.C. Finley, D.T. Lawson, R.D. Wolford, D.K. Eddington, and W.M. Rabinowitz, "New Levels of Speech Recognition with Cochlear Implants," *Nature*, forthcoming.

[14] Subcontract from Boston University. Professor H. Steven Colburn, Principal Investigator.

[15] P.M. Zurek, "Probability Distributions of Interaural Phase and Level Differences in Binaural Detection Stimuli," submitted to *J. Acoust. Soc. Am.*

1.6 Clinical Applications of Binaural Hearing

Sponsor

National Institutes of Health
Grant FV00428 [16]

Project Staff

Dr. Patrick M. Zurek

Work on clinical applications of binaural hearing has focused on comparisons between the performance of listeners with sensorineural impairments and listeners with normal hearing on tests of binaural detection, localization, and contralateral masking. The results show, as expected, that impairments often lead to reduced performance in these tests, and that performance is correlated across tests. However, correlation between performance on these tests and audiometric configuration is relatively weak; unexplained intersubject variance remains disturbingly large.

1.7 Tactile Communication of Speech

Sponsor

National Institutes of Health
Grant 5 R01 DC00126

Project Staff

Lorraine A. Delhorne, Nathaniel I. Durlach, Dr. William M. Rabinowitz, Dr. Charlotte M. Reed, Dr. Mandayam A. Srinivasan

Previous research on (1) tactual communication of speech among the deaf-blind in which the tactual stimulation is achieved by direct physical contact with the speaker and (2) tactual aids that transform acoustic signals into patterns of tactual stimulation and thus function at a distance has led us to the following conclusions: (1) The tactual sense is capable of receiving continuous speech at nearly normal speaking rates with nearly zero error rates; (2) Subjects are capable of integrating a relatively impoverished tactual signal with visual speechreading to achieve essentially normal speech-reception performance; (3) Limitations on the speech-reception performance obtained with current tactual aids are due primarily to inadequacies in the design of the aids and/or in the training received with these aids; and (4) There are no fundamental scientific obstacles to eliminating these inadequacies and achieving much improved speech reception for a wide range of patients. Conclusions (1) and (2) are based on (a) extrapolations of results obtained with relatively crude experimental devices on subjects with relatively limited training;[17] (b) tactual communication performance exhibited by the deaf-blind using direct-contact methods;[18] and (c) preliminary results on the ability of individuals who are experienced in the visual reception of Cued Speech to integrate visual speechreading with direct-contact tactual cueing. Conclusions (3) and (4) are essentially corollaries of conclusions (1) and (2).

With the above research as background, our ultimate general goal can be stated simply as follows: To develop schemes for processing acoustic signals and displaying these processed signals to the tactual sense so that, when accompanied by equivalent training, they provide speech-reception performance comparable to that demonstrated for the direct-contact methods. Discussion of our progress during the past year is divided into the following subsections: (a) Basic study of encoding and display schemes, (b) Tactual supplements to speechreading, (c) Evaluation of practical aids, and (d) Completion of work on natural methods of

---

[16] Subcontract from University of Connecticut. Dr. Janet D. Koehnke, Principal Investigator.

[17] N.I. Durlach, C.E. Sherrick, and J.D. Miller, "Sensory Substitution: Visual and Tactual Methods," chapter in *Speech Communication Aids for the Hearing Impaired: Current Status and Needed Research,* Report of CHABA Working Group 95 by C.S. Watson, R.A. Dobie, N.I. Durlach, H. Levitt, J.D. Miller, C.E. Sherrick, F.B. Simmons, G.A. Studebaker, R.S. Tyler, and G.P. Widin, forthcoming; C.M. Reed, N.I. Durlach, and L.D. Braida, "Research on Tactile Communication of Speech: A Review," *ASHA Monograph Number 20,* 1982; C.E. Sherrick, "Basic and Applied Research on Tactile Aids for Deaf People: Progress and Prospects," *J. Acoust. Soc. Am.* 75: 1325-1342 (1984).

[18] C.M. Reed, W.M. Rabinowitz, N.I. Durlach, L.D. Braida, S. Conway-Fithian, and M.C. Schultz, "Research on the Tadoma Method of Speech Communication," *J. Acoust. Soc. Am.* 77: 247-257 (1985).

tactual communication. Recent reports of our work are available in Reed et al.;[19] and Tan et al.[20]

1.7.1 Basic Study of Encoding and Display Schemes

Previous research on transmitting information through the tactual (i.e., cutaneous, proprioceptive, kinesthetic) sense has been confined almost exclusively to stimulation of the skin; manipulation of joint angles (i.e., hand postures) has been essentially ignored. Research is now underway to determine information transfer rates achieved by manipulation of joint angles, as well as by both joint angle manipulation and cutaneous stimulation combined. New devices to drive the hand are being developed and preliminary discrimination and identification experiments are being performed. One issue of particular interest concerns the extent to which subjects highly experienced in outputting via manual manipulation (such as typists and pianists) are exceptionally good at learning to receiving information manually.

1.7.2 Tactual Supplements to Speechreading

Research in this area over the past year has been concerned with comparing the effectiveness of a simple, low-bandwidth supplement to speechreading presented auditorally versus tactually. The signal consisted of a 200-Hz tone modulated by the envelope of an octave band of speech centered at 500 Hz. The resulting signal was used to drive a high-performance single-channel vibrator for tactile stimulation or Koss earphones for auditory stimulation. Preliminary results indicate a consistent improvement in speechreading using the single-channel vibrator; however, this benefit is small compared to that obtained with the auditory supplement. Various hypotheses concerning the observed difference in performance between the tactile and auditory supplements are now being examined.

1.7.3 Evaluation of Practical Aids

Experiments are being conducted to compare segmental resolution through a wearable tactile device (the seven-channel Tactaid VII which uses zero-crossing analysis to track the first two speech formants) and a laboratory version of the Queen's University tactile aid (a nine-channel device which operates using a traditional vocoder principle). Results currently available indicate roughly similar performance through the two devices. An initial evaluation of a profoundly hearing-impaired adult (who had worn a Tactaid VII for approximately two months prior to testing) indicate substantial benefits to speechreading for segments but only modest benefits for sentence materials. During the coming year, we plan to re-test this subject as well as to provide Tactaid VII devices to additional subjects who will participate in periodic evaluations.

1.7.4 Completion of Work on Natural Methods of Tactual Communication

During the past year, we have continued work on our detailed statistical analysis of measurements of speech produced by Tadoma users (in Tadoma, speech is understood by using the hand to sense the mechanical actions of the face associated with speech production); data collection and analysis for a study of the visual reception of sign language as a function of presentation rate to serve as a reference for previous results on the tactual reception of sign language; and further studies of the tactual reception of Cued Speech in conjunction with both speechreading and Tadoma.

---

[19] C.M. Reed, N.I. Durlach, L.D. Braida, and M.C. Schultz, "Analytic Study of the Tadoma Method: Effects of Hand Position on Segmental Speech Perception," *J. Speech Hear. Res.* 32: 921-929 (1989); C.M. Reed, N.I. Durlach, L.A. Delhorne, W.M. Rabinowitz, and K.W. Grant, "Research on Tactual Communication of Speech: Idea, Issues, and Findings," *Volta Rev.* 91: 65-78 (1989); Also in *Research on the Use of Sensory Aids for Hearing-Impaired People,* ed. N.S. McGarr; C.M. Reed, L.A. Delhorne, N.I. Durlach, and S.D. Fischer, "A Study of the Tactual and Visual Reception of Fingerspelling," *J. Speech Hear. Res.* 33: 786-797 (1990); C.M. Reed, W.M. Rabinowitz, N.I. Durlach, L.A. Delhorne, L.D. Braida, J.C. Pemberton, B.D. Mulcahey, and D.L. Washington, "Analytic Study of the Tadoma Method: Improving Performance through the Use of Supplementary Tactual Displays," submitted to *J. Speech Hear. Res.*; C.M. Reed, N.I. Durlach, and L.A. Delhorne, "Natural Methods of Tactual Communication," chapter in *Tactile Aids for the Hearing Impaired,* ed. Ian R. Summers (New York: Taylor and Francis Ltd., forthcoming).

[20] H.Z. Tan, W.M. Rabinowitz, and N.I. Durlach, "Analysis of a Synthetic Tadoma System as a Multidimensional Tactile Display," *J. Acoust. Soc. Am.* 86: 981-988 (1989).

1.8 Super Auditory Localization for Improved Human-Machine Interfaces

Sponsor

U.S. Air Force - Office of Scientific Research
Grant AFOSR 90-200

Project Staff

Nathaniel I. Durlach, Dr. Richard M. Held, Dr. Xiao Dong Pang, Dr. William M. Rabinowitz, Dr. Patrick M. Zurek

The normal human auditory system suffers from a number of deficiencies in its ability to localize sound sources. The auditory system determines the distance or elevation of a source poorly, is substantially worse at detecting changes in azimuth when the source is off to the side than when it is in front or back, and occasionally makes front-back confusions when the head is motionless. However, when localization is considered in the context of human-machine interfaces such as those employed in teleoperator or virtual-environment systems, there is an opportunity to recode source location in a manner that improves localization. In other words, one can transform the acoustical cues available to the listener for determing source location (i.e., alter the manner in which source location is represented in the binaural acoustic stimulus) in such a way that the listener achieves super localization.

The principal research questions in attempting to achieve super localization concern the ability of the human operator to adapt to such transformations and to switch back and forth between the normal cue system and the altered cue system rapidly and reliably. Although certain consequences of these transformations can be predicted theoretically from our models of normal human audition, those involving perceptual learning and adaptation cannot be predicted. A major goal of the research is to determine, understand, and model the perceptual effects of these transformations.

The planned research involves the study of adaptation to a wide range of transformations using a specially designed virtual-environment system for presenting the transformed localization cues, a variety of training procedures to achieve adaptation, and localization tests to measure adaptation that include detection and localization in multiple-source environments and dynamic tests of localization constancy, as well as discrimination and identification of single sources. To the extent that reliable and reversible adaptation can be demonstrated, the results of this research will provide important new options for improved interface design. Further background in this area can be found in Durlach.[21]

During the past year, our efforts have been directed primarily towards the development of appropriate facilities for this work.

Our desire to incorporate reverberation into head-related transfer functions (HRTFs) for virtual auditory displays has resulted in some suggested changes in the Convolvotron, a key device for creating virtual auditory environments. Numerous discussions between our staff and the manufacturer of the Convolvotron have lead to an outline for improvement of the filter length, memory size, computational method, speed, and data structure of the system. Also, at our request, the manufacturer has developed a new software package for making HRTF measurements in a reverberant environment using the Convolvotron. The modified system is currently under evaluation in our laboratory.

In order to be able to measure HRTFs for individual listeners, a computer-controlled speaker placement system is being constructed with a speaker mounted on an 8-ft. diameter ring which can be driven in two degrees of freedom for placing the speaker anywhere on the surface of a sphere whose center coincides with the center of subjects's head. The mechanical structure of the system has been completed, including the ring, the platform, the motors, the driving mechanism, and the sensing mechanism for motor control. A master's thesis has been outlined to implement the remaining control mechanisms, measure HRTFs, incorporate the HRTFs into the Convolvotron, and conduct and analyze the relevant experiments.

A mechanical head-tracker with six degrees of freedom has been designed and is under construction in the laboratory. The purpose of this tracking device is to overcome three major problems with the currently available (Polhemus) tracker: restricted work space, time delay, and electromagnetic interference. The mechanical tracker will provide a much larger operating range than the Polhemus tracker (9-ft. radius as opposed to 2-ft.), will be essentially immune to electromagnetic interference, and will have delays

[21] N.I. Durlach, "Auditory Localization in Teleoperator and Virtual-Environment Systems: Ideas, Issues, and Problems," *Percept.*, forthcoming.

less than 100 microseconds (from a 25 kHz A/D convertor). The construction of the mechanical head-tracker and its interface with a PC are expected to be completed within the next few months.

A complete software system for conducting localization and adaptation experiments has been developed. This system includes a menu-driven user interface for entering and displaying experimental parameters, and a "controller" for calibrating spatial coordinate systems, controlling stimulus presentations (both probabilistically and temporally), and prompting, recording, storing, and organizing subject responses. The initial transformations implemented include rotation of the interaural axis, expansion and contraction of the interaural axis, and exponentiation of HRTFs.[22] A computer-controlled visual display is available in the form of spatially distributed light bulbs. In addition to conventional keyboard control, manual control of sound source location has been made available through the use of a Power Glove. Preliminary observations suggest that the use of these non-auditory inputs improves externalization of virtual acoustic targets.

A DEC 5000 work station with a graphics engine has been purchased and a graduate student has begun to develop software for generating 3-D visual stimuli for a head-mounted visual display (to be integrated with the auditory display).

A preliminary analysis has been made of algorithms for achieving interaural expansion. The algorithms considered are those of Durlach and Pang[22] and Van Veen and Jenison.[23] The second set, unlike the first, are linear. Thus, they should be superior in multiple jammer environments (to the extent that the approximations are acceptable). For virtual auditory environments, however, where the experimenter has separate control of individual sound sources, issues other than linearity dominate.

1.9 Research on Reduced-Capability Human Hands

Sponsor

U.S. Navy - Office of Naval Research
Grant N00014-90-J-1935

Project Staff

Lorraine A. Delhorne, Nathaniel I. Durlach, Dr. Xiao Dong Pang, Dr. Mandayam A. Srinivasan

The general objectives of our research on hand function are to increase basic knowledge of manual sensing and manipulation, aid in the design and evaluation of artificial hands for robotic and teleoperator systems, and improve clinical diagnosis and treatment of hand impairments. Reports of some of our previous work in this general area are available in Durlach et al.[24] and Pang et al.[25]

The particular research being conducted in this grant focuses on the ability of the human hand to sense and manipulate the environment under various types of constraints. Such constrained hand performance is being studied in connection with hand-design questions in the area of teleoperator systems. Determination of how performance degrades as various capabilities of the normal human hand are eliminated provides important background for hand-design decisions. The constraints to be studied are imposed by experimental gloves and local anesthetics, as well as by various types of hand impairments (resulting from injuries, birth defects, or diseases).

Efforts in the first area have involved (1) interaction with clinics to establish a flow of patients with appropriately impaired hands, (2) study of techniques for constructing experimental gloves that reduce tactile sensitivity in a controllable manner, and (3) selection and acquisition of materials for constructing various types of splints for limiting movement and force output of the hand. The technique for glove construction that appears most promising involves the dipping of latex finger cots in plastic coating material.

---

[22] N.I. Durlach and X.D. Pang, "Interaural Magnification," *J. Acoust. Soc. Am.* 80: 1849-1850 (1986).

[23] B. Van Veen and R. Jenison, "Auditory Space Expansion via Linear Filtering," *J. Acoust. Soc. Am.*, forthcoming.

[24] N.I. Durlach, L.A. Delhorne, A. Wong, W.Y. Ko, W.M. Rabinowitz, and J.M. Hollerbach, "Manual Discrimination and Identification of Length by the Finger-Span Method," *Percept. Psychophys.* 46(1): 29-38 (1989).

[25] X.D. Pang, H.Z. Tan, and N.I. Durlach, "Manual Discrimination of Force Using Active Finger Motion," *Percept. Psychophys.*, forthcoming.

Efforts in the second area have involved (1) conceptual analysis of how various types of manual tasks/tests relate to various underlying sensimotor capabilities of the hand; (2) selection of specific tasks/ tests in the clinical domain, the elementary analytic domain, the general functional domain, and the teleoperator operational domain; and (3) development of facilities for performing these tasks/tests and for recording hand actions during the tasks/tests.

1.10 Skin Biomechanics

Sponsor

National Institutes of Health
Grant 5 R29 DC00625

Project Staff

Dr. Mandayam A. Srinivasan

Whenever we touch an object, the source of all tactile information is the spatio-temporal distribution of mechanical loads on the skin at the contact interface. The relationship between these loads and the resulting stresses and strains at the nerve terminals within the skin plays a fundamental role in the neural coding of tactile information. Although empirical determination of the stress or strain state of a mechanoreceptor is not possible at present, mechanistic models of the skin and subcutaneous tissues enable prediction and verification of peripheral neural response. The research under this grant is directed towards applying theoretical and computational mechanics to analyze the biomechanical aspects of touch—the mechanics of contact, the transmission of the mechanical signals through the skin, and their transduction into neural impulses by the mechanoreceptors.

1.10.1 Determination of Geometric and Material Properties of the Primate Fingertip

The first step in performing mechanistic analyses of the primate fingertip is to determine its geometric and material properties. We have indented the fingerpads of humans and monkeys in vivo using a line load delivered by a sharp wedge, and photographed the resulting skin surface deflections. We have shown that the homogeneous elastic model of the fingertip only roughly approximates the experimental data, while a simple alternative model, which views the fingertip as an elastic membrane filled with an incompressible fluid (like a "waterbed"), predicted the observed profiles very well.[26] We are planning more experiments to determine the external and internal geometry of the primate fingertip as well as its material properties.

1.10.2 Finite Element Analyses of Two-dimensional Models

We have performed finite element analysis on a series of mechanistic models of the fingerpad under a variety of mechanical stimuli. The models range from a semi-infinite medium to cylindrical distal phalanx, composed of either a homogeneous elastic material or a thick elastic shell containing a fluid. Simulations of the mechanistic aspects of neurophysiological experiments involving mapping of receptive fields with single point loads, determination of spatial resolution of two-point stimuli, and indentations by single bars as well as periodic and aperiodic gratings have been carried out. The results show, for example, that the strain energy density at the receptor site is a leading contender for the relevant stimulus that causes the responses recorded from slowly adapting afferent fibers. More generally, we have demonstrated the power of computational mechanics in investigating the relationship between tactile stimuli imposed on the skin and the resulting peripheral neural response. The analyses are being extended both in terms of the mechanical stimuli applied on the fingerpad as well as the geometrical and material properties of the fingertip.

1.10.3 Tactile Sensing of Shapes and Softness

We have been collaborating with Dr. LaMotte of Yale University School of Medicine in conducting psychophysical and neurophysiological studies of the encoding of shapes and degree of softness in mechanoreceptive afferents. Based on a theoretical analysis of the mechanics of contact, we have demonstrated that the receptors respond to the low-pass filtered versions of surface pressures.[27] Thus, curvature of the skin surface under an

[26] M.A. Srinivasan, "Surface Deflection of Primate Fingertip Under Line Load," *J. Biomech.* 22(4): 343-349 (1989).

[27] M.A. Srinivasan and R.H. LaMotte, "Encoding of Shape in the Responses of Cutaneous Mechanoreceptors," in *Information Processing in the Somatosensory System*, eds: O. Franzen and J. Westman, Wenner-Gren Interna-

object, which we know from differential geometry is approximated by the second spatial derivative of surface deflection, is coded without differentiating (which is a noise enhancing process), but by exploiting its relation to surface pressure. We will be using our finite element models to further explore the neural coding of shapes and softness.

1.10.4 Development of a Computational Theory of Touch

Although the "hardware" of the tactile apparatus in humans and robots is different, they have the common feature of mechanosensors embedded in a deformable medium. Thus the computational problem of coding (predicting sensor response for a given mechanical stimulus at the surface) and decoding (inferring the mechanical stimulus at the surface by suitably processing the sensor response) need similar mechanistic analyses for their solution. We have developed such a "computational theory" for an idealized medium subjected to arbitrary pressure or displacement loading conditions, and give explicit formulae for the coding and decoding problems.[28]

In collaboration with Dr. Annaswamy of the Department of Aerospace and Mechanical Engineering, Boston University, we have investigated some of the identification and control problems that occur in the context of manipulation, when compliance is present in the end-effectors as well as in the object.[29] In order to understand the fundamental aspects of these tasks, we have analyzed the problem of identification of compliant objects with a single finger contact, was well as under a two-finger grasp. Assuming that the finger and the compliant object are constrained to deform along a single spatial dimension, we have carried out parameter identification using either force or displacement inputs to the rigid backing of the end-effector. Based on this analysis, control strategies are developed to achieve a desired manipulation of the object in the workspace. Animated graphical renderings are being developed to visually illustrate the presence of absence of slipping and crushing during an active manipulation task. The theoretical results can be used to generate testable hypotheses for human or robot experiments on tactual sense.

1.11 Publications

Annaswamy, A.M., and M.A. Srinivasan. "Adaptive Control for Grasping and Manipulation of Compliant Objects with Compliant Fingerpads." Accepted for presentation at the American Control Conference, Boston, June 1991.

Annaswamy, A.M., and M.A. Srinivasan. "Manipulation of Compliant Objects with Compliant Fingerpads: Identification and Control Issues." *Proceedings of the IEEE Conference on Decision and Control,* Hawaii, December 1990.

Braida, L.D. "Crossmodal Integration in the Identification of Consonant Segments." *Quart. J. Exper. Psych.* (1991). Forthcoming.

Braida, L.D. "Two Types of Audiovisual Integration for the Identification of Speech Segments." *J. Acoust. Soc. Am.* 88: S82 (1990).

Delhorne, L.A., J.M. Besing, C.M., Reed, and N.I. Durlach. "Tactual Cued Speech as a Supplement to Speechreading." *ASHA* 32: 73 (1990).

Durlach, N.I. "Auditory Localization in Teleoperator and Virtual Environment Systems." *Percept.* Forthcoming.

Grant, K.W., L.D. Braida, and R.J. Renn. "Single-band Envelope Cues as an Aid to Speechreading." *Quart. J. Exper. Psych.* (1991). Forthcoming.

Grant, K.W., and L.D. Braida. "Evaluating the Articulation Index for Audiovisual Input." *J. Acoust. Soc. Am.* (1991). Forthcoming.

Koehnke, J., and P.M. Zurek. "Localization and Binaural Detection with Monaural and Binaural

tional Symposium Series (New York: Macmillan Press, 1990); M.A. Srinivasan and R.H. LaMotte, "Tactile Discrimination and Representation of Texture, Shape, and Softness," in *Human-Machine Interfaces for Teleoperators and Virtual Environments,* eds. N.I. Durlach, T. Sheridan, and S. Ellis, *NASA Report* (1990), forthcoming.

[28] M.A. Srinivasan, "Tactile Sensing in Humans and Robots: Computational Theory and Algorithms," Newman Lab. Tech. Rep., Dept. of Mech. Eng., MIT, 1988.

[29] A.M. Annaswamy and M.A. Srinivasan, "Manipulation of Compliant Objects with Compliant Fingerpads: Identification and Control Issues," *Proceedings of the IEEE Conference on Decision and Control,* Hawaii, December 1990; A.M. Annaswamy and M.A. Srinivasan, "Adaptive Control for Grasping and Manipulation of Compliant Objects with Compliant Fingerpads," accepted for presentation at the American Control Conference, Boston, June 1991.

Amplification." *J. Acoust. Soc. Am.* 88: S169 (1990).

LaMotte, R.H., and M.A. Srinivasan. "Surface Microgeometry: Neural encoding and Perception." In *Information Processing in the Somatosensory System.* Eds. O. Franzen and J. Westman. Wenner-Gren International Symposium Series. New York: Macmillan Press, 1990.

Pang, X.D., H.Z. Tan, and N.I. Durlach. "Manual Discrimination of Force Using Active Finger Motion." *Percept. Psychophys.* (1990). Forthcoming.

Peterson, P.M., S.-M. Wei, W.M. Rabinowitz, and P.M. Zurek. "Robustness of an Adaptive Beamforming Method for Hearing Aids." *Acta Otolaryngologica Suppl.* 469: 85-90 (1990).

Rankovic, C.M., R.L. Freyman, and P.M. Zurek. "Potential Benefits of Varying the Frequency-gain Characteristic for Speech Reception in Noise." Submitted to *J. Acoust. Soc. Am.*

Rankovic, C.M., and P.M. Zurek. "Rollover with High-frequency Emphasis." *J. Acoust. Soc. Am.* 87: S87 (1990).

Reed, C.M., L.A. Delhorne, N.I. Durlach, and S.D. Fischer. "A Study of the Tactual and Visual Reception of Fingerspelling." *J. Speech Hear. Res.* 33: 786-797 (1990).

Reed, C.M., N.I. Durlach, and L.A. Delhorne. "Natural Methods of Tactual Communication." In *Tactile Aids for the Hearing Impaired.* Ed. Ian R. Summers. New York: Taylor and Francis. Forthcoming.

Reed, C.M., M.H. Power, N.I. Durlach, L.D. Braida, K.K. Foss, J.A. Reid, and S.R. Dubois. "Development and Testing of Artificial Low-Frequency Speech Codes." *J. Rehab. Res. Dev.* 28 (1991). Forthcoming.

Srinivasan, M.A. "Tactual Interfaces: The Human Perceiver." In *Human-Machine Interfaces for Teleoperators and Virtual Environments. NASA Report.* Eds. N.I. Durlach, T. Sheridan, and S. Ellis. Washington, D.C.: NASA, 1990.

Srinivasan, M.A., and R.H. LaMotte. "Tactile Discrimination and Representation of Texture, Shape, and Softness." In *NASA Report.* Eds. N.I. Durlach, T. Sheridan, and S. Ellis. Washington, D.C.: NASA, 1990.

Srinivasan, M.A., J.M. Whitehouse, and R.H. LaMotte. "Tactile Detection of Slip: Surface Microgeometry and Peripheral Neural Codes." *J. Neurophys.* 63 (6): 1323-1332 (1990).

Srinivasan, M.A., and R.H. LaMotte. "Encoding of Shape in the Responses of Cutaneous Mechanoreceptors." In *Information Processing in the Somatosensory System.* Eds. O. Franzen and J. Westman. Wenner-Gren International Symposium Series. New York: Macmillan Press, 1990.

Wilson, B.S., C.C. Finley, D.T. Lawson, R.D. Wolford, D.K. Eddington, and W.M. Rabinowitz. "New Levels of Speech Recognition with Cochlear Implants." *Nature.* Forthcoming.

Zurek, P.M., J.E. Greenberg, and P.M. Peterson. "Sensitivity to Design Parameters in an Adaptive-beamforming Hearing Aid." *Proc. ICASSP '90,* pp. 1129-1132.

Zurek, P.M., and C.M. Rankovic. "Potential Benefits of Varying the Frequency-gain Characteristic for Speech Reception in Noise." *J. Acoust. Soc. Am.* 87: S87 (1990).

Theses

Ito, Y. *Auditory Discrimination of Power Spectra for Roving Two-Tone Stimuli.* Ph.D. diss. Dept. of Electr. Eng. and Comput. Sci., MIT, 1990.

Millier, K.M. *Intelligibility of Vowels Represented by Multiple Intra-speaker Tokens.* S.B. thesis. Dept. of Elect. Eng. and Comput. Sci., MIT, 1990.

Taylor, L. *Token Variability of Intra-speaker Speech: Fricative Consonant Sounds.* S.B. thesis. Dept. of Electr. Eng. and Comput. Sci. MIT, 1990.

Wang, L. *Two Talker Activity Labelling by Humans.* S.B. thesis. Dept. of Electr. Eng. and Comput. Sci., MIT, 1990.

Section 3 Auditory Physiology

Chapter 1 Signal Transmission in the Auditory System

Chapter 1. Signal Transmission in the Auditory System

Academic and Research Staff

Professor Lawrence S. Frishkopf, Professor Nelson Y.S. Kiang, Professor William T. Peake, Professor William M. Siebert, Professor Thomas F. Weiss, Dr. Alice M. Berglund, Dr. Peter A. Cariani, Dr. Robin L. Davis, Dr. Bertrand Delgutte, Dr. Donald K. Eddington, Dr. Dennis M. Freeman, Dr. Barbara C. Fullerton, Dr. Miriam Furst, Dr. Jill C. Gardner, Dr. John J. Guinan, Jr., Dr. James B. Kobler, Dr. Robert A. Levine, Dr. Xiao Dong Pang, Dr. William M. Rabinowitz, Dr. John J. Rosowski

Visiting Scientists and Research Affiliates

Ellen Carlisle, Patricia A. Cuneo, Debra S. Louison, Dr. Jay T. Rubinstein, Frank J. Stefanov-Wagner, David A. Steffens, Meng Y. Zhu

Graduate Students

Kristin J. Dana, Scott B.C. Dynes, Farzad Ehsani, Michael P. McCue, Jennifer R. Melcher, Michael E. Ravicz, Steven M. Stufflebeam, Jenny S. Yu

Technical and Support Staff

Janice L. Balzer

1.1 Introduction

Sponsors

Health Sciences Fund
National Institutes of Health
Grants 5 R01 DC00194, 8 P01 DC00119, 5 R01 DC00473, 5 R01 DC00238, 5 T32 DC00006, 5 P01 DC00361, 5 R01 DC00235
Peoples Republic of China Fellowship
Unisys Corporation Doctoral Fellowship
Whitaker Health Sciences Fellowship

Research on the auditory system is carried out in cooperation with two laboratories at the Massachusetts Eye and Ear Infirmary (MEEI). Investigations of signal transmission in the auditory system involve the Eaton-Peabody Laboratory for Auditory Physiology. Our long-term objective is to determine the anatomical structures and physiological mechanisms that underlie vertebrate hearing and to apply that knowledge to clinical problems. Studies of cochlear implants in humans are carried out at the MEEI Cochlear Implant Laboratory. The ultimate goal of these devices is to provide speech communication for the deaf through electric stimulation of intracochlear electrodes to elicit patterns of auditory nerve fiber activity that the brain can learn to interpret.

1.2 Signal Transmission in the External and Middle Ear

1.2.1 Structure-Function Relations in Middle Ears

Project Staff

Professor William T. Peake, Dr. John J. Rosowski

The goal of this project is to investigate and formulate rules which relate the structure of the external and middle ears of land-dwelling vertebrates to hearing function. This goal is being achieved by testing and refining acoustic and mechanical models of the auditory periphery with new measurements of external and middle structure and function. In the past year, we have advanced the applications of our external- and middle-ear modeling efforts into new areas. Our work on the structure of the ear in the earliest (250 million years old) mammals has resulted in two manuscripts accepted for publication[1] which derive predictions of auditory function of these mammals from their middle-ear structure. These

[1] J.J. Rosowski and A. Graybeal, "What Did Morganucodon Hear?" *Zool. J. Linnean Soc.*, forthcoming; J.J. Rosowski, "Hearing in Transitional Mammals: Predictions from the Middle-ear Anatomy and Hearing Capabilities

predictions are consistent with the view that the suite of adaptations that define mammals (e.g., homeothermy, hair, soft palate and the mammalian jaw and ear) all evolved simultaneously, allowing these animals to develop a nocturnal life style.

We have also used our models of the auditory periphery to explain observations that the ear is most easily damaged by sounds with intense middle-frequency (1-10 kHz) spectral components.[2] Our investigations of the effects of the middle-ear cavity on auditory function continued; measurements were made of the cavities' contribution to the middle-ear input impedance in the gerbil,[3] an animal with a hypertrophied middle-ear air space. An expanded model of the effect of the middle-ear air space was also developed[4] in order to investigate the effect of direct acoustic stimulation of the cochlear windows by middle-ear sound pressure. We have also submitted a paper critiquing some common measures of the performance of the auditory periphery.[5]

1.2.2 Basic and Clinical Studies of the Auditory System: External and Middle Ears.

Project Staff

Professor William T. Peake, Dr. John J. Rosowski

The goals of this project are to understand the workings of the normal and pathological human external and middle ear. The techniques used include the interaction of measurements of the acoustics and mechanics of the human auditory periphery with acoustic and mechanical models of ear performance.

The work on this project has proceeded on three fronts:

1. A manuscript indicating that temporal bones extracted from cadavers are valid models of the human middle ear was published.[6]
2. Additional work with temporal bones has addressed the issue of what are the modes of ossicular motion.[7] The results suggest that the malleus rotates at sound frequencies below 1 kHz. However, at higher frequencies, the malleus also translates and may bend.
3. Model investigations of the effects of direct acoustic stimulation of the cochlear windows[8] indicate that the residual hearing observed in many middle-ear pathologies may be completely explained by the action of sound on the cochlear windows. The resultant models allow quantitative predictions of the effects of various middle-ear reconstruction techniques on hearing.

---

of Extant Mammals," in *The Evolutionary Biology of Hearing,* eds. A.N. Popper, R.R. Ray and D.B. Webster (New York: Springer-Verlag, forthcoming).

2 J.J. Rosowski, "The Effects of External- and Middle-ear Filtering on Auditory Threshold and Noise-induced Hearing Loss," *J. Acoust. Soc. Am.*, forthcoming.

3 M.E. Ravicz, J.J. Rosowski, and H.F. Voigt, "Acoustic Impedance Measurements in the Gerbil Ear," *J. Acoust. Soc. Am.* 87 (Suppl. 1): S101 (1990).

4 W.T. Peake, J.J. Rosowski, and T.J. Lynch III, "Acoustic Coupling to Cochlear Windows," Abstracts of the 15th Midwinter Meeting of the Association for Research in Otolaryngology, St. Petersburg, Florida, February 1991, forthcoming.

5 W.T. Peake and J.J. Rosowski, "Impedance Matching, Optimum Velocity and Ideal Middle Ears," *Hear. Res.*, forthcoming.

6 J.J. Rosowski, S.N. Merchant, P.J. Davis, K.M. Donahue, and M.D. Coltrera, "Cadaver Middle Ears as Models for Living Ears: Comparisons of Middle-ear Input Immittance," *J. Otol. Rhinol. Laryngol.* 99: 402-412 (1990).

7 K.M. Donahue, J.J. Rosowski, and W.T. Peake. "Can the Motion of the Human Malleus Be Described as Pure Rotation?," Abstracts of the Fifteenth Midwinter Meeting of the Association for Research in Otolaryngology, St. Petersburg, Florida, February 1991, forthcoming.

8 W.T. Peake, J.J. Rosowski, and T.J. Lynch III, "Acoustic Coupling to Cochlear Windows," Abstracts of the 15th Midwinter Meeting of the Association for Research in Otolaryngology, St. Petersburg, Florida, February 1991, forthcoming.

Publications and Papers Presented

Donahue, K.M., J.J. Rosowski, and W.T. Peake. "Can the Motion of the Human Malleus Be Described As Pure Rotation?" Abstracts of the 15th Midwinter Meeting of the Association for Research in Otolaryngology, St. Petersburg, Florida, February 1991. Forthcoming.

Peake, W.T., J.J. Rosowski, and T.J. Lynch III. "Acoustic Coupling to Cochlear Windows." Abstracts of the 15th Midwinter Meeting of the Association for Research in Otolaryngology. St. Petersburg, Florida, February 1991. Forthcoming.

Peake, W.T., and J.J. Rosowski. "Impedance Matching, Optimum Velocity and Ideal Middle Ears." *Hear. Res.* Forthcoming.

Ravicz, M.E., J.J. Rosowski, and H.F. Voigt. "Acoustic Impedance Measurements in the Gerbil Ear." *J. Acoust. Soc. Am.* 87 (Suppl. 1): S101 (1990).

Rosowski, J.J. "The Effects of External- and Middle-ear Filtering on Auditory Threshold and Noise-induced Hearing Loss." *J. Acoust. Soc. Am.* Forthcoming.

Rosowski, J.J., "Hearing in Transitional Mammals: Predictions from the Middle-ear Anatomy and Hearing Capabilities of Extant Mammals." A talk presented at the Symposium on the Evolutionary Biology of Hearing, Sarasota, Florida, May 1990.

Rosowski, J.J. "Hearing in Transitional Mammals: Predictions from the Middle-ear Anatomy and Hearing Capabilities of Extant Mammals." In *The Evolutionary Biology of Hearing.* Eds. A.N. Popper, R.R. Ray and D.B. Webster. New York: Springer-Verlag. Forthcoming.

Rosowski, J.J., and A. Graybeal. "What Did Morganucodon Hear?" *Zool. J. Linnean Soc.* Forthcoming.

Rosowski, J.J., S.N. Merchant, P.J. Davis, K.M. Donahue, and M.D. Coltrera. "Cadaver Middle Ears as Models for Living Ears: Comparisons of Middle-ear Input Immittance." *Ann. Otol. Rhin. Laryngol.* 99: 402-412 (1990).

1.3 Cochlear Mechanisms

Project Staff

Professor Thomas F. Weiss, Professor Lawrence S. Frishkopf, Dr. Dennis M. Freeman, Kristin J. Dana, Farzad Ehsani

The results of several studies, described in last year's Progress Report, have now been published.[9] The progress described below focuses primarily on newer projects.

Our longer-term goal is to investigate the micromechanical mechanisms by which vibrations of macroscopic inner ear structures are conveyed to the receptor (hair) cells. For this purpose, we have developed *in vitro* preparations to (1) place a dissected portion of an auditory receptor organ in a chamber on the stage of a compound microscope; (2) perfuse the tissue with artificial lymph solutions; (3) stimulate the organ hydrodynamically; and (4) measure displacements of inner ear structures in response to changes in solution composition and to audio frequency hydrodynamic stimulation. We have developed both an isolated preparation of the cochlear duct of the alligator lizard and isolated tectorial membrane (TM) preparations of the chick and alligator lizard cochlea.

Measurement of the osmotic response of the receptor organ is one way to measure the viability of the organ. This measurement can give insight into mechanisms of ion transport in the cells of the organ. Measurement of the osmotic response of the TM to changes in solution composition can yield information about the physical-chemical properties of the TM. To investigate these osmotic responses, we have devised a video microscopy system that consists of a compound microscope, displacement detector, video camera, video digitizer, and personal computer. We can routinely measure the location of a microscopic object in three dimensions with respect to a reference location with this system. The height of the object along the optical axis of the microscope is measured by bringing the object into focus in the microscope and measuring the height of the

[9] D.M. Freeman and T.F. Weiss, "Superposition of Hydrodynamic Forces on a Hair Bundle," *Hear. Res.* 48: 1-16 (1990); D.M. Freeman and T.F. Weiss, "Hydrodynamic Forces on Hair Bundles at Low Frequencies," *Hear. Res.* 48: 17-30 (1990); D.M. Freeman and T.F. Weiss, "Hydrodynamic Forces on Hair Bundles at High Frequencies," *Hear. Res.* 48: 31-36 (1990); D.M. Freeman and T.F. Weiss, "Hydrodynamic Analysis of a Two-dimensional Model for Micromechanical Resonance of Free-standing Hair Bundles," *Hear. Res.* 48: 37-68 (1990); D.M. Freeman, "Anatomical Model of the Cochlea of the Alligator Lizard," *Hear. Res.* 49: 29-38 (1990); R.C. Kidd and T.F. Weiss, "Mechanisms that Degrade Timing Information in the Cochlea," *Hear. Res.* 49: 181-208 (1990).

microscope stage with a displacement detector. The location of the object in the plane perpendicular to the optical axis is measured by displaying the microscope field on a video terminal and using a mouse-controlled cursor that is superimposed on the video image. Clicking the mouse results in acquisition of all three coordinates of an object, which are then placed in a file along with the time of data acquisition. In addition, the video images can be acquired, image-processed, and saved in files. Software has been written that allows us to measure the locations of beads (microspheres $1 - 5\ \mu m$ in diameter) on cochlear structures and to acquire images during an experiment. Experimental results—absolute bead locations as a function of time, Euclidean distances between beads as a function of time, sequences of images—can be displayed during the experiment.

With the video microscopy system we have continued to examine the osmotic response of the isolated auditory receptor organ of the alligator lizard to perfusion with artificial lymph solutions. The principal finding of this study is that the cochlear duct of the alligator lizard swells in some isoosmotic solutions but not in others. The duct swells in solutions that contain both potassium and chloride ions, but does not swell if either sodium is substituted for potassium or gluconate is substituted for chloride. A manuscript is being prepared which describes these results and their implications for mechanisms of ion transport in hair cells; the ototoxicity of endolymph, which may play a role in Ménière's disease; and the use of *in vitro* preparations.

In collaboration with Dr. Douglas A. Cotanche of the Anatomy Department at the Boston University Medical School, we have developed an isolated TM preparation for studying the physical-chemical properties of the TM. The intact TM is microdissected from the auditory receptor organ of either chick or alligator lizard and cemented onto the surface of an experimental chamber using a tissue adhesive. Beads are allowed to settle on the TM and the positions of each bead in three dimensions is measured with the video microscopy system as solutions of different composition are perfused through the chamber. Video images of the TM have also been obtained with the video microscopy system.

The isolated TM preparation has several advantages over preparations in which the TM is in place surmounting the receptor organ. In studies of shrinkage/swelling of the TM, using this method eliminates a possible ambiguity caused by shrinkage/swelling of the underlying tissue. Furthermore, structural features of the TM are more readily visualized when TM is isolated than when it is in place in the receptor organ. Preliminary results from both chick and alligator lizard TMs reveal that both the dimensions and microstructure of the TM are critically dependent on the composition of the bathing solution. Changes in osmolarity and ionic strength produced very large (>500%), rapid changes in dimensions. Large (100%) changes in dimensions and microstructure were seen when the sodium, potassium, and calcium content of artificial lymph solutions were changed even though the solutions were isoosmotic and had the same ionic strength.

Publications

Freeman, D.M., and T.F. Weiss. "Superposition of Hydrodynamic Forces on a Hair Bundle." *Hear. Res.* 48: 1-16 (1990).

Freeman, D.M., and T.F. Weiss. "Hydrodynamic Forces on Hair Bundles at Low Frequencies." *Hear. Res.* 48: 17-30 (1990).

Freeman, D.M., and T.F. Weiss. "Hydrodynamic Forces on Hair Bundles at High Frequencies." *Hear. Res.* 48: 31-36 (1990).

Freeman, D.M., and T.F. Weiss. "Hydrodynamic Analysis of a Two-dimensional Model for Micromechanical Resonance of Free-standing Hair Bundles." *Hear. Res.* 48: 37-68 (1990).

Freeman, D.M. "Anatomical Model of the Cochlea of the Alligator Lizard." *Hear. Res.* 49: 29-38 (1990).

Kidd, R.C., and T.F. Weiss. "Mechanisms That Degrade Timing Information in the Cochlea." *Hear. Res.* 49: 181-208 (1990).

1.3.1 Regeneration of Primary-auditory Neurons in vitro

Project Staff

Dr. Robin L. Davis

To determine whether intrinsically-regulated growth features contribute to the precise quality of regeneration observed in the lower vertebrate auditory system, neurite regeneration was studied from individual goldfish primary-auditory neurons placed in the homogenous conditions of tissue culture. We observed stereotyped morphology and timing of neurite outgrowth *in vitro* and the properties observed from these same neurons *in vivo*. These findings suggest that some morphological properties of neurite regeneration, as well as the way in which the growth was attained, may be

important endogenously-determined features in adult regenerating primary-auditory neurons.

Publications

Davis, R.L. "Conditioning Lesions Promote Primary-auditory Neurite Regeneration *in vitro*." *Abstr. Assoc. Res. Otolaryngol.* 13: 316-317 (1990).

Davis, R.L., and W.F. Sewell. "Neurite Regeneration from Single Primary-auditory Neurons *in vitro*." Submitted to *J. Neurosci.*

Davis, R.L. "Specificity of VIIIth Nerve Regeneration in Lower Vertebrates." *J. Exp. Zool.* (mini-review from a neurosciences symposium, Molecular and Cellular Events in Development and Regeneration, submitted for review).

1.3.2 Stimulus Coding in the Auditory Nerve and Cochlear Nucleus

Project Staff

Dr. Bertrand Delgutte, Dr. Peter A. Cariani

The goal of our research is to understand neural mechanisms for processing of complex acoustic stimuli at the level of the auditory nerve and cochlear nucleus. Our modeling work on nonlinear responses of auditory-nerve fibers to complex stimuli has progressed. A particular focus of this model is on suppression phenomena, which play a key role in masking and speech processing.

We have investigated how this model might be used to develop improved analysis-synthesis systems for telecommunications.[10] This work is based on the premise that auditory models only respond to features of the acoustic signal that are perceptually relevant. Indeed, the model response to speech processed by a high-quality speech coding system resembled more the response to natural speech than the response to a poor-quality coder. We further showed that nonlinear processing in the model helps to predict the relative salience of selected spectral manipulations for speech-like stimuli.

We have analyzed data on the responses of auditory-nerve fibers at very low sound levels.[11] These kinds of data are important for understanding physiological substrates of behavioral thresholds and may shed light on cochlear mechanisms in a range where nonlinear phenomena are likely to be less prominent. Results show that the growth of driven discharge rate with sound pressure for tones at the characteristic frequency (CF) is well approximated by a power function. The exponent of this function is greater for fibers with low spontaneous rates (SR) of discharge than for high-SR fibers. The detection-theoretic measure d' also shows a power-law behavior as a function of sound pressure, but the mean exponent was about the same for all fibers. Thresholds based on d' were lower for high-SR fibers than for low-SR fibers, suggesting that high-SR fibers are most appropriate for signal detection. Rate-level functions for tones at frequencies other than the CF also showed a power-law behavior. The exponent was larger for tones below the CF than for tones above the CF. This frequency dependence is probably of mechanical origin because the growth of basilar-membrane motion shows a similar dependence.

We are beginning to investigate possible neural mechanisms for the representation of periodicities of complex waveforms in the auditory nerve and the cochlear nucleus. We are conducting a series of experiments on the responses of auditory-nerve fibers to speech-like, single-formant stimuli with fundamental frequency that is systematically varied. Specifically, we are investigating whether auditory nerve fibers show an enhanced response when their CF is a small multiple of the fundamental frequency, which is predicted by rate-place models of auditory processing. Preliminary results suggest that these enhanced responses are most prominent for low-CF fibers and high fundamental frequencies; this is consistent with filter-bank models of cochlear processing.

Neurons with "chopper" response patterns in the cochlear nucleus show enhanced synchronization to the fundamental frequency of amplitude modulated tones when this modulation frequency is close to the "intrinsic oscillation" or "chopping" frequency of the cell.[12] We are developing a simple neuron model to ascertain whether threshold

---

[10] B. Delgutte, "Physiological Models of Masking and Speech Processing," *J. Acoust. Soc. Am.* 87: S13 (1990).

[11] B. Delgutte, "Power-law Behavior of the Discharge Rates of Auditory-nerve Fibers at Low Sound Levels," Fifteenth Midwinter Meeting, Association of Research in Otolaryngology, St. Petersburg, Florida, February 1991, forthcoming.

[12] D.O. Kim, J.G. Sirianni, and S.O. Chang, "Responses of DCN-PVCN Neurons and Auditory Nerve Fibers in

accommodation can account for this behavior and whether these kinds of neurons could play a role in periodicity detection. We plan to utilize complex waveforms, periodic and aperiodic click trains, noise, and speech-like sounds to investigate the temporal responses of chopper neurons.

During the past year, two previously-submitted manuscripts have been published.[13]

1.3.3 Electrical Stimulation of the Auditory Nerve

Project Staff

Dr. Bertrand Delgutte, Scott B.C. Dynes

This research aims at understanding physiological mechanisms of electrical stimulation to help design improved cochlear implants. We are recording the responses of auditory-nerve fibers to electric currents applied through electrodes inserted into the cochlea. In one series of experiments, the threshold of auditory-nerve fibers is measured as a function of the duration of brief rectangular current pulses. These very basic experiments are important for understanding not only stimulation of the auditory nerve, but also stimulation of myelinated fibers in general. Preliminary results suggest that the threshold for long pulses was about 10-dB lower for cathodal currents than for anodal currents, consistent with the predictions of a biophysical model of myelinated nerve fibers.[14] Time constants describing the decrease in threshold with pulse duration were lower for anodal currents than for cathodal currents, contrary to model predictions. In another series of experiments, the threshold of auditory-nerve fibers for stimulation through one intracochlear electrode is measured while a subthreshold current is applied through another electrode. These experiments study "electrode interactions" that are likely to limit the performance of certain multiple-channel cochlear implants. Preliminary results suggest that the threshold current varies linearly with the subthreshold current; this is consistent with the notion that these electrode interactions are due to linear summation of the electric fields produced by stimulation of each electrode.

Publications and Papers Presented

Delgutte, B. "Physiological Mechanisms of Psychophysical Masking: Observations from Auditory-nerve Fibers." *J. Acoust. Soc. Am.* 87: 791-809 (1990).

Delgutte, B. "Two-tone Suppression in Auditory-nerve Fibers: Dependence on Suppressor Frequency and Level." *Hear. Res.* 49: 225-246 (1990).

Delgutte, B. "Physiological Models of Masking and Speech Processing." *J. Acoust. Soc. Am.* 87: S13 (1990).

Delgutte, B. "Power-law Behavior of the Discharge Rates of Auditory-nerve Fibers at Low Sound Levels." Paper presented at the 15th Midwinter Meeting, Association for Research in Otolaryngology, St. Petersburg, Florida, February 1991. Forthcoming.

1.4 Middle-Ear Muscle Reflex

Project Staff

Dr. John J. Guinan, Jr., Dr. James B. Kobler, Michael P. McCue

Our aim is to determine the structural and functional basis of the acoustically elicited middle-ear muscle reflexes.

Our previous work has shown that stapedius motoneurons can be divided into categories based on the laterality of their response to sound and that these categories are partly spatially segregated in the brainstem. Stapedius motoneurons which respond to contralateral sound have their cell bodies in one location, those which respond to sound in either ear in another location, and so forth. During the past year, we have attacked the question of whether there is also spatial segregation in the organization of stapedius motor fibers as they enter the stapedius muscle. In other muscle systems which show central segregation, there is also peripheral segregation.

Unanesthetized Decerebrate Cats to AM and Pure Tones: Analysis with Autocorrelation/Power-spectrum," Hear. Res. 45: 95-113 (1990).

[13] B. Delgutte, "Physiological Mechanisms of Psychophysical Masking: Observations from Auditory-nerve Fibers," *J. Acoust. Soc. Am.* 87: 791-809 (1990): B. Delgutte, "Two-tone Suppression in Auditory-nerve Fibers: Dependence on Suppressor Frequency and Level," *Hear. Res.* 49: 225-246 (1990).

[14] J.T. Rubinstein, "Analytical Theory for Extracellular Stimulation of Nerve with Focal Electrodes. II. Passive Myelinated Axon," *Biophys. J.*, forthcoming.

We have attacked this question by two methods. First, we have examined the locations of labeled cells following injections of single fascicles of the stapedius nerve with HRP and compared these patterns with those produced by injections of the whole stapedius muscle. All of the individual fascicles received innervation from all four brainstem regions which have stapedius motoneurons. This pattern rules out strict segregation within individual fascicles, but considering that the proportions of labeled cell bodies in each region varied from one case to the next, there may be some weak segregation.

Our second method was to analyze the distribution of unit types obtained in recordings from individual fascicles. There were fascicles which contained stapedius motoneurons in each of the four laterality types, fascicles which contained stapedius motoneurons of only one type, and everything in between. A statistical analysis of these data suggests that the distribution could not have been produced by a random selection of unit types from a large pool. This is consistent with some segregation of stapedius motoneurons present at the level of the fascicles entering the stapedius. The function of this segregation for the stapedius is not clear. The general principal of the presence of peripheral segregation if there is central segregation is upheld, but the degree of segregation peripherally may be less than it is centrally.

During the past year, data analysis and writing have been done to prepare for publication our results on the responses to sound and and axon conduction velocities of stapedius motoneurons (These data provide the basis for the division of stapedius motoneurons into response-type groups.)

We have begun work on a project to measure the overall change in transmission, ΔT, produced by middle-ear muscles to determine whether the maximum ΔT is substantially different for crossed, uncrossed and binaurally-evoked stapedius reflexes. To measure ΔT, we have assembled acoustic systems which have two sound sources and a microphone in each ear canal and have built a suitable computer-controlled signal analysis system. We are now beginning work on measurement techniques for determining the mechanical output of the middle ear.

1.5 Cochlear Efferent System

Project Staff

Dr. John J. Guinan, Jr., Michael P. McCue

Our aim is to understand the physiological effects produced by medial olivocochlear (MOC) efferents which terminate on outer hair cells in the mammalian cochlea. It has been proposed that (1) a major role of medial olivocochlear efferents is to control the cochlear amplifier and (2) the mechanical output of the cochlear amplifier produces traveling waves in both dirctions along the cochlea with the backward waves producing stimulus frequency otoacoustic emissions (SFEs).

To test these hypotheses, the effect of efferents on SFEs was determined by measuring changes in the ear canal sound pressure, ΔP, produced by stimulation of medial efferents.[15] For most probe tones, ΔP amplitude was a few dB lower than the amplitude of the SFE and ΔP phase was opposite that of the SFE. These data indicate that efferent stimulation inhibits the SFE. In addition, the efferent-induced change in the compound action potential of the auditory nerve ($\Delta N1$) was compared to ΔP using tone pips (for $\Delta N1$) and tones (for ΔP) of the same frequency and level. As the amplitude of the efferent effect was varied by changing efferent shock rate or amplitude, $\Delta N1$ was approximately proportional to ΔP. These data are consistent with the hypothesis that efferents control the gain of an amplifier which is responsible for the sensitivity of the cochlea. In contrast to previous work which has shown that efferents affect emissions generated by cochlear nonlinearities, the present work demonstrates that an efferent effect on an emission may be generated primarily by linear processes and may directly reflect efferent effects on the cochlear amplifier.

Efferent activity and two-tone suppression might affect the cochlear amplifier at different sites and produce similar effects. Their effect on stimulus-frequency otoacoustic emissions (SFEs) in cats was compared by measuring the vector change in ear-canal sound pressure. The results indicate that contributions to the SFE originate along a large fraction of the length of the cochlea and that SFEs may provide a "window" into the action of the cochlear amplifier.[16]

---

[15] J.J. Guinan, Jr., "Inhibition of Stimulus Frequency Emissions by Medial Olivocochlear Efferent Neurons in Cats," Association for Research in Otolaryngology, Abstracts 14, forthcoming.

[16] J.J. Guinan, Jr., "Changes in Stimulus Frequency Otoacoustic Emissions Produced by Two-tone Suppression and

We have published a paper which shows the signal processing properties of a group of brainstem auditory neurons.[17]

Work has begun on a project to determine the correspondence between the number of medial efferents that fire and the effects produced. Our intention is to evoke activity in medial efferents with brainstem shocks and determine the percentage of them which fire by analyzing recordings from single medial efferent fibers. The effects of this efferent activity will be assessed by measuring changes in N1. The results are intended to determine the size of the effect of a single efferent fiber on auditory-nerve responses, and how these effects summate (i.e., linearly, or with saturation, etc).

Publications

Guinan, J.J., Jr. "Inhibition of Stimulus Frequency Emissions by Medial Olivocochlear Efferent Neurons in Cats." Association for Research in Otolaryngology, Abstracts 14. Forthcoming.

Guinan, J.J., Jr. "Changes in Stimulus Frequency Otoacoustic Emissions Produced by Two-tone Suppression and Efferent Stimulation in Cats." *Proceedings of the 1990 Conference on the Mechanics and Biophysics of Hearing.* Forthcoming.

Guinan, J.J., Jr., and R.Y.S. Li. "Signal Processing in Brainstem Auditory Neurons which Receive Giant Endings (Calyces of Held) in the Medial Nucleus of the Trapezoid Body of the Cat." *Hear. Res.* 49: 321-334 (1990).

1.5.1 The Generators of the Brainstem Auditory Evoked Potential

Project Staff

Professor Nelson Y.S. Kiang, Professor William T. Peake, Dr. Barbara C. Fullerton, Jennifer R. Melcher

When a punctate sound is presented to the ear, a time-varying potential can be recorded from electrode pairs on the surface of the head. The potential waveform at short latencies (< 10 msec following the stimulus) is distinguished from the potential at longer latencies by a characteristic series of deflections, each about one msec in duration. Similar waveforms have been measured in every mammalian species in which recordings have been attempted. It is believed that the short-latency potential is generated by cells in the auditory nerve and brainstem. Thus, this potential is called the brainstem auditory evoked potential (BAEP).

The goal of Melcher's thesis is to better understand which cells generate the different components of the BAEP. In previous years progress has been made along two lines: (1) a series of lesion experiments were begun, and (2) a model for BAEP generation was developed. The model relates the activity of individual cells in the auditory pathway to the BAEP and has served as a guide for designing and interpreting the experiments. The lesion experiments involve injecting a neurotoxin into different parts of the cat brainstem and correlating the resulting cell loss with changes in the BAEP.

The lesion experiments and a preliminary analysis of the cell loss in each case were completed during the last year. We have determined that two of the BAEP components are generated by cells in separate pathways within the auditory system. A more refined assessment of cell loss is in progress.

Publication

Melcher, J.R., B.C. Fullerton, J.J. Guinan, N.Y.S. Kiang, and I.M. Knudson. "Cellular Generators of the Brainstem Auditory Evoked Potential in Cat." Poster presentation at the 20th Annual Meeting of the Society for Neuroscience, St. Louis, Missouri, October 28-November 2, 1990.

1.6 Cochlear Implants

Project A: Models of Current Spread and Nerve Excitation during Intracochlear Stimulation

Project Staff

Dr. Donald K. Eddington, Dr. Jay T. Rubinstein

The basic function of a cochlear prosthesis is to elicit patterns of activity on the array of surviving

Efferent Stimulation in Cats," *Proceedings of the 1990 Conference on the Mechanics and Biophysics of Hearing,* forthcoming.

[17] J.J. Guinan, Jr., and R.Y.S. Li, "Signal Processing in Brainstem Auditory Neurons Which Receive Giant Endings (Calyces of Held) in the Medial Nucleus of the Trapezoid Body of the Cat," *Hearing Res.* 49: 321-334 (1990).

auditory nerve fibers by stimulating electrodes that are placed in and/or around the cochlea. By modulating these patterns of neural activity, these devices attempt to present information that the implanted subject can learn to interpret.

The spike activity patterns elicited by electrical stimulation depend on several factors: (1) the complex, electrically heterogeneous structure of the cochlea; (2) the geometry and placement of the stimulating electrodes, (3) the stimulus waveform, and (4) the distribution of excitable auditory nerve fibers. An understanding of how these factors interact to determine the activity patterns is fundamental to designing better devices and interpreting the results of experiments involving intracochlear stimulation of animal and human subjects. As a first step towards understanding this interaction, the goal of this project is to construct a software model of the cochlea that predicts the distribution of potential produced by the stimulation of arbitrarily placed, intracochlear electrodes, and to use these potential distributions as inputs that drive models of auditory nerve fibers.

Last year, we continued the development of the three-dimensional, finite element model of the human cochlea for prediction of the potential distribution produced in this structure by electrical stimulation of model electrodes of arbitrary position and geometry. We have begun (1) investigating different numerical techniques that will allow us to specify anisotropic media and (2) porting the model to a Thinking Machine computer to reduce computational time. Continued measurements of potential at unstimulated electrodes made in ten subjects implanted with intracochlear electrodes confirmed the asymmetric potential distributions predicted by the model. Psychophysical measures of the interaction between two electrodes stimulated simultaneously also exhibited the predicted asymmetries in the 13 subjects measured to date.

We have also begun work on the development of linear and nonlinear models of extracellular excitation of myelinated and unmyelinated nerve fibers. Psychophysical measures have confirmed model predictions that an electrical stimulus composed of a single, biphasic pulse of subthreshold amplitude produces a residual membrane depolarization that can reduce the threshold of a second pulse when it follows the first within several hundred microseconds. The 100 us time constant of this sensitization effect as measured psychophysically is consistent with the time constant of the residual depolarization predicted by the model.

Publications

Eddington, D.K. "An Electroanatomical Model of Intracochlear Electrical Stimulation." Paper presented at the Second International Cochlear Implant Symposium, Iowa City, Iowa, June 4-8, 1990.

Rubinstein, J.T. "An Analytical Model for Electrical Stimulation of Nerve 2: Passive Myelinated Axon." *Biophys. J.* Forthcoming.

Project B: Psychophysical Measures and their Correlation with Speech Reception

Project Staff

Dr. Donald K. Eddington

One striking aspect of speech reception measurements made with subjects using cochlear implants is the wide range of performance. This project is designed to identify basic psychophysical measures that correlate with the subject's speech reception ability. These correlations should help us to both identify basic performance deficits that might be overcome with alternative processing schemes and to relate correlations found between pathology and psychophysical measures in experimental animals to their potential effect on speech reception.

We have reported correlations of speech reception with two psychophysical measures [threshold ($r = -0.78$) and interaction ($= -0.86$)] in 16 subjects. These correlations are consistent with an interpretation that the density of excitable fibers that remain in each subject is one underlying factor important for speech reception.

Publication

Eddington, D.K. "Psychophysical Correlates of Speech Reception in Subjects Using Multichannel Cochlear Implants." Paper presented at the Second International Cochlear Implant Symposium, Iowa City, Iowa, June 4-8, 1990.

Project C: Cues Used by the Brain to Assign Pitch Based on Electrode Position

Project Staff

Dr. Donald K. Eddington

Subjects with intracochlear electrodes provide a unique opportunity to elicit activity patterns in the array of auditory nerve fibers that cannot be elic-

ited in normal hearing individuals using acoustic stimuli. This opportunity to present novel inputs to the brain and to determine how human subjects perceive them provides a powerful tool for probing the processing mechanisms of the "central processor." We have been using this tool to identify cues that the brain uses to determine the relative pitch of perceptions produced by two electrical stimuli that are temporally but not spatially equivalent. Preliminary results in three subjects indicate that the subjects use the apical boundary of excitation when assigning relative pitch to these stimuli.

Project D: 3D Reconstruction and Display of Data Obtained from Computerized Tomography (CT) of the Temporal Bone

Project Staff

Meng Y. Zhu

The goal of this project is to construct 3D computer representations of the inner ear structures by reconstructing the x-ray attenuation data from a sequence of parallel slices obtained during CT scanning. In order to optimize the resolution of the representation, raw CT data are used in the reconstruction rather than the image data derived from a down-sampling process. One use of these 3D representations is to compute intracochlear electrode positions in individual human subjects. These positions are helpful in interpreting the results of psychophysical measures such as electrode interaction and can be used to customize our models of current spread for individual subjects. Considerable effort has also been invested in designing software for the display of these 3D structures.

1.7 Anatomical Basis for the Relationships Between Binaural Hearing and Brainstem Auditory Evoked Potentials in Humans

Project Staff

Dr. Jill C. Gardner, Dr. Robert A. Levine, Dr. Barbara C. Fullerton, Ellen Carlisle, Steven M. Stufflebeam

In ongoing studies, we have been making behavioral and physiological measurements on patients with multiple sclerosis (MS) who show specific losses in auditory functions. We are investigating whether these functions, which involve using cues to determine the lateral position of sounds (auditory lateralization), depend on the integrity of the brainstem auditory pathway. We are using nuclear magnetic resonance (nmr) imaging to localize lesions, which occur in multiple sclerosis, with respect to the nuclei and fiber tracts of the auditory pathway in the brainstem.

We have had good initial success correlating the sites of brainstem lesions to the performance of the MS patients on a variety of tasks. Over 50% of the patients we have examined showed deficits in auditory lateralization although their hearing appeared to be otherwise normal. In the nmr scans, some of the abnormalities were focal and clearly defined, typical of what has been described in MS, while others were diffuse, and in some cases covered a considerable extent of the brainstem. All of the subjects with lesions in the brainstem auditory pathway performed abnormally on some aspect of the lateralization tasks. The subjects with diffuse lesions showed deficits far more severe than the MS group as a whole.

Previous studies, which for the most part focused on abnormalities in the cerebral cortex, have found little relationship between nmr "lesions" and the symptoms of MS patients. Our initial analysis of the data indicates that there are clear correlations between the extent of lesions, the psychoacoustics and a physiological measure, and the brainstem auditory evoked potential, which is widely used clinically. Our data suggest that we may be seeing a variety of abnormalities in the nmr scans that have not been previously described. Our efforts at the present are directed toward developing methodologies for characterizing the normal brainstem and defining and quantifying MS related abnormalities in magnetic resonance scans.

Publications

Furst, M., J.C. Gardner, R.A. Levine, B. Fullerton, and P. Cuneo. "Localizing the Brainstem Auditory Pathway in Human Magnetic Resonance Images: An Algorithm Matching MR Scans to a Computerized Anatomic Atlas." Paper presented at the Association for Research in Otolaryngology, 14th Midwinter Meeting, St. Petersburg, Florida, February 1990.

Gardner, J.C., M. Furst, R.A. Levine, B. Fullerton, and B.R. Rosen. "An Anatomic Atlas and Mapping Algorithm for Localizing the Brainstem Auditory Pathway on Magnetic Resonance Scans." Paper presented at the Society of Magnetic Resonance in Medicine, Ninth Annual Meeting, New York, 1990.

From left, graduate student Donna K. Hendrix, Professor Lawrence S. Frishkopf, Professor Thomas F. Weiss, and Research Scientist Dr. Dennis M. Freeman are shown with plastic models of the inner ear of a lizard (magnified 50 times).

Section 4 Linguistics

Chapter 1 Linguistics

Chapter 1. Linguistics

Academic and Research Staff

Professor Morris Halle, Professor Noam A. Chomsky

1.1 Introduction

The work of the Linguistics group is directed towards a better understanding of the mental capacities of human beings through the study of the nature, acquisition and use of language. Language is a uniquely human faculty: only humans appear to be capable of learning and using a language, and every normal human acquires knowledge of one or more languages.

We are trying to understand how this linguistic knowledge is represented in the speaker's mind. The central issues of linguistics research are:

1. What is the nature of linguistic knowledge? What do speakers of a particular language such as Latvian, Spanish or Walpiri know, and how does knowledge of one language ressemble or differ from that of another language?
2. How do speakers acquire this knowledge?
3. How do speakers put this knowledge to use in producing and understanding utterances?
4. What are the physiological mechanisms that provide the material basis for storage, acquisition and utilization of linguistic knowledge?

Our ability to answer these questions differs considerably, and our research reflects these differences. At present, we have progressed further with regard to answering the questions posed by item one and have made less progress with item four. Currently, our research is heavily concentrated on issues concerned with the nature of the knowledge that characterizes fluent speakers of various languages. However, we are making a significant effort to solve the other questions also.

We are studying these topics along a number of parallel lines. Linguists have investigated the principles by which words are concatenated to form meaningful sentences. These principles have been the primary domain of inquiry into the disciplines of syntax and semantics. Phonology studies the sound structure of words while morphology examines the manner in which different languages combine different meaning-bearing units (specifically, stems, prefixes, suffixes and infixes) to form words. The latter topic has attracted increasing interest in recent years and will probably become more prominent in our research efforts in the future.

1.2 Abstracts of Doctoral Dissertations

The following are abstracts of dissertations submitted to the Department of Linguistics and Philosophy in partial fulfillment of the requirements for the degree of Doctor of Philosophy in Linguistics.

1.2.1 On the Nature of Tone

Zhiming Bao

Abstract

This thesis addresses two issues: the feature geometry of tone and the formal relation of tone with respect to other aspects of phonological representation.

The tonal geometry I propose can be stated simply: tone (t) consists of register (r) and contour (c):

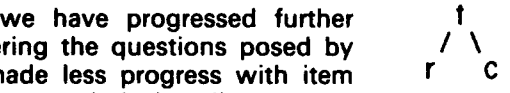

r is specified by the laryngeal feature [stiff], and c by the laryngeal feature [slack]. In addition, c is allowed to branch. The structures of r and c are below.

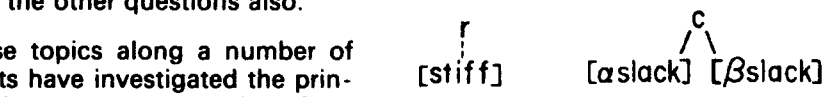

Since tone is phonetically executed by the VC node, it is claimed that the geometry of tone is a substructure of the geometry of laryngeal features. The geometry of laryngeal features is shown below (CT=cricothyriod; VOC=vocalis):

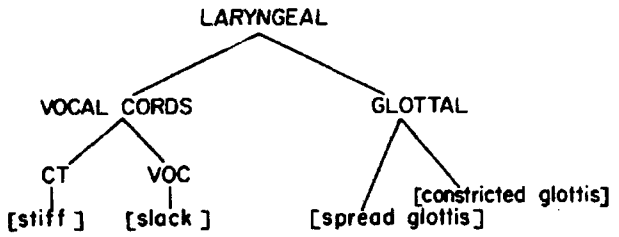

It is speculated that register is executed by the articulator CT; and contour by the articulator VOC over time.

I argue against a tone plane. The mapping of tones to tone bearing units (TBU) is an adjunction process: tone is adjoined to the tone bearing unit. Given that the rime is the TBU, tone mapping creates the structure below:

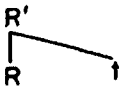

Thus, tones form a tier on the syllable plane, rather than an independent plane. This accounts for structure-dependency of tone stability.

After tone sandhi rules have been applied, t is linked to the laryngeal node of the head of TBU through the process of segmentalization. This allows tone to be phonetically realized on vowels or other segments which may be the head of tone bearing units.

1.2.2 A Formal Study of Syllable, Tone, Stress and Domain in Chinese Languages

San Duanmu

Abstract

This thesis makes a close examination of syllable, tone and stress in Chinese languages to find out general properties that are shared by all natural languages. It offers the following related claims:

1. All Chinese syllables have the following uniform underlying structure:

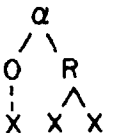

2. The general tonal model is as follows:

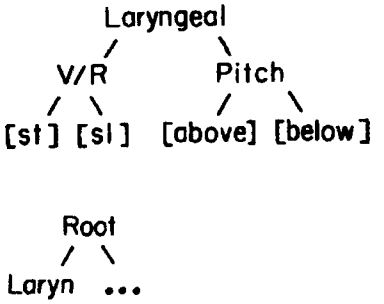

where the tonal structure is part of the feature geometry under a Root node. The V/R node represents both consonant voicing and tonal register. The Pitch node is specified for tone-bearing segments only.

3. The tone bearing unit is the moraic segment, or equivalently, the segment in the rime, whether it is a vowel or any consonant. A geminate has two Roots and may serve as two tone bearing units.

4. Contour segments do not exist. Their absence is attributed to a universal principle called the No Contour Principle (NCP), which is given as follows:

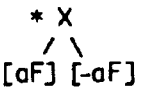

5. The tonal domain is the stress domain. Most syntax-phonology mismatches are due to lack of stress in some constituents.

1.2.3 Slavic Aspect and Its Implications

Peter Francis Kipka

Abstract

The goal of this thesis is to explore a new theory of verbal aspect. The theory is motivated primarily by a consideration of morphological and syntactico-semantic data from Slavic, but as a module of Universal Grammar it can be shown to be of much more general applicability. Thus Slavic aspect is contrasted with what can be found in a variety of other languages. The proposed system of representation is derivational in character: Final aspectual structures are built up by a small number of operations from lexical representations. The theory posits only two aspectual primitives (the point and the box, yielding perfectivity and imperfectivity in Slavic in a direct fashion).

Chapter 1 begins with an overview of much of the relevant data from the Slavic language Polish. Morphological and syntactico-semantic reflexes of aspect are identified and correlated. This leads directly to a formulation of the theory. The workings of the latter are demonstrated with respect to Polish verbs of motion. Its applicability to other languages (including English) is also discussed; some of the key factors contributing to language differences are the different means of lexical underspecification of aspectual structures.

Chapter 2 examines further data from Slavic. It is shown how double-aspect phenomena, inherent perfectivity, and habituals can be construed as providing support for a theory of the type envisaged here. The proposed theory (its primitives, operations, and conditions) is summarized in this chapter.

Chapter 3 is an exploration of the connection between aspect and prepositional notions. Core prepositions (or their equivalents) are taken to be interaction-denoting categories, a view that is contrasted with locationist hypotheses. Some aspectual consequences of this view are developed.

Finally, Chapter 4 continues the study of extra-Slavic and prima facie extra-aspectural implications of the theory here proposed. The dative alternation in English is examined, as are the English locative alternation, Georgian medial verbs, and restrictions on English 're-' prefixation. Light is shed on these phenomena, which at the same time provide empirical support for such theoretical devices as aspectual zerohood, box-layering, and lexical underspecification.

1.2.4 Conditions on X^0-Movement

Yafei Li

Abstract

X^0-movement is subject not only to the Empty Category Principle (ECP), as is widely accepted by now, but also to such principles as Binding Condition C (BCC) and the Subjacency Condition (SC). This multiprinciple constraining on X^0-movement further supports the similarity between it and XP-movement, which is also constrained by all these principles of the Universal Grammar. Empirically, it enables us not only to explain certain data not explained in a theory based solely on the ECP, but also to provide a unified analysis to such diverse phenomena as verb-incorporation (VI), clitic-climbing (CC), and predicate-clefing (PC).

Theoretical background is laid out in Chapter 1, in which the notion of variables is modified to cover X^0-traces resulting from moving a lexical head to a functional head. This, in turn, makes such an X^0-trace fall into the domain of BCC. In Chapter 2, it is shown that since cross-linguistically only a small set of verbs can trigger VI, a problem arises if X^0-movement is constrained only by the ECP, but can be readily explained by BCC plus the modified definition of variables. The environments in which CC takes place constitute a highly limited superset of those for VI. Chapter 3 argues that the similar requirements of the two phenomena on their structural environments results from BCC, while the difference derives from applying the SC and intermediate trace deletion in CC but not in VI. Chapter 4 studies PC, which requires an even looser restriction on the environments. Again, BCC and SC play crucial roles in determining when PC is possible, with the looser constraint attributed to the presence of a resumptive verb filling the D-structure position of the clefted one.

1.2.5 The A/A-bar Distinction and Movement Theory

Anoop Kumar Mahajan

Abstract

This thesis argues for a reformulation of the A/A-bar distinction in the theory of syntax. In the first part of this thesis, it is shown that this reformulation is forced by both theoretical considerations raised by VP internal subject theories and also certain empirical considerations relating to scrambling operations in Hindi. Evidence for the reformulation includes locality constraints on movement, weak crossover phenomena, reconstruction effects and binding properties associated with movement. This evidence also leads to a new approach to the study of scrambling phenomena. It is suggested that scrambling operations that move NPs may belong to two different kinds of syntactic operations—an operation of a functional projection internal to IP (with properties similar to a rule lie Passive) and an operation that adjoins the scrambled NP to a maximal projection (with properties similar to a rule like QR). The approach developed here yields a framework that seems to be promising for the study of variation found with respect to scrambling phenomena in natural languages.

The second part of this thesis argues that a language that does not have overt wh-movement at s-structure may not have wh-movement to SPEC CP at LF either. It is argued that in a language like Hindi, the wh-phrases simply undergo QR at LF. This operation adjoins a wh-phrase to the nearest IP. We show that this approach yields a number of consequences that are desirable in Hindi, a language that at first glance seems to be mixed between a language with overt wh-movement in syntax as well as wh-in-situ. We discuss some aspects of wide scope quantification in Hindi and some other languages and show that the absence of sh-movemnet ot SPEC CP at LF yields certain effects that would be surprising under the approaches that permit wh-movement to SPEC CP at LF.

1.2.6 Structure and Stress in the Phonology of Russian

Janis Leanne Melvold

Abstract

This thesis investigates the interaction between phonology and morphology in the stress system of Russian. Russian has an accent-based stress system, in which morphemes are characterized by two accentural properties: [±accented, ±dominant] Dominant morphemes trigger deaccentuation of the stem to which they attach.

Works surface with one stress, regardless of whether they contain zero or several lexically accented morphemes. I show that the stress rule in Russian applies cyclically, assigning stress to the leftmost accented vowel. Words with an accented root have stress fixed on the root. In the inflectional paradigm of work with unaccented roots, stress alternated between the initial and final vowels, depending on the accentural property of the inflectional suffix. I refer to this as *mobile* stress.

In Chapter 1, I observe an important correlation between stress and the derivational status of words. The generalization is the following: mobile stress occurs only in nonderived word or words derived from a nonsyllabic derivational suffix. To account for this fact, I show that it is crucial to assume not only that the stress rule is cyclic, but that all suffixes are cyclic. My analysis poses a challenge to theories which argue that morphemes which delete previously assigned metrical structure are necessarily cyclic while thoses which preserve previously assigned structure are noncyclic.

I adopt the framework of autosegmental phonology, whereby segmental, syllabification, and metrical processes operate on independent planes linked to a series of timing slots. Since vowels are the only stressable elements in Russian, they are the only elements represented on the stress plane. This allows us to explain the fact that a nonsyllabic morpheme which triggers a cyclic rule on the segmental plane fails to trigger the cyclic stress rule, which operates on the stress plane.

In Chapter 2, I introduce a class of apparent counterexamples to the claim that mobile stress can only occur in words derived from a nonsyllabic suffix. All of the problematic cases involve morphemes which exhibit vowel-zero alternations. I argue that these morphemes contain abstract vowels which consist of a floating feature matrix. Furthermore, I present both segmental and metrical

evidence to show that there are three distinct abstract vowels in Russian.

Chapter 3 addresses certain complexities in the adjectival system, which involve rules of post-accentuation and retraction.

Verbs exhibit stress alternations not found among other lexical categories. These alternations result from vowel sequences which are unique to derived verb stems. In Chapter Four, I show that stress assignment in these verbs involves a complex interaction between the stress rule, syllabification, and vowel truncation rules.

The thesis thus provides strong evidence for current theories of abstract elements in phonology and suggests a different view of cyclicity than the one recently proposed by Halle and Vergnaud (1987) and Halle and Kenstowicz (1989). These authors have argued that only the dominant (stress-deleting) morphemes are cyclic. This thesis shows that both dominant and nondominant morphemes consitute cyclic domains, but the structural properties of a morpheme may prevent application of a cyclic rule on a particular plane.

1.2.7 Issues in the Phonology of Prominence

Scott Meredith

Abstract

A theory of the interaction of phonology and phonetics in the prosodic domains of fundamental frequency, duration, and intensity is developed. Metrical constituent structure in the framework of Halle and Vergnaud 1987 is shown to be the fundamental representation of information of these prosodic domains, integrating phonological categories of tone and syllable weight with phonetic parameters of pitch, duration, and intensity.

The theory is illustrated by reference to three detailed case studies in the prosody of Tibetan, Beijing Mandarin Chinese, and English. For Tibetan, it is shown that the status of syllable nuclei in abstract metrical structure correlates with complexity of surface tonal realization. For Beijing Mandarin Chinese, it is shown that abstract metrical structure describing the location of stress is partially dependent on lexical tone quality of syllables. For English, it is argued that tonological primitives are not interposed between abstract metrical structure and surface fundamental frequency generation.

1.2.8 Negation in Syntax: On the Nature of Functional Categories and Projections

Miren Itziar Laka Mugarza

The central concern of this work is the syntactic nature of negation in Universal Grammar, and its relation to other functional elements in the Syntax.

The study argues that negation is not a syntactic category on its own; rather, it is one of the values of a more abstract syntactic category, nate Σ, which includes other sentence operators, such as affirmation and emphasis (Chapter 2). It is also argued that the syntactic feature (negation) surfaces in other syntactic categories besides Σ. In particular, the existence of (N) (negative). Complementizers is defended; this accounts for a range of phenomena in various languages: across-the-clause licensing of Negative Polarity Items in English, the distribution of the -nik complementizer in Basque, and the nature of Dubitative Subjunctive in Romance (Chapter 3).

Chapter 1 argues for the existence of a universal requirement that inflectional heads such as negation (Σ) must be c-commanded by the syntactic head Tense at S-structure. Assuming this requirement, a unified account is provided for apparently unrelated phenomena induced by negation in English and Basque.

Chapter 2 alsc presents an account of the phenomenon of "double negation" in Romance, in terms of the category Σ and its projection ΣP. It is argued that preverbal instance of the elements that induce "double negation," such as nadie, nada ningun etc., involve movement of the item in question to the specifier of ΣP, which is headed by a phonologically non-overt negative element. Also, "yes" and "no" answers are discussed in relation to the Σ Projection. It is argued that such answers make crucial use of this syntactic category, and parametric differences between the three languages under study (English, Spanish and Basque) are considered in support of the hypothesis.

The structure of Inflection in Spanish is considered in Chapter 3. The nature of Subjunctive and its relation to Negation and Imperative Mood is discussed. A proposal is made concerning the inflectional structure of Spanish, this proposal is shown to generate exhaustively the entire verbal paradigm of this language, and it predicts a number of language-particular properties of Spanish.

Appendices

Appendix A. RLE Publications and Papers Presented

The first section of this bibliography includes papers and talks presented by RLE faculty, staff and students during 1990 and is in alphabetical order by conference name. Reprints of these papers may be obtained by contacting the authors directly.

Section 2 includes an alphabetical listing by author of journal articles that were published, accepted or submitted for publication. Book chapters by RLE authors are listed in Section 3. Section 4 of this bibliography lists RLE general publications and technical reports, and Section 5 is a list of RLE theses submitted during 1990. Section 6 contains miscellaneous publications.

A.1 Meeting Papers

A.1.1 Papers Presented

Acoustical Society of America Meeting, College Park, Pennsylvania, May 20-25, 1990.

Huffman, M.K. "An Acoustic Study of the Timing of Contextual Nasalization in English."

Perkell, J.S., and M.L. Matthies. "Timing of Upper Lip Protrusion Gestures for the Vowel /u/."

Rabinowitz, W.M., D.R. Henderson, C.M. Reed, L.A. Delhorne, and N.I. Durlach. "Continuing Evaluation of a Synthetic Tadoma System."

Rankovic, C.M., and P.M. Zurek. "Rollover with High-Frequency Emphasis."

Ravicz, M.E., J.J. Rosowski, and H.F. Voigt. "Acoustic Impedance Measurements in the Gerbil Ear."

Zurek, P.M., and C.M. Rankovic. "Potential Benefits of Varying the Frequency-Gain Characteristic for Speech Reception in Noise."

Acoustical Society of America, 120th Meeting, San Diego, California, November 26-30, 1990.

Huffman, M.K. "The Role of F1 Amplitude in Producing Nasal Percepts."

Advanced Heterostructure Transistors, Kailua-Kona, Hawaii, December 3-8, 1990.

Smith, H.I., K. Ismail, and D.A. Antoniadis. "Investigations of Field-Effect-Controlled Mesoscopic Structures Fabricated with X-ray Nanolithography."

AIRSAR Workshop 1990 at the Jet Propulsion Laboratory, Pasadena, California, June 7, 1990.

Yueh, S.H., J.A. Kong, and R.T. Shin. "Calibration of Polarimetric Radars Using In-Scene Reflectors."

American Chemical Society Meeting, Washington, D.C., August 1990.

Ceyer, S.T. "Collision Induced Absorption of H into Ni(111)."

American Geophysical Union, Fall Meeting, San Francisco, California, December 3-7, 1990.

Ram, A.K., and A. Bers. "Space-Time Analysis of Electromagnetic Instabilities With Application to Auroral Kilometric Radiation."

American Physical Society Division of Plasma Physics, 32nd Annual Meeting, Cincinnati, Ohio, November 12-16, 1990.

Basu, B., and B. Coppi. "Plasma Collective Modes Driven by Velocity Gradients."

Bers, A., V. Fuchs, and C. Chow. "Single-Pass Absorption in Ion-Cyclotron Heating" (poster session).

Betti, R., J.U. Brackbill, B. Coppi, and J.P. Freidberg. "Nonlinear Ballooning Modes."

Chow, C., A.K. Ram, and A. Bers. "Spatio-Temporal Chaos and Quasiperiodicity in the Nonlinear Three Wave Interaction" (poster session).

Conde, M.E., G. Bekefi, and J.S. Wurtele. "The MIT 35 GHz Free Electron Laser Amplifier."

Coppi, B. "The Isotopic Effect on Plasma Confinement."

Coppi, B. "The Ignitor Ultimo Experiment."

Coppi, B., and F. Pegoraro. "Current Density and Energy Transport in High Temperature Plasmas."

Coppi, A.C., and B. Coppi. "Excitation of Macroscopic Plasma Modes Under Fusion Burn Conditions."

Coppi, B., R.C. Englade, M. Nassi, F. Pegoraro, L.E. Sugiyama. "Current Density Transport, Confinement and Fusion Burn Conditions."

Englade, R., P.T. Bonoli, M. Porkolab, and A. Kritz. "Simulations of Electron Cyclotron Heating in CIT with a Combined Code."

Englade, R., and B. Coppi. "Anomalous Thermal Transport and Plasma Collective Modes."

Kupfer, K., A. Bers, and A.K. Ram. "Stochastic Electron Transport Induced by Lower-Hybrid Current Drive Wave Fields" (poster session).

Migliuolo, S. "Resistive Internal Modes in High Temperature Plasmas."

Nassi, M., L.E. Sugiyama, S. Jardin, and N. Pomphrey. "Free Boundary Simulation of Ignition in a High Field Tokamak."

Ram, A.K., C. Chow, and A. Bers. "Bandwidth of Scattered Radiation in Laser-Plasma Interactions" (poster session).

Squire, J.P., M. Porkolab, S.C. Luckhardt, J. Colborn, and J. Villasenor. "Magnetic Fluctuation and Hard X-ray Measurements in High Poloidal Beta Plasma Equilibria on Versator II."

Sugiyama, L.E., and B. Coppi. "Thermal Transport Coefficient for Well-Confined Ohmic Plasmas."

Sugiyama, L.E., and M. Nassi. "Free Boundary Simulation of Current Ramp in a High Field Tokamak."

American Physical Society Meeting, Anaheim, California, March 12-16, 1990.

Broekaert, T.P.E., P.F. Bagwell, T.P. Orlando, and C.G. Fonstad. "Resonant Tunneling Diodes and Transistors with One, Two, or Three Dimensional Emitter."

Marko, J.F. "Density Functional Theory of Phase Transitions in Fluids of Anisotropic Particles."

Ranganathan, R., J. Kaminsky, B.D. McCombe, K. Elcess, and C.G. Fonstad. "Free Electron Laser Studies of the Saturation of Cyclotron Resonance in a <111>-InGaAs/GaAs Strained Layer Superlattice."

Rappe, A.M., K.M. Rabe, E. Kaxiras, and J.D. Joannopoulos. "Optimized Pseudopotentials."

Walrod, D.B., S.Y. Auyang, P.A. Wolff, and W. Tsang. "Enhancement of Optical Nonlinearities Due to Band Nonparabolicity in AlInSb/InSb Superlattices."

American Physical Society, Spring Meeting, Washington, D.C., April 16-19, 1990.

DiRienzo, A.C., G. Bekefi, and J.S. Wurtele. "The M.I.T. 35 GHz Cyclotron Autoresonance Maser (CARM) Amplifier."

Jerby, E., J.S. Wurtele, and G. Bekefi. "Observations of Periodic Bursts of Emission From a Free Electron Laser Oscillator."

American Speech, Language and Hearing Association, Seattle, Washington, November 15-20, 1990.

Delhorne, L.A., J.M. Besing, C.M. Reed, and N.I. Durlach. "Tactual Cued Speech as a Supplement to Speechreading."

Anomalous Absorption Conference, 20th Annual, Traverse City, Michigan, July 9-13, 1990.

Chow, C.C., A Bers, and A.K. Ram. "Bandwidth of Scattered Radiation in Laser-Plasma Interactions."

Applications of Superconductivity Conference, Snowmass, Colorado, September 24-26, 1990.

Face, D.W., S.D. Brorson, A. Kazeroonian, T.K. Cheng, G.L. Doll, M.S. Dresselhaus, G. Dresselhaus, E.P. Ippen, T. Venkatesan, X.D. Wu, and A. Inam. "Femtosecond Thermomodulation Studies of Low and High-Tc Superconductors."

Association for Research in Otolaryngology, 14th Midwinter Meeting, St. Petersburg, Florida, February 4-8, 1990.

Davis, R.L. "Conditioning Lesions Promote Primary-Auditory Neurite Regeneration in Vitro."

Furst, M., J.C. Gardner, R.A. Levine, B. Fullerton, and P. Cuneo. "Localizing the Brainstem Auditory Pathway in Human Magnetic Resonance Images: An Algorithm Matching MR Scans to a Computerized Anatomic Atlas."

Association for Research in Vision and Ophthalmology, Annual Meeting, Sarasota, Florida, April 29 - May 5, 1990.

Huang, D., C. Lin, J. Wang, J.G. Fujimoto, and C.A. Puliafito. "High Resolution Measurement of Corneal and Anterior Eye Structure Using Optical Coherence Domain Reflectometry."

Chemistry at Surfaces Symposium, University of California, Irvine, California, October 1990.

Cever, S.T. "Adsorbate Synthesis with Molecular Beams."

Cold Fusion Conference, First Annual, Salt Lake City, Utah, March 28-31, 1990.

Hagelstein, P.L. "Status of Coherent Fusion Theory."

Conference on Lasers and Electro-Optics/International Quantum Electronics Conference, Anaheim, California, May 21-25, 1990.

Basu, S., and P.L. Hagelstein. "Unstable Resonators for XUV Lasers."

Basu, S., M.H. Muendel, J.P. Braud, D. Tauber, S. Kaushik, and P.L. Hagelstein. "Development of a Table-Top XUV Laser at 196Å in Ni-Like MO."

Birngruber, R., Y. Hefetz, T. Deutsch, C.A. Puliafito, and J.G. Fujimoto. "Single-Picosecond Pulse Photodisruption in Ocular Structures."

Braud, J.P. "Whisper-Gallery Mirrors as Unstable Resonators for Short-Wavelength Lasers."

Corcoran, C., and R.H. Rediker. "Operation of Five Discrete Diode Lasers as a Coherent Ensemble by Fiber-Coupling into an External Cavity."

DelCorno, A., G. Gabetta, G.C. Reali, V. Kubecek, and J. Marek. "Shortening of Pulses from an Active-Passive Mode-locked Nd:YAG Laser Through Two-photon Absorption in GaAs" (poster session).

Fujimoto, J.G. "Femtosecond Lasers and Ultrafast Measurement Techniques" (short course).

Goodberlet, J., J. Jacobson, J.G. Fujimoto, P.A. Schulz, and T.Y. Fan. "Self-starting Additive Pulse Mode-locking of a Diode Pumped Nd:YAG Laser."

Goodberlet, J., J. Wang, P. Schulz, and J.G. Fujimoto. "Self-Starting Additive Pulse Mode-Locking Characterization with a $Ti:Al_2O_3$ Laser."

Hall, K.L., Y. Lai, E.P. Ippen, and G. Eisenstein. "Short Pulse Gain Saturation in a 1.5 μm Multiple Quantum Well Optical Amplifier."

Haus, H.A., and Y. Lai. "Quantization of Solitons" (invited paper).

Helmerson, K., M. Xiao, and D. Pritchard. "Radiative Decay of Densely Confined Atoms."

Huang, D., J. Wang, J.G. Fujimoto, C. Lin, and C.A. Puliafito. "Measurement of Intraocular Structure by Optical Coherence Domain Reflectometry."

Huxley, J.M., L.Y. Liu, E.P. Ippen, and H.A. Haus. "Self-Starting Additive Pulse Mode-Locking of 1.06- and 1.32-μm Nd:YAG Lasers."

Kaushik, S., S. Basu, and P. Hagelstein. "Design Studies of the MIT 194Å Ni-Like MO Laser."

Moores, J.D., K. Bergman, H.A. Haus, and E.P. Ippen. "Optical Switching Using Fiber Ring Reflectors."

Pang, L.Y., E.S. Kintzer, and J.G. Fujimoto. "High Power Two-stage Injection Locking of Laser Diode Arrays."

Phillips, M.R., E.P. Ippen, H.A. Haus, and J.C. Vlcek. "Subpicosecond Optical Nonlinearities Below the Band-Edge of InGaAs/InAlAs Quantum Wells."

Shapiro, J.H., S.R. Shepard, and N.C. Wong. "Fourier Theory, Uncertainty Relations, and Quantum Phase."

Wong, N.C., K.W. Leong, and J.H. Shapiro. "Nonclassical Intensity Correlation from a Type-I Phase-Matched Optical Parametric Oscillator."

Conference on Neural Networks for Computing, Snowbird, Utah, April 1990.

Wyatt, J.L., Jr., D. Standley, and B. Horn. "Local Computation of Useful Global Quantities Using Linear Resistive-Grid Networks" (poster session).

Consortium for Superconducting Electronics Signal Distribution and Conditioning Networks, AT&T Bell Laboratories, Holmdel, New Jersey, October 28, 1990.

Sheen, D.M., S.M. Ali, D.E. Oates, R.S. Withers, and J.A. Kong. "Current Distribution in Superconducting Strip Transmission Lines."

Defense Advanced Research Projects Agency (DARPA) Microsystems and Prototyping

Meeting, Semiannual, University of North Carolina, Chapel Hill, North Carolina, October 3, 1990.

Devadas, S. "Synthesis for Testability."

Design Automation Conference, Orlando, Florida, June 24-28, 1990.

McCormick, S.P., and J. Allen. "Waveform Moment Methods for Improved Interconnection Analysis."

Device Research Conference, 48th Annual, Santa Barbara, California, June 25-27, 1990.

Eugster, C.C., J.A. del Alamo, and M.J. Rooks. "Ballistic Transport in a Novel Grated Quantum Wire."

Kuo, T.Y., K.W. Goossen, J.E. Cunningham, W.Y. Jan, C.G. Fonstad, and F. Ren. "Monolayer Be d-doped Heterostructure Bipolar Transistor Fabricated Using Doping Selective Base Contact."

Digital Signal Processing Workshop, Fourth, Mohawk Mountain House, New Paltz, New York, September 16-19, 1990.

Alkhairy, A., K. Christian, and J. Lim. "A New Algorithm for Optimal Filter Design with Arbitrary Phase."

Wornell, G.W., and A.V. Oppenheim. "Fractal Signal Modeling and Processing Using Wavelets."

Division of Atomic, Molecular, and Optical Physics Conference, Monterey, California, May 1990.

Pritchard, D.E. "Atom Optics."

EESof Users Group Meeting, Dallas, Texas, May 8, 1990.

Meskoob, B., J.C. Vlcek, H. Sato, S. Prasad, G. Fonstad, and M-K. Vai. "Characterization of InGaAs/InAlAs/InP Emitter-Down Heterojunction Bipolar Transistors at Microwave Frequencies."

Electrical Engineering Department Collegium, Minneapolis, Minnesota, October 18, 1990.

Melngailis, J. "Focused Ion Beam Microfabrication."

Electron, Ion and Photon Beam Symposium, San Antonio, Texas, May 29 - June 1, 1990.

Murguia, J.E., C.R. Musil, M.I. Shepard, H. Lezec, D.A. Antoniadis, and J. Melngailis. "Merging Focused Ion Beam Patterning and Optical Lithography in Device and Circuit Fabrication."

Tao, T., J-S. Ro, J. Melngailis, Z. Xue, and H.D. Kaesz. "Focused Ion Beam Induced Deposition of Platinum."

Electronic Materials Conference, Santa Barbara, California, June 27-29, 1990.

Vlcek, J.C., and C.G. Fonstad. "Precise Control of Time-dependent MBE Flux Profiles - Application to InGaAlAs/InP Alloys."

European Materials Research Society Meeting, Strasbourg, France, May 1990.

Kolodziejski, L.A. "Semimagnetic Semiconductor Superlattices: MBE Growth and Characterization."

European Research Conference on Quantum Optics, Davos, Switzerland, October 1-5, 1990.

Kleppner, D. "Eigenstates of Chaos."

Pritchard, D.E. "Atom Interferometry."

Evolutionary Biology of Hearing Symposium, Sarasota, Florida, May 19-24, 1990.

Rosowski, J.J., and A. Graybeal. "Hearing in Transitional Mammals: Predictions from the Anatomy and Hearing Capabilities of Extant Terrestial Vertebrates."

Gordon Conference on the Dynamics of Simple Systems in Chemistry and Physics, Proctor Academy, New Hampshire, August 15, 1990.

Kleppner, D. "Eigenstates of Chaos."

Gordon Conference on Organometallic Chemistry, Wolfeboro, New Hampshire, June 1990.

Ceyer, S.T. "The Activation and Reactions of CH_4 on Ni(111)."

Hawaii Conference on System Sciences, 23rd, Kona, Hawaii, January 2-7, 1990.

Devadas, S., A.R. Newton. "Exact Algorithms for Output Encoding, State Assignment and Four- Level Boolean Minimization."

Human-Machine Interfaces for Teleoperators and Virtual Environments, Meeting, Santa Barbara, California, March 4-9, 1990.

Pang, X.D., H.Z. Tan, and N.I. Durlach. "Manual Discrimination of Force."

Srinivasan, M.A., and R.H. LaMotte. "Tactual Interfaces for Telepresence: The Human Perceiver" (invited talk).

Srinivasan, M.A., and R.H. LaMotte. "Tactile Discrimination and Representation of Texture, Shape, and Softness" (poster presentation).

IEEE Communications Workshop, 20th, Ojai, California, June 23-28, 1990.

Lim, J.S. "Advanced Television Systems."

IEEE International Conference on Acoustics, Speech and Signal Processing, 1990, Albuquerque, New Mexico, April 3-6, 1990.

Beckmann, P.E., and B.R. Musicus "Fault-Tolerant Round Robin A/D Converter System."

Brandstein, M.S., P.A. Monta, J.C. Hardwick, and J.S. Lim "A Real-Time Implementation of the Improved MBE Speech Coder."

Tabei, M., and M. Ueda. "Backprojection with Fourier Series Expansion and FFT."

Zurek, P.M., J.E. Greenberg, and P.M. Peterson. "Sensitivity to Design Parameters in an Adaptive-Beamforming Hearing Aid."

IEEE International Conference on Plasma Science, 1990, Oakland, California, May 21-23, 1990.

Conde, M.E., G. Bekefi, and J.S. Wurtele. "A 35 GHz Free Electron Laser Amplifier Operating with High Guide Magnetic Field."

IEEE International Electronics Manufacturing Technology Symposium, Washington, D.C., October 2-3, 1990.

McIlrath, M. "CAFE - The MIT Computer Aided Fabrication Environment."

IEEE International Symposium on Circuits and Systems, New Orleans, Louisiana, May 1-3, 1990.

Devadas, S., and K. Keutzer. "Validatable Non-robust Delay-Fault Testable Circuits Via Logic Synthesis."

Neto, L.S., J. White, and L. Vidigal. "On Exponential Fitting for Circuit Simulation."

IEEE United States Activities Board Workshop, Washington, D.C., November 12-13, 1990.

Lim, J.S "Progress at MIT's Advanced Television Research Program."

IEEE Workshop on Micrometer and Submicrometer Lithography, New Orleans, Louisiana, January 29 - February 2, 1990.

Melngailis, J. "Focused Ion Beam Lithography and Implantation."

International Cochlear Implant Symposium, Second, Iowa City, Iowa, June 3-9, 1990.

Eddington, D.K. "An Electroanatomical Model of Intracochlear Electrical Stimulation."

Eddington, D.K. "Psychophysical Correlates of Speech Reception in Subjects Using Multichannel Cochlear Implants."

Rabinowitz, W.M., and D.K. Eddington. "Effects of Channel-To-Electrode Mappings with the Symbion Cochlear Prosthesis."

International Conference of Atomic Physics, Ann Arbor, Michigan, July 1990.

Pritchard, D.E. "Atom Optics."

International Conference on Computer-Aided Design, Santa Clara, California, November 11-15, 1990.

Silveira, L.M., A. Lumsdaine, and J.K. White. "Parallel Simulation Algorithms for Grid-Based Analog Signal Processors."

International Conference on Consumer Electronics, Rosemont, Illinois, June 3-7, 1990.

Lim, J.S. "Advanced Television Systems."

International Conference on Directions in Electromagnetic Wave Modeling, New York, New York, October 22-24, 1990.

Nghiem, S.V., J.A. Kong, and T.Le Toan. "Electromagnetic Wave Modeling for Remote Sensing."

International Conference on Lasers 1990, San Diego, California, December 10-12, 1990.

Hung, T-Y., and P.L. Hagelstein. "Whisper Gallery Mirrors Reflectivities from 100Å to 500Å."

Muendel, M.H., and P.L. Hagelstein. "Short-pulse Glass Slab Amplifier."

International Conference on Metallorganic Vapor Phase Epitaxy, Fifth, Aachen, Germany, June 18-21, 1990.

Karam, N.H., A. Mastrovita, V. Haven, K. Ismail, S. Pennycock, and H.I. Smith. "Patterning and Overgrowth of Nanostructure Quantum Well Wire Arrays."

International Conference on Molecular Beam Epitaxy, Sixth, LaJolla, California, August 17-31, 1990.

Bahl, S.R., W.J. Azzam, and J.A. del Alamo. "Orientation Dependence of Mismatched InAlAs/InGaAs HFETs."

International Conference on the Physics of Semiconductors, 20th, Thessaloniki, Greece, August 6-10, 1990.

Liu, C.T., D.C. Tsui, M. Shayegan, K. Ismail, D.A. Antoniadis, and H.I. Smith. "Observation of Landau Level Splitting in Two-Dimensional Lateral Surface Superlattices."

Toriumi, A., K. Ismail, M. Burkhardt, D.A. Antoniadis, and H.I. Smith. "Resonant Magneto-Conductance in a Two-Dimensional Lateral-Surface-Superlattice."

International Conference on Plasma Physics and Controlled Nuclear Fusion Research, 13th, Washington, D.C., October 1-6, 1990.

Coppi, B. "The Isotopic Effect on Plasma Confinement."

Coppi, B., R.C. Englade, M. Nassi, F. Pegoraro, and L.E. Sugiyama. "Current Density Transport, Confinement and Fusion Burn Conditions."

International Conference on Solid State Devices and Materials, Sendai, Japan, August 23-26, 1990.

Kuo, T.Y., K.W. Goossen, J.E. Cunningham, C.G. Fonstad, F. Ren, and W. Jan. "Elimination of Emitter-Mesa Etching and Complete Planarization of Heterojunction Bipolar Transistors via Doping Selective Base Contact and Selective Hole Epitaxy."

International Geoscience and Remote Sensing Symposium, Tenth Annual, University of Maryland, College Park, Maryland, May 20-24, 1990.

Lim, H.H., S.H. Yueh, R.T. Shin, and J.A. Kong. "Correlation Function for a Random Collection of Discrete Scatterers."

Nghiem, S.V., J.A. Kong, and R.T. Shin. "Study of Polarimetric Response of Sea Ice With Layered Random Medium Model."

Yueh, S.H., J.A. Kong, and R.T. Shin. "Calibration of Polarimetric Radars Using In-Scene Reflectors."

Yueh, S.H., J.A. Kong, R.T. Shin, and H.A. Zebker. "Statistical Modelling for Polarimetric Remote Sensing of Earth Terrain."

International School on Physics of Semiconducting Compounds, Jaszowiec, Poland, April 1990.

Kolodziejski, L.A. "Modern Growth Technologies of Semimagnetic Semiconductors."

International Sherwood Theory Conference, Annual, Williamsburg, Virginia, April 22-25, 1990.

Coppi, B., and F. Pegoraro. "Symmetries and Global Transport Equations."

Kupfer, K., A. Bers, and A.K. Ram. "Guiding Center Stochasticity in a Tokamak."

Ram, A.K., and A. Bers. "Propagation of Ion-Bernstein Waves in Toroidal Plasmas."

Sugiyama, L.E., and M. Nassi. "Time Dependent Effects and the Current Ramp Phase in D-T Ignition."

International Symposium on Electron, Ion, and Photon Beams, 34th, San Antonia, Texas, May 29-June 1, 1990.

Moel, A., M.L. Schattenburg, J.M. Carter, and H.I. Smith. "A Compact, Low-Cost System for Sub-100 nm X-ray Lithography."

Schattenburg, M.L., K. Early, Y-C. Ku, W. Chu, M.I. Shepard, S-C. The, H.I. Smith, D.W. Peters, R.D. Frankel, D.R. Kelly, and J.P. Drumheller. "Fabrication and Testing of 0.1 μm-linewidth Microgap X-ray Masks."

International Test Conference, Washington, D.C., September 10-13, 1990.

Devadas, S., and K. Keutzer "Design of Integrated Circuits Fully Testable for Delay-Faults and Multifaults."

International X-ray Laser Conference, Second, University of York, York, England, September 17-21, 1990.

Hagelstein, P.L., S. Basu, M.H. Muendel, J.P. Braud, D. Tauber, S. Kaushik, J. Goodberlet, T-Y. Hung, and S. Maxon. "The MIT Short-Wavelength Laser Project: A Status Report."

Japan-U.S. Seminar on Focused Ion Beams and Applications, Second, Portland, Oregon, December 3-7, 1990.

Dubner, A.D., A. Wagner, J. Melngailis, and C.V. Thompson. "The Role of the Ion/Solid Interaction in Ion Beam Induced Deposition of Gold."

Hartney, M.A., D.C. Shaver, M.I. Shepard, J.S. Huh, and J. Melngailis. "Silylation Using Focused Ion Beam Lithography."

Lezec, H.J., C.R. Musil, J. Melngailis, L.J. Mahoney, and J.D. Woodhouse. "Dose Rate

Effects in Focused Ion Beam Implantation of Si into GaAs."

Murguia, J.E., M.I. Shepard, J. Melngailis, A.L. Lattes, and S.C. Munroe. "Increase in Silicon CCD Speed with Focused Ion Beam Implanted Channels."

JASON (July, August, September, October, November) Meeting, General Atomics Corporation, San Diego, California, July 19, 1990.

Wornell, G.W. "Wavelet-Based Representations in Fractal Signal Modeling."

Materials Research Society, Spring Meeting, San Francisco, California, April 17, 1990.

Floro, J.A., and C.V. Thompson. "Epitaxial Grain Growth and Orientation Metals Metastability in Heteroepitaxial Thin Films."

Materials Research Society, Fall Meeting, Boston, Massachusetts, November 26-December 1, 1990.

Liu, C.T., D.C. Tsui, M. Santos, M. Shayegan, K. Ismail, D.A. Antoniadis, and H.I. Smith. "Magnetoresistance of Two-Dimensional Electrons in a Two-Dimensional Lateral Surface Superlattice."

Mechanics and Biophysics of Hearing Meeting, University of Wisconsin, Madison, Wisconsin, June 24-29, 1990.

Guinan, J.J., Jr. "Changes in Stimulus Frequency Otoacoustic Emissions Produced by Two-Tone Suppression and Efferent Stimulation in Cats."

Molecular Beam Epitaxy Conference, Sixth International, San Diego, California, August 27-31, 1990.

Singer, R.A., and C.G. Fonstad. "MBE Growth of InGaAs and InAlAs on (111) B InP."

Vlcek, J.C., and C.G. Fonstad. "Precise Computer Control of the MBE Process - Application to Graded InGaAlAs/InP Alloys."

Molecular Beam Epitaxy Workshop, Fifth New England, Cambridge, Massachusetts, April 17, 1990.

Blanck, H. "Characterization of GaAs Grown Patterned Si-substrates for Optoelectronic Devices."

Vlcek, J.C. "Control of Compositional Grading and Abruptness in InGaAlAs Heteroepitaxy."

National Association of Broadcasters Meeting, Atlanta, Georgia, March 30 - April 4, 1990.

Lim, J.S. "Research on Advanced Television Systems at MIT."

NATO Advanced Research Workshop on Resonant Tunneling in Semiconductors: Physics and Applications, El Escorial, Spain, 1990.

Bagwell, P.F., T.P. Orlando, and A. Kumar. "Low-Dimensional Resonant Tunneling."

NATO Advanced Study Institute on Waveguide Optoelectronics, Glasgow, Scotland, August 3-11, 1990.

Fujimoto, J.G. "Femtosecond Techniques for the Characterization of Nonlinear and Linear Properties of Waveguide Devices and Studies of All Optical Switching."

Neural Networks for Computing, Meeting, Snowbird, Utah, April 3-6, 1990.

Wyatt, J., D. Standley, and B. Horn. "Local Computation of Useful Global Quantities Using Linear Resistive Grid Networks" (poster session).

Neutral-Atom Interferometry and DeBroglie Optics Workshop, Sante Fe, New Mexico, January 15-16, 1990.

Keith, D. "A Three Grating Atom Interferometer."

Pritchard, D.E. "Atom Diffraction and Atom Interferometers."

Nonlinear Optics '90: Materials, Phenomena and Devices, Kauai, Hawaii, July 16-20, 1990.

Shapiro, J.H., S.R. Shepard, and N.C. Wong. "Fourier Theory, Number-Ket Causality, and Rational Phase States."

NSF/CBMS Regional Conference on Wavelets, University of Lowell, Lowell, Massachusetts, June 11-15, 1990.

Wornell, G.W., and A.V. Oppenheim. "Wavelet-Based Representations for Fractal Modeling" (poster session).

OCEANS '90 Conference, Washington, D.C., September 24-26, 1990.

Melville, W.K., R.H. Stewart, J.A. Kong, W.C. Keller, D. Arnold, A.T. Jessup, and E. Lamarre. "Measurements of Sea-state Bias at Ku and C Bands."

Optical Society of America Topical Meeting on Ultrafast Phenomena, Monterey, California, May 14-17, 1990.

Brorson, S.D., A. Kazeroonian, J.S. Moodera, D.W. Face, T.K. Cheng, E.P. Ippen, M.S. Dresselhaus, G. Dresselhaus, G.L. Doll, T. Venkatesan, X.D. Wu, and A. Inam. "Femtosecond Thermomodulation Study of Conventional and High-Tc Superconductors."

Optical Society of America, Annual Meeting, Boston, Massachusetts, November 4-9, 1990.

Bergman, K., and H.A. Haus. "Squeezed Pulse Vacuum from Fiber-Ring Interferometer."

Goodberlet, J., J. Jacobson, G. Gabetta, P.A. Schulz, T.Y. Fan, and J.G. Fujimoto. "Ultrashort Pulse Generation with Additive Pulse Modelocking in Solid State Lasers."

Keith, D. "Two Particle Correlation Experiments with Massive Particles."

Kleppner, D. "Eigenstates of Chaos" (invited talk).

Kolodziejski, L.A. "Chemical Beam Epitaxy for Advanced Optoelectronic Devices."

Wong, N.C. "Optical Frequency Measurement and Synthesis Using Optical Parametric Oscillators."

Wong, N.C., K.W. Leong, and J.H. Shapiro. "Quantum Correlation and Absorption Spectroscopy in an Optical Parametric Oscillator."

Picture Coding Symposium, Cambridge, Massachusetts, March 25-27, 1990.

Picard, R.W. "A Staggered-DCT Decreases Perceived Blockiness."

Pritchard, D.E. "Atom Optics."

Semiconductor Research Corporation/Defense Advanced Research Projects Agency Computer-Integrated Manufacturing of Integrated Circuits Workshop, Fifth Annual, University of California Berkeley, Berkeley, California, August 15-16, 1990.

Troxel, D.E., and M.B. McIlrath. "The MIT Process Flow Representation - Application to Fabrication."

Society of Magnetic Resonance in Medicine, Ninth Annual Meeting, New York, 1990.

Gardner, J.C., M. Furst, R.A. Levine, B. Fullerton, and B.R. Rosen. "An Anatomic Atlas and Mapping Algorithm for Localizing the Brainstem Auditory Pathway on Magnetic Resonance Scans."

Society of Motion Picture and Television Engineers Technical Conference, 132nd, New York, New York, October 13-17, 1990.

Bace, M.M., and J.S. Lim. "A Receiver-Compatible System for Channel Noise Reduction."

Hajjahmad, I., and J.S. Lim. "Image Coding with Progressive Scanning as an Alternative to Interlaced Scanning."

Monta, P., and J.S. Lim. "Source Adaptive Processing for ATV System Design."

Society of Neuroscience, 20th Annual Meeting, St. Louis, Missouri, October 28-November 2, 1990.

Melcher, J.R., B.C. Fullerton, J.J. Guinan, Jr., N.Y.S. Kiang, and I.M. Knudson. "Cellular Generators of the Brainstem Auditory Evoked Potential in the Cat" (poster session).

Society of Photo-Optical Instrumentation Engineers (SPIE) Opto-Electronics Laser 1990 Conference, Los Angeles, California, January 14-19, 1990.

Anderson, K.K., M.J. LaGasse, H.A. Haus, and J.G. Fujimoto. "Femtosecond Studies of Nonlinear Optical Switching in GaAs Waveguides Using Time Domain Interferometry."

DiRienzo, A., and G. Bekefi. "The MIT 35 GHz Cyclotron Autoresonance Maser (CARM) Amplifier."

Hannon, S.M., and J.H. Shapiro. "Active-Passive Detection of Multipixel Targets."

SPIE International Society for Optical Engineering, San Diego, California, March 3-17, 1990.

LaGasse, M.J., K.K. Anderson, C.A. Wang, H.A. Haus, and J.G. Fujimoto. "Femtosecond Investigations of Optical Switching and $\chi^{(3)}$ in GaAs Waveguides."

SPIE International Symposium on Optical and Optoelectronic Applied Science and Engineering, San Diego, California, July 8-13, 1990.

Habashy, T.M., M. Moldoveanu, and J.A. Kong. "Inversion of Permittivity and Conductivity Profiles Employing Transverse-Magnetic Polarized Monochromatic Data."

Speech Research Symposium, Maritime Institute of Technology, Linthicum, Maryland, October 16-17, 1990.

Brandstein, M.S., P.A. Monta, J.C. Hardwick, and J.S. Lim. "A Real-Time Implementation of the Improved MBE Speech Coder."

Symposium on the Evolutionary Biology of Hearing, Sarasota, Florida, May 1990.

Rosowski, J.J. "Hearing in Transitional Mammals: Predictions from the Middle-Ear Anatomy and Hearing Capabilities of Extant Mammals" (talk).

Symposium on Nonlinear Fiber Pulse Processing, Grasmere, England, September 10-13, 1990.

Lai, Y., and H.A. Haus. "Quantum Theory of Solitons in Optical Fibers."

Symposium on Quantum Aspects of Nonlinear Systems, Essen, Germany, July 16-20, 1990.

Kleppner, D. "Eigenstates of Chaos."

Topical Meeting on Ultrafast Phenomena, Monterey, California, May 14-17, 1990.

Goodberlet, J., J. Jacobson, J. Wang, and J.G. Fujimoto. "Ultrashort Pulse Generation with Additive Pulse Modelocking in Solid State Lasers: Ti:Al_2O_3, Diode Pumped Nd:YAG and Nd:YLF."

Goodberlet, J., J. Jacobson, J. Wang, and P. Schulz. "Additive Pulse Mode-Locking in Ti:Al_2O_3 Diode Pumped Nd:YAG, and Nd:YLF."

Hou, A.S., R.S. Tucker, and E.P. Ippen. "Chirp in Actively Modelocked Diode Lasers."

Union of Radio Science International Commission F Meeting, Hyannis, Massachusetts, May 15-17, 1990.

Melville, W.K., J.A. Kong, R.H. Stewart, W.C. Keller, D. Arnold, A.T. Jessup, and E. Lamarre. "Measurements of Sea-State Bias at Ku and C Bands."

Nghiem, S.V., J.A. Kong, R.T. Shin, H.A. Yueh, and R.G. Onstott. "Theoretical Models and Experimental Measurements For Polarimetric Remote Sensing of Snow and Sea Ice."

Nghiem, S.V., J.A. Kong, and T. LeToan. "Application of Layered Random Medium Model to Polarimetric Remote Sensing of Vegetation."

Union of Radio Science National Meeting, Boulder, Colorado, January 3-5, 1990.

Han, H.C., J.A. Kong, T.M. Habashy, and M.D. Grossi. "Principles of VLF Antenna Array Design in Magnetized Plasmas."

United States-Japan Seminar on Quantum Electronic Manipulation of Atoms and Fields, Kyoto, Japan, September 3-7, 1990.

Shapiro, J.H. "Going Through a Quantum Phase."

US/USSR Symposium on the Physics of Optical Phenomena and Their Use as Probes of Matter, Fourth Binational, Irvine, California, January 22-26, 1990.

Fujimoto, J.G. "Femtosecond Photoemission Studies of Image Potential and Electron Dynamics in Metals."

Workshop on Chaos and Transport in Fluids and Plasmas, College Park, Maryland, April 26-27, 1990.

Kupfer, K., A. Bers, and A.K. Ram. "Guiding Center Stochasticity by Electrostatic Waves."

Workshop on Compound Semiconductor Materials and Devices, San Francisco, California, February 19-21, 1990.

Bahl, S.R., and J.A. del Alamo. "Strained InAlAs/n^+-InGaAs HFETs."

A.1.2 Papers To Be Presented

American Astronomical Society Meeting, 177th, Philadelphia, Pennsylvania, January 13-17, 1991.

Markert, T., M.L. Schattenburg, T. Isobe, J. Bauer, C. Canizares, J. O'Connor, J. Porter, and H.I. Smith. "Investigations of Materials for Ultra-Thin Window X-ray Detectors."

American Control Conference, Boston, Massachusetts, June 1991.

Annaswamy, A.M., and M.A. Srinivasan. "Adaptive Control for Grasping and Manipulation of Compliant Objects with Compliant Fingerpads."

American Physical Society, General Meeting, Cincinnati, Ohio, March 18-22, 1991.

Alerhand, O.L. "Equilibrium Properties of Steps on Si(100)." *Bull. Am. Phys.* 36(3):587 (1991).

Bagwell, P.F., and A. Kumar. "Evolution of the Quantized Ballistic Conductance with Increasing Disorder in Narrow Wire Arrays."

Berker, A.N. "Quenched Fluctuation Induced Second-Order Phase Transitions." *Bull. Am. Phys.* 36(3):439 (1991).

Liu, C.T., S. Luryi, and P.A. Garbinski. "Quench of Hot-Electron Real-Space-Transfer by Electronic Screening."

Park, S.L., P.F. Bagwell, A. Yen, D.A. Antoniadis, H.I. Smith, T.P. Orlando, and M.A. Kastner. "Magnetotransport in Multiple Narrow Si Inversion Channels Opened Electrostatically Into a Two-Dimensional Electron Gas."

Rittenhouse, G., H.I. Smith, J.M. Graybeal, B. Meyerson. "A Novel Structure for a Three-Terminal Superconducting Resonant Tunneling Device."

Zhao, Y., D.C. Tsui, S.J. Allen, K. Ismail, H.I. Smith, and D.A. Antoniadis. "Spectroscopy of 2-Deg in a Grid Gate Patterned Heterostructure."

American Vacuum Society Meeting, Seattle, Washington, Fall 1991.

Kolodziejski, L.A. "Chemical Beam Epitaxy of II-VI/III-V Heterostructures."

Association for Research on Otolaryngology, 15th Midwinter Meeting, St. Petersburg, Florida, February 1991.

Delgutte, B. "Power-law Behavior of the Discharge Rates of Auditory-nerve Fibers at Low Sound Levels."

Design Automation Conference, 28th, San Francisco, California, June 1991.

Cheng, K-T., S. Devadas, and K. Keutzer. "Robust Delay-Fault Test Generation and Synethesis for Testability Under a Standard Scan Methodology."

Devadas, S., K. Keutzer, and S. Malik. "A Synthesis-Based Approach to Test Generation and Compaction for Multifaults."

IEEE International Symposium on Circuits and Systems, Singapore, June 1991.

Bryan, M.J., S. Devadas, and K. Keutzer. "Analysis and Design of Regular Structures for Robust Dynamic Fault Testability."

Ghosh, A., and S. Devadas. "Implicit Depth-First Transversal of Sequential Machines."

International Conference on Acoustics, Speech, and Signal Processing, Toronto, Ontario, Canada, May 14-17, 1991.

Covell, M.M., and J. Richardson. "A New, Efficient Structure for the Short-Time Fourier Transform, with an Application in Code-Division Sonar Imaging."

Preisig, J.C. "A Robust High Resolution Array Processing Algorithm Based Upon Minmax Criteria."

Tabei, M., B.R. Musicus, and M. Ueda. "A Maximum Likelihood Estimator for Frequency and Decay Rate."

Wornell, G.W., and A.V. Oppenheim. "Communication Over Fractal Channels."

International Conference on Computer Design: VLSI in Computers and Processors, Cambridge, Massachusetts, October 1991.

Asher, P., S. Devadas, and A. Ghosh. "Boolean Satisfiability and Equivalence Checking Using General Binary Decision Diagrams."

Devadas, S., K. Keutzer, and A.S. Krishnakumar. "Design Verification and Reachability Analysis Using Algebraic Manipulation."

International Symposium on Electron, Ion and Photon Beams, 35th, Seattle, Washington, May 28-31, 1991.

Anderson, E.H., V. Bögli, M. Schattenburg, D. Kern, and H.I. Smith. "Metrology of Electron Beam Lithography Systems Using Holographically Produced Reference Samples."

Chu, W., S.A. Rishton, M.L. Schattenburg, D.P. Kern, and H.I. Smith. "Fabrication of 50 nm Line and Space X-ray Masks in Thick Au Using a 50 keV Electron Beam."

Ku, Y.C., L-P. Ng, R. Carpenter, K. Lu, and H.I. Smith. "In Situ Stress Monitoring and Deposition of Zero Stress W Absorber for X-ray Masks."

Moel, A., W. Chu, K. Early, Y.C. Ku, E.E. Moon, M.L. Schattenburg, J.M. Bauer, F. Tsai, F.W. Griffith, L.E. Haas, and H.I. Smith. "Fabrication and Characterization of High-Flatness Mesa-Etched Silicon Nitride X-ray Masks."

Schattenburg, M.L., K. Li, R.T. Shin, J.A. Kong, and H.I. Smith. "Electromagnetic Calculation of Soft X-ray Diffraction from Nanometer-scale Gold Structures."

Smith, H.I., S.D. Hector, M.L. Schattenburg, and E.H. Anderson. "A New Approach to High Fidelity E-Beam Lithography Based on an In Situ, Golobal Fiducial Grid."

Progress in Electromagnetics Research Symposium, Cambridge, Massachusetts, July 1-5, 1991.

Schattenburg, M.L., K. Li, R.T. Shin, J.A. Kong, and H.I. Smith. "Calculation of Soft X-ray Diffraction from Nanometer-Scale Gold Structures Using a Finite-Element Time-Domain Method."

Society of Photo-Optical Instrumentation Engineers (SPIE) Opto- Electronics Laser 1991 Conference, Orlando, Florida, April 1-5, 1991.

Green, Jr., T.J., J.H. Shapiro, and M.M. Menon. "Target Detection Performance Using 3-D Laser Radar Images."

Mentle, R.E., and J.H. Shapiro. "Track-While-Image in the Presence of Background."

A.1.3 Published Meeting Papers

Alerhand, O.L., A.N. Berker, J.D. Joannopoulos, and D. Vanderbilt. "Phase Transitions on Misoriented Si(100) Surfaces." *Proceedings of the 20th International Conference on the Physics of Semiconductors,* Thessaloniki, Greece, August 6-10, 1990.

Alerhand, O.L., E.Kaxiras, J.D. Joannopoulos, and G. Turner. "Kinetics and Growth Channels in GaAs Epitaxy on Si(100)." *Proceedings of the 20th International Conference on the Physics of Semiconductors,* Thessaloniki, Greece, August 6-10, 1990.

Anderson, K.K., M.J. LaGasse, H.A. Haus, and J.G. Fujimoto. "Femtosecond Studies of Nonlinear Optical Switching in GaAs Waveguides Using Time Domain Interferometry." *Proceedings of the International Society for Optical Engineering (SPIE),* 1216:2-12, Los Angeles, California, January 16-19, 1990.

Annaswamy, A.M., and M.A. Srinivasan. "Manipulation of Compliant Objects with Compliant Fingerpads: Identification and Control Issues." *Proceedings of the Conference on Decision and Control,* Hawaii, December 1990.

Ashar, P., S. Devadas, and A.R. Newton. "Testability-Driven Decomposition of Large Finite State Machines." *Proceedings of the International Conference on Computer Design: VLSI in Computers and Processors,* Boston, Massachusetts, September 1990.

Ashar, P., S. Devadas, and K. Keutzer. "Testability Properties of Multilevel Logic Networks Derived From Binary Decision Diagrams." *Proceedings of the Conference on Advanced Research in VLSI,* Santa Cruz, California, March 1991.

Ashar, P., A. Ghosh, S. Devadas, and K. Keutzer. "Implicit State Transition Graphs: Applications to Sequential Logic Synthesis and Test." *Proceedings of the International Conference on Computer-Aided Design,* Santa Clara, California, November 11-15, 1990.

Bahl, S.R., and J.A. del Alamo. "An InAlAs/n^+-InGaAs Heterostructure Field-Effect Transistor with an In-Enriched Channel." *Proceedings of the Second International Conference on Indium Phosphide and Related Materials,* pp. 100-103, Denver, Colorado, April 23-25, 1990.

Bahl, S.R., and J.A. del Alamo. "A Quantized-Channel InAlAs/n^+-InGaAs HFET with High Breakdown Voltage." *Extended Abstracts of the Fall Meeting of the Materials Research Society,* EA-21:117-120, Boston, Massachusetts, November 26-December 1, 1990.

Bossi, D.E., W.D. Goodhue, M.C. Finn, K. Rauschenbach, and R.H. Rediker. "Fabrication and Enhanced Performance of Reduced-Confinement GaAlAs Tapered-Waveguide Antennas." *1990 Technical Digest of the Optical Society of America,* Series 5:41-42, Anaheim, California, May 21-26, 1990.

Brandstein, M.S., P.A. Monta, J.C. Hardwick, and J.S. Lim. "A Real-Time Implementation of the Improved MBE Speech Coder." *Proceedings of the 1990 IEEE International Conference on Acoustics, Speech, and Signal Processing,* Albuquerque, New Mexico, April 3-6, 1990.

Broekaert, T.P.E., and C.G. Fonstad. "AlAs Etch-Step Layers for InGaAlAs/InP Heterostructure Devices and Circuits." *Technical Digest of the 1990 International Electron Devices Meeting,* IEEE 1990, pp.339-342, Piscataway, New Jersey.

Bryan, M.J., S. Devadas, and K. Keutzer. "Testability-Preserving Circuit Transformations." *Proceedings of the International Conference on Computer-Aided Design,* Santa Clara, California, November 11-15, 1990.

Butzburger, J., M. Ostendorf, P.J. Price, and S. Shattuck-Hufnagel. "Isolated Word Intonation Recognition Using Hidden Markov Models." *Proceedings of the 1990 IEEE International Conference on Acoustics, Speech, and Signal Processing,* pp. 773-776, Albuquerque, New Mexico, April 3-6, 1990.

Corcoran, C., and R.H. Rediker. "Operation of Five Discrete Diode Lasers as a Coherent Ensemble by Fiber-Coupling into an External Cavity." *1990 Technical Digest of the Optical Society of America,* Series 7:552-554, Anaheim, California, May 21-26, 1990.

Devadas, S., and K. Keutzer. "An Automata-Theoretic Approach to Behavioral Equivalence." *Proceedings of the International Conference on Computer-Aided Design,* Santa Clara, California, November 11-15, 1990.

Devadas, S., K. Keutzer, and A. Ghosh. "Recent Progress in VLSI Synthesis for Testability." *Proceedings of the VLSI Test Symposium,* Atlantic City, New Jersey, April 1991.

Devadas, S., and K. Keutzer. "Design of Integrated Circuits Fully Testable for Delay Faults and Multifaults." *Proceedings of the International Test Conference,* Washington, D.C., September 1990.

DiRienzo, A., and G. Bekefi. "The MIT 35 GHz Cyclotron Autoresonance Maser (CARM) Amplifier." *Proceedings of the International Society for Optical Engineering (SPIE),* Vol. 1226, Los Angeles, California, January 16-19, 1990.

Elfadel, I., and R. Picard. "Miscibility Matrices Explain the Behavior of Grayscale Textures Generated by Gibbs Random Fields." *SPIE Proceedings on Intelligent Robots and Computer Vision IX,* OE/Boston '90, Boston, Massachusetts, November 4-9, 1990.

Goodberlet, J., J. Jacobson, J.G. Fujimoto, P.A. Schulz, and T.Y. Fan. "Self-starting Additive Pulse Mode-locking of a Diode Pumped Nd:YAG Laser." *Technical Digest of the Conference on Lasers and Electro-Optics,* Anaheim, California, May 21-25, 1990.

Goodberlet, J., J. Jacobson, J. Wang, P.A. Schulz, T.Y. Fan, and J.G. Fujimoto. "Additive Pulse Modelocking in $Ti:Al_2O_3$ Diode Pumped Nd:YAG and Nd:YLF." *Technical Digest of the Ultrafast Phenomena Topical Meeting,* Monterey, California, May 14-17, 1990.

Goodberlet, J., J. Wang, P.A. Schulz, and J.G. Fujimoto. "Self-starting Additive Pulse Mode-locking Characterization with a $Ti:Al_2O_3$ Laser." *Technical Digest of the Conference on Lasers and Electro-Optics,* Anaheim, California, May 21-25, 1990.

Ghosh, A., S. Devadas, and A.R. Newton. "Heuristic Minimization of Boolean Relations Using Testing Techniques." *Proceedings of the International Conference on Computer Design: VLSI in Computers and Processors,* Boston, Massachusetts, September 1990.

Ghosh, A., S. Devadas, and A.R. Newton. "Synthesis for Sequential Logic Testability Using Register-Transfer Level Descriptions." *Proceedings of the International Test Conference,* Washington, D.C., September 10-13, 1990.

Hagelstein, P.L. "Coherent Fusion Mechanisms." *Proceedings of the Conference on Anomalous Processes in Deuterated Metals,* Brigham Young University, Utah, October 1990.

Hagelstein, P.L. "On the Partial-Wave Method for Self-Energy Calculations in Non-hydrogenic Ions." *Proceedings of the First International Conference on Coherent Radiation Processes in Strong Fields,* Catholic University, Washington, D.C., June 1990.

Hannon, S.M., and J.H. Shapiro. "Active-Passive Detection of Multipixel Targets." *Proceedings of the International Society for Optical Engineering (SPIE),* Vol. 1222 (Laser Radar V):2-23 (1990), Los Angeles, California, January 16-19, 1990.

Keast, C.L., and C.G. Sodini. "A CCD/CMOS Process for Integrated Image Acquisition and Early Vision Signal Processing." *SPIE Proceedings on Charge-Coupled Devices and Solid State Sensors,* pp. 152-161, Santa Clara, California, February 1990.

Kupfer, K., A. Bers, and A.K. Ram. "Guiding Center Stochasticity in a Tokamak." *Proceedings of the International Sherwood Theory Meeting,* Williamsburg, Virginia, April 23-25, 1990.

Kupfer, K., A. Bers, and A.K. Ram. "Guiding Center Stochasticity and Transport Induced by Electrostatic Waves." *Proceedings of the Topical Conference on Research Trends in Nonlinear and Relativistic Effects in Plasmas,* LaJolla Institute, LaJolla, California, February 5-8, 1990.

Lumsdaine, A., J. Wyatt, and I. Elfadel. "Nonlinear Analog Networks for Image Smoothing and Segmentation." *Proceedings of the IEEE International Symposium on Circuits and Systems,* pp. 987-991, New Orleans, Louisiana, May 1-3, 1990.

McIlrath, M.B., and D.S. Boning. "Integrating Semiconductor Process Design and Manufacture Using a Unified Process Flow Representation." *Proceedings of the Second Rensselaer International Conference on Computer Integrated Manufacturing,* Troy, New York, May 21-23, 1990.

Melngailis, J., P.G. Blauner, A.D. Dubner, J.S. Ro, T. Tao, and C.V. Thompson. "Focused Ion

Beam Induced Deposition." *Proceedings of the International Symposium on Process Physics and Modeling in Semiconductor Technology/Electrochemical Society Meeting,* Montreal, Quebec, Canada, May 6-11, 1990.

Muendel, M.H., and P.L. Hagelstein. "High Repetition Rate, Tabletop X-ray Lasers." *Proceedings of the International Society for Optical Engineering (SPIE),* Vol. 1229:87-96, Los Angeles, California, January 16-19, 1990.

Muendel, M.H., and P.L. Hagelstein. "Analysis of a Soft X-ray Frequency Doubler." *Proceedings of the International Conference on Lasers '89,* pp. 34-36, New Orleans, Louisiana, December 3-8, 1989.

Musicus, B.R., A. Aliphas, and A.J. Wei. "A Prototype for a Fault Tolerant Parallel Digital Signal Processor." *Proceedings of the IEEE Application Specific Array Processor Conference,* Princeton, New Jersy, September 5-7, 1990.

Pritchard, D.E., and B.G. Oldaker. "Light Forces and Atom Diffraction—An Illustrated Summary." *Proceedings, Sixth Rochester Conference on Coherence and Quantum Optics,* (Coherence and Quantum Optics VI:937-942), University of Rochester, Rochester, New York, June 26-28, 1989.

Ram, A.K., and A. Bers. "Propagation of Ion-Bernstein Waves in Toroidal Plasmas." *Proceedings of the International Sherwood Theory Meeting,* Williamsburg, Virginia, April 23-25, 1990.

Rosenkranz, P.W. "Oxygen Line Emission as a Measure of Temperature in the Upper Stratosphere and Mesosphere." *Proceedings of the Tenth Annual International Geoscience and Remote Sensing Symposium,* pp. 1185-1188, University of Maryland, College Park, Maryland, May 20-24, 1990.

Shapiro, J.H., S.R. Shepard, and N.C. Wong. "Coherent Phase States and Squeezed Phase States." *Proceedings, Sixth Rochester Conference on Coherence and Quantum Optics,* (Coherence and Quantum Optics VI), University of Rochester, Rochester, New York, June 26-28, 1989.

Shapiro, J.H., S.R. Shepard, and N.C. Wong. "A New Number-Phase Uncertainty Principle." *Proceedings, Sixth Rochester Conference on Coherence and Quantum Optics,* (Coherence and Quantum Optics VI), University of Rochester, Rochester, New York, June 26-28, 1989.

Standley, D.L. "Stability in a Class of Resistive Grid Networks Containing Active Device Realizations of Nonlinear Resistors." *Proceedings of the IEEE International Symposium on Circuits and Systems,* pp. 1474-1477, New Orleans, Louisiana, May 1-3, 1990.

Stevens, K.N., and C.A. Bickley. "Higher-level Control Parameters for a Formant Synthesizer." *Proceedings of the First International Conference on Speech Synthesis,* pp. 63-66, Autrans, France, 1990.

Tabei, M., and M. Ueda. "Backprojection with Fourier Series Expansion and FFT." *Proceedings of the 1990 IEEE International Conference on Acoustics, Speech, and Signal Processing,* Albuquerque, New Mexico, April 3-6, 1990.

Veilleux, N., M. Ostendorf, S. Shattuck-Hufnagel, and P.J. Price. "Markov Modeling of Prosodic Phrases." *Proceedings of the 1990 IEEE International Conference on Acoustics, Speech, and Signal Processing,* pp. 777-780, Albuquerque, New Mexico, April 3-6, 1990.

Vleck, J.C., and C.G. Fonstad. "Molecular Beams Epitaxial Growth Techniques for Graded-Composition InGaAs/InP Alloys." *Proceedings of the Second International Conference on InP and Related Materials,* pp. 135-138, IEEE 1990, Piscataway, New Jersey.

Wyatt, Jr., J.L., and M. Ilic. "Time-Domain Reactive Power Concepts for Nonlinear, Nonsinusoidal or Nonperiodic Networks." *Proceedings of the IEEE International Symposium on Circuits and Systems,* pp. 387-390, New Orleans, Louisiana, May 1-3, 1990.

Yang, W., and A.M. Chiang. "A Full Fill-Factor CCD Imager with Integrated Signal Processors." *Proceedings of the IEEE International Solid State Circuits Conference,* pp. 218-219, San Francisco, California, February 1990.

Yen, A., R.A. Ghanbari, Y-C. Ku, W. Chu, M.L. Schattenburg, J.M. Carter, and H.I. Smith. "X-ray Masks with Large-Area 100 nm-Period Gratings for Quantum- Effect Device Applications." *Proceedings of the International Conference on Microlithography, Microcircuit Engineering 90,* Leuven, Belgium, September 18-20, 1990.

A.1.4 Meeting Papers Accepted For Publication

Bickley, C.A. "Vocal-fold Vibration in a Computer Model of a Larynx." *Proceedings of the Vocal Fold Physiology Conference,* Stockholm, Sweden.

Halle, M., and K.N. Stevens. "Knowledge of Language and the Sounds of Speech." *Proceedings of the Symposium on Music. Language, Speech, and Brain.* Stockholm, Sweden.

Huang, C.B. "Effects of Context, Stress, and Speech Style on American Vowels." *Proceedings of the International Conference on Spoken Language Processing '90,* Kobe, Japan.

Keith, D.W., and D. E. Pritchard. "Atom Optics." *Proceedings of NATO Advanced Study Institute on New Frontiers in Quantum Electrodynamics and Quantum Optics,* Istanbul, Turkey.

Lee, H., S.M. Ali, and J.A. Kong. "Hybrid-Mode Analysis of High-Tc Superconducting Planar Transmission Lines." *Progress in Electromagnetics Research Symposium,* Cambridge, Massachusetts, July 1-5, 1991.

Stevens, K.N. "Vocal-fold Vibration for Obstruent Consonants." *Proceedings of the Vocal Fold Physiology Conference,* Stockholm, Sweden.

A.2 Journal Articles

A.2.1 Published Journal Articles

Alerhand, O.L., A.N. Berker, J.D. Joannopoulos, D. Vanderbilt, R.J. Hamers, and J.E. Demuth. "Finite-Temperature Phase Diagram of Vicinal Si(100) Surfaces." *Phys. Rev. Lett.* 64(20):2406-2409 (1990).

Alerhand, O.L., A.N. Berker, J.D. Joannopoulos, D. Vanderbilt, R.J. Hamers, and J.E. Demuth. "Alerhand et al. Reply." *Phys. Rev. Lett.* 66(7):962 (1991).

Allen, J. "Performance-Directed Synthesis of VLSI Systems." *Proc. IEEE* 78(2):336-355 (1990).

Anderson, K.K., M.J. LaGasse, H.A. Haus, and J.G. Fujimoto. "Femtosecond Time Domain Techniques for Characterization of Linear and Nonlinear Optical Properties in GaAs Waveguides." *Proc. Mat. Res. Soc. Symp.* 167:51-60 (1990).

Anderson, K.K., M.J. LaGasse, C.A. Wang, J.G. Fujimoto, and H.A. Haus. "Femtosecond Dynamics of the Nonlinear Index Near the Band Edge in AlGaAs Waveguides." *Appl. Phys. Lett.* 56(19):1834-1836 (1990).

Ashar, P., S. Devadas, and A.R. Newton. "Optimum and Heuristic Algorithms for a Formulation of Finite State Machine Decomposition." *IEEE Trans. Comput.-Aided Des.* 10(3):296-310 (1991).

Ashar, P., S. Devadas, and A.R. Newton. "Irredundant Interacting Sequential Machines Via Optimal Logic Synthesis." *IEEE Trans. Comput.-Aided Des.* 10(3):311-325 (1991).

Azzam, W.J., and J.A. del Alamo. "An All-Electrical Floating-Gate Transmission Line Model Technique for Measuring Source Resistance in Heterostructure Field-Effect Transistors." *IEEE Trans. Electron Devices* 37(9):2105-2107 (1990).

Bagwell, P.F. "Evanescent Modes and Scattering in Quasi-One-Dimensional Wires." *Phys. Rev. B* 41:354-371 (1990).

Bagwell, P.F. "Solution of Dyson's Equation in a Quasi-One-Dimensional Wire." *J. Phys. Condens. Matter* 2:6179 (1990).

Bagwell, P.F., T.P.E. Broekaert, T.P. Orlando, and C.G. Fonstad. "Resonant Tunneling Diodes and Transistors with a One, Two, and Three Dimensional Electron Emitter." *J. Appl. Phys.* 68(9):4634-4646 (1990).

Basu, S., and P.L. Hagelstein. "Design Analysis of a Short Wavelength Laser in an Unstable Resonator Cavity." *J. Appl. Phys.* 69(4):1853-1861 (1991).

Beckerle, J.D., A.D. Johnson, and S.T. Ceyer. "Collision Induced Desorption of Physisorbed CH_4 from Ni(111): Experiments and Simulations." *J. Chem. Phys.* 93:4047 (1990).

Berker, A.N. "Harris Criterion for Direct and Orthogonal Quenched Randomness." *Phys. Rev. B* 42(13):8640-8642 (1990).

Bers, A., V. Fuchs, and C.C. Chow. "Single-Pass Absorption in Ion-Cyclotron Heating." *Bull. Amer. Phys. Soc.* 35:2047 (1990).

Binder, B.T., P.T. Yu, J.H. Shapiro, and J.K. Bounds. "An Atmospheric Optical Ring Network." *IEEE Trans. Commun.* 38(1):74-81 (1990).

Bossi, D.E., W.D. Goodhue, M.C. Finn, K. Rauschenbach, J.W. Bales, and R.H. Rediker. "Reduced-Confinement Antennas for GaAlAs Integrated Optical Waveguides." *Appl. Phys. Lett.* 56(5):420-422 (1990).

Boyce, S.E. "Coarticulatory Organization for Lip Rounding in Turkish and English." *J. Acoust. Soc. Am.* 88(6):2584-2595 (1990).

Boyce, S.E., R.A. Krakow, F. Bell-Berti, and C.E. Gelfer. "Converging Sources of Evidence for Dissecting Articulatory Movements into Core Gestures." *J. Phon.* 18:173-188 (1990).

Braida, L.D. "Two Types of Audiovisual Integration for the Identification of Speech Segments." *J. Acoust. Soc. Am.* 88: S82 (1990).

Broekaert, T.P.E., P.F. Bagwell, T.P. Orlando, and C.G. Fonstad. "Resonant Tunneling Diodes and Transistors with a One, Two, or Three Dimensional Electron Emitter" (abstract). *Bull. Amer. Phys. Soc.* 35:298 (1990).

Broekaert, T.P.E., and C.G. Fonstad. "$In_{0.53}Ga_{0.47}As/AlAs$ Resonant Tunneling Diodes with Peak Current Densities in Excess of 450 kA/cm^2," *J. Appl. Phys.* 68(8):4310-4312 (1990).

Brorson, S.D., H. Yokoyama, E.P. Ippen. "Spontaneous Emission Rate Alteration in Optical Waveguide Structures." *IEEE J. Quantum Electron.* 26(9):1492-1499 (1990).

Brorson, S.D., A. Kazeroonian, J.S. Moodera, D.W. Face, T.K. Cheng, E.P. Ippen, M.S. Dresselhaus, G. Dresselhaus, G.L. Doll, T. Venkatesan, X.D. Wu, and A. Inam. "Femtosecond Thermomodulation Study of Conventional and High-Tc Superconductors." *Ultrafast Phenomena VII* 53:354-356 (1990).

Brorson, S.D., A. Kazeroonian, D.W. Face, T.K. Cheng, G.L. Doll, M.S. Dresselhaus, G. Dresselhaus, E.P. Ippen, T. Venkatesan, X.D. Wu, and A. Inam. "Femtosecond Thermomodulation Study of High-Tc Superconductors." *Solid State Commun.* 74(12):1305-1308 (1990).

Brorson, S.D., A. Kazeroonian, J.S. Moodera, D.W. Face, T.K. Cheng, E.P. Ippen, M.S. Dresselhaus, and G. Dresselhaus. "Femtosecond Room-Temperature Measurement of the Electron-Phonon Coupling Constant λ in Metallic Superconductors." *Phys. Rev. Lett.* 64(18):2172-2175 (1990).

Burns, G.F., H. Blanck, and C.G. Fonstad. "Low-threshold GaAs/AlGaAs Graded-index Separate-confinement Heterostructure Lasers Grown by Molecular Beam Epitaxy on Oxide-masked Si Substrates." *Appl. Phys. Lett.* 56(25):2499-2501 (1990).

Cammarata, R.C., C.V. Thompson, C. Haydelden, and K-N. Tu. "Silicide Precipitation and Silicon Crystallization in Nickel Implanted Amorphous Silicon Thin Films." *J. Mater. Res.* 5:2133 (1990).

Ceyer, S.T. "New Mechanisms for Chemistry at Surfaces." *Science* 294:133 (1990).

Chakraborty, B., N. Reed, C. Kane, and P.A. Lee. "Spiral Phases and Time-Reversal-Violating Resonating-Valence-Bond States of Doped Antiferromagnets." *Phys. Rev. B* 42(7):4819-4822 (1990).

Cheng, T.K., S.D. Brorson, A.S. Kazeroonian, M.S. Dresselhaus, and E.P. Ippen. "Impulsive Excitation of Coherent Phonons Observed in Reflection in Bismuth and Antimony." *Appl. Phys. Lett.* 57(10):1004-1006 (1990).

Cho, J., and C.V. Thompson. "Electromigration-Induced Failures in Interconnects with Bimodel Grain Size Distributions." *J. Elec. Mater.* 19:1207 (1990).

Chow, C.C., V. Fuchs, and A. Bers. "Reflection at the Resonance Layer of the Fast Alfven Wave in Ion Cyclotron Heating." *Phys. Fluids B* 2(9):2185-2190 (1990).

Chow, C.C., A.K. Ram, and A. Bers. "Spatio-Temporal Chaos and Quasiperiodicity in the Nonlinear Three Wave Interaction." *Bull. Amer. Phys. Soc.* 35:2006 (1990).

Chow, C.C., V. Fuchs, and A. Bers. "The Dispersion Relation for D^3(He) Ion-Cyclotron Resonance Heating." *Phys. Fluids B* 2:1089 (1990).

Clevenger, L.A., and C.V. Thompson. "Explosive Silicidation in Nickel/Amorphous-Silicon Multilayer Thin Films." *J. Appl. Phys.* 67:2894 (1990).

Clevenger, L.A., and C.V. Thompson. "Nucleation Limited Phase Selection During Reactions in Nickel Amorphous-Silicon Multilayer Thin Films." *J. Appl. Phys.* 67:1325 (1990).

Coppi, B., S. Migliuolo, F. Pegoraro, and F. Porcelli. "Global Modes and High-energy Particles in Ignited Plasmas." *Phys. Fluids B* 2(5):927-943 (1990).

Coppi, B., S. Migliuolo, and Y-K. Pu. "Candidate Mode for Electron Thermal Energy Transport in Multi-keV Plasmas." *Phys. Fluids B* 2(10):2322-2333 (1990).

Cornell, E.A., R.M. Weisskoff, K.R. Boyce, R.W. Flanagan, Jr., G.P. Lafyatis, and D.E. Pritchard. "Cornell et al. Reply." *Phys. Rev. Lett.* 64(17):2099 (1990).

Cornell, E.A., R.M. Weisskoff, K.R. Boyce, and D.E. Pritchard. "Mode Coupling in a Penning Trap: π Pulses and a Classical Avoided Crossing." *Phys. Rev. A* 41(1):312-315 (1990).

Davis, R.L. "Conditioning Lesions Promote Primary-Auditory Neurite Regeneration in vitro." *Assoc. Res. Otolaryngol.* Abstract 13:316-317 (1990).

DeAvillez, R.R., L.A. Clevenger, C.V. Thompson, and K-N. Tu. "Quantitative Investigation of Titanium/Amorphous-Silicon Multilayer Thin Film Reactions." *J. Mater. Res.* 4:593 (1990).

del Alamo, J.A., and C.C. Eugster. "Quantum Field-Effect Directional Coupler." *Appl. Phys. Lett.* 56:78 (1990).

Delgutte, B. "Physiological Mechanisms of Psychophysical Masking: Observations From Auditory-Nerve Fibers." *J. Acoust. Soc. Am.* 87:791-809 (1990).

Delgutte, B. "Two-Tone Suppression in Auditory-Nerve Fibers: Dependence on Suppressor Frequency and Level." *Hear. Res.* 49:225-246 (1990).

Delgutte, B. "Physiological Models of Masking and Speech Processing." *J. Acoust. Soc. Am.* 87: S13 (1990).

Delhorne, L.A., J.M. Besing, C.M. Reed, and N.I. Durlach. "Tactual Cued Speech as a Supplement to Speechreading." *J. Am. Speech Hear. Assoc.* 32:73 (1990).

Devadas, S. "Optimal Layout Via Boolean Satisfiability." *Inter. J. Comput.-Aided VLSI Des.* 2(2):251-262 (1990).

Devadas, S., H-K.T. Ma, A.R. Newton, and A. Sangiovanni-Vincentelli. "Irredundant Sequential Machines Via Optimal Logic Synthesis." *IEEE Trans. Comput.-Aided Des.* 9(1):8-18 (1990).

Devadas, S., and H-K.T. Ma. "Easily Testable PLA-based Finite State Machines." *IEEE Trans. Comput.-Aided Des.* 9(5):611-614 (1990).

Devadas, S., and K. Keutzer. "A Unified Approach to the Synthesis of Fully Testable Sequential Machines." *IEEE Trans. Comput.-Aided Des.* 10(1):39-50 (1991).

Devadas, S., and A.R. Newton. "Exact Algorithms for Output Encoding, State Assignment and Four-Level Boolean Minimization." *IEEE Trans. Comput.-Aided Des.* 10(1):13-27 (1991).

Early, K., M.L. Schattenburg, and H.I. Smith. "Absence of Resolution Degradation in X-ray Lithography for λ from 4.5nm to 0.83nm." *Microelectron. Eng.* 11:317-321 (1990).

Eugster, C.C., and P.L. Hagelstein. "X-ray Detection Using the Quantum Well Exciton Nonlinearity." *IEEE J. Quantum Electron.* 26(1):75-84 (1990).

Feidenhans'l, R., F. Grey, R.L. Johnson, S.G.J. Mochrie, J. Bohr, and M. Nielsen. "Oxygen Chemisorption on Cu(110): A Structured Determination by X-ray Diffraction." *Phys. Rev. B* 41:5420 (1990).

Field, S.B., M.A. Kastner, U. Meirav, J.H.F. Scott-Thomas, D.A. Antoniadis, H.I. Smith, and S.J. Wind. "Conductance Oscillations Periodic in the Density of One-Dimensional Electron Gases." *Phys. Rev. B* 42(6):3523-3536 (1990).

Freeman, D.M. "Anatomical Model of the Cochlea of the Alligator Lizard." *Hear. Res.* 49:29-38 (1990).

Freeman, D.M., and T.F. Weiss. "Hydrodynamic Forces on Hair Bundles at Low Frequencies." *Hear. Res.* 48:17-30 (1990).

Freeman, D.M., and T.F. Weiss. "Hydrodynamic Forces on Hair Bundles at High Frequencies." *Hear. Res.* 48:31-36 (1990).

Freeman, D.M., and T.F. Weiss. "Superposition of Hydrodynamic Forces on a Hair Bundle." *Hear. Res.* 48:1-16 (1990).

Freeman, D.M., and T.F. Weiss. "Hydrodynamic Analysis of a Two-Dimensional Model for Micromechanical Resonance of Free-Standing Hair Bundles." *Hear. Res.* 48:37-68 (1990).

Frost, H.J., C.V. Thompson, and D.T. Walton. "Simulation of Thin Film Grain Structures: I. Grain Growth Stagnation." *Acta Metallurgica Mater.* 38:1455 (1990).

Gasiewski, A.J., J.W. Barrett, P.G. Bonanni, and D.H. Staelin. "Aircraft-based Radiometric

Imaging of Tropospheric Temperature and Precipitation Using the 118.75-GHz Oxygen Resonance." *J. Appl. Meterorol.* 29(7):620-632 (1990).

Gasiewski, A.J., and D.H. Staelin. "Numerical Modeling of Passive Microwave O_2 Observations Over Precipitation." *Radio Sci.* 25(3):217-235 (1990).

Gentile, T.R., B.J. Hughey, D. Kleppner, and T.W. Ducas. "Microwave Spectroscopy of Calcium Rydberg States." *Phys. Rev. A.* 42(1):440-451 (1990).

Gibbs, D., B.M. Ocko, D.M. Zehner, and S.G.J. Mochrie. "Structure and Phases of the Au(001) Surface: In-Plane Structure." *Phys. Rev. B* 42(12):7330-7344 (1990).

Gold, A. "Enhanced Plasmon Anomaly in the Dynamical Conductivity of Heterostructures with Large Spacer." *Phys. Rev. B* 41(6):3608-3619 (1990).

Gold, A. "Temperature Dependence of Mobility in $Al_xGa_{1-x}As$/GaAs Heterostructures for Impurity Scattering." *Phys. Rev. B* 41(12):8537-8540 (1990).

Gold, A., and A. Ghazali. "Analytical Results for Semiconductor Quantum-Well Wire: Plasmons, Shallow Impurity States, and Mobility." *Phys. Rev. B* 41(11):7626-7640 (1990).

Gold, A., and A. Ghazali. "Exchange Effects in a Quasi-One-Dimensional Electron Gas." *Phys. Rev. B* 41(12):8318-8322 (1990).

Goodberlet, J., J. Jacobson, J.G. Fujimoto, P.A. Schulz, and T.Y. Fan. "Self-starting Additive-pulse Mode-locked Diode-pumped Nd:YAG Laser." *Opt. Lett.* 15(9):504-506 (1990).

Goodberlet, J., J. Jacobson, J. Wang, J.G. Fujimoto, T.Y. Fan, and P.A. Schulz. "Ultrashort Pulse Generation with Additive Pulse Modelocking in Solid State Lasers: $Ti:Al_2O_3$, Diode Pumped Nd:YAG and Nd:YLF." *Ultrafast Phenomena VII* 53:11-13 (1990).

Goodberlet, J., J. Wang, J.G. Fujimoto, and P.A. Schulz. "Starting Dynamics of Additive-Pulse Mode Locking in the $Ti:Al_2O_3$ Laser." *Opt. Lett.* 15(22):1300-1302 (1990).

Goodhue, W.D., D.E. Bossi, M.C. Finn, J.W. Bales, and R.H. Rediker. "Reduced-Confinement GaAlAs Tapered-Waveguide Antenna Grown by Molecular-Beam Epitaxy." *J. Vac Sci Technol. B* 8(2):349-351 (1990).

Gould, P.L., P.J. Martin, G.A. Ruff, R.E. Stoner, J-L. Picque', and D.E. Pritchard. "Momentum Transfer to Atoms by a Standing Light Wave: Transition from Diffraction to Diffusion." *Phys. Rev. A* 43(1):585-588 (1991).

Griffith, M., G. Langston, M. Heflin, S. Conner, J. Lehar, and B. Burke. "The Third MIT-Green Bank 5 GHz Survey." *Astrophys. J.* 74(1):129-180 (1990).

Guinan, J.J., Jr., and R.Y.S. Li. "Signal Processing in Brainstem Auditory Neurons Which Receive Giant Endings (Calyces of Held) in the Medial Nucleus of the Trapezoid Body of the Cat." *Hear. Res.* 49:321-334 (1990).

Habashy, T.M., S.M. Ali, and J.A. Kong. "Input Impedance Parameters and Radiation Pattern of Cylindrical-Rectangular and Wraparound Microstrip Antennas." *IEEE Trans. Antennas Propag.* 38(5):722-731 (1990).

Hall, K.L., E.P. Ippen, and G. Eisenstein. "Bias-lead Monitoring of Ultrafast Nonlinearities in InGaAsP Diode Laser Amplifiers." *Appl. Phys. Lett.* 57(2):129-131 (1990).

Hall, K.L., Y. Lai, E.P. Ippen, G. Eisenstein, and U. Koren. "Femtosecond Gain Dynamics and Saturation Behavior in InGaAsP Multiple Quantum Well Optical Amplifiers." *Appl. Phys. Lett.* 57(27):2888-2890 (1990).

Hall, K.L., J. Mark, E.P. Ippen, and G. Eisenstein. "Femtosecond Gain Dynamics in InGaAsP Optical Amplifiers." *Appl. Phys. Lett.* 56(18):1740-1742 (1990).

Haus, H.A., and Y. Lai. "Quantum Theory of Soliton Squeezing: A Linearized Approach." *J. Opt. Soc. Am. B* 7(3):386-392 (1990).

Hillman, R.E., E.B. Holmberg, J.S. Perkell, M. Walsh, and C. Vaughn. "Phonatory Function Associated with Hyperfunctionally Related Vocal Fold Lesions." *J. Voice* 4:52-63 (1990).

Ho, S.T., P. Kumar, and J.H. Shapiro. "Quantum Theory of Nondegenerate Multiwave Mixing III. Application to Single-Beam Squeezing." *J. Opt. Soc. Am. B* 8(1):37-57 (1991).

Hughey, B.J., T.R. Gentile, D. Kleppner, and T.W. Ducas. "Experimental Study of Small Ensembles of Atoms in a Microwave Cavity." *Phys. Rev. A* 41(11):6245-6254 (1990).

Hughey, B.J., T.R. Gentile, D. Kleppner, and T.W. Ducas. "A Split High-Q Superconducting

Cavity." *Rev. Sci. Instrum.* 61(7):1940-1945 (1990).

Huh, J.S., M.I. Shepard, and J. Melngailis. "Focused Ion Beam Lithography." *J. Vac. Sci. Technol. B* 1:173-175 (1991).

Hui, K., and A.N. Berker. "Random-Field Mechanism in Random-Bond Multicritical Systems." *J. Appl. Phys.* 67(9):5991 (1990).

Huxley, J.M., P. Mataloni, R.W. Schoenlein, J.G. Fujimoto, E.P. Ippen, and G.M. Carter. "Femtosecond Excited-State Dynamics of Polydiacetylene." *Appl. Phys. Lett.* 56(16):1600-1602 (1990).

Ippen, E.P., L.Y. Liu, and H.A. Haus. "Self-Starting Condition for Additive-Pulse Mode-Locked Lasers." *Opt. Lett.* 15(3):183-185 (1990).

Ismail, K., M. Burkhardt, H.I. Smith, N.H. Karam, and P.A. Sekula-Moise. "Patterning and Characterization of Large-Area Quantum-Wire Arrays." *Appl. Phys. Lett.* 58(14):1539-1541 (1991).

Iu, C., G.R. Welch, M.M. Kash, D. Kleppner, D. Delande, and J.C. Gay. "The Diamagnetic Rydberg Atom: Confrontation of Calculated and Observed Spectra." *Phys. Rev. Lett.* 66:145 (1991).

Jiran, E., and C.V. Thompson. "Capillary Instabilities in Thin Films." *J. Elec. Mater.* 19:1155 (1990).

Kane, C.L., P.A. Lee, T.K. Ng, B. Chakraborty, and N. Read. "Mean-Field Theory of the Spiral Phases of a Doped Antiferromagnet." *Phys. Rev. B* 41(4):2653-2656 (1990).

Kiang, J.F., S.M. Ali, and J.A. Kong. "Integral Equation Solution to the Guidance and Leakage Properties of Coupled Dielectric Strip Waveguides." *IEEE Trans. Microwave Theory Tech.* 38(2):193-203 (1990).

Kidd, R.C., and T.F. Weiss. "Mechanisms that Degrade Timing Information in the Cochlea." *Hear. Res.* 49:181-208 (1990).

Kim, H-J., and C.V. Thompson. "The Effects of Dopants on Surface-Energy-Driven Secondary Grain Growth in Silicon Films." *J. Appl. Phys.* 67:757 (1990).

Kinaret, J.M., and P.A. Lee. "Exchange Interaction in a Quantum Wire in a Strong Magnetic Field." *Phys. Rev. B* 42(18):768-773 (1990).

Kinaret, J.M., and P.A. Lee. "Conductance of a Disordered Narrow Wire in a Strong Magnetic Field." *Phys. Rev. B.* 43(5):3847-3855 (1991).

Kirkwood, R., I.H. Hutchinson, S.C. Luckhardt, M. Porkolab, and J.P. Squire. "Measurement of Suprathermal Electron Confinement by Cyclotron Transmission." *Phys. Fluids B* 2(6):1421-1426 (1990).

Klatt, D.H., and L.C. Klatt. "Analysis, Synthesis, and Perception of Voice Quality Variations Among Female and Male Talkers." *J. Acoust. Soc. Am.* 87(2):820-857 (1990).

Kleppner, D. "With Apologies to Casimir." *Physics Today* October:9-10 (1990).

Kleppner, D., C. Iu, and G.R. Welch. "Positive Energy Spectoscopy of the Diamagnetic Lithium System." *Comments At. Mol. Phys.* 25:301 (1991).

Koehnke, J., and P.M. Zurek. "Localization and Binaural Detection with Monaural and Binaural Amplification." *J. Acoust. Soc. Am.* 88: S169 (1990).

Ku, Y.C., H.I. Smith, and I. Plotnik. "Low Stress Tungsten Absorber for X-ray Masks." *Microelectron. Eng.* 11:303-308 (1990).

Kumar, A., and P.F. Bagwell. "Resonant Tunneling in a Multi-Channel Wire." *Solid State Commun.* 75(12):949-953 (1990).

Kuo, T.Y., T.H. Chiu, J.E. Cunningham, K.W. Goosen, C.G. Fonstad, and F. Ren. "Heterostructure Bipolar Transistor Employing Carbon-Doped Base Grown with Trimethyl-Ga and Arsine." *Electron. Lett.* 26:1260-1262 (1990).

Kuo, T.Y., J.E. Cunningham, K.W. Goosen, W.Y. Jan, C.G. Fonstad, and F. Ren. "Monolayer Be S-doped Heterostructure Bipolar Transistor - Fabricated Using Doping Selecting Base Contact." *Electron. Lett.* 26:1187-1188 (1990).

Kupfer, K., A. Bers, and A.K. Ram. "Stochastic Electron Transport Induced by Lower-Hybrid Current Drive Wave Fields." *Bull. Amer. Phys. Soc.* 35:1984-1985 (1990).

LaGasse, M.J., K.K. Anderson, C.A. Wang, H.A. Haus, and J.G. Fujimoto. "Femtosecond Investigations of Optical Switching and $\chi^{(3)}$ in GaAs Waveguides." *SPIE Proceedings,* Vol. 1282 Ultrafast Laser Probe Phenomena in Bulk and

Microstructure Semiconductors III:59-70 (1990).

LaGasse, M.J., K.K. Anderson, C.A. Wang, H.A. Haus, and J.G. Fujimoto. "Femtosecond Measurements of the Nonresonant Nonlinear Index in AlGaAs." *Appl. Phys. Lett.* 56(5):417-419 (1990).

Lai, Y., K.L. Hall, E.P. Ippen, and G. Eisenstein. "Short Pulse Gain Saturation in InGaAsP Diode Laser Amplifiers." *IEEE Photonics Tech. Lett.* 2(10):711-713 (1990).

Lai, Y., and H.A. Haus. "Quantum Theory of Self-Induced Transparency Solitons: A Linearization Approach." *Phys. Rev. A* 42(5):2925-2934 (1990).

Lam, C.W., S.M. Ali, and J.A. Kong. "The Propagation Characteristics of Signal Lines with Crossing Strips in Multilayered Anisotropic Media." *J. Electromag. Waves Appl.* 4(10):1005-1021 (1990).

Langston, G.I., S.R. Conner, J. Lehar, B.F. Burke, and K.W. Weiler. "Galaxy Mass Deduced from the Structure of Einstein Ring MG1654+1346." *Nature* 344(6261):43-45 (1990).

Langston, G.I., S.R. Conner, M.B. Heflin, J. Lehar, and B.F. Burke. "Faint Radio Sources and Gravitational Lensing." *Astrophys. J.* 353:34-38 (1990).

Lee, C.F., R.T. Shin, J.A. Kong, and B.J. McCartin. "Absorbing Boundary Conditions on Circular and Elliptic Boundaries." *J. Electromag. Waves Appl.* 4(10):945-962 (1990).

Leong, K.W., N.C. Wong, and J.H. Shapiro. "Non-classical Intensity Correlation from a Type I Phase-Matched Optical Parametric Oscillator." *Opt. Lett.* 15(19):1058-1060 (1990).

Liou, C-Y., and B.R. Musicus. "A Separable Cross-Entropy Approach to Power Spectral Estimation." *IEEE Trans. Acoust., Speech, Signal Process.* 38(1):105-113 (1990).

Liu, L.Y., J.M. Huxley, E.P. Ippen, and H.A. Haus. "Self-starting Additive-pulse Mode Locking of a Nd:YAG Laser." *Opt. Lett.* 15(10):553-555 (1990).

Liu, C.T., K. Nakamura, D.C. Tsui, K. Ismail, D.A. Antoniadis, and H.I. Smith. "Far-Infrared Transmission Measurements on Grid-Gate GaAs/AlGaAs Lateral-Surface-Superlattice Structures." *J. Surface Sci.* 228:527 (1990).

Liu, C.T., D.C. Tsui, M. Shayegan, K. Ismail, D.A. Antoniadis, and H.I. Smith. "Oscillatory Density-of-States of Landau Bands in a Two-Dimensional Lateral Surface Superlattice." *Solid State Commun.* 75:395-399 (1990).

Liu, C.T., D.C. Tsui, M. Shayegan, K. Ismail, D.A. Antoniadis, and H.I. Smith. "Observation of Landau Level Splitting in Magneto-Capacitance Measurements on GaAs/AlGaAs Two-Dimensional Surface Superlattice Structures." *Bull. Amer. Phys.* 35:597 (1990).

Ma, E., and C.V. Thompson. "Self-Propagating Explosive Reactions in Al/Ni Multilayer Thin Films." *Appl. Phys. Lett.* B7:1262 (1990).

Manuel, S.Y. "The Role of Contrast in Limiting Vowel-to-Vowel Coarticulation in Different Languages." *J. Acoust. Soc. Am.* 88(3):1286-1298 (1990).

Meirav, U., M.A. Kastner, and S.J. Wind. "Single-Electron Charging and Periodic Conductance Resonances in GaAs Nanostructures." *Phys. Rev. Lett.* 65(6):771-774 (1990).

Migita, M., A. Taike, and H. Yamamoto. "ZnSe p-n Junctions Produced by Metalorganic Molecular-Beam Epitaxy." *J. Appl. Phys.* 68:880-882 (1990).

Migliuolo, S., and A.K. Sen. "Effects of a Nonuniform Equilibrium Electric Field on Ion Temperature Gradient Instabilities." *Phys. Fluids B* 2(12):3047-3051 (1990).

Mochrie, S.G.J., D.M. Zehner, B.M. Ocko, and D. Gibbs. "Structure and Phases of the Au(001) Surface: X-ray Scattering Measurements." *Phys. Rev. Lett.* 64(24):2925-2928 (1990).

Moel, A., M.L. Schattenburg, J.M. Carter, and H.I. Smith. "A Compact, Low-cost System for Sub-100 nm X-ray Lithography." *J. Vac. Sci. Technol. B* 8(6):1648-1651 (1990).

Murguia, J.E., C.R. Musil, M.I. Shepard, H. Lezec, D.A. Antoniadis, and J. Melngailis. "Merging Focused Ion Beam Patterning and Optical Lithography in Device and Circuit Fabrication." *J. Vac. Sci. Technol. B* 8(6):1374-1379 (1990).

Nagaosa, N., and P.A. Lee. "Normal-State Properties of the Uniform Resonating-Valence-Bond State." *Phys. Rev. Lett.* 64(20):2450-2453 (1990).

Netz, R.R., and A.N. Berker. "Monte Carlo Mean-Field Theory and Frustrated Systems in Two

and Three Dimensions." *Phys. Rev. Lett.* 66(3):377-380 (1991).

Oldaker, B.G., P.J. Martin, P.L. Gould, M. Xiao, and D.E. Pritchard. "Experimental Study of Sub-Poissonian Statistics in the Transfer of Momentum from Light to Atoms." *Phys. Rev. Lett.* 65(13):1555-1558 (1990).

Peterson, P.M., S-M. Wei, W.M. Rabinowitz, and P.M. Zurek. "Robustness of an Adaptive Beamforming Method for Hearing Aids." *Acta Oto-Larngol. Suppl.* 469:85-90 (1990).

Prasad, S., W. Lee, and C.G. Fonstad. "Reply to 'Comments on Unilateral Gain of Hetrojunction Bipolar Transistors at Microwave Frequencies.'" *IEEE Trans. Electron. Dev.* 37:826 (1990).

Qiu, J., Q-D. Qian, R.L. Gunshor, M. Kobayashi, D.R. Menke, D. Li, and N. Otsuka. "Influence of GaAs Surface Stoichiometry on the Interface State Density of As-Grown Epitaxial ZnSe/Epitaxial GaAs Heterostructures." *Appl. Phys. Lett.* 56(13):1272-1274 (1990).

Ram, A.K., and A. Bers. "Space-Time Analysis of Electromagnetic Instabilities with Application to Auroral Kilometric Radiation." *EOS Trans. Amer. Geophys. Union* 71(43):1532 (1990).

Ram, A.K., C.C. Chow, and A. Bers. "Bandwidth of Scattered Radiation in Laser-Plasma Interactions." *Bull. Amer. Phys. Soc.* 35:2126 (1990).

Ramesh, S., N. Kobayashi, and Y. Horikoshi. "Migration-Enhanced Epitaxy Growth and Characterization of High-Quality ZnSe/GaAs Superlattices." *Appl. Phys. Lett.* 57(11):1102-1104 (1990).

Rankovic, C.M., and P.M. Zurek. "Rollover with High-frequency Emphasis." *J. Acoust. Soc. Am.* 87: S87 (1990).

Rappe, A.M., K.M. Rabe, E. Kaxiras, and J.D. Joannopoulos. "Optimized Pseudopotentials." *Phys. Rev. B* 41(2):1227-1230 (1990).

Ravicz, M.E., J.J. Rosowski, and H.F. Voigt. "Acoustic Impedance Measurements in the Gerbil Ear." *J. Acoust. Soc. Am.* 87(Suppl.1): S101 (1990).

Reed, C.M., L.A. Delhorne, N.I. Durlach, and S.D. Fischer. "A Study of the Tactual and Visual Reception of Fingerspelling." *J. Speech Hear. Res.* 33:786-797 (1990).

Rosowski, J.J., P.J. Davis, K.M. Donahue, S.N. Merchant, and M.D. Coltrera. "Cadaver Middle Ears as Models for Living Ears: Comparisons of Middle Ear Input Immittance." *Ann. Otol., Rhinol., Laryngol.* 99(5):403-412 (1990).

Sato, H., J.C. Vlcek, C.G. Fonstad, B. Meskoob, and S. Prasad. "InGaAs/InAlAs/InP Collector - Up Microwave Heterojunction Bipolar Transistors." *Electron. Dev. Lett.* 11:457-459 (1990).

Schattenburg, M.L., K. Early, Y-C. Chu, M.I. Shepard, S-C. The, H.I. Smith, D.W. Peters, R.D. Frankel, D.R. Kelly, and J.P. Drumheller. "Fabrication and Testing of 0.1-μm-linewidth Microgap X-ray Masks." *J. Vac. Sci. Technol. B* 8(6).1604-1608 (1990).

Schattenburg, M.L., E.H. Anderson, and H.I. Smith. "X-ray/VUV Transmission Gratings for Astrophysical and Laboratory Applications." *Phys. Scr.* 41:13-20 (1990).

Schoenlein, R.W., J.G. Fujimoto, G.L. Eesley, and T.W. Capehart. "Femtosecond Dynamics of the n=2 Image-Potential State on Ag(100)." *Phys. Rev. B* 41(8):5436-5439 (1990).

Scott-Thomas, J.H.F., M.A. Kastner, S.B. Field, H.I. Smith, and D.A. Antoniadis. "Conductance Oscillations of 1-Dimensional Hole and Electron Gases." *Bull. Amer. Phys. Soc.* 35:731 (1990).

Secker-Walker, H.E., and C.L. Searle. "Time-domain Analysis of Auditory-nerve-fiber Firing Rates." *J. Acoust. Soc. Am.* 88(3):1427-1436 (1990).

Sheen, D.M., S.M. Ali, M.D. Abouzahra, and J.A. Kong. "Application of the Three-Dimensional Finite-Difference Time-Domain Method to the Analysis of Planar Microstrip Circuits." *IEEE Trans. Microwave Theory Tech.* 38(7):849-857 (1990).

Shirasaki, M., and H.A. Haus. "Squeezing of Pulses in a Nonlinear Interferometer." *J. Opt. Soc. Am. B* 7(1):30-34 (1990).

Smith, H.I., and D.A. Antoniadis. "Seeking a Radically New Electronics." *Tech. Rev.* 93:26-40 (1990).

Smith, H.I., and H.G. Craighead. "Nanofabrication." *Phys. Today* (February):24-30 (1990).

Smith, H.I., K. Ismail, M.L. Schattenburg, and D.A. Antoniadis. "Sub-100nm Electronic Devices

and Quantum-Effects Research Using X-ray Nanolithography." *Microelectron. Eng.* 11:53-59 (1990).

Srinivasan, M.A., J.M. Whitehouse, and R.H. LaMotte. "Tactile Detection of Slip: Surface Microgeometry and Peripheral Neural Codes." *J. Neurosphysiol.* 63(6):1323-1332 (1990).

Stoner, R., S.C. Chen, and G. Bekefi. "A Planar Electromagnet Microwiggler for Free Electron Lasers." *IEEE Trans. Plasma Sci.* 18(3):387-391 (1990).

Tao, T., J. Ro, J. Melngailis, Z. Xue, and H.D. Kaesz. "Focused Ion Beam Induced Deposition of Platinum." *J. Vac. Sci. Technol. B* 8(6):1826-1829 (1990).

Tao, T., W. Wilkinson, and J. Melngailis. "Focused Ion Beam Induced Deposition of Platinum for Repair Processes." *J. Vac. Sci. Technol. B* 1:162-164 (1991).

Tarnow, E., P. Dallot, P.D. Bristowe, J.D. Joannopoulos, G.P. Francis, and M.C. Payne. "Structural Complexity in Grain Boundaries with Covalent Bonding." *Phys. Rev. B* 42(6):3644-3657 (1990).

Thompson, C.V. "Grain Growth in Thin Films." *Annu. Rev. Mater. Sci.* 20:245-268 (1990).

Thompson, C.V., J. Floro, and H.I. Smith. "Epitaxial Grain Growth in Thin Metal Films." *J. Appl. Phys.* 67:4099-4104 (1990).

Toriumi, A., K. Ismail, M. Burkhardt, D.A. Antoniadis, and H.I. Smith. "Resonant Magneto-Capacitance in a Two-Dimensional Lateral-Surface Superlattice." *Phys. Rev. B* 41:12346-12349 (1990).

Venkateswaran, U.D., L.J. Cui, M. Li, B.A. Weinstein, K. Elcess, C.G. Fonstad, and C. Mailhoit. "Strain Mapping in (111)- and (100)-InGaAs/GaAs Superlattices." *Appl. Phys. Lett.* 56:286-288 (1990).

Venkateswaran, U.D., T. Burnett, L.J. Cui, M. Li, B.A. Weinstein, J.M. Kim, C.R. Wie, K. Elcess, C.G. Fonstad, and C. Mailhoit. "Comparison and Spatial Profiling of Strain in [001] and [111] InGaAs/GaAs Superlattices from Raman and X-ray Experiments." *Phys. Rev. B* 42:3100-3108 (1990).

Veysoglu, M.E., H.A. Yueh, R.T. Shin, and J.A. Kong. "Polarimetric Passive Remote Sensing of Periodic Surfaces." *J. Electromag. Waves Appl.* 5(3):267-280 (1991).

Weiner, A.M., D.E. Leaird, G.P. Wiederrecht, and K.A. Nelson. "Femtosecond Pulse Sequences Used for Optical Manipulation of Molecular Motion." *Science* 247:1317-1319 (1990).

Weinstein, E., M. Feder, and A.V. Oppenheim. "Sequential Algorithms for Parameter Estimation Based on the Kullback-Leibler Information Measure." *IEEE Trans. Acoust., Speech, Signal Process.* 38(9): 1652-1654 (1990).

Wodicka, G.R., K.N. Stevens, H.L. Golub, and D.C. Shannon. "Spectral Characteristics of Sound Transmission in the Human Respiratory System." *IEEE Trans. Biomed. Eng.* 37(12):1130-1134 (1990).

Wong, N.C. "Optical Frequency Division Using an Optical Parametric Oscillator." *Opt. Lett.* 15(20):1129-1131 (1990).

Wong, N.C., K.W. Leong, and J.H. Shapiro. "Quantum Correlation and Absorption Spectroscopy in an Optical Parametric Oscillator in the Presence of Pump Noise." *Opt. Lett.* 15(16):891-893 (1990).

Wornell, G.W. "A Karhunen-Loeve-like Expansion for 1/f Processes via Wavelets." *IEEE Trans. Inf. Theory* 36(4):859-861 (1990).

Wurtele, J.S., G. Bekefi, R. Chu, and K. Xu. "Prebunching in a Collective Raman Free-Electron Laser Amplifier." *Phys. Fluids B* 2(2):401-406 (1990).

Xu, K., and G. Bekefi. "Experimental Study of Multiple Frequency Effects in a Free Electron Laser Amplifier." *Phys. Fluids B* 2(3):678-680 (1990).

Yen, A., R.A. Ghanbari, E.H. Anderson, and H.I. Smith. "Fabricaton of 100 nm-Period Gratings Using Achromatic Holographic Lithography." *Microelectron. Eng.* 11:201-205 (1990).

Yokoyama, H., K. Nishi, T. Anan, H. Yamada, S.D. Brorson, and E.P. Ippen. "Enhanced Spontaneous Emission from GaAs Quantum Wells in Monolithic Microcavities." *Appl. Phys. Lett.* 57(26):2814-2816 (1990).

Yueh, H.A., J.A. Kong, R.M. Barnes, and R.T. Shin. "Calibration of Polarimetric Radar Using In-scene Reflectors." *J. Electromag. Waves Appl.* 4(1):27-49 (1990).

Yueh, H.A., R.T. Shin, and J.A. Kong. "Scattering from Randomly Oriented Scatterers with Strong

Permittivity Fluctuations." *J. Electromag. Waves Appl.* 4(10):983-1004 (1990).

Zakhor, A. "Reconstruction of Two-Dimensional Signals from Level Crossings." *IEEE Proc.* 78(1):31-55 (1990).

Zurek, P.M., and C.M. Rankovic. "Potential Benefits of Varying the Frequency-Gain Characteristic for Speech Reception in Noise." *J. Acoust. Soc. Am.* 87: S87 (1990).

A.2.2 Journal Articles Accepted for Publication

Bahl, S.R., W.J. Azzam, and J.A. del Alamo. "Orientation Dependence of Mismatched InAlAs/InGaAs HFETs." *J. Crystal Growth.*

Basu, S. "Possibility of X-ray Detection Using Quantum Wells." *IEEE J. Quantum Electron.*

Bossi, D.E., W.D. Goodhue, L.M. Johnson, and R.H. Rediker. "Reduced-Confinement GaAlAs Tapered Waveguide Antennas for Enhanced Far-Field Beam Directionality." *IEEE J. Quantum Electron.*

Braida, L.D. "Crossmodal Integration in the Identification of Consonant Segments." *Quart. J. Exp. Psychol.*

Braud, J.P., and P.L. Hagelstein. "Whispering-Gallery Laser Resonators - Part I: Diffraction of Whispering-Gallery Modes." *IEEE J. Quantum Electron.*

Bryan, M.J., S. Devadas, and K. Keutzer. "Analysis and Design of Regular Structures for Robust Dynamic Fault Testability." *Inter. J. Comput.-Aided VLSI Des.*

Burrus, C.S., A.W. Soewito, and R.A. Gopinath. "Least Squared Error FIR Filter Design with Transition Bands." *IEEE Trans. Acoust., Speech, Signal Process.*

Chu, N.C., J.A. Kong, H.A. Yueh, S.V. Nghiem, J.C. Fleischman, S. Ayasli, and R.T. Shin. "Variance of Phase Fluctuations of Waves Propagation Through a Random Medium." *J. Electromag. Waves Appl.*

Clevenger, L.A., C.V. Thompson, R.R. deAville, and E. Ma. "Nucleation Controlled Phase Selection in Vanadium/Amorphous-Silicon Multilayer Thin Films." *J. Vac. Sci. Tech. A.*

Devadas, S. "Delay Test Generation for Sychronous Sequential Circuits." *Inter. J. Comput.-Aided VLSI Des.*

Devadas, S. "Optimization of Interacting Finite State Machines Using Sequential Don't Cares." *IEEE Trans. Comput.-Aided Des.*

Devadas, S., and K. Keutzer. "Synthesis of Robust Delay-Fault Testable Circuits: Theory." *IEEE Trans. Comput.-Aided Des.*

Devadas, S., and K. Keutzer. "An Automata-Theoretic Approach to Behaviorial Equivalence." *Intern. J. Comput.-Aided VLSI Des.*

Devadas, S., and K. Keutzer. "Synthesis of Robust Delay-Fault Testable Circuits: Practice." *IEEE Trans. Comput.-Aided Des.*

Devadas, S., K. Keutzer, and J.K. White. "Estimation of Power Dissipation in CMOS Combinational Circuits Using Boolean Function Manipulation." *IEEE Trans. Comput.-Aided Des.*

Durlach, N.I. "Auditory Localization in Teleoperator and Virtual Environment Systems." *Perception.*

Frank, L.R., A.P. Crawley, and B.R. Musicus. "Arbitrary Temporal Sampling of Flow Through the Cardiac Cycle with Fast Spin Echoes." *J. Mag. Res.*

Ghosh, A., S. Devadas, and A.R. Newton. "Test Generation and Verification of Highly Sequential Circuits." *IEEE Trans. Comput.-Aided Des.*

Grant, K.W., L.D. Braida, and R.J. Renn. "Single-band Envelope Cues as an Aid to Speechreading." *Quart. J. Exp. Psychol.*

Grant, K.W., and L.D. Braida. "Evaluating the Articulation Index for Audiovisual Input." *J. Acoust. Soc. Am.*

Griffith, M., G. Langston, M. Heflin, S. Conner, and B. Burke. "The Fourth MIT-Green Bank 5 GHz Survey." *Astrophys. J.*

Habashy, T.M., S.M. Ali, J.A. Kong, and M.D. Grossi. "Dyadic Green's Functions in a Planar Stratified, Arbrarily Magnetized Linear Plasma." *Radio Sci.*

Hartney, M.A., D.C. Shaver, M.I. Shepard, J.S. Huh, and J. Melngailis. "Silylation of Focused Ion Beam Exposed Resists." *Appl. Phys. Lett.*

Haus, H.A., and W.P. Huang. "Coupled Mode Theory." *IEEE Proc.*

Huang, K.G., D. Gibbs, D.M. Zehner, A.R. Sandy, and S.G.J. Mochrie. "Phase Behavior of the Au(111) Surface: Discommensurations and Kinks." *Phys. Rev. Lett.*

Ismail, K., P.F. Bagwell, T.P. Orlando, D.A. Antoniadis, and H.I. Smith. "Quantum Phenomena in Field-Effect-Controlled Semiconductor Nanostructures." *IEEE Proc.*

Kazeroonian, A.S., T.L. Cheng, S.D. Brorson, Q. Li, E.P. Ippen, X.D. Wu, T. Venkatesan, S. Etemad, M.S. Dresselhaus, and G. Dresselhaus. "Probing the Fermi Level of $Y_{1-x}Pr_xBa_2Cu_3O_{7-\delta}$ by Femtosecond Spectroscopy." *Solid State Commun.*

Keane, D.T., P.A. Bancel, G.L. Jordan-Sweet, G.A. Held, A. Mak, and R.J. Birgeneau. "Evidence for Two-Step Disordering of the Au(110) 1 x 2 Reconstructed Surface" *Surf. Sci.*

Lezec, H.J., C.R. Musil, J. Melngailis, L.J. Mahoney, and J.D. Woodhouse. "Dose-Rate Effects in Focused-Ion Beam Implantation of Si into GaAs." *J. Vac. Sci. Technol. B.*

Liou, C-Y., and B.R. Musicus. "Approximation of Structured Covariance Matrices via Minimum Cross Entropy." *IEEE Trans. Acoust. Speech, Signal Process.*

Lumsdaine, A., J.L. Wyatt, Jr., and I.M. Elfadel. "Nonlinear Analog Networks for Image Smoothing and Segmentation." *J. VLSI Sig. Process.*

Melngailis, J. "Focused Ion Beam Induced Deposition - A Review." *SPIE Proc.* Vol. 1465.

Migliuolo, S. "Collisional Viscosity and Ion FLR Effects on Resistive Internal Kink Modes." *Nuclear Fusion.*

Mollenauer, L.F., S.G. Evangelides, and H.A. Haus. "Long Distance Soliton Propagation Using Lumped Amplifiers and Dispersion-Shifted Fiber." *J. Light Tech.*

Moores, J.D., K. Bergman, H.A. Haus, and E.P. Ippen. "Optical Switching Using Fiber Ring Reflectors." *J. Opt. Soc. Am. B.*

Moores, J.D., K. Bergman, H.A. Haus, and E.P. Ippen. "Demonstration of Optical Switching via Solitary Wave Collisions in a Fiber Ring Reflector." *Opt. Lett.*

Murgia, J.E., M.I. Shepard, J. Melngailis, A.L. Lattes, and S.C. Munroe. "Increase in Speed of Silicon CCD's with Channels Implanted using a Focused Ion Beam." *J. Vac. Sci. Technol.*

Needels, M., J.D. Joannopoulos, Y. Bar-Yam, and S.T. Pantelides. "Oxygen Complexes in Silicon." *Phys. Rev. B.*

Pang, X.D., H.Z. Tan, and N.I. Durlach. "Manual Discrimination of Force Using Active Finger Motion." *Percep. Psychophys.*

Peake, W.T., and J.J. Rosowski. "Impedance Matching, Optimum Velocity and Ideal Middle Ears." *Hear. Res.*

Perkell, J.S., E.B. Holmberg, R.E. Hillman. "A System for Signal Processing and Data Extraction from Aerodynamic, Acoustic and Electroglottographic Signals in the Study of Voice Production." *J. Acoust. Soc. Am.*

Ram, A.K., and A. Bers. "Propagation and Damping of Mode Converted Ion-Bernstein Waves in Toroidal Plasmas." *Phys. Fluids B.*

Rediker, R.H., K.A. Rauschenbach, and R.P. Schloss. "Operation of a Coherent Ensemble of Five Diode Lasers in an External Cavity." *IEEE J. Quantum Electron.*

Reed, C.M., M.H. Power, N.I. Durlach, L.D. Braida, K.K. Foss, J.A. Reid, and S.R. Dubois. "Development and Testing of Artificial Low-Frequency Speech Codes." *J. Rehabil. Res. Dev.*

Reichelt, M., J. White, and J. Allen. "Waveform Relaxation for Transient Two-Dimensional Simulation of MOS Devices." *IEEE Trans. Comput-Aided Des.*

Rosowski, J.J. "The Effects of External- and Middle-Ear Filtering on Auditory Threshold and Noise-Induced Hearing Loss." *J. Acoust. Soc. Am.*

Rosowski, J.J., and A. Graybeal. "What Did Morganucodon Hear?" *Zool. J. Linnean Soc.*

Rubinstein, J.T. "An Analytical Model for Electrical Stimulation of Nerve 2: Passive Myelinated Axon." *Biophys. J.*

Sandy, A.R., S.G.J. Mochrie, D.M. Zehner, K.G. Huang, and D. Gibbs. "Phase Behavior of the Au(111) Surface: X-ray Scattering Studies." *Phys. Rev. B.*

Sarpeshkar, R., J.L. Wyatt, Jr., N.C. Lu, and P.D. Gerber. "Mismatch Sensitivity of a Simultaneously Latched CMOS Sense Amplifier." *IEEE J. Solid-State Circuits.*

Schoenlein, R.W., J.G. Fujimoto, G.L. Eesley, and T.W. Capehart. "Femtosecond Relaxation Dynamics of Image-Potential States." *Phys. Rev. B.*

Shapiro, J.H., S.R. Shepard. "New Perspectives on Quantum Phase Measurement." *Phys. Rev. A.*

Shirasaki, M., and H.A. Haus. "Noise Reduction in Quantum Nondemolition Measurement of Nonlinear Mach-Zehnder Interferometer Using Squeezed Vacuum." *J. Opt. Soc. Amer. B.*

Stevens, K.N., and C.A. Bickley. "Constraints among Parameters Simplify Control of Klatt Formant Synthesizer." *J. Phon.*

Tulintseff, A.N., S.M. Ali, and J.A. Kong. "Input Impedance of a Probe-Fed Stacked Circular Microstrip Antenna." *IEEE Trans. Antennas Propag.*

Vlcek, J.C., and C.G. Fonstad. "Precise Computer Control of the MBE Process - Application of Graded InGaAlAs/InP Alloys." *J. Cryst. Growth.*

Wilson, B.S., C.C. Finley, D.T. Lawson, R.D. Wolford, D.K. Eddington, and W.M. Rabinowitz. "New Levels of Speech Recognition with Cochlear Implants." *Nature.*

Wornell, G.W., and A.V. Oppenheim. "Estimation of Fractal Signals From Noisy Measurements Using Wavelets." *IEEE Trans. Acoust., Speech, Signal Proc.*

Yoo, B.S., X.C. Liu, A. Petrou, J-P. Cheng, A.A. Reeder, B.D. McCombe, K. Elcess, and C.G. Fonstad. "Optical and Intrared Studies of (111) InGaAs/AlGaAs Strained-Layer Superlattices." *J. Superlattices Microstruct.*

Yueh, S.H., and J.A. Kong. "Analysis of Diffraction from Chiral Gratings." *J. Electromag. Waves Appl.*

Yueh, H.A., J.A. Kong, R.T. Shin, H.A. Zebker, and T. LeToan. "K-distribution and Multi-Frequency Polarimetric Terrain Radar Clutter." *J. Electromag. Waves Appl.*

A.2.3 Journal Articles Submitted for Publication

Abernathy, D.L., S.G.J. Mochrie, D.M. Zehner, G. Gröbel, and D. Gibbs. "Orientational Epitaxy and Lateral Structure of the Hexagonally Reconstructed Pt(001) and Au(001) Surfaces." *Phys. Rev. B.*

Alerhand, O.L., A.N. Berker, J.D. Joannopoulos, D. Vanderbilt, R.J. Hamers, and J.E. Demuth. "Reply to Comment LTK412 by N.C. Bartlett, T.L. Einstein, and C. Rottman." *Phys. Rev. Lett.*

Ali, S.M., T.M. Habashy, and J.A. Kong. "Dyadic Green's Functions for Multilayered Uniaxially Anisotropic Media." *J. Electromag. Waves Appl.*

Bagwell, P.F., and A. Kumar. "Comment on Effects of Channel Opening and Disorder on the Conductance of Narrow Wires." *Phys. Rev. B.*

Bahl, S.R., W.J. Azzam, and J.A. del Alamo. "Strained-Insulator InAlAs/n^+-InGaAs Heterostructure Field- Effect Transistors." *IEEE Trans. Electron Dev.*

Beckmann, P.E., and B.R. Musicus. "Fault-Tolerant Round-Robin A/D Converter System." *IEEE Trans. Circuits Syst.*

Bergman, K., and H.A. Haus. "Squeezing in Fibers with Optical Pulses." *Opt. Lett.*

Broekaert, T.P.E., and C.G. Fonstad. "AlAs Etch-Stop Layers for InGaAlAs/InP Heterostructure Devices and Circuits." *IEEE Trans. Electron. Dev.*

Corcoran, C., and R.H. Rediker. "Operation as a Coherent Ensemble of Five Discrete Diode Lasers Fiber-Coupled into an External Cavity." *Appl. Phys. Lett.*

Davis, R.L., and W.F. Sewell. "Neurite Regeneration From Single Primary-Auditory Neurons in vito." *J. Neurosci.*

Geis, M.W., and H.I. Smith. "Large-Area Mosaic Diamond Films Approaching Single-Crystal Quality." *Appl. Phys. Lett.*

Gibbs, D., G. Gröbel, M. Zehner, D.L. Abernathy, and S.G.J. Mochrie. "Rotational Transformation of the Pt(001) Surface." *Phys. Rev. Lett.*

Gu, Q., D.M. Sheen, S.M. Ali, and J.A. Kong. "Transient Analysis in Frequency-Dependent

Systems with Nonlinear Terminations." *IEEE Trans. Microwave Theory Tech.*

Hagelstein, P.L. "Design of a Nearly Stigmatic Toroidal Spectrometer." *Appl. Opt.*

Hagelstein, P.L. "Coherent Neutron Transfer Reactions." *J. Fusion Tech.*

Hagelstein, P.L., and I.L. Chuang. "Approximations to the Single Photon Exchange Interaction with Full Retardation." *J. Phys. B.*

Halle, M., and K.N. Stevens. "The Postalveolar Fricatives of Polish." *Osamu Fijimura Festschrift.*

Haus, H.A. "Quantum Noise in Soliton-Like Repeater System." *J. Opt. Soc. Am. B.*

Haus, H.A., U. Keller, and W.H. Knox. "A Theory of Coupled Cavity Modelocking with a Resonant Nonlinearity." *J. Opt. Soc. Am. B.*

Ho, S.T., N.C. Wong, and J.H. Shapiro. "Single-Beam Squeezed State Generation in Sodium Vapor and its Self-Focusing Limitations." *Opt. Lett.*

Ismail, K., F. Legoues, N.H. Karam, J. Carter, and H.I. Smith. "High Quality GaAs on Sawtooth-Patterned Si Substrates." *Appl. Phys. Lett.*

Kumar, A., and P.F. Bagwell. "Resonant Tunneling in a Quasi-One-Dimensional Wire: Influence of Evanescent Modes." *Phys. Rev. B.*

Kumar, A., S.E. Laux, and F. Stern. "Electron States in a GaAs Quantum Dot in a Magnetic Field." *Phys. Rev. B.*

Kuo, C.C., P.W. Rosenkranz, and D.H. Staelin. "Statistical Iterative Scheme for Estimating Atmospheric Relative Humidity Profiles." *IEEE Trans. Geosci. Remote Sens.*

Lam, C.W., S.M. Ali, and J.A. Kong. "Finite-Difference Time-Domain Method for Single and Coupled Microstrip Lines." *IEEE Trans. Microwave Theory Tech.*

Lane, H., J.S. Perkell, M. Svirsky, and J. Webster. "Changes in Speech Breathing Following Cochlear Implant in Postlingually Deafened Adults." *J. Speech Hear. Res.*

Liu, C.T., D.C. Tsui, M. Shayegan, K. Ismail, D.A. Antoniadis, and H.I. Smith. "Guiding-Center-Drift Resonance of Two-Dimensional Electrons in a Grid-Gate Superlattice Potential." *Appl. Phys. Lett.*

Mak, A., K. Evans-Lutterodt, K. Blum, D.Y. Noh, J.D. Brock, G.A. Held, and R.J. Birgeneau. "Synchrotron X-ray Diffraction Study of the Disordering of the Ge(111) Surface at High Temperatures." *Phys. Rev. Lett.*

Meir, Y., N. Wingreen, and P.A. Lee. "Transport Through a Strongly Interacting Electron System: Theory of Periodic Conductance Oscillations." *Phys. Rev. Lett.*

Milios, E.E., and S.H. Nawab. "Acoustic Tracking from CPA Time, Amplitude, and Frequency at Spatially Distributed Sensors." *J. Acoust. Soc. Am.*

Muendel, M.H., and P.L. Hagelstein. "Four-Wave Frequency Conversion of Coherent Soft X-rays." *Phys. Rev. A.*

Muendel, M.H., P.L. Hagelstein, and L.B. DaSilva. "Predicted Four-Wave Mixing Rates for Neonlike Yttrium X-ray Laser Radiation in a Sodiumlike Calcium Plasma." *Phys. Rev. A.*

Musicus, B.R., and W.S. Song. "Fault-Tolerant Digital Signal Processing via Generalized Likelihood Ratio Tests." *IEEE Trans. Acoust., Speech, Signal Process.*

Musicus, B.R., and W.S. Song. "Fault-Tolerant Architecture for a Parallel Digital Signal Processing Machine." *IEEE Trans. Computing.*

Ocko, B.M., D. Gibbs, K.G. Huang, D.M Zehner, and S.G.J. Mochrie. "Structure and Phases of the Au(001) Surface: X-ray Reflectivity." *Phys. Rev. B.*

Payne, M., D. Allan, M. Teter, and J.D. Joannopoulos. "Iterative Minimization Techniques for Ab-Initio Total Energy Calculations." *Rev. Modern Phys.*

Peng, L-H., T.P.E. Broekaert, W-Y. Choi, C.G. Fonstad, and V. Jones. "Defect Activated Infrared Multi-phonon Excitation in Fe-doped Semi-insulating InP." *Appl. Phys. Lett.*

Perkell, J.S., and M.H. Cohen. "Token-to-token Variation of Tongue-body Vowel Targets: the Effect of Context." *Osamu Fijimura Festschrift.*

Perkell, J.S., and M.L. Matthies. "Temporal Measures of Labial Coarticulation for the Vowel /u/." *J. Acoust. Soc. Am.*

Rankovic, C.M., R.L. Freyman, and P.M. Zurek. "Potential Benefits of Varying the Frequency-

Gain Characteristic for Speech Reception in Noise." *J. Acoust. Soc. Am.*

Reed, C.M., W.M. Rabinowitz, N.I. Durlach, L.A. Delhorne, L.D. Braida, J.C. Pemberton, B.D. Mulcahey, and D.L. Washington. "Analytic Study of the Tadoma Method: Improving Performance Through the Use of Supplementary Tactual Displays." *J. Speech Hear. Res.*

Schattenburg, M.L., C.R. Canizares, D. Dewey, K.A. Flanagan, M.A. Hamnett, A.M. Levine, K.S.K. Lum, R. Manikkalingam, T.H. Markert, and H.I. Smith. "Transmission Grating Spectroscopy and the Advanced X-ray Astrophysics Facility (AXAF)." *Opt. Eng.*

Shattuck-Hufnagel, S. "The Role of Word and Syllable Structure in Phonological Encoding in English." *Cognition* (special issue).

Tabei, M., B. Musicus, and M. Ueda. "A Maximum Likelihood Estimator for Frequency and Decay Rate." *IEEE Trans. Acoust., Speech, Signal Process.*

Tsuk, M.J., and J.A. Kong. "A Hybrid Method for the Calculation of the Resistance and Inductance of Transmission Lines with Arbitrary Cross-Sections." *IEEE Trans. Microwave Theory Tech.*

Tulintseff, A.N., S.M. Ali, and J.A. Kong. "Resonant Frequencies of Stacked Circular Microstrip Antennas." *IEEE Proc.*

Umminger, C.B., and C.G. Sodini. "Switched Capacitor Networks for Monolithic Image Processing Systems." *IEEE J. Solid-State Circuits.*

A.3 Books/Chapters in Books

Alerhand, O.L., A.N. Berker, J. D. Joannopoulos, and D. Vanderbilt. "Phase Transitions on Misoriented Si(100) Surfaces." In *Proceedings of the 20th International Conference on the Physics of Semiconductors.* Ed. J.D. Joannopoulos. Singapore: World Scientific, 1990.

Atkins, R.G., R.T. Shin, and J.A. Kong. "A Neural Net Method for High Range Resolution Target Classification." In *Progress in Electromagnetic Research* 4(7):255-292. Ed. J.A. Kong. New York: Elsevier, 1990.

Berker, A.N., and K. Hui. "Absence of Temperature-Driven First-Order Phase Transitions in Systems with Random Bonds." In *Science and Technology of Nanostructured Magnetic Materials.* Eds. G.C. Hadjipanayis, G. Prinz, and L. Paretti. New York: Plenum Press, 1990.

Braud, J.P. "Adiabatic Whisper-Gallery Cavities for EUV and Soft X-ray Laser Cavities." In *Proceedings of the International Conference on Lasers '89,* Society for Optical and Quantum Electronics, pp. 37-39. Eds. D.G. Harris and T.M. Shay. McLean, Virginia: STS Press, 1990.

Ceyer, S.T., D.J. Gladstone, M. McGonigal, and M.T. Schulberg. "Molecular Beams: Probes of the Dynamics of Reactions on Surfaces." In *Physical Methods of Chemistry,* Second Edition. Eds. B.W. Rossiter, J.F. Hamilton, and R. C. Baetzold. New York: Wiley, 1991.

Gentile, T.R., B.J. Hughey, T.W. Ducas, and D. Kleppner. "Experimental Study of Two-Photon Rabi Oscillations." In *Coherence and Quantum Optics VI.* Ed. J.H. Eberly et al. New York: Plenum Press, 1990.

Hughey, B.J., T.R. Gentile, T.W. Ducas, and D. Kleppner. "Atom-Photon Interaction Modified by a Microwave Cavity." In *Coherence and Quantum Optics VI.* Ed. J.H. Eberly et al. New York: Plenum Press, 1990.

Keith, D.W., and D.E. Pritchard. "Atom Optics." In *New Frontiers in Quantum Electrodynamics and Quantum Optics.* Ed. A.O. Barut. New York: Plenum Press, 1990.

Kiang, J.F., S.M. Ali, and J.A. Kong. "Modelling of Lossy Microstrip Lines with Finite Thickness." In *Progress in Electromagnetic Research* 4(3):85-117. Ed. J.A. Kong. New York: Elsevier, 1990.

Kolodziejski, L.A., R.L. Gunshor, A.V. Nurmikko, and N. Otsuka. "Molecular Beam Epitaxy of Wide Gap II-VI Semiconductor Heterostructures." In *Molecular Beam Epitaxy.* Eds. R.F.C. Farrow, and J.R. Arthur. New York: Noyes Publishers, 1991.

Kolodziejski, L.A., and J.J. Coleman. *Quantum Well Heterostructures and Superlattices.* Piscataway, New Jersey: IEEE Publications, 1991.

Kong, J.A., S.H. Yueh, H.H. Lim, R.T. Shin, and J.J. van Zyl. "Classification and Maximum Contrast of Earth Terrain Using Polarimetric Synthetic Aperture Radar Images." In *Progress in Electromagnetic Research* 3(6):327-370. Ed. J.A. Kong. New York: Elsevier, 1990.

LaMotte, R.H., and M.A. Srinivasan. "Surface Microgeometry: Neural Encoding and Perception." In *Information Processing in the Somatosensory System,* Wenner-Gren International Symposium Series. Eds. O. Franzen, and J. Westman. New York: Macmillan Publishing, 1990.

Lee, C.F., R.T. Shin, and J.A. Kong. "Fine Difference Method for Electromagnetic Scattering Problems." In *Progress in Electromagnetic Research* 4(11):373-442. Ed. J.A. Kong. New York: Elsevier, 1990.

Lee, P.A. "Normal State Properties of the Oxide Superconductors: A Review." In *High Temperature Superconductivity Proceedings,* p. 96. Ed. K.S. Bedell et al. Reading, Massachusetts: Addison-Wesley, 1990.

McKay, S.R., and A.N. Berker. "Magnetization of the d-Dimensional Random-Field Ising Model: An Intermediate Critical Dimension." In *New Trends in Magnetism.* Eds. M.D. Coutinho-Filho and S.M. Rezende. Singapore: World Scientific, 1990.

Nelson, K.A. "Impulsive Stimulated Raman Scattering with Single-pulse and Multiple-pulse Excitation." In *Proceedings of the 12th International Conference on Raman Spectroscopy,* pp. 19-22. Eds. J.R. Durig and J.F. Sullivan. Chichester: Wiley, 1990.

Mochrie, S.G.J., D. Gibbs, and D.M. Zehner. "X-ray and Neutron Scattering Studies of the Structure and Phase Behavior of Interfaces." In *Physics News in 1990.* New York: American Institute of Physics, Forthcoming.

Nghiem, S.V., M. Borgeaud, J.A. Kong, and R.T. Shin. "Polarimetric Remote Sensing of Geophysical Media with Layer Random Medium Model." In *Progress in Electromagnetic Research* 1(3):1-73. Ed. J.A. Kong. New York: Elsevier, 1990.

Perkell, J.S. "Testing Theories of Speech Production, Implications of Some Detailed Analyses of Variable Articulatory Data." In *Speech Production and Speech Modeling.* Eds. W.J. Hardcastle and A. Marchal. Boston, Massachusetts: Kluwer Academic Publishers, 1990.

Pritchard, D.E. "Atom Optics." In *Yearbook of Science and Technology.* New York: McGraw-Hill, 1990.

Ram, A.K., and A. Bers. "Absolute Versus Convective Analysis of Instabilities in Space Plasmas." In *SPI Conference Proceedings and Reprint Series,* Number 10. Eds. T. Chang, G.B. Crew, and J.R. Jasperse. Cambridge, Massachusetts: Scientific Publishers, 1991.

Reed, C.M., N.I. Durlach, and L.A. Delhorne. "Natural Methods of Tactual Communication." In *Tactile Aids for the Hearing Impaired.* Ed. I.R. Summers. New York: Taylor and Francis Ltd., 1990.

Rosowski, J.J. "Hearing in Transitional Mammals: Predictions From the Middle-Ear Anatomy and Hearing Capabilities of Extant Mammals." In *The Evolutionary Biology of Hearing.* Eds. A.N. Popper, R.R. Ray, and D.B. Webster. New York: Springer-Verlag. Forthcoming.

Shapiro, J.H., S.R. Shepard, and N.C. Wong. "A New Number-Phase Uncertainty Principle." In *Coherence and Quantum Optics VI.* Eds. L. Mandel, E. Wolf, and J.H. Eberly. New York: Plenum Press, 1990.

Shapiro, J.H., S.R. Shepard, and N.C. Wong. "Coherent Phase States and Squeezed Phase States." In *Coherence and Quantum Optics VI.* Eds. L. Mandel, E. Wolf, and J.H. Eberly. New York: Plenum Press, 1990.

Srinivasan, M.A., and R.H. LaMotte. "Encoding of Shape in the Responses of Cutaneous Mechanoreceptors." In *Information Processing in the Somatosensory System,* Wenner-Gren International Symposium Series. Eds. O. Franzen, and J. Westman. New York: Macmillan Publishing, 1990.

Srinivasan, M.A. "Tactual Interfaces: The Human Perceiver." In *Human-Machine Interfaces for Teleoperators and Virtual Environments.* Eds. N.I. Durlach, T. Sheridan, and S. Ellis. NASA Report, 1990.

Srinivasan, M.A, and R.H. LaMotte. "Tactile Discrimination and Representation of Texture, Shape, and Softness." In *Human-Machine Interfaces for Teleoperators and Virtual Environments.* Eds. N.I. Durlach, T. Sheridan, and S. Ellis. NASA Report, 1990.

Stevens, K.N. "Some Factors Influencing the Precision Required for Articulatory Targets: Comments on Keating's Paper." In *Papers in Laboratory Phonology I.* Eds. J.C. Kingston and M.E. Beckman. Cambridge: Cambridge University Press, 1990.

Weiner, A.M., D.E. Leaird, G.P. Wiederrecht, M.J. Banet, and K.A. Nelson. "Spectroscopy with Shaped Femtosecond Pulses: Styles for the 1990s." In *Picosecond and Femtosecond Spec-*

troscopy from Laboratory to Real World, SPIE Proc. 1209:185-197. Ed. K.A. Nelson. Bellingham, Washington: SPIE, 1990.

Weiner, A.M., D.E. Leaird, G.P. Wiederrecht, and K.A. Nelson. "Femtosecond Optical Control Over Molecular Motion." In *Physics News in 1990,* pp. 25-26. Ed. P.F. Schewe. New York: AIP, 1990.

Yueh, S.H., J.A. Kong, J.K. Jao, R.T. Shin, H.A. Zebker, T. LeToan, and H. Öttl. "K-distribution and Polarimetric Terrain Radar Clutter." In *Progress in Electromagnetic Research* 3(4):237-275. Ed. J.A. Kong. New York: Elsevier, 1990.

Yueh, S.H., J.A. Kong, and R.T. Shin. "Calibration of Polarimetric Radars Using In-Scene Reflectors." In *Progress in Electromagnetic Research* 3(9):451-510. Ed. J.A. Kong. New York: Elsevier, 1990.

A.4 RLE Publications

These materials, except those as noted, may be obtained by writing the Communications Office, Building 36-412, Research Laboratory of Electronics, Massachusetts Institute of Technology, Cambridge, Massachusetts 02139-4307, at the listed cost.

Prepayment is required. Please include a check payable to MIT RLE and allow six to eight weeks for surface mail. For foreign airmail, include an additional $4.00 for each report ordered.

RLE currents 3(2): (1990). Topic: Image Processing at RLE. 20 pp. No charge.

RLE currents 4(1): (1990). Topic: Radio Astronomy at RLE. 20 pp. No charge.

RLE Progress Report No. 132: January - December 1989. MIT, 1990. 404 pp. No charge.

Bace, M.M. *A Receiver-Compatible Noise Reduction System.* RLE TR-553. MIT, 1990. $14.00.

Baylon, D.M., and J.S. Lim. *Transform/Subband Analysis and Synthesis of Signals.* RLE TR-559. MIT, 1990. $6.00.

Beckman, P.E., and B.R. Musicus. *Fault-Tolerant Round Robin A/D Converter System.* RLE TR-561. MIT, 1990. $10.00.

Brorson, S.D. *Femtosecond Thermomodulation Measurements of Transport and Relaxation in Metals and Superconductors.* RLE TR-557. MIT, 1990. $17.00.

Cobra, D.T. *Estimation and Correction of Geometric Distortions in Side-Scan Sonar Images.* RLE TR-556. MIT, 1990. $14.00.

Piot, J. *Adaptive Frequency Modulation for Satellite Television Systems.* RLE TR-554. MIT, 1990. $15.00.

Randolph, M.A. *Syllable-based Constraints on Properties of English Sounds.* RLE TR-555. MIT, 1990. $17.00.

Song, W.S., and B.R. Musicus. *A Fault-Tolerant Multiprocessor Architecture for Digital Signal Processing Applications.* RLE TR-552. MIT, 1990. $15.00.

Tom, A.S. *Channel Equalization and Interference Reduction Using Scrambling and Adaptive Amplitude Modulation.* RLE TR-558. MIT, 1990. $14.00.

Weinstein, E., A.V. Oppenheim, and M. Feder. *Signal Enhancement Using Single and Multi-Sensor Measurements.* RLE TR-560. MIT, 1990. $8.00.

Zangi, K.C. *A Novel QMF Design Algorithm.* RLE TR-551. MIT, 1990. $10.00.

A.5 Theses

Akerson, J.J. *A Monolithic Dual-Gate Mesfet Circuit for L-Band Mixers.* S.M. thesis, Dept. of Electr. Eng. and Comput. Sci., MIT, 1990.

Amparan, A.B. *Measurements of Antireflection Coatings on AlGaAs Diode Lasers.* S.B. thesis, Dept. of Electr. Eng. and Comput. Sci., MIT, 1990.

Bagwell, P.F. *Quantum Mechanical Transport in Submicron Electronic Devices.* Ph.D. diss., Dept. of Electr. Eng. and Comput. Sci., MIT, 1990.

Bossi, D.E. *Reduced-Confinement GaAlAs Tapered Waveguide Antennas.* Ph.D. diss., Dept. of Electr. Eng. and Comput. Sci., MIT, 1990.

Brabson, A.R. *Stimulated Brillouin Scattering in a Fiber Reflector Ring.* S.M. thesis, Dept. of Electr. Eng. and Comput. Sci., MIT, 1990.

Cho, J. *Effect of Microstructure of Aluminum Alloys on the Electromigration-Limited Reliability of VLSI Interconnects.* Ph.D. diss., Dept. of Mater. Sci. and Eng., MIT, 1990.

Chu, N.C. *Phase Fluctuations of Waves Propagating Through a Random Medium.* S.M. thesis, Dept. of Electr. Eng. and Comput. Sci., MIT, 1990.

Cornell, E.A. *Mass Spectroscopy Using Single Ion Cyclotron Resonance.* Ph.D. diss., Dept. of Physics, MIT, 1990.

DiRienzo, A.C. *Experimental Observations of Microwave Emission from a 35 GHz Cyclotron Autoresonance Maser.* Ph.D. diss., Dept. of Physics, MIT, 1990.

Duanmu, S. *A Formal Study of Syllable, Tone, Stress and Domain in Chinese Languages.* Ph.D. diss., Dept. of Linguistics and Philosophy, MIT, 1990.

Dubner, A.D. *Mechanisms of Ion Beam Induced Deposition.* Ph.D. diss., Dept. of Mater. Sci. and Eng., MIT, 1990.

Goodberlet, J.G. *Passively Mode-Locked Ti:Al_2O_3 Laser with a Nonlinear External Cavity.* S.M. thesis, Dept. of Electr. Eng. and Comput. Sci., MIT, 1990.

Hannon, S.M. *Detection Processing for Multidimensional Laser Radars.* Ph.D. diss., Dept. of Electr. Eng. and Comput. Sci., MIT, 1990.

Heflin, M.B.. *Milliarcsecond Structure of the Radio Source 2016+112.* Ph.D. diss., Dept. of Physics, MIT, 1990.

Hendrix, D.K. *Development of an In Vitro Preparation of the Alligator Lizard Cochlear Duct.* S.M. thesis, Dept. of Electr. Eng. and Comput. Sci., MIT, 1990.

Hou, A.S. *Chirp in Actively Modelocked Diode Lasers.* S.B. and S.M. thesis, Dept. of Electr. Eng. and Comput. Sci., MIT, 1990.

Ito, Y. *Auditory Discrimination of Power Spectra for Roving Two-Tone Stimuli.* Ph.D. diss., Dept. of Electr. Eng. and Comput. Sci., MIT, 1990.

Iu, C. *Energy Level Structure of Atoms in Magnetic Fields.* Ph.D. diss., Dept. of Physics, MIT, 1990.

Jiran, E. *Capillary Instabilities in Thin, Solid Films.* Ph.D. diss., Dept. of Mater. Sci. and Eng., MIT, 1990.

Kashani, A. *A Reservation-based Scheduler for CAFE.* S.M. thesis, Dept. of Electr. Eng. and Comput. Sci., MIT, 1990.

Khatri, F.I. *Simulations of Additive Pulse Modelocked Laser Start-Up.* S.B. thesis, Dept. of Electr. Eng. and Comput. Sci., MIT, 1990.

Lee, C.F. *Finite Difference Method for Electromagnetic Scattering Problems.* Ph.D. diss., Dept. of Electr. Eng. and Comput. Sci., MIT, 1990.

Leong, K.W. *Intensity Quantum Noise Reduction with an Above-Threshold Optical Parametric Oscillator.* Ph.D. diss., Dept. of Electr. Eng. and Comput. Sci., MIT, 1990.

Millier, K.M. *Intelligibility of Vowels Represented by Multiple Intra-Speaker Tokens.* S.B. thesis, Dept. of Electr. Eng. and Comput. Sci., MIT, 1990.

Oldaker, B.G. *Multi-Photon Momentum Transfer from Light to Atoms.* Ph.D. diss., Dept. of Physics, MIT, 1990.

Ma, J. *The Effects of Probe Correction Error on the Planar Near-Field Calibration of a Beacon Tracking Antenna.* S.B. and S.M. thesis, Dept. of Electr. Eng. and Comput. Sci., MIT, 1990.

McCann, P. *Heteroepitaxial Growth of IV-VI Semiconductors on Barium Flouride.* Ph.D. diss., Dept. of Mater. Sci. and Eng., MIT, 1990.

Meirav, U. *Single Electron Charging and Periodic Conductance Oscillations Gallium Arsenide Nanostructures.* Ph.D. diss., Dept. of Physics, MIT, 1990.

Mentle, R.E. *Laser Radar Performance Theory for Track-While-Image Operation.* S.M. thesis, Dept. of Electr. Eng. and Comput. Sci., MIT, 1990.

Moskowitz, W.P. *Differential Cross Sections for Na_2-Ar Collisions.* Ph.D. diss., Dept. of Physics, MIT, 1990.

Oldaker, B.G. *Multi-Photon Momentum Transfer from Light to Atoms.* Ph.D. diss., Dept. of Physics, MIT, 1990.

Park, S.L. *The Anomalous Magnetoresistance of the Electron Gas in a Restricted Geometry.* Ph.D. diss., Dept. of Physics, MIT, 1990.

Phillips, M.R. *Near Band-gap Optical Nonlinearities in InGaAs/InAlAs Multiple Quantum Well Structures.* Ph.D. diss., Dept. of Electr. Eng. and Comput. Sci., MIT, 1990.

Schulberg, M.T. *The Reaction of Molecular Fluorine with Silicon(100): Adsorption, Desorption, and Scattering Dynamics.* Ph.D. diss., Dept. of Chem., MIT, 1990.

Schwonek, J.P. *A Study of a Cold Atomic Hydrogen Beam Source.* S.B. thesis, Dept. of Physics, MIT, 1990.

Scott-Thomas, J.L. *Conductance Oscillations Periodic in the Charge Density of One-Dimensional MOSFET Structures.* Ph.D. diss., Dept. of Physics, MIT, 1990.

Taylor, L. *Token Variability of Intra-Speaker Speech: Fricative Consonant Sounds.* S.B. thesis, Dept. of Electr. Eng. and Comput. Sci., MIT, 1990.

The, S.C *A Self-Aligned NMOS Process Using X-ray Lithography.* S.M. thesis, Dept. of Electr. Eng. and Comput. Sci., MIT, 1990.

Tsuk, M.J. *Propagation and Interference in Lossy Microelectronic Integrated Circuits.* Ph.D. diss., Dept. of Electr. Eng. and Comput. Sci., MIT, 1990.

Tulintseff, A.N. *A Theoretical Analysis of a Probe-Fed Stacked Circular Microstrip Antenna.* Ph.D. diss., Dept. of Electr. Eng. and Comput. Sci., MIT, 1990.

Umminger, C.B. *Switched Capacitor Networks for Machine Vision.* S.M. thesis, Dept. of Electr. Eng. and Comput. Sci., MIT, 1990.

Wang, L. *Two Talker Activity Labelling by Humans.* S.B. thesis, Dept. of Electr. Eng. and Comput. Sci., MIT, 1990.

Yang, W. *The Architecture and Design of CCD Processors for Computer Vision.* Ph.D. diss., Dept. of Electr. Eng. and Comput. Sci., MIT, 1990.

A.6 Miscellaneous

Chow, C.C., V. Fuchs, and A. Bers. "Reflection at the Resonance Layer of the Fast Alfvén Wave in Ion Cyclotron Heating." *Plasma Fusion Center Report* PFC/JA-90-2. MIT, 1990.

Chow, C.C., A.K. Ram, and A. Bers. "Bandwidth of Scattered Radiation in Laser-Plasma Interactions." *Plasma Fusion Center Report* PFC/JA-90-24. MIT, 1990.

Davis, R.L. "Specificity of VIIIth Nerve Regeneration in Lower Vertebrates." *J. Exp. Zool.* (mini-review from a neurosciences symposium entitled: "Molecular and Cellular Events in Development and Regeneration," submitted for review).

Kupfer, K., A. Bers, and A.K. Ram. "Guiding Center Stochasticity and Transport Induced by Electrostatic Waves." *Plasma Fusion Center Report* PFC/JA-90-22. MIT, 1990.

Ram, A.K., and A. Bers. "Absolute Versus Convective Analysis of Instabilities in Space Plasmas." *Plasma Fusion Center Report* PFC/JA-91-2. MIT, 1991.

Ram, A.K., and A. Bers. "Propagation and Damping of Mode Converted Ion-Bernstein Waves in Toroidal Plasmas." *Plasma Fusion Center Report* PFC/JA-90-20. MIT, 1990.

Troxel, D. "CAFE - The MIT Computer Aided Fabrication Environment." *Microsystems Technology Laboratories Microsystems Research Review.* MIT, 1990.

Appendix B. Current RLE Personnel

Director: Jonathan Allen
Associate Director: Daniel Kleppner

Professors

Jonathan Allen
Dimitri A. Antoniadis
Arthur B. Baggeroer
George Bekefi
A. Nihat Berker
Abraham Bers
Robert J. Birgeneau
Amar G. Bose
Louis D. Braida
Bernard E. Burke
Sylvia T. Ceyer
Sow-Hsin Chen
Bruno Coppi
Shaoul Ezekiel
Clifton G. Fonstad, Jr.
Lawrence S. Frishkopf
Hermann A. Haus
Albert Hill[1]
Erich P. Ippen
John D. Joannopoulos
Marc A. Kastner
Nelson Y.-S. Kiang
John G. King
Daniel Kleppner
Jin A. Kong
Patrick A. Lee
Jerome Y. Lettvin[1]
Jae S. Lim
Alan V. Oppenheim
William T. Peake
Miklos Porkolab
David E. Pritchard
William F. Schreiber
Campbell L. Searle
Jeffrey H. Shapiro
William M. Siebert
Henry I. Smith
David H. Staelin
Kenneth N. Stevens
Julius A. Stratton[1]
Donald E. Troxel
Thomas F. Weiss
Jerome B. Wiesner[1]
John L. Wyatt, Jr.
Henry J. Zimmermann[1]

Associate Professors

Jesus A. del Alamo
James G. Fujimoto
Peter L. Hagelstein
Keith A. Nelson
Carl V. Thompson III
Jacob K. White

Assistant Professors

Boris Altshuler
Srinivas Devadas
John M. Graybeal
Jacqueline N. Hewitt
Qing Hu
Leslie A. Kolodziejski
Simon G.J. Mochrie
Jonathan S. Wurtele

Senior Research Scientists

Nathaniel I. Durlach
John Melngailis
Joseph S. Perkell
Robert H. Rediker

Principal Research Scientists

John J. Guinan, Jr.
William M. Rabinowitz
Charlotte M. Reed
Philip W. Rosenkranz
Patrick M. Zurek

---

[1] Professor Emeritus.

Postdoctoral Fellows and Associates

Alice M. Berglund
Joan M. Besing
Suzanne Boyce
Peter A. Cariani
Arnaldo Dal Pino
Marie K. Huffman
Chun-Ho Iu
Wolfgang Ketterle
Yulin Li
Robert D. Meade
Son Van Nghiem
David Pullman
Christine M. Rankovic
Mario A. Svirsky
Rosalie M. Uchanski
Xin Xu
Simon H. Yueh

Research Scientists and Research Specialists

Sami M. Ali
Giovanni Aliberti
John W. Barrett
Santanu Basu
James M. Carter
Bertrand Delgutte
Lorraine A. Delhorne
Donald K. Eddington
Ronald C. Englade
Edward W. Fitzgerald
David W. Foss
Dennis M. Freeman
Seth M. Hall
Wilberto Martinez
Ivan Mastovsky
Melanie L. Matthies
Michael B. McIlrath
Stefano Migliuolo
Xiao Dong Pang
Abhay K. Ram
Barbara A. Roman
John J. Rosowski
Stefanie Shattuck-Hufnagel
Stephen C. Shepard
Mandayam A. Srinivasan
Linda E. Sugiyama
Ngai Chuen Wong
Ying-Ching E. Yang

Visiting Scientists

Lucio H. Acioli
Sunny Y.C. Auyang
Vladimir Barsukov
Giuseppe Bertin
Corine A. Bickley
Tomaz Catunda
Paolo Detragiache
Theodore W. Ducas
Carol Y. Espy-Wilson
Richard L. Freyman
Gad Geiger
Bernard Gold
Qizheng Gu
Yan-an Han
Toru Hara
Tetsuo Ichikawa
Lance G. Joneckis
Arthur K. Jordan
Janet D. Koehnke
Jack Kotik
James H. Kukula
Pierandrea Lo Nostro
Neil A. Macmillan
Alexander Martin
Antonio Mecozzi
Takahide Mizuno
Phylis Morrison
Kazunori Naganuma
Guilia A. Nassi
Marco Nassi
Kevin O'Neill
Karen L. Payton
Harold R. Raemer
Ramdas L. Ram-Mohan
Stanley J. Rosenthal
Masataka Shirasaki
Dominique J. Vignaud
Leonid E. Zakharov

Research Affiliates

John S. Barlow
Herbert J. Bernstein
Frank S. Cardarelli
Giuseppe Gabetta
Richard S. Goldhor
Philip R. Hemmer
Robert E. Hillman
Eva B. Holmberg
Caroline B. Huang
Joseph A. Jarrell
John D. Kierstead
Harlan Lane
John I. Makhoul
Bruce R. Musicus
Leonard L. Picard
Mara G. Prentiss
Stephen A. Raymond
Carol C. Ringo
Joseph F. Rizzo
Jay T. Rubinstein
Robert T. Shin
Richard J. Solomon
Frank J. Stefanov-Wagner
David A. Steffens
Jane W. Webster
Meng Yu Zhu

Research Assistants

Abeer Alwan
Michael Ames
Robert C. Armstrong
David V. Arnold
William W. Au
Babak Ayazifar
Ali J. Azarbayejani
Matthew M. Bace
Sandeep Bahl
Donald G. Baltus
David S. Barwick
David M. Baylon
Keren Bergman
Pierino G. Bonanni
Kevin R. Boyce
Michael Brandstein
John P. Braud
Tom P. Broekaert
Martin Burkhardt
Edmond Chalom
Claudio Chamon
Pin-P. Chang
Jyh-Shing Chen
Shiufun Cheung
Kyeongjae Cho
Kevin G. Christian
William Chu
Samuel R. Conner
Christopher J. Corcoran
Christopher A. Coronado
Kiran Dandekar
John T. Delisle
Daniel J. DiLorenzo
Paul Duchnowski
Scott B. Dynes
Kathleen R. Early
Farzad Ehsani
Christopher R. Ekstrom
John D. Ellithorpe
Darin Ernst
Marina Frants
Joseph A. Frisbie
Eric M. Fuchs
Thomas J. Green, Jr.
Mark E. Griffith
Ibrahim Hajjahmad
Katherine L. Hall
Hsiu C. Han
John C. Hardwick
Scott Hector
Michael R. Hee
Eason Ho
Jeffrey R. Holley
Chih-Chien Hsu
David Huang
Gregory T. Huang
Charles T. Hultgren
Janice M. Huxley
Erik B. Iverson
Hong Jiao
Michael A. Joffe
Mark A. Johnson
Abbas Kashani
Sumanth Kaushik
David W. Keith
Farzana I. Khatri
Songmin Kim
Wolfgang G. Knecht
Kenneth C. Kupfer
Yinchieh Lai
Cheung-Wei Lam
Kevin Lam
Suzanne D. Lau-Shiple
Dicky Lee
Hongsing Lee
Darren L. Leigh
Kenneth S. Liao
Harold H. Lim
Jennifer A. Lloyd
Robert I. Lutwak
Gregory R. Martin
Paul S. Martin
Robert E. Mentle
Alberto M. Moel
Michael C. Moldoveanu
Peter A. Monta
John D. Moores
Martin Muendel
Christian R. Musil
Keith S. Nabors
Vasant Natarajan
Julien J. Nicolas
John H. Oates
Scott N. Paine
Hanalabos Papadopoulos
Brian K. Pheiffer
Matthew H. Power
James C. Preisig
Khalid Rahmat
Malini Ramaswamy
Mark W. Reichelt
George E. Rittenhouse
Jae-Sang Ro
Partha Saha
Jon C. Sandberg
Hugh E. Secker-Walker
Mark N. Seidel
Mohamad S. Shahriar
David M. Sheen
Gennady Shvets
Luis M. Silveira
Richard A. Singer
Stephen P. Smith
Richard E. Stoner
Chi-Kuang Sun
Ke-Xun Sun
Lon E. Sunshine
Mohammad A. Tassoudji
Ricardo Telichevesky
Michael J. Tsuk
Morrison Ulman
Murat E. Veysoglu
Jesus Noel Villasenor
James Vlcek
David B. Walrod
Jing Wang
Robert J. Webster
Lorin F. Wilde
Timothy A. Wilson
Albert R. Woo
Gregory W. Wornell
Rolf A. Wyss
Jiqing Xia
Julius J. Yang
Chang D. Yoo
Peter T. Yu
Kambiz C. Zangi
Farhad Zarinetchi
Michael L. Zerkle

Teaching Assistants

Grace H. Chen
Chee W. Chia
Christopher A. Crowley
Ibrahim M. Elfadel
Yoshiko Ito
Joseph M. Jacobson
Kimberly Pace
Michael J. Schwartz
Andrew C. Singer

Graduate Students

Ashraf S. Alkhairy
John G. Apostolopoulos
Tomas A. Arias
Robert G. Atkins
Paul E. Beckmann
Karl K. Berggren
Scott I. Berkenblit
Riccardo Betti
Saurav Bhatta
Bradley T. Binder
John Buck
Bruce L. Carvalho
Claudio L. Cesar
Szu-Li Chang
Curtis S. Chen
Jerry C. Chen
Marilyn Y. Chen
Tak K. Cheng
Yiu Y. Chu
Isaac L. Chuang
Manoel E. Conde
Michael W. Courtney
Kevin M. Cuomo
Kristin Dana
Kendall Davis
Frank DiFilippo
Andy B. Dobrzeniecki
David J. Dougherty
Andre B. Fletcher
Jerrold A. Floro
Ethan B. Foxman
Seth A. Gordon
Reza A. Ghanbari
Julie E. Greenberg
Xuan H. Guo
Troy D. Hamnond
Helen M. Hanson
John F. Heanue
Olivier Herbelot
Lori K. Herold
William R. Hollaway
Steven H. Isabelle
Mark Jablonski
Jacek Jachner
Zoher Z. Karu
Raymond T. Klann
Warren M. Lam
Joseph Lehar
Gadi Lenz
Henri J. Lezec
Kevin Li
Hai P. Longworth
Andrew Lumsdaine
Christine M. Martin
Michael M. McCue
Ignacio S. McQuirk
Scott E. Meredith
Malini V. Narayanan
Aradhana Narula
James M. Njeru
Janet L. Pan
Timothy G. Reese
Michael D. Richard
Michael T. Richey
Timothy T. Rueger
Stephen F. Scherock
Amelia H. Shen
Scott R. Shepard
Barbara G. Shinn
Jared P. Squire
Robert W. Stadler
David G. Steel
Kohichi R. Tamura
Veena Trehan
Christopher B. Umminger
Filip Van Aelten
Taylen J. Wong
Xinglong Yan
Chan Yoo
Saed Younis

Undergraduate Students

John G. Abbamondi
Joseph K. Abedi
Gregory S. Adams
Mustafa K. Ahmed
Santosh Ananthraman
Christopher B. Anderson
Alexandar Angelus
Susan E. Bach
Kelly S. Bai
John E. Berberian
Stephen Bertram
Michele M. Bierbaum
Adam D. Brand
Bennett Brown
Stephanie Byrne
Vinay Chandra
Venkatesh R. Chari
George Chen
Stephanie M. Cheng
Patrick Chou
Daniel J. Chung
Michael W. Connell
Hooman Davoudiasl
Michael D. Dickens
Komlin O. Edoh
Mauricio A. Escobar
Leslie Fan
Juan Ferrera
Charles G. Freeman
Curtis A. Gabrielson
John M. Gachora
Swaroop Gantela
Boris Golubovic
Andrew H. Grant
Darby A. Hailes
John M. Hedgcock
Barry E. Hemmerdinger
Anna M. Ison
Mario A. Jimenez-Garate
Anthony C. Kam
Jerome Khohayting
Peter Khoury
Weng-Yew Ko
Shing Kong
Abhijit Kulkarni
Gloria W. Lau
Adnan H. Lawai
Chee-Heng Lee
Kenneth S. Lee
Michael H. Lim
Ronald G. Lovejoy
Sandra Y. Ma
Allison M. Marino
Matthew J. Marjanovic
Laura Marmorstein
Laura J. Mayfield
Michael J. McQuirk

Anna W. Men
Mark D. Messier
Michael W. Minnich
David Mitchell
Euclid E. Moon
Pablo Munguia
Arvind Narayana
Quinin T. Ndibongo
Kathryn M. Nelson
Lee P. Ng
Luong V. Nguyen
Son C. Nguyen
Lynn E. Niles
Francis D. Njie
Daniel B. Olster
John E. Oswald
Prashun R. Patel
Thomas J. Paul
Joel R. Phillips
Lisa Primiano
Jo-Ana Quirch
Charles A. Reisman
Rebecca J. Renn
Alexander P. Rigopulos
William W. Roberts
Charles D. Robinson
Anthony R. Salas
Shahir Salyani
Sumeet Sandhu
Gary J. Tarnowski
Colin J. Taylor
Quan M. Tran
Trac D. Tran
Roderick D. Tranum
Flora S. Tsai
Quentin Turchette
Timothy Ueng
Evren R. Unver
Benjamin Van Roy
Li-Fang Wang
Michele A. Wang
Lead Wey
Monnica Williams
Joshua N. Winn
Diana Wong
Derrick Yim
Yee-Chien C. Ying

Administrative Staff

Donald F. Duffy
Virginia R. Lauricella
Barbara J. Passero
John S. Peck
Gerrard F. Power
William H. Smith
Vicky-Lynn Taylor
Donna Maria Ticchi

Support and Technical Staff

Robert W. Aalerud
Mary C. Aldridge
Janice L. Balzer
Felicia G. Brady
Margery E. Brothers
Manuel Cabral, Jr.
Donald A. Clements
John F. Cook
Carol A. Costa
Ann K. Dix
Francis M. Doughty
Laura B. Doughty
Dorothy A. Fleischer
Deborah A. Gage
Donna L. Gale
Mary S. Greene
Debra L. Harring
Maureen C. Howard
Wendy E. Hunter
Barbara A. King
Cynthia Y. Kopf
Kit-Wah F. Lai
Sarah L. Larson
Lisbeth N. Lauritzen
Edward R. Lavalle
Cynthia LeBlanc
Anh Lieu
Wei Ming-Yu Lin
Catherine Lorusso
Eleanora M. Luongo
Rita C. McKinnon
Gina L.B. Milton
Mark K. Mondol
Susan E. Nelson
Donald K. North
Robert H. Priest
Brian E. Ray
Bruce A. Russell
Maxine P. Samuels
Clare F. Smith
Arlene E. Wint
Mary J. Ziegler

In Memoriam

Arthur Berg (1915 - 1990)

Younes Borki (1971 - 1990)

Professor Emeritus Edward L. Bowles (1888 - 1991)

Professor Emeritus and Senior Lecturer Joseph C.R. Licklider (1915 - 1990)

Professor James R. Melcher (1936 - 1991)

The tradition of service continues. . . Sponsored Research Technical Staff John W. Barrett (above) of RLE's Radio Astronomy Group completed 40 years of service in RLE on May 7, 1991. Shown holding his RadLab badge is John B. Sanroma (below), former Instrument Maker in both the Rad-Lab (1942-1945) and RLE (1946-1969).

Appendix C. RLE Research Support Index

Project Staff and Subject Index

Project Staff and Subject Index

A

B

C

D

E

F

G

H

I

J

K

L

M

N

O

P

Q

R

S

T

U

V

W

X

Y

Z